2007 Rocky Mountain Section Friends of the Pleistocene Field Trip—Quaternary Geology of the San Luis Basin of Colorado and New Mexico, September 7–9, 2007

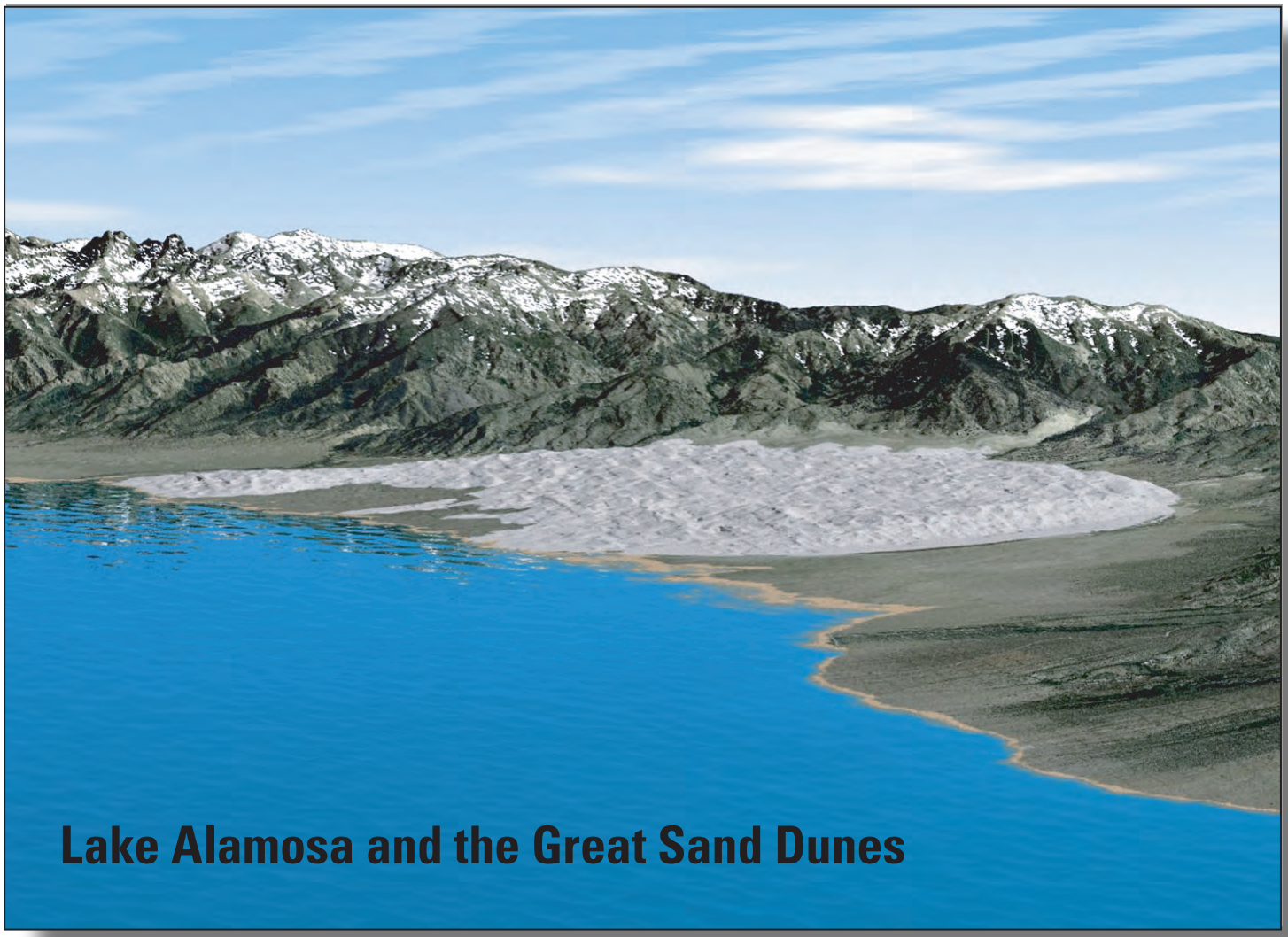

Open-File Report 2007–1193

U.S. Department of the Interior
U.S. Geological Survey

2007 Rocky Mountain Section Friends of the Pleistocene Field Trip—Quaternary Geology of the San Luis Basin of Colorado and New Mexico, September 7–9, 2007

By Michael N. Machette, Mary-Margaret Coates, and Margo L. Johnson

Open-File Report 2007–1193

U.S. Department of the Interior
U.S. Geological Survey

U.S. Department of the Interior
DIRK KEMPTHORNE, Secretary

U.S. Geological Survey
Mark D. Myers, Director

U.S. Geological Survey, Reston, Virginia: 2007

For product and ordering information:
World Wide Web: http://www.usgs.gov/pubprod
Telephone: 1-888-ASK-USGS

For more information on the USGS—the Federal source for science about the Earth,
its natural and living resources, natural hazards, and the environment:
World Wide Web: http://www.usgs.gov
Telephone: 1-888-ASK-USGS

Any use of trade, product, or firm names is for descriptive purposes only and does not imply endorsement by the U.S. Government.

This publication has not been reviewed for stratigraphic nomenclature.

Although this report is in the public domain, permission must be secured from the individual copyright owners to reproduce any copyrighted materials contained within this report.

Suggested citation:
Machette, M.N., Coates, M-M., and Johnson, M.L., 2007, 2007 Rocky Mountain Section Friends of the Pleistocene Field Trip—Quaternary geology of the San Luis Basin of Colorado and New Mexico, September 7–9, 2007: U.S. Geological Survey Open-File Report 2007–1193, 197 p.; available at <http://pubs.usgs.gov/of/2007/1193

Cover
A modern restoration of Lake Alamosa. View to the northeast from above the San Luis Hills, southeast of Alamosa, Colo. Visualization created in Visual Nature Studio (v. 2.7, 3D Nature Co.) by Paco Van Sistine (USGS) using 30-m DEM and a lake elevation of 7,660 ft (2,335 m).

Contents

Field-Trip Leaders vii
Prologue viii
Friends of the Pleistocene Rocky Mountain Section List of Annual Trips....x
Field Trip Guidebook
Chapter A — Field-Trip Day 1—Quaternary geology of Great Sand Dunes National Park and Preserve, southern Colorado (*Valdez, Forman, McCalpin, Madole, Machette, Schumann, Rupert, Mahan, Bunch*) 3
Orientation for Day 1—Friday, Sept. 7, 2006....3
Stop A1—Development and eolian geomorphology of Great Sand Dunes (*Valdez*)....7
Stop A2—Optical dating of episodic dune movement at Great Sand Dunes National Park and Preserve (*Forman*)....11
Stop A3—Paleoseismology of range-front fault scarps at Great Sand Dunes (*McCalpin*) 19
Stop A4—Parabolic dune migration across the southern sand sheet (*Forman*)....24
Stop A5—Cattle-guard Paleoindian site (*Bunch, Jodry*) 30
Stop A6—Medano Ranch area (*Madole, Mahan, Rupert*) 30
Stop A7—Sabkha overlook (*Valdez*)....36
Stop A8 (optional)—Closed basin overflow and origin of Hansen Bluff (*Valdez*)....38
Stop A9 (optional)—Middle and late Holocene eolian sand dunes (*Machette*)....40
Stop A10—Late Pleistocene to early Holocene wetland deposits in the Mr. Peat pit (*Machette, Schumann)*....42

Chapter B — Field-Trip Day 2—Quaternary geology of Lake Alamosa and the Costilla Plain, southern Colorado (*Machette, Thompson, Marchetti, Kirkham*) 53
Orientation for Day 2—Saturday, Sept. 8, 2007....53
Stop B1—Deposits of Lake Alamosa at the Bachus pit (*Machette*)....57
Stop B2—Soil on intermediate-age alluvium (post–Lake Alamosa), Sanford, Colo. (*Machette*)....61
Stop B3—Soils on and experimental dating of lacustrine gravels of Lake Alamosa at Saddleback Mountain (*Machette, Marchetti*) 63
Stop B4—Overview of the Rio Grande outlet (*Machette, Thompson*)....71
Stop B5 (optional) —Lagoons and barrier bars of ancient Lake Alamosa (*Machette*)....78
Stop B6 (optional)—And the wind blows—Fluted ventifacts on the ancient shore of Lake Alamosa (*Machette*) 81
Stop B7 (optional)—Hansen Bluff—Alamosa Formation (*Machette*) 85
Stop B8—Mesita Hill: An early Pleistocene volcano adrift in a sea of dirt (*Machette, Thompson, Kirkham*) 89
Stop B9—Landslides and the Sangre de Cristo fault zone along San Pedro Mesa (*Machette*)....100

Chapter C—Field-Trip Day 3—Quaternary geology of Sunshine Valley and associated neotectonics along the Latir Peaks section of the Southern Sangre de Cristo fault zone (*Ruleman, Shroba, Thompson)* 111
Overview....111
Stop C1—Volcanic and geomorphic setting of the Sunshine Valley and Taos Plateau (*Thompson, Ruleman*) 112
Stop C2—Highest depositional surface within Sunshine Valley (*Ruleman, Shroba*)...114
Stop C3—Faulted Servilleta Basalt (3.66–4.75 Ma) at Latir Creek (*Ruleman*) 116
Stop C4—Old Alluvium (unit Qao2) overlying Servilleta Basalt and Santa Fe Formation (*Shroba, Ruleman*)....120
Stop C5—Ute Mountain volcanic rocks and fan deposits and surficial geology of northern Sunshine Valley (*Thompson, Shroba*)....121
Stop C6—Faulted alluvium at Jaroso Canyon, Latir Peaks section of the southern Sangre de Cristo fault zone (*Ruleman*) 125
Stop C7—Piedmont fault scarp on Cedro Canyon fan (*Ruleman*) 128

Papers
Chapter D—Ground-water age and flow at Great Sand Dunes National Monument, south-central Colorado (*Rupert and Plummer*) 135
Chapter E—Dating and stratigraphy of middle to late Holocene eolian sand deposits in the San Luis Basin, east of Alamosa, Colorado (*Machette and Puseman*)....139
Chapter F—Late Pleistocene to early Holocene paleoecology of the Mr. Peat wetland deposit, Alamosa County, Colorado (*Schumann and Machette)* 147
Chapter G—Ancient Lake Alamosa and the Pliocene to middle Pleistocene evolution of the Rio Grande (*Machette, Marchetti, and Thompson)* 157
Chapter H—Geology of Mesita volcano, Colorado—Eruptive history and implications for basin sedimentation during the Quaternary (*Thompson, Machette, Shroba, and Ruleman*) 169
Chapter I—Possible role of eolian sediment in the genesis of bouldery debris-flow deposits on the lower flanks of Ute Mountain, northern Taos Plateau volcanic field, New Mexico (*Shroba, Thompson, and Ruleman)* 181
Chapter J—An overview of the Sangre de Cristo fault system and new insights into interactions between Quaternary faults in the northern Rio Grande rift (*Ruleman and Machette*) 187

Conversion Factors

Units of measure

The U.S. Geological Survey uses international units of measure (meters, kilometers, kilograms, etc), so our normal policy is to use only these units. However, because this guidebook deals with distances that are always shown in miles on road signs and automobile odometers, and because all of the detailed topographic maps (1:24,000-scale) use feet as the measure of elevation, we feel compelled to provide both units. Thus, for this report our convention for reporting units of measure will be as follows:

For distances, we use kilometers (and miles)

For elevations, we use feet (and meters) asl (above sea level)

For thickness in measured section and heights above or below some datum (such as stream level or canyon rim), we use only metric (meters or kilometers).

For areas and volumes, we use only metric (cm^2, m^2, or km^2; cm^3, m^3, or km^3)

For weights, we use only metric (grams or kilograms)

The following table lists conversion factors useful for this report:

Multiply SI unit	By	To obtain English unit
	Length	
centimeter (cm)	0.3937	inch (in.)
millimeter (mm)	0.03937	inch (in.)
meter (m)	3.281	foot (ft)
kilometer (km)	0.6214	mile (mi)
	Area	
square centimeter (cm^2)	0.1550	square inch (ft^2)
square centimeter (cm^2)	0.001076	square foot (ft^2)
square meter (m^2)	10.76	square foot (ft^2)
square meter (m^2)	0.0002471	acre
square kilometer (km^2)	247.1	acre
square kilometer (km^2)	0.3861	square mile (mi^2)

Temperature in degrees Celsius (°C) may be converted to degrees Fahrenheit (°F) as follows:
°F=(1.8×°C)+32

Temperature in degrees Fahrenheit (°F) may be converted to degrees Celsius (°C) as follows:
°C=(°F–32)/1.8

Vertical coordinate information is referenced to the insert datum name (and abbreviation) here, for instance, “North American Vertical Datum of 1988 (NAVD 88)”

Horizontal coordinate information is referenced to the insert datum name (and abbreviation) here, for instance, “North American Datum of 1983 (NAD 83)”

Altitude, as used in this report, refers to distance above the vertical datum.

Abbreviations Used in This Report

Units of measure	
^{14}C	carbon 14 (radiocarbon)
^{14}C yr	radiocarbon years
asl	above sea level
cal yr B.P.	calibrated years before present
cm	centimeter, centimeters
cm/yr	centimeters per year
ft	foot, feet
ft/mi	feet per mile
g	gram
g/cm^2	gram per square centimeter
Gy	Gray (a measure of absorbed dose for luminescence dating)
ka	thousands of years ago
km	kilometers
k.y.	thousands of years (duration of time)
m	meter, meters
m/s	meters per second
m/yr	meters per year
mGy/yr	milli-Grays per year
mi	miles
mm	millimeter, millimeters
mm/yr	millimeters per year
mW/cm^2	milliwatts per square centimeter
nm	nanometers
nT	nano-Tesla
s	second, seconds
torr	unit of pressure; 1 torr = 133.322368 pascals
wt percent	weight percent
yr	year

Initialisms	
AMS	accelerator mass spectrometry
BLM	Bureau of Land Management
B.P.	before present
DP	drift potential
EROS	Earth Resources Observation System
ETM	enhanced thematic mapper
FOP	Friends of the Pleistocene
GSDNPP	Great Sand Dunes National Park and Preserve
HF	hydrofluoric acid
ICP-MS	inductively coupled plasma–mass spectrometry
IRSL	infrared stimulated luminescence
M	moment magnitude
M_w	moment magnitude
M_s	moment magnitude
MAP	mean annual precipitation
MAT	mean annual temperature
NAD27	North American Datum of 1927
NOSAMS	National Ocean Sciences Accelerator Mass Spectrometry facility
NPS	U.S. National Park Service
OIS	oxygen-isotope stage
OSL	optically stimulated luminescence
PD	parabolic dune
PE	paleoevent
PDSI	Palmer Drought Severity Index
RDD	resultant drift direction
RDP	resultant drift potential
RDP/DP	ratio of resultant drift potential to resultant drift direction
RMMP	(private company)
SAR	single aliquot regeneration
SCS	Soil Conservation Service
TCN	terrestrial cosmogenic nuclide
U.S.A.	United States of America
USGS	U.S. Geological Survey
UTM	Universal Transverse Mercator

Edited by Michael N. Machette, Mary-Margaret Coates, and Margo L. Johnson

Field-trip leaders:

Day 1—Andrew Valdez, Steve Forman, Richard Madole, Jim McCalpin, Michael Machette, Mike Rupert, Randy Schumann, Shannon Mahan, Pegi Jodry, and Fred Bunch

Day 2—Michael Machette, Ren Thompson, David Marchetti, and Robert Kirkham

Day 3—Cal Ruleman, Ren Thompson, Ralph Shroba, and David Marchetti

2007 Rocky Mountain Cell Friends of the Pleistocene Field Trip—Quaternary Geology of the San Luis Basin of Colorado and New Mexico, September 7–9, 2007

Prologue

Welcome to the 2007 Rocky Mountain Cell Friends of the Pleistocene Field Trip, which will concentrate on the Quaternary geology of the San Luis Basin of Colorado and New Mexico. To our best knowledge, Friends of the Pleistocene (FOP) has never run a trip through the San Luis Basin, although former trips in the region reviewed the "Northern Rio Grande rift" in 1987 and the "Landscape History and Processes on the Pajarito Plateau" in 1996. After nearly a decade, the FOP has returned to the Rio Grande rift, but to an area that has rarely hosted a trip with a Quaternary focus. The objective of FOP trips is to review—in the field—new and exciting research on Quaternary geoscience, typically research being conducted by graduate students. In our case, the research is more topically oriented around three areas of the San Luis Basin, and it is being conducted by a wide range of Federal, State, academic, and consulting geologists.

This year's trip is ambitious—we will spend our first day mainly on the Holocene record around Great Sand Dunes National Park and Preserve, the second day on the Quaternary stratigraphy around the San Luis Hills, including evidence for Lake Alamosa and the 1.0 Ma Mesita volcano, and wrap up the trip's third day in the Costilla Plain and Sunshine Valley reviewing alluvial stratigraphy, the history of the Rio Grande, and evidence for young movement on the Sangre de Cristo fault zone.

In the tradition of FOP trips, we will be camping along the field trip route for this meeting. On the night before our trip, we will be at the Great Sand Dunes National Park and Preserve's Pinyon Flats Campground, a group facility located about 2 miles north of the Visitors Center. After the first day's trip, we will dine and camp in the Bachus pit, about 3 miles southwest of Alamosa. For the final night (after day 2), we will bed down at La Junta Campground at the Bureau of Land Management (BLM) Wild and Scenic Rivers State Recreation Area, west of Questa, New Mexico, overlooking a majestic canyons of the Rio Grande and Red River.

This is the 48th meeting of the Rocky Mountain Section of FOP, which was initiated by Gerry Richmond (USGS-Denver, deceased) in 1952 (see the following table, which lists all the Rocky Mountain Section field trips). The Rocky Mountain Section has been inactive for three years owing to a series of problems, including an unfortunate cancellation of Dennis Dahms' trip to the southern Wind River Range in 2005. Hopefully, this year's trip will provide the logistical initiative and scientific momentum for future Friends of the Pleistocene trips in the Rocky Mountain region.

Michael Machette
Organizer and Editor

2007 FOP Rocky Mountain Section

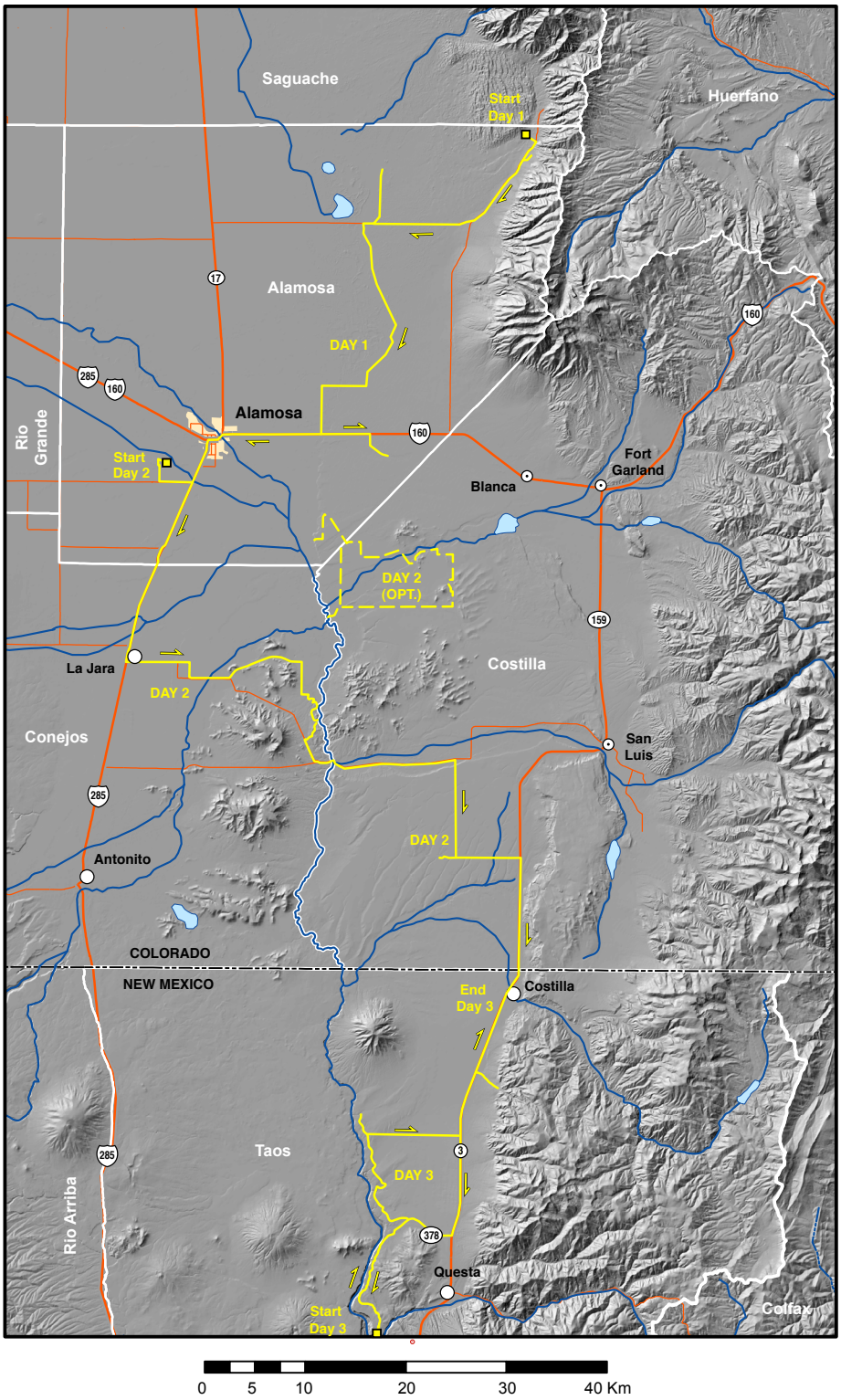

Figure 1. Route map for the FOP trip, days 1, 2, and 3. More detailed maps for each day are included in chapters A, B, and C (respectively) in this volume.

FRIENDS OF THE PLEISTOCENE ROCKY MOUNTAIN SECTION LIST OF ANNUAL TRIPS

This section (or cell) was organized by Gerry Richmond in May 1952 at the Rocky Mountain Section meeting of the Geological Society of America at Salt Lake City, Utah

No.	Year	Date	Area or title and leaders
1	1952	Oct. 4–5	Rocky Mountain National Park, Colorado: Gerald Richmond
2	1953	Oct. 3–4	Twin Lakes area, Colorado: Gerald Richmond
3	1954	Oct. 9–10	Medicine Bow–Laramie area, Wyoming: S.H. Knight
---	1955–1957		No trip conducted
4	1958	Sept. 5–7	Jackson Hole area, Wyoming: J.D. Love, John Montagne
5	1959	Sept. 12–13	Pinedale and Lander areas, Wyoming: Gerald Richmond
6	1960	Sept. 10–11	Little Cottonwood Creek area, Salt Lake County, Utah: Henry Goode, Roger Morrison
7	1961	Aug. 25–26	Bear Lake Valley, Utah–Idaho, to American Falls, Idaho: J. Stewart Williams, Donald Trimble, Allan Willard, Verlyn Parker
8	1962	Aug. 24–26	Twin Falls to Glenns Ferry, Idaho (Snake River Canyon): Harold Malde, Howard Powers, Dwight Taylor
9	1963	Aug. 23–24	Madison River Valley and Yellowstone River Valley from Hayden Valley to Pine Creek, Montana: John Good, J.D. Love, John Montagne
10	1964	Aug. 28–30	Quaternary geology of the Duncan-Virden-Safford area, New Mexico: Roger Morrison
---	1965		No FOP trips, in light of the 1965 INQUA meeting in Boulder, Colo.
11	1966	Aug. 26–28	Landscape evolution and soil genesis in the Rio Grande region, southern New Mexico (Desert Project, Soil Investigations, Soil Conservation Service): John Hawley, Leland Gile
12	1967	Aug. 25–27	Western Snake River Plain, Idaho: Harold Malde
13	1968	Sept. 21–22	San Pedro Valley and Murray Springs archeological site, Arizona: Vance Haynes, Larry Aggenbroad, Peter Mehringer, Paul Martin, Everett Lindsay, William Wasley, Thomas Hemmings
14	1969	Oct. 4–5	Jordan Valley, Utah: Richard Van Horn, Edward Weakly
15	1970	Oct. 2–4	San Francisco Peaks (Flagstaff area): Troy Péwé, R.G. Updike
16	1971	Oct. 9–10	Bishop–Mono Lakes area, California: Michael Sheridan
17	1972	Sept. 9–10	Canon City–Westcliffe area (Wet Mountain Valley), Colorado: Glenn Scott, Richard Taylor, Rudy Epis
18	1973	Sept. 15–16	Mt. Sopris–Thomas Lakes area, Colorado: Peter Birkeland, Ralph Shroba, James Yount
19	1974	Sept. 6–7	West Yellowstone–Gallatin River–Three Forks area, Montana: John Montagne, Cliff Montagne, Ken Pierce, Leslie Davis
20	1975	Oct. 17–18	Southern High Plains, Texas: C.C. Reeves, Jr., James Goolsby, Charles Johnson, Eileen Johnson, John Hawley
21	1976	Aug. 27–28	Plains of southern Alberta (Canada): Chester Beaty, Rene Barendregt, John Dormaar, Stuart Harris, Archie Stalker
22	1977	Aug. 2–3	Natural Trap cave, Lovell, Wyoming: B. Miles Gilbert
23	1978	July 29–30	Hot Springs Mammoth site, South Dakota: L.D. Agenbroad
24	1979	July 9–10	Agate Basin archeological site, Wyoming: George Frison
---	1980		No trip conducted
25	1981	Sept. 19–20	Roaring Fork Valley and Twin Lakes and Chalk Creek areas, central Colorado: Alan Nelson, Lucy Piety, Ralph Shroba
26	1982	Sept. 17–19	Little Valley, Jordan Valley, and Beaver Basin, Utah: William Scott, Michael Machette, Ralph Shroba, William McCoy
27	1983	Aug. 26–28	Three trips—(1) Jokulhlaups in to the Sanpoil arm of glacial Lake Columbia, Washington: Brian Atwater; (2) Jokulhlaups near Spokane, Washington, and Lewiston, Idaho: Richard Waitt; (3) Glacial sequence near McCall, Idaho: Steven Colman, Ken Pierce, Richard Fosberg

28	1984	Aug. 10–11	Northern Bighorn Basin, Wyoming–Montana: Marith Reheis, Dale Ritter, Robert Palmquist
29	1985	Sept. 19–20	Animas Valley, Colorado–New Mexico: Mary Gillam, Robert Blair
30	1986	Sept. 6–7	Yellowstone National Park, Wyoming–Montana–Idaho: William Locke, Grant Meyer, Wayne Hamilton, John Montagne, David Nash, Steven Personius, Ken Pierce, Gerald Richmond
31	1987	Oct. 8–11	Northern Rio Grande rift, New Mexico: Dave Dethier, Chuck Harrington, Dave Love, Chris Menges, Steve Wells, John Wesling, Ralph Shroba
32	1988	Oct. 14–15	Tonto Basin, central Arizona: Larry Anderson, Lucy Piety, Dale Nations, Jim Faulds, Joel Sturm, Cathy Wellendorf
33	1989	Aug. 17–21	Wind River Mountains, Wyoming: Peter Birkeland, Curt Sorenson, Ralph Shroba, Dennis Dahm, Bob Hall
34	1990	Aug. 15–19	Quaternary geology of the western Madison Range, Madison Valley, Tobacco Root Range, and Jefferson Valley: Robert Hall, Ken Adams, Bill Locke, Scott Lundstrom, and ten others
35	1991	Oct. 11–13	Lake Bonneville stratigraphy and Quaternary volcanism in the Sevier and Black Rock Deserts, Utah: Charles (Jack) Oviatt (ed.), William McCoy, William Nash
36	1992	Sept. 11–13	Quaternary geology of Jackson Hole, Wyoming: Ken Pierce, John Good
37	1993	Sept. 10–12	Quaternary geology of the Mission Valley, Montana: Dan Levish, Dean Ostenaa, Ralph Klinger
38	1994	Aug. 13–14	Quaternary geology of the Wind River Basin, Wyoming: Oliver Chadwick, Bob Hall, Gene Kelley, Ronald Amundson, John Gosse, Fred Phillips, Cheryl Jaworoski
39	1995	Aug. 25–27	Late Pleistocene–Holocene evolution of the northeastern Yellowstone landscape: Grant Meyer (ed.), James Anderson, Matthew Bingham, Peter O'Hara, Eric Simpson, Kenneth Pierce
40	1996	Sept. 12–15	Landscape history and processes on the Pajarito Plateau, northern New Mexico: Steve Reneau, Eric McDonald, Craig Allen, David Broxton, Jamie Gardner, Rory Gauthier, Keith Kelson, William Phillips, Bradford Wilcox
41	1997	Oct. 12–14	The active geologic environment of central Colorado—Aspen–Glenwood Springs area, Colorado: Jim McCalpin (ed.), Bob Kirkham, Bruce Stover, Jim White
42	1998	Sept. 10–13	Soil, water, and earthquakes around Socorro, New Mexico: Bruce Harrison (ed.), Dave Love, Carol Treadwell-Stietz, Dennis McMahon, Michael Machette, Allen Gellis, Milan Pavih, Missy Eppes, Fred Phillips, John Hawley, Frank Pazzaglia, and Dan Koning. Included premeeting (Sept. 10) and postmeeting (Sept. 13) trips
43	1999	Sept. 10–12	Quaternary and environmental geology of the southwestern San Juan Mountains, Colorado: Mary Gillam, Robert Blair, Stanley Church, Scott Elias, Robert Kirkham, Thomas Perry, Fred Phillips, and others
44	2000	Sept. 22–24	Red Gate to Blue Gate–Lava-boulder diamicts and gravel, Aquarius Plateau through Waterpocket Fold (Capitol Reef), Utah: Richard Waitt (ed.), Thure Cerling, Dave Marchetti, Lee Kreutzer, Adrienne Anderson
45	2001	Oct. 12–14	Plio-Pleistocene stratigraphy and geomorphology of the central part of the Albuquerque Basin: Sean Connell, David Love, John Sorrell, Bruce Harrison
46	2002	Oct. 11–13	Quaternary stratigraphy and tectonics, and Late Prehistoric agriculture of the Safford Basin (Gila and San Simon River valleys), Graham County, Arizona: Brenda Houser, Philip Pearthree, Jeffry Homburg, Lawrence Thrasher
47	2003	Sept. 5–7	Fan-tastic, flaming, firn-filled fluvial FOP [central Idaho]: Jennifer Pierce (ed.), Grant Meyer, Charlie Luce, Tom Black, Glenn Thackray, Spencer Wood
---	2004		No trip conducted
---	2005	July 29–31 (canceled)	Glacial stratigraphy, erosion, and paleoenvironments of the southern Wind River Range, Sinks Canyon, Lander, Wyoming: Dennis Dahms
---	2006		No trip conducted
48	2007	Sept. 7–9	Quaternary geology of the San Luis basin, southern Colorado and northern New Mexico: Michael Machette, Cal Ruleman, Ralph Shroba, David Marchetti, Ren Thompson, Andrew Valdez, Steve Forman, and others

Frontispiece, Chapter A. Autumn view of the dunes and Sangre de Cristo Mountains from Zapata Falls Recreation Area. National Park Service photograph by Patrick Myers.

Chapter A — Field Trip Day 1 Quaternary Geology of Great Sand Dunes National Park and Preserve, Southern Colorado

By Andrew Valdez, Steve Forman, Richard Madole, James McCalpin, Michael Machette, Randy Schumann, Mike Rupert, Shannon Mahan, and Fred Bunch

Orientation for Day 1 — Friday, Sept. 7, 2006

Speakers: Michael Machette and Fred Bunch
Location: Dunes parking lot, Great Sand Dunes National Park and Preserve
1.1 road mi (1.8 km) southwest of Pinyon Flats Campground
0.9 road mi (1.4 km) northwest of the Park's Visitor Center
Zapata Ranch 7.5' quadrangle
GPS: NAD27, Zone 13, 454450 m E., 4176800 m N.
Elevation: 8,060 ft

Welcome to the 2007 Rocky Mountain Section Friends of the Pleistocene (FOP) field trip to the San Luis Basin. An introduction to this year's FOP trip will be presented by field trip organizer Michael Machette (USGS) and we'll discuss some basic aspects of field trip logistics and our general route through the San Luis Basin for the next three days (see fig. A1). A brief discussion of the Quaternary geology of local area will be presented using posters. Finally, Fred Bunch of the National Park Service (NPS), Chief of Resource Management at Great Sand Dunes National Park and Preserve (GSD-NPP), will welcome our group and provide an overview of the Park (http://www.nps.gov/grsa).

Overview

Day 1 will focus on surficial deposits of the eastern Alamosa Basin, a subbasin of the Rio Grande rift (fig A–1). The dominant feature is an eolian system that appears to be fed by a playa lake system. Most of the research conducted in this area has focused on modern (Holocene) geological and hydrological processes as well as on archeology of the same time period. Few details are known about the geologic history of the eolian deposits. It was once assumed that the dunes were a product of glacial outwash and dated to around 12,000 yr B.P. Drilling during groundwater exploration has revealed that the eolian sand extends hundreds of feet into the subsurface, so potentially they could be much older than 12,000 years as the creation of accommodation space in a rift valley is a slow process. Where penetrated, the eolian sands start within about 10 feet of a lacustrine deposit known locally as the blue clay layer. If this clay is from Lake Alamosa (discussed on day 2), then the eolian system may have been initiated by the lake retreat (see cover photo) and been a continuous feature since.

The trip begins at the terminal end of the eolian system, the main dune field of Great Sand Dunes (fig A–2), proceeds up the wind gradient into an extensive playa system, and then heads south where eolian sand thins and stream erosion has exposed some peat deposits. NPS geologist Andrew Valdez will present an overview of the eolian system and the geologic processes that influence its development. Figure A–3, which is a genetic classification of eolian sand dunes based on processes, vegetation, and topography, provides a basis for much of the discussion of dunes and dune forms. Steve Foreman, University of Illinois, Chicago, has used optically stimulated luminescence (OSL) dating on samples collected near the main dune field and on the sand sheet. He will be talking about the depositional history of the dunes and how parabolic dunes respond to climatic variations. Rifting creates the depositional setting of the basin. To understand that setting, Jim McCalpin, GeoHaz Consultants, conducted a paleoseismology study on exposed fault scarps, and he present his results. The irregular surface of the sand sheet must have been a productive hunting ground for Paleoindians, as Pegi Jodry of the Smithsonian Institution will explain. Rich Madole, U.S. Geological Survey (USGS), has developed a Quaternary stratigraphy for the upper eolian deposits and mapped the deposits based upon his stratigraphic identifications. Rich will explain his logic and keys to identifying these units. Next up, Mike Rupert, USGS, will present his findings

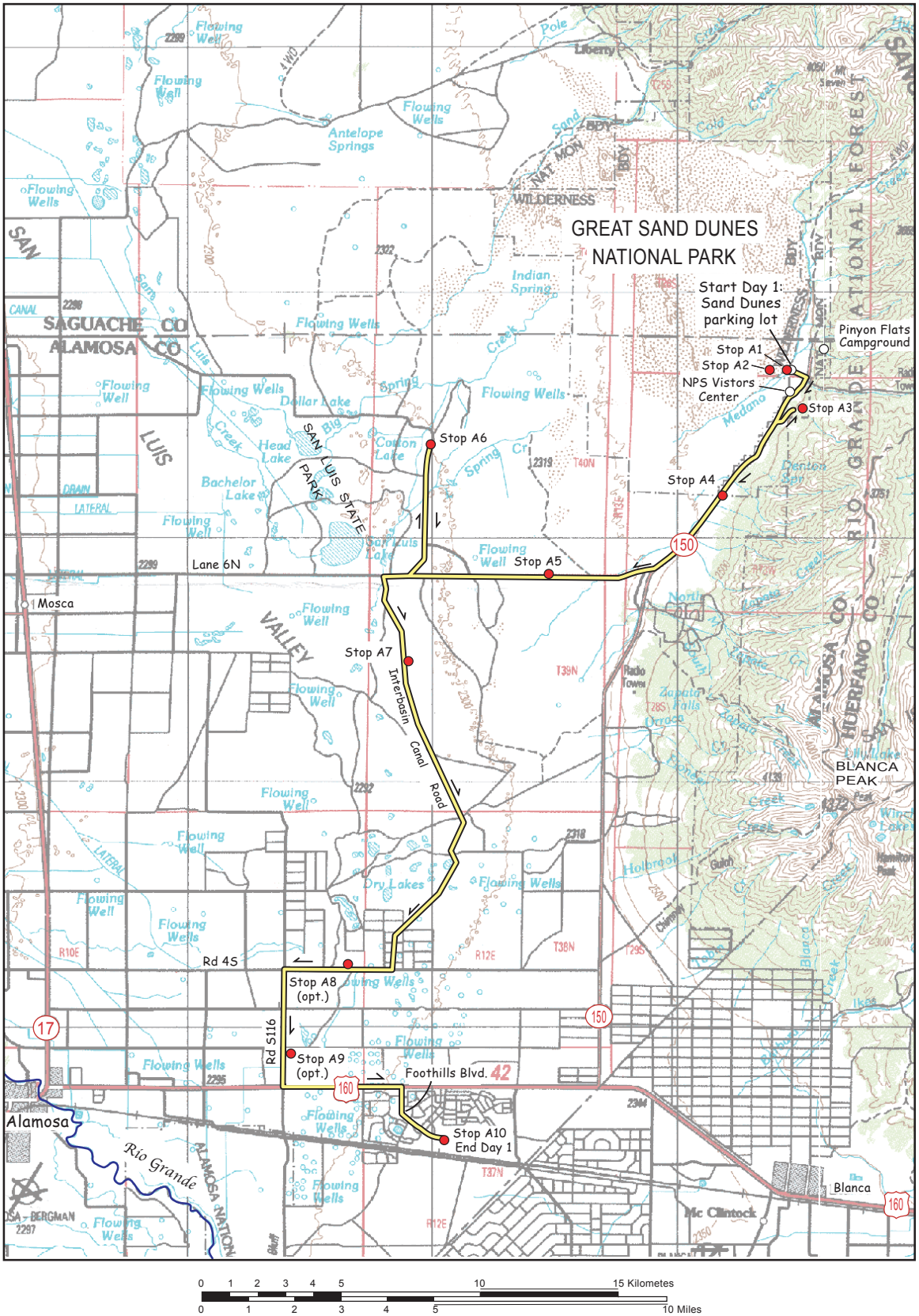

Figure A-1. Route and stops of field trip day 2.

on dating groundwater. The several aquifers in the Alamosa Basin each contain water with a distinct residence time. The trip will then proceed along the edge of the playa lake area for a closer examination of the features of the sabkha; quick stops will be led by Andrew Valdez, Michael Machette, and Randy Schumann. The field trip ends at a paleostream valley east of Alamosa where peat and tufa deposits indicate a vastly different environment than that of the present.

The day ends with a catered dinner at the Bachus pit (stop B1), which serves as our official FOP campground in Alamosa. It's a few miles southwest of Alamosa and the starting point for day 2. However, Alamosa has numerous other restaurants, motels, and camping options.

Acknowledgments

We would not be able to visit any of the stops on this or other days of the field trip without the permission of the landowners. Therefore, we would like to thank the following for allowing access to their properties during day 1 of the field trip:

Stops A1–A3: National Park Service, Mosca, Colo.
Stop A4: Patty Vittoria, owner, Great Sand Dunes Oasis (general store)
Stop A5: National Park Service, Mosca, Colo., and Medano Ranch (The Nature Conservancy)
Stop A6: National Park Service, Mosca, Colo., and Zapata Ranch (The Nature Conservancy)
Stop A7: U.S. Bureau of Reclamation, Closed Basin Division, Alamosa, Colo.
Stop A8: U.S. Bureau of Reclamation, Closed Basin Division, Alamosa, Colo.
Stop A9: The Cisneros family, Alamosa, Colo. (no trespassing please)
Stop A10: Adrian Absmeier, Absmeier Landscaping (previously RMMP), Alamosa, Colo.

In addition, we appreciate the constructive and helpful comments of Margaret Berry (USGS) and Daniel Muhs (USGS), who reviewed a preliminary version of this manuscript. However, any errors that may remain are the responsibility of the authors.

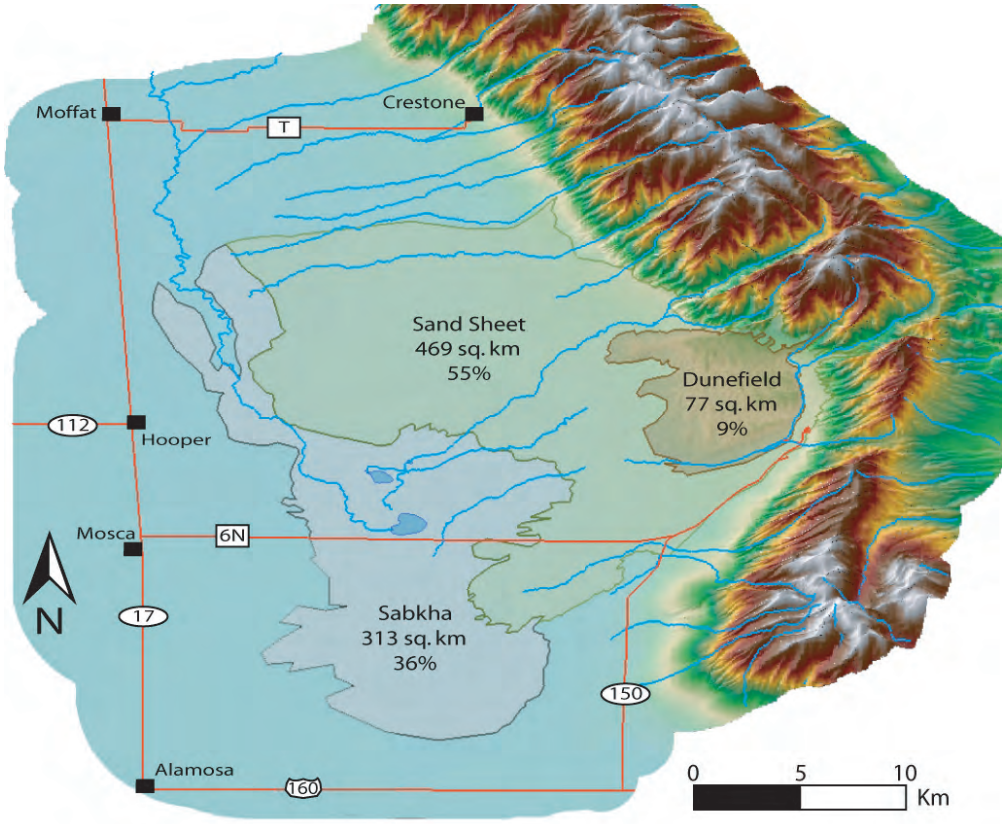

Figure A–2. Aerial view of the Great Sand Dunes and adjacent parts of the San Luis Valley and Sangre de Cristo Mountains. The dune field, sand sheet, and sabkha are subjects of the field trip. A digital elevation model is draped over topography to create a three-dimensional image of the area.

Toward a Genetic Classification of Aeolian Sand Dunes

Kevin R. Mulligan, Department of Economics and Geography, Texas Tech University Lubbock, Texas
Vatche P. Tchakerian, Department of Geography and Geology & Geophysics, Texas A&M University, College Station, Texas

Aeolian sand dunes occur in a wide variety of forms in many different environmental settings. Although several notable attempts have been made to classify dune forms (e.g. Hack, 1941; McKee, 1979; Pye and Tsoar, 1990; Cooke *et. al.*, 1993; Lancaster, 1995; Livingstone and Warren, 1996; Thomas, 1997), the problem of dune classification is complicated by the diverse terminology used in the literature and a lack of consensus among geomorphologists. More importantly, most dune classification systems fail to emphasize the genetic linkage between different dune types. In many situations dune morphologies can be represented as part of a continuum from one dune type to another.

The purpose of this paper is to outline a simple dune classification system that stresses the genetic linkage between the different types of dunes controlled by autogenic processes, vegetation and topography.

Dunes Related to Autogenic Processes
In the first case, dunes controlled by autogenic processes reflect bedform self-organization and the nature of dune morphology is largely a function of the wind regime, sand supply and time. Over very long time scales these dunes can become part of larger draas or ergs in depositional basins or sinks.

Dunes Related to Vegetation
In the second case, vegetation is considered to be an important controlling variable and dunes are classified as part of a continuum reflecting the degree of sand accumulation or deflation. In the absence of vegetation (either natural or human induced), these dunes can take on the form of autogenic dunes.

Dunes Related to Topography
Lastly, dunes are classified in relation to topography, expressed as either sloped terrain or cliffed terrain. In this case, dune forms are controlled by their relative position with respect to the dominant wind direction and slope.

REFERENCES

Cooke, R., Warren, A., and Goudie, A., 1993, *Desert Geomorphology*, UCL Press, London, p. 526.

Hack, J.T., 1941, Dunes of the western Navaho county, *Geographical Review*, v. 31, p. 240-263.

Lancaster, N., 1995, *Geomorphology of Desert Dunes*, Routledge Press, London, 290 p.

Livingstone, I., and Warren, A., 1996, *Aeolian Geomorphology*, Longman, Essex, 211 p.

McKee, E.D., 1979, Introduction to a study of global sand seas. In E.D. McKee (ed) *A Study of Global Sand Seas*, U.S.G.S. Professional Paper 1052, p. 1-19.

Pye, K., and Tsoar, H., 1990, *Aeolian Sand and Sand Dunes*, Unwin Hyman, London, 396 p.

Thomas, D.S.G., 1997, *Arid Zone Geomorphology*, John Wiley and Sons, London, 713 p.

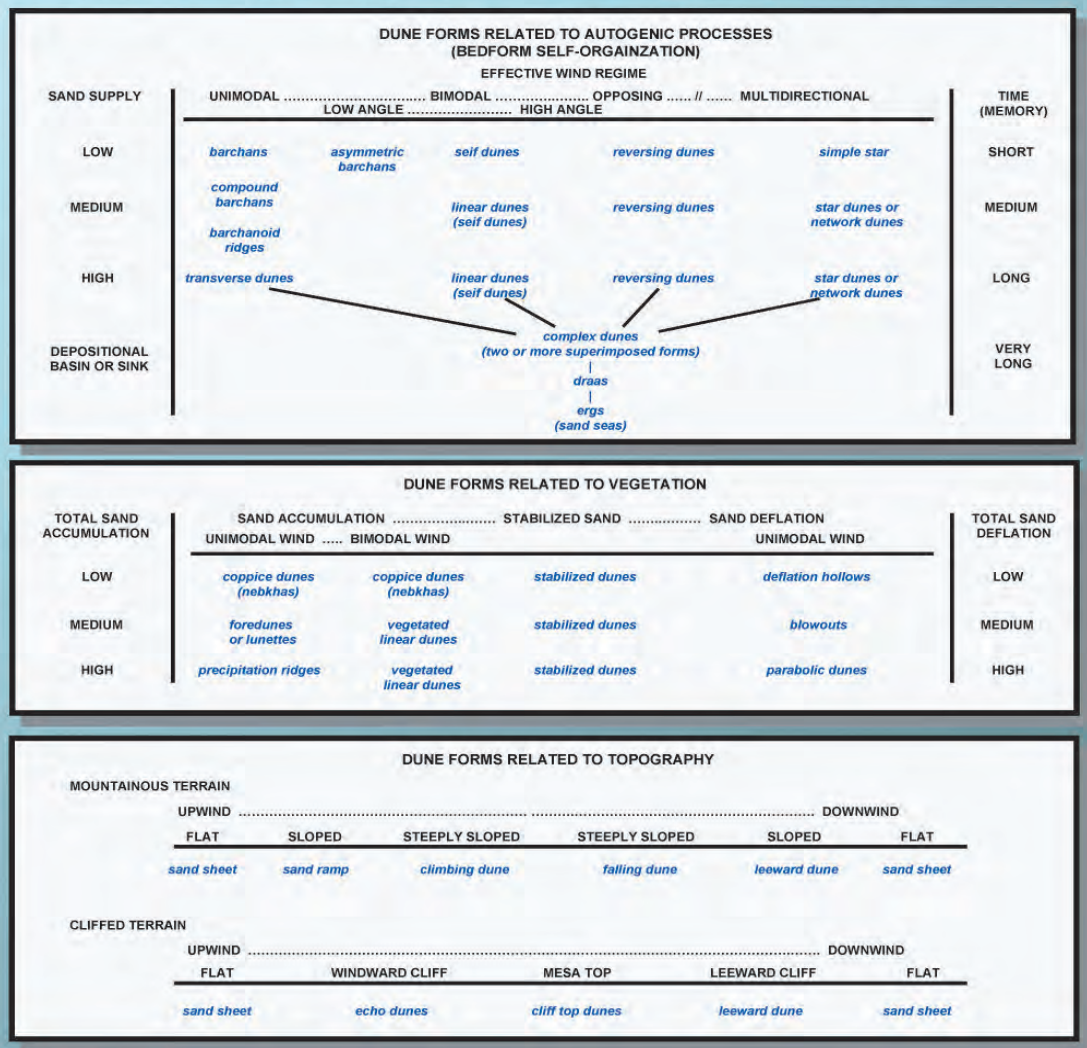

Figure A–3. A genetic classification of eolian sand dunes (Mulligan and Tchakerian, written commun. to Andrew Valdez, 2006).

Stop A1 — Development and Eolian Geomorphology of Great Sand Dunes

Speaker: Andrew Valdez
Location: Medano Creek, 200 m west of Dunes Picnic Area, Great Sand Dunes National Park and Preserve
Zapata Ranch 7.5' quadrangle
GPS: NAD27, Zone 13, 454300 m E., 4176740 m N.
Elevation: 8,060 ft

Synopsis

The Alamosa Basin contains several eolian sand deposits that extend from the axis of the basin (its topographic low points) eastward to the Sangre de Cristo Mountains. With increasing elevation these sand deposits transition from a sabkha to a sand sheet, then to a dune field, and finally into sand ramps. The setting for the eolian deposits is created by the sediment-filled San Luis Basin (upper Rio Grande rift), and dunes are modified by variations in wind regime, transport of sand by streams, the presence of vegetation, and near-surface groundwater. The interaction of these processes results in multiple sand deposits and also causes variations in dune configuration and dune types.

Discussion

The Great Sand Dunes eolian system is located in south-central Colorado, U.S.A., in a physiographic area known as the San Luis Valley (fig. A1–1). The San Luis Valley occupies the San Luis Basin, which is part of the Rio Grande rift, an eastern portion of the Basin and Range Province. It is bound by the San Juan Mountains on the west and the Sangre de Cristo Mountains on the east. Eolian deposits are well developed in the Alamosa subbasin, which is the northern part of the San Luis Basin.

The eolian system changes along a topographic gradient from sabkha to sheet sand to dune field and terminates as a sand ramp (fig. A1–2). In a simple view, this system can be described as a process whereby (1) streams deposit sand in sabkha areas; (2) wind transports the sand across the sand sheet; and (3) sand is ultimately deposited in the dune field and up onto a sand ramp (Fryberger, 1990a). The extent of the Great Sand Dunes eolian system can be traced upwind to the playa area, suggesting that the sand had its sources in a playa system (Madole and Romig, 2002).

Dune types also differ along this topographic gradient (fig. A1–3). Vegetation-related dune forms develop on the lower gradient where sand movement is inhibited. As the gradient and amount of sand exposure increases, autogenic (self-organizing) dunes are formed. Along the mountain front, topography controls the development of dunes. Coppice dunes and lunettes (crescent- or tongue-shaped dunes) are common near the sabkha, whereas blowouts, parabolic dunes, and transverse dunes develop downwind of the sabkha. Reversing and star dunes are the primary dune types of the dune field.

The variation in sand deposits and dune types results from the interaction of five geologic processes that are fundamental to the development of the eolian system. At Great Sand Dunes these processes are (1) crustal rifting, extension, uplift, and basin formation, all leading to topography favorable for sediment deposition; (2) sand transport by stream flow; (3) sand transport related to wind regime; (4) sand stabilization by vegetation growth; and (5) sand cementation by evaporite minerals. Rifting creates a closed basin allowing sand to accumulate. It also is responsible for the development of a playa-lake system and the configuration of the Sangre de Cristo Mountains, which provide topographic controls on wind flow. Wind regime controls dune type and behavior; streams modify the perimeter of the dune field, and vegetation stabilizes surfaces.

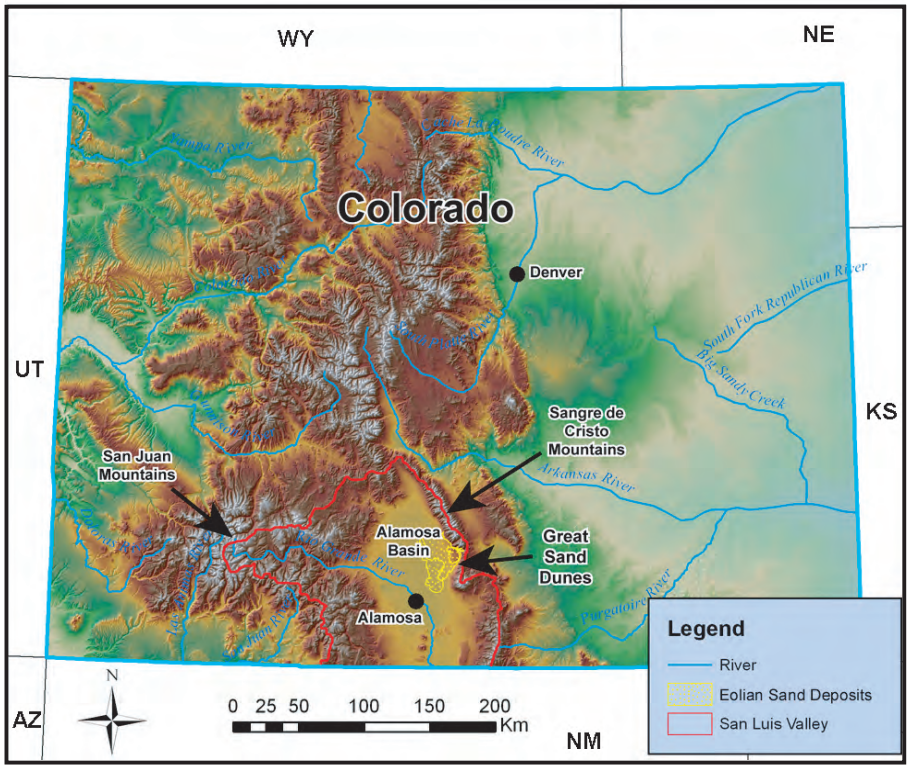

Figure A1–1. Location of San Luis Valley and Great Sand Dunes in southern Colorado.

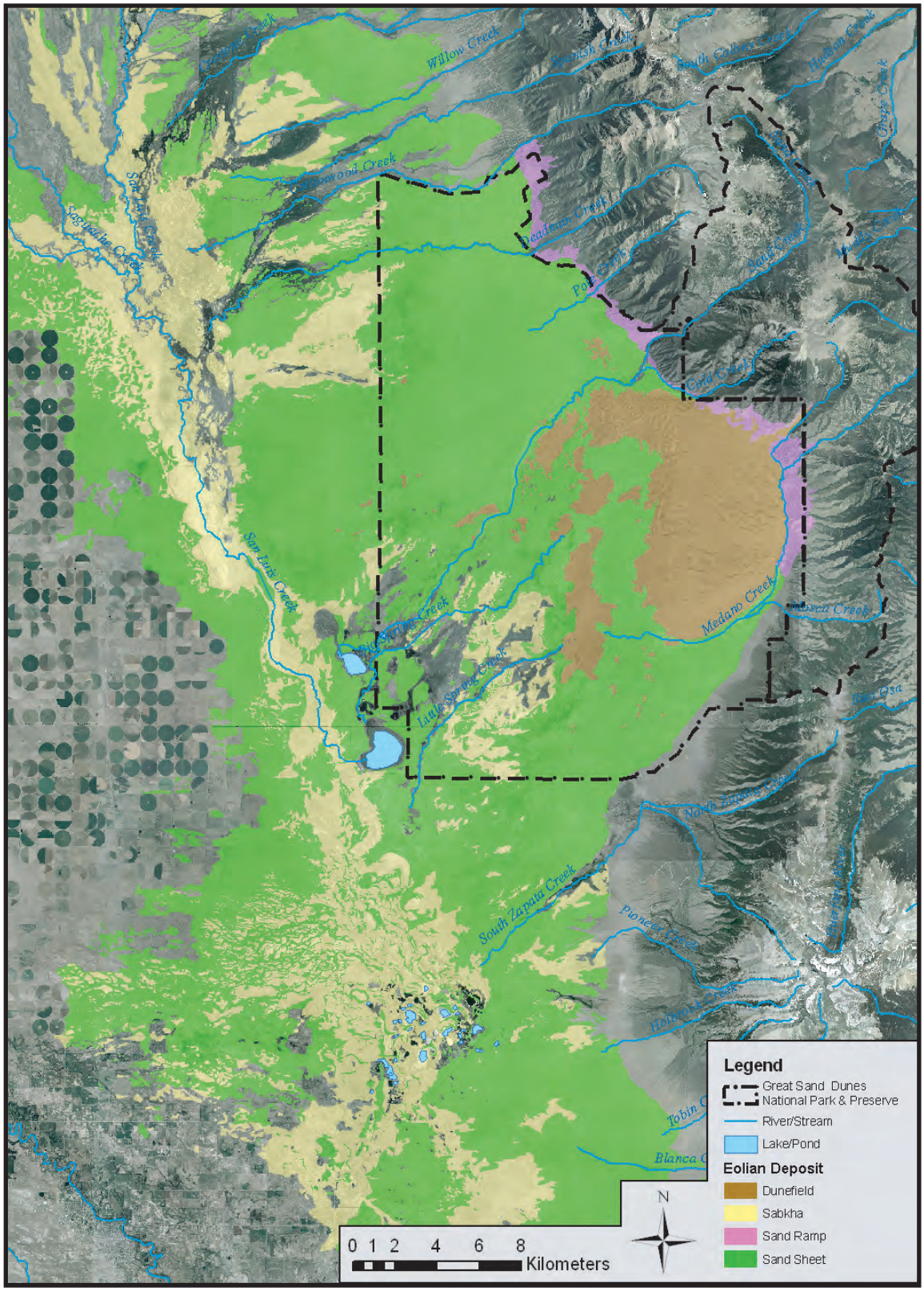

Figure A1–2. Eolian sand deposits near Great Sand Dunes, southern Colorado. Dashed line shows boundary of Great Sand Dunes National Park and Preserve; larger lakes are part of San Luis Lakes State Park.

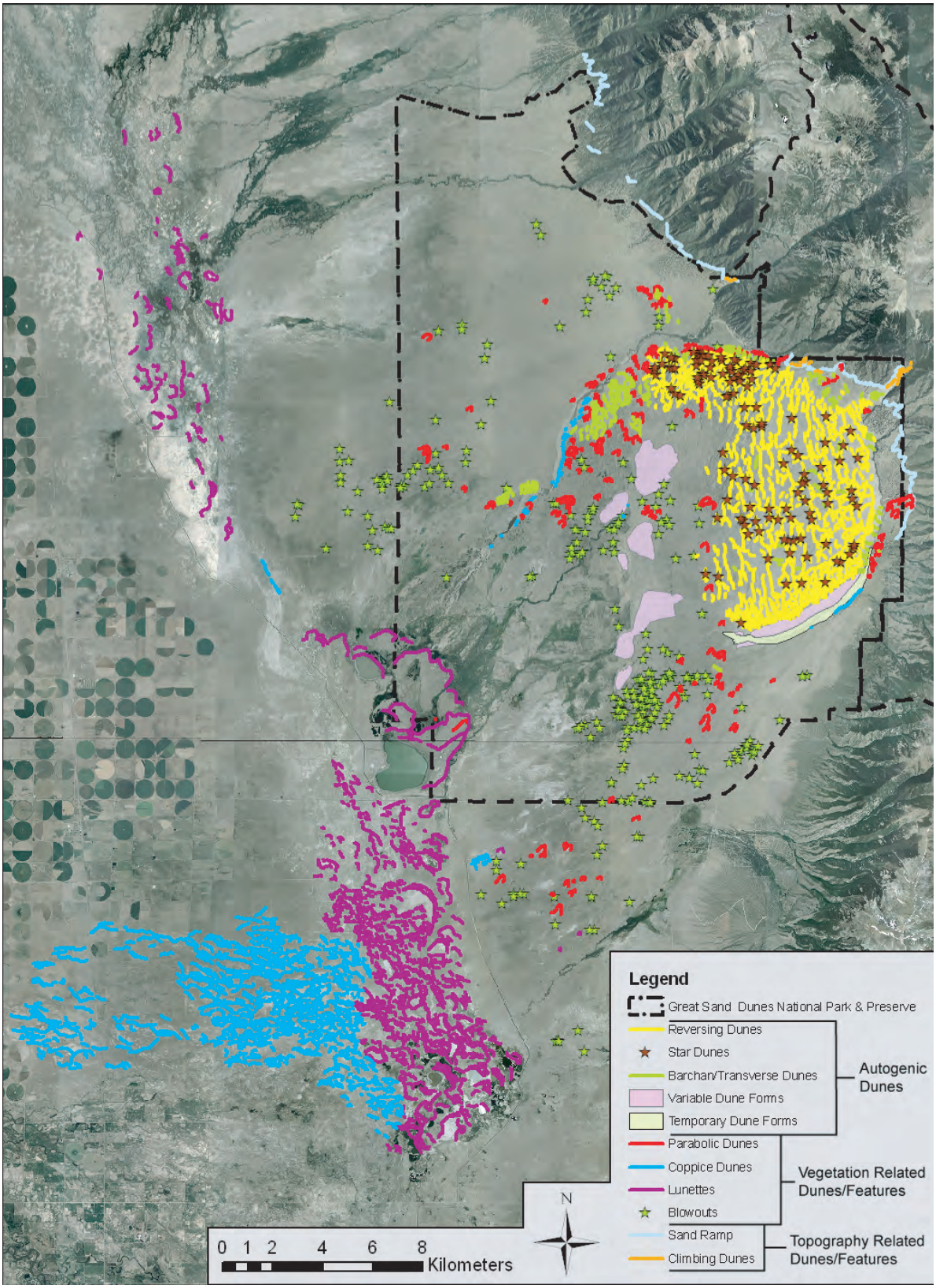

Figure A1–3. Dune types near Great Sand Dunes, Colorado.

Areas that have near-surface groundwater have sediments that are commonly cemented by evaporite minerals.

The Great Sand Dunes sabkha has formed where basin subsidence is greatest and a depression, known locally as the "closed basin," has developed. Playa lakes are common here and because the water-table gradient is flat, the primary means of water outflow is through evaporation, resulting in saline groundwater. Sabkhas can also form when deflation lowers the ground surface to the groundwater's capillary fringe. Sodium carbonate, calcite, and other evaporite minerals precipitate, cementing the sand to form a sabkha (Krystinik, 1990). The primary features of the sabkha are mineralized salt flats, fine-grained lake deposits, coppice dunes, and lunettes.

As the topographic gradient increases toward the east, the ground surface rises above the capillary fringe zone and sand sheets accumulate on the piedmont, which is mostly covered by vegetation dominated by shrubs and grasses. The north and south ends of the sand sheet have a planar surface marked by parabolic dunes developed around their margin. The average rate of parabolic dune migration has been measured at about 10 m/yr (Marin and others, 2005), but the rate increases during intervals of drought (Forman and others, 2006), such as the one we have had this decade. Conversely, the central sand sheet is currently less vegetated and has parabolic and transverse dune forms superimposed on it. The unvegetated areas have dunes that transition with time between dome, transverse, and reversing dunes. Sand ramps with climbing dunes form where the sand sheet laps onto the mountain front.

The Great Sand Dunes (dune field) covers 78 km^2. The dune field is a classic draa—a large sand dune tens of kilometers long and hundreds of meters high, often with smaller dunes on the leeward and windward faces. It has five depositional centers of greater sand thickness. Each deposition center can also be considered a draa (fig. A1–4). The primary dune types are reversing and star dunes. The tallest dune reaches a height of 229 m above the plain of the valley floor. The dune field is crescent-shaped and has three areas of distinct dune development: the (1) Sand Creek star dune complex, (2) central dune field, and (3) Medano Creek dune ridge (fig. A1–4). The Sand Creek star dune complex has reversing dune ridges radiating out from central high points that form the star dunes. The central dune field is composed of large north-south trending reversing dunes separated by large troughs. The Medano Creek dune ridge has more closely spaced, north-south-trending dune ridges and a secondary dune ridge that trends northeast, filling the troughs of the north-south-trending dunes. Along the dune field margins and adjacent to the creeks are smaller dunes that transition between dome, barchan, barchanoid ridge, transverse, and reversing dunes depending on wind conditions and sand supply.

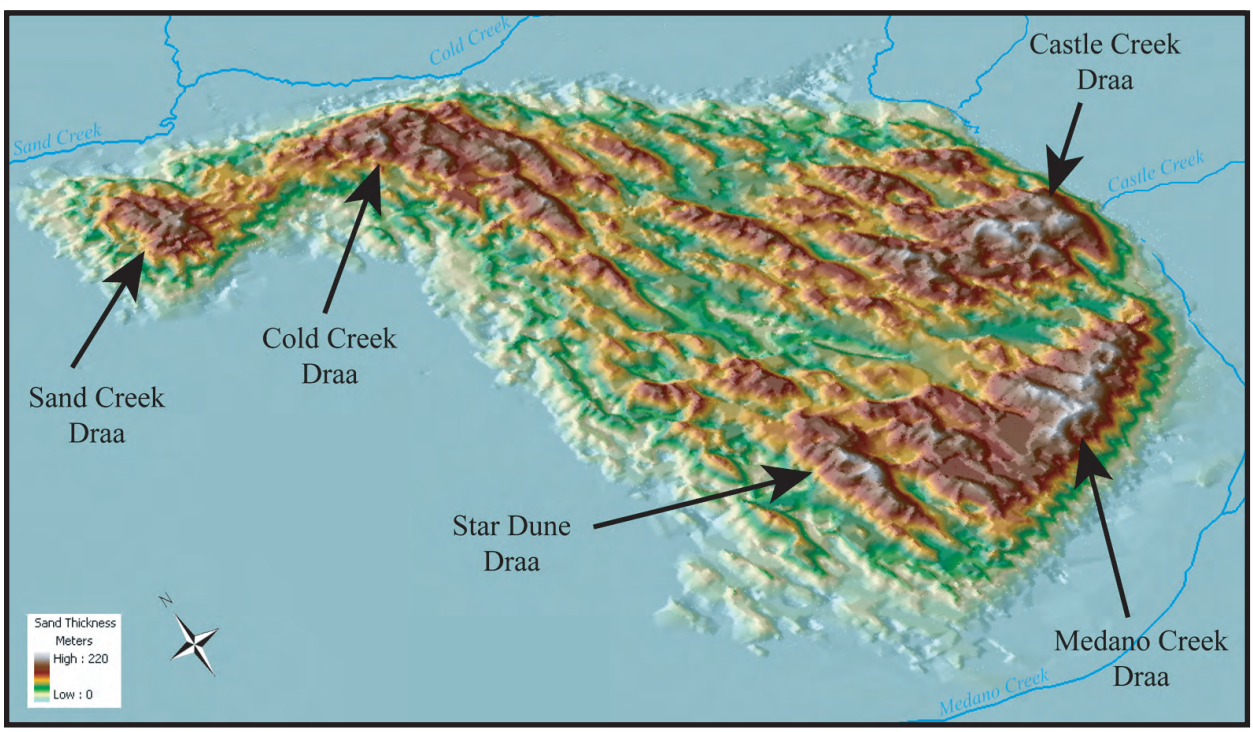

Figure A1–4. Sand thickness within the main dune field of Great Sand Dunes, southern Colorado. The main dune field is about 10 km (north-south) by 6 km (east-west).

Stop A2 — Optical Dating of Episodic Dune Movement at Great Sand Dunes National Park and Preserve

Speaker: Steve Forman
Location: Base of main dune field, 600 m west of Dunes Picnic Area, Great Sand Dunes National Park and Preserve
Zapata Ranch 7.5' quadrangle
GPS: NAD27, Zone 13, 453850 m E., 4177020 m N.
Elevation: 8,060 ft

Synopsis

The Great Sand Dunes National Park and Preserve in the San Luis Valley, Colo., contains a variety of eolian landforms that reflect Holocene drought variability. The most spectacular is a dune field banked against the Sangre de Cristo Mountains, which is fronted by an extensive sand sheet with stabilized parabolic dunes. Stratigraphic exposures of parabolic dunes on the sand sheet and associated luminescence dating of quartz grains by single aliquot regeneration (SAR) protocols indicate eolian deposition of unknown magnitude occurred about 1290–940, 715±80, 320±30, and 200–120 years ago and in the 20th Century. Preliminary SAR ages from the dune field near Medano Creek indicate sand movement about 300 years ago. Eleven drought intervals are inferred from the tree-ring record of the past 1,300 years at Great Sand Dunes and are potentially associated with dune movement, although only 5 eolian depositional events are currently recognized in the stratigraphic record. There is evidence for eolian transport associated with dune movement in the 13th Century, which may coincide with the "Great Drought," a 26-year-long dry interval identified in the tree ring record and associated with migration of Anasazi people from the Four Corners areas to wetter areas in southern New Mexico. This nascent chronology indicates that the transport of eolian sand across San Luis Valley was episodic in the late Holocene; appreciable dune migration in the 8th, 10–13th, and 19th Centuries ultimately nourished the dune field against the Sangre de Cristo Mountains.

Discussion

Many intermountain basins in the western United States are mantled by complex sequences of eolian deposits, a testament to the significant drought variability in the Holocene (Gaylord, 1989; Morrison, 1991; Stokes and Gaylord, 1993; Forman and Pierson, 2003; Lancaster and Tchakerian, 2003). Numerous studies in the past two decades document compelling evidence for large-scale and repeated reactivation of dune systems in the Great Basin and adjacent western Great Plains during the Holocene and as recently as <2,000 years ago (for example, Wells and others, 1990; Forman and others, 1992, 1995, 2001; Madole, 1994, 1995; Muhs and others, 1996, 1997; Stokes and Swinehart, 1997; Wolfe and others, 2001; 2002; Goble and others, 2004; Mason and others, 2004). Tree-ring time series from across North America show severe multidecadal droughts during the 13th and 16th Centuries (Woodhouse and Overpeck, 1998; Stahle and others, 2000) and in the middle 18th Century for the Rocky Mountains. These droughts surpassed conditions during the driest years of the 20th Century (Woodhouse and others, 2002; Fye and others, 2003). A late 13th Century dry period in the southwestern United States, referred to as the "Great Drought" (Larson and others, 1996), is associated with large-scale environmental degradation and was one of many factors for depopulation of Anasazi centers (Fish and Fish, 1994; Lekson, 2001, 2002; Nelson and Schachner, 2002). This stop examines the record of eolian sand deposition in the Park (fig. A2–1). Questions remain as to whether or not dunes in intermountain, semiarid landscapes have been reactivated with droughts in the past 2000 years (Woodhouse and Overpeck, 1998). To address this question, we have employed recent advances in optically stimulated luminescence dating, specifically single-aliquot regeneration (Murray and Wintle, 2000, 2003) protocols, to provide the first quantitative dosimetric-based ages on formation of parabolic dunes in the sand-sheet area, upwind of the main dune field (fig. A2–1).

Geomorphic Setting

The Great Sand Dunes National Park and Preserve, with an area of 104 km^2, is located in the San Luis Valley, southern Colorado, in a small reentrant of the Sangre de Cristo Mountains (fig. A2–1*A*). The sand for these dunes is derived mainly from alluvium of the Rio Grande River, blown by prevailing southwesterly winds across the San Luis Valley (Johnson, 1967). The original sources of this sand are the volcanic rocks that form the San Juan Mountains on the western side of the valley and smaller amounts of crystalline and sedimentary rocks from the Sangre de Cristo Mountains on the valley's eastern side (Johnson, 1967; Wiegand, 1977).

The most prominent feature in the Park is a massive active dune field that is banked against the Sangre de Cristo Mountains (fig. A2–1*B*). This dune field is a complex of active and sinuous transverse to barchanoid ridges, generally oriented north-northwest–south-southeast and north-south. On top of the transverse dunes, toward the north and southwest, star dunes have formed in response to locally complex wind directions. Reversing dunes also formed at the crest of the primary ridges in response to short-term winds blowing from the northeast (Wiegand, 1977). The main dune field is confined between two perennial sandy-bed streams that flow westward from the Sangre de Cristo Mountains—Sand Creek to the north and west and Medano Creek to the east and south (fig. A2–1*C*). Although the flow of these streams rarely extends more than 3.5 km from the mountain front, it may reach 8 km

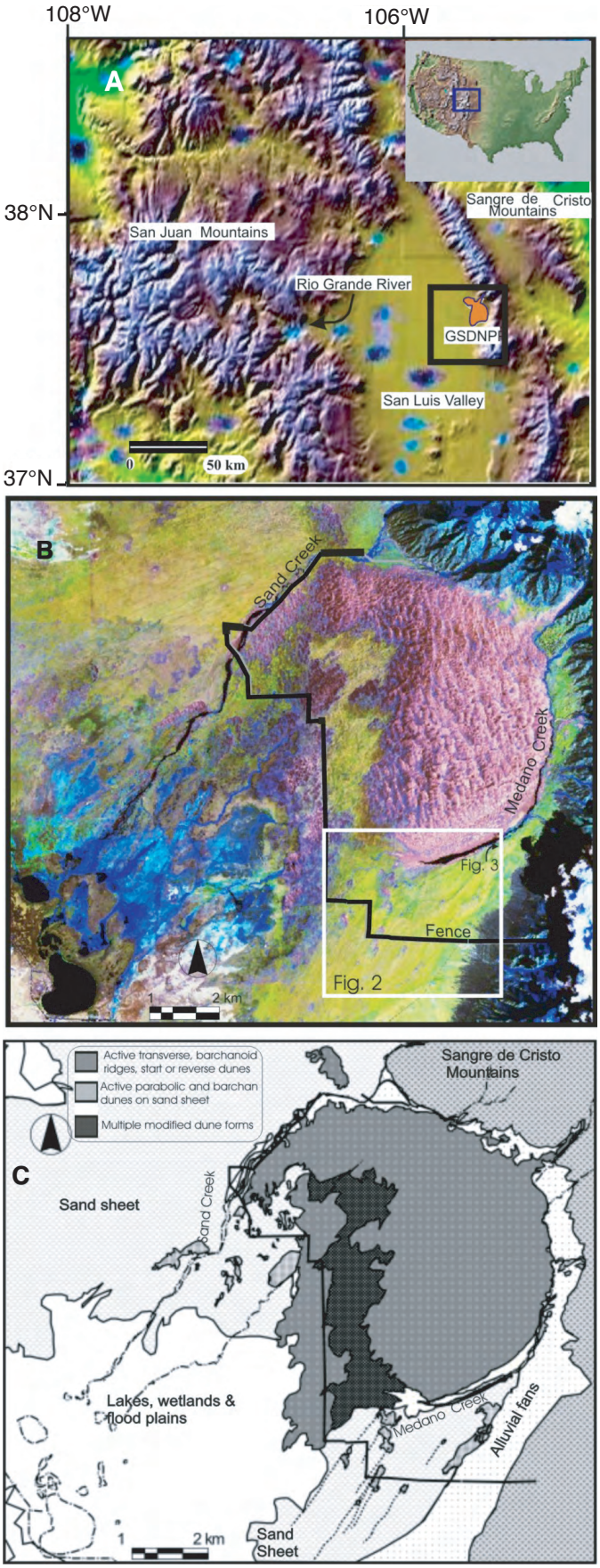

Figure A2–1. Index maps for the Great San Dunes National Park and Preserve in Colorado. *A*, Digital terrain model of the Park. San Luis Valley is bounded by San Juan and Sangre de Cristo Mountains to the west and east, respectively. *B*, False color composition (bands 5 in red, 4 in green and 7 in blue) of the Landsat 7 enhanced thematic mapper image acquired on July 26, 1999. The active dunes are shown in red tones, the sand sheet in magenta and blue, mountainous vegetation in dark green and brown, and the water in dark blue and black. *C*, Surficial geologic map of the Park. The southeast sand-sheet area is the focus of this study (from Forman and others, 2006).

during peak flow from May to July (Johnson, 1967; Wiegand, 1977). During floods, sand is eroded from the dunes by the creeks and is carried back toward the sand sheet (Fryberger, 1999); when the creeks dry, eolian sand is blown across the creeks' beds back into the main dune field (Johnson, 1967; Wiegand, 1977; Fryberger, 1999).

A vegetated low-relief sand sheet bounds the dune field for hundreds of kilometers to the north, west, and south. Scattered active parabolic dunes are distinctive on the south and southwestern areas of the sand sheet. These parabolic dunes have arms (McKee, 1979, p. 9) anchored by a variety of grasses and shrubs. The arms are as long as 3.5 km and are oriented 35°–40° NE., in response to predominant winds from the west-southwest (figs. A2–1 and A2–2). The arms, observed in aerial photographs as long parallel ridges, were originally interpreted by Johnson (1967) as longitudinal dunes, but Wiegand (1977) later recognized them as arms of parabolic dunes. Active barchan and reversing dunes oriented 40º–50° NE. are also superimposed on the sand sheet, near the western margin of the main dune field. Some of these barchan dunes are scattered, but the dunes next to Sand and Indian Creeks often coalesce to form compound barchanoid ridges with reverse tops. Alternatively, these dunes may be a hybrid dune type (for example, Carson and MacLean, 1986).

The climate of the San Luis Valley is arid with a mean annual precipitation of 15±8 cm/yr (1948–2002); however, orographic controls in the Park generate a locally wetter climate, with a mean annual precipitation 24±11 cm/yr (National Climatic Data Center, 1950–2002). More than 67 percent of the yearly precipitation occurs as scattered showers in spring and thunderstorms in summer. August is the wettest month with 50 percent of the total summer precipitation. The mean annual temperature at GSDNPP is approximately 6.7°C (Wiegand, 1977); summers and autumns are usually temperate, and they have average temperatures of 21.6°C and 19°C, respectively, and a maximum monthly temperature of 26.5°C in August (1950–2002) (National Climatic Data Center, 1950–2002).

Opposing wind regimens prevail at Great Sand Dunes (Wiegand, 1977). The southwest winds blow throughout the year, whereas winds from the northeast are both seasonal (July, August, and September) and diurnal (cold air flowing from the mountains at night) (Johnson, 1967; Wiegand, 1977). The synoptic-scale circulation of the Rocky Mountain region and the topographic configuration of the San Luis Valley are reflected in the wind pattern. Upper-level cyclonic storm centers move eastward across central North America along a track that passes north of Colorado during most of the year. Storm tracks during winter lie south of Colorado, also producing surface winds from the southwest (Wiegand, 1977). Northeast winds reflect a local orographically influenced circulation pattern caused by the presence of tall peaks coupled with low

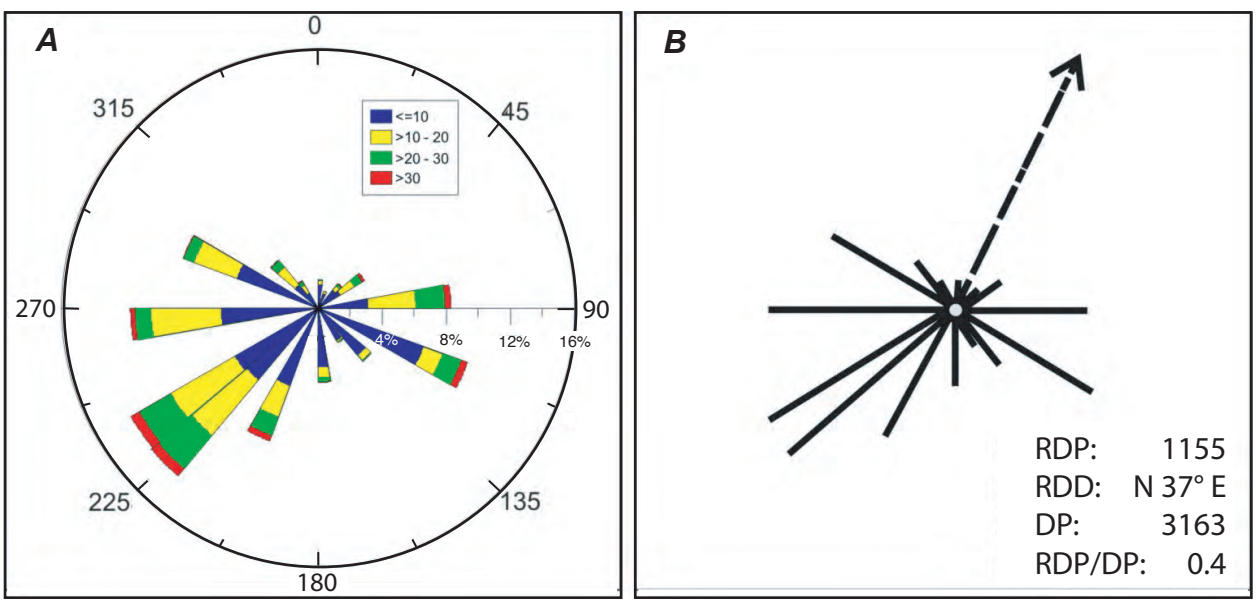

Figure A2–2. Wind roses and sand drift potential for Great Sand Dunes National Park and Preserve. *A*, Wind roses generated from data from July 2002 to April 2003. Wind velocity represented by color: blue, velocities ≤10 m/s; yellow, velocities >10 m/s. *B*, Sand drift potential from vectorial analyses of the wind data from part *A*, following Fryberger and Dean (1979, p. 147). The data are based on calculations of over 10,000 wind measurements every 10 minutes during an interval of 3 years, which form a unique data set that yields relative high values of resultant drift potential and drift potential. Abbreviations: RDP, resultant drift potential; RDD, resultant drift direction; DP, drift potential; RDP/DP, ratio of resultant drift potential to resultant drift direction.

mountain passes that funnel winds through them. These winds may also reflect a thermal convection cell produced by differential heating and cooling between the mountains and the valley (Wiegand, 1977; Alexander, 1979). Wind data collected at Great Sand Dunes show a strong southwestern component, with wind directions of similar magnitude originating from the southeast and northwest. The drift potential for sand movement has a resultant drift direction of N. 37° E., coinciding with parabolic dune orientation (fig. A2–2).

Optical Dating

Optically stimulated luminescence (OSL) geochronology is based on the time-dependent dosimetric properties of silicate minerals, predominately quartz (Aitken, 1998). The single-aliquot regenerative (SAR) (Murray and Wintle, 2000, 2003) method was used to estimate the equivalent dose of the 150–250 μm quartz fractions from dune sands. Eolian sands at Great Sand Dunes are mineralogically immature, consisting of well-sorted medium sand, with median grain sizes ranging from 290 to 350 μm, composed of 51.7 percent volcanic rock fragments, 27.8 percent quartz, and the remaining grains of mixed lithology (Wiegand, 1977). The quartz fraction was isolated by density separations using the heavy liquid Na–polytungstate, and a 40-minute immersion in hydrofluoric acid (HF) was applied to etch the outer 10+ microns of grains, which are affected by alpha radiation (Mejdahl and Christiansen, 1994). The purity of the quartz separate was evaluated by petrographic inspection and point counting of a representative aliquot. Samples that show >1 percent of nonquartz minerals are retreated with HF and again checked petrographically. Duplicate or triplicate reaction with HF is often needed to obtain a pure quartz separate. The purity of quartz separates from selected samples is tested by exposing small aliquots to infrared excitation (880 μm), which preferentially excites feldspar minerals. Samples measured showed only weak emissions (<300 counts) with infrared excitation, indicating a spectrally pure quartz extract.

An automated Risø TL/OSL–DA–15 system (Bøtter-Jensen and others, 2000) was used for SAR analyses. Blue light excitation (470±20 nm) was produced by an array of 30 light-emitting diodes that delivers about 15 mW/cm^2 to the sample position at 90 percent power. A Thorn EMI 9235 QA photomultiplier tube coupled with three 3-mm-thick Hoya U-340 detection filters, transmitting between 290 and 370 nm, measured photon emissions. Laboratory irradiations used a calibrated ^{90}Sr/^{90}Y beta source coupled with the Risø reader. All SAR emissions were integrated over the first 0.8 s of stimulation out of 500 s of measurement, with background based on emissions for the last 90- to 100-s interval.

Before the application of SAR protocols, a series of experiments evaluated the effect of preheating at 180°, 200°, 220°, and 240°C on the regenerative signal (Murray and Wintle, 2000). These experiments show that preheat temperatures of 200°C yielded the highest and most consistent equivalent doses; therefore aliquots were preheated at this temperature for 10 s for the SAR protocols. Tests for dose recovery were also performed and for samples the last dose coincides well with the initial dose (at 1-sigma errors).

A critical analysis for luminescence dating is the dose rate, which is an estimate of the amount of ionizing radiation acting upon the sediment during the burial period. The contents of U and Th (each assumed to be in secular equilibrium in their decay series) and ^{40}K were determined by inductively coupled plasma–mass spectrometry (ICP-MS) analysis by Activation Laboratory LTD, of Ontario, Canada. The beta and gamma doses were adjusted according to grain diameter to compensate for mass attenuation (Fain and others, 1999). A small cosmic ray component between 0.31 and 0.22±0.01 mGy/yr, depending on depth of sediment, was included in the estimated dose rate (Prescott and Hutton, 1994). A moisture content of 5±2 percent was assumed, which is between field capacity and hydroscopic limit for sandy soils in semiarid environments (Brady, 1974, p. 191–193). The dose rate for these samples is relatively high at about 5 mGy/yr, reflecting the abundances of mica and associated minerals in mafic and granite rock fragments.

At many study localities, near-surface eolian sand has yielded SAR ages between 50 and 20 years. To verify that such young SAR ages are truly finite estimates, sample UIC1077, which yielded an age of 20±2 yr, was subsequently reset with 2 h of solar exposure. This “zero-age” sample yielded no SAR age (that is, 0 yr). However, the associated error is large (80 yr) because of the low signal-to-noise ratio (<5). Similar young but apparently accurate ages have been previously reported for other eolian systems (for example, Bailey and others, 2001; Ballarini and others, 2003; Stokes and others, 2004; Forman and others, 2005).

Backhoe Trenches A and B Across Parabolic Dune Arms

Two backhoe trenches (A and B) were excavated across stabilized limbs of parabolic dunes in the sand sheet area to reveal their stratigraphy (fig. A2–3). These trenches were difficult to excavate because of the inherent instability of the sand; therefore, the depth of excavation was limited to about 2 m. There was a noticeable lack of paleosols exposed in the trenches, compared to what has been found in other eolian sand depositional sequences in the western United States (for example, see Forman and others, 2001).

The basal unit (A–1) exposed in trench A is a moderately well sorted, medium- to coarse-grained sand having common, scattered angular to subrounded (pea-gravel size) clasts, 2–5 mm in diameter (fig. A2–4). The median particle size for this unit is 370 to 310 μm (n=5). Grain lithology includes fragments of gneiss and mafic rock and feldspar and quartz minerals. Numerous burrow fills indicate considerable bioturbation, but in places millimeter-scale, low-angle, cross-stratification is preserved, with beds dipping to west. The upper 40 cm of unit A–1 contains the most abundant coarse sand

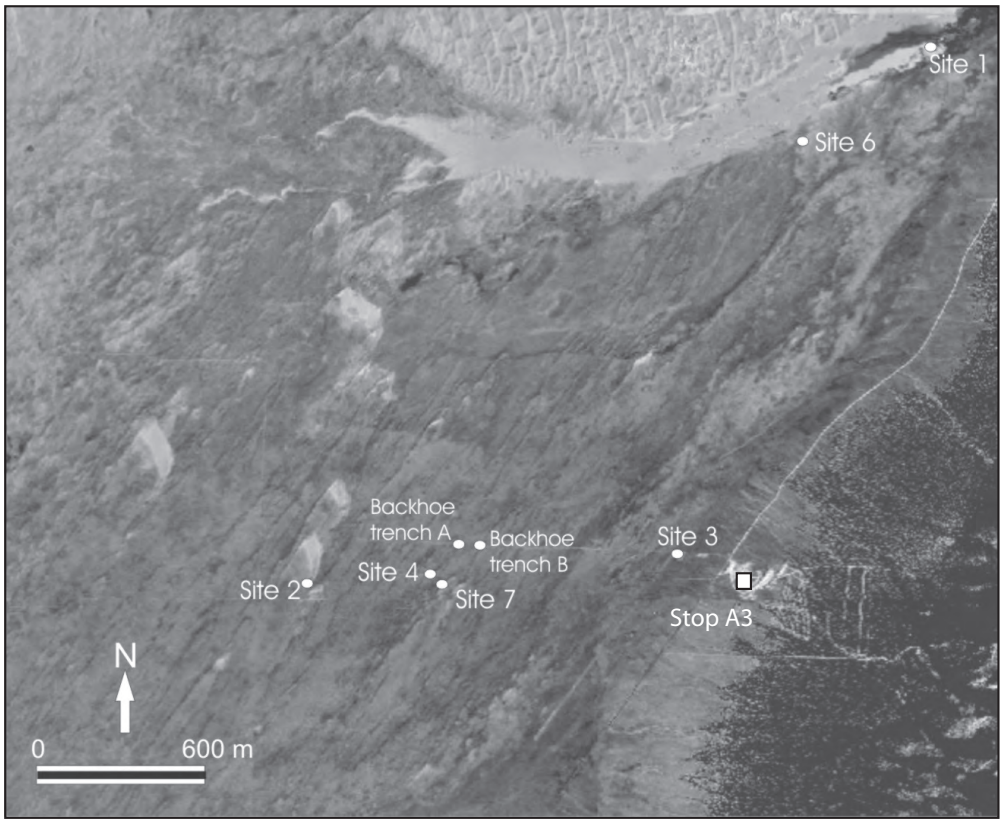

Figure A2–3. Sand dunes at and west of stop A3. Sites and trenches are those mentioned in the text.

and gravel, reflecting lag deposition prior to the emplacement of the overlying unit A–2. Unit A–2 is a well-sorted medium sand having grain and clast lithologies similar to those of unit A–1. The median particle size for unit A–2 is 310 to 270 μm (n=7) and is somewhat finer than underlying unit A–1. The sediment in unit A–2 often appears massive, but in places millimeter- to centimeter-scale bed fragments are preserved, particularly in the lower 30 cm. The surface soil is weakly developed as marked by a weak 20- to 25-cm-thick cambic horizon. SAR dating of quartz grains from units A–1 and A–2 indicate an unconformity, with the basal unit (A–1) yielding ages of 940±80 yr (UIC1086) and 700±75 (UIC1137) yr and the overlying unit A–2 giving ages of 210±30 yr (UIC1238), 230±30 yr (UIC1138), and 170±30 yr (UIC1235).

Backhoe trench B through an adjacent parabolic arm ~200 m east of backhoe trench A has similar lithostratigraphy (Fig. A2–4), but the boundary between upper and lower units is less clear. The lower unit (B–1) is a well-sorted medium sand that exhibits 2- to 30-cm-long bed fragments in the upper 40 cm with horizontal and subhorizontal bedding dipping to the east in the basal 40 cm. Upper unit (B–2) is a massive, well-sorted, medium sand, with common 2–5 mm diameter gravel in the upper 20 cm. This unit has been extensively burrowed. A lag of coarse sand and pebbles marks the boundary between units B–1 and B–2. Quartz grains from unit B–1 yielded SAR ages of 710±70 yr (UIC1260) and 735±90 yr (UIC1260), similar to the ages of basal sediments in backhoe-trench A. Sediments from unit B–2 yielded an SAR age of 120±20 yr (UIC1259), confirming the presence of a lacuna between units B–1 and B–2.

Sedimentary Structure and Age of the Dune Field Adjacent to Medano Creek

A striking and defining landform at Great Sand Dunes National Park and Preserve is the massive dune field that lies adjacent to the western margin of the Sangre de Cristo Mountains. Questions remain on the age and origin of this dune field. One that we address herein is, “Did the dune field expand during periods of eolian transport in the past 1,500 years on the adjacent sand sheet?” Recently we have initiated research that couples OSL dating with detailed sedimentologic assessments to determine the age or ages of the dune field.

The dune field is demarcated by star dunes that reflect multiple wind directions. The flanks of the dune field, near Medano Creek, host 10- to 30-m-high reversing dunes with noticeable interdunal scour. Exposures in the dunes show water-bearing, cohesive sand that has high- and low-angle dune cross bedding. These sediments often contain 5–20 percent water that reflects local perched water tables within the dune field; the wet sediment provides grain cohesion and resistance against eolian erosion and transport (Chen and others, 2004). Water-bearing eolian sediment has been observed in many exposures adjacent to Medano Creek and in boreholes into the dune field. Thus, the upper 20–50 m of sand is mobile;

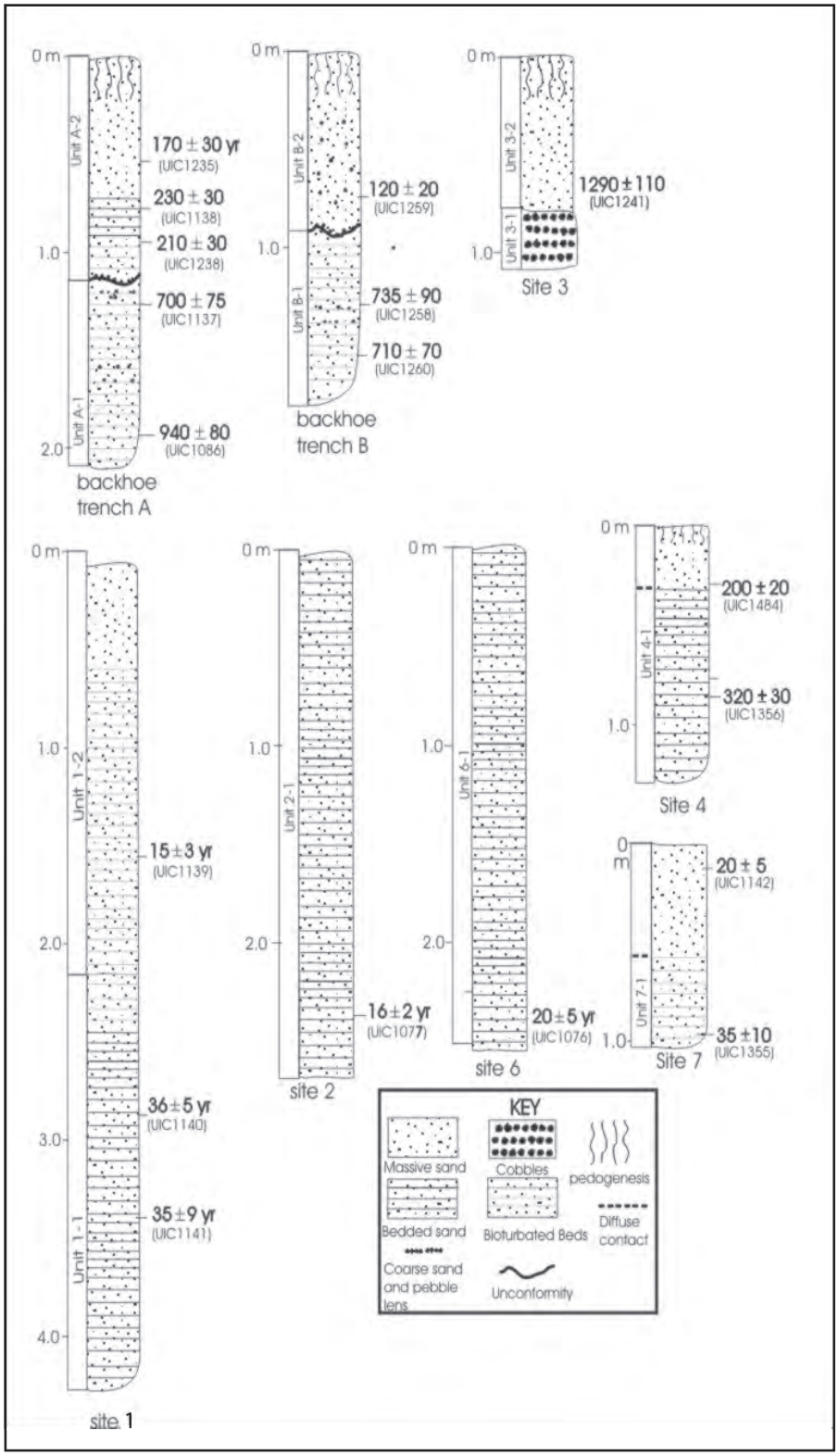

Figure A2–4. Stratigraphic sections of eolian sand deposits at sites and trenches west of stop A3, as shown in figure A2–3.

it forms star, barchan, transverse, and reversing dunes, whereas the subjacent moisture-bearing sand is cohesive and forms a boundary for eolian transport.

Preliminary OSL dating of eolian sand from these water-bearing sands indicates that the lower sand is about 270 years old, whereas the uppermost sand was deposited in the past 60 years (fig. A2–5). These early results indicate that part of the dune field adjacent to Medano Creek was accreted in the past 300 years.

Eolian Sand Depositional History

In the past 1,300 years there have been at least 13 droughts of sufficient magnitude to result in dune remobilization to varying extent at GSDNPP. These droughts are inferred from the tree-ring-derived Palmer Drought Severity Index (PDSI) and annual precipitation records (fig. A2–6). The severest droughts, lasting decades and with broad impact across North America, occurred during the 8th, 11th, 13th and 16th Centuries (Woodhouse and Overpeck, 1998; Stahle and others, 2000). These droughts were equal to or more severe than the driest conditions in the 20th Century for which we have documented changes in dune migration and vegetation coverage at in the Park (Marin and others, 2005). Our field- and laboratory-based study provides a conservative assessment of dune reactivation or formation with at least seven potential events at about 1280±100, 715±80, 310±30, 200±20, 130±10 years ago, and in the 20th Century. However, some of the severest droughts are not represented in the stratigraphic record; thus, this incomplete assessment reflects the paucity of well-dated stratigraphic localities and the vagaries of erosion and deposition in parabolic dune systems. The nascent chronology does indicate that the transport of eolian sand across San Luis Valley, ultimately nourishing the dune field against the Sangre de Cristo Mountains, was an episodic process during the late Holocene, with appreciable dune migration in the 8th, 10–13th, and 19th Centuries.

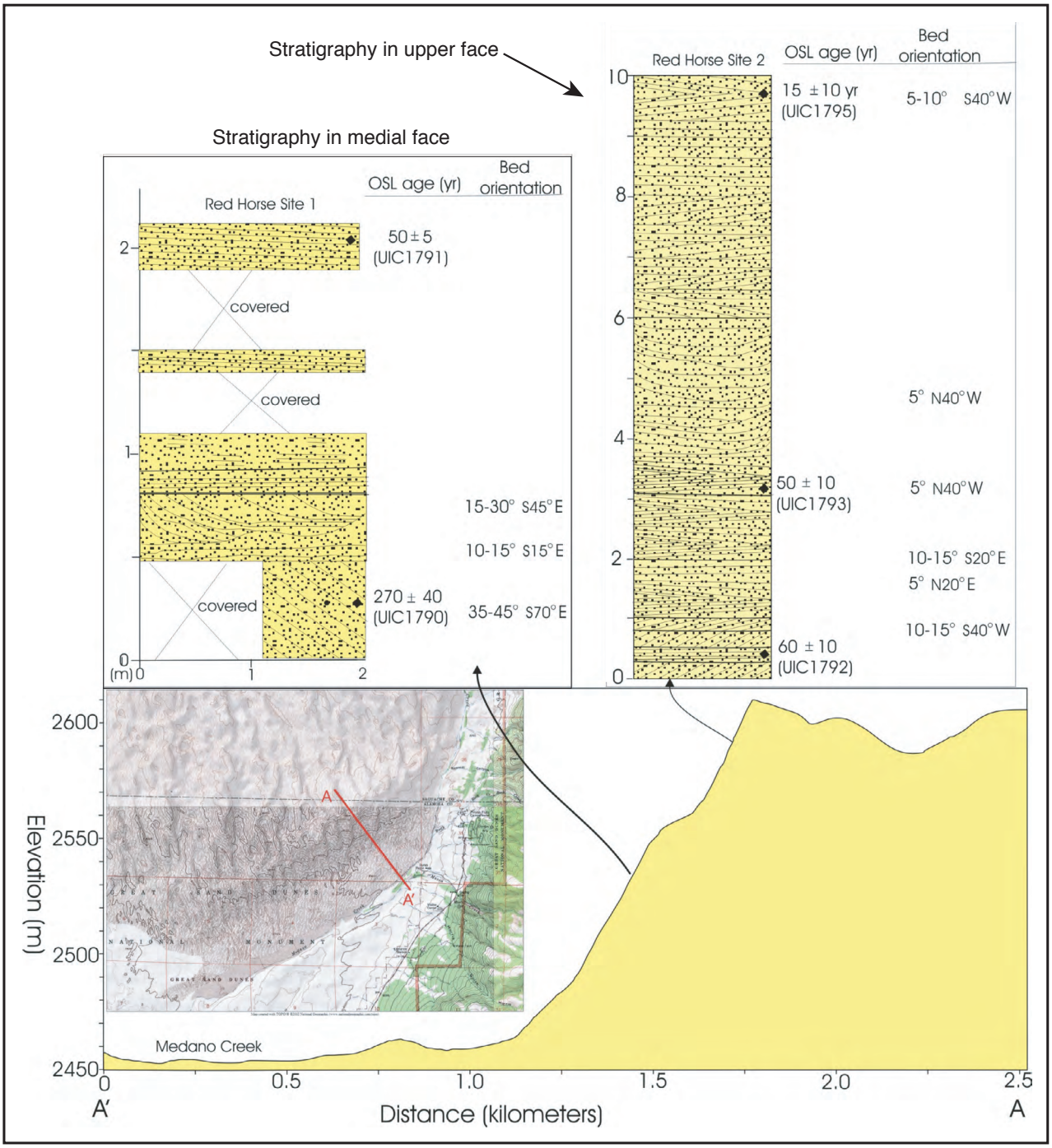

Figure A2–5. Optically stimulated luminescence ages of eolian sand deposits on the accreting face of the large dune west of stop A1.

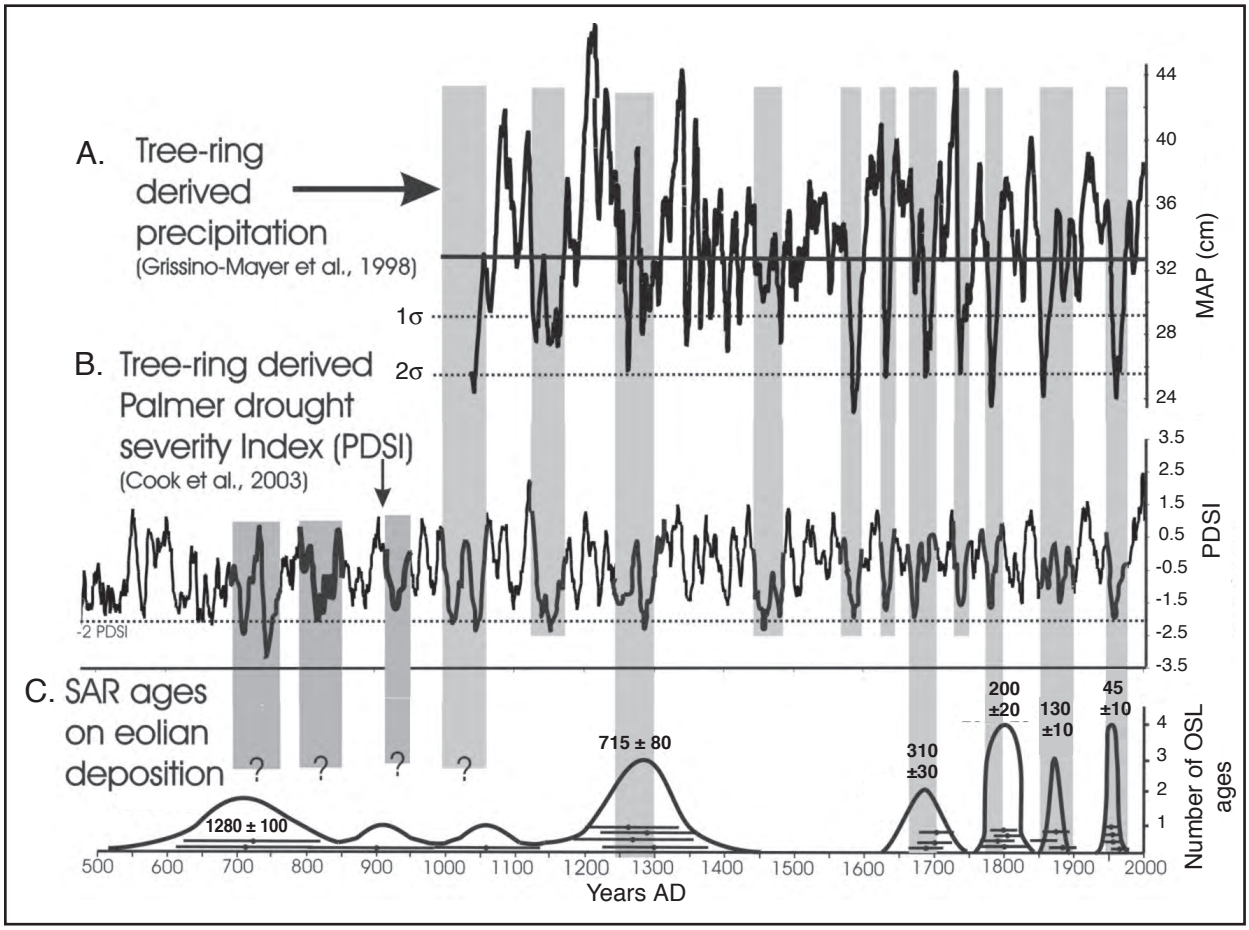

Figure A2–6. Climatic data and times of eolian sand deposition. *A*, Inferred mean annual precipitation (MAP) since AD 1000 near lower treeline at Great Sand Dunes National Park and Preserve (GSDNPP) from tree-ring time series (Grissino-Mayer and others, 1998). *B*, Inferred summer Palmer Drought Severity Index (PDSI) for upper treeline since AD 500 from tree-ring time series (point #132: 37.5° N., 105.0° W.; Cook and others, 2003). *C*, Frequency distribution showing 2-sigma range of single-aliquot regeneration (SAR) ages on eolian sand depositional events at GSDNPP. Horizontal black bars indicate individual SAR ages. Vertical grey bars indicate possible correspondence between eolian depositional events and droughts in the tree-ring record. There is greater uncertainty in associating drought where there is just a single SAR age constraining eolian depositional events as is shown by shorter grey bands ending in a question mark.

Stop A3 — Paleoseismology of Range-Front Fault Scarps at Great Sand Dunes

Speaker: James McCalpin
Location: Great Sand Dunes National Park and Preserve, near NPS residential water tank
Zapata Ranch 7.5' quadrangle
GPS: NAD27, Zone 13, 455170 m E., 4175333 m N.
Elevation: 8,320 ft

Synopsis

At this stop we will examine fault scarps on Quaternary deposits along the range-front traces of the northern Sangre de Cristo normal fault zone. In 2002 and 2003, a research team from the Crestone Science Center mapped fault scarps and excavated four trenches for paleoseismology in the Morris Gulch and Visitor Center areas (fig. A3–1). The trenches across the Morris Gulch scarps exposed evidence for two post-Pinedale (post-15 ka to 35 ka) surface-rupturing earthquakes, each with vertical displacements of about 1.7–2.3 m. Those displacements alone imply that the earthquakes had moment magnitudes of about 6.9–7.0. The most recent event occurred about 5.3–5.5 ka, whereas the prior event occurred sometime in the early Holocene or latest Pleistocene (10–15 ka?). Thus, the recurrence interval could range from 4.5 to 9.7 k.y. The most-recent-event elapsed time of 5.3–5.5 k.y. composes 55–122 percent of the most recent recurrence interval. In contrast, a trench across the scarp directly below the GSDNPP Visitor Center failed to expose a tectonic fault but instead exposed an old landslide(?) failure plane. The scarp is probably caused by stream erosion, which unweighted the toe of the failed material. Therefore, we interpret the Visitor Center scarp as a probable fluvial scarp eroded by ancestral Medano Creek that poses no direct threat to the Visitor Center. The only infrastructure at the Park directly threatened by future fault surface rupture is the water tank, which stores potable water for the park headquarters and employee housing area. However, all structures in the Park would be subjected to strong ground shaking in the event of an **M** 7 earthquake. This ground shaking could reach horizontal and vertical accelerations of as much as 0.5–1 g and last for 30–40 s. However, with a return time of about 5,000 to 10,000 years for such earthquakes, the annual probability of such strong ground shaking is on the order of 1/5,000 to 1/10,000. A more complete discussion of these subjects is included in a comprehensive contract report to the National Park Service (McCalpin, 2006).

Tectonic Setting

The Park lies astride the northern Sangre de Cristo fault zone, which is the eastern-margin fault of the San Luis Valley. This fault zone is a west-dipping, normal, and the master fault of the San Luis Valley, which is in turn two east-tilted half-grabens and an intervening horst. Geophysical data suggest that the total Neogene throw on the northern Sangre de Cristo fault zone is at least 4 km (Brister and Gries, 1994). The Mapco State geothermal test well drilled in the graben 5 km west of Great Sand Dunes reached Precambrian basement at a depth of 2.9 km, but it was not located in the deepest gravity low (see also fig. A7–1, stop A7). Thus, the depth of basin-filling sediment probably exceeds 3 km in depth.

The fault zone has remained active into the Holocene, as evidenced by single-event fault scarps that displace Holocene deposits about 1.5–2.5 m (McCalpin, 1982). Mapping of older deposits such as Pinedale, Bull Lake, and pre-Bull Lake alluvial fans is based on topographic location, geomorphic expression, and soils. These three groups of glacial-age deposits have range-front fault scarps 3–8 m high, 5–13 m high, and as much as 85 m high, respectively. Given its length (about 120 km), its average vertical slip rate (0.1–0.3 mm/yr), and its recent movement (mid-Holocene), the northern Sangre de Cristo fault zone is considered Colorado's most active and hazardous fault.

The fault zone was divided into three sections by Widmann and others (1998). Stop A3 is on the Zapata section, a linear, 23- to 27-km-long section of the fault zone that trends N. 10° E. from the western foot of Blanca Peak to Medano Creek, north of which the northern Sangre de Cristo Range changes strike by 45°, suggesting that it may be a section boundary (see discussion in chapter J, this volume).

Quaternary Faulting on the Zapata Section

Fault scarps are more or less continuous across the heads of range-front alluvial fans in the Zapata section, all of which were assigned to the Pinedale glaciation by McCalpin (1982) (fig. A3–1). Where the fault zone is expressed as a single fault scarp, its vertical surface offset (vertical separation) ranges from 2.8 to 6.0 m. In several places south of the Park there are two closely spaced, parallel, down-to-the-west fault scarps at the fanhead, and these double scarps have combined vertical surface offsets of 5.9–7.2 m. In general, surface offsets increase southward from the Pinon Flats Campground in GSDNPP (3.4 m) to South Arrastre Creek (7.2 m), a distance of 6 km, in deposits of presumably identical age. The fault zone is expressed at the range front by a single trace, and pre-Pinedale-age deposits on the hanging wall are everywhere buried by Pinedale fans. Generally along the northern Sangre de Cristo fault zone, pre-Pinedale deposits are exposed only if multiple parallel traces exist with sufficient late Quaternary throw to bring up pre-Pinedale deposits in a fault-bounded sliver. [NOTE: the published 1:24,000-scale USGS geologic maps (Johnson and others, 1989; Bruce and Johnson, 1991) do not map the range-front Quaternary fault scarps, but instead generalize the fault zone as a dotted line placed arbitrarily across the upper to middle parts of the alluvial fans.]

The southern end of the Zapata section is difficult to identify because scarps south of South Arrastre Creek are no

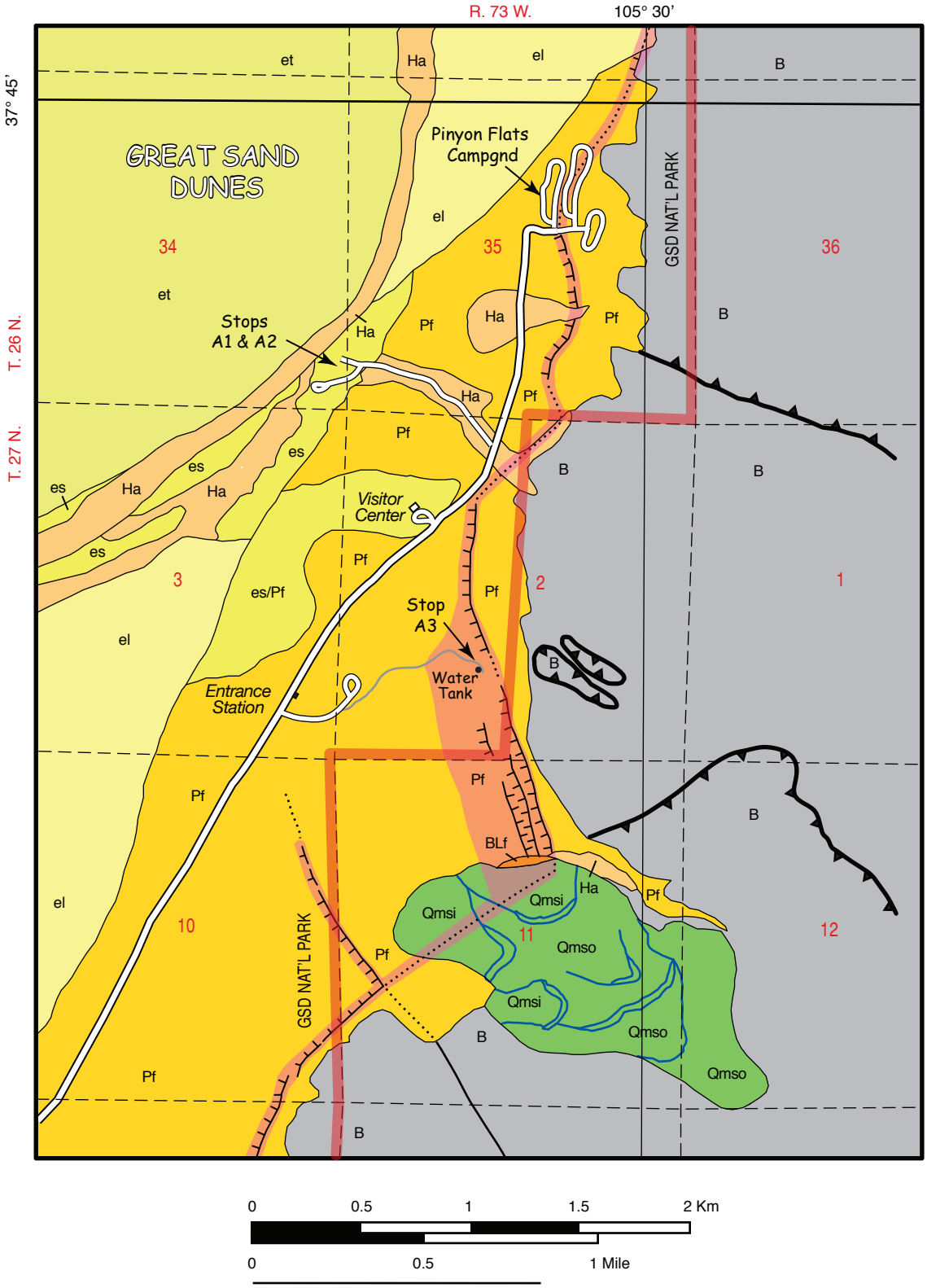

Figure A3–1. Geology of Great Sand Dunes National Park in the vicinity of the Visitors Center. Geologic units and mapping modified slightly from McCalpin (2006). Eolian sand units: et, transverse dunes; el, longitudinal dunes; es, undivided sand. Alluvial units: Ha, Holocene; Pf, Pinedale (late Pleistocene); BLf, Bull Lake (late middle Pleistocene). Landslide deposit units: Qmsi, younger; Qmso, older. Other units: B, bedrock (undivided Pennsylvanian Minturn Formation and Precambrian granitic gneiss). Shaded zone along faults indicates high hazard from surface fault rupture. Morris Gulch and trenches shown on figure A3–2.

longer continuous along the base of the range front. Instead, the southernmost Quaternary fault scarp is an anomalous 2.6 km-long scarp that crosses Urraca Creek, 14.7 km south of this stop. The anomalous scarp trends N. 10° W. and lies 1.7 km west of the range front, at the toe (rather than the head) of the alluvial fan. It is also 5 km south of the nearest range-front scarp. On this short scarp, early Holocene deposits are displaced 2.0–2.1 m vertically, Bull Lake deposits 6.1–7.1 m, and pre-Bull Lake deposits 8.4–10.6 m vertically (McCalpin, 1982). The paleoearthquake responsible for faulting the early Holocene deposit occurred about 5 ka.

What We See at Stop A3 (Water Tank)

Stop A–3 shows several fault scarps on the Pinedale-age (inferred) alluvial fan of Morris Gulch (fig. A3–2). Compared to fault scarps elsewhere in the section, this fault scarp is anomalous in several ways: (1) there are four parallel fault scarps (A, B, C, D) of subequal height in a zone 300 m wide; (2) the scarps trend north-northwest, but the range front trends north-northeast; and (3) owing to their north-northwest trend, the scarps obliquely cross contours and some stream flow has followed along their bases.

Paleoseismology of the Morris Gulch Scarps

The Morris Gulch scarps (A–D) represent two surface-faulting events that displace the surface of a Pinedale-age alluvial fan in a wide zone of parallel scarps. The cumulative vertical displacement across the scarps is on the order of 8 m, which is slightly greater than the 5.2–7.2 m of throw calculated for scarps south of Morris Gulch (McCalpin, 2006). Trenches B, C, and D indicate that the per-event displacement on each scarp during these events ranges from about 1.5 m (the 3 m net displacement on scarp B, divided by 2), to 1.7 m (single-event displacement from trench C; see fig. A3–3), to 1.65 m (net displacement of 3.3 m in trench D, divided by two). The average cumulative displacement per event on all three scarps would thus range from 3.15 m (without the single scarp C event) to 4.85 m (with the scarp C displacement), if we neglect any component of back-rotation between the scarps. These displacements of 3.15–4.85 m are roughly similar to those measured south of Morris Gulch, where the average per-event displacement was 3.15 m.

Those per-event displacements imply earthquakes of moment magnitude (**M**) 6.96–7.10 if the displacements are assumed to be the maximum that occurred in the event, or **M** 7.10–7.22 if they are assumed to represent an average displacement (Wells and Coppersmith, 1994). The larger magnitude is probably a better estimate, considering the fact that each surface rupture was associated with meter-scale displacement on at least 3, and perhaps 4, parallel fault strands.

The radiocarbon ages from this study indicate that the most recent event occurred about 4.8–5.3 ka, at least on scarp D. Simultaneous rupture on scarps B and C is supported by the overall stratigraphy in their respective trenches. This age is similar to the age of surface rupture deduced by McCalpin (1982) at the Urraca Creek trench south of the Monument, which had a closely limiting maximum of about 5.5 ka. The timing of the paleoevent (PE) is not constrained by numerical ages but must be post-Pinedale. The degree of soil development in trench B suggests that the interevent time between the most recent event (PE1) and PE2 is on the same order as the

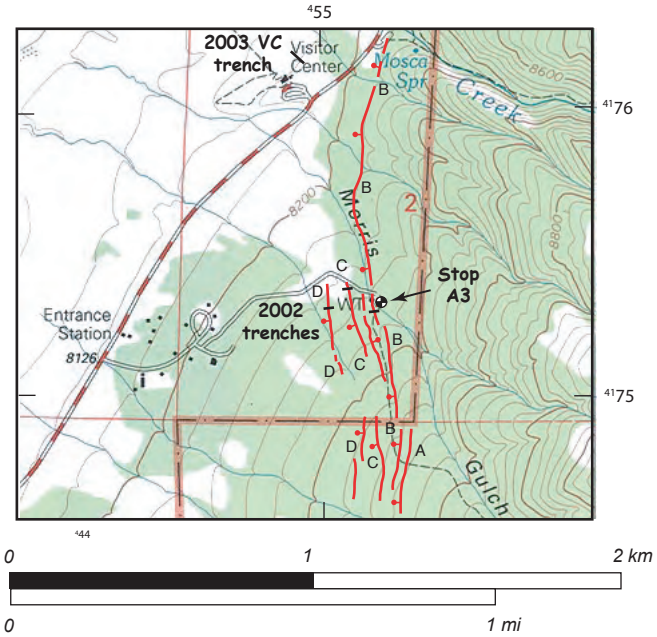

Figure A3–2. Faults on the alluvial fan of Morris Gulch and location of stop A3, Water Tank trench site. Red lines A–D, fault strands with ball on downthrown side; black bars, trenches. Map scanned from Zapata Ranch, Colorado, 7.5-minute topographic map.

Figure A3–3. Trenching operations during 2002 at scarp C. View to the northwest from the top of the fault scarp. Dunes visible in background.

time between the most recent event and present, or roughly 5,000 years. However, McCalpin (1982) estimated that the long-term (post-Bull Lake) recurrence on the Zapata section of the northern Sangre de Cristo fault zone was on the order of 10–20 k.y.

Large Bedrock Landslide South of Morris Gulch

South of Morris Gulch, fault scarps end at the flank of a west-protruding bedrock ridge but then reappear at the range front south of the ridge (red lines in fig. A3–4). The surface morphology of this ridge does not resemble that of any other ridge along the range front of the Sangre de Cristo Mountains. Rather than being a narrow-crested, steep, erosional ridge as is typical of faceted-spur range fronts, this ridge has a broad, low-gradient crest composed of alternating benches and scarps (yellow lines in fig. A3–4). In addition, there are several closed or nearly closed depressions on the ridge crest. Overall, the ridge looks like a giant landslide, yet the entire ridge is mapped as Precambrian gneiss by Bruce and Johnson (1991).

Field reconnaissance reveals that outcrops of Precambrian gneiss do exist throughout the ridge crest, but the foliation directions are random. Gullies cut into the flanks of the ridge expose outcrops of red sandstones and siltstones of the late Paleozoic Minturn Formation about 10–15 m below the ridge crest. As shown by Bruce and Johnson (1991), this part of the Sangre de Cristo range is composed of thrust sheets of Precambrian gneiss thrust eastward over Paleozoic sedimentary rocks; the thrust strikes N. 5° E. to N. 10° E. and dips 19° W.

It appears that the landslide ridge is underlain by a thin sheet of highly fractured Precambrian gneiss no more than 10–15 m thick, lying on a Laramide thrust fault that dips west at about 19°. The moderately steep dip of this thrust fault toward the valley and its weak (?) material properties have combined to induce incipient westward landsliding and dismemberment of the Precambrian slab. Westward slippage was probably also induced by the strong earthquake shaking that accompanies **M**>7 earthquakes on the northern Sangre de Cristo fault zone here roughly every 10,000 years (see discussion in McCalpin, 2006). As the range has been uplifted above the valley floor, this west-dipping Laramide thrust fault has been progressively “daylighted” on the range-front slopes. The daylighting removes the lateral support from the downslope end of the west-tilted slab of gneiss, allowing it to begin to stretch and extend valleyward.

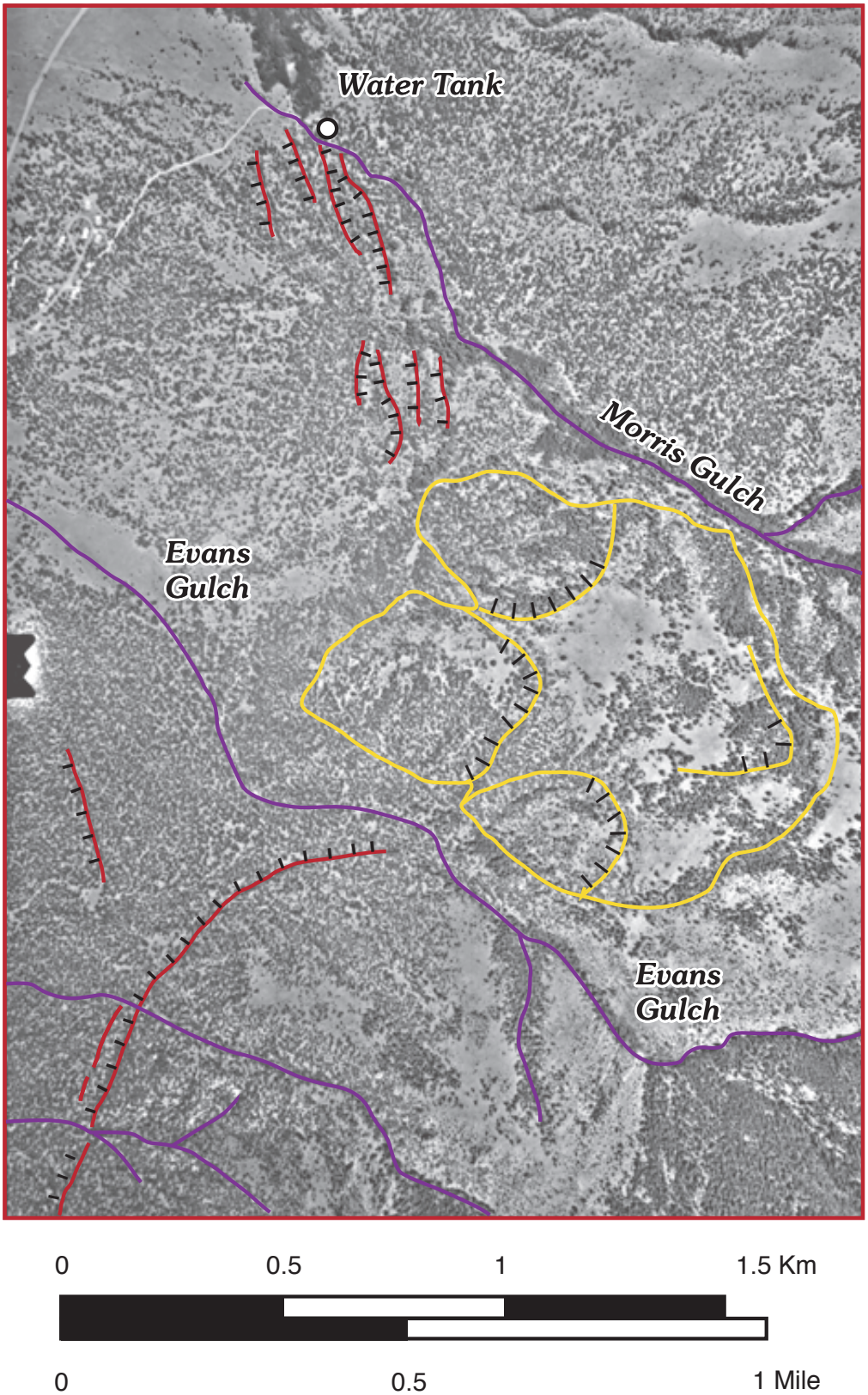

Figure A3–4. Fault scarps (red lines), landslides (yellow lines), and stream drainages (blue lines) along and adjacent to Morris Gulch. Location of Water Tank shown on figures A3–1 and A3–2.

Stop A4 — Parabolic Dune Migration Across the Southern Sand Sheet

Speaker: Steve Forman
Location: Great Sand Dunes Oasis (general store) parking lot
Zapata Ranch 7.5' quadrangle
GPS: NAD27, Zone 13, 451720 m E., 4171630 m N.
Elevation: 7,970 ft

Synopsis

The Great Sand Dunes National Park and Preserve in Colorado contains one of the largest and tallest intermountain dune systems in North America (fig. A2–1). This active dune field rises to heights of 250 m above the San Luis Valley, is banked against the Sangre de Cristo Mountains, and contains a rich variety of dune types. The response of the Park's dune system to well-documented droughts that affected large parts of western North America in the past 70 years (1930s, 1950s, 1960–64, 1971–74, 1977–81, 1989–90, and 2000–04) is the focus of both recent and other ongoing research (Marin and others, 2005).

The focus of this study is the sand sheet area, which fronts the dune field to the north, south, and west. The sand sheet harbors mostly vegetated and stabilized kilometer-long parabolic and barchanoid dunes that indicate dominant winds from the west-southwest. The distinct morphology of these dunes, well-defined wind formational processes, and readily identifiable forms in remotely sensed images provide straightforward targets to assess changes in dune position. To evaluate the response of these active parabolic and barchanoid dunes, a time series of aerial photographs and remotely sensed images from 1936 to 1999 was studied by image analysis and geographic information system (GIS) techniques and complemented with field assessment. The extent of dune migration was evaluated with respect to climate parameters, such as precipitation and the Palmer Drought Severity Index (PDSI), to understand better the landscape's response to varying levels of drought in the 20th Century. This stop provides insight into how semiarid landscapes respond to drought and quantifies thresholds and rates for dune migration at Great Sand Dunes National Park.

Discussion

Understanding dune dynamics in the western United States is critical to assessing semiarid landscape response to past climate variability (Overpeck, 1996; Woodhouse and Overpeck, 1998; Forman and others, 2001). The stratigraphic and geomorphic records of eolian deposition in the Basin and Range Province and Great Plains serve as proxies for the timing and magnitude of large-scale droughts in the past 10,000 years of sufficient severity for the widespread movement and accumulation of eolian sand (for example, Wells and others, 1990; Forman and others, 2001, 2006; Forman and Pierson, 2003; Mason and others, 2004). A variety of paleoclimatic studies in central North America show possible relationships between episodes of past eolian activity and drought intervals for the past 2,000 years (for example, Muhs and others, 1997; Woodhouse and Overpeck, 1998 and references within; Forman and others, 2001, 2006; Wolfe and others, 2001; Forman and Pierson, 2003). Periods of aridity in the western United States directly affects growing season moisture and vegetation; this lack of moisture is associated with reduction in rainfall and increases in evapotranspiration (Schlesinger and others, 1990; Lancaster, 1997). However, sustained drought in semiarid areas is associated with complex surficial processes that promote the heterogeneous distribution of soil nutrients leading to degradation of grasslands and subsequent invasion by desert shrubs (Shulka and Mintz, 1982; Schlesinger and others, 1990; Huenneke and others, 2002). Other surface disturbances such as grazers and off-road vehicles increase soil heterogeneity and erosion, enhancing the availability of sediments for eolian entrainment (Schlesinger and others, 1990). Questions remain on the sensitivity of dune systems in semiarid landscapes, such as that at Great Sand Dunes, to drought variability in the 20th and beginning of the 21st Centuries.

Remote Sensing of Eolian Landforms

Remote sensing and GIS techniques are powerful tools for registering land surface changes and for quantifying dune migration at Great Sand Dunes. This stop will highlight a digital database of 15 remotely sensed images that are used to understand changing surficial processes with evolving drought conditions at Great Sand Dunes. Fourteen sets of aerial photographs that cover all or a portion of the area were obtained from Great Sand Dunes and scanned into digital format with an original resolution of 0.8 m/pixel. This database contains aerial photography from 1936, 1937, 1938, 1941, 1953, 1955, 1957, 1966, 1975, 1979, 1981, 1983, 1988, 1995, and 1998 (table A4–1). A Landsat Enhanced Thematic Mapper Plus (ETM+) image from 26 July 1999 (Path 33, Row 34) processed with radiometric, geometric, and precise correction of parallax error was added to the database (fig. A4–1, table A4–1). This image served as a reference to assess dune position and land cover changes. False color composition images from the Landsat ETM+ using visible (1, 2, and 3) and infrared (4, 5, and 7) bands (25-m resolution) and panchromatic (10-m resolution) are superb for identifying large-scale dune forms and to separate active eolian sand from areas covered by vegetation or water (Marin and others, 2005). To facilitate georeferencing and later comparison among images, the 1998 digital orthoquadrangle from the U.S. Geological Survey (Terraserver, 2004) at 2-m resolution and the ETM+ image were coregistered using image-to-image methods having first-order polynomial model universal transverse Mercator (UTM) coordinates (Zone 13, Clarke 1866 spheroid, and NAD

27 datum). Aerial photographs were coregistered with a 1998 orthoquadrangle using the same georeferenced model. Digital mosaics for each set of data were produced from the respective georeferenced aerial photographs. These mosaics have a spatial resolution of 2 m and errors ranging from 5 to 45 m, depending on the number and location of control points (that is, roads, buildings, and fence lines) in the image-to-image coregistration (table A4–1). The largest errors (42–45 m) were generated in the registration process of digital mosaics (1953, 1966, and 1979) provided for GRSDNPP by Hammond (1998). However, despite these spatial resolution and georeferencing errors, the images are appropriate for tracking decadal positional changes of individual and compound parabolic and barchan dunes, with total dune migrations between 150 and 650 m in the past 63 years. Additional geographic and topographic information for geomorphic assessments is from a digital terrain model (30 m resolution) from the U.S. Geological Survey (Mapmart, 2004). ENVI 3.4 and ERDAS Imagine 8.2 programs are used for imagery preparation, georeferencing, combination, and enhancement. GIS-ARC/View 3.2 is used for visual and quantitative analyses of landscape elements and to document changes in dune coverage, extent and form, vegetation cover, and water resources.

Quantitative Analysis of Parabolic Dune Migration From 1936 to 1999

The position of well-formed parabolic dunes (PD) on the sand sheet (figs. A4–1 and A4–2) is tracked using 16 sets of remote sensing data from 1936 to 1999 (table A4–1). The parabolic dunes are conspicuous on the images as elongated, “hairpin” forms that often occur in an en echelon configuration, forming compound parabolic dunes (fig. A4–2). The arms of the parabolic dunes are mostly vegetated by grasses and shrubs and can be traced for up to about 3.5 km. Individual dunes are conspicuous in images from the 1930s, whereas compound parabolic dunes are common in the late 20th Century (figs. A4–2 and A4–3). Today, these dunes are as much as 4 m high and are oriented N. 35° E. to N. 40° E., reflecting predominantly southwesterly winds (fig. A4–2). Dune migration is associated with blowout of the parabolic dune rim and downwind migration of the slip face (Greeley and Iversen, 1987, p.172–173).

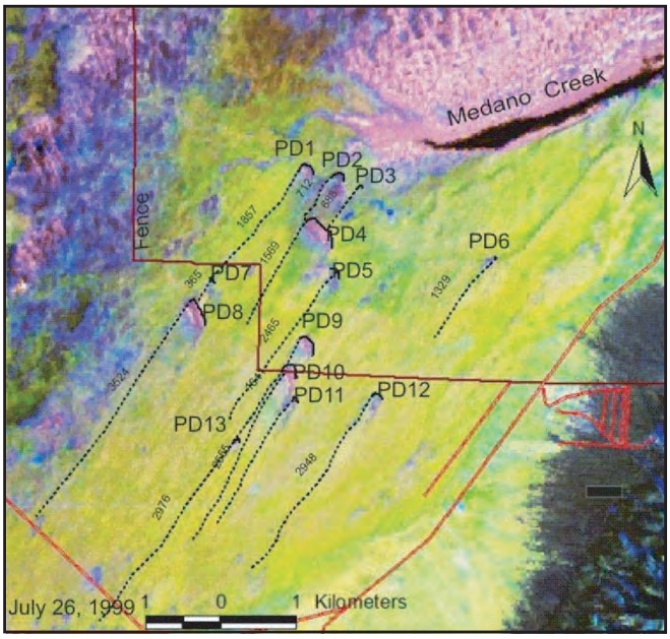

Figure A4–1. Digital terrain model of the southwest part of Great Sand Dunes National Park and Preserve. The southeast sand-sheet area (with site numbers, such as PD12) is the focus of this study (modified from Forman and others, 2006).

Changes in position of 13 parabolic dunes (PD1–PD13) were tracked on the remote sensing imagery time series (table A4–2, fig. A4–3). This analysis provides estimates for net, total, and rate of dune migration and associated errors (table A4–2). The extent of dune migration was assessed relative to a mosaic of the oldest aerial photographs that were taken on 12 August 1936 (table A4–1). The dunes on these photos range in length from about 0.7–3.5 km and are readily identified on images from all years (figs. A4–2 and A4–3, table A4–2). The longest parabolic dunes (about 3.5–2.5 km) are present to the south of the Park fence where the arms are minimally disturbed by a road that goes to San Luis Lake (parabolic dunes 5, 8, 10, 12, and 13 in fig. A4–3, table A4–2). North of the Park fence, the arms of parabolic dunes are truncated, merging into compound forms and often reworking sand from previously stabilized arms.

Evaluating dune migration at GSDNPP is constrained by the temporal spacing of aerial photographic coverage. Assessment of completeness in the geologic record stresses that the estimated rate of change increases with number of dated observations and that calculated rates often are underestimates (Sadler and Strauss, 1990; Sadler, 2004). Thus, estimates of the rate of dune migration in the Park may be minima, reflecting the variable time interval (1 to 13 years) between images. However, dune migration rates for successive years and for decadal intervals with more than three mosaics may provide close to finite estimates, specifically when longer time steps do not result in a reduction in rate compared with shorter intervals.

The 13 parabolic dunes monitored between 1936 and 1938 yield an apparent range of velocities between 2 and 70 m/yr, with an average velocity of 16 m/yr (table A4–2, fig. A4–4). Between 1938 and 1941, 12 of the 13 dunes (all except PD3) accelerated to one of the highest velocities measured (16 to 46 m/yr); the highest average migration rate was 32 m/yr (table A4–2). Dune migration rates decreased from 1941 to 1953, ranging from 0.3 to 10 m/yr and averaging 5 m/yr. Subsequently, between 1953 and 1955 drift rates increased for 7 (PD1, PD2, PD3, PD4, PD8, PD9, and PD11) of the 13 dunes; the rates ranged from 1 to 44 m/yr with an average 14 m/yr for all 13 dunes. The slowest rates of dune migration of (<10 m/yr) were registered between

Table A4–1. Remote-sensing imagery used to assess migration of parabolic and barchan dunes at Great Sand Dunes National Park and Preserve.

Georeferenced mosaics	Original scale	Pixel size (m)	RMS[c] (m)	UTM coordinates location[d]				Coverage GSDNPP (percent)	Source[e]
				ULX	ULY	LRX	LRY		
August 12, 1936	1:31,680	2	39	440838	4190169	456246	4162357	70	GSDNPP and SCS
September 26, 1937	1:20,000	2	35	442267	4188903	446869	4176191	30	GSDNPP and SCS
August 9, 1938	1:30,000	2	11	446927	4175580	451861	4170556	30	GSDNPP and SCS
November 15, 1941	1:20,000	2	15	438492	4185984	459420	4160848	80	National Archives
October, 1953	1:53,000	2	44	436028	4192183	458292	4167447	100	Hammond, 1998
August 22, 1955	1:20,000	2	42	442778	4179184	456050	4165752	50	GSDNPP and SCS
September 25, 1957	1:20,000	2	7	444438	4187469	450192	4181533	20	GSDNPP and SCS
July 2, 1966	1:20,157	2	45	440050	4190136	457322	4167314	50	Hammond, 1998
September 25, 1975	1:80,000	2	7	430687	4193302	448539	4169846	50	GSDNPP and SCS
September 5, 1979	1:78,000	2	45	433723	4193002	457619	4164562	100	Hammond, 1998
June 11, 1981	1:40.000	2	18	442549	4190336	456813	4154912	95	GSDNPP and SCS
September 16, 1983	1:58,000	2	18	444570	4190779	456576	4166533	90	GSDNPP and SCS
September 4, 1988	1:40,000	2	18	438702	4188794	457400	4169686	90	GSDNPP and SCS
July 26, 1995	1:24,000	2	21	443239	4175190	453843	4168622	30	GSDNPP and SCS
September 6, 1998	1:40,000		5	441653	4188608	457641	4164558	100	GSDNPP, SCS, USGS
PAN[a] July 26, 1999		10	10	422266	4194108	460791	4157533	100	EROS Data Center
IR/VISIBLE[b]		25	25	422266	4194108	460791	4157533	100	EROS Data Center

[a]Panchromatic band of the Landsat enhanced thematic mapper image.

[b]Infrared (bands 4, 5, and 7) and visible (bands 1, 2, and 3) of the Landsat enhanced thematic mapper image.

[c]Root mean squared error associated with the georeference process.

[d]ULX, ULY: Upper left X and Y coordinates. LRX, LRY: Lower right X and Y coordinates. Corresponds with UTM Zone 13, spheroid: Clarke 1866 and datum: NAD27.

[e]EROS, Earth Resources Observation System; GSDNPP, Great Sand Dunes National Park and Preserve; SCS, Soil Conservation Service; USGS, U.S. Geological Survey.

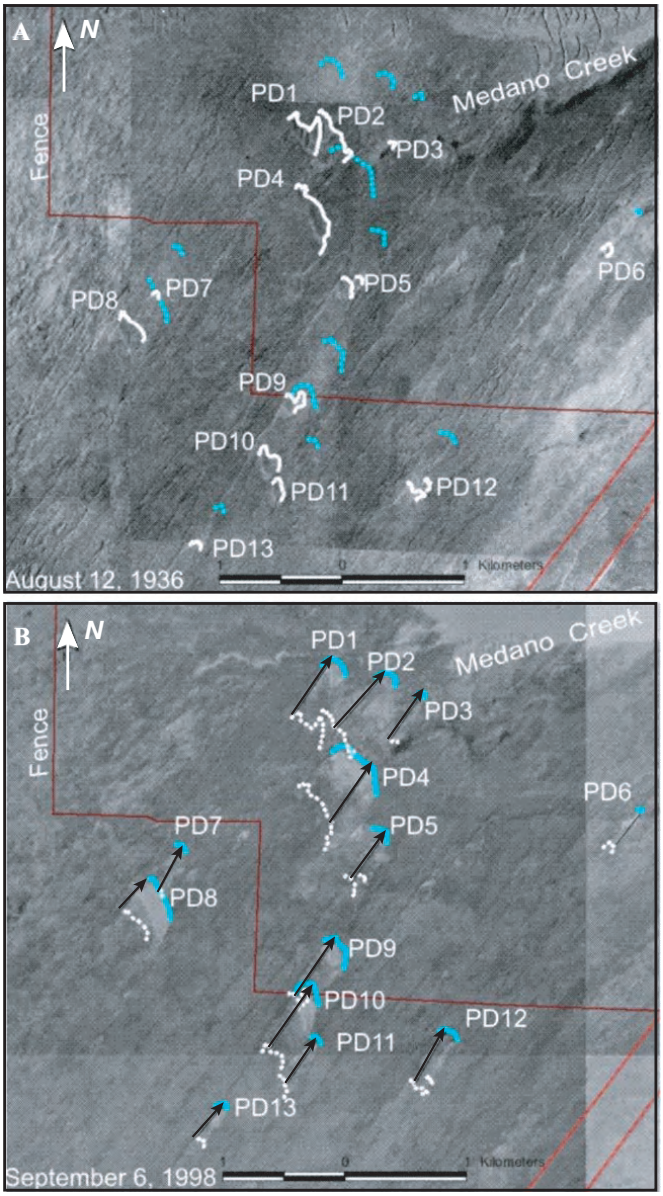

Figure A4–2. Aerial images of parabolic dunes in the Great Sand Dunes National Park and Preserve. Labels refer to studied dunes (that is, for instance, PD1). *A*, Aerial photograph from August 12, 1936. Solid white lines show the position of the parabolic dunes in 1936, and the dotted blue lines represent the position of the same dunes on a Landsat image from July 26, 1999. *B*, Aerial photograph from September 6, 1998. Solid blue lines show the position of the parabolic dunes on a Landsat image from July 26, 1999, and dotted white lines show the location of the dunes on August 12, 1936 (part *A*). Black arrows show the direction and magnitude of the dune advance in 63 years (modified from Forman and others, 2006).

1955 and 1979, followed by acceleration of 9 (PD4, PD5, PD6, PD7, PD8, PD9, PD10, PD11, and PD13) of the 13 dunes between 1979 and 1981 at velocities ranging from 2 to 37 m/yr and averaging 16 m/yr for all dunes (table A4–2). Dunes were relatively quiescent between 1981 and 1983; 8 of the 13 dunes yielded velocities of <8 m/yr. For the past 25 years (between 1983 and 1988, 1988 and 1995, and 1995 and 1998), dune migration rates remained low and velocities were <10 m/yr for at least 7 of the 13 dunes. The position of parabolic dunes between 1998 and 1999 changed dramatically, with 12 of the 13 dunes accelerating to 14 to 76 m/yr and 6 of the dunes (PD4, PD6, PD9, PD10, PD11, and PD13) showing the highest drift velocities yet measured (table A4–2). The average dune migration rate between 1998 and 1999 was 30 m/yr, which is similar to migration rates for the period 1938–1941, in which all dunes registered either the highest or next to highest recorded velocities (table A4–2, fig. A4–4).

Summary

In summary, the total parabolic dune migration from 1936 to 1999 for the 13 measured dunes ranges from 313–665 m toward the northeast; corresponding average rates for individual dunes range from 5–11 m/yr with an average rate of about 8±1.6 m/yr for all dunes (table A4–2, fig. A4–3). A significant observation is that between 1936 and 1999 the largest dunes with active areas of 0.04 km^2 to 0.23 km^2 (PD1, PD2, PD8, PD9, and PD10) show average migration rates (about 9 m/yr) that are 30 percent greater than rates (about 6 m/yr) observed for smaller dunes with areas of <0.004 km^2 (PD3, PD5, PD6, PD7, PD11, PD12, and PD13). Nearly half of the total dune migration between 1936 and 1999 occurred prior to 1955, mostly associated with drought intervals in the 1930s and 1950s. Approximately 30 percent of dune migration occurred between 1955 and 1981 and 15 percent from 1981 to 1995. As much as 10 percent of the total dune drift occurred since 1995 and 1998 for dunes 4, 7, 11, and 12 and dunes 6, 10, and 13 (respectively) reflecting drought conditions in the late 20 Century (table A4–2).

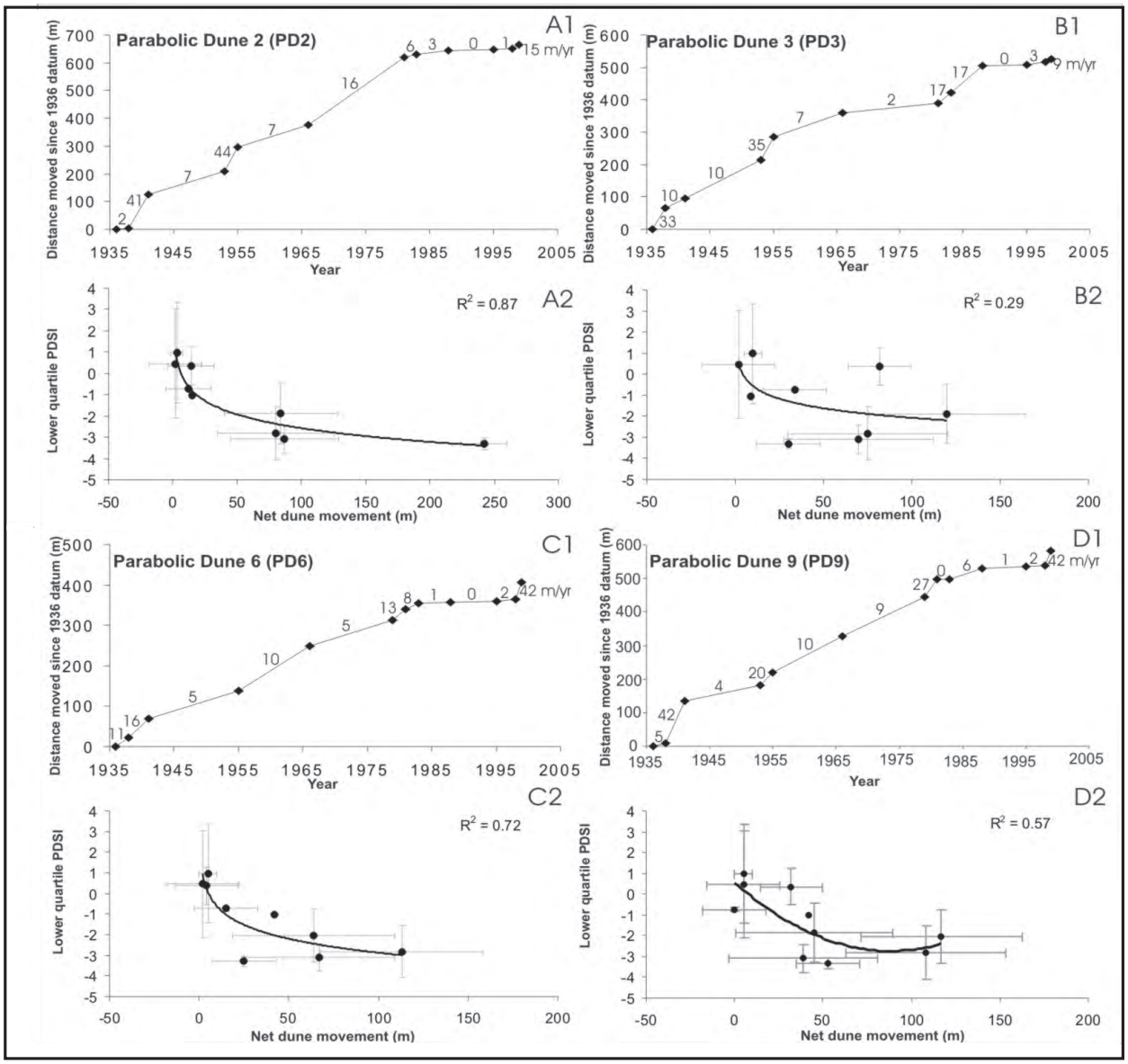

Figure A4–3. Quantitative analysis of parabolic dune migration rate from georeferenced mosaics of imagery from 1936 to 1999 (table A4–1, fig. A4–2). Graphs A1, B1, C1, and D1 show absolute migration (in meters) for parabolic dunes 2, 3, 6, and 9 relative to their position in 1936. The numbers adjacent to line segments are dune migration rates (meters/year). Graphs A2, B2, C2, and D2 show the logarithmic relation between net parabolic dune migration and the Palmer Drought Severity Index (PDSI) lower quartile. Shown are 1-sigma PDSI errors and net dune migration errors, reflecting the root mean squared errors from mosaicking and georeferencing images (table A4–2).

Table A4–2. Migration of parabolic dunes (PD) measured from 1936 to 1999 at the Great Sand Dunes National Park and Preserve (GRSA) and associated Palmer Drought Severity Index (PDSI).

Intervals	Net migration of parabolic dunes (m)														Migration rates for parabolic dunes (m/yr)														PDSI [b]
	PD1	PD2	PD3	PD4	PD5	PD6	PD7	PD8	PD9	PD10	PD11	PD12	PD13	Error (m)[a]	PD1	PD2	PD3	PD4	PD5	PD6	PD7	PD8	PD9	PD10	PD11	PD12	PD13	Ave. rate[c]	lowest 25%
1998-99	14	15	9	48	2	42	16	25	42	76	42	22	32	10	14	15	9	48	2	42	16	25	42	76	42	22	32	**30 ± 20**	-1.0
1995-98	0	3	10	44	3	5	3	26	5	21	30	17	31	5	0	1	3	15	1	2	1	9	2	7	10	6	10	5 ± 5	1.0 ± 2.4
1988-95	46	2	2	46	1	2	63	28	5	85	19	22	7	21	7	<1	0	7	0	0	9	4	1	12	3	3	1	4 ± 4	0.5 ± 2.6
1983-88	15	14	82	22	16	4	62	39	32	40	4	18	6	18	3	3	16	4	3	1	12	8	6	8	1	4	1	5 ± 5	0.4 ± 0.9
1981-83	53	12	34	0	0	15	2	5	0	12	43	0	27	18	27	6	17	0	0	8	1	3	0	6	22	0	14	8 ± 9	-0.7 ± 0.1
1979-81	na	na	na	37	74	25	40	43	53	13	25	9	3	18	na	na	na	19	37	13	20	22	27	6	13	5	2	**16 ± 11**	-3.0 ± 0.3
1966-79	na	na	na	18	65	64	3	72	117	121	8	5	41	45	na	na	na	1	5	5	0	6	9	9	1	<1	3	4 ± 3	-2.0 ± 1.3
1966-81	47	242	30	na	na	na	na	na	na	na	na	na	na	18	3	16	2	na	na	na	na	na	na	na	na	na	na	7 ± 8	-3.3 ± 0.3
1955-66	140	80	75	94	74	113	33	7	108	67	79	156	6	45	13	7	7	9	7	10	3	1	10	6	7	14	1	7 ± 4	-2.8 ± 1.3
1953-55	26	87	70	13	8	na	4	69	39	1	21	2	12	42	13	44	35	7	4	na	2	35	20	1	11	1	6	**15 ± 15**	-3.1 ± 0.7
1941-55	na	na	na	na	na	67	na	na	na	na	na	na	na	42	na	na	na	na	na	5	na	na	na	na	na	na	na	5	-3.1 ± 0.7
1941-53	79	84	120	92	117	na	18	4	45	100	33	39	50	44	7	7	10	8	10	na	2	<1	4	8	3	3	4	5 ± 3	-1.9 ± 1.4
1938-41	138	123	29	97	100	48	106	71	126	89	113	110	89	15	46	41	10	32	33	16	35	24	42	30	38	37	30	**32 ± 10**	
1936-38	5	3	65	20	23	22	25	139	10	15	62	6	9	11	3	2	33	10	12	11	13	70	5	8	31	3	5	**16 ± 19**	
Total dune movement (m)	563	665	526	531	483	407	375	528	582	640	479	406	313	Dune movement rate 1936-1999 (m/yr)	8.9	10.6	8.4	8.4	7.7	6.5	6.0	8.4	9.2	10.2	7.6	6.4	5.0	7.9 ± 1.6	
Arms length (m)	1857	712	688	1569	2465	1329	365	3524	1641	2555	1940	2948	2976	Minimum inferred age (yr)[d]	209	67	82	187	320	204	61	420	178	250	255	461	595		

[a] Root Mean Squared error associated to the georeference process.
[b] Palmer Drought Severity Index from 1950 to 2003, National Climatic Data Center, 2004 www.ncdc.noaa.gov/oa/ncdc.html.
[c] Bold figures indicate significant migration rates, above long-term average.
[d] Ages calculated by dividing parabolic arm length by dune migration rate for 1936-99.

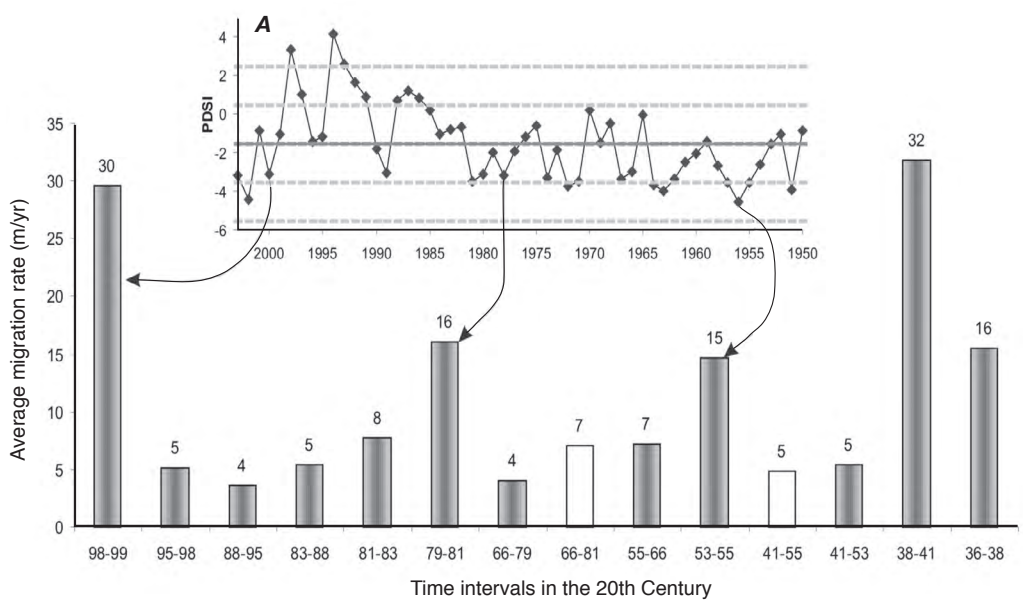

Fig A4–4. Migration rate for parabolic dunes over during measured time intervals in the 20th Century (from Marín and others, 2005). Shaded black bars indicate average drift rate for more than 3 parabolic dunes; white bar indicates average drift rate for fewer than 3 parabolic dunes. Inset graph (*A*) is the lower quartile time series of corresponding Palmer Drought Severity Index for the Great Sand Dunes National Park and Preserve.

Stop A5 — Cattle-Guard Paleoindian Site

Speaker: Fred Bunch and (or) Pedi Jodry
Location: Cattle Guard archeological site, Alamosa County Lane 6N.
Medano Ranch 7.5' quadrangle
GPS: NAD27, Zone 13, 444530 m E., 4168410 m N.
Elevation: 7,636 ft.

Discussion

Stewart's "Cattle-guard" site is an outstanding example of a Folsom bison kill site. Over 9,000 years ago, nomadic hunters killed 49 bison at this location (fig. A5–1). These bison (*Bison antiquus*) were a great deal larger than modern bison. Archaeologists from the Smithsonian Institution have been studying this site for two decades (see for example Jodry, 1987; Jodry and others, 1989; Jodry and Stanford, 1992), and the results of their research here have contributed greatly to the body of knowledge regarding Paleoindian tools and kill sites.

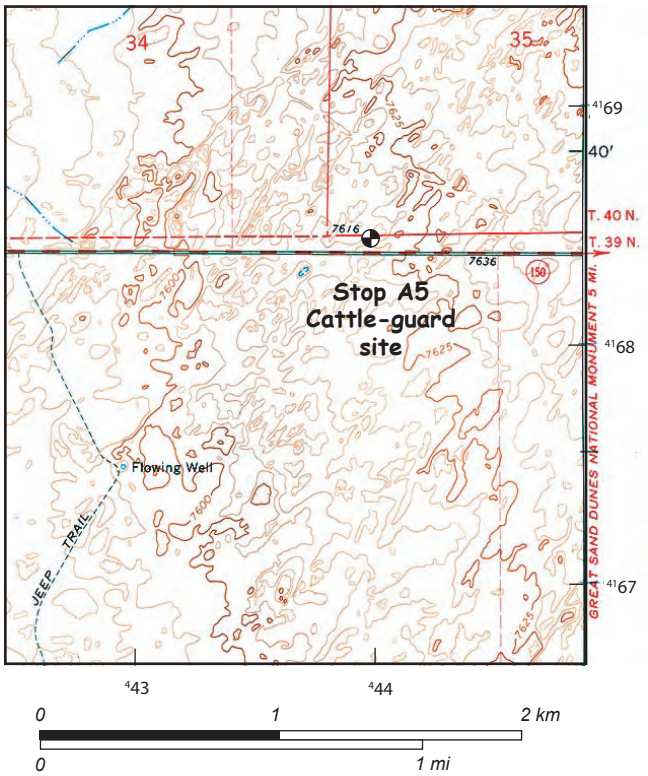

Figure A5–1. Topography around stop A5, Stewart's Cattle-guard site. Map scanned from Medano Ranch, Colorado, 7.5-minute topographic map.

Stop A6 — Medano Ranch Area

Speakers: Richard Madole, Shannon Mahan, and Michael Rupert
Location: Near former Medano Ranch headquarters
Medano Ranch 7.5' quadrangle
GPS: NAD27, Zone 13, 441650 m E., 4176460 m N.
Elevation: 7,650–7,665 ft

Medano Ranch

The Medano Ranch is one of the oldest continuously operated ranches in the San Luis Valley. The headquarters area of the ranch was established during the early years of the range cattle industry in Colorado when the Dickey brothers from Ohio brought large numbers of Texas cattle into the area. The Dickeys sold their beef to the booming mining camps of Leadville to the north. A post office was established at the ranch in 1877 with William Dickey as postmaster. In 1882, the Dickeys sold the ranch to Adee and Durkee (of the seasoning fame) who have been described as "cattle kings" with the largest beef production in the valley. The tenure of Adee and Durkee was impacted by severe weather, a steep drop in cattle prices, and the economic effects of the panic of 1890. In 1894, George Adams bought the ranch and sold it seven years later to Loren Sylvester of Monte Vista and Richard Holsford of Iowa, but cattle raising continued to be a depressed industry and in 1907 they sold the ranch back to the bank that had loaned them the money.

George W. Linger acquired the ranch in 1912 and ushered it into the modern era, changing it into fed-cattle business and introducing white-faced Herefords. Following George Linger's death in an airplane crash in 1921, his children continued the operation until 1947 when the ranch was sold to Malcolm Stewart, a Texas oilman. Stewart in turn sold the ranch in 1988 to Hisa Ota and others who started raising bison as well as cattle. Ota sold the ranch to the Nature Conservancy in late

summer of 1999. When the Nature Conservancy purchased the Zapata-Medano Ranch, they came into ownership of about 103,000 acres on the east side of the San Luis Valley bordering Great Sand Dunes on the north and the Rio Grande National Forest to the east. As a result, they became owners of one of the largest bison herds in Colorado.

The buildings at the Medano Ranch Headquarters were listed on the National Register of Historic Places in February 2004. The Nature Conservancy bison operation is centered on this portion of the Medano-Zapata. This portion of the property is also included within the newly authorized boundaries of the adjacent Great Sand Dunes National Park and Preserve located to the east. We'll discuss two intertwined topics at stop A6 on the Medano Ranch: the Quaternary stratigraphy in the Great Sand Dunes area (stop 6.1) and dating of ground water at Great Sand Dunes (stop 6.2)

Stop A6.1 — Overview of Quaternary Stratigraphy in the Great Sand Dunes Area

Speakers: Richard Madole and Shannon Mahan

Synopsis

At this stop, we will review eolian sand stratigraphy and also briefly discuss the noneolian deposits (fluvial, lacustrine, paludal, and sheetwash) in the area. Stop A6.1 is on eolian sand (unit Qes2; fig. A6.1–1) that ranges in age from middle Holocene (defined here as 8–4 ka) to the early part of late Holocene time. Sand from just below the thin, case-hardened $CaCO_3$-bonded ledge seen here has an estimated age of 3,640±260 OSL yr B.P. Eolian sand of unit Qes3 forms the "hills" 2 km to the southwest, which are less than 1,000 years old. Latest Pleistocene eolian sand (unit Qes1) is not visible at this stop. However, most of the area within view is underlain by upper Pleistocene sediment, chiefly alluvium, at shallow depths (1–6 m).

Discussion

A nearly continuous belt of windblown sand of variable width extends along the east side of the San Luis Valley between Rito Alto Creek on the north and the Dry Lakes area on the south, a distance of about 70 km. The Great Sand Dunes cover about 12 percent of this sand area. Although most of the eolian sand at the surface is Holocene, stratigraphic and geomorphic evidence indicate that eolian sand has been accumulating here since late-middle Pleistocene time. Within and adjacent to deposits of eolian sand are large areas of sediment that accumulated in lakes, ponds, marshes, and alluvial flats on the lower piedmont slope and basin floor. Stop A6.1 is in an area where noneolian sediment, mostly alluvium, is particularly widespread (fig. A6.1–1). Alluvium is the dominant noneolian surficial material present. Most alluvium consists of poorly sorted sand and fine- to coarse-pebble gravel. In addition, thin (1.0–1.5 m) deposits of calcareous silty fine sand and sandy silt are extensive in some places. These deposits are probably "river-end"

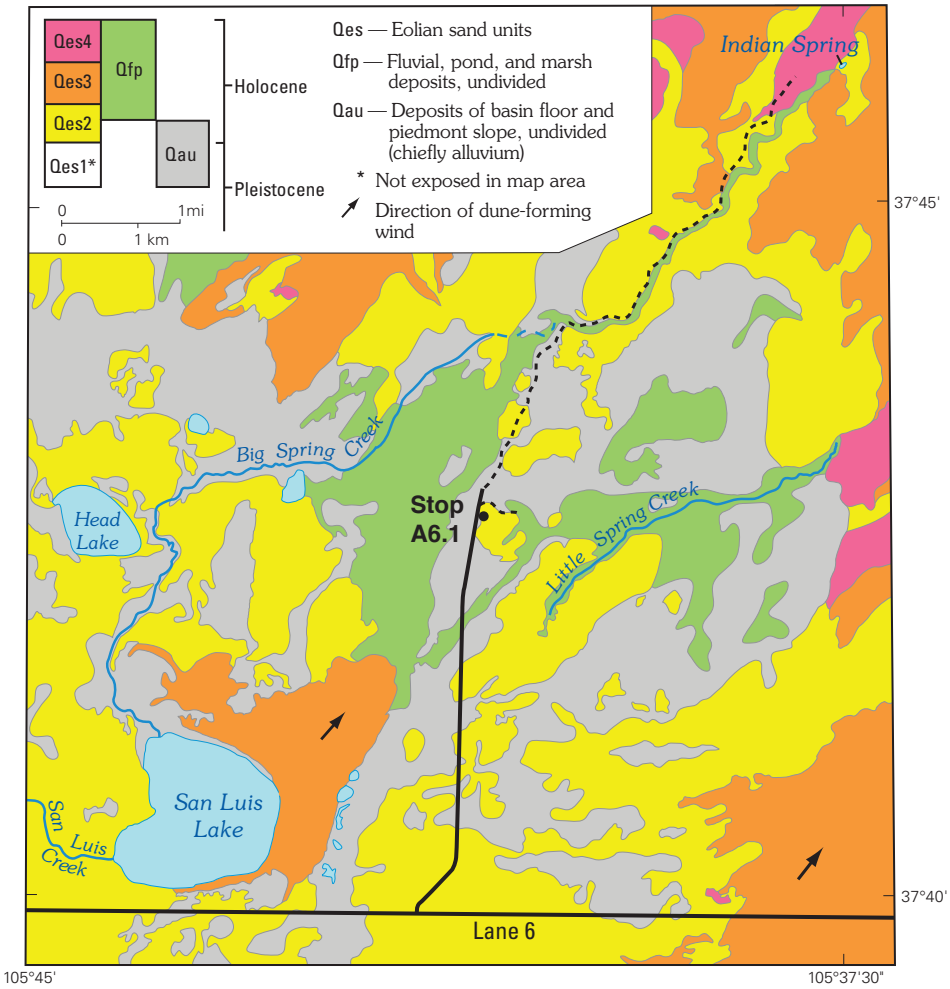

Figure A6.1–1. Eolian, fluvial and alluvial deposits in the vicinity of stop A6.1. (Derived from Richard Madole, unpub. data, 2007).

sediment that was delivered to the lower piedmont slope and basin floor primarily by sheetwash and ephemeral streams that originated higher on the piedmont slope. Differences in degree of soil development and a few radiocarbon ages indicate that some of the alluvium is late Pleistocene and some is Holocene. In several places, a veneer (0.5–1.5 m) of Holocene alluvium overlies Pleistocene alluvium.

Eolian sand can be divided into four mappable units on the basis of physical properties, topographic expression of dunes, differences in degree of soil development, and stratigraphic relations (fig. A6.1–2). The youngest unit (Qes4) consists of sand that has been active during historic time. It is at the surface in about 15 percent of the eolian sand area. Most of unit Qes4 blankets the Great Dunes, but smaller deposits also are present elsewhere. The next oldest unit (Qes3) was deposited episodically between about 1,300 and 300 years ago. This age range is based partly on radiocarbon ages from this area and partly on correlations with similar deposits on the plains of eastern Colorado for which there is more numerical age control. Unit Qes3 is at the surface in about 60 percent of the eolian sand area. It forms (1) fields of parabolic dunes north, northwest, and southwest of the Great Sand Dunes National Park and Preserve, (2) lunette dunes in southern part of the area, and (3) compound parabolic dunes that extend northeast from San Luis Lake, the leeward edge of which are visible (looking southwest) from this stop (fig. A6.1–1).

Unit Qes2 includes sand that was deposited at different times during the middle Holocene (8–4 cal yr ka) and early part of the late Holocene (4–0 cal yr ka). It is at the surface in about 25 percent of the area, primarily the west-central part (fig. A6.1–3) and in broad-crested lunette dunes in the southern part. Unlike unit Qes3, which is noncalcareous and has little or no soil development, unit Qes2 has a very weakly developed soil in most places and everywhere contains secondary $CaCO_3$ in the upper 1–1.5 m. We are on unit Qes2 at this stop. Eolian sand from just below the thin ledge formed here by case-hardened, $CaCO_3$-bonded sand has an estimated age of 3,640±260 OSL yr B.P. (fig. A6.1–4).

Unit Qes1 is of late Pleistocene age. Little is known about its lateral extent and material properties because younger deposits—eolian sand, alluvium, and lacustrine sediment—bury it in most places. Exposures of unit Qes1 are primarily in stream banks, blowouts, and excavations (fig. A6.1–5). Except for the Great Dunes, the area within view from stop A6.1 is underlain at shallow depths (1–6 m) by late Pleistocene sediment, chiefly alluvium.

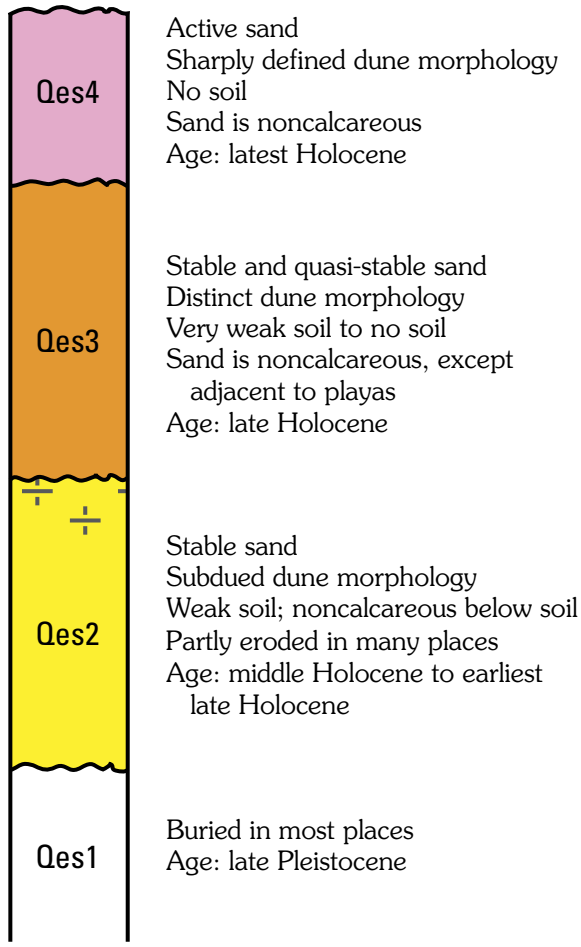

Figure A6.1–2. Composite section of eolian sands. Four mappable units defined on the basis of physical properties, topographic expression of dunes, differences in degree of soil development, and stratigraphic relations.

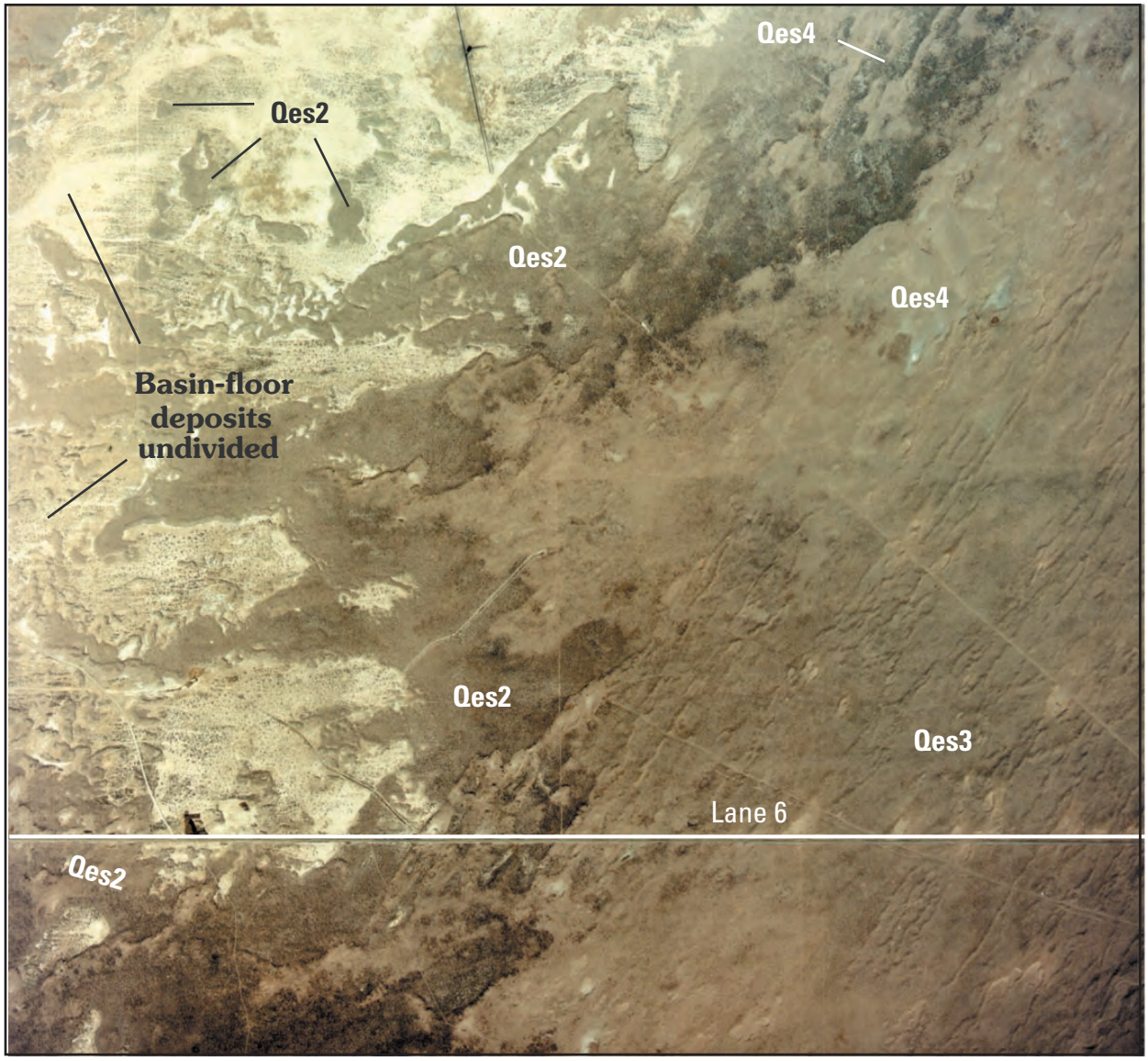

Figures A6.1–3. Typical distribution of three of the four eolian sand units shown in figure A6.1–2. We travel down Lane 6 on the way to stop A6.

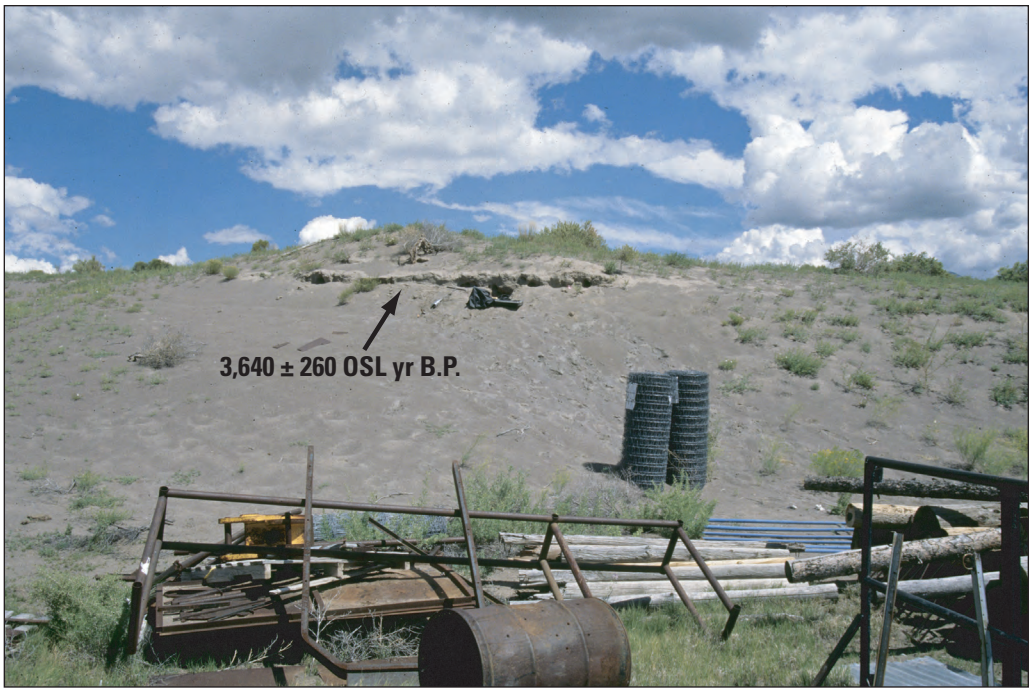

Figures A6.1–4. Age of eolian sand of unit Qes2 has an estimated age of 3640±260 OSL yr B.P. Sample is from below the thin ledge of case-hardened, $CaCO_3$-bonded sand.

Figure A6.1–5. Exposures of unit Qes1, the oldest of four sand units, are primarily in stream banks, excavations, and blowouts as shown in this photograph.

Stop A6.2 — Dating Groundwater at Great Sand Dunes National Park and Preserve

Speaker: Michael Rupert

Overview

There are the two principal aquifers at the Great Sand Dunes National Park and Preserve: a shallow unconfined aquifer and a deeper confined aquifer. Ground water in the unconfined aquifer is recharged by Medano and Sand Creeks near the Sangre de Cristo Mountain front, flows underneath the main dune field, and discharges to Big and Little Spring Creeks on the western margin of the dune field. It takes more than 60 years for the ground water to flow from Medano and Sand Creeks to Big and Little Spring Creeks (fig. A6.2–1), a distance of about 10 km (chapter D, this volume). During this time, ground water in the upper part of the unconfined aquifer is recharged by numerous precipitation events. This recharge from precipitation events causes the apparent ages determined using chlorofluorocarbons and tritium to become younger, because relatively young precipitation water is mixing with older waters derived from Medano and Sand Creeks. Radiocarbon dating of ground water in the confined aquifer (well Y) indicates it is about 30,000 years old (plus or minus 3,000 years). The peak of the last major ice advance (Pinedale glacial, OIS 2) occurred about 20,000 years ago; ground water from the confined aquifer is much older than that. A more complete discussion of these subjects is included in chapter D of this volume.

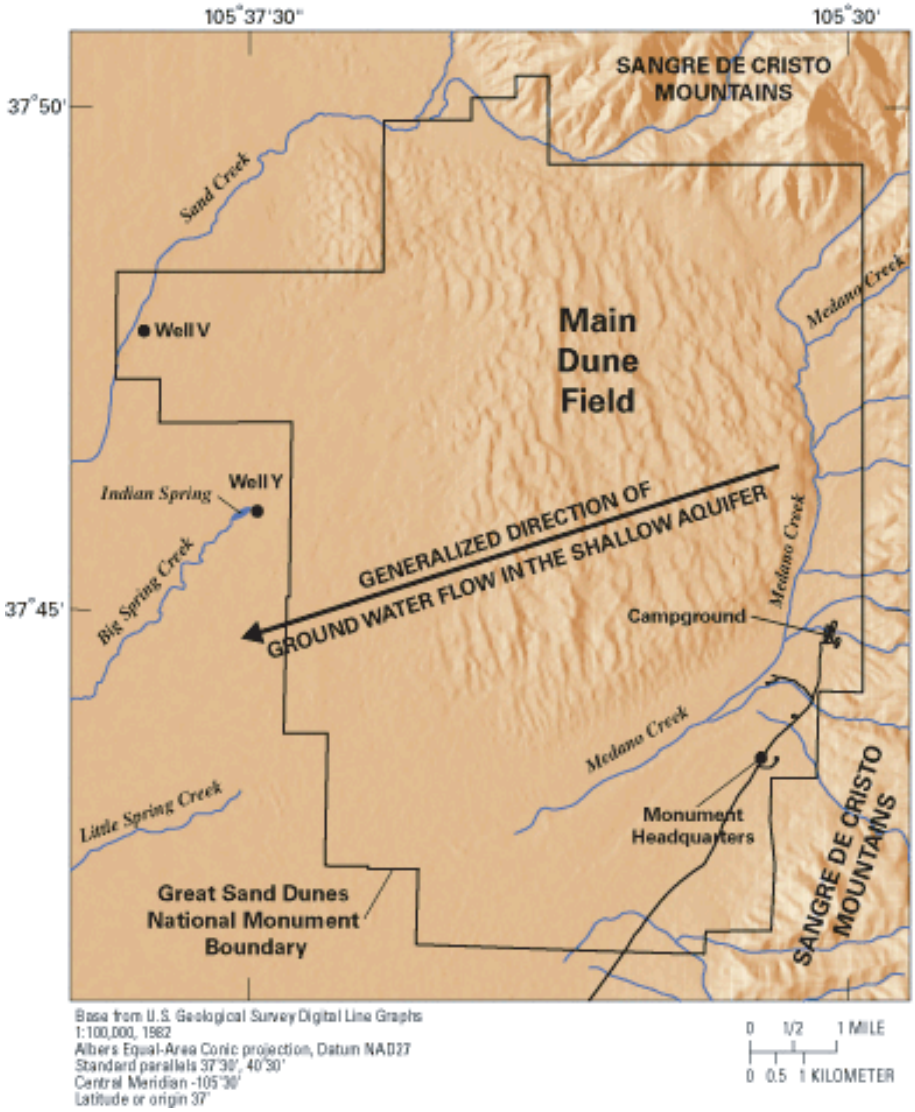

Figure A6.2–1. Generalized direction of ground-water flow beneath the Great Sand Dunes (main field).

Stop A7 — Sabkha overlook

Speaker: Andrew Valdez
Location: Closed Basin Canal, Zapata Ranch
Medano Ranch 7.5' quadrangle
GPS: NAD27, Zone 13, 438810 m E., 4164850 m N.
Elevation: 7,525 ft

Synopsis

This stop allows a close examination of a sabkha (salt-encrusted plain). Sabkhas form in areas of internal drainage where basin subsidence exceeds stream deposition, although wind deflation may also contribute to formation of local depressions. Playa formation is common and appears to be a critical factor in the accumulation of adjacent eolian sand deposits. Little is known about how Pleistocene climates would have affected the area and the input of sand. A group discussion on possible Pleistocene climatic effects will be sought.

Discussion

Sabkha is an Arabic term that refers to a salt-encrusted plain. The geologic definition refers to a coastal environment characterized by evaporites and eolian deposits. In the literature, it has been adapted to include similar environments away from coastlines, such as playas. At Great Sand Dunes, areas of sabkha are also found upgradient from the playas where deflation lowers the ground surface to the groundwater capillary fringe, and evaporation from that fringe produces evaporites.

The subsurface, rift structure of the Alamosa subbasin (of the San Luis Basin) exerts some control over the current basin surface in a manner that leads to the maintenance of the current eolian system. Drilling and geophysical-based petroleum exploration indicates that the basin is asymmetrical, dips to the east, and is subdivided into different crustal blocks (fig. A7–1). The western block is the moderately deep Monte Vista half graben. In the center, but in the subsurface, is the Alamosa horst. This elevated block may be spatially related to the San Luis Hills horst that is exposed south of the Alamosa subbasin (see chapter B). The eastern block is the relatively deeper and younger Baca graben. Here, basin-fill sediment of the Santa Fe Group (upper Cenozoic) is estimated to be as much as 5.6 km thick (Brister and Gries, 1994). Subsidence of the Baca graben and possibly wind deflation of the surface has created a subtle depression known locally as the “closed basin” since the area normally lacks external drainage. A playa or lake system has developed along the axis of the closed basin. During wet periods, the playas can fill to the point of overflowing the closed basin and thus become ephemeral tributaries to the Rio Grande. The last known occurrence of overflow was in the 1920s. Currently there is little opportunity for the basin to fill as most of the surface water is diverted for agricultural use upgradient from the playas.

The playa system commonly is associated with a poorly lithified, sandy deposit. The water-table gradient of the area is essentially flat, so the only known output of water is by evapotranspiration. This factor has resulted in saline water conditions and the precipitation of evaporite minerals and

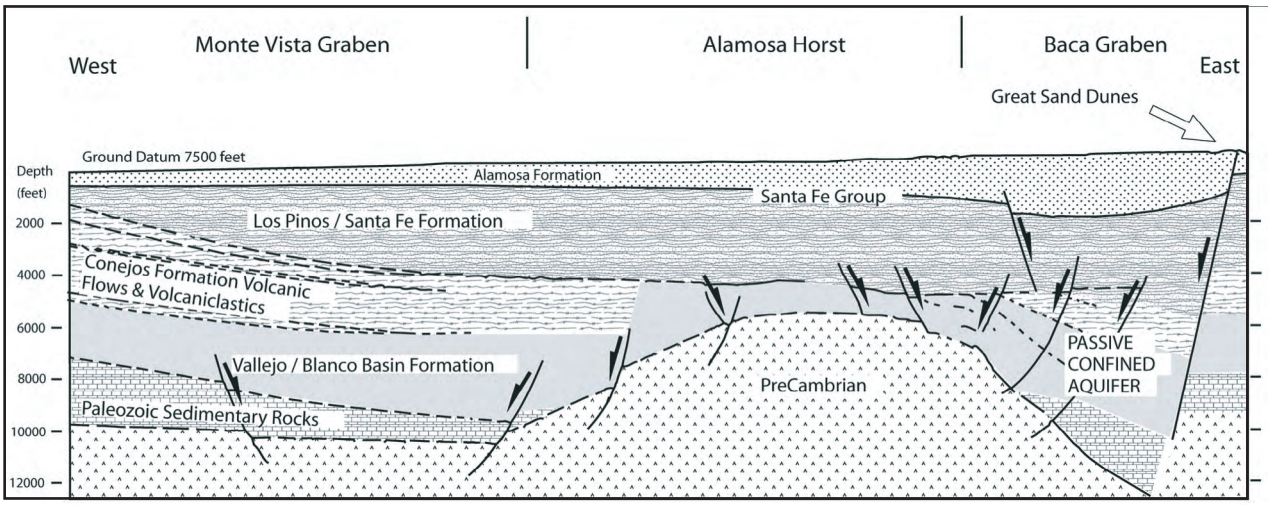

Figure A7–1. Geologic cross section of the San Luis Basin at the latitude of the Great Sand Dunes (37° 39' N.). Modified from Brister and Gries, 1994.

diagenesis of the sand (Krystinik, 1990). The most common evaporite is sodium bicarbonate (Fryberger, 1990b), likely in the mineral form of trona (H.N. Dixon, oral commun., 2006). U.S. Geological Survey research in the late 1970s and early 1980s subdivided the Great Sand Dunes eolian system into different depositional provinces. The playa area was termed "Province I, Dry Lakes" (Andrews, 1981). Later, USGS researchers identified the evaporite environment as a sabkha (Krystinik, 1990).

The majority of Great Sand Dunes' surficial eolian deposits can be traced upwind to the playa lake area, indicating that the processes that form the playa provide the fluvial source for eolian deflation (Madole and Romig, 2002). Without the development of playas, it is unlikely that eolian deposits would develop on the scale we see today. The process leading to the accumulation of eolian deposits requires that streams periodically fill playas; wave action concentrates sand on the beaches; and when the playa dries, beach sand is exposed to the wind and results in deposition of eolian sand downwind from the playa. The eolian sand forms lunettes (crescent- or tongue-shaped dunes) around playas, which tend to be round. In this area, they form on the northeast side of the playas because the dominate wind direction is from the southwest (Fig. A7–2).

The eolian system has resulted in formation of Great Sand Dunes downwind from the San Luis lakes, which are in the lowest and wettest part of the closed basin. Sand is plentiful enough in this system to promote dune development as indicated by active dune or vegetated dune forms. Eolian deposits exist north and south of the lakes, but the deposits generally consist of a thin veneer of sand and dunes are uncommon.

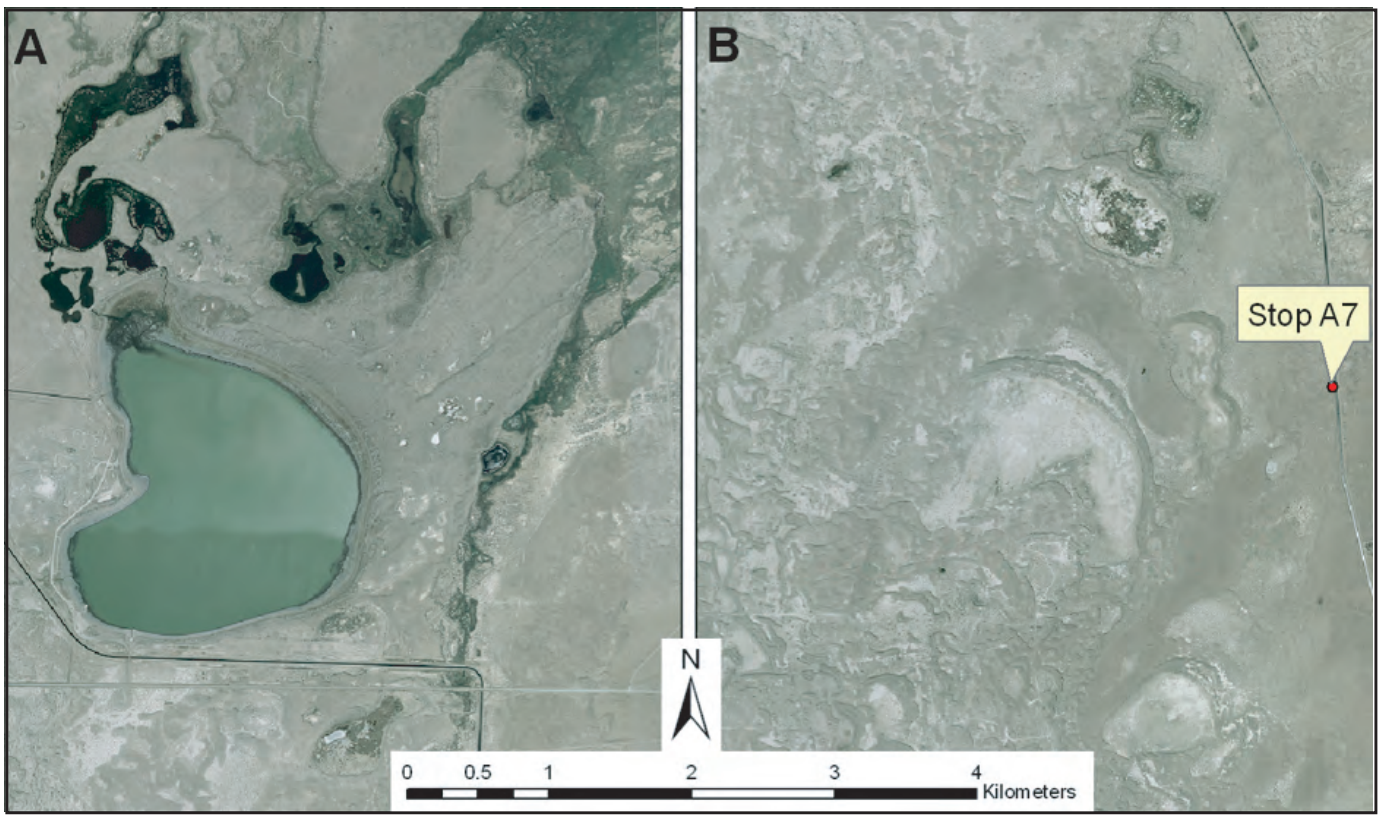

Figure A7–2. San Luis Lake and sabhka south of San Luis Lakes. *A*, San Luis Lake. *B*, Sahbka and dunes west of stop A7, about 3 km (2 mi) south of Lane 6 and San Luis Lake.

Stop A8 (Optional) — Closed Basin Overflow and Origin of Hansen Bluff

Author: Andrew Valdez
Location: Closed Basin Canal, Zapata Ranch
Medano Ranch 7.5' quadrangle
GPS: NAD27, Zone 13, 436490 m E., 4152416 m N.
Elevation: 7,522 ft

Synopsis

As this stop we will see the overflow point between the closed basin (stop A7) and the Rio Grande. Hansen Bluff, which is as much as 20 m high to the south (stop B7), extends north to this area, where it can be traced as a subtle fluvial scarp cut into the broad piedmont of the Sangre de Cristo Mountains. Historic accounts note that the closed basin did overflow during the 1920s, but now most of this stream water is diverted for agricultural use, so the opportunity for the basin to fill is reduced in all but extremely large-discharge years.

Discussion

Hansen Bluff is a north-south trending, 24-km-long topographic break in the otherwise planar surface of the Alamosa subbasin (fig. A8–1). The bluff extends from the southern end of the depression known as the "closed basin" to near the confluence of the Rio Grande and Trinchera Creek. The southern half is parallel to the trend of the Rio Grande and is positioned on the eastern edge of its topographic floodplain, adjacent to the Hansen Ranch (its namesake, stop B7). The Rio Grande and Hansen Bluff diverge from each other north of the bluff's midpoint where the trend of the river flow changes from south to southwest. The bluff's expression is subtle where it begins in the north, with a height of 1 m. The bluff's height increases with distance southward. Along the Rio Grande floodplain it reaches a height of 20 m (Siebenthal, 1910; McCalpin, 1996). At stop B7, the type section of the Alamosa Formation, Machette discusses the sediments exposed in Hansen Bluff (chapter B, this volume).

The origin of the bluff has long been a curiosity. Along the Rio Grande floodplain to the south, the scarp appears to be the result of lateral river erosion, but if so, why do the bluff and river diverge? Explanations include speculation about the Rio Grande approaching from a more northern position as well as the bluff being controlled by an underlying fault.

Interpretation of aerial photography suggests that the northern part of the bluff is a stream-cut escarpment, albeit low (fig. A8–2). The feature is sinuous, suggesting river loops and oxbow meanders. The northernmost extent begins near the point where a water-filled closed basin would overflow. The overflow point was determined by examining ponding in the small playas of the area. Adjacent to the bluff are dry stream channels, and the crescentic shape of the bluff mimics the oxbow pattern of the streambed, indicating lateral stream erosion. This pattern can be seen along the entire length of the bluff but is pronounced north of Highway 160. The extent of lateral stream erosion determines where valley margins are but, in this case, the area to the west of the overflow is essentially flat. Therefore, it lacks the sloping piedmont that would lead to formation of stream-cut escarpments. East of the overflow, the land gently slopes upward in a broad piedmont to the Sangre de Cristo Mountains and scarps can form in response to lateral erosion. Hansen Bluff appears, therefore, to be the eastern margin of an asymmetrical stream valley. The northern portion would have been cut by overflow from the closed basin and the southern portion by the Rio Grande. The height of the bluff increases southward as the overflow stream adjusts to the lower base level of the Rio Grande.

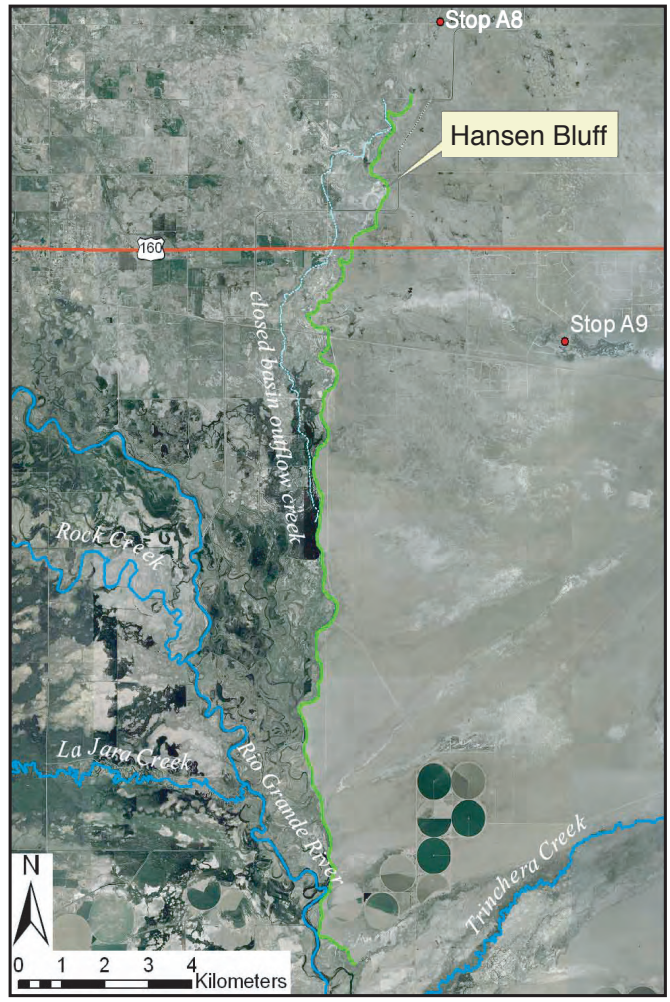

Figure A8–1. Hansen Bluff, the Rio Grande, and its tributary streams.

Historic accounts show that the closed basin did overflow during the 1920s. Water to fill the closed basin comes from the numerous streams that currently flow into it, including Saguache Creek, San Luis Creek, and Sand Creek. Most of this stream water is now diverted for agricultural use, so the closed basin can fill only during extremely large-discharge years (when supply exceeds agricultural use). Precipitation values reconstructed from tree-ring data (fig. A8–3) indicate that the 10-year (decadal) precipitation average has been cyclic during the last millennium. During wet periods, such as the first half of the 13th Century, the closed basin may have been filled frequently. Interpretation of aerial photography also suggests during extreme precipitation years, water from the Rio Grande fan system can enter the closed basin (R.F. Madole, oral commun., 2006).

Aeromagnetic data suggests possible subsurface faulting beneath the south end of Hansen Bluff, perhaps related to the Alamosa horst (V.J.S Grauch, written commun., 2007) or northern extension of Lasauses fault (Burroughs, 1972; Rogers, 1984), so the possibility exists for some structural influence on the bluff as well. However, the bluff has the sinuous shape associated with fluvial systems rather than that of a scarp formed by a normal fault (see also stop B7, chapter B, this volume).

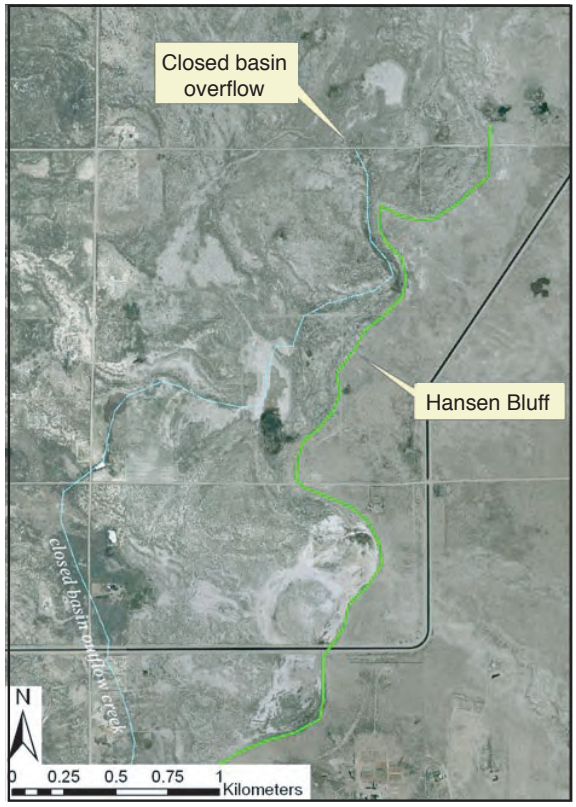

Figure A8–2. Hansen Bluff and the closed-basin overflow channel.

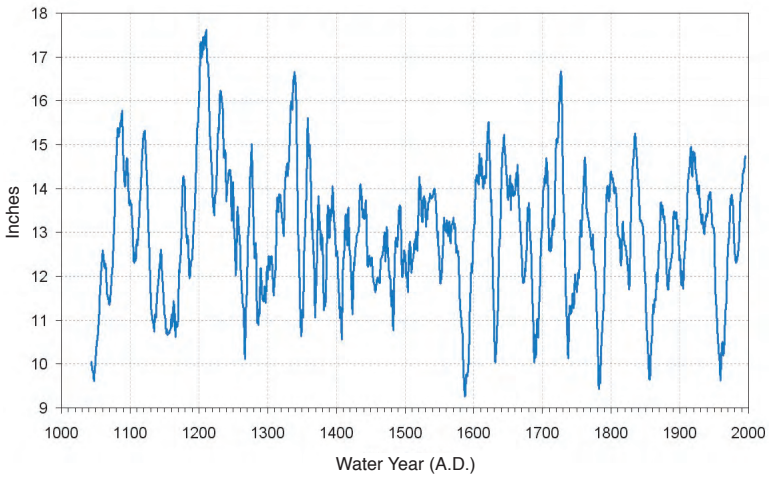

Figure A8–3. Decadal precipitation records for the Great Sand Dunes as interpreted from tree-ring data (modified from Grissino-Mayer and others, 1997).

Stop A9 (Optional) — Middle and Late Holocene Eolian Sand Dunes

Author: Michael Machette
Location: Baca Lane pit (informal name, private property)
Southeast corner of County Road 6S and Road S116 (Baca Lane), about 6 mi east of Alamosa, Colo.
Baldy 7.5' quadrangle (Sta. BA–MM04–25)
GPS: NAD27, Zone 13, 433910 m E., 4148955 m N.
Elevation: 7,525 ft (at gated entrance to pit)

Synopsis

This optional stop is at a restricted site (private property, trespassing not allowed) where a borrow pit was excavated into a stratified eolian sand dune. As part of his reconnaissance mapping of the Alamosa area in the summer of 2005, Machette made a quick description of the sand sequence, sampled organic materials and charcoal from buried soils that mark depositional hiatuses in the sequence of sands, and noted artifacts associated with a hearth site. Three samples of charcoal separated from the buried soils date from about 2800 to 5560 cal yr. This interval is a longer time sequence than normally exposed or seen in the basin or at Great Sand Dunes to the north (see stops A2 and A4, this chapter). The dating and stratigraphy of middle to late Holocene eolian sands exposed in the Baca pit are discussed more completely in chapter E of this volume.

Discussion

This stop is one of the few places in the Alamosa area where we can see a sequence of stratified Holocene eolian sand deposits separated by well-formed, organic-rich soils (buried A horizons). Unfortunately, this site is on private property that is posted as NO TRESPASSING, so please respect the landowner's rights. This area, and in particular the southeast corner of County Road 6S and Road S116 (Baca Lane), is characterized by largely stabilized sand dunes and interspersed blowouts that expose playa-like, organic-rich sediment. The site was discovered during the course of geologic mapping of the north-central part of the Alamosa sheet (M.N. Machette and Ren Thompson, unpub. mapping, 2007). Figure A9–1, which shows the surficial geology around field trip stop A9, has been modified from Machette and Thompson's (2005) 1:50,000-scale map.

In the summer of 2005 Machette made a quick description of the sand sequence, photographed the site (fig. A9–2),

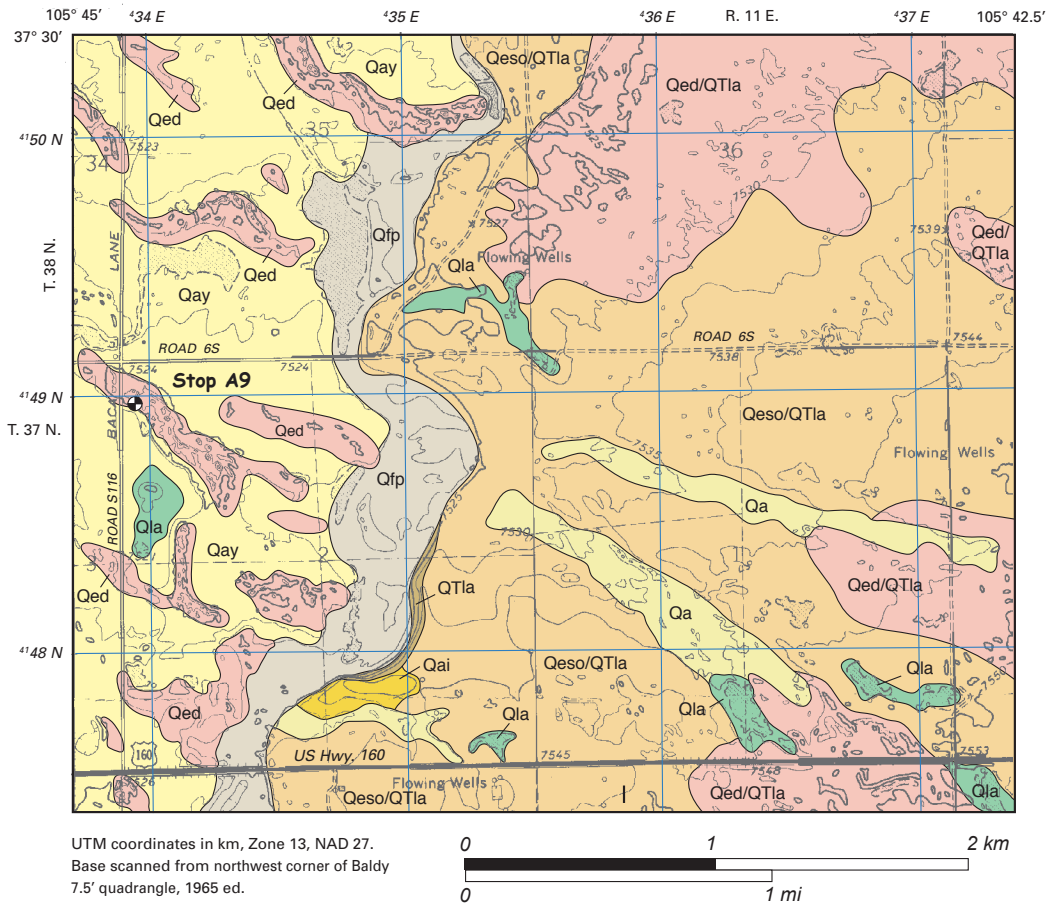

Figure A9–1. Eolian, alluvial, and lacustrine deposits at and east of stop A9. Map units: Qed, eolian dune sand; Qeso, older eolian sand; Qfp, floodplain alluvium; Qa, Holocene alluvium; Qla, Holocene lake and playa deposits; Qay, young (latest Pleistocene) alluvium; Qai, intermediate (middle Pleistocene) alluvium; QTla, Alamosa Formation. Geology simplified from M.N. Machette and Ren Thompson, unpub. mapping, 2007.

sampled organic materials and charcoal from buried soils, and noted artifacts associated with a hearth site. Flotation of bulk samples from the Baca Lane pit (site BA–MM04–25) resulted in recovery of charcoal and other charred plant remains for radiocarbon dating. Rabbitbrush charcoal in samples R2 and R4, saltbush charcoal in sample R2, greasewood charcoal in samples R2 and R4, and Chenopodiaceae charcoal in samples R1, R2, and R4 all were present in sufficient quantities for accelerator mass spectrometry radiocarbon analysis. Only sample R3 yielded insufficient charcoal or other charred organics for dating. A more complete discussion of this site is included in chapter E of this volume.

Three samples of charcoal separated from the buried soils that mark depositional hiatuses in the sequence of sands gave radiocarbon ages at about 2800 cal yr, 3900 cal yr, and 5560 cal yr (table A9–1), which is a much longer sequence than is normally exposed or seen in the basin. Animal and plant remains in these samples reveal paleo-vegetation that is similar to that of the present, as well as evidence of human occupation in the period between about 2.8 ka and 3.9 ka.

Paleoenvironments During the Late and Middle Holocene

Climatic and environmental conditions at the Baca Lane site appear to have fluctuated from moist to dry at least four times (that is, four eolian sand units with intercalated soils) during the past 6,000 years. During moister conditions, the sand was stable and soil organic matter accumulated at or near the surface of the dunes. Without OSL dating of the eolian sand, we cannot estimate how long it took each sand unit to accumulate (intervals of instability and sand transport) or the duration of soil formation (intervals of stability and no, or minimal, sand transport). Nevertheless, it appears that, on average, these sand dunes undergo periodic stabilization every 1–2 k.y.

The recovered charcoal types represent local shrubs that were processes as food sources by the prehistoric occupants of the site. Charred seeds of *Chenopodium* (goosefoot), *Portulaca* (purslane), *Sporobolus* (dropseed), and *Oxalis* (wood sorrel) were found in the samples that were processed. Samples R1 through R4 span 2.8 ka to about 5.56 ka, which equates to late and middle Holocene time. During these times, early man appears to have been occupying this area during the late summer or fall seasons when these seed resources are available for harvesting. Charred bone fragments recovered from all four samples most likely reflect processing of meat and fish (sample R1).

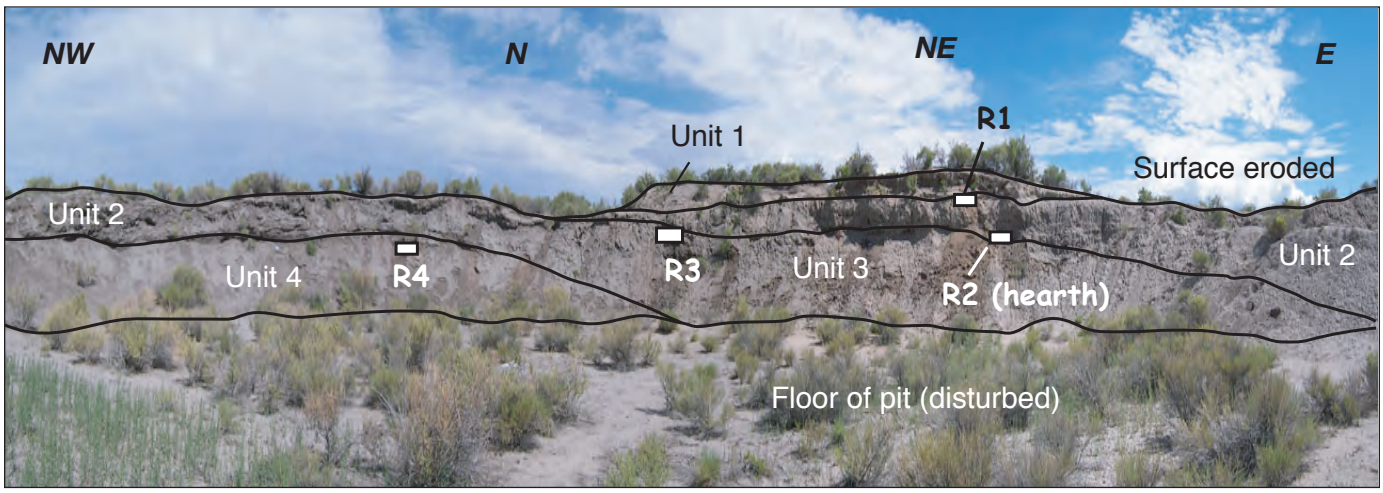

Figure A9–2. Stratigraphic units and soils exposed in the Baca Lane pit (sand borrow pit). Sampled soils are shown as R1 to R4 from eolian sand units 2, 3, and 4. View is to the northwest (on left) sweeping to the east (on right). The total vertical exposure in the pit is about 4 m. Image has 1.5x vertical exaggeration.

Table A9–1. Radiocarbon age determinations from charcoal samples at stop A9.

[Reported radiocarbon ages have 1-sigma errors; calendar-corrected ages have two 2-sigma errors. The radiocarbon ages were calendar corrected using the radiocarbon calibration program (CALIB REV. 5.0.1 of Stuiver and others, 2005; see also Stuvier and Reimer, 1993)]

USGS sample number (position)	Type and weight of charcoal	NOSAMS accession number	$\delta^{13}C$	Radiocarbon ages and errors (^{14}C yr B.P.)	Calendar ages and errors (years)
BA–MM04–25R1 (Soil on unit 2)	Artiplex (Saltbush), 0.025 g	OS–52749	–23.38	2700±35	2804±54
BA–MM04–25R2 (Hearth at base of unit 2, on unit 3)	Artiplex (Saltbush), 0.038 g	OS–52750	–11.21	3590±55	3905±98
BA–MM04–25R4 (Soil on unit 4)	Unidentified hardwood, 0.015g	OS–52751	–25.62	4820±45	5560±90

Stop A10 — Late Pleistocene to early Holocene wetland deposits in the Mr. Peat pit

Speakers: Michael Machette and Randy Schumann
Location: North edge of Mr. Peat pit, which extends about 2 mi east-west along an unnamed drainage.
Location is about 2 mi south of U.S. Highway 160 and about 10 mi east of Alamosa, Colo.
Baldy 7.5' quadrangle (Stations BA–MM05–73 and –74, BA–MM06–76)
GPS: NAD27, Zone 13, 440123 m E., 4145465 m N.
Elevation: 7,590 ft (at north edge of pit on section–line fence)

Synopsis

This stop provides an opportunity to see peat-rich wetland deposits related to paleospring waters that flowed down a now-abandoned late Pleistocene glacial-meltwater stream channel. The peat deposits have been commercially mined from what is known as the “Mr. Peat” pit by RMMP (Alamosa, Colo.) since about 1950. In the summer of 2006, we excavated four pits in these deposits to understand better the timing and duration of peat accumulation, facies of the peats, the age of underlying fossil-bearing alluvial deposits, and the age and origin of overlying tufa deposits. Radiocarbon dating of the peats show that most of the wetland deposits accumulated from 13.5 ka to about 11.6 ka and that deposition continued until middle Holocene time (4.3–6.7 ka), whereas locally overlying tufaceous spring deposits started to accumulate about 6.7 ka and that accumulation continued until about 3.9 ka. The peats lie in a late-glacial-age paleovalley that is underlain by well-bedded sand and sandy fluvial gravel. An organic seam in the alluvium about 1.4 m below the peat yielded an age of 14.4 ka, whereas OSL dating of the alluvium yielded a variety of stratigraphically consistent and inconsistent ages (6.5–34.3 ka) for sands below the peats. The dating, stratigraphy, and paleoecology of the Mr. Peat pit are discussed more completely in chapter F of this volume.

Discussion

This stop focuses on a spectacular, abandoned stream valley where we can see a sequence of stratified peats and overlying tufaceous spring deposits. A second smaller valley is located about 1 km to the northeast, and shallow peat deposits can be seen where the valley crosses U.S. Highway 160 (see fig. A10–1). In the fall of 2005, Machette found these peat-filled valleys during mapping of the surficial geology of the north-central part of the Alamosa sheet (M.N. Machette and Ren Thompson, unpub. mapping, 2007). Figure A10–1, which shows the surficial geology around field trip stop A10, has been modified from the previously cited 1:50,000-scale map.

Local Geology

The Mr. Peat pit is located south of U.S. Highway 160, which is the main highway across the San Luis valley. It connects Fort Garland on the east to Alamosa at the Rio Grande, and Monte Vista and Del Norte on the west. The pit is about 1.3 mi (2 km) south of the highway, in a west-trending, slightly entrenched stream valley (unnamed). The peats, which have been extensively mined, extend about a 1.5 km to the east and west of this stop (figs. A10–2 and A10–3). The stream valley is incised into gently west-sloping piedmont covered by eolian dune and cover sands (Holocene to upper Pleistocene). The piedmont is largely a relict basin floor of ancient Lake Alamosa (chapter G, this volume) of middle Pleistocene age.

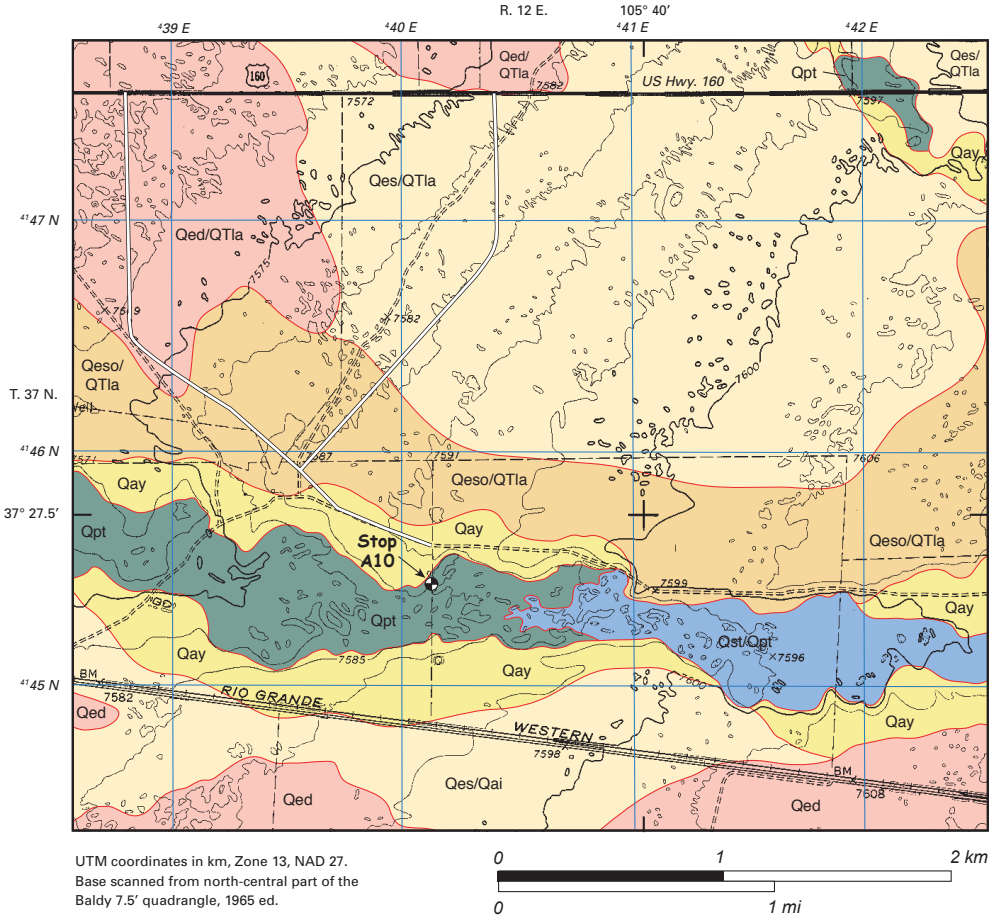

Figure A10–1. Paleospring deposits in unnamed valley east of Alamosa, Colo. Map units: Qed, eolian dune sand; Qes, eolian sand; Qeso, older eolian sand; Qpt, peat deposits; Qts, tufa from springs; Qay, young (latest Pleistocene) alluvium; Qai, intermediate (middle Pleistocene) alluvium; QTla, Alamosa Formation. Geology simplified from Machette and Thompson, unpub. mapping, 2007. Extensive subdivision roads (only two are shown) north of stop A10 were built after topographic base map was constructed.

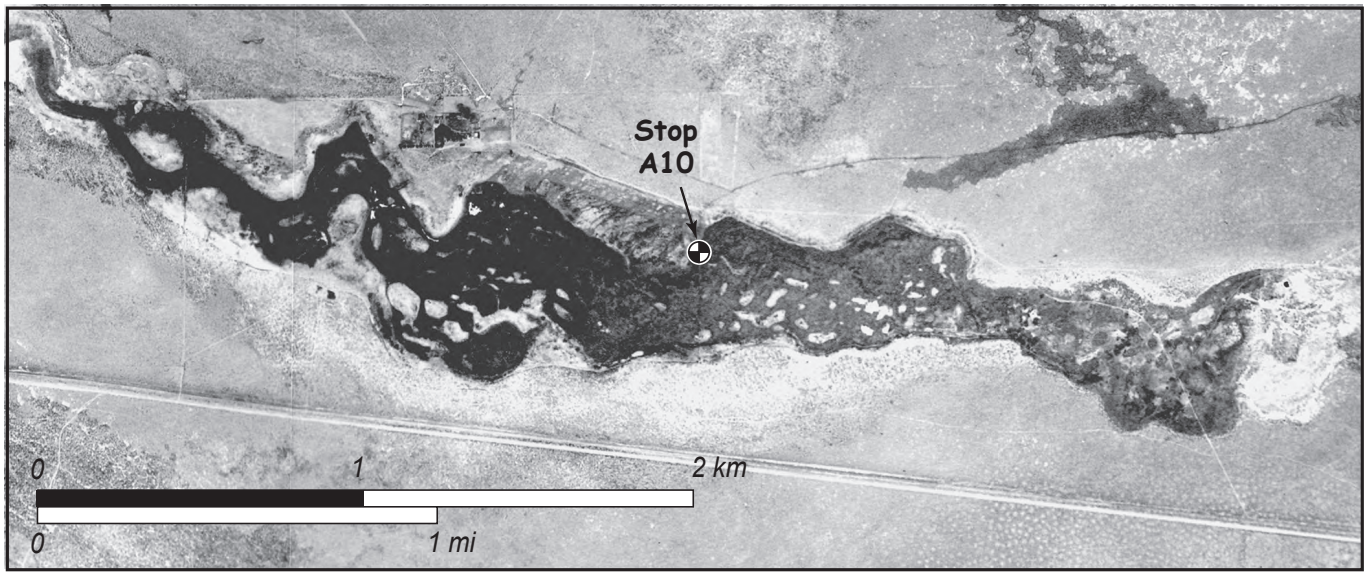

Figure A10–2. Area around the Mr. Peat pit, stop A10. This vintage aerial photograph taken in 1938 by the Soil Conservation Service, well before the peat was mined.

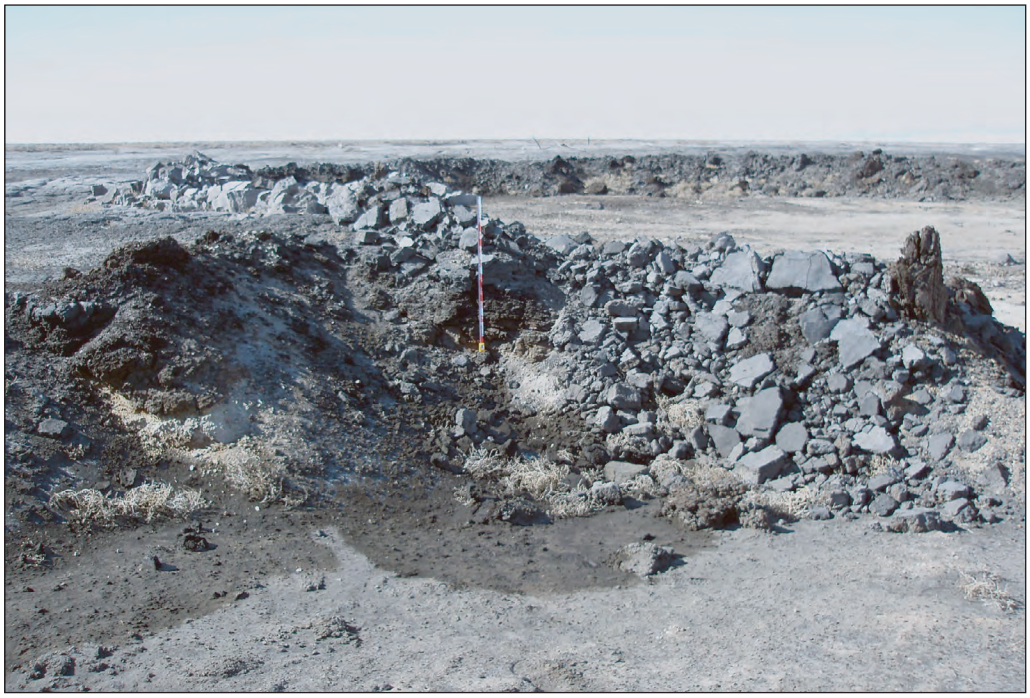

Figure A10–3. Actively mined peat in the Mr. Peat pit, stop A10. Photograph taken in October, 2006. Stadia rod (1.8 m long) for scale.

Shallow lacustrine and interbedded fluvial sediment under the piedmont are part of the uppermost part of the Alamosa Formation (middle Pleistocene to Pliocene). The Alamosa Formation is considered to be time equivalent to the upper part of the Santa Fe Group (middle Pleistocene to Pliocene, Machette and Thompson, unpub. mapping, 2007).

Mr. Peat Pit

In the summer of 2006, we excavated four pits in these deposits to understand better the timing and duration of peat accumulation, facies of the peats, the age of underlying fossil-bearing alluvial deposits and the age and origin of overlying tufa deposits. Fifteen radiocarbon samples were collected from the Mr. Peat pit: two from natural exposures and the remainder from the four trenches we excavated. The woody peats contained whole, fresh fragments of plant material, which were hand picked after ultrasonic cleaning in distilled water. The remaining samples were separated by Kathy Puseman of Paleo Research, Inc. (see also chapter F, this volume). Snails were found in the tufa samples, whereas organic matter or charcoal was concentrated from the remaining samples of organic silt and mucky peat (see table A10–1). All of the concentrated materials (either organic or inorganic) were sent to the radiocarbon laboratory at Woods Hole Oceanographic Institute (WHOI) for accelerator mass spectrometry radiocarbon dating. In addition, four samples of sand that did not contain datable organic matter were collected for OSL dating.

Stratigraphy

From our 2005 reconnaissance, it appeared that the stratigraphy of the Mr. Peat pit consisted of basal fluvial deposits, peats, and tufa mounds (upward in section). This basic stratigraphy was confirmed in four trenches and scattered fresh exposures in and adjacent to the pit, as shown in figure A10–4. The lower fluvial section is based on trench 3, which is shown in more detail in the accompanying paper (chapter F) in this volume, whereas the peat section is based on a composite of trenches 1 and 2.

The peat has three main facies: (1) a mucky (nondescript) black peat with scattered plant fragments, (2) a brown, woody peat that is composed almost entirely of fresh-appearing wood and plant fragments, and (3) a light to medium gray, porous (low density) organic silt. The mucky peat is commonly the basal facies and the dry peat is commonly the uppermost facies, although not all three facies are always present or preserved in the pit.

In the eastern part of the valley, the peats are locally overlain by tufa deposits. At the site of our first trench, the tufas are concentrated in round, domed mounds that are >25 cm to as much as 1 m thick (figs. F–7 and F–8, chapter F, this volume). Downstream, the tufas become less continuous and thinner, pinching out by the location of this field trip stop. Capping the entire section is a mantle of locally derived eolian sand that is composed of quartz and feldspar sands and of reworked fragments (typically granule size) of tufa and peat. A sample of these sands (MRP–DL1) was dated at about 1.6 ka by OSL techniques (see fig. F–4, chapter F in this volume).

Table A10–1. Radiocarbon ages from samples collected at Mr. Peat pit.

[Samples arranged in descending stratigraphic order (see fig. A10-3). Reported radiocarbon ages have one 1-sigma errors; calendar-corrected ages have two 2-sigma errors. The radiocarbon ages were calendar corrected using the radiocarbon calibration program (CALIB REV. 5.0.1 of Stuiver and others, 2005; see also Stuvier and Reimer, 1993). A more complete listing of laboratory parameters is included in table F–1 of chapter F, this volume]

USGS sample number	Material dated	Depth in section (cm)	NOSAMS accession number	Radiocarbon ages and errors (^{14}C yr B.P.)	Calendar ages used for discussion (ka)
BA–MM05–74	Snail shell in tufa	Grab sample	OS–53176	3580±30	3.9
MRP–A6	Snail shell in tufa	53–60	OS–57406	5880±45	6.7
MRP–B4	Dry peat	80–85	OS–57942	3850±85	4.3
BA–MM05–73	Dry peat	85–90	OS–53707	5880±50	6.7
MRP–A4	Woody peat	100–105	OS–56477	9960±40	11.3
MRP–B2	Woody peat	100–105	OS–56641	10150±55	11.8
MRP–A3	Woody peat	115–120	OS–56395	10250±55	12.0
MRP–A2(2)	Moss in organic silt	20–25	OS–57712	9930±60	11.3
MRP–A2(1)	Stems and roots in organic silt	80–85	OS–57672	10550±40	12.5
MRP–B1	Mucky peat	125–130	OS–57499	11350±45	13.2
MRP–A1	Mucky peat	155–160	OS–57714	11600±65	13.4
MRP–C1	Stems and roots in alluvium	Grab sample	OS–57740	12350±60	14.3

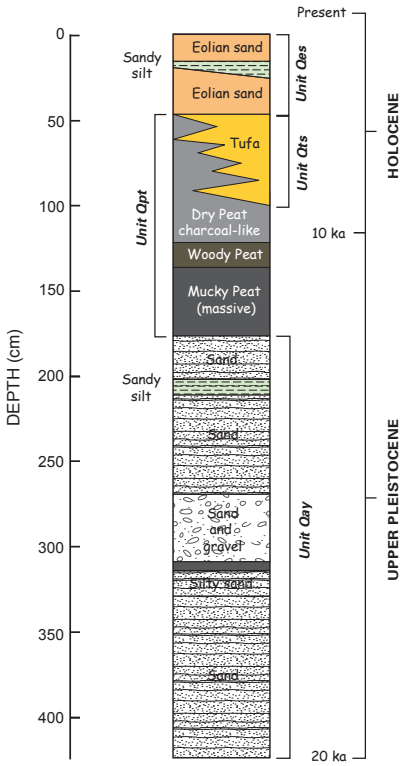

Figure A10–4. Composite stratigraphic section at the Mr. Peat pit, field-trip stop A10. Section described and sampled by Michael Machette, Randall Schumann, and Shannon Mahan, July 5–7, 2006.

Radiocarbon and OSL dating

Twelve radiocarbon samples and four OSL samples were processed for dating. The radiocarbon ages (see Table A10–1) were run at Woods Hole Oceanographic Institute National Ocean Sciences Accelerator Mass Spectrometry Facility (WHOI-NOSAMS) (http://nosams.whoi.edu/index.html), whereas the OSL ages were determined by Shannon A. Mahan (USGS). (See chapter F of this volume for a more complete discussion of sample preparation and dating results.)

In general, the radiocarbon ages are in proper stratigraphic order; the oldest ages come from the basal mucky peat and the youngest ages come from the organic silt and coeval tufa deposits. Most of the peat deposits accumulated from 13.5 ka to about 11.6 ka although deposition continued until middle Holocene time (4.3–6.7 ka), whereas locally overlying tufaceous spring deposits started to accumulate at about 6.7 ka and deposition continued until about 3.9 ka. The underlying sand and sandy fluvial gravel contained an organic seam located about 1.4 m below the peat that yielded an age of 14.3 ka, whereas IRSL and OSL dating of the alluvium yielded ages as young as 6.45 ka as old as 34.3 ka (see chapter F (this volume) for a more complete discussion of the luminescence dating).

Paleoenvironments During the Late Pleistocene to Middle Holocene

On the basis of these dating studies, we suggest that during the late Pleistocene, glacial-fed streams flowing west into the Rio Grande entrenched and backfilled valleys. By 15–20 ka, these stream channels had aggraded to within 5–10 m of the piedmont slope that they flowed across. High water tables on the piedmont intersected the paleostream valley and probably caused persistent spring discharge that might have been localized by faults in the underlying Alamosa Formation (see discussion in chapter F, this volume). Marsh-like or cienega wetland conditions in the valley caused slow accumulation of peats, but as ground-water levels fell, deposition shifted to charcoal-like dry peats and tufa.

References Cited

Aitken, M.J., 1998, An introduction to optical dating—The dating of Quaternary sediments by the use of photon-stimulated luminescence: New York, Oxford University Press, 280 p.

Alexander, B., 1979, Geology of Great Sand Dunes—A preliminary review of the literature: Unpublished National Park Service report, Great Sand Dunes National Park and Preserve library, 58 p.

Andrews, S., 1981, Sedimentology of Great Sand Dunes, Colorado, *in* Ethridge, F.G., and Flores, R.M., eds., Recent and ancient nonmarine depositional environments—Models for exploration: Tulsa, Oklahoma, Society of Economic Paleontologists and Mineralogists Special Publication 31, p. 279–291.

Bailey, S.D., Wintle, A.G., Duller, G.A.T., and Bristow, C.S., 2001, Sand deposition during the last millennium at Aberffraw, Anglesey, North Wales as determined by OSL dating of quartz: Quaternary Science Reviews, v. 20, p. 701–704.

Ballarini, M., Wallinga, J., Murray, A., van Heteren, S., Oost, A.P., Bos, A. J.J., and van Eijk, C. W.E., 2003, Optical dating of young coastal dunes on a decadal time scale: Quaternary Science Reviews, v. 22, p. 1011–1017.

Bøtter-Jensen, L., Bulur, E., Duller, G.A.T., and Murray, A.S., 2000, Advances in luminescence instrument systems: Radiation Measurements, v. 32, p. 523–528.

Brady, N.C., 1974, The nature and properties of soils, 8th ed.: New York, Macmillan Publishing, 639 p.

Brister, B.S., and Gries, R.R., 1994, Tertiary Stratigraphy and tectonic development of the Alamosa Basin (northern San Luis Basin), Rio Grande rift, south-central Colorado, *in* Keller, G.R., and Cather, S.M., eds., Basins of the Rio Grande rift—Structure, stratigraphy, and tectonic setting: Geological Society of America Special Paper 291, p. 39–58.

Bruce, R.M., and Johnson, B.R., 1991, Reconnaissance geologic map of parts of the Zapata Ranch and Mosca Pass quadrangles, Alamosa and Huerfano Counties, Colorado: U.S. Geological Survey Miscellaneous Field Studies Map MF–2168, scale 1:24,000.

Burroughs, R.L., 1972, Geology of the San Luis Hills, south-central Colorado: Albuquerque, University of New Mexico, Ph.D. dissertation, 139 p.

Carson, M.A., and MacLean, P.A., 1986, Development of hybrid dunes—The William River dunefield, northwest Saskatchewan, Canada: Canadian Journal of Earth Sciences, v. 23, p. 1974–1990.

Chen, J.S., Li, L., Wang, J.Y., Barry, D.A., Sheng, X.F., Gu, W.Z., Zhao, X., and Chen, L., 2004, Groundwater maintains dune landscape: Nature, v. 432, p. 459–460.

Cook, E.R., Krusic, P.J., and Woodhouse, C.A., 2003, North American drought atlas: Intergovernmental Panel on Climate Change Workshop on Droughts, Nov. 2003, v. 1–3 (http://www.ngdc.noaa.gov/paleo/newpsdi.html).

Fain, J., Soumana, S., Montret, M., Miallier, D., Pilleyre, T., and Sanzelle, S., 1999, Luminescence and ESR dating—Beta-dose attenuation for various grain shapes calculated by a Monte-Carlo method: Quaternary Science Reviews, v. 18, p. 231-234.

Fish, S.K., and Fish, P.R., 1994, Prehistoric desert farmers of the Southwest: Annual Review of Anthropology, v. 23, p. 83–108.

Forman, S.L., Goetz, A.F.H., and Yuhas, R.H., 1992, Large scale stabilized dunes on the High Plains of Colorado—Understanding the landscape response to Holocene climates with the aid of images from space: Geology, v. 20, p. 145–148.

Forman, S.L., Marín, L., Pierson, J., Gómez, J., Miller, G.H., and Webb, R.S., 2005, Aeolian sand depositional records from western Nebraska—Landscape response to droughts in the past 1500 years: The Holocene, v. 15, no. 7, p. 973–981.

Forman, S.L., Oglesby, R., Markgraf, V., and Stafford, T., 1995, Paleoclimatic significance of late Quaternary eolian deposition on the Piedmont and High Plains, central United States: Global and Planetary Change, v. 11, p. 35–55.

Forman, S.L., Oglesby, R., and Webb, R.S., 2001, Temporal and spatial patterns of Holocene dune activity on the Great Plains of North America—Megadroughts and climate links: Global and Planetary Change, v. 29, p. 1–29.

Forman, S.L., and Pierson, J., 2003, Formation of linear and parabolic dunes on the eastern Snake River Plain, Idaho, in the nineteenth century: Geomorphology, v. 56, p. 189–200.

Forman, S.L., Spaeth, M., Marín, L., Pierson, J., and Gómez, J., 2006, Episodic late Holocene dune movements on the sand sheet area, Great Sand Dunes National Park and Preserve, San Luis Valley, Colorado: Quaternary Research, v. 66, p. 97–108.

Fryberger, S.G., 1990a, Depositional Models for Modern Eolian Sand Seas (Chap. 6) *in* Fryberger, S.G., Krystinik, L.F., and Schenk, C.J., eds., Modern and ancient eolian deposits—Petroleum exploration and production: Denver, Rocky Mountain Section Society of Economic Paleontologists and Mineralogists, p. 6–5

Fryberger, S.G., 1990b, Great Sand Dunes depositional system—An overview (Chap. 1), *in* Modern and ancient eolian deposits—Petroleum exploration and production: Denver, Rocky Mountain Section Society of Economic Paleontologists and Mineralogists, p. 1–3.

Fryberger, S.G., 1999, Overview of the eolian depositional system, Great Sand Dunes National Monument and vicinity, *in* Schenk, C.J., ed., Hydrologic, geologic and biologic research at Great Sand Dunes National Monument, Colorado: National Park Service Research Symposium 1, Denver, Colorado, Proceedings, p. 195–214.

Fryberger, S.G., and Dean, G., 1979, Dune forms and wind regime, *in* McKee, E.D., ed., A study of global sand seas: U.S. Geological Survey Professional Paper 1052, p. 137–169.

Fye, F.K., Stahle, D.W., and Cook, E.R., 2003, Paleoclimatic analogs to twentieth-century moisture regimes across the United States: Bulletin of the American Meteorological Society, v. 84, p. 901–915.

Gaylord, D.R., 1989, Holocene paleoclimatic fluctuations revealed from dune and interdune strata in Wyoming: Journal of Arid Environments, v. 18, p. 123–138.

Goble, R.J., Mason, J.A., Loope, D.B., Swinehart, J.B., and Loope, D.B., 2004, Optical and radiocarbon ages of stacked paleosols and dune sands in the Nebraska Sand Hills, USA: Quaternary Science Reviews, v. 23, p. 1173–1182.

Greeley, R., and Iversen, J.D., 1987, Wind as a geological process on Earth, Mars, Venus and Titan: New York, Cambridge University Press, 333 p.

Grissino-Mayer, H.D., Baisan, C.H., Swetnam, C.W., 1998, A multicentury reconstruction of precipitation for Great Sand Dunes National Monument, southwestern Colorado: Final report submitted to Mid-continent Ecological Science Center for the National Park Service.

Hammond, D.J., 1998, Measuring changes in areal extent of historic wetlands at Great Sand Dunes National Monument, Colorado 1936–1995: Fort Collins, Colorado State University, M.S. thesis, 56 p.

Huenneke, L.F., Anderson, J.P., Remmenga, M., and Schlesinger, W.H., 2002, Desertification alters patterns of above ground net primary production in Chihuahuan ecosystems: Global Change Biology, v. 8, p. 247–264.

Jodry, M.A., 1987, Stewart's Cattle Guard site—A Folsom site in southern Colorado—A report on the 1981 and 1983 field seasons: Austin, University of Texas Department of Anthropology, unpublished M.A. thesis.

Jodry, M.A., and Stanford, D.J., 1992 Stewart's Cattle Guard site—An analysis of Bison remains in a Folsom kill–butchery campsite, *in* Stanford, D.J., and Day, J.S., eds., Ice age hunters of the Rockies: Niwot, University Press of Colorado, p. 101–168.

Jodry, M.A., Shafer, D.S., Stanford, D.J., and Davis, O.K., 1989, Late Quaternary environments and human adaptation in the San Luis valley, south-central Colorado, *in* Harmon, E. J., ed., Water in the valley—A 1989 perspective on water supplies, issues, and solutions in the San Luis Valley, Colorado: Colorado Ground-Water Association Guidebook, 8th annual field trip, p. 189–208.

Johnson, B.R., Bruce, R.M., and Lindsey, D.A., 1989, Reconnaissance geologic map of the Medano Pass quadrangle and part of the Liberty quadrangle, Alamosa, Huerfano, and Saguache Counties, Colorado: U.S. Geological Survey Miscellaneous Field Studies Map MF–2089, scale 1:24,000.

Johnson, R.B., 1967, The Great Sand Dunes of southern Colorado: U. S. Geological Survey Professional Paper 575–C, p. C177–C183.

Krystinik, L.F., 1990, Early diagenesis in continental eolian deposits (Chap. 8), *in* Fryberger, S.G., Krystinik, L.F., and Schenk, C.J., eds., Modern and ancient eolian deposits—Petroleum exploration and production: Denver, Colorado, Rocky Mountain Section Society of Economic Paleontologists and Mineralogists, p. 8–1.

Lancaster, N., 1997, Response of eolian geomorphic systems to minor climate change—Examples from the southern Californian deserts: Geomorphology, v. 19, no. 3–4, p. 333–347.

Lancaster, N., and Tchakerian, V.P., 2003, Late Quaternary eolian dynamics, Mojave Desert, California, *in* Enzel, Y., Wells, S.G., and Lancaster, N., eds., Paleoenvironments and paleohydrology of the Mojave and southern Great Basin deserts: Geological Society of America Special Paper 368, p. 231–249.

Larson, D.O., Neff, H., Graybill, D.A., Michaelsen, J., and Ambos, E., 1996, Risk, climatic variability, and the study of southwestern prehistory—An evolutionary perspective: American Antiquity, v. 61, p. 217–241.

Lekson, S.H., 2001, Casas Grandes and its hinterland—Prehistoric regional organization in northwest Mexico: Journal of Field Archaeology, v. 28, p. 216–222.

Lekson, S.H., 2002, Anasazi America—Seventeen centuries on the road from center place: American Antiquity, v. 67, p. 172–173.

Machette, M.N., and Thompson, R.A., 2005, Preliminary geologic map of the northwestern part of the Alamosa ½° x 1° quadrangle, Alamosa and Conejos Counties, Colorado: U.S. Geological Survey Open-File Report 2005–1392, 1 sheet, 1:50,000 scale.

Madole, R.F., 1994, Stratigraphic evidence of desertification in the west-central Great Plains within the past 1000 yr: Geology, v. 22, p. 483–486.

Madole, R.F., 1995, Spatial and temporal patterns of Late Quaternary eolian deposition, eastern Colorado, U. S. A.: Quaternary Science Reviews, v. 14, p. 155–178.

Madole, R.F., and Romig, J.H., 2002, The Great Sand Dunes (GSD) of south-central Colorado—Origin and implications [abs.]: Geological Society of America Abstracts with Programs, v. 34, no. 6, p. 275.

Mapmart, 2004: http://*www.mapmart.com* (last accessed in 2005)

Marín, L., Forman, S. L., Valdez, A., and Bunch, F., 2005, 20th Century dune migration at the Great Sand Dunes National Park and Preserve, Colorado and relation to drought variability: Geomorphology, v. 70, p. 163–183.

Mason, J.A., Swinehart, J.B., Globe, R.J. and Loope, D.B., 2004, Late Holocene dune activity linked to hydrological drought, Nebraska Sand Hills, USA: The Holocene, v. 14, p. 209–217.

McCalpin, J.P., 1982, Quaternary geology and neotectonics of the west flank of the northern Sangre de Cristo Mountains, south-central Colorado: Colorado School of Mines Quarterly, v. 77, no. 3, 97 p.

McCalpin, J.P., 1996, General geology of the northern San Luis Valley, Colorado (in section II, Geology and geohydrology), *in* Thompson, R.A., Hudson, M.R., and Pillmore, C.L., eds., Geologic excursions to the Rocky Mountains and beyond—Field trip guidebook for 1996 Annual Meeting of the Geological Society of America, Denver, Colorado, October 28–31: Colorado Geological Survey Special Publication 44, 11 p. (CD-ROM).

McCalpin, J.P., 2006, Active faults and seismic hazards to infrastructure at Great Sand Dunes National Monument and Preserve: Crestone, Colorado, GEO-HAZ Consulting, Inc., 49 p., 1 oversize plate.

McKee, E.D., 1979, A study of global sand seas: U.S. Geological Survey Professional Paper 1052, 429 p.

Mejdahl, V., and Christiansen, H.H., 1994, Procedures used for luminescence dating of sediments: Boreas, v. 13, p. 403–406.

Morrison, R.B., ed., 1991, Quaternary nonglacial geology—Conterminous U.S.: Boulder, Colorado, Geological Society of America, The Geology of North America, v. K–2, 672 p.

Muhs, D.R., Stafford, T.W., Beann, J., Mahan, S.A., Burdett, J., Skipp, G., and Rowland, Z.M., 1997, Holocene eolian activity in the Minot dune field, North Dakota: Canadian Journal of Earth Sciences, v. 34, p. 1442–1459.

Muhs, D.R., Stafford, T.W., Cowherd, S.D., Mahan, S.A., Kihl, R., Maat, P.B., Bush, C.A., and Nehring, J., 1996, Origin of the late Quaternary dune fields of northeastern Colorado: Geomorphology, v. 17, p. 129–149.

Muhs, D.R., Stafford, T.W., Swinehart, J.B., Cowherd, S.D., Mahan, S.A., Bush, C.A. Madole, R.F. and Maat, P.B., 1997, Late Holocene eolian activity in the mineralogically mature Nebraska Sand Hills: Quaternary Research, v. 48, no. 2, p. 162–176.

Murray, A.S., and Wintle, A.G., 2000, Quartz OSL—Effects of thermal treatment and their relevance to laboratory dating procedures: Radiation Measurements, v. 32, p. 387–400.

Murray, A.S., and Wintle, A.G., 2003, The single aliquot regenerative dose protocol—Potential for improvements in reliability: Radiation Measurements, v. 37, p. 377–381.

National Climatic Data Center, 1950–2002: U.S. Department of Commerce, NOAA Satellite and Information Service. http;//www.ncdc.noaa.gov/oa/ncdc.html.

Nelson, M.C., and Schachner, G., 2002, Understanding abandonments in the North American Southwest: Journal of Archaeological Research, v. 10, p. 167–206.

Overpeck, J.T., 1996, Warm climate surprises: Science, v. 271, p. 1820–1821.

Prescott, J.R., and Hutton, J.T., 1994, Cosmic-ray contributions to dose rates for luminescence and ESR dating—Large depths and long-term time variations: Radiation Measurements, v. 23, p. 497–500.

Rogers, K.L., 1984, A paleontologic analysis of the Alamosa Formation (south-central Colorado; Pleistocene, Irvingtonian), *in* Baldridge, W.S., Dickerson, P.W., Riecher, E., and Zidek, J., eds., Rio Grande rift—Northern New Mexico: New Mexico Geological Society 35th Annual Field Conference, Guidebook, v. 35, p. 151–155.

Sadler, P.M., 2004, Quantitative biostratigraphy—Achieving finer resolution in global correlation: Annual Review of Earth and Planetary Sciences, v. 32, p. 187–213.

Sadler, P.M., and Strauss, D.J., 1990, Estimation of completeness of stratigraphical sections using empirical data and theoretical models: Journal of the Geological Society, v. 147, p. 471–485.

Schlesinger, W.H., Reynolds, J.F., Cunningham, G.L., Huenneke, L.F., Jarrel, W.M., Virginia, R.A., and Whitford, W.G., 1990, Biological feedbacks in global desertification: Science, v. 247, p. 1043–1048.

Shulka, J. and Mintz, Y., 1982, Influence of land-surface evapotranspiration on the Earth's climate: Science, v. 215, p. 1498–1501.

Siebenthal, C.E., 1910, Geology and water resources of the San Luis Valley, Colorado: U.S. Geological Survey Water-Supply Report 240, 128 p.

Stahle, D.W., Cook, E.R., Cleaveland, M.K., Therrell, M.D., Meko, D.M., Grissino-Mayer, H.D., Watson, E., and Luckman, B.H., 2000, Tree-ring data document 16th Century megadrought over North America: EOS, Transactions of the American Geophysical Union, v. 81, p. 121–125.

Stokes, S., Bailey, R.M., Fedoroff, N., and O'Marah, K.E., 2004, Optical dating of aeolian dynamism on the West African Sahelian margin: Geomorphology, v. 59, p. 281–291.

Stokes, S., and Gaylord, D.R., 1993, Optical dating of Holocene dune sands in the Ferris dune field, Wyoming: Quaternary Research, v. 39, p. 274–281.

Stokes, S., and Swinehart, J.B., 1997, Middle- and late-Holocene dune reactivation in the Nebraska Sand Hills, USA: The Holocene, v. 7, p. 263–272.

Stuiver, Minze, and Reimer, P.J., 1993, Extended ^{14}C database and revised CALIB 3.0 ^{14}C age calibration program: Radiocarbon, v. 35, no. 1, p. 215–230.

Stuvier, Minze, Reimer, P.J., and Reimer, Ron, 2005, CALIB Radiocarbon Calibration, v. 5.0.1 [online program], http://radiocarbon.pa.qub.ac.uk/calib/ (last accessed in 2006; to be used in conjunction with Stuiver and Reimer, 1993).

Terraserver, 2004: *http://terraserver.microsoft.com* (last accessed in 2005)

Wells, D.L., and Coppersmith, K.J., 1994, Empirical relationships among magnitude, rupture length, rupture area, and surface displacement: Bulletin of the Seismological Society of America, v. 84, p. 974–1002.

Wells, S.G., McFadden, L.D., and Schulz, J.D., 1990, Eolian landscape evolution and soil formation in the Chaco dune field, southern Colorado Plateau, New Mexico: Geomorphology, v. 3, p. 517–546.

Widmann, B.L., Kirkham, R.M., and Rogers, W.P., 1998, Preliminary Quaternary fault and fold map and database of Colorado: Colorado Geological Survey Open-File Report 98–8, 331 p.

Wiegland, J.P., 1977, Dune morphology and sedimentology at Great Sand Dunes National Monument: Fort Collins, Colorado State University, unpublished M.S. thesis.

Wolfe, S.A., Huntley, D.J., David, P.P., Ollerhead, J., Sauchyn, D.J., and MacDonald, G.M., 2001, Late 18th century drought-induced sand dune activity, Great Sand Hills, Saskatchewan: Canadian Journal of Earth Sciences, v. 38, 105–117.

Wolfe, S.A., Ollerhead, J., and Lian, O.B., 2002, Holocene eolian activity in south-central Saskatchewan and the southern Canadian Prairies: Geographie Physique et Quaternaire, v. 56, p. 215–227.

Woodhouse, C.A., Lukas, J.J., and Brown, P.M., 2002, Drought in the western Great Plains, 1845–56—Impacts and implications: Bulletin of the American Meteorological Society, v. 83, p. 1485–1493.

Woodhouse, C.A. and Overpeck, J.T., 1998, 2000 years of drought variability in the central United States: Bulletin of the American Meteorological Society, v. 79, p. 2693–271.

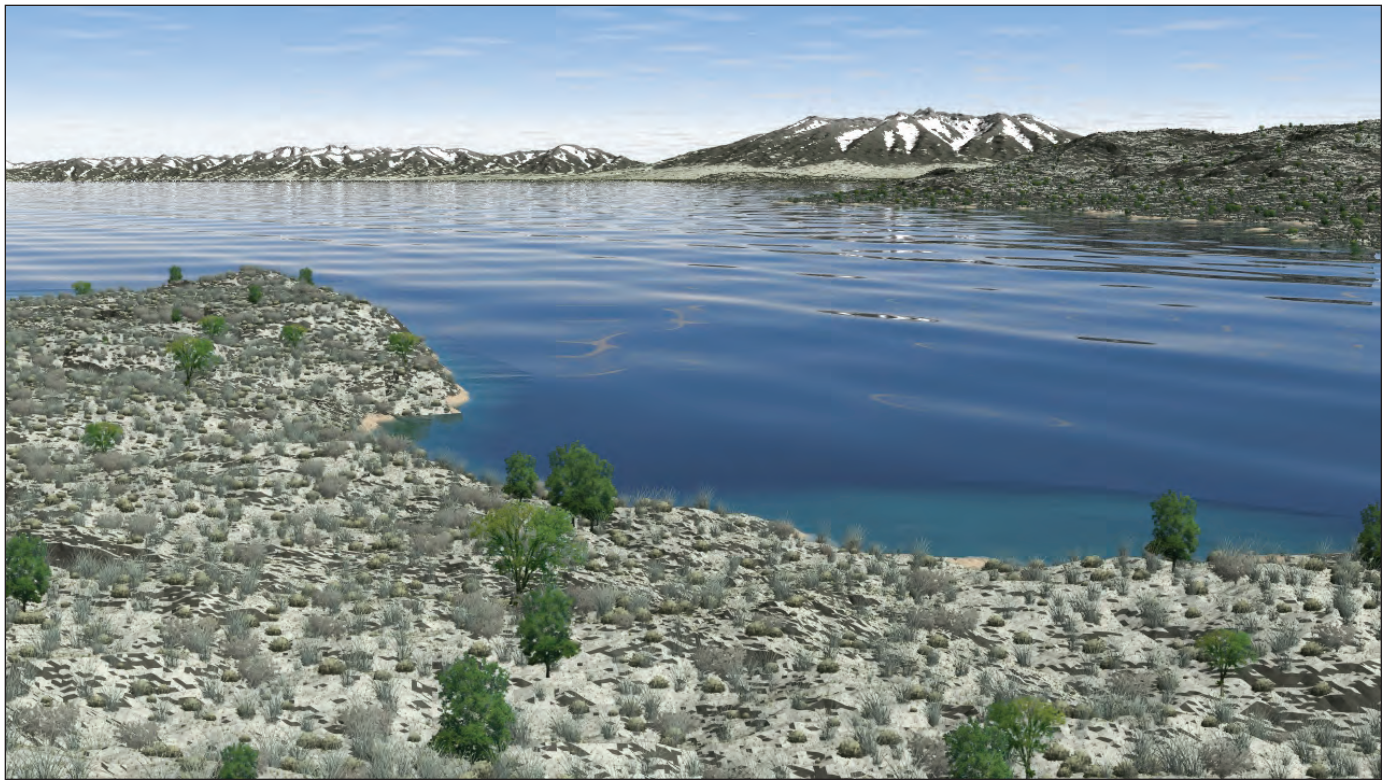

Frontispiece, Chapter B. Re-creation of Lake Alamosa. View to the northeast from the San Luis Hills (see Stop B4). Highest peak in the background is Blanca Peak at 14,345 ft asl. Visualization created in Visual Nature Studio (v. 2.7, 3D Nature Co.) by Paco Van Sistine (USGS) using 30-m DEM and a lake elevation of 7,660 ft (2,335 m).

Chapter B — Field Trip Day 2 Quaternary Geology of Lake Alamosa and the Costilla Plain, Southern Colorado

By Michael Machette, Ren Thompson, David Marchetti, and Robert Kirkham

Orientation for Day 2 — Saturday, Sept. 8, 2007

Speakers: Michael Machette and Ren Thompson
Location: Near center of Bachus pit, Road S106, about 3 mi (5 km) southwest of Alamosa, Colo. (camping location for previous day).
Alamosa West 7.5' quadrangle
GPS: NAD27, Zone 13, 418200 m E., 4144720 m N.
Elevation: 7,560 ft (2,304 m) asl at top of pit

Synopsis

On this day's field trip, we will discuss various aspects of middle Pleistocene to Pliocene Lake Alamosa, including its extent, relict geomorphic features, and age. In addition, we will see the ancient outlet of the lake and review its overflow through the Costilla Plain and into New Mexico (one subject of field-trip day 3). We will visit Mesita Cone, a 1.0-Ma basaltic vent on the Costilla Plain and stop along the base of San Pedro Mesa to discuss landslide and fault hazards along the southern Sangre de Cristo fault zone. In addition, the field-trip log contains information for optional stops B5, B6, and B7.

Introduction

Today's field-trip route is rather long (96 mi, 155 km), starting near Alamosa and ending in northern New Mexico at the Wild and Scenic Rivers Recreation Area. Most of the trip is on paved roads, but we'll be off road for about 10 mi (16 km) going to and from stop B4, which overlooks the Rio Grande. Vehicles with high ground clearance are recommended for at least this part of the trip.

Today's route is divided into three parts, only two of which we'll do on this trip. The morning portion includes stops B1–B4 and the afternoon portion includes a walking tour at stop B8 and an overview at stop B9. An optional leg that uses county gravel roads northeast of our lunch stop (B4) includes three stops (B5–B7) and is recommended for another time. After stop B9, we have a 45-minute drive (27 mi, 43.5 km) south to our campground at La Junta Point (New Mexico), which is the departure point for day 3 (chapter C).

Morning Stops

The first leg for day 2 (fig. B–1) focuses on rarely exposed sediment of Lake Alamosa (stops B1 and B3) and landforms constructed during its last and highest stand (stops B3 and B4). In addition, we'll see post-lake alluvial deposits that lie unconformably on lake sediment and show reversals of topography (stop B2). Relations at these stops are discussed in detail in chapter G, which documents the Pliocene to Pleistocene history of Lake Alamosa.

Optional Stops

An optional leg for day 2 (fig. B–2) includes three stops: (1) stop B5: barrier bar, spit, and lagoonal features that were formed during Lake Alamosa's highest stand (see also chapter G, this volume); (2) stop B6: spectacular wind-eroded rocks (ventifacts) along the southeastern margin of Lake Alamosa; and (3) B7: proposed type section for the Alamosa Formation, which is the basin-fill sediment of Lake Alamosa (stop B4). This last stop is at Hansen Bluff (see also stop A8, chapter A, this volume), a river-cut bluff that exposes early Pleistocene sediment that contains diverse faunal and floral remains, two volcanic ashes, and a well-documented magnetostratigraphic record.

Afternoon Stops

The last leg for day 2 (fig. B–3) focuses on a 1.0-Ma basalt volcano (Mesita Hill, stop B8) that is in the center of the Costilla Plain. We'll spend nearly 2 hours here reviewing the eruptive history of the

CHAPTER B

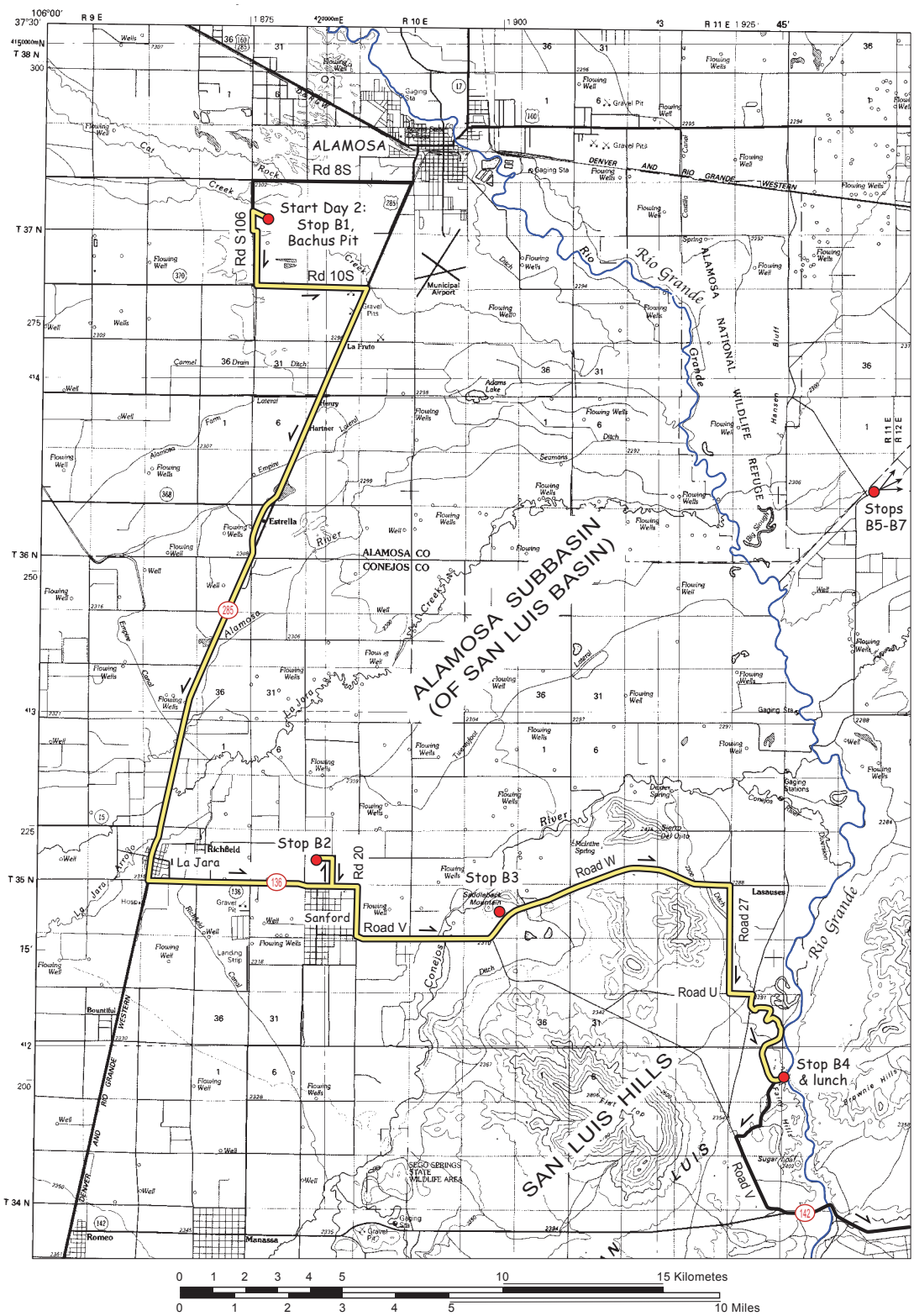

Figure B–1. Route and stops on morning of field-trip day 2. Stops B5, B6, and B7 (to the northeast of our route; shown as red dots) are optional and will not be visited.

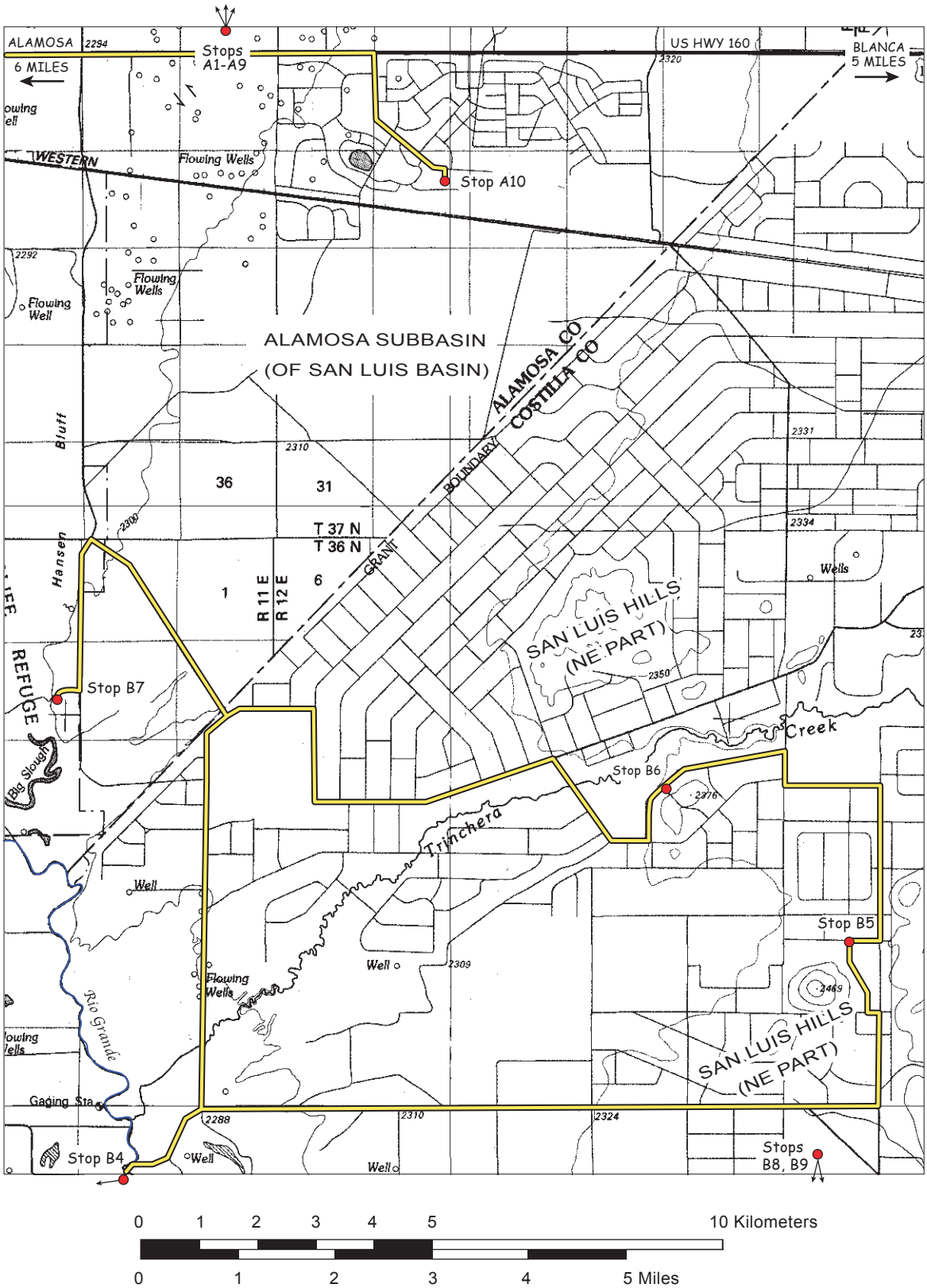

Figure B–2. Optional stops on field-trip day 2. Stops B4, B5, and B6 (to the northeast of the day 2 route; stops shown as red dots) will not be visited.

volcano, discussing the possibility that the volcano was nearly buried between 1.0 Ma and about 500 ka, and examining the western, faulted flank of the volcano. From there, we travel about 10 mi (16 km) southeast to the base of San Pedro Mesa to discuss landslide and fault hazards along the southern Sangre de Cristo fault zone, which is the southern part of the larger Sangre de Cristo fault system. This fault system has the highest documented Quaternary slip rates in the Rio Grande rift, which extends from at least Leadville, Colo. (on the north), to the Big Bend region of west Texas and to Chihuahua, Mexico (on the south).

Acknowledgments

None of the stops on this or other days of the field trip would be possible to visit without the permission of the landowners. We gratefully thank the following for allowing access to their properties during day 2 of the field trip:

Stop B1: Daniel Russell, owner, Bachus pit, Alamosa, Colo.

Stop B2: Lynn and Linda Mortensen, owners, Mortensen pit, Sanford, Colo.

Stop B3: Bureau of Land Management (public property), Monte Vista, Colo.

Stop B4: Bureau of Land Management (public property), Monte Vista, Colo.

Stop B5: Costilla County (public property), San Luis, Colo.

Stop B6: Costilla County (public property), San Luis, Colo.

Stop B7: Alamosa Wildlife Refuge, Alamosa, Colo.

Stop B8: Hecla Mining (Butte, Montana), owner, Hake and Jake Mine, Mesita, Colo.

Stop B9: Evan Melby, Melby Ranch Properties, LLC, Ventura, Calif.

In addition, we appreciate the constructive and helpful comments of James Cole (USGS) and Richard Madole (USGS-Emeritus), who reviewed a preliminary version of this manuscript. However, any errors that may remain are the responsibility of the authors.

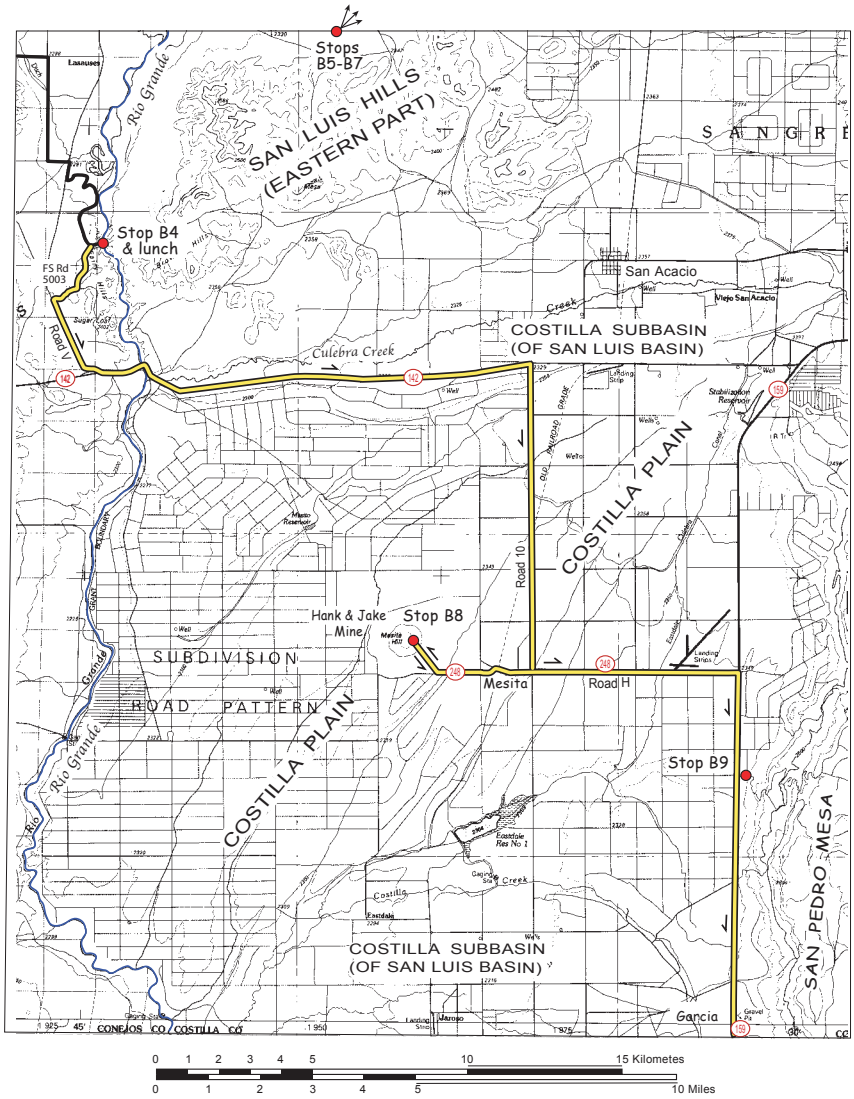

Figure B–3. Route and stops on afternoon of field-trip day 2. Stops B5, B6, and B7 (to the northeast of the day 2 route; stops shown as red dots) are optional and will not be visited on this trip.

Stop B1 — Deposits of Lake Alamosa at the Bachus Pit

Speaker: Michael Machette
Location: Various locations around perimeter of Bachus pit
Alamosa West 7.5' quadrangle
GPS: NAD27, Zone 13, 418900 m E., 4144720 m N., near center of Bachus pit
Elevation: About 7,540 ft (2,298 m) asl at base of pit; about 7,562 (2,305 m) asl at top of pit

Synopsis

Exposures within the Bachus pit show evidence of transgression and regression of Lake Alamosa, followed by incision of alluvial channels graded to post-lake base levels. The Bachus pit is one of the few places in the lake basin where lake deposits are well exposed; elsewhere, post-lake surficial deposits, high water tables, and strong efflorescence of gypsum typically obscure exposures of lacustrine sediment.

The Bachus pit extracts sand and pebble-size gravel for local use (mainly fill material). Although the pit walls change with continued mining, the base of the pit is controlled by fine-grained, water-saturated silt and clay deposited by Lake Alamosa prior to its last transgression and subsequent overflow. The walls of the pit expose well-sorted, sandy, small-pebble gravel that represents transgressive and regressive near shore and low-energy beach deposits. Between these deposits is sandy silt (deeper water phase of the lake) that is finely laminated and contorted by pressure loading from the overlying sedimentary package. The entire lacustrine section is capped, unconformably, by several meters of fine-grained alluvium that was deposited in response to falling base levels as the lake emptied through an outlet at the Fairy Hills. This alluvium is capped by loess and has relict soils, but their discontinuous Bt and Bw horizons (disturbed by animal burrows) are suggestive of middle Pleistocene age.

Sediment in the Bachus pit, together with high-energy near-shore gravel seen at stop B3 and lagoonal features seen at stop B7, are new and important stratigraphic and geomorphic evidence for the culmination and subsequent overflow of ancient Lake Alamosa.

Introduction

The Bachus pit is owned by Dan Russell of Alamosa (fig. B1–1). Dan earned a BS in Geology from Adams State College in the 1970s and currently owns and operates a land-surveying company in Alamosa. Dan's strong and enduring connection to geology is obvious from his enthusiastic support of our mapping of the Quaternary geology in this area (Machette and Thompson, 2005) and topical studies of Lake Alamosa. As a result, the Friends of the Pleistocene awarded Dan Russell its "Most Cooperative Landowner, 2007" award at its annual meeting in the Bachus pit on September 7, 2007.

Figure B1–1. Entrance to the Bachus pit, camping site for day 1 and first stop of day 2.

The Bachus pit produces well-graded sand and pebble-size gravel: the maximum gravel size is only 2–3 cm owing to its long transport distances from the eastern margin of the San Juan Mountains. Coarse gravel is so rare in the area that it is hauled from pits in coarser grained alluvial fans located about 15 km to the southwest. The Bachus pit supplies ungraded and graded sand and gravel to local contractors for use as backfill. Although the pit walls change with continued mining, the base of the pit is controlled by fine-grained, water-saturated silts and clays deposited by Lake Alamosa prior to its last transgression and subsequent overflow (see discussion in chapter G).

Local Geology

The Bachus pit is located on an east-trending topographic ridge that extends from west of our mapping area (longitude 106° W.) almost to U.S. Highway 285 (Alamosa to Antonito). Although the ridge is only about 20 ft (6 m) above the surrounding landscape, its elevated position is well above the local water table; thus, this and other similar ridges in the area are dry. They typically are the sites of churches, cemeteries, silage and sand pits, and stock ponds. This ridge is relatively planar and has a gentle east slope of less than 0.002 (that is, 2 m/km or 10 ft/mi) (fig. B1–2).

The ridge is composed of intermediate-age (middle Pleistocene) alluvium 2–3 m thick that rests unconformably on lacustrine sediment of the Alamosa Formation (see chapter G for a discussion of Lake Alamosa). Adjacent to the ridge are

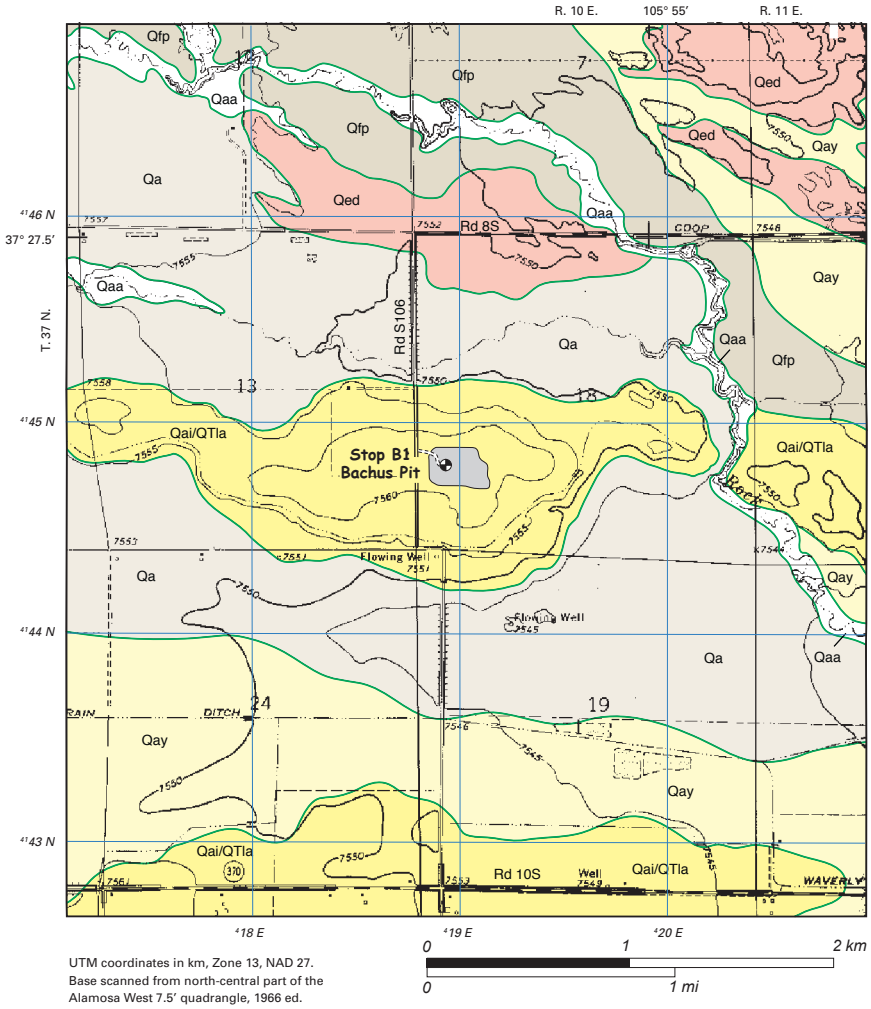

Figure B1–2. Surficial deposits and underlying near-shore lacustrine deposits of Lake Alamosa. Map units: Qe, Holocene eolian sand; Qaa, active alluvium; Qa, Holocene alluvium; Qfp, floodplain alluvium; Qay, younger (latest Pleistocene) alluvium, Qai, intermediate (middle Pleistocene) alluvium; QTla, Alamosa Formation. Geology modified from Machette and Thompson, 2005.

slightly lower valleys floored by latest Pleistocene to Holocene alluvium (fig. B1–2) and Holocene eolian sand.

Quaternary Stratigraphy

The Bachus pit has been extensively mined; the main product is sandy pebble gravel and silty sand. The pit floor is relatively flat and controlled by underlying lacustrine silt and sand (unit 5, fig. B1–3) that is commonly water-saturated at this elevation (about 7,540 ft or 2,298 m asl). Above the floor of the pit is sandy small-pebble gravel that represents transgressive near-shore, low-energy beach deposits of Lake Alamosa (unit 4, fig. B1–3). The transgressive deposits are not exposed in the west wall of the pit but were visible in 2005 on the north and east walls (exposures depend on activity in the pit and regrading of the pit walls). The near-shore sandy gravel is typically heavily stained by iron and manganese oxides, which in some locations are abundant enough to cement beds of gravel.

The transgressive deposits are overlain by sandy silt (deeper water phase of lake, unit 3 of fig. B1–3) that is finely laminated and contorted by pressure loading from the overlying sedimentary deposits (fig. B1–4). Over the silt is more sandy pebble gravel that represents regressive near-shore deposits related to drawdown of the lake (unit 2, figs. B1–3 and B1–4). We know that these are regressive deposits because they contain rip-up clasts of lake-bottom mud (derived from unit 3, fig. B1–5). Altogether, the entire cycle of lake sediment (units 2–4, fig. B1–3) is only about 3 m thick.

The Bachus pit is at an altitude of about 7,540–7,562 ft (2,298–2,305 m) asl, which is 100–120 ft (30–35 m) below the threshold (overflow) elevation of Lake Alamosa in the San Luis Hills. Thus, during the highest stand of Lake Alamosa, the Bachus pit was under about 30–35 m of water and well into the southwestern part of the lake. For example, the high-shoreline contour (7,660 ft or 2,335 m asl) is on the west side of the Monte Vista Wildlife Refuge, which is about 20 km to the west.

Above the lacustrine sediment is several meters of intermediate-age alluvial deposits (unit Qai) and loess (unit 1, fig. B1–3 and B1–4). The alluvium is relatively fine grained owing to its long transport distance from source areas in the eastern part of the San Juan Mountains. After water level in Lake Alamosa dropped, the lake floor was probably mantled by thin and discontinuous regressive near-shore deposits and deeper-water fine-grained deposits, all of which were eroded and reworked in alluvial channels that coursed across the newly exposed lake bottom. Wind erosion of the lacustrine sediment resulted in deposition of a 0.5–1 m thick layer of loess (silt and sand) that caps the alluvium. Relict soils formed on the loess and alluvium are disturbed by animal burrowing but show discontinuous Bt and Bw horizons suggestive of middle Pleistocene age (better exposures will be seen at stop B2).

Geologic History

The sediments exposed in the Bachus pit represent the last deep-water cycle of Lake Alamosa, which we believe culminated in overflow at about 440 ka (chapter G, this volume). This package may be thinner than those deposited during older

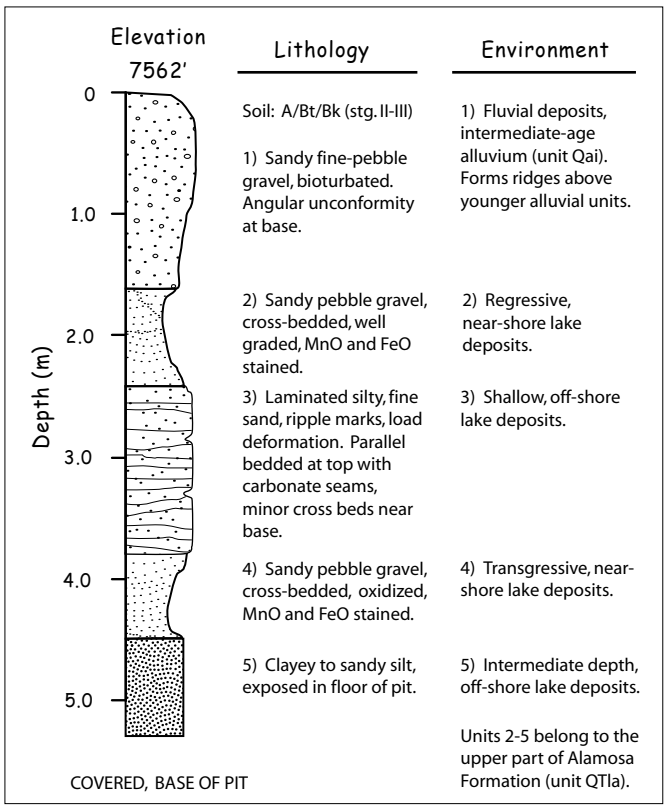

Figure B1–3. Schematic section of deposits exposed at field-trip stop B1 on west wall of the Bachus pit, as exposed in June 2004.

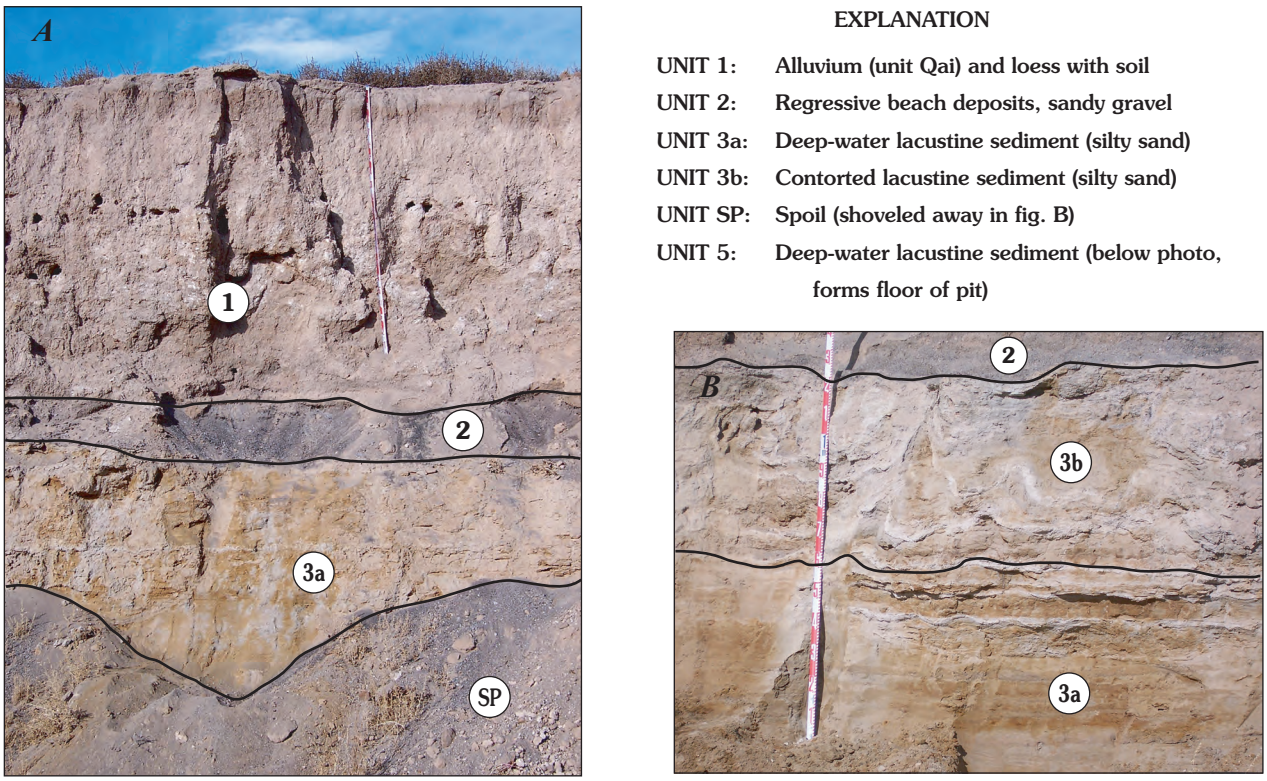

Figure B1–4. Exposures on the west wall of the Bachus pit. *A*, Alluvium (unit Qai) and loess deposits over lacustrine gravel and silty sands. Tape measure is extended 2 m. *B*, Closeup view of contorted lacustrine silty sand beds (unit 3b), which are rippled and well laminated (see unit 3a). Contortions in unit 3b are probably the result of penecontemporaneous loading by the overlying lacustrine and alluvial deposits, rather than by liquifaction (no feeder dikes were noted). Vertical exposure in this view is about 1.5 m.

cycles of the lake; the entire regressive phase of the sediment package is related to lowering of the lake as its waters flowed over and cut through the bedrock threshold in the Fairy Hills (see field-trip stop B4). If the lake had receded by evaporation, we would expect to see a thicker, coarsening-upwards section of sediment between units 3a and 2 (fig. B1–4) as the shoreline approached this site from the west and conditions changed from deep, quiet-water to shallow, near-shore conditions, rather than an abrupt unconformity between these units.

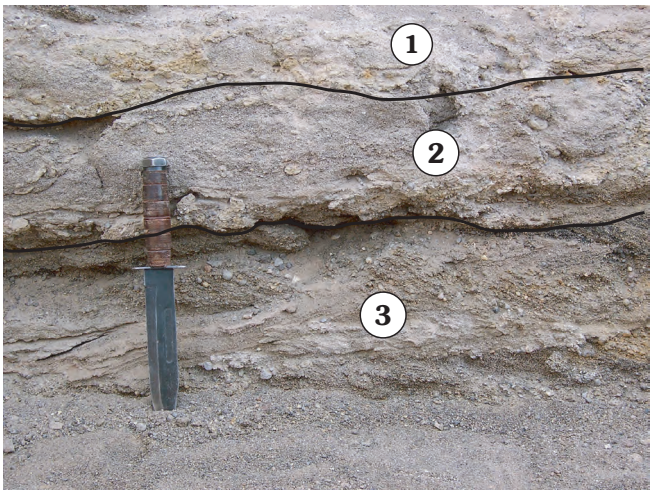

EXPLANATION

1: Layer with rip-up clasts of silty sand

2: Medium sand, crudely bedded

3: Sandy pebble gravel (1 cm max. clasts) and cross-bedded sand

Figure B1–5. Exposed lacustrine deposits on north wall of the Bachus pit. Silty oxidized clasts (1) in upper part of view are pieces of lake sediment ripped up during regression f the lake. Knife is about 20 cm long. All of these deposits are part of unit 5 in figure B1–3.

As the lake dropped, so did base level for the tributary streams emanating from the eastern part of the San Juan Mountains and streams heading on the exposed lake floor. The largest of these streams flowed northeast and east toward the Rio Grande's outlet from the Alamosa subbasin. Stream channels that cut into the exposed lake-bottom sediment became preferentially filled with alluvium (unit Qai, fig. B1–6) as the region was transformed from an exposed lake bottom to a gentle piedmont slope. However, the slightly more resistant nature of the alluvium-filled channels led to topographic reversal through time, just as basalt-filled channels become topographically reversed when less resistant bedrock is eroded preferentially.

Conclusions

The Bachus pit contains excellent exposures of sediments deposited during and after the last cycle of Pliocene to middle Pleistocene Lake Alamosa. The lacustrine sediments represent the uppermost preserved part of the Alamosa Formation (Siebenthal, 1910), which underlies almost the entire San Luis Valley north of the San Luis Hills. This uppermost part of the Alamosa Formation (about 700–440 ka) is missing from Hansen Bluff (see stop B5) owing to local erosion. Nevertheless, because this bluff is well exposed and contains abundant fossils, it is considered to be the type area of the formation as described by Siebenthal (1910). Thus, the sediments in the Bachus pit, together with high-energy, near-shore gravels seen at stop B3 and lagoonal features seen at stop B7, are new and important stratigraphic and geomorphic evidence for the culmination and subsequent overflow of Lake Alamosa.

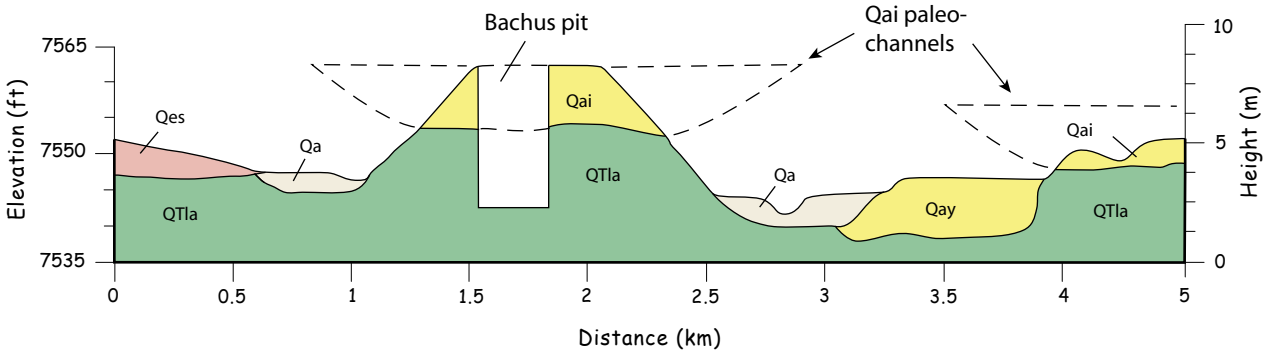

Figure B1–6. Schematic cross section through the ridge on which the Bachus pit is excavated showing position of Qai paleochannels cut into lacustrine deposits. Geologic units: Qes, Holocene eolian sand; Qa, undivided Holocene alluvium; Qay, young (latest Pleistocene) alluvium; Qai, intermediate (middle Pleistocene) alluvium; QTla, lacustrine sediment of the Alamosa Formation (Pliocene to middle Pleistocene). Geology from Machette and Thompson (2005). Vertical exaggeration is 50x.

Stop B2 — Soil on Intermediate-Age Alluvium (Post-Lake Alamosa), Sanford, Colo.

Speaker: Michael Machette
Location: Mortensen gravel pit, on low ridge about 0.6 mi (1km) north of city center of Sanford, Colo.
La Jara 7.5' quadrangle (Station LJ–MM04–19)
GPS: NAD27, Zone 13, 419880 m E., 4125652 m N.
Elevation: Top of pit is at 7,590 ft asl (2,313 m)

Synopsis

This pit exposes a thick, well-developed calcic soil formed in sandy pebble gravel that Machette and Thompson (2005) mapped as intermediate-age alluvium (unit Qai). The soil clearly represents hundreds of thousands of years of soil formation; it has a remarkable Bk horizon (stage III morphology) for this altitude (nearly 7,600 ft or 2,316 m asl). This stop is on a wide, north-trending ridge (informally named Sanford Ridge) that is only about 3–4 m above adjacent, younger alluvial surfaces. Similar to the geomorphology at stop 1, Sanford Ridge represents a reversal of topography: unit Qai gravel was deposited in a broad channel cut into lacustrine deposits (unit QTla) after Lake Alamosa had overflowed and dropped to a lower level. This relationship is common in the southwestern part of the lake basin.

Introduction

The Mortensen pit is an inactive sand and gravel pit that is owned by Lynn and Linda Mortensen of Sanford (fig. B2–1). The pit is adjacent to several reservoirs that retain irrigation water from deep wells. The pit and reservoirs are in a low, broad, north- to northeast-trending ridge of middle Pleistocene alluvium that is only about 3–4 m above surrounding surfaces formed on latest Pleistocene and Holocene alluvium (fig. B2–1). The ridge is informally named after the town of Sanford. Sanford Ridge is relatively tabular and has a gentle north slope of about 0.0016 (that is, 1.6 m/km or 8 ft/mi) as measured from the La Jara 7.5-minute topographic map. It extends about 10 km in a north-south direction (see mapping of Thompson and Machette, 1989) and is one of several in the southwestern part of the Alamosa subbasin (of the San Luis Basin) that reflect inverted topography, as discussed at stop 1. Sanford is a small Mormon farming community, whereas many of the adjacent communities (such as La Jara) are primarily Hispanic.

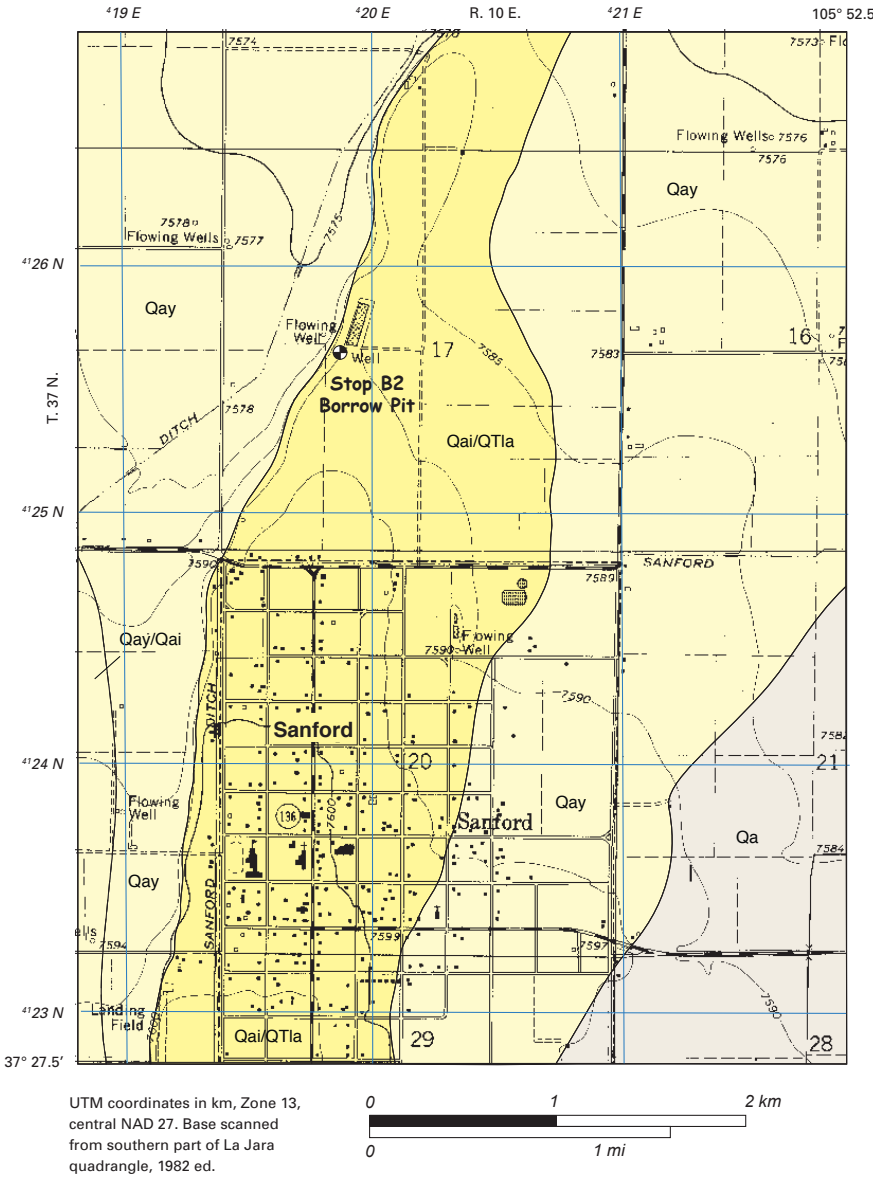

Figure B2–1. Alluvial deposits in the vicinity of the Sanford, Colo.; stop B2 is at the Mortensen sand and gravel pit. Map units: Qa, Holocene alluvium; Qay, younger (latest Pleistocene) alluvium; Qai, intermediate (middle Pleistocene) alluvium; QTla, Alamosa Formation (buried lacustrine deposits). Geology modified from Machette and Thompson, 2005.

Local Geology

The Mortensen pit is in alluvium composed of sand and pebble gravel, which has maximum clast sizes of 3–4 cm. Most clasts are derived from Tertiary volcanic rocks of the San Juan Mountains, either deposited directly from the source area or recycled from older alluvium (unit Qao) preserved above the ancient shorelines of Lake Alamosa to the southwest. At this stop and Sanford (in general), we are 20–25 m below the maximum shoreline elevation of Lake Alamosa, which is about 7,660 ft (2,335 m) asl. The material in the pit and underlying Sanford Ridge is mapped as intermediate-age alluvium (unit Qai, fig. B2–1) and may be only 2–3 m thick and, if so, rests unconformably on lacustrine sediment (unit QTla) of the Alamosa Formation (see chapter G in this volume for a discussion of Lake Alamosa). Sanford Ridge is surrounded by slightly lower surfaces formed on latest Pleistocene to Holocene alluvium (fig. B1–2). Shallow pits in these younger materials typically fill with water owing to a high water table in this part of the Alamosa subbasin. All of the alluvium in this area has been deposited by the Conejos River and adjacent tributary streams, which flow east and northeast from the eastern foothills of the San Juan Mountains.

Soils in the Mortensen Pit

As previously mentioned, exposures of alluvium at low elevations in this part of the Alamosa subbasin (of the San Luis Basin) are rare and then often water saturated. However, owing to the slightly higher elevation of Sanford Ridge with respect to adjacent surfaces, this pit is typically dry. The pit is on the western margin of the ridge, but the soils we see here have formed since the ridge was geomorphically isolated by downcutting (some unknown amount of time after deposition of alluvial unit Qai).

Soils exposed in the south wall of the pit (fig. B2–2) reflect varying degrees of development probably as a result of the site's relatively high altitude (7,590 ft or 2,313 m asl). Older soils at high elevations in the southwestern United States typically have formed in alternating climates (glacial, interglacial) that can cause losses and accumulations of carbonate both through time and space owing to vertical or lateral flow of water through the soil (see Machette, 1985). The two soils shown in figure B2–2 have differing characteristics: the soil at locality 1 has an A/Bt/Btk/Bk profile, whereas the soil at locality 2 (only 10 m to the west) has a Btk/Bk profile. The lack of A and Bt horizons at locality 2 probably reflect erosion of the soil along the margin of Sanford Ridge; conversely, its stronger and thicker Bk horizon may reflect lateral soil water flow (to the west) that has enhanced the accumulation of carbonate (that is, some of the carbonate may have precipitated from laterally flowing groundwater).

We made a quick description of the soil at locality 1 (fig. B2–3) several years ago but do not have laboratory data on its physical or chemical properties. Nevertheless, the thickness of the soil (<155 cm), presence of an argillic (Bt and Btk) horizon, and the strong carbonate morphology (stage III) suggest that this soil represents hundreds of thousands of years of formation at an altitude that is relatively high for accumulation of pedogenic carbonate.

Geologic History

The sediments exposed in the Mortensen pit reflect alluvial channel cutting and subsequent topographic reversal in response to drawdown of Lake Alamosa, which we believe occurred at about 440 ka (chapter G, this volume). As the lake dropped, so did base level for the streams emanating from the eastern part of the San Juan Mountains (such as the Rio Conejos and Rio Grande) and streams heading on the exposed lake floor, such as at stop B1. Stream channels cut into the exposed lake bottom sediment became filled with gravelly alluvium (unit Qai, fig. B2–1) as the area was transformed from a lake bottom to a piedmont slope, and the slightly more resistant alluvium in thick channels led to topographic reversal through time. This relationship is common in the southwestern part of the lake basin. Subsequent erosion (eolian and fluvial) of the lake deposits (mainly silts here) caused a topographic reversal,

Figure B2–2. South wall of the Mortensen pit (informal name). Pit is not active, and exposures are poor. However, 1–1.5 m of soil is exposed at the two labeled spots. Locality 1—Argillic B horizon over discontinuous Bk horizon. This is the locality for the soil profile shown in fig. B2–3. Locality 2—A and weak B horizons over well developed Bk horizon. View to south; town of Sanford is in background, about 1 km to south.

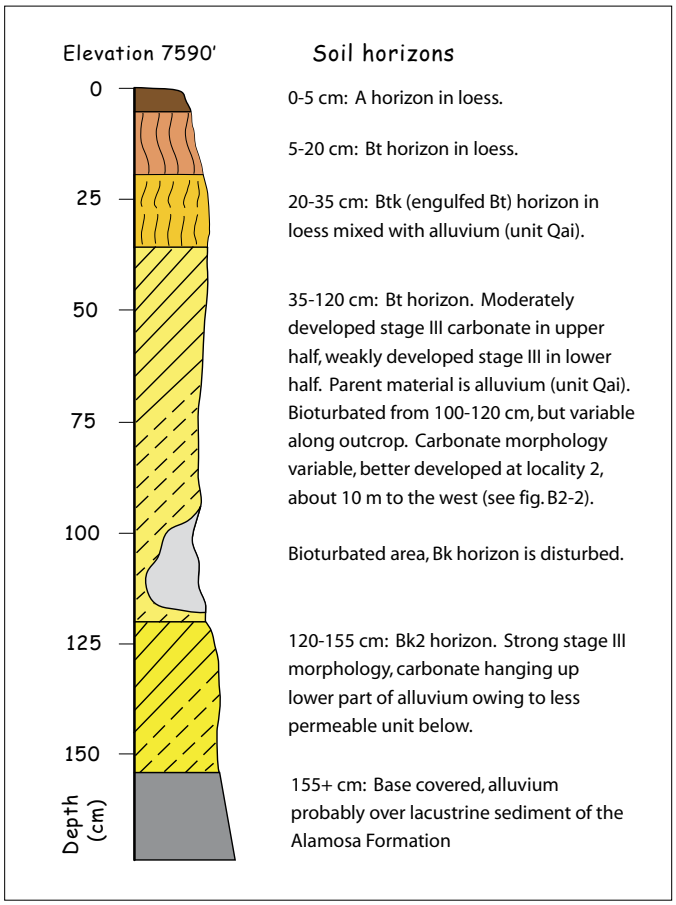

Figure B2–3. Schematic section showing soil profile at locality 1 (fig. B2–2), south wall of the Mortensen pit, as of June 2004.

such that unit Qai sits above younger alluvial deposits. In fact, just from inspecting topographic maps of the area it is obvious that most of the cemeteries are built on ridges of unit Qai alluvium for two reasons: they are high and dry.

The unit Qai ridges seen at this and the previous stop extend basinward to minimum elevations of about 7,530–7,540 ft or 2,295–2,298 m) asl, which probably reflect the base level of the Rio Grande once the gorge was cut through the San Luis Hills. The Rio Grande's channel is presently at about 7,500 ft (2,286 m) asl at the same latitude as the distal ends of the unit Qai ridges, thus there has been about 30–40 ft (9–12 m) of additional stream incision since the gorge was cut through the Fairy Hills (see stop B4).

Conclusions

The Mortensen pit contains excellent but shallow exposures of strongly developed soils on intermediate-age (unit Qai) alluvium. The alluvium fills channels of the ancient Rio Conejos, which extended its course basinward after middle Pleistocene Lake Alamosa was drained. The lacustrine sediment beneath stop B2 represents the uppermost preserved part of the Alamosa Formation, which underlies almost the entire San Luis Valley north of the San Luis Hills. Thus, the Mortensen pit is an excellent location to observe the degree of soil development on alluvium that postdates the draining of ancient Lake Alamosa. These soils represent hundreds of thousands of years of formation, but they are not as strongly developed as the soils on the highest shoreline deposits of Lake Alamosa (see stops B3 and B4), which appears to have culminated in overflow at about 440 ka (see more complete discussion of Lake Alamosa in chapter G, this volume).

Stop B3 — Soils on and Experimental Dating of Lacustrine Gravels of Lake Alamosa at Saddleback Mountain

Speakers: Michael Machette and David Marchetti
Location: Gravel spits on south face of Saddleback Mountain, about 3 mi (4.8 km) east of Sanford, Colo.; 1.5 mi northeast of bridge over Rio Costilla
Pikes Stockade 7.5' quadrangle (Stations PS–MM04–29a, PS–MM04–29b, and PS–MM05–72)
GPS: NAD27, Zone 13, 425340 m E., 4123725 m N.
Elevation: About 7,575 ft (2,309 m) asl (base of slope at turn off from paved road)

Synopsis

This stop is a key location for understanding the extent and age of Lake Alamosa. Two spits perched on the southern side of Saddleback Mountain provide unequivocal evidence for the presence of a large ancient lake (Lake Alamosa) that occupied the San Luis Basin, probably during the Pliocene and Pleistocene. Soils on these spits show strong development of calcic (Bk) horizons, which suggest a middle Pleistocene age for the spits.

The lower (stop B3.1) and upper (stop B3.2) spits were trenched in order to describe the soils formed on the lacustrine gravels and to sample for a variety of experimental cosmogenic nuclide and U/Th dating techniques. At the time this report was written, only surface-exposure dating using ^{3}He isotopes had been completed. This technique yielded an age of 439±6 ka from a single bedrock boulder (stop B3.3); thus, for the purposes of discussions of Lake Alamosa we use a time of 440 ka for its overflow and the Rio Grande's subsequent incision of the Fairy Hills.

Introduction

Saddleback Mountain, the elongate bedrock ridge north of the road, is formed by subhorizontal volcanic flows of the upper Oligocene to Miocene Hinsdale Formation (fig. B3–1). These flows are silicic alkali-olivine basalts with as much as 40 percent phenocrysts of olivine and clinopyroxene. In the San Luis Hills, these basalts have been dated at about 26 Ma (see Thompson and Machette, 1989; Dan Miggins, written commun., 2006). At Lake Alamosa's highest stand (about 7,660 ft asl), Saddleback Mountain was an island in the southern part of the lake. At this elevation, the lake extended westward to the eastern margin of the San Juan Mountains (near Monte Vista) and northward, nearly to Saguache, a distance of about 55 mi (88 km). Thus the lake had a long fetch to the northwest, and during large storms waves eroded the northern face of Saddleback Mountain and other bedrock hills to the east of this stop.

Local Geology and Climate

Young gravelly alluvium (units Qaa, Qaa, Qfp, and Qay) that surrounds the northern and western sides Saddleback Mountain was deposited by the Rio Conejos, which eroded into a preexisting platform of fine-grained lacustrine sediment of the Alamosa Formation (unit QTla, fig. B3–1). However, to the east and south of Saddleback Mountain both coarse- and fine-grained deposits of Lake Alamosa are preserved to the leeward (south) of the mountain. The fine-grained deposits are poorly exposed and highly eroded, whereas the coarse-grained deposits are preserved in gravelly spits on the south side of Saddleback Mountain and as gravel-capped, bedrock-cored saddles between hills (note: the road east from here passes through such a saddle). Younger lacustrine deposits (unit Qla, fig. B3–1), which are probably reworked from sediment of the Alamosa Formation, typically occupy playas in topographic depressions, such as the one south of Saddleback Mountain.

The bouldery spits at stop 3, rich in basaltic clasts of the Hinsdale Formation, are key to understanding the extent and age of Lake Alamosa. Two spits are present here; at most localities only one spit, shoreline or barrier bar is preserved at these elevations. However, multiple barrier bars and back-bar lagoons such as at stop B6 record a rising Lake Alamosa, prior to its overflow through the Fairy Hills (see stop B4). Here at stop 3, we have an opportunity to see constructional features of Lake Alamosa, a Pliocene to middle Pleistocene lake that occupied most of the San Luis Basin north of the San Luis Hills.

The spits at stop B3 were formed by long-shore (southwest) transport of eroded bedrock blocks and subsequent deposition of sandy cobble to boulder gravels on the leeside of Saddleback Mountain (figs. B3–2, B3–3). The tops of both spits are planar and gently east sloping, which reflects deposition into deepening water to the south and southeast of Saddleback Mountain.

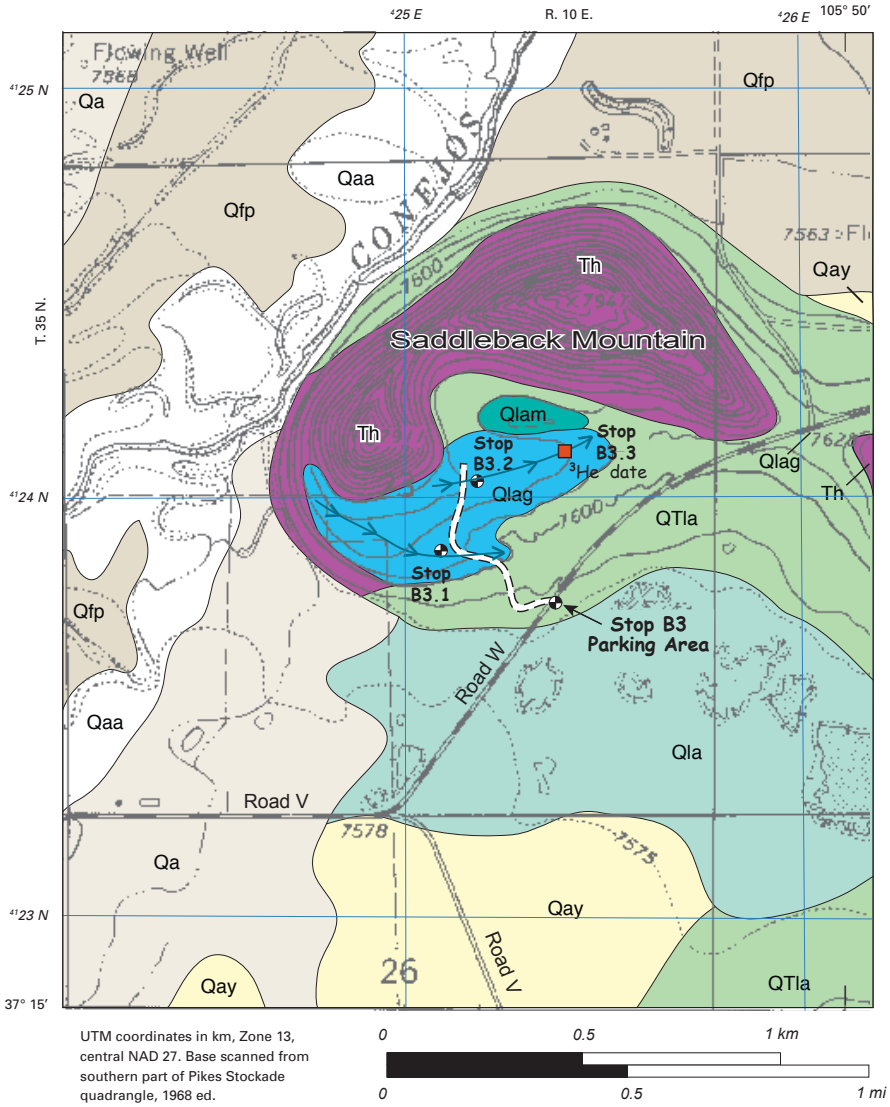

Figure B3–1. Bedrock, alluvial deposits, and lacustrine deposits of Lake Alamosa. Map units: Qaa, active alluvium; Qa, Holocene alluvium; Qfp, floodplain alluvium; Qay, younger (late Pleistocene) alluvium, Qla, lacustrine deposits (post-Lake Alamosa); Qlag (gravelly) and Qlam (lagoonal) near-shore deposits of Lake Alamosa (middle Pleistocene part of QTla); QTla, Alamosa Formation (undivided, fine grained deposits here), and Hinsdale Formation (26 Ma). Geology modified from Machette and Thompson, 2005.

The elevation in this part of the basin ranges from about 7,550 to 8,000 ft asl, so it is a little surprising (to Machette) to find abundant, thick calcic soils on the older landscapes (see also, stops B1 and B2). However, the climatic conditions are conducive to their formation now and apparently in the past also. Modern climatic conditions in Alamosa, about 15 mi (24 km) to the north of this stop, are cold (41°F or 5°C mean annual temperature (MAT)) and relatively dry (about 7 in. or 180 mm mean annual precipitation (MAP)) on average for the year (see http://www.wrcc.dri.edu). These conditions are well within the normal limits of pedocal formation (see Machette, 1985). Rainfall increases slightly across the basin as you gain distance from the San Juan Mountains, which creates a strong rain shadow in the San Luis Valley. Glacial climates must have been considerably colder and probably drier than present, thus preventing massive leaching of calcium carbonate from the soil.

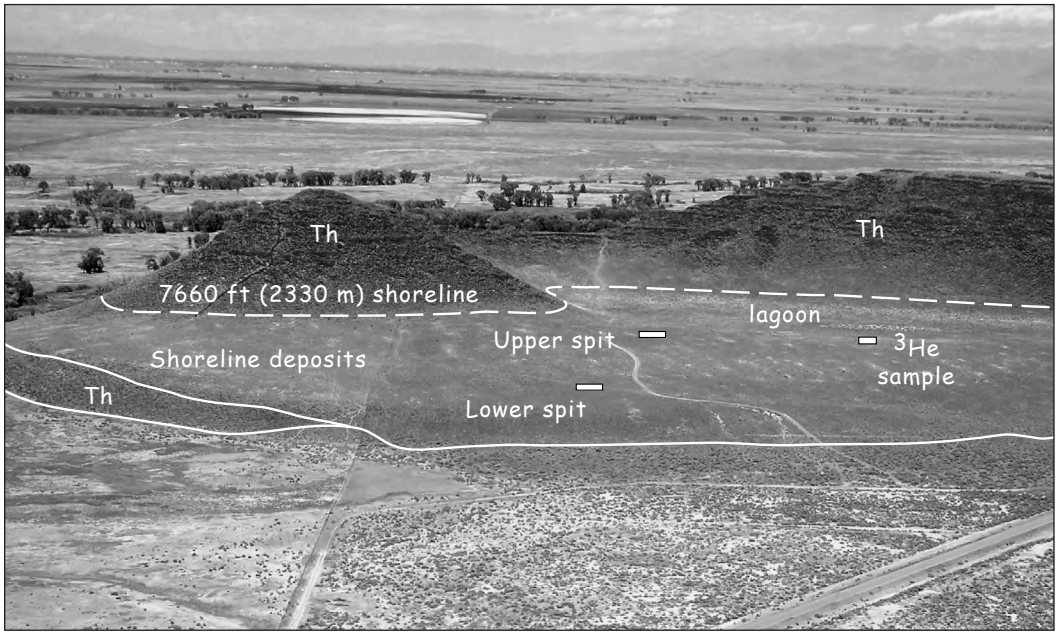

Figure B3–2. Oblique aerial photograph of the south side of Saddleback Mountain, location of stop B3. Unit Th, Hinsdale Formation (upper Oligocene andesitic basalt). View to the northeast.

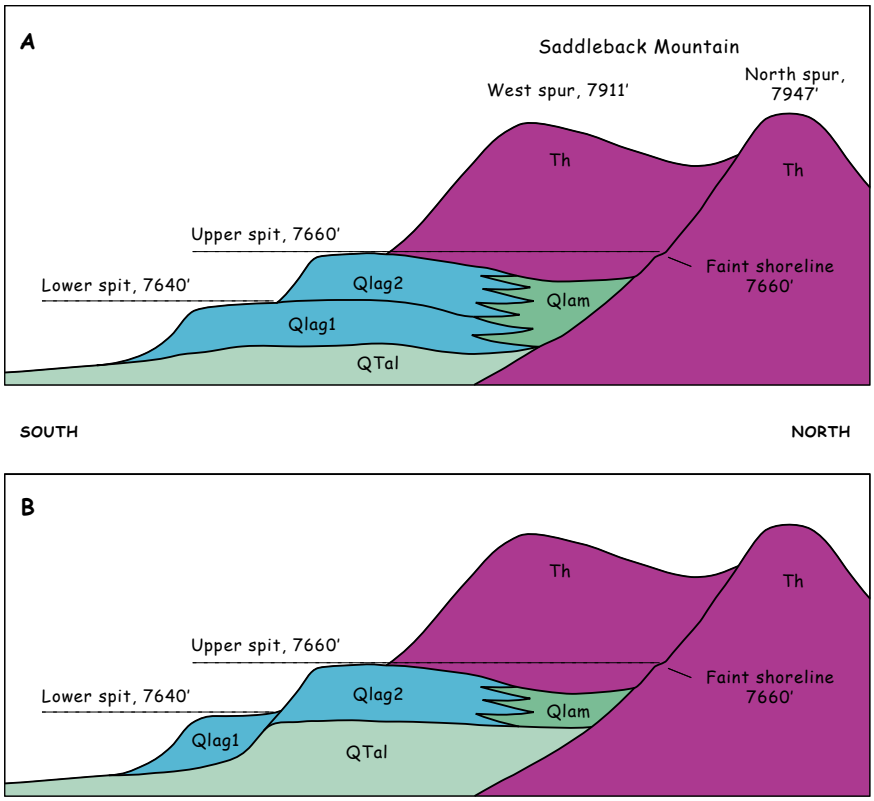

Fig. B3–3. Schematic cross section of surficial and bedrock geology at Saddleback Mountain, location of stop B3. *A*) Stacked spits (Qlag1 is older than Olag2). *B*) Superposed spits (Qlag1 is younger than Olag2). Map units: Qlam, lagoonal deposits of Lake Alamosa; Qlag, gravel (spit) deposits of Lake Alamosa (Qlag1, lower spit; Qlag2, upper spit); QTal, Alamosa Formation, undivided; Th, Hinsdale Formation (upper Oligocene andesitic basalt). View to the west. Based on geologic mapping of Machette and Thompson, 2005.

Stop B3.1 — Lower Spit, Soil Profile

Location: Lower of two spits, filled soil pit
Pikes Stockade 7.5' quadrangle (Station PS–MM04–29b)
GPS: NAD27, Zone 13, 425107 m E., 4123885 m N.
Elevation: 7,640 ft (2,329 m) asl

Overview

The lower spit has a very well developed calcic soil that is morphologically identical to the soil on the upper spit (stop B3.2), but it is not as well developed in terms of thickness and total carbonate. In New Mexico to the south, similar calcic soils are formed on middle Pleistocene deposits. Considering the site's semiarid climate and high elevation (7,640 ft or 2,329 m asl), this soil is particularly well developed in a noncalcareous sandy basalt-rich gravel.

Soil Development

The soil is formed in basaltic gravel (fig. B3.1–1) that has no easily weatherable source of Ca^{++}. The entire Bk horizon is about 95 cm thick and has a maximum stage III morphology with a maximum of 50 percent $CaCO_3$ in the <2 mm portion of the Bk2 horizon (fig. B3.1–2). Texturally, the parent material for this soil is a sandy silt, with about 25 percent <2 mm matrix in a coarse cobble to boulder gravel. Textural analyses of the soil (see data in table B3.2–1) show a dominance of sand in the profile, but the silty component (as much as 41 percent) may be lacustrine in origin or be deeply translocated dust. Chittick analyses of the lowest Bk subhorizon show 3.8 percent $CaCO_3$ in the <2 mm fraction; thus, we estimated that the parent material has only 1.0 percent $CaCO_3$ in the <2 mm fraction.

At lower elevations of about 4,500–5,500 ft (1,370–1,675 m) asl in New Mexico to the south, morphologically similar soils are middle Pleistocene in age (Machette, 1985; Machette and others, 1997). Thus, the relict calcic soil on the lower spit is particularly well developed considering it is in a semiarid climate and at a high elevation (7,640 ft or 2,329 m asl).

Although we cannot prove the stratigraphic relations between the lower and upper spits, we consider the lower one to be slightly younger and project under the upper spit (as shown schematically in fig. B3–3A). If the lower spit is younger than the upper spit (fig. B3–3B), it would be evidence for a multistage drawdown of the lake (rather than a single drop) as the Rio Grande cut a gorge through the Fairy Hills (see stop B4) in an intermittent manner.

Figure B3.1–1. Soil- and cosmogenic-sampling pit at stop B3.1 on the lower spit (unit Qlag1) at Saddleback Mountain. Pit is about 2.5 m deep in coarse sandy gravel. View to the southwest.

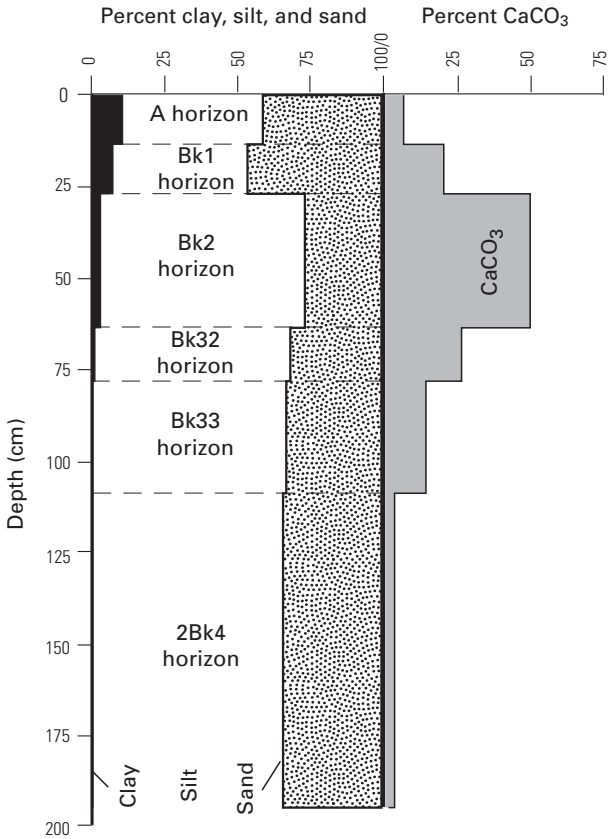

Figure B3.1–2. Profile data for soil on lower spit, stop B3.1.

Stop B3.2 — Upper Spit, Soil Profile and Experimental Dating

Location: Upper of two spits, filled soil pit.
Pikes Stockade 7.5' quadrangle (Station PS–MM04–29a)
GPS: NAD27, Zone 13, 425136 m E., 4124048 m N.
Elevation: 7,660 ft (2,335 m) asl

Overview

The upper spit has a very well developed calcic soil that is morphologically identical to the soil on the lower spit, but it contains about 30 percent more calcium carbonate (on a total profile basis). The Bk horizon (undivided) is about 40 cm thicker and has a maximum of 64 percent $CaCO_3$ in the <2 mm portion of the Bk2 horizon.

Marchetti obtained a single ^3He surface-exposure age of 439±6 ka for a large boulder on this spit (see discussion in stop B3.3 and chapter G). However, in order to date the spit further, we sampled for three other experimental techniques: U-series dating of carbonate pendants and terrestrial cosmogenic nuclide (chlorine and helium) dating of soil-depth profiles. Unfortunately, none of the results from these other techniques were available when this discussion was written in the spring of 2007.

Soil Development

Soils on the upper and lower two spits (and two other sites) were described by Alan Stuebe (fig. B3.2–1) of the National Resource Conservation Service in Alamosa. Janet Slate (USGS) and Michael Machette sampled for soil and cosmogenic-chlorine analyses at the same time. The backhoe pits in the soils were about 2.5 m deep, but they quickly filled with loose materials so we sampled from the bottom up.

Figure B3.2–1. Alan Stuebe preparing to describe the soil on the upper spit (unit Qlag2) at Saddleback Mountain, stop B3.1. Alan is with the National Resource Conservation Service (formerly SCS) in Alamosa and has mapped tens of thousands of square kilometers of soils in the San Luis Valley.

As with the lower spit, this soil is formed in basaltic gravel (fig. B3.1–1) and thus has no easily weatherable source of Ca^{++}. The entire Bk horizon is about 150 cm thick and has a maximum stage III morphology and about 64 percent $CaCO_3$ in the <2 mm portion of the Bk2 horizon (fig. B3.2–2). The parent material for this soil is very gravelly sandy silt that contains about 25 percent <2 mm matrix in a coarse cobble to boulder gravel. Textural analyses of the soil (fig. B3.2–3; see also data in table B3.2–1) shows a dominance of silt (as much as 65 percent) in the <2 mm fraction; thus, much of the silt may be lacustrine in origin or deeply translocated eolian dust. The lowest Bk subhorizon has an estimated 4 percent $CaCO_3$ in the <2 mm fraction; thus, we assumed that the parent material has only 1.0 percent $CaCO_3$ in the <2 mm fraction (these assumptions are based on the soil on the lower spit).

Carbonate Accumulation

We have calculated calcium carbonate accumulation rates at this site for comparison with rates at other sites in New Mexico, mainly as a relative dating tool. One can approximate the total amount of $CaCO_3$ in a soil profile from the following parameters for each horizon as shown in table B3.2–1: thickness (column C), percent <2 mm fraction (column H), percent $CaCO_3$ in the <2 mm fraction (column I), and bulk density of the <2 mm fraction (column J). For a more complete discussion of this method, see Machette (1978, 1985). The only fraction of pedogenic $CaCO_3$ not accounted for in the following discussion are the thick pendants (rinds) that have accumulated on the base of some clasts. We suspect that this component might add as much as 10 percent to the calculations shown in table B3.2–1.

The two soils that we analyzed have quite different amounts of pedogenic $CaCO_3$: the lower spit (stop B3.1) has about 26.6 g of $CaCO_3$ per cm^2 column through the soil, whereas the upper spit (stop B3.2) has about 35.0 g (30 percent more). Using 30±5 g as an average value and a duration of soil formation of 440 ka (see following discussion of ^3H dating, stop B3.3) yields a long-term accumulation rate of about 0.074 g/cm^2/1,000 yr. The upper spit contains the most carbonate; using its 35 g content yields a rate of about 0.080 g/cm^2/1,000 yr. By comparison, soils that Machette (1985) considered to be about 0.5 Ma in New Mexico had much higher calculated accumulation rates of 0.2–0.4 g/cm^2/1,000 yr. However, new dating control for the deposits that host these soils show that they may be as much as five times older than considered in 1985, reducing the New Mexico accumulation rates to only 0.04–0.08 g/cm^2/1,000 yr. Thus, the maximum rate of 0.080 g/cm^2/1,000 yr calculated for that this stop suggests that calcic soils in the San Luis basin may have accumulated as fast as those in Albuquerque.

The calculated total pedogenic $CaCO_3$ contents of 26.6–35 g per cm^2 of soil column from the spits reflects only the $CaCO_3$ retained in their soils. The wide variability in the amount and morphology of $CaCO_3$ seen in soils in this area suggests that former glacial or pluvial climates and vegetation (for instance, forests) may have caused leaching and

Table B3.2–1. Physical and calcium carbonate data for relict soils on spits of Lake Alamosa, Saddleback Mountain, stop B3.

Sample	Depth (thickness) (cm)	Horizon	<2 mm texture	Percent sand, 64–2000 µm	Percent silt, 2–64 µm	Percent clay, <2 µm	Percent <2 mm	$CaCO_3$ content (percent)	Bulk density (g/cm^3)	$CaCO_3$ concentration (g/cm^3)	Horizon $CaCO_3$ (g/cm^2)	Cumulative profile $CaCO_3$ (g/cm^2)
A	B	C	D	E	F	G	H	I	J	K	L	M
Stop B3.1. Soil from lower spit, Saddleback Mountain (samples PS–MM04–29b)												
–S1	0–14 (14)	A	Silty sand	60.6	29.1	10.3	95	6.1	1.55e	0.10	1.3	1.3
–S2	14–27 (13)	Bk1	Silty sand	59.9	33.4	6.7	50	20.0	1.77	0.18	2.3	3.6
–S3	27–64 (37)	Bk2	Silty sand	56.2	41.0	2.8	45	50.2	1.70e	0.38	14.2	17.8
–S4	64–79 (45)	Bk32	Sand	81.9	16.8	1.3	35	25.9	1.65e	0.15	6.7	24.5
NS	79–109 (30)	Bk33	Sand	85e	14e	1e	35e	15e	1.6e	0.08	2.5	27.0
–S5	109–195 (86)	2Bk4	Sand	91.0	8.3	0.7	25	3.8	1.6e	0.02	1.3	28.3
NS	(195)	PM	Sand	-----	-----	-----	50e	1.0	1.55e	0.008	–1.7	26.6
Stop B3.2. Soil from upper spit, Saddleback Mountain (samples PS–MM04–29a)												
–S1	2–11 (9)	A	Silty sand	42.2	44.9	12.9	95	8.7	1.54	0.127	1.1	1.1
–S2	11–38 (27)	Bk1	Silty sand	47.4	43.5	9.1	40	28.7	1.6e	0.18	5.0	6.1
–S3	38–83 (45)	Bk2	Sandy silt	26.9	64.9	8.2	35	64.3	1.7e	0.38	17.2	23.3
–S4	83–147 (64)	Bk3	Sandy silt	32.4	59.8	7.8	35	21.6	1.6e	0.12	7.7	31.0
–S5	147–160 (13)	Bk4	Sandy silt	33.9	56.1	10.0	30	26.7	1.6e	0.13	4.1	35.1
NS	160–220 (60)	2Ck	Sandy silt	35e	60e	5e	25	4.0e	1.55e	0.04	1.6	36.7
NS	(220)	PM	Sandy silt	-----	-----	-----	50e	1.0	1.55e	0.008	–1.7	35.0

Abbreviations: e, estimated value; NS, not sampled (or analyzed); PM, parent material.

Notes on calculated values:

Column C—PM, parent material. Values assumed based on typical noncalcareous, sandy beach (spit) gravels. These are used to calculate primary carbonate (see Machette, 1978 and 1985; Machette and others, 1997).

Column K—Concentration of $CaCO_3$ (g/cm^3) in each horizon calculated as column H (percent)/100 x column I (percent)/100 x column J (g/cm^3).

Column L—Total $CaCO_3$ (g/cm^2) in each horizon calculated as column B (cm) x column K (g/cm^3).

Column M—Cumulative $CaCO_3$ (g/cm^2) in each profile is calculated as sum of values in column L, from the surface though the entire Bk horizon.

Figure B3.2–2. Upper 1.2 m of calcic soil formed on the upper spit (unit Qlag2) at Saddleback Mountain, stop B3.2. Backhoe excavating arm for scale.

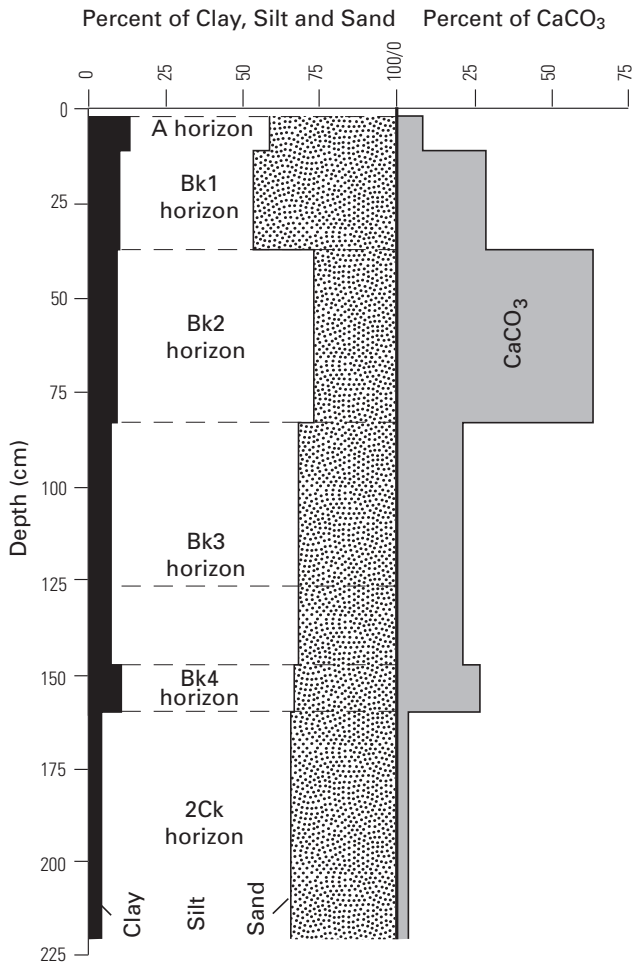

Figure B3.2–3. Profile data for soil on the upper spit, stop B3.2.

losses of previously accumulated $CaCO_3$. As one moves upslope to higher, forested elevations, $CaCO_3$ accumulations in soils become discontinuous and spotty, even at the outcrop level. Thus, as one approaches the pedocal-pedalfer boundary at high elevation or moist sites, studies of total pedogenic $CaCO_3$ contents make it more difficult to assume steady-state processes for soil formation in this region (Machette, 1985; Birkeland, 1999).

Experimental Age Dating

In an effort to date the highest (and youngest) shorelines of Lake Alamosa, we have focused on these spits. In addition to the relative degree of soil development and the calculations of total $CaCO_3$ accumulation, we are attempting to use a variety of isotopic techniques to date the time of deposition of the spits. These spits have been trenched several times to sample for specific dating techniques:

1. Surface-exposure dating (basalt boulders) using ^{3}He isotopes. These analyses were done in 2006 at the University of Utah's Noble Gas Laboratory (Salt Lake City) by David Marchetti (see Machette and Marchetti, 2006). This technique can date the exposure of eroded boulders that have been at the surface as long as 1.0 million years if they have the appropriate mineralogy (olivine or pyroxene).

2. Terrestrial cosmogenic nuclide profile dating using ^{3}He isotopes. David Marchetti is performing these analyses at the University of Utah's Noble Gas Laboratory (Salt Lake City). This technique uses small gravel clasts collected through a vertical profile at least 2–3 m deep and can date deposits as old as 1 Ma if they have the appropriate mineralogy (olivine or pyroxene).

3. Terrestrial cosmogenic nuclide profile dating using ^{36}Cl isotopes. These analyses are being performed by the PRIME Lab at Purdue University (Lafayette, Indiana) and the modeling work is being done in cooperation with Fred Phillips of New Mexico Institute of Mining and Technology (Socorro). This technique (see Gosse and Phillips, 2001) uses small gravel clasts collected through a vertical profile at least 2–3 m deep, and it can date deposits as old as 300 ka.

4. Experimental U/Th dating using a laser-ablation mass-spectrometer techniques (see Sharp and others, 2005). These analyses are being done as part of a cooperative project with Warren Sharp at the University of California at Berkeley Geoscience Center. This technique uses calcium-carbonate rinds on the bases of large clasts. The best rinds are typically in the Bk horizon of a thick calcic soil. The technique can date deposits as old as 750 ka if they have small amounts of detrital thorium, are dense (not porous), and are a closed system (for example, no dissolution and reprecipitation).

At the time this report was written (spring 2007), only the surface-exposure dating using ^{3}He isotopes had been completed. This technique yielded an age of about 439±6 ka for the boulder; thus, for the purposes of discussions of Lake Alamosa we use a time of 440 ka for its overflow and lowering.

Stop B3.3 — Upper Spit, ^{3}He Surface-Exposure Dating

Location: 1-m-diameter basalt boulder on upper spit
Pikes Stockade 7.5' quadrangle (Station PS–MM05–72)
GPS: NAD27, Zone 13, 425353 m E., 4125111 m N.
Elevation: 7,650 ft (2,332 m) asl

Overview

The upper spit has a large number of basalt boulders at the surface but most of them have been eroded by sand blasting (formation of ventifacts), or may have been split or spalled by weathering processes such as freeze-thaw, fires, or thermal expansion. The largest unweathered-appearing boulder on this upper spit is located about 220 m east of the soil pit (stop B3.2). Cosmogenic surface-exposure dating of this single 1-m diameter, best-candidate boulder (sample PS–MM05–72He) yielded a ^{3}He age of 439±6 ka, which should reflect the length of time that this boulder has been exposed to cosmic radiation and thus provide a minimum time for the overflow and draining of Lake Alamosa.

Figure B3.3–1. Largest boulder on the upper spit of Saddleback Mountain. The upper 2–3 cm (left of the GPS receiver) of this 1-m-wide boulder was sampled for ^{3}He surface-exposure dating. Notebook (15 x 25 cm) for scale. Sample locality is shown on figures B3–1 and B3–2.

^{3}He Surface Exposure Dating—Results

Although the other dating results (see below) are still pending, we have been able to date the upper spit at Saddleback Mountain (stop B3.3) using ^{3}He isotopes. At this locality, the spits are composed almost entirely of reworked basalt boulders and lacustrine silty sand. The basalt boulders start out as angular blocks, but they are rounded and abraded in the surf zone as they are transported (slowly) around the west side of the Saddleback Mountain, a minimum of about 400 m to 1 km. The largest exposed basalt boulder is 1 m in diameter (fig. B3.3–1), of which 30–40 cm is exposed above the ground surface. The basalt boulders have mineralogy suitable for ^{3}He dating since they contain phenocrysts of olivine and pyroxene, two minerals that retain cosmogenic He isotopes. At least three sources of error common to surface exposure dating could be at play here:

1. Inheritance of ^{3}He isotopes from rock surfaces that were exposed to cosmic radiation—this makes reported ages too old,
2. Excessive erosion of a boulder surface (owing to various processes)—this makes reported ages too young, and
3. Shielding of a boulder surface (by snow or sand)—this makes reported ages too young.

Various strategies are employed to minimize or eliminate these potential errors, such as selecting long-transported boulders (error source 1), selecting rounded, nonpitted, or fresh-appearing boulders (error source), and selecting large (high) boulders in areas of minimum sand cover. We believe that we selected the best possible boulder for dating on these spits; however, a larger dated number of boulders (such as 6–8) would allow us to see if there is a preferred exposure age. Since so few boulders are candidates for this method, we have pursued other allied dating techniques (see following discussion).

A pyroxene separate from the surface of the large boulder (sample PS–MM05–72He) yielded a preliminary ^{3}He exposure age of 439±6 ka. This age was determined using the total ^{3}He concentration and an absolute ^{3}He production rate of 116 atoms gram^{-1} year^{-1} (Licciardi and others, 1999) that was scaled to the sample's altitude and latitude using Lal (1991) (see table B3.3–1). Pyroxenes from rocks with older (>1–2 Ma) crystallization ages can have significant noncosmogenic ^{3}He from nucleogenic reactions on ^{6}Li (^{6}Li (n, α) ^{3}H$\rightarrow^3$He). Marchetti and Cerling (2005) and Marchetti and others (2005) used samples shielded from cosmic radiation to account for noncosmogenic ^{3}He in pyroxenes from intermediate volcanic rocks exposed on the western edge of the Colorado Plateaus Province in Utah.

The volcanic rocks in those studies are remarkably similar in terms of crystallization age (~25 Ma) and petrology to the sample we dated in this study (~26 Ma; Hinsdale Formation, unit Th on fig. B3–1). Applying the ^{3}He/^{4}He shielded correction of Marchetti and others (2005) to the He data of the sample in this study changes the exposure age only slightly, from 439 to 431±6 ka (see table B3.3–2), and does not change our interpretation of the age of the spits. A more complete discussion of ^{3}He surface-exposure dating is included in chapter G, this volume.

Table B3.3–1. Sampling data for ^{3}He surface-exposure dating of basalt at stop B3.3.

Sample	Latitude (N)	Longitude (W)	Altitude (m)	Topo shielding factor	Self-shielding factor	Total shielding factor	^{3}He Production Rate (atoms g^{-1} year^{-1})*
PS-MM05-72c	37.262416	105.842416	2324	0.999	0.942	0.941	598

*Determined using an absolute ^{3}He production rate of 116 atoms g^{-1} yr^{-1} (Licciardi et al., 1999) that was scaled using Lal (1991). No corrections for potential snow shielding were applied to the production rate.

Table B3.3–2. He isotope data for cosmogenic surface-exposure dating of basalt at stop B3.3.

Sample	$^4He_{total}$ (10^{12} atoms g^{-1})	$^3He_{total}$ (10^6 atoms g^{-1})	$^3He/^4He$ fusion	^3He_c (10^6 atoms g^{-1})	^3He_c %	Exposure age (ka) ± 2σ
PS-MM05-72c	22.92±0.06	262.5±3.5	1.15 x 10^{-5}	262.5±3.5	100	**439 ± 6**
PS-MM05-72c*	22.92±0.06	262.5±3.5	1.15 x 10^{-5}	257.7±3.5	98.2	**431 ± 6**

*Sample corrected using an estimated $^3He/^4He$ correction. The ^3He_c (cosmogenic) component was determined using the following relationship: $^3He_c = {}^3He_{total} - ({}^4He_{total} \times {}^3He/^4He_{shielded})$. Where the $^3He/^4He_{shielded}$ is from Marchetti et al. (2005), and is 2.08x10^{-6}.

Conclusions

Using the ^{3}He surface exposure date of 439 ka, we conclude that the upper spit at Saddleback Mountain was deposited at about 440 ka, which roughly corresponds with the glaciation during marine oxygen-isotope stage 12 which, in turn, appears to have ended between 452 ka and 427 ka (see chapter G). Marine oxygen-isotope stage 12 is associated with one of coldest glacial climates and, by inference, most extensive glaciations in North America (see fig. G–5, chapter G, this volume). The age of 440 ka should reflect the time since this boulder was exposed to cosmic radiation, and thus it provides a minimum time for the overflow and draining of Lake Alamosa.

Stop B4 — Overview of the Rio Grande Outlet

Speakers: Michael Machette and Ren Thompson
Location: Overlook, east of BLM Road 5003, west side of Rio Grande, about 3.6 mi (5.8 km) south of Lasauses, Colo.; about 1.5 mi southeast of Lasauses Cemetery
Mesito Reservoir 7.5' quadrangle
GPS: NAD27, Zone 13, 433780 m E., 4118190 m N.
Elevation: 7,610 ft (2,319 m) asl (turn around point overlooking river)

Synopsis

This scenic overview of the Rio Grande is located near the overflow point of Lake Alamosa. The gap between the Fairy Hills and Brownie Hills to the south of here is the lowest point in the San Luis Hills, and thus it represented the first opportunity for a rising Lake Alamosa to overtop a hydrologic sill. Overflow of the lake through the Fairy Hills cut a deep, narrow gorge and allowed the lake waters to drain southward across the Costilla Plain and northern Taos Plateau, eventually joining the Red River and Rio Grande, west of Questa, N. Mex. In addition, stop 4 is near the point where Jacob Fowler described the first account of Lake Alamosa—in 1811–12.

On the route to our lunch stop (B4), we drove uphill and across a bedrock-cored saddle, just north of stop B4.1. This saddle is covered with small rounded pebbles of reworked volcanic rock from the adjacent slopes. These gravels represent low-energy, beach (shoreline) deposits of Lake Alamosa at its highest stand (about 7,660 ft or 2,335 m asl). A soil pit excavated about 20 m west of this gravel road exposed sandy

pebble to small cobble gravel that was deposited just offshore (west of) the highest shoreline. Further west, gullies expose fine-grained sand, silt, and marl that represent deeper water, offshore deposits (Alamosa Formation) of Lake Alamosa.

Discussion

Our lunch site on this small rounded hill of Tertiary volcanic rock provides a popular and scenic overview of the Rio Grande, opposite the Indian Cave. Here, we are located near the overflow point of Lake Alamosa and below a bedrock sill (to the west of the fork in BLM Road 5003) at about 7,650 ft (2,332 m) asl. This sill is devoid of gravel, probably having been swept clean during the overflow of the lake. About a half mile (0.8 km) north (at optional stop 4.1), abundant well-rounded pebbles attest to wave action and shoreline erosion at elevations of 7,650–7,660 ft (2,332–2,335 m) asl, which is about 185 ft (56 m) above the present river channel.

The gap between the Fairy Hills and Brownie Hills is the lowest point in the San Luis Hills, and thus it represented the first opportunity for a rising Lake Alamosa to overtop a hydrologic sill. Overflow of the lake though the Fairy Hills cut a deep, narrow gorge and allowed the lake waters to drain southward across the Costilla Plain and northern Taos Plateau, eventually joining the Red River and Rio Grande, west of Questa, N. Mex.

In 1821–22, Jacob Fowler made his way up the Rio Grande on a hunting and trapping expedition. This expedition preceded those of pioneer scientists and geographers such as Hayden and Powell by more than 50 years and settlement of the area by about 30 years. (San Luis, the oldest town in Colorado, was established in 1854.) Fowler was obviously a keen observer of topography and geography. His journals include this prescient passage that is particularly relevant to our lunch stop, probably near where he recorded the following note (from Siebenthal, 1910, p. 112–114).

> *"I Have no doubt but the River from the Head of those Rocks up for about one Hundred miles Has once been a lake of about from forty to fifty miles Wide and about two Hundred feet deep—and that the running and dashing of the Watter Has Woren a Way the Rocks So as to form the present Chanel."*

We suspect that Jacob Flower made this observation from the San Luis Hills (probably in the Fairy Hills, above the river's gorge near here), looking north into the upper San Luis Valley. Jacob accurately estimated the size, depth and overflow history of the lake—185 years ago (see chapter G for a full discussion of Lake Alamosa).

A half century later, in 1875, F.V. Hayden led a team of scientists through the San Luis Valley. In his report dated 1877, geologist F.M. Endlich (1877) reports the following about the valley (our additions are in brackets):

> *"Judging from the evident deflection of rivers, the failure of mountain-streams to carry specimens of the rock through which they pass into the valley for any distance, . . . and the cañoned outlet of the Rio Grande, I have come to the conclusion that at one time San Luis Valley was covered by two large lakes, the northern and the southern* [there is no evidence for a southern lake on the Costilla Plain]. *These I have named . . . Coronado's Lakes. Of these the former covered about 1,400 square miles [3,626 km^2]; the latter 300 square miles* [777 km^2]. *I have alluded to the cañon near station 105, cut through the trachyte* [Conejos Formation]. *It is about three miles* [5 km] *in length, and its general direction is perfectly straight. In case that narrow passage* [gorge through the Fairy-Brownie Hills], *which I assume to have been opened by seismic force, should be closed today, the result would be an accumulation of water in the northern end of the San Luis Valley, the formation of a lake. This lake would reach a certain depth of water, consequently increase in area until the slight rise southwest of Fort Garland would be overcome, and it would flow over into the southern region* [Costilla Plain] . . . . *It may seem curious that no heavy deposits of alkali or old 'shore-lines' mark the presence of these ancient lakes. If, however, the assumption that the Grande found a sudden egress through the deep fissure produced by a volcanic earthquake is true, there is no reason why the waters should not have flown off by far too rapidly to permit of the formation of either . . ." (p. 147 in Hayden's 1875 "Ninth Annual Report" dated 1877).*

Not surprisingly, many of the details reported by the Hayden team have proved wrong, such as the presence of a southern lake, eastern flow path for the Rio Grande, and lack of shoreline (related) features, but Hayden accurately suspected that fault weakened rocks led to quick and easy erosion of the canyon through the Fairy–Brownie Hills. It seems unlikely that an earthquake caused a fissure and sudden draining of the lake, but rather that the discharge was the result of a rising lake that overtopped a natural bedrock sill during pluvial conditions (see chapter G).

Local Geology

Upper Oligocene intrusive and extrusive rocks of the Conejos Formation (fig. B4–1) dominate the bedrock geology in the San Luis Hills (see also Thompson and Machette, 1989). These hills are the surface expression of a large northeast-southwest-trending horst that divides the sedimentary fill of

the San Luis Basin into subbasins. To the north of the hills, the Alamosa subbasin is primarily an east-tilted half graben, although seismic reflection and geophysical data show internal complications (such as two grabens and an intervening horst). To the southeast of the San Luis Hills, the Costilla subbasin extends into New Mexico as far south as Questa. The Costilla subbasin contains the Culebra graben on the east (Fort Garland south to Sanchez Reservoir), San Pedro Mesa (a Precambrian-cored Miocene horst) and the Costilla Plain on the west. We will traverse the Costilla Plains later today (stops B8 and B9).

The lower part of the Conejos Formation is exposed throughout the Fairy and Brownie Hills. Most of the bedrock is 29- to 30-Ma andesitic to porphyritic dacite flows, but dacite dikes with north to north-northeast trends are common (note a prominent weathered dike along BLM Road 5003 on our way south from this stop; fig. B4–2). Although unmapped by Thompson and Machette (1989), Burroughs (1972) mentioned a major north-south-trending Neogene fault (the Lasauses fault) that parallels the course of the Rio Grande. There is little stratigraphic evidence for this fault (Conejos against Conejos). However, extensive subparallel dikes and hydrothermally altered rock in this area seem to support extensive deformation and weakening of the bedrock (Conejos Formation) in the eventual outlet area for Lake Alamosa.

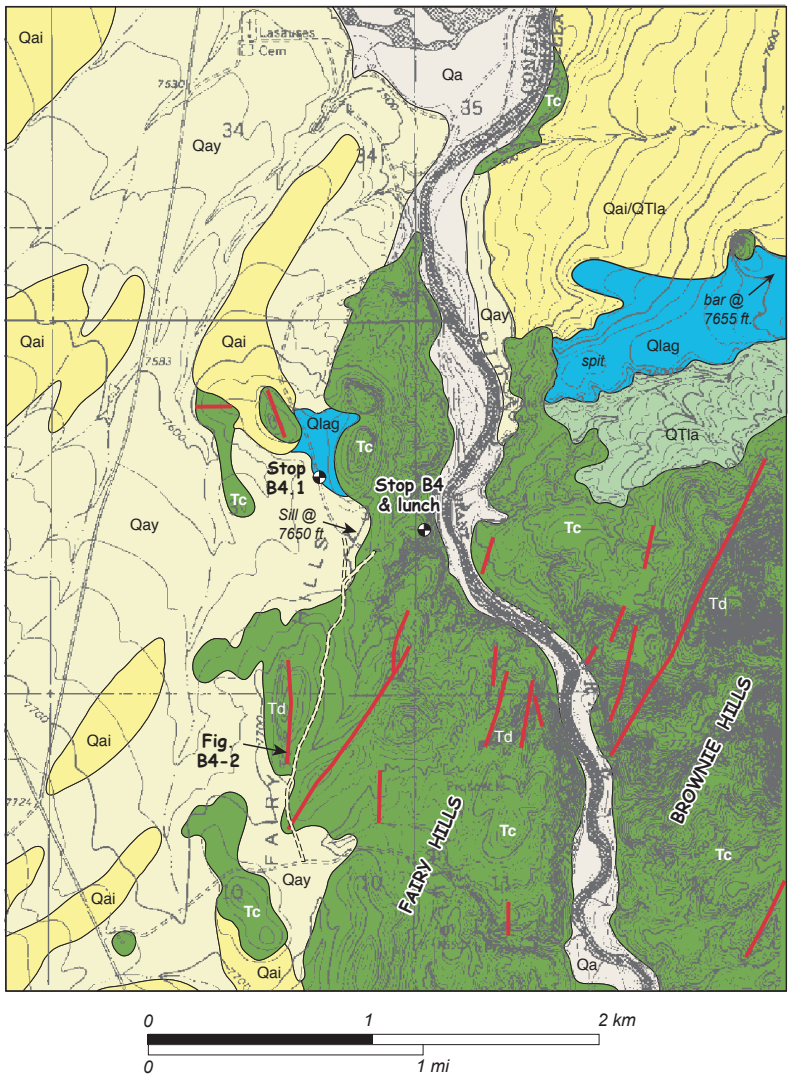

Figure B4–1. Bedrock and surficial deposits near the overflow threshold (sill) of Lake Alamosa and canyon that the Rio Grande cut through the Fairy and Brownie Hills. Map units: Qa, Holocene alluvium; Qay, younger (latest Pleistocene) alluvium; Qai, intermediate alluvium (middle Pleistocene) ; Qlag, near-shore, coarse-grained deposits of Lake Alamosa (uppermost part of unit QTla); QTla, Alamosa Formation (undivided, middle Pleistocene to Pliocene); Tc and Td (dikes) of the Conejos Formation (29–30 Ma). Bedrock geology modified from Thompson and Machette (1989), surficial geology simplified from Machette and Thompson (2005). Base from Manassa NE and Mesito Reservoir quadrangles.

Before an outlet for the lake was carved through the San Luis Hills, they were a formidable barrier to southward-flowing streams. The rocks of the San Luis horst extend from near Antonito on the southwest to about 5 mi (8 km) southwest of Blanca on the northeast. In essence, these hills blocked the entire south margin of the Alamosa subbasin. In addition, eruption of theoliitic flood basalts (for example, the Servilleta Basalt) from 4.8 to 3.7 Ma also blocked possible southward drainage (or drainages) from the San Luis Basin. These flows extended north from the Taos Plateau at least to the areas of La Jara on the west and Fort Garland on the east. Thus, by middle Pliocene time (about 3.5 Ma), drainage southward from the Alamosa subbasin was blocked across the entire width of the San Luis Valley (fig. G–6, chapter G, this volume). Although it is undated, we assume that the lacustrine sediment at the base of the Alamosa Formation is at least this old (3.5 Ma).

Sedimentation in the closed Alamosa subbasin led to aggradation of the basin floor, although Pliocene to Pleistocene movement on the Sangre de Cristo fault system probably continued to keep the eastern side of the basin somewhat lower. As with classic, one-sided grabens (such as Death Valley), fans on the passive (west) side of the San Luis Valley are very large, whereas the east-side fans tend to be more compact owing to downdropping and continued burial.

By middle Pleistocene time, Lake Alamosa had grown laterally to such an extent that it occupied most of the Alamosa subbasin. The single ^{3}He-exposure date from basalt in the upper spit at stop 3.3 suggests that the lake reached its highest (topographic) level at about 440 ka during oxygen-isotope stage (OIS) 12, which was one of the major continental glaciations in the northern hemisphere (see chapter G for more details and references). At a water level of 7,660 ft (2,335 m asl), Lake Alamosa would have surrounded many of the isolated

Figure B4–2. Weathered dacite dike (upper Oligocene Conejos Formation) in the Fairy Hills. This 5-m-high dike is on the west side of BLM Road 5003, about 1 mile south-southwest of stop B4. View to the west.

hills in this area and formed an embayment into the Fairy-Brownie Hills, as shown in figure B4–3.

From our lunch stop (B4), one would have looked northwest across the Lake Alamosa (fig. B4–4) about 30 mi (48 km) to see the Sangre de Cristo Mountains and Blanca Peak, which at 14,345 ft (4,372 m) asl, is the highest point between Pikes Peak and the San Juan Mountains. At its highest elevation of 7,660 ft (2,335 m) asl, Lake Alamosa would have occupied most of the San Luis Valley north of here. As such, the lake would have been 105 km (65 mi) from north to south and as much as 48 km (30 mi) from west to east (along the route of Highway 160; see chapter G, this volume). The 7,660 ft contour extends west to the Monte Vista Wildlife Refuge and beneath Monte Vista (town), north to a point several miles southwest of Saguache and south of Mineral Hot Springs in the north end of the valley and then south along the east margin of the valley. The contour is coincident with several natural springs that emerge from the western base of the Great Sand Dunes.

Long Spit, Across River

Due east of stop B4, waves from the lake eroded Tertiary rocks of the Brownie Hills and deposited a long and wide southwest-trending spit that extended into the southernmost bay of the lake. The spit is underlain by sandy well-rounded gravel about 5–15 m thick that rests on a platform of Tertiary volcanic rock. This spit extends west about 1.4 km from an isolated bedrock hill at 7,660 ft (2,335 m) asl to the vicinity of Indian Cave, where the top of the spit is at about 7,620 ft (2,322 m) asl (fig. B4–5). This spit is one of the longest, but not volumetrically largest, in the basin. The largest spit is probably the one on the south side of Sierra Del Ojito, which is located about 5 km east of stop B3 and north of Road W (see mapping of Machette and Thompson, 2005).

Overflow and Erosion

When Lake Alamosa rose to 7,660 ft (2,335 m) asl, water could spill south over the low divide between the Fairy Hills (on the west) and the Brownie Hills (on the east). There may

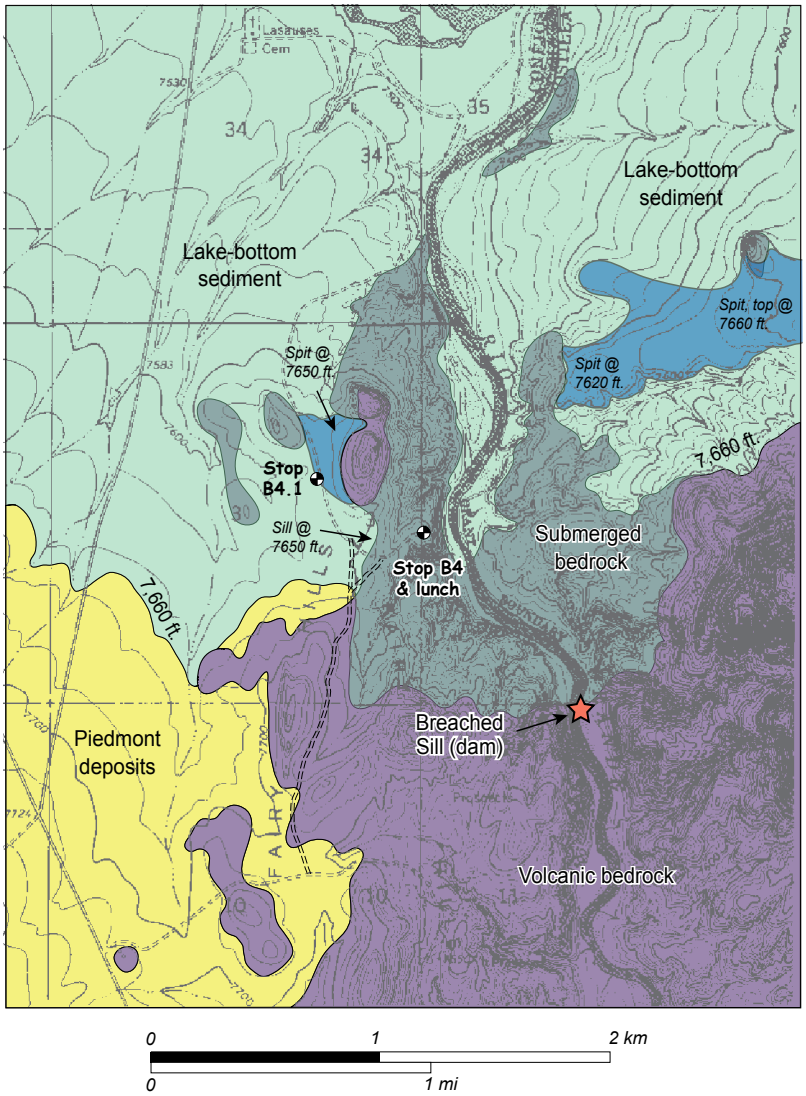

Figure B4–3. Schematic map showing extent of bedrock, surficial, and lacustrine deposits at highest (overflow) level of Lake Alamosa, about 7,660 ft, prior to overflow. Stop B4.1 is a drive by, past the site of a trench in sandy spit deposits. A threshold sill floored by bedrock is crossed before dropping into the canyon for stop B4. Base map scanned from Manassa NE and Mesito Reservoir quadrangles.

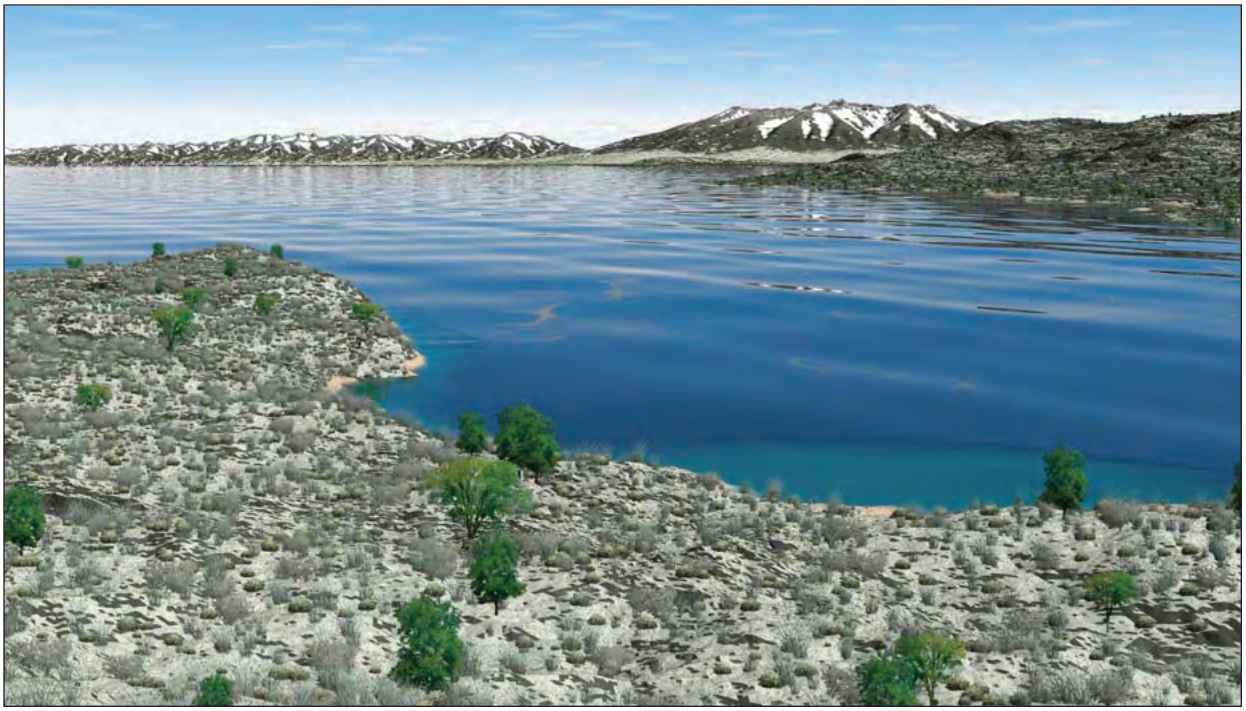

Figure B4–4. Re-creation of Lake Alamosa. View to the northeast from the area of stop B4. Highest peak in the background is Blanca Peak at 14,345 ft asl. Visualization created in Visual Nature Studio (v. 2.7, 3D Nature Co.) by Paco Van Sistine (USGS) using 30-m DEM and a lake elevation of 7,660 ft (2,335 m).

Figure B4–5. Long, west-sloping spit of Lake Alamosa. Top of spit descends from 7,660 ft at head to 7,620 ft at toe, above the "Indian Cave." View to the east with the eastern portion of the San Luis Hills in the middle ground and Blanca Peak in the background (upper left).

have been several pathways to the south, one of which is now abandoned but intact at the top of the hill to the west of us (fig. B4–3, sill at 7,650 ft or 2,332 m asl). This sill has no gravel on it, now, probably owing to scouring. The southward-flowing water must have found a softer avenue (along the river's present course) and cut a deep gorge through the Tertiary volcanic rock (fig. B4–6). We don't know how deeply or how quickly the gorge was cut, but there are several lines of evidence to suggest it was cut quickly and rather deeply.

First, in most cases the preserved barrier bars, lagoons (see stop B7), and spits (stops B3 and B4) are preserved at a very restricted range of elevations—typically 7,640–7,670 ft (2,329–2,337 m) asl. The highest ones are located in the southeastern part of the basin (south of stop B5), where storm surge coupled with wave action generated by the lake's long fetch may have formed higher than normal shorelines. Where multiple shoreline features are preserved (for example, the two spits at stop B3 or the two stacked bars and lagoons at stop B7), they are constructional features that are typically related to lake transgression rather than regression. Also, the Alamosa subbasin lacks the repetitious shorelines characteristic of slow drawdown, such as between the Provo and Gilbert shorelines of latest Pleistocene Lake Bonneville that Machette had previously mapped in Utah Valley (Utah).

Second, the isolated topographic ridges associated with intermediate-age (unit Qai) alluvial channels (stops B1 and B2) are graded to base levels that are relatively low

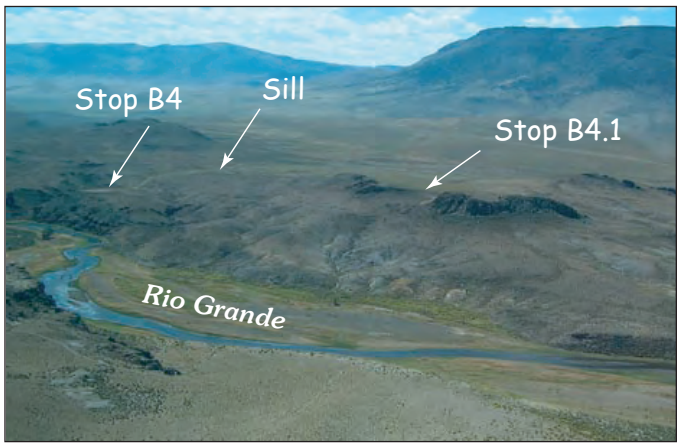

Figure B4–6. Canyon of the Rio Grande in the Fairy Hills, south of Lasauses. The sill, at 7,650 ft, is 185 ft (56 m) above the Rio Grande (elev. 7,465 ft here). View to the southwest; western portion of San Luis Hills in the background.

(7,530–7,540 ft or 2,295–2,298 m asl), perhaps only 30–40 ft (9–12 m) above the present channel of the Rio Grande. If these channels formed in response to lake lowering, then the canyon of the Rio Grande must have been cut deeply as a result of overtopping, perhaps excavating as much as 45 m of the 55 m of relief between the Lake Alamosa overflow and present river level.

Finally, although we suspect a catastrophic draining of the lake, we don't know if this was accomplished in a month, a year, a decade, or a hundred years. Nevertheless, it was probably accomplished in just a "moment of geologic time." O'Connor (1992) reports that the catastrophic overflow of Lake Bonneville and coincident downcutting through Red Rock Pass (about 108 m, Currey, 1990) might have been accomplished in as little as a month. Surely, the cutting associated with Lake Alamosa's overflow took longer since the entire gorge is in Tertiary bedrock, whereas much of the cutting at Red Rocks Pass was through surficial deposits and into bedrock. Although Lake Bonneville was several orders of magnitude larger than Lake Alamosa and thus had a much greater volume of water for cutting, we consider both events to be geologically instantaneous.

Interestingly, we have not found large-scale outbreak deposits along the Rio Grande to the south, which are characteristic of the Bonneville flood across the Snake River Plain. There is one feature that might be suggestive of catastrophic overflow from Lake Alamosa. Where the Rio Grande leaves the San Luis Hills and enters the Costilla Plain, the intermediate-age (post Lake Alamosa) terraces of the river (units Qam1 and Qam2 of Thomson and Machette, 1989) become extremely wide. In map pattern, these terraces suggest that the Rio Grande excavated widely and deeply into older alluvium (unit Qao) and the underlying Santa Fe Group sediment (unit QTsf) before flowing south across and cutting into Pliocene Servilleta Basalt of the Taos Plateau.

Path of the Rio Grande

Prior to overflow of Lake Alamosa, the Rio Grande probably had its headwaters in the present Red River basin (see Wells and others, 1987). Streams draining from the Sangre de Cristo Mountains north of Questa to San Luis probably drained out into Sunshine Valley and the Costilla Plain, both of which were largely closed or poorly drained basins (see field-trip discussions in chapter C and discussion of the Rio Grande in chapter G).

The modern Rio Grande north of Questa probably has been in the same channel since Lake Alamosa overflowed in middle Pleistocene time (440 ka) owing to progressive incision through the Servilleta Basalt. Upon exiting the Fairy Hills, the overflow entered the lower, southward-flowing part of Culebra Creek (where the bridge on Highway 142 crosses the present Rio Grande, fig. B–1 and B–3). From here, the overflow took a southerly route following the lowest ground between the southwest-sloping Costilla Plain and the southeast-sloping piedmonts of the San Luis Hills. Santa Fe Group basin-fill sediment containing abundant Precambrian clasts extends across the entire Costilla Plain and into Punche Valley, west of the present Rio Grande, indicating that the Santa Fe sediment and the unconformable cap of older gravel (unit Qao) that forms the Costilla Plain predates overflow of the lake. At the south end of the Costilla Plain (near the New Mexico–Colorado border), the overflowing lake water excavated basin-fill sediment and exhumed some previously buried Servilleta Basalt. The overflow continued to the south, generally taking a course along east margin of the east-dipping Servilleta Basalt (see stops C2 and C3). Finally, the overflow coursed between Cerro Chieflo and Guadalupe Mountain (near Cerro, N. Mex.) and entered the canyon of the Rio Grande (Red River) at La Junta Point (stop C1). At 440 ka, this river junction had the same geometry, but the Rio Grande above the junction may have looked much like the present day Niagara Falls. Since 440 ka, the falls have migrated headward about 10 km north as evidence by a 180-m-high steepened gradient (ancient knickpoint) in the Rio Grande (Wells and others, 1987). North of Cerro Chieflo, the modern Rio Grande has a shallower gorge that extends north into Colorado along a much shallower gradient.

Stop B4.1 (Optional) — Rounded Pebble Gravel of Lake Alamosa, Filled Soil Pit

Location: BLM Road 5003, west side of Rio Grande, about 1 mi (1.6 km) southeast of Lasauses Cemetery
Manassas NE 7.5' quadrangle (Station MNE–MM04–33a)
GPS: NAD27, Zone 13, 425136 m E., 4124048 m N.
Elevation: 7,650 ft (2,332 m) asl (just below maximum shoreline at 7,660 ft or 2,335 m asl)

Synopsis

This general area has well-rounded pebble gravels eroded from Tertiary volcanic rocks that form a sill for Lake Alamosa. The highest gravels are found along and slightly (5 m) above this part of BLM Road 5003. They record a maximum lake level of about 7,650–7,660 ft (2,332–2,335 m) asl, which is consistent with the elevations of barrier-bar lagoons to the northeast (optional stop B6). A soil pit was excavated about 20 m (65 ft) west of the road for cosmogenic nuclide dating, but the soil in the pit was extensively bioturbated and thus unsuitable for sampling. Nevertheless, the pit revealed very sandy pebble to small-cobble gravel that was deposited in a near-shore (shallow) beach environment.

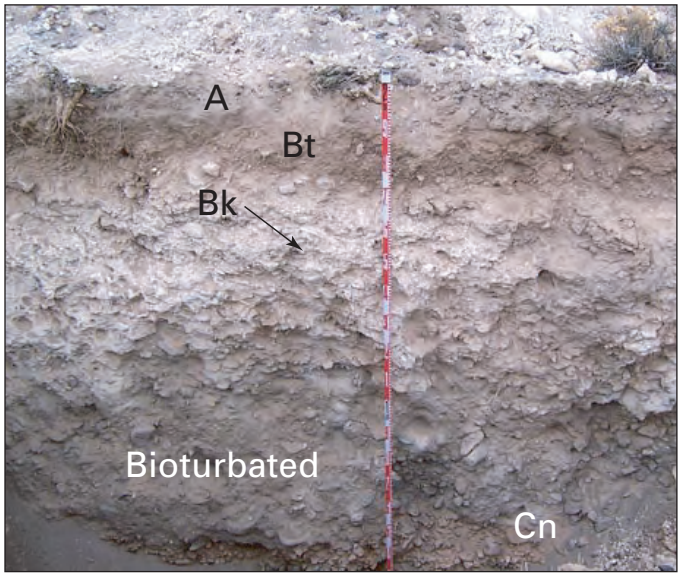

Figure B4.1–1. Strong calcic soil developed on sandy gravel at stop B4.1. This pit was not sampled for cosmogenic dating owing to extensive bioturbation of the lower part of the soil. Nevertheless, the Bk horizon is an indicator of middle Pleistocene age. Tape measure is extended 1.6 m in this view.

Discussion

On the route to the lunch stop (B4), we climbed uphill and crossed a bedrock-cored saddle just north of stop B4.1. This saddle is covered with small rounded pebbles (generally <2 cm in diameter) of locally reworked volcanic rocks. These gravels represent nearshore (shallow) beach deposits of Lake Alamosa at its highest stand (about 7,660 ft or 2,335 m asl).

A soil pit excavated along this gravel road exposed sandy pebble to small-cobble gravel (fig. B4.1–1) that was deposited just offshore (west of) the high shoreline. Further west and topographically lower, stream gullies expose fine-grained sand, silts and marls that represent deeper water deposits (Alamosa Formation) of Lake Alamosa.

The calcic soil in this pit (table B4.1–1) showed development comparable to that at stop B3 (the upper and lower spits). The calcic part of the soil (Bk horizon) extends from 41 cm to 194 cm (1.5 m thick), but it appears to have engulfed a former Bt horizon (see clay contents for 22–93 cm, table B4.1–1). Some of this clay is probably from loess (similar to the present A horizon) that was incorporated into the sandy gravel parent material, but some may be pedogenic since clay films were noted on ped faces and in pores. We described this soil but didn't sample it for physical analyses or cosmogenic dating owing to extensive bioturbation. The strength, thickness, and morphology of the Btk and Bk horizons are similar to the soils in similar age deposits at stop B3 (the upper and lower spits).

Table B4.1–1.Soil profile on sandy gravels at stop B4.1

Depth (cm)	Horizon	Soil texture	Estimated clay content (percent)	Ca CO_3 morphology	Color, <2 mm, dry	Geologic origin
0–22	A	Loam	13	Stage I	*10YR4/2*	Loess
22–41	Btk1	Gravelly loam	22	Stage II	*10YR5/3*	Lacustrine
41–93	Btk2	Gravelly sandy loam	20	Stage III	*10YR5/2*	Lacustrine
93–141	Bk3	Gravelly loamy sand	4	Stage III	*10YR6/2*	Lacustrine, horizon is bioturbated
141–194	Bk4	Gravelly loamy fine sand	4	Stage II–III	*10YR5/3*	Lacustrine, horizon is bioturbated
194+	2Cn	Fine sand to gravelly fine sand	2	Stage I or none	*10YR3/2*	Sand and sandy gravel beds (lacustrine)

Stop B5 (Optional) — Lagoons and Barrier Bars of Ancient Lake Alamosa

Author: Michael Machette

Location: Appleblossum Lane (north-south) and 24th Street N (east-west), Trinchera Creek Estates; about 8 mi (13 km) southwest of Blanca, Colo.
Blanca SE 7.5' quadrangle (BSE–MM05–67)
GPS: NAD27, Zone 13, 446639 m E., 4132967 m N.
Elevation: 7,650 ft (2,332 m) asl (at road intersection)

Synopsis

From this road intersection, you can see two sets of bay-mouth barrier bars that have blocked a north-trending shallow stream valley. The bars impounded the drainage and formed lagoons, which have been playas since Lake Alamosa was drained. The lower bar (to the north of us) has elevations of 7,645–7,655 ft (2,310–2,333 m) asl and declines in height from northeast to southwest, in the direction of its propagation. The upper bar (the Appleblossum bar) spans the stream valley and has a medial east-west elevation of about 7,662 ft (2,312 m) asl; it is attached to bedrock that borders the valley on both ends. A soil pit excavated on the crest of this bar penetrated sandy, well-rounded pebble to boulder gravel and laminated sands, all of which were deposited in shallow water. The soil on this barrier bar has a discontinuous 65-cm-thick Bk horizon, and it is not as well developed as the soils on the upper and lower spits of Saddle Mountain (stop B3) or in shoreline deposits in the Fairly Hills (stop B4.1). A second, exploratory pit on the margin of the playa south of the Appleblossum bar exposed unbedded silt and sand that is extensively bioturbated.

Discussion

This stop is located along the southeast margin of ancient Lake Alamosa, about 13 mi (20 km) northeast of the lake's outlet (stop B4). We were first attracted to this area by unusual topographic features that are near the highest shorelines of Lake Alamosa, specifically between about 7,640 ft (2,329 m) and 7,665 ft (2,336 m) asl (fig. B5–1). This area is covered by the northwestern part of the Blanca SE 7.5-minute topographic map, which has 10-ft contours. We first noted numerous closed depressions, typically 5–10 ft deep, but locally as much as 20 ft deep. Closed depressions can be formed by numerous processes, such as dissolution (sinkholes), eolian deflation (blowouts), or blockage (by volcanic flows, debris flows, sand dunes, or lacustrine spits and bars).

The first two processes—solution collapse and deflation—seemed unreasonable because the surficial deposits in this area are typically sand and gravel (alluvium) and underlain by a platform of volcanic rock (upper Oligocene Conejos Formation as mapped by Michael Machette and Ren Thompson, unpub. mapping, 2007). Thus, we conclude that these closed depressions were formed by blockage by lacustrine spits and bars related to high shorelines of Lake Alamosa. In addition, we are amazed that these easily eroded features could still be so well preserved since their creation in middle Pleistocene time (about 440 ka). In the western United States, geomorphic evidence of ancient lakes in this time range is rarely seen. For example, Reheis and others' (2002) Kirk Bryan Award–winning paper (for 2007) on ancient Pliocene to middle Pleistocene lakes in the western Great Basin documents sedimentary evidence for lakes that are 650 ka and older, but shoreline notches or constructional features (such as bars) were found at only three (of many) locations—Thorne Bar, Lone Mountain, and Lone Tree Hill—all in Nevada (fig. 1, Reheis and others, 2002).

Local Geology

The lacustrine spits, bars, and lagoons are formed along the margin of a series of unnamed bedrock hills composed primarily of andesite flows, breccias, and lahars of the Conejos Formation (about 29–30 Ma, upper Oligocene). Longshore drift along the southern shores of Lake Alamosa built a series of gravelly bars that blocked embayments and valleys that existed before Lake Alamosa rose above about 7,640 ft asl (fig. B5–1). On the north side of the hills (at this stop) the bars were built by west to southwest currents, whereas on the south side of these hills the currents were easterly.

Faint shorelines are preserved on the windward (west and north) side of the hills, but shoreline notches dating from the ancient lake's high stand are completely covered, presumably with eolian sand and bedrock-derived colluvium. At certain times of the day and from certain perspectives, these shorelines are apparent as horizontal breaks in slope and different types of vegetation grow on the sandy colluvium and bare bedrock. For example, on a previous field trip USGS Scientist Emeritus Jim Erdman noticed that spike dropseed *(Sporobolus contractus)*, a cool-season bunchgrass, is "aspect dominant" (the plant that dominates the landscape) on sandy deposits along the shorelines at Saddleback Mountain (Erdman, written commun., 2007). So these breaks in slope and vegetation changes are the most conspicuous signatures of the middle Pleistocene shorelines in the San Luis Valley.

Barrier Bars and Lagoons

In this area, we were interested in trenching one of the bar or lagoon features to characterize the texture and bedding of the deposits, the soils formed on a bar, and to sample underlying lake gravel for cosmogenic dating (^{36}Cl). As you will notice from the topographic map of the area (Blanca SE quadrangle; a portion is shown on fig. B5–1), the area was subdivided for land sales in the 1970s. This scheme is typical of many areas in southern Colorado and New Mexico—potential buyers are

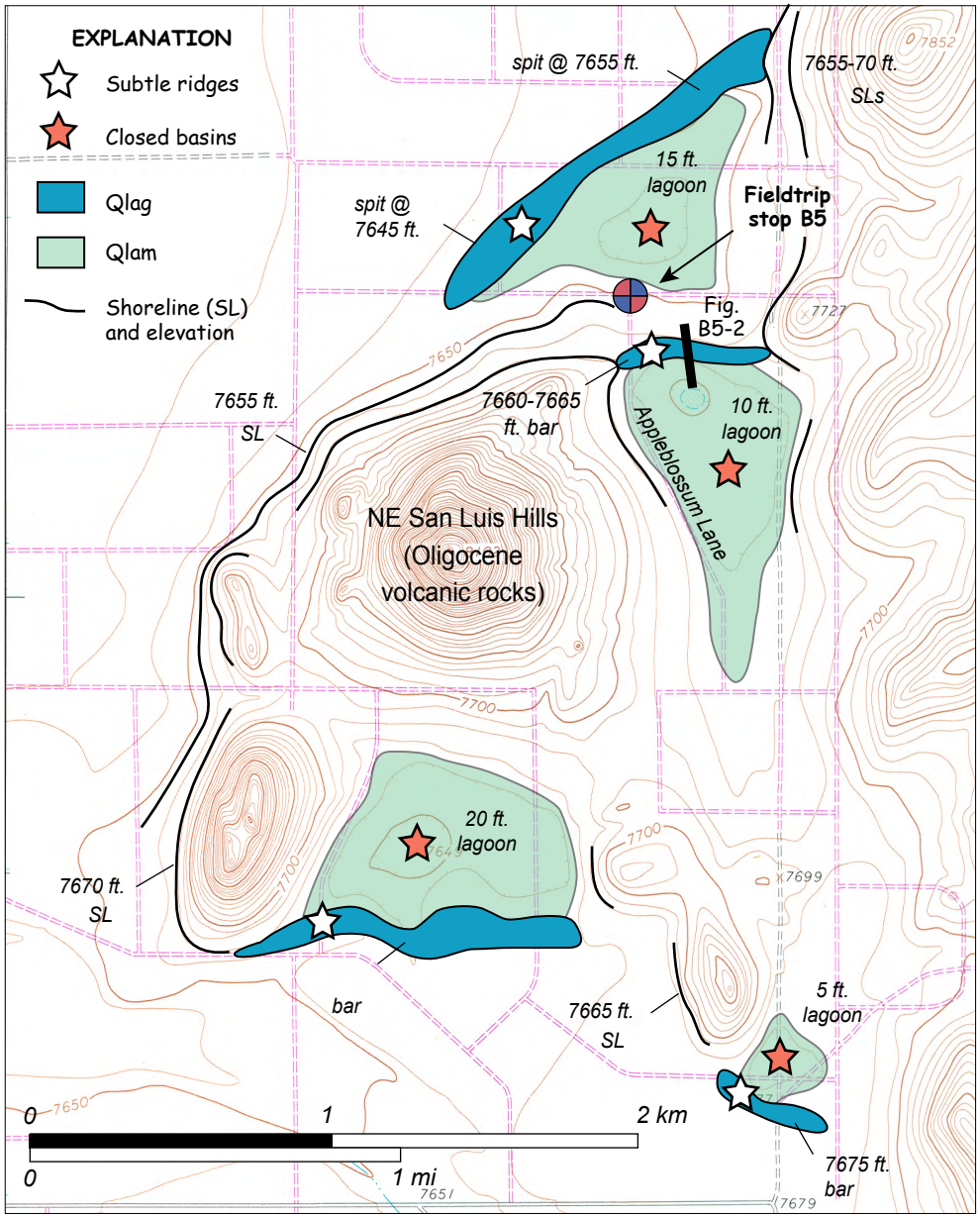

Figure B5–1. Lacustrine features of Lake Alamosa near stop B5. Map unit Qlag is coarse-grained (sandy gravel), whereas unit Qlam is finer grained (sand, silt and clay). Base map scanned from Blanca SE quadrangle.

shown stunning photographs of the mountains (Sangre de Cristo Mountains, 20 km to the east), trout fishing in streams (not here), and so forth, with the lure of inexpensive property for retirement or vacation homes. Look around—now, almost 40 years later and not a neighbor in sight!

In this subdivision tract, which is unit 6 (of 8) in Trinchera Creek Estates, there are no permanent residents or houses. The roads in this development were platted and graded in 1982, 25 years ago. There is no accompanying infrastructure such as water, sewer, power, or phone. In addition, landowners here do not have water rights, so drilling a well is not permitted. As a result, most of these lots (which are typically 5 acres) are not likely to be developed for residential use. Nevertheless, the developer and county officials recognized that closed depressions occasionally hold water that would be a flood hazard. Thus, the three larger and deeper lagoons shown in figure B5–1 were set aside as "Public Use Exempt" land in the development plan. "Public Use Exempt" land is typically used for parks or open areas and these are under county ownership. Even though taxes on these 5-acre parcels are about $30 per year, most of the parcels have been repurchased by local real estate companies or have reverted to county ownership because the owners have defaulted on their taxes. Here is your retirement opportunity and a chance to build a home on the shores of (ancient) Lake Alamosa.

We trenched the crest of the east-west-trending bar here, which is informally named for Appleblossum Lane, the graded dirt road on the west side of the lagoon (fig. B5–1). The pit was about 3 m deep and exposed a strong calcic soil in sandy gravel over laminated sand. The gravelly bar deposits (upper 2.7 m) coarsen downwards, partly as a result of accumulation and incorporation of sandy eolian deposits in the upper meter of the deposits. The lower part of the pit encountered well-laminated silty to sandy deposits that appear to be a backwater (lagoonal) facies. Figure B5–2 shows a schematic cross section through the bay-mouth bar and lagoon that is based on our topographic profile, the pit, and a second trench on the south side of the barrier bar. The second trench exposed massive, bioturbated sandy silts with lenses and stringers of lacustrine gravel. We have interpreted this bar as being deposited as the lake rose in elevation, such that individual gravel packages climb across and bury the southern, leeward slopes of previous bars and intertongue with finer-grained lagoonal deposits.

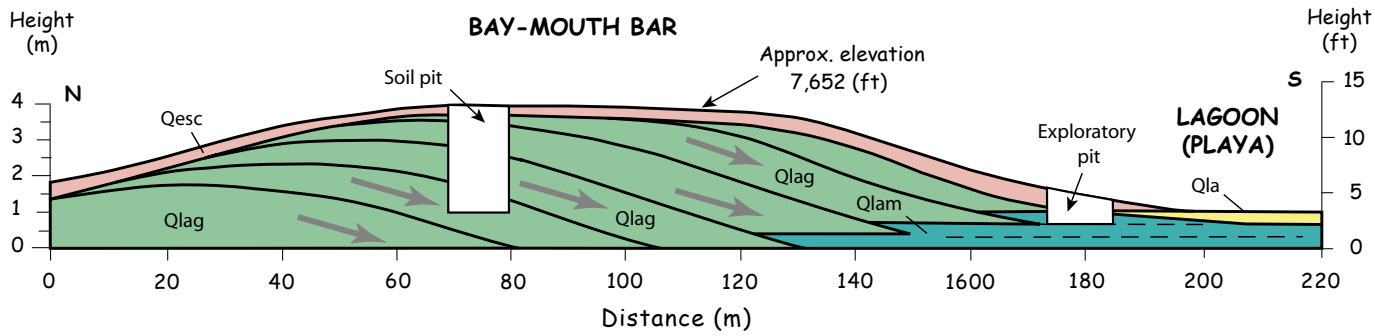

Figure B5–2. Topographic profile and schematic cross section through bay-mouth bar and lagoon at stop B5. Gray arrows show probable direction of transport across bar as it grew to the south. Map units: Qesc, eolian sand and colluvium; Qla, playa deposits; Qlag (coarse-grained) and Qlam (fine-grained), bar deposits of the Alamosa Formation. Topographic profile measured by Robert Schultz (Colorado Division of Water Resources, Mosca) and Harland Goldstein (USGS, Denver) along line shown in fig. B5–1. Vertical exaggeration is about 6x. Geology based on mapping of Michael Machette and Ren Thompson, unpub. mapping, 2007.

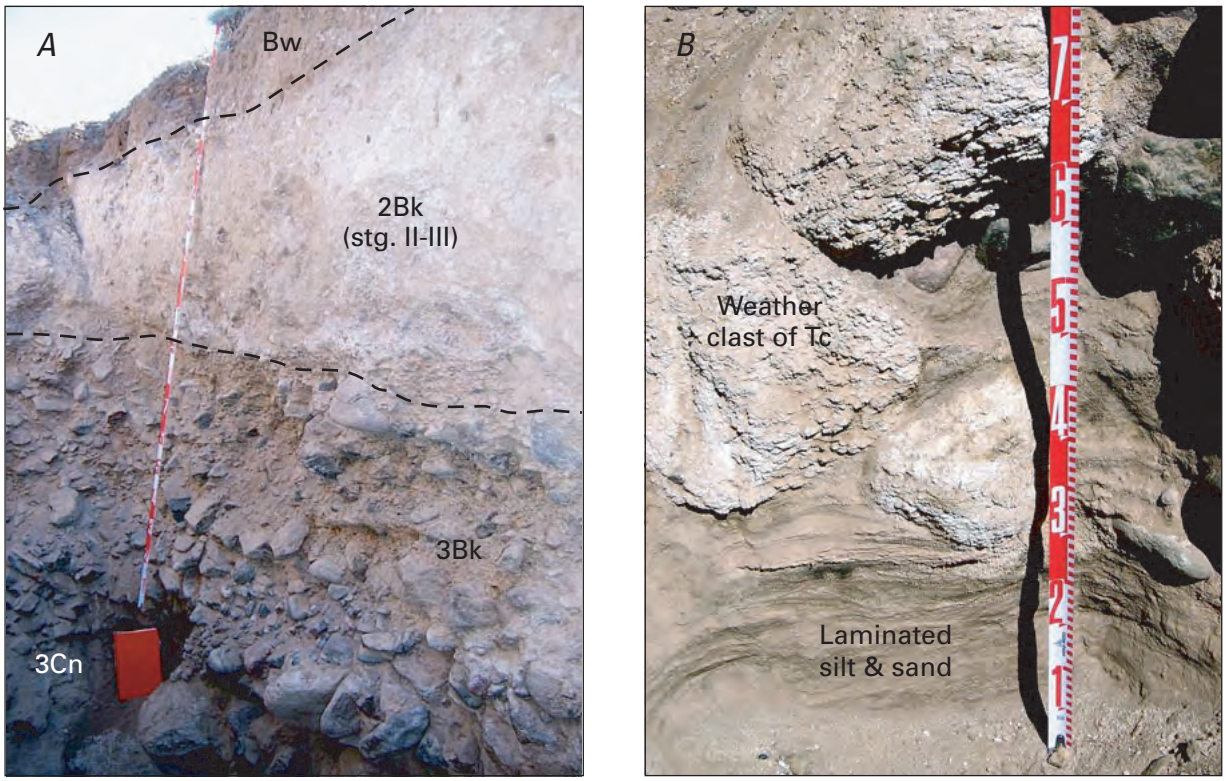

Figure B5–3. Soil pit on upper bay-mouth bar at stop B5. *A* , Calcic soil in upper part of bar deposits. Upper parent material is a gravelly sand; lower parent materials (2 and 3) are sandy, pebble to cobble gravels (subangular to well rounded). Tape measure (2 m long) and field notebook for scale. *B*, Coarse gravel (weathered clasts of unit Tc, Conejos Formation) within and over laminated silt and sand (unit 4) at base of pit.

Soil Pit in Bar

The soil on the Appleblossum Lane bar is not as well developed as soils on the spits at stop B3 or on the spit that formed on the south side of Sierra Del Ojito (see mapping of Machette and Thompson, 2005). The B horizon here is poorly formed (Bw with minor carbonate in lower half; see figs. B5–3A and B5–4). The upper 36 cm of the profile are formed in slightly gravelly sand (mainly eolian), whereas the next 66 cm (down to 100 cm) is formed in sandy pebble gravel (parent material 2). The 2 Bk (and subhorizons) are visibly whitened but have only about 5–7 percent $CaCO_3$ in the <2 mm fraction of the soil, which composes about 75–80 percent of the unit. The low gravel and high sand content of the 2Bk horizon (from 36 to 110 cm) probably reflects burial of the gravel spit and deposition of sand in the final stages of the lake filling. To the south of stop B5, the subtle 1-m-high bar at an elevation of 7,670 ft (2,337 m) asl (fig. B5–1) is the highest lacustrine feature that we have found in the San Luis Valley.

Although the Bk horizon is weakly developed in terms of carbonate and morphology (stage II–III), there is a weak clay bulge (3–4 percent clay, <2 mm fraction) and abundant silt, some of which might have been translocated from the surface or upper horizons (or both). The 2Bk3 horizon (at 78–100 cm) and 3Bk horizon (110 to 145 cm) contain almost 20 percent silt, which is quite a bit for a lacustrine pebbly sand (unit 2) and sandy gravel (unit 3).

Although it is undated, we consider the Appleblossum Lane bar (and similar features shown in fig. B5–1) to have formed at the same time as the spits at Saddleback Mountain (stop B3). They all fall in a restricted elevation range and were deposited as Lake Alamosa rose to its final and highest level (about 7,660 ft or 2,335 m asl) and overflowed its hydrologic sill in the Fairy Hills (stop B4).

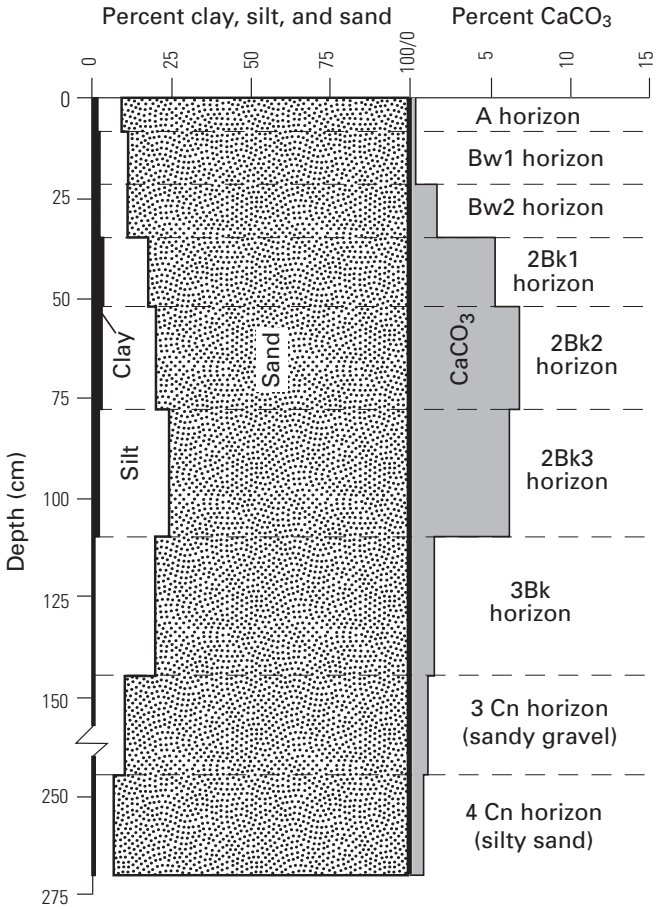

Figure B5–4. Profile data for soil on crest of barrier bar, stop B5. Note break in vertical axis from 160–240 cm (within 3Cn horizon).

Stop B6 (Optional) — And the Wind Blows—Fluted Ventifacts on the Ancient Shore of Lake Alamosa

Author: Michael Machette

Location: Thatcher Road (unmarked), S side of Trinchera Creek, about 8.2 mi (13.2 km) southwest of Blanca, Colo.
Lasauses 7.5' quadrangle (LaS–MM04–38)
GPS: NAD27, Zone 13, 4432787 m E., 4135480 m N.
Elevation: 7,655 ft (2,336 m) (at crest of road)

Synopsis

This ridge of resistant volcanic rocks of the Conejos Formation shows evidence of prolonged erosion from sand blasting (the presence of ventifacts). Finger-size troughs, cones, and broad mullions on the windward and leeward sides of intact bedrock blocks reflect hundreds of thousands of years of wind erosion at a location where sand is available and the wind is funneled into a valley. The base of this ridge was cut by the highest stand of Lake Alamosa (elevation 7,660 ft or 2,335 m asl) at this site, and there is a persistent gravel bench from here south along bedrock hills for at least 1 km on the southeast side of Trinchera Creek. The ridge may have been initially cut as part of the channel of Trinchera Creek, but this cutting would have predated the highest stand of Lake Alamosa, about 440 ka. Ventifacts are present hundreds of meters south and tens of meters above the ridge, thus eliminating water erosion as a significant factor in their formation.

Local Geology

This stop is located on southeast margin of ancient Lake Alamosa at an elevation of 7,660 ft (2,335 m) asl, which is commonly the highest elevation at which we find lacustrine spits (stops B3 and B4), barrier bars and lagoons (stop B5), and eroded shorelines (this stop). The bedrock in this area is upper Oligocene porphyritic andesite flows, breccias, and lahars of the Conejos Formation (unit Tc, fig. B6–1) (Thompson and Machette, 1989). Of these rock types, the flows are particularly resistant to erosion and thus form small hills, buttes, and ridges, such as the one at this stop.

The base of this ridge was cut by the highest stand of Lake Alamosa, and there is a persistent gravel bench from here south for at least 1 km (0.6 mi) on the west side of the hills. Further south, a prominent saddle between hills of volcanic rock is covered with locally derived beach gravel. Shallow road cuts through this gravel show strong calcic soil development (see also stops B3 and B4.1) that supports our inference of a middle Pleistocene age. South of the hills shown in figure B6–1, the lake deposited a long spit (unit Qlag) that extends southwest for at least 1 km on the west side of the hills and south of Trinchera Creek.

Trinchera Creek occupies the narrow valley to the north of this stop and is one of the few eastern tributaries to the Rio Grande that flows on a perennial basis. This stream originates in the Sangre de Cristo Mountains east of Blanca Peak and flows westward through the Garland mesas (southeast of Fort Garland), across the central Sangre de Cristo fault zone, and into the San Luis Basin. There are older (unit Qao), intermediate (unit Qai), and younger terraces (unit Qay) along the margins of Trinchera Creek from near Smith Reservoir (south of Blanca) west to the Rio Grande, a distance of about 13 mi (21 km) (fig. B6–1).

The older alluvium (unit Qao) generally predates the highest stand of Lake Alamosa as mapped by Machette and Thompson (2005) and Michael Machette and Ren Thompson (unpub. mapping, 2007), although some elements of unit Qao may be coeval with the lake. Conversely, the intermediate-age alluvium (unit Qai) is always mapped as younger than the lake deposits (unit QTla, Alamosa Formation), as demonstrated at stops B1 and B2. Intermediate alluvium was graded to lowering base levels as the Rio Grande became established as a through-going stream through the San Luis Hills. Likewise, the younger alluvium (unit Qay) and Holocene alluvium (units Qa, Qfp, and Qaa; fig. B6–1) form terraces and the modern floodplain and channels of Trinchera Creek. No significant eolian deposits have been mapped in the area around stop B6, but most of the piedmont to the north and west of here is mantled by latest Pleistocene to Holocene eolian sand (units Qed, Qes, and Qeso of Michael Machette and Ren Thompson, unpub. mapping, 2007; see also fig. B7–1 at Hansen Bluff). This area seems to be a corridor of sand transport, rather than a repository of eolian sand.

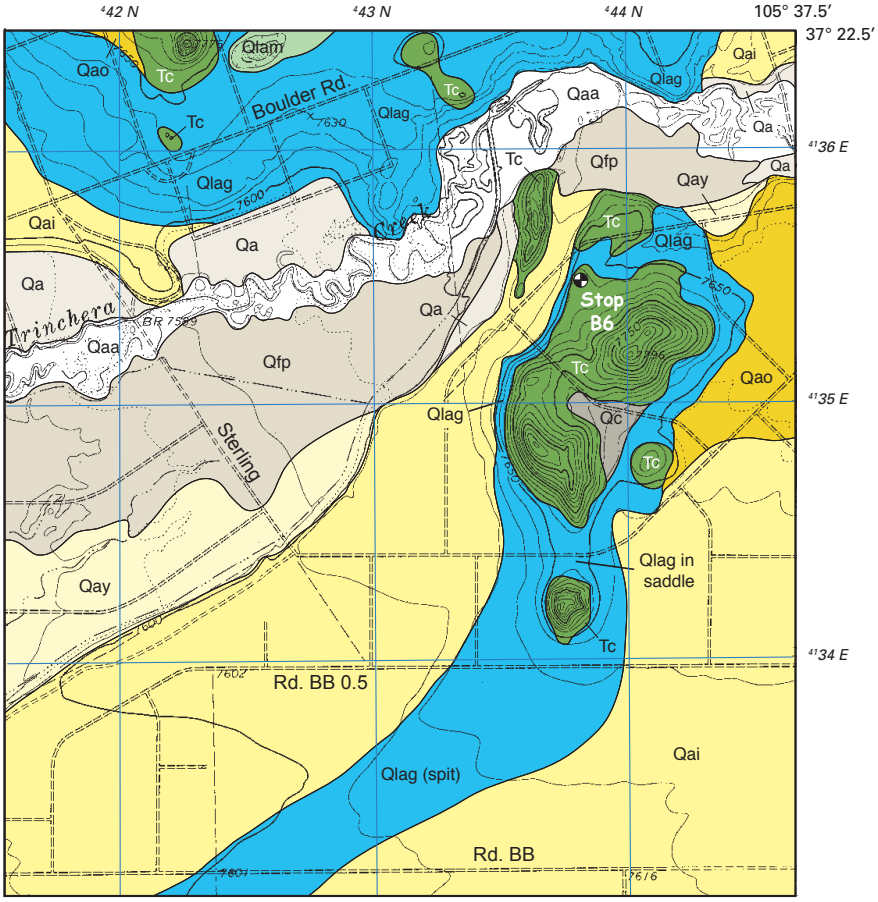

UTM coordinates in km, Zone 13, central NAD 27. Base scanned from northeastern corner of Lasauses quadrangle, 1968 ed.

0 0.5 1 2 km
0 0.5 1 mi

Figure B6–1. Bedrock, alluvial deposits, and lacustrine deposits of Lake Alamosa at stop B6, along Trinchera Creek. Map units: Qaa, active alluvium; Qa, Holocene alluvium; Qfp, floodplain alluvium; Qay, younger (latest Pleistocene) alluvium; Qai, intermediate alluvium (late to middle Pleistocene); Qao, older alluvium (middle Pleistocene); Qc, colluvium; Qlag (coarse-grained) and Qlam (fine-grained) near-shore coarse-grained deposits of Lake Alamosa (middle Pleistocene, uppermost part of unit QTla); and volcanic rocks of the Conejos Formation (29–30 Ma). Geology modified from Michael Machette and Ren Thompson, unpub. mapping, 2007.

Ventifacts (modified from Wikipedia (http://www.wikipedia.org/); see also selected references)

> *"Ventifacts are rocks that have been abraded, grooved, or polished by wind driven sand. These geomorphic features are most typically found in arid environments where there is little vegetation to interfere with eolian particle transport, where there are frequently strong winds, and where there is a steady but not overwhelming supply of sand. Ventifacts can be abraded to eye-catching natural sculptures [see fig. B6–2] . . . . Individual stones, such as those forming desert pavement, are often found with grooved, etched, surfaces where these same wind driven processes have slowly worn away the rock. When ancient ventifacts are preserved without being moved or disturbed, they may serve as ancient wind indicators. The wind direction at the time the ventifacts formed will be parallel to grooves or striations cut in the rock."*

Julie Laity (Geography Dept., California State University, Northridge), who is an authority on wind erosion in the southwestern United States, made the following observations on the basis of photographs of the ventifacts at stop B6:

1. On the basis of the scale, beveling of the form, and the degree of fluting, the area appears to have received sustained abrasion. The scale of the ventifact-form features (such as flutes) increases with the strength of the wind. Is there any sand in the area today? [No.] Sand is not always present in large quantities in fossil ventifact fields, as the area may have been largely a corridor of transportation.

2. Normally, ventifacts appear in topographic positions where water fluting is unlikely (for example, near hill crests). However, I have seen ventifacts within relict channels—some are found south of Ludlow, Calif., where the wind blew sand down the channel after streamflow ceased (assumed climatic change)—but this occurrence is rare. Are your ventifacts found in an area where the wind would accelerate (near a hill crest or in a topographic saddle)? [Yes.]

With reference to the Wikipedia discussion and Dr. Laity's observations, this site has the following attributes that are conducive to their formation:

1. Climate, present and past: Modern conditions are cold (41°F or 5°C, MAT) and relatively dry (about 7 in. or 180 mm, mean annual precipitation (MAP)) in Alamosa (see http://www.wrcc.dri.edu) about 20 mi (32 km) to the west. The elevation in this part of the basin ranges from about 7,550 ft to 8,000 ft (2,301 m to 2,438 m) asl. Glacial climates must have been considerably colder and probably drier than present.

2. Sand is and has been available from the floor of ancient Lake Alamosa and later from terraces and stream channels of Trinchera Creek.

3. Wind conditions. The monthly mean wind speed varies from 5 to 12 mph (2.2 to 5.4 m/s) and averages 8 mph (3.6 m/s). However, monthly peak gusts have been 48 to 67 mph (21.5 to 30.0 m/s) from the southwest>west>northwest in the past two decades in Alamosa (see http://www.wrcc.dri.edu).

4. Topography. This site is along a north-south ridge, perpendicular to the prevailing winds (southwest to northwest). In addition, there is higher topography in the form of bedrock-cored hills to the north and south of Trinchera Creek (fig. B6–1). These conditions are conducive to accelerating ambient winds by a venturi effect.

However, the presence of flutes on the leeward (east) side of the blocks is a bit troubling. Laity (written commun., 2007) says that "it is uncommon for these type of ventifacts to form on the leeward side: in having looked at thousands of ventifacts at dozens of sites . . , erosion is always on the windward side of the rock. . . . Furthermore, I stood for about three hours in a hellacious sand storm in the Mojave observing ventifact formation: no abrasion occurred on the leeward side—in most cases, it is mantled (and thus protected) by sand falling out of suspension or by a wind tail."

Thus, one must consider whether there have also been strong westerly winds at this site, or whether the flutes on the east side of the bedrock blocks might be of another (fluvial?) origin.

The ventifacts at stop B6 formed on wind-polished blocks of porphyritic andesite (unit Tc, fig. B6–1); they are characterized by finger-size troughs, percussion cones, and broad mullions on the front and back sides of intact bedrock (fig. B6–2). These features reflect hundreds of thousands of years of wind erosion at a location where sand is available and the wind is strong. Further east, near Smith Reservoir (south of Blanca), dreikanter-type (three-sided) ventifacts are well developed on blocks of Servilleta Basalt—Pliocene tholeiitic flood basalts that are common to the south of the San Luis Hills (see stops in chapter C). This basalt appears to have been at or near the surface since it was emplaced about 3.7 Ma.

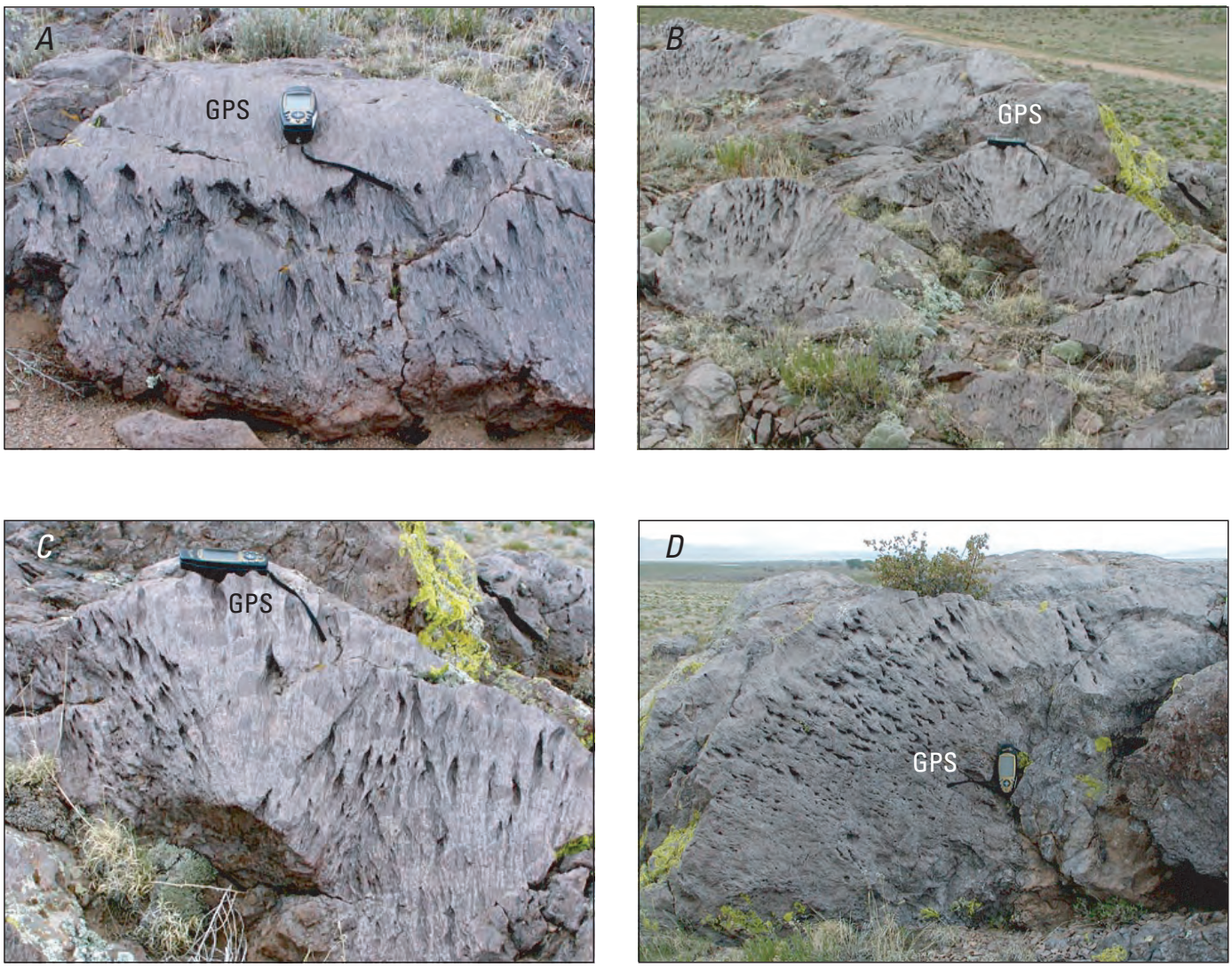

Figure B6–2. Ventifacts in upper Oligocene porphyritic andesite (Conejos Formation). GPS (15 cm long) for scale. *A*, Flutes in leeward (east) side of large wind-polished boulder. View to west (upwind). *B*, Broader view of flutes in leeward (east) side of large wind-polished boulders. Note variations in orientation. View to west (upwind). *C*, Closeup view of flutes shown in *B*. Note that the flutes cut across flow bands and clasts within the andesite. *D*, Radially oriented cones and flutes in windward (west) side of large wind-polished boulder. View to east (downwind).

Stop B7 (Optional) — Hansen Bluff—Alamosa Formation

Author: Michael Machette
Location: Hansen Bluff
Alamosa East 7.5' quadrangle (BSE–MM04–23)
GPS: NAD27, Zone 13, 433322 m E., 4136731 m N.
Elevation: About 7,525 ft (2,294 m) asl (Wildlife Refuge parking lot below measured section D of Rogers and others, 1985)

Synopsis

Although we don't have time to visit this site, Hansen Bluff (fig. B7–1) is one of the most important locations in terms of understanding the Alamosa Formation. Karel Rogers and her colleagues conducted integrated, multidisciplinary studies of these bluffs in the late 1970s and early 1980s and published a number of excellent papers describing the Quaternary geology, environments of deposition, faunal and floral remains, magnetostratigraphy, and age control for the section. They followed up by drilling a 127-m-long core to extend the sedimentary record into the Pliocene. The main contributions that we have made at Hansen Bluff are to map the local geology, to recognize a stratigraphic unconformity between the fine-grained Alamosa Formation and the overlying coarser sandy gravel beds (older alluvium, unit Qao), and to suggest how these deposits fit into the broader history of Lake Alamosa.

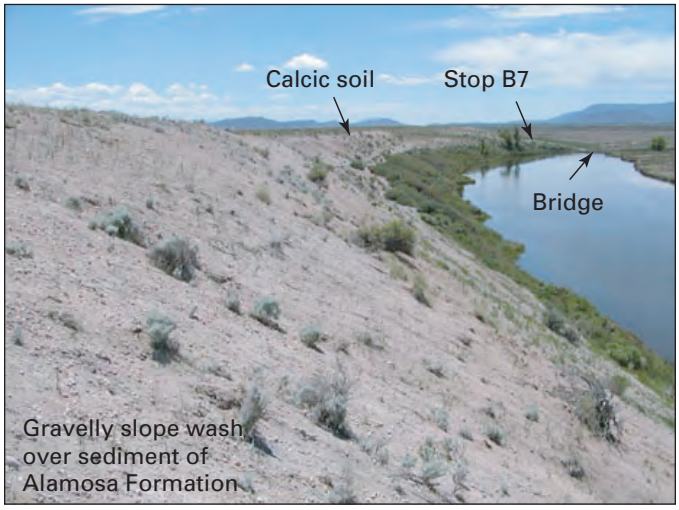

Figure B7–1. View of Hansen Bluff looking south from scenic drive near northernmost measured section (C) of Rogers (1984, fig. 1). Meander loop of the Rio Grande to right; San Luis Hills in the background. Location is 433378 mE, 4137274 mN (UTM Zone 13, NAD 83).

Discussion

Past Work

When vertebrate paleontologist Karel Rogers was at Adams State College (Alamosa, Colo.) in the 1970s and early 1980s, she assembled a team of paleontogists and geologists to study Hansen Bluff, a series of low stream-cut banks that lie just east of the Holocene channel of the Rio Grande, about 15 km east-southeast of Alamosa. Her colleagues included several USGS scientists who have retired (Rick Forrester) or passed away (Charles Reppening and J. Platt Bradbury) in the past few years. In the late 1970s, exposures of the bluffs were better and the area was not yet part of the Alamosa National Wildlife Refuge. Over a span of a decade they conducted detailed, multidisciplinary studies of these bluffs and published a number of excellent papers describing the geology, ecology, depositional environments, faunal and floral remains, magnetostratigraphy, and age control for the section. They followed up by drilling an additional 127 m to further extend the sedimentary record into the Pliocene. Among their many papers, those that are most important to the stratigraphy of the Alamosa Formation include an initial overview by Rogers (1984), a review paper by Rogers and others (1985) that is difficult to find (now), a specialized paper focusing on the Alamosa local fauna by Rogers (1987), a paper on the magnetostratigraphy, ages and sedimentation rates by Rogers and Larson (1992), and a final comprehensive review paper by Rogers and 11 others (1992).

Roughly sixty years earlier, USGS geologist Claude E. Siebenthal had described the sediments along Hansen Bluff, which he named for the bluff bank opposite the Hansen Ranch (Siebenthal, 1910, p. 11). Siebenthal conducted the first comprehensive survey of the geology and water resources of the San Luis Valley, completing his fieldwork in 1904 and the report in 1906. (He states that "untoward circumstances have intervened to prevent the publication of the report until the present" [1910]). Siebenthal's report focused on the groundwater potential of a prime and growing agricultural area in Colorado and provided the first stratigraphic evidence for a large and ancient lake, which he alluded to but did not name. Siebenthal's (1910, p. 40–41) measured section of the Alamosa Formation at Hansen Bluff is somewhat generalized, but it includes various colored sands, pebbly sandy, and drab clay totaling 61.5 ft (about 19 m), including several beds with laminae (lake beds). Siebenthal found a great number of freshwater shells in the bluff and reported that drill holes around the valley had brought up fossils (bird or fish bones) as well as wood, rootlets, leaves, seeds and peaty moss. He speculated that sediment of the Alamosa Formation was likely of late Pliocene or early Pleistocene age (not a bad guess for 110 years ago).

By the 1980s, Rogers and her team had a much larger and more sophisticated tool bag to investigate the bluff than

Siebenthal. In addition to excellent paleontological reference collections, they had tephrochronlogy and magnetostratigraphy to provide time lines. For the purposes of this field trip, we are most interested in the age control that Rogers and her team provided for the Alamosa Formation at Hansen Bluff.

There is no type locality for the Alamosa Formation, which is commonly 300–500 m thick in the subsurface (Siebenthal, 1910). Because so little of its sediment is exposed in the San Luis Basin, Hansen Bluff should be considered as the type section for the upper (Quaternary) part of the Alamosa Formation.

Local Geology

The main contributions that we have made at Hansen Bluff are to map the local geology, to recognize a stratigraphic unconformity between the fine-grained Alamosa Formation and the overlying coarser sandy gravel beds (older alluvium, unit Qao), and to suggest how these deposits fit into the broader history of Lake Alamosa.

Only the upper part of the Alamosa Formation is exposed at Hansen Bluff. This unit is mapped as QTla (Pliocene to middle Pleistocene), although Rogers (1984) established that the exposed section is early Pleistocene (late Irvingtonian). Overlying the Alamosa Formation is sandy pebble to small cobble gravel (3–6 cm diameter clasts), which has a 1-m-thick, stage III calcic soil (fig. B7–2). The alluvium is derived from the Sangre de Cristo Mountains (including Blanca Peak), but it may also be reworked from basin-fill sediment of the Santa Fe Group, which is exposed near Fort Garland. Precambrian rock (such as gneiss, quartzite, and granite) is exposed only in the Sangre de Cristo Mountains, whereas Tertiary volcanic rock dominates the San Juan Mountains and its foothills west of the valley. Thus, the type of rock clasts in alluvium (Precambrian basement versus Tertiary volcanic rock) is a reliable indicator of source area and transport direction in this part of the San Luis Basin sediments.

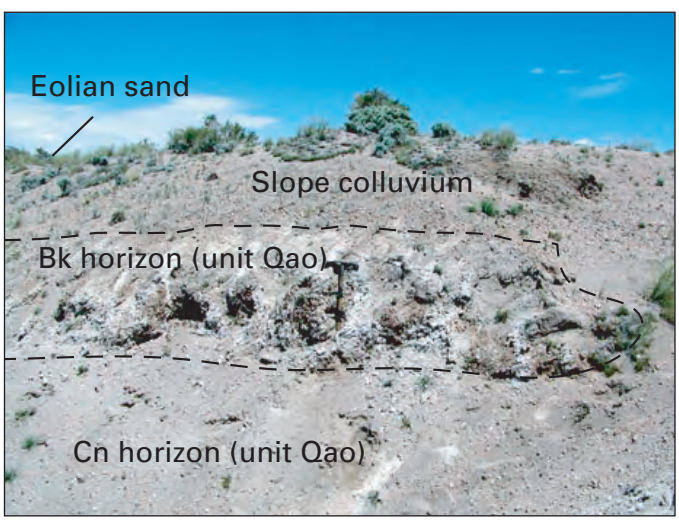

Figure B7–2. Strong but discontinuous calcic soil (Bk, stage III morphology) that caps Hansen Bluff. Soil pick (60 cm long) for scale. Location about 0.5 km north of stop B7, but this soil is representative of development in older alluvium (unit Qao) along bluff. View to the east.

To the east of Hansen Bluff, there are a series of sand-covered, piedmont-slope deposits at high, intermediate, and low levels: these are mapped as units Qao, Qai, and Qay, respectively (fig. B7–3). All of these deposits lie unconformably on the Alamosa Formation. The upper 8 ft (2.5 m) of Siebenthal's (1910) section is listed as "Recent" gravelly slope (slope colluvium) and indurated conglomerate (Bk horizon in sandy gravel), which we map as unit Qao. At this location, the surface of unit Qao is about 20 m (65–70 ft) above Holocene alluvium of the Rio Grande (units Qaa, Qfp, and Qa, fig. B7–3). The surface of Qai, which is inset into Qao as southwest-trending terrace deposits, projects about 15 m (50 ft) above the Holocene alluvium. Unit Qay is not widespread in this area, but it fills channels that project to only 3 m (10 ft) above the Holocene alluvium. All of the elevated alluvial surfaces were truncated along the bluff by lateral migration of the Rio Grande during the late Pleistocene and Holocene.

The cover of eolian sand east of the Hansen Bluff is quite impressive. Sand dunes (unit Qed) are concentrated along the bluff's western edge, but an extensive sheet of cover sands and coppice dunes extends several kilometers to the east. These sands are mapped (simply) as unit Qes, although older components (unit Qeso, Machette and Thompson, 2005; Michael Machette and Ren Thompson, unpub. mapping, 2007) are found in areas of blowouts in unit Qes cover. The older sands have Bw to weak Bt (argillic) horizons over stage I–II Bk horizons. We suspect that these older sands are of late or latest Pleistocene age.

Some authors have suggested that Hansen Bluff is an uplifted fault block (for example, Rogers, 1984), although there is little evidence or requirement for such a fault. Burroughs (1972) showed the bluff as a fault-line escarpment of the Lasauses fault, which extends north-south along the Rio Grande through the Fairy Hills (stop B4). However, there are no fault scarps on middle Quaternary or younger surficial deposits either to the north or south of Hansen Bluff, so there need not be a fault. We suspect that the Lasauses fault is a Neogene structure that has not been active in the Quaternary.

Hansen Bluff—Stratigraphy and Age

The age of the Alamosa Formation exposed in Hansen Bluff is based on a variety of data and assumptions (see discussion of Rogers and Larson, 1992). Two tephra beds (volcanic ashes) were exposed during the excavations: the upper tephra was identified as the Bishop ash, which was erupted from Long Valley caldera in eastern California at about 0.74 Ma. A second tephra was found about a meter lower in section, but it was not typed to a unique source and, thus, is of unknown age (and little use to us). A third tephra, the 2.02 Ma Huckleberry Ridge ash from the Yellowstone area

of northwestern Wyoming, was found in an adjacent drill hole, 78 m below the surface.

The two identified ashes are now considered to be slightly older (0.76 Ma Bishop Ash, Sarna-Wojcicki and others, 2000; 2.06 Ma Huckleberry Ridge ash, Lanphere and others, 2002; respectively) as a result of better radiometric dating ($^{40}Ar/^{39}Ar$) and laboratory calibrations. The Bishop Ash lies about 11 m above the base of the 17-m-high exposure at Hansen Bluff. The total sediment package between the 0.76 Ma and 2.06 Ma tephras is about 84 m thick. Thus, 84 m of sediment deposited in 1.30 m.y. yields a long-term (average) sedimentation rate of 6.5 cm per 1,000 yr. A more important assumption here is that of constant sedimentation, which is a first-order approximation that Rogers had to make. Because Lake Alamosa was a climatically driven lake, the sedimentation rates should have fluctuated greatly depending on the position of lake level, environment of deposition, and climate (all factors recognized by Rogers and her colleagues). On the basis of sedimentation rate, Rogers and Larson (1992) estimated that the Hansen Bluff section ranges from about 0.67 Ma and 0.9 Ma, with the Alamosa Formation extending back to at least 2.6 Ma at the bottom of the drill hole (at 127 m depth).

Rogers and Larson (1992, fig. 2) assembled a magnetostraphic record for the Alamosa Formation surface exposures (Hansen Bluff) and cored section, using the two dated ash beds to anchor the magnetic polarity zonation (fig. B7–4). The Bishop Ash is normally magnetized and lies at the base of the Bruhnes Normal Chron (0–0.78 Ma). Conversely, the Huckleberry Ridge Ash (at 2.06 Ma) lies within one of the Reunion normal events within the Matuyama Reversed Chron in the late Pliocene (Rogers and Larson, 1992, fig. 2). On the basis of depth and sedimentation rate, the base of the drill hole appears to be in the Gauss Normal Chron, and thus is >2.48 Ma.

For comparison, we have used a recent composite benthic oxygen-isotope record (Lisiecki and Raymo, 2005) to infer possible correlations with major glacial and interglacial stages for the exposed section at Hansen Bluff (fig. B7–4). If the upper part of the section were about 0.67 Ma, this would correlate with OIS 17 (a major interglacial interval), whereas the basal part of the section (0.9 Ma) would correlate with a time just before OIS 22 (a major glacial interval). Within the exposed section, there should be a sedimentary record of climatically oscillating Lake Alamosa (and an adjacent piedmont) that contains three major glacial cycles (OIS 22, 20,

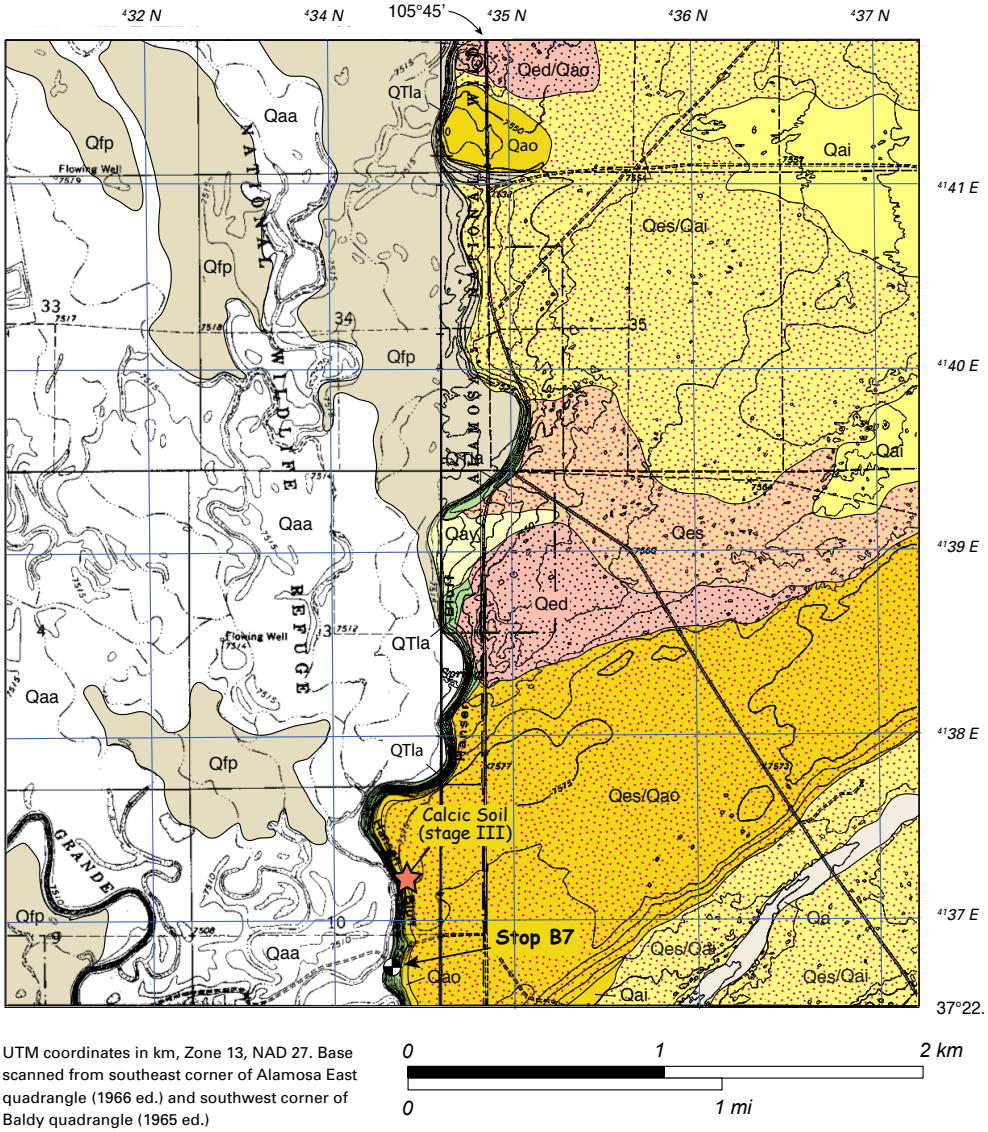

UTM coordinates in km, Zone 13, NAD 27. Base scanned from southeast corner of Alamosa East quadrangle (1966 ed.) and southwest corner of Baldy quadrangle (1965 ed.)

Figure B7–3. Hansen Bluff, suggested type section for the Alamosa Formation. Map units: Qes, eolian sand; Qed, dune sand; Qaa, active alluvium; Qfp, floodplain alluvium; Qa, undivided Holocene alluvium; Qay, younger alluvium (late Pleistocene); Qai, intermediate alluvium (late to middle Pleistocene); Qao, old alluvium (middle Pleistocene); and QTla, Alamosa Formation. Photographs shown in figures B7–1 and B7–2 were taken at location marked by red star (calcic soil). Geology modified from Machette and Thompson (2005) and Michael Machette and Ren Thompson, unpub. mapping, 2007).

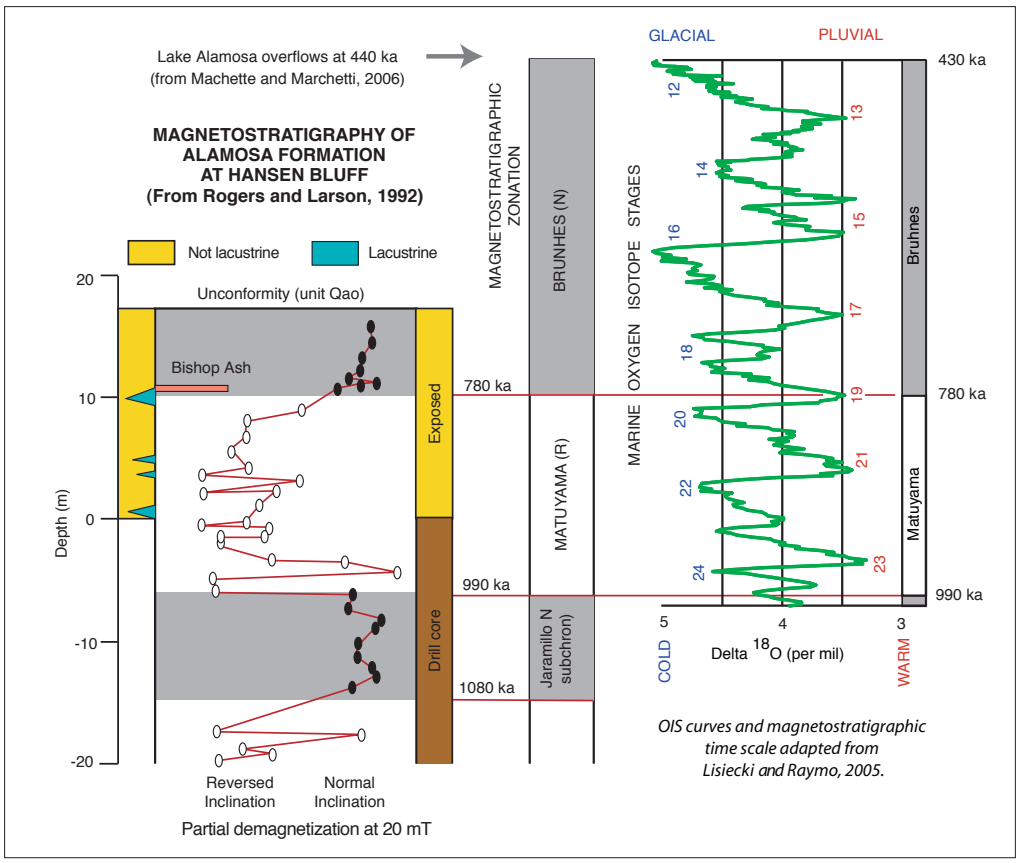

Figure B7–4. Magnetostratigraphic record at Hansen Bluff (modified from Rogers and Larsen, 1992, fig. 2). Upper 17 m of sediment are exposed; lower sediment is from drill core. Record is modified to fit magnetostratigraphic zonation and ages of Lisiecki and Raymo (2005). Interpretation of lacustrine versus nonlacustrine environments of deposition are from Rogers (1984, fig 3). By our interpretation, the upper part (ca. 670–440 ka) of the Alamosa Formation is not preserved at Hansen Bluff.

and 18) and all or parts of four interglacial cycles (OIS 23, 21, 19, and 17).

If our model of a climatically driven Lake Alamosa is correct (see chapter G), then the glacial cycles should relate to deep, large lakes (such as the records show for Lake Bonneville and Lake Lahontan, see Reheis and others, 2002), and the interglacial cycles should relate to shallow, restricted lakes (or playas). The sedimentologic and fossil records at Hansen Bluff (Rogers, 1984; Rogers and others, 1985) show only four intervals of lacustrine sedimentation (Rogers, 1984, fig. 3). We plotted these lacustrine versus nonlacustrine intervals on the left side of figure B7–4, strictly for comparison with the glacial records from marine oxygen isotope stages (Lisiecki and Raymo, 2005). These correlations suggest that Lake Alamosa rose to the level of Hansen Bluff (about 7,520–7,560 ft or 2,292–2,304 m asl) four times from 0.9 to 0.67 Ma, but not for long each time (because most lake beds are thin). The portions of lacustrine beds in the section do not appear to map simply into the chronology of glacial events inferred from the marine oxygen-isotope data (assuming linear sedimentation rates), but they do support our inference of recurrent, high stands in Lake Alamosa during the early to middle Quaternary.

Stop B8 — Mesita Hill: An Early Pleistocene Volcano Adrift in a Sea of Dirt

Speakers: Michael Machette, Ren Thompson, and Bob Kirkham

Location: Entrance to Jake and Hank Mine (cinder quarry) at Mesita Hill, about 2 mi (3.2 km) west-northwest of Mesita, Colo.
Sky Valley Ranch 7.5' quadrangle
GPS: NAD27, Zone 13, 443580 m E., 4106700 m N.
Elevation: 7,800 ft (2,377 m) asl (at entrance gate)

Synopsis

Mesita Hill is an early Pleistocene basaltic shield volcano in the Costilla Plain between San Pedro Mesa and the Rio Grande. With an $^{40}Ar/^{39}Ar$ age of 1.03±0.01 Ma (Appelt, 1998), the volcano is the youngest eruptive center within the San Luis Basin and in the Rio Grande rift north of Albuquerque, N. Mex. Younger volcanoes, generally considered to be associated with crustal extension, exist further north in west-central Colorado, including Dotsero "crater" (4,150±30 ^{14}C yrs B.P., Giegengack, 1962) and Willow Peak volcano (0.28±0.04 Ma, Kunk and others, 2002), but they are well outside of the present physiographic boundary of the rift. The Mesita volcano is cut by an intrarift fault, informally known as the Mesita fault (figs. B8–1 and B8–2). The fault shows recurrent post-4 Ma movement including offset of the western flank of Mesita volcano, offset of middle Pleistocene alluvium of the Costilla Plain, and offset of late-middle and late Pleistocene alluvium of the Costilla drainage south of Mesita.

Stop B8 includes a walking traverse from the parking area on the south side of the reclaimed quarry pit, skirting the east side of the remaining pit to the north end of the cinder quarry, followed by a short excursion (about 0.5 km) to the northern flank of the volcano and subsequent return to the starting point by a route along the footwall of the Mesita fault. There are three principal topics of discussion planned for stop B8 that correspond with stops along the walking traverse delineated on figure B8.1. The first stop (stop B8.1) provides an opportunity to discuss the volcanic history of this beautifully exposed basaltic cone and flows and to examine sedimentary deposits and structures preserved on the north rim of the excavation pit. The origin of these sedimentary deposits has been the subject of some debate that centers on the posteruption geologic history of Mesita Hill, whether Mesita Hill is a primary feature or an exhumed feature, and the associated geologic histories involved these vastly different interpretations. This debate will be examined in light of the observed deposits and models for basin evolution and the origin of the Costilla Plain. The second topic (stop B8.2) involves a discussion of the results of cosmogenic dating of lava flows and its application to surface-exposure dating at Mesita volcano. The final stop (stop B8.3) on our volcano tour provides an overview of the Mesita fault, a down-to-west intrabasin fault with recurrent Quaternary movement that cuts the 1.0 Ma basalt flows on the west side of the volcano.

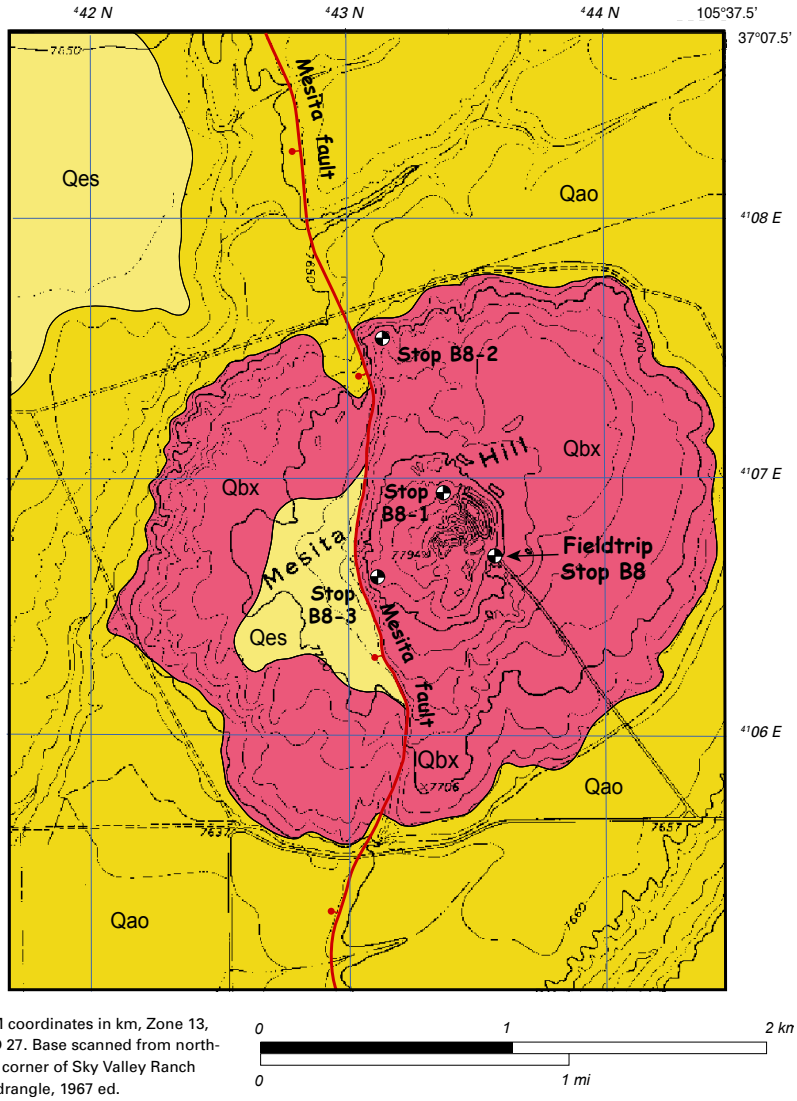

Figure B8–1. Geologic map showing Mesita Cone, a 1.0 Ma volcano. Map units: Qes, eolian sand; Qao, old alluvium (Costilla Plain); Qbx, basalt of Mesita Cone. Geology modified from Thompson and Machette (1989).

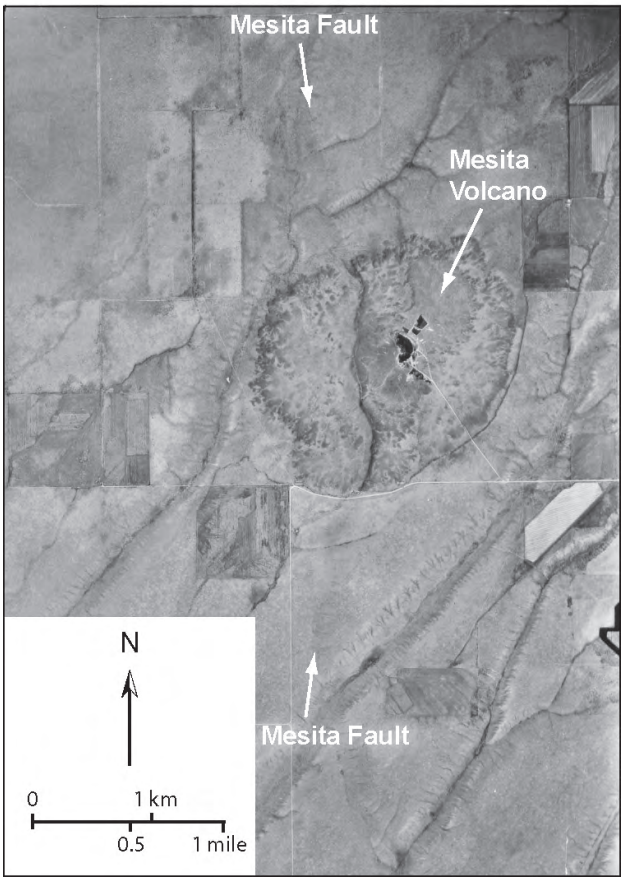

Figure B8–2. Aerial photograph taken in 1953 showing Mesita fault (white arrows) cutting 1.0 Ma Mesita volcano and middle Pleistocene alluvium (unit Qao of Thompson and Machette, 1989). Also visible are early excavations associated with the Hank and Jake Mine (quarry in Mesita cone).

Stop B8.1 — Cinder Pit (Reclaimed), Mesita Volcano

Location: Main cinder pit
Sky Valley Ranch 7.5' quadrangle
GPS: NAD27, Zone 13, 443406 m E., 4106841 m N.
Elevation: 7,750–7,780 ft (2,362–2,371 m) asl

Discussion

Johnson (1969) originally mapped Mesita volcano at a scale of 1:250,000 on the geologic map of the Trinidad 1° x 2° quadrangle. Colton (1976) also mapped the volcano at a scale of 1:250,000 and was the first to map the Mesita fault that cuts the volcano (fig. B8–1). Epis (1977) conducted a detailed study of the volcano as part of an unpublished ground-water availability study by Zorich-Erker Engineering, Inc. (1980) that included a 1:24,000-scale map and cross section of Mesita volcano and adjacent Costilla Plain (figs. B8.1–1 and B8.1–2). Thompson and Machette (1989) show the volcano on their 1:50,000-scale map of the San Luis Hills area, but they incorrectly assumed it was Pliocene in age, prior to the 1.0 Ma $^{40}Ar/^{39}Ar$ age determination of Appelt (1998). These documents and the results of new interpretations presented in Thompson and others (chapter H, this volume) are the basis for discussion at this stop.

Epis (1977) and Thompson and Machette (this volume) map the central part of the volcano as predominantly consisting of near-vent pyroclastic deposits associated with the eruption of Mesita volcano. Epis described the vent area as being composed predominantly of cinders—a resource that was developed by the Mickelsen family in 1950 or 1951. George Oringdulph, Sr., and Henry Quiller acquired the property in the mid-1950s and mined there until 1981 when they sold the operation. The property changed ownership a few times since then, but Hecla Mining Company (Coeur d'Alene, Idaho) ended up with the property in the mid-1980s when they bought out Ranchers Exploration (mining history from Rob Oringdulph, oral commun., 2006). The mine operated until the late 1990s but is now scheduled for reclamation by the owner. Although mining had disturbed some, but not all, of the important stratigraphic relationships that were preserved near the edifice of the volcano, the reclamation activities scheduled for

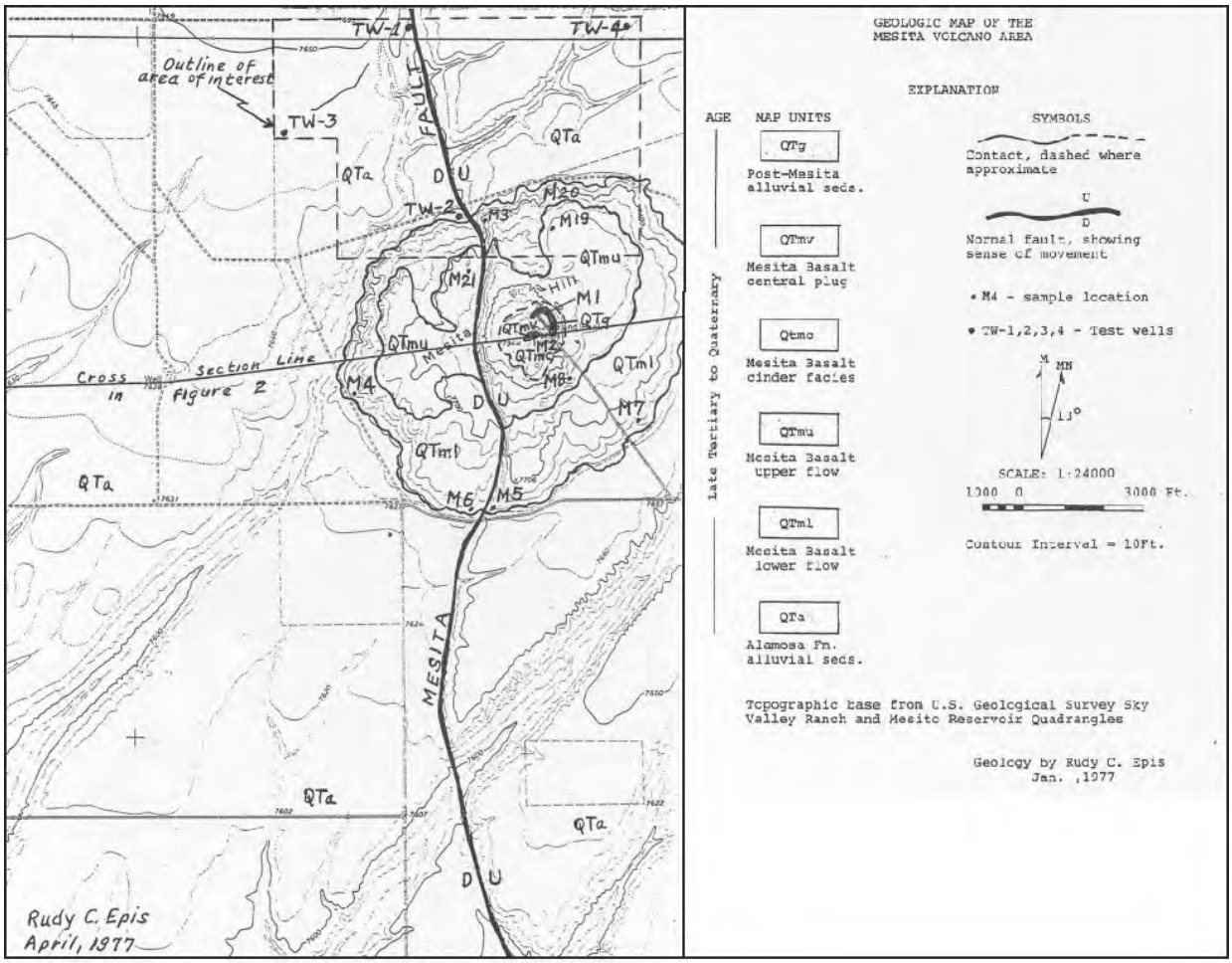

Figure B8.1–1. Geologic map of Mesita Hill reproduced from Epis (1977). USGS topographic base of 1967 compiled from photography flown in 1965.

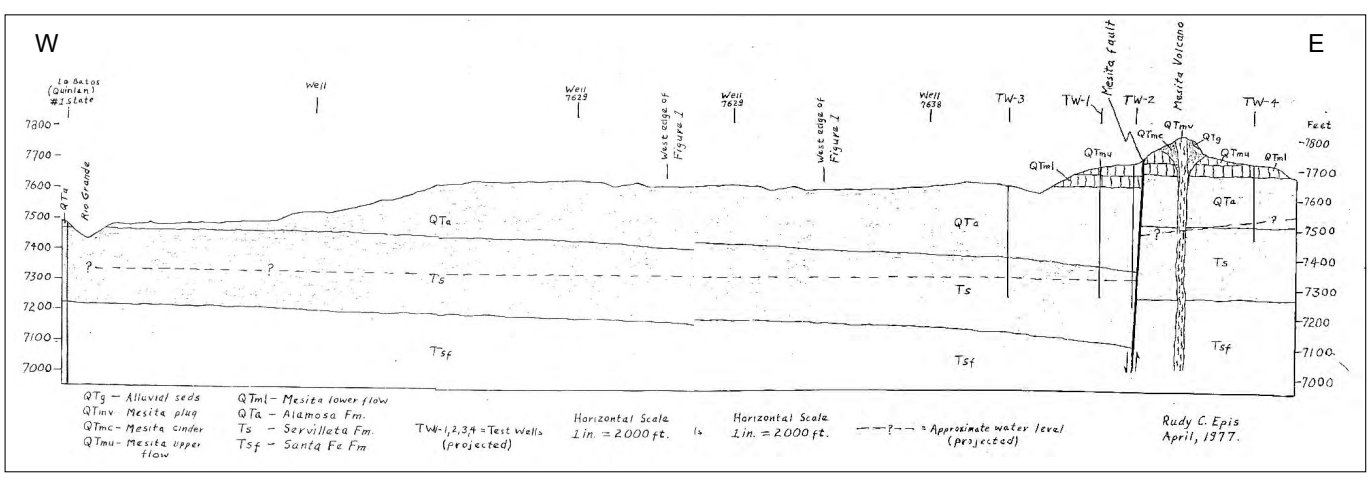

Figure B8.1–2. Geologic cross section through Mesita Hill, reproduced from Epis (fig. 2, 1977).

this summer (2007) will destroy what remains of the quarry and primary stratigraphic relations preserved therein.

Mesita volcano is a low-relief shield consisting of a symmetric summit cone built on a platform of lava flows. The existing USGS Sky Valley Ranch quadrangle, compiled photogrammetrically in 1967 from aerial photographs taken in 1965, demonstrates that the preexcavation summit cone of Mesita volcano rose to an elevation of approximately 7,810 ft, approximately 60 ft (18 m) above the top of the plateau-forming lava flows underlying the cone. In 1965, quarry operations were restricted to a small pit on the northeast shoulder of the summit cone (fig. B8.1–1) and the original summit was undisturbed. The lava-flow plateau underlying the cinder cone comprises two eruptive phases of compositionally similar lava denoted in figures B8.1–1 and B8.1–2 as map units QTml and QTmu respectively. The lower unit (QTml) was incorrectly described by Epis (1977) as a single lava flow, but in fact it contains multiple lava flows, the boundaries of which are distinct on aerial photographs (Thompson and others, chapter H, this volume) and preserved flow contacts in the footwall of the Mesita fault. The upper unit (QTmu) represents late stage eruption of lava prior to cessation of volcanic activity. This final phase of eruption was likely Strombolian in character and was responsible for the formation of the cinder cone and the thin lava flows extending both northeast and west from the current summit cone.

On the basis of limited geochemical data, all of the Mesita volcano lava flows and near-vent deposits are basaltic andesite, similar in composition to other small-volume eruptions of the Taos Plateau volcanic field. Petrographically, the rocks are weakly porphyritic to microporphyritic with pilotaxitic texture. Phenocrysts, where present, are predominantly plagioclase with lesser amounts of olivine. The rock's microcrystalline groundmass consists of plagioclase, pyroxene, olivine, and iron-titanium oxides. Ubiquitous but scarce xenocrysts of plagioclase and lesser quartz can be as large as 1 cm and are characteristic of other small-volume eruptive centers in the region, resulting in the informal usage of the term XBA (xenocrystic basaltic andesite) to describe such rocks (Lipman and Mehnert, 1979; Thompson and Lipman, 1994a,b). In spite of the propensity of these rocks to have excess "old" argon resulting from disaggregation and possible magmatic recycling of xenocrysts of Precambrian age, Appelt's (1998) $^{40}Ar/^{39}Ar$ age of 1.03±0.01 Ma from groundmass yielded a reasonable plateau age. Unfortunately, since we only have Appelt's reported sample locality to go on, we don't know if the sample was collected from "in place" rock (unit Qtmu) or a block of material stockpiled from quarry. If the sample were collected from a natural outcrop, it would date the younger of the two lava-flow sequences.

Beautiful examples of cinder, spatter, spatter agglutinate, incipient lava flows, and bombs are exposed within the remaining quarry pit. The bombs are primarily of the spindle variety, characteristic of Strombolian eruptions of basaltic andesite. Notably absent are dikes of similar composition that are commonly found in cinder quarries. This absence likely reflects the short-lived nature of the eruptive activity at Mesita volcano. Preexcavation aerial photography taken in 1936 shows two northwest-trending dikes that cut the northern end of the cinder cone and may have served as vent areas for at least part of the eruption cycle. Epis (1977) maps a central vent "plug" (figs. B8.1–1 and B8.1–2), but no evidence for this plug is visible in the earlier photographs or in the remaining pit quarry. Regardless of the exact location or geometry of the vent area, the eruption could have occurred over a period as short as a few days to weeks.

A small remnant of sedimentary deposits locally overlies volcanic rocks on the northeast flank of the Mesita volcano. Epis (1977) provided the first record of these deposits, but Robert Kirkham and Eric Harmon (2006, oral commun. to Kirkham) also observed the sediments in the mid-1970s. Epis mapped the deposit as a crescent-shaped remnant of sediment on the north and northeast rim of the volcano (fig. B8.1–1). His report is an appendix to an unpublished document by Zorich-Erker Engineering, Inc. (1980). Because this document is difficult to obtain, Epis' 1977 map is reproduced herein as figure B8.1–1. The remnant of sediment is the dark-shaded area labeled "QTg" on his map. Epis refers to these deposits as "Post-Mesita alluvial sediments" and described them as "alluvial muds, sands, and gravels." This evidence led Epis to conclude, "the region was formerly buried by alluvial sediments and is now being exhumed and dissected by the entrenchment of the Rio Grande and its tributary drainages." Kirkham (2006) also pointed out the remnant of sediment and stated that its presence suggested the volcano could be an exhumed feature.

Unfortunately, some outcrops of the sediment have been removed or disturbed by mining activities. Figure B8.1–3 shows these sediments in the north wall of the mine pit, as they appeared in 2006. As part of planned reclamation activities by the Hecla Mining Company for the summer of 2007, the pit may be reclaimed. These sediments and features may be disturbed, buried, or completely removed prior to the FOP field trip.

The sediment in the remnant consists of beds of very poorly sorted to moderately well sorted, weakly bedded to nonstratified, silty medium-grained to very fine grained sand, sandy silt, and gravelly sand. The matrix is arkosic, not volcaniclastic. Most pebble- and cobble-size clasts are composed of angular to subangular basalt (cinders, scoria, and flow rock) that is locally derived from Mesita volcano, although rare subrounded pebbles of quartz and gneiss are present. Although the volcanic clasts are reworked as colluvium, the enclosing matrix sediment is arkosic. Machette and Thompson believe that that the matrix might be eolian sediment derived from arkosic sands (upper part of Santa Fe Group) that underlie the adjacent Costilla Plains, whereas the volcanic clasts are certainly locally derived (colluvium) (see discussion in chapter H, this volume). Conversely, Kirkham believes that the arkosic sediment is water laid and part of a once more extensive (and thicker) basin-fill sequence. The main question about the perched sedimentary package of Epis (1977) comes down to (1) whether wind was capable of transporting the rare,

Figure B8.1–3. Photographs of sediments preserved on the north rim of existing quarry (stop B8.1). *A*, Unconformity between primary pyroclastic deposits (a), volcanic colluvium (b), and overlying sedimentary deposits (c). *B*, Pebble- to cobble-size volcanic and Precambrian(?) clasts in sediments overlying volcanic deposits. *C*, Closeup view of sedimentary structures and clasts near basal contact with volcanic deposits. Photographs by R.M. Kirkham, 2006.

small (1–2 cm) pebbles of quartz and gneiss found within the sedimentary deposit or (2) whether this is a remnant of fluvial sediment deposited on the volcanic cone and now preserved ≳30 m (100 ft) above the Costilla Plains. If the volcano was buried or nearly buried by sediment and subsequently exhumed, its evolution could be characterized by the cross sections shown in figure B8.1–4. Exhumation must have occurred prior to deposition of the middle Pleistocene older alluvium of Thompson and Machette (1989; unit Qao), which is estimated to be 500±100 ka.

However, the exhumation model proposed by Epis (1977) and supported by Kirkham (2006) introduces local and regional complexities not consistent with other geomorphic and geologic observations. For example, if one raises the unit Qao surface of Thompson and Machette (1989) to an elevation of 7,777 ft (the elevation of the sediments observed at stop B8.1), it dramatically increases the amount of basin-fill sediment that would have covered the Costilla Plain and encroached upon the San Luis Hills, and it should have left a geologic signature on the early Pleistocene landscape well beyond Mesita Hill—in fact, around the entire margin of the Costilla Plain, according to Machette and Thompson.

Locally, these fluvial deposits would have completely covered the lower flanks of Mesita volcano and much of the summit cone. Although the summit cone has all but been removed by mining operations, the lower flanks of the volcano, including pressure ridges and ramp structures associated with primary emplacement, are well preserved (Thompson and others, chapter H this volume). Fresh-appearing aa surfaces appear little modified by alluvial processes, such as bed-load scouring or local channel cut and fill. Exotic clasts of gneiss and quartz are seldom observed as lag deposits over much of the volcano, particularly in filled depressions on the aa surfaces. Results from an ongoing effort to cosmogenically date the flows using ^{3}He techniques (stop B8.2) may help to resolve the burial history of the volcano. A surface-exposure age near 1 Ma (the time of the eruption) would support an interpretation that the basalt flows were never buried, whereas an exposure age much less than 1 Ma would support burial and exhumation of the flows (and by inference the cone).

If sedimentation of the Santa Fe Group was 30 m (100 ft) higher, then one could predict its extent throughout the Costilla Plain (and west to the San Luis Hills). Using a depositional surface pinned at 7,777 ft at Mesita volcano and parallel to that mapped for the unit Qao alluvium by Thompson and Machette (1989) would lead to burial of the 5.3 Ma Culebra volcano (just south of the intersection of State Highway 142 and the Rio Grande, fig. B–3). It would extend part way up

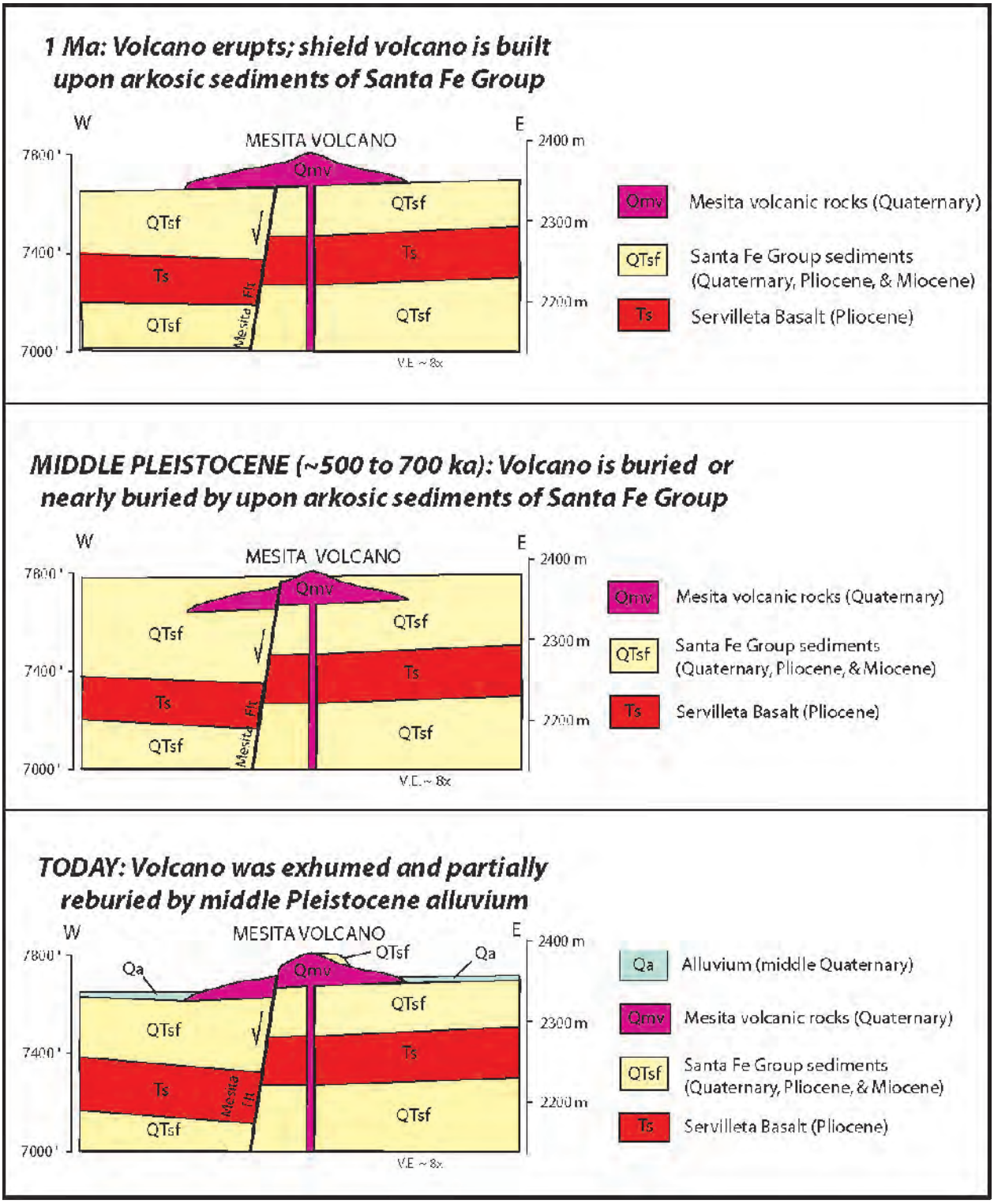

Figure B8.1–4. Schematic geologic cross sections showing geomorphic evolution of Mesita Hill proposed by Kirkham (2006), based on map relations depicted in Epis (1977).

the higher mesas of the San Luis and Fairy Hills (underlain by Conejos Formation volcanic deposits) and could have buried the eventual spillway area of Lake Alamosa (stop B4). Although the lower flanks of Culebra volcano contain clasts of Precambrian rock related to a paleochannel of the Rio Culebra, no exotic clasts are found near the summit region, suggesting the unit Qao surface never exceeded an elevation of about 7,635 ft at the position of the Rio Grande. Additionally, mapping in the Fairy Hills region of the San Luis Hills has revealed no remnants of Precambrian-rich alluvial sediments that would correlate with the perched sediment on Mesita volcano. Perhaps most intriguing about the hypothesis of 30 m higher deposition on the Costilla Plain is the implication that alluvial sediments of the Rio Culebra drainage could have extended northwest into the Fairy Hills, above the hydrologic threshold for Lake Alamosa at stop B4. No sedimentologic evidence exists for a higher level of basin filling—with the exception of the "fluvial sediment" on Mesita cone.

Mapping of sediment of the Santa Fe Group in the San Luis area (Machette and others, 2007) suggests that Santa Fe deposition continued into the middle Quaternary. About 4.5 km (2.8 mi) northeast of San Luis, Colo., Machette found volcanic ash interbedded in the uppermost part of the Santa Fe Group. This ash (sample SL–MM06–9) consists of nicely preserved, angular, predominantly solid, ribbed, and platy glass shards that match well with bimodal Lava Creek B (639±2 ka) volcanic glass samples from the Yellowstone caldera of northwestern Wyoming (Elmira Wan, USGS, written commun., 2006). The ash bed is overlain by several meters of slightly deformed sediment (unit QTsf) that is unconformably truncated by older alluvium (unit Qao). Thus, in the San Luis area (about 10 km north-northeast of stop B8), the upper part of the Santa Fe Group may be as young as 600 ka.

The overflow of Lake Alamosa occurred at about 440 ka (see Machette and others, chapter G, this volume), which led to downcutting of the Rio Grande and its tributary streams (such as Rio Culebra and Rio Costilla) on the Costilla Plain. If one presumes an approximate age of 500 ka for the pre-overflow unit Qao deposits, including the perched deposits at Mesita Hill, then there may have been only a very short period of time (60 k.y.) for basin-wide exhumation after the end of Santa Fe Group sedimentation. The tectonic or climatic driver for such rapid and complete denudation of the basin is unclear and the geologic impact of such a widespread erosion event has not been identified elsewhere in the basin.

Stop B8.2 (Optional) — ^{3}He Dating of Basalt Flows, North Flank of Mesita Volcano

Location: North flank of Mesita Volcano
Sky Valley Ranch 7.5' quadrangle (SVR–MM06–124)
GPS: NAD27, Zone 13, 443130 m E., 41067505 m N.
Elevation: 7,740 ft (2,359 m) asl

Synopsis

The second topic for discussion at the Mesita volcano (stop B8.2) involves cosmogenic ^{3}He surface-exposure dating of lava flows as a technique for resolving the burial history of the volcano, as discussed at stop B8.1. If the cosmogenic dating yields an exposure age near 1 Ma, then the volcano probably is a relict feature that was never buried. If the exposure age is much less than 1 Ma, then the volcano probably is an exhumed feature. Samples were being processed in the spring of 2007, with anticipation of having results by the time of the field trip (September 2007).

Discussion

In the fall of 2006, we collected three samples of flows from the Mesita Volcano for cosmogenic ^{3}He surface-exposure age. The samples were taken from slightly weathered flow surfaces located on the north flank of the volcano (fig. B8.2–1). At the time this field-trip guidebook was written (spring 2007), we are in the process of separating and concentrating the minerals olivine and pyroxene from the basalt. Once mineral separates are obtained, we will crush the separates under vacuum and determine the ^{3}He/^{4}He inventory in mantle-derived fluid inclusions. The samples will then be degassed at about 1400°C and the total concentrations of ^{3}He and ^{4}He will be measured by mass spectrometry. Cosmogenic ^{3}He concentrations will be determined using the mantle correction, and exposure ages will be determined using the latest ^{3}He production rate and cosmogenic scaling factors. Since ^{3}He is a stable isotope, the temporal limit

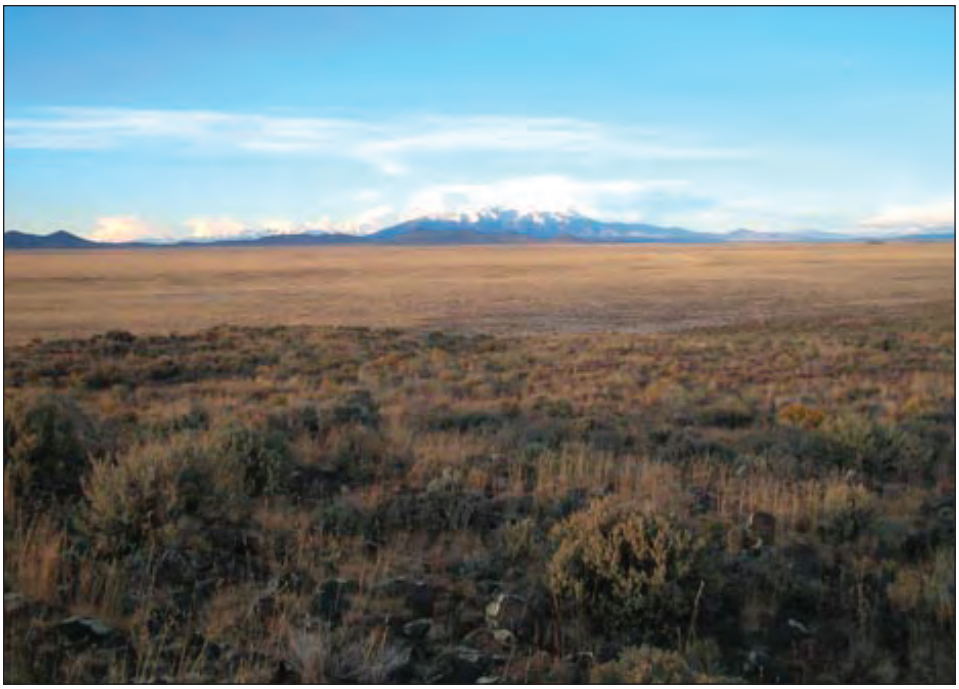

Figure B8.2–1. Surface morphology of basalts on the north flank of Mesita Volcano in foreground. View to the north shows northeast part of the San Luis Hills in the middle distance on the left and Blanca Peak is in the background. Photograph taken in October, 2006.

Figure B8.2–2. Locality on north flank of Mesita volcano that we sampled for ^{3}He surface-exposure dating. Machette, Thompson, and Shroba are shown from left to right, respectively.

of the dating method is constrained only by the erosion rate of the surface that is being sampled. Cosmogenic ^{3}He exposure ages in excess of several million years have been obtained in slowly eroding landscapes around the world (for example, Chile's Atacama Desert, Dry Valleys of Antarctica). See stop B3.3 for a discussion of the ^{3}He surface-exposure dating of basalts on spits of Lake Alamosa.

Strategy for Age Dating

The goal of sampling at B8.2 is simply to determine the exposure duration of the Mesita Volcano flow surfaces (fig. B8.2–2). We will use these data to test the plausibility of the burial or nonburial hypotheses discussed at stop B8.1. If the Mesita Cone and nearby Costilla Plain were not buried by some unknown thickness of alluvium (the burial hypothesis), then the exposure ages of the surfaces we sampled should be close to 1.0 Ma—which is the crystallization age of the Mesita Cone—and the ages should approach 1.0 Ma when a reasonable erosion rate is added into the age determination. If, however, the cone and Costilla Plain were buried by alluvium for a significant amount of time (such as 500 k.y.), then the exposure ages should be considerably younger than 1.0 Ma and not approach 1.0 Ma even when corrected for potential erosion rates.

Stop B8.3 — The Mesita Fault

Location: West flank of Mesita Volcano
Sky Valley Ranch 7.5' quadrangle
GPS: NAD27, Zone 13, 443100 m E., 4106660 m N.
Elevation: 7,820 ft (2,383 m) asl (upthrown block of fault)

Synopsis

Basalt flows dated at 1.0 Ma (stop B8.1) on the western margin of the Mesita volcano are displaced as much as 13 m by the Mesita fault, a down-to-the-west intrabasin fault that shows a well-documented history of progressive growth since Pliocene time. Quaternary alluvial deposits (mainly to the south of the volcano) are offset progressively less with decreasing age, whereas middle Pliocene flows of Servilleta Basalt (about 4.0±0.3 Ma) are offset substantially more than the 1.0 Ma basalt flows of the Mesita volcano. The offset of five geologic datums of Pliocene to late Quaternary age allows us to calculate long-term and interval slip rates through time, which on this fault are relatively constant at about 0.012 mm/yr. For comparison, the southern Sangre de Cristo fault zone shows an order of magnitude higher slip rates (see chapters C and J, this volume).

Discussion

The Mesita fault has been mapped from about 5 km (3 mi) north of Mesita Hill, south across the Costilla Plain 7 km (4.3 mi) into northern New Mexico. The southernmost mappable trace is on the northeast flank of Ute Mountain (recent mapping of the Sunshine and Ute Mountain areas by C.A. Ruleman, unpub. mapping, 2007). The fault's 22-km-long scarp (fig. B8.3–1) was first mapped by Colton (1976) as part of a reconnaissance study of landslides. The Mesita fault (#108 in Kirkham and Rogers, 1981, p. 25) forms a conspicuous west-facing scarp along the eastern side of the Sky Valley Ranch and Mesito Reservoir quadrangles, where it downdrops the west side of the Mesita cone by about 13 m (Kirkham and Rogers, 1981). Machette and Personius (1984) reported various amounts of offset of Quaternary alluvium along the fault, and Personius and Machette (1984) summarized the

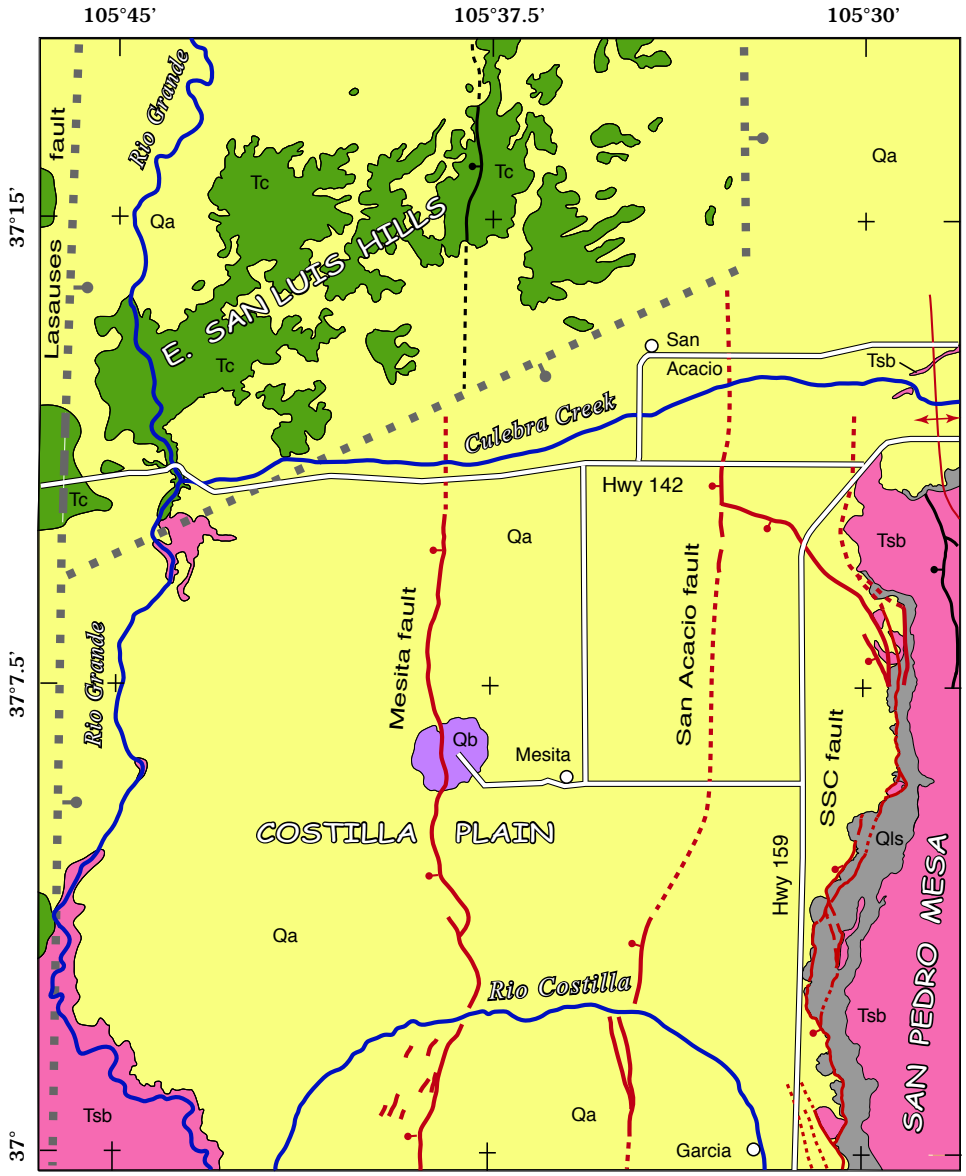

Figure B8.3–1. Costilla Plain (in Colorado) showing Quaternary faults (red lines) and older structures (black lines). Major Neogene faults that block out the San Luis Hills are shown by thicker gray dashed or dotted lines. Bedrock units lumped into the following: Qb, Mesita basalt (1.0 Ma); Tsb, Servilleta and age-equivalent basalts; Tc, Oligocene volcanic rocks. Quaternary units shown as Qa, with exception of landslide deposits (Qls) along San Pedro Mesa. SSC fault: southern Sangre de Cristo fault zone. Geology modified from Thompson and Machette (1989) and Thompson and others (2007).

fault in a regional overview of Quaternary faulting in northern New Mexico and southern Colorado. The Mesita fault is shown as structure 2015 in the U.S. Geological Survey Quaternary fault and fold database (see http://earthquake.usgs.gov/regional/qfaults/).

Quaternary Faulting

The intrabasin Mesita fault is positioned midway between the Sangre de Cristo fault zone on the east and the San Luis Hills on the west (fig. B8.3–1). To the south, the Mesita fault ends northeast of Ute Mountain where extension is transferred in an opposite sense to the intrabasin, down-to-the-east Sunshine Valley fault (see discussion in chapter C, this volume). The southern Sangre de Cristo fault zone, which is the main east-bounding structure for the Rio Grande rift in this region, is rather complex here. This 250-km-long fault system has three discrete fault zones, herein described from north to south. (See chapter J, this volume, for a more complete discussion of the Sangre de Cristo fault system and new designations of its individual fault zones.)

1. Northern fault zone: Extends about 104 km from Poncha Pass across the northern part of the San Luis Valley, along the west margin of Sangre de Cristo Mountains, east of the Great Sand Dunes and to the south flank of the Blanca Peak massif;

2. Central fault zone: Extends about 60 km from the south flank of the Blanca Peak massif through Fort Garland, along the west margin of Culebra Range and east side of the Culebra graben to the border with New Mexico; and

3. Southern fault zone: Extends about 96 km from southeast of San Acacio along the west side of San Pedro Mesa (stop B9) and the Sangre de Cristo Mountains of New Mexico to southeast of Taos at Talpa (see Personius and Machette, 1984), where it merges with the northeast-trending Embudo fault.

As part of their mapping of the San Luis Hills, Thompson and Machette (1989) measured the surface offset of Pleistocene alluvial deposits along the Mesita fault. The Mesita cone is surrounded by an apron of flows that spread outward from the eruptive center; a flow near our parking site (see location under B8) was dated at 1.01±0.03 Ma by Appelt (1998). Scarps formed on flows on the west side of the cone show consistent down-to-the-west offset of 8–10 m, less than the 13 m reported by Kirkham and Rogers (1981) probably owing to a blanket of eolian sand that covers parts of hanging-wall (western) block. The scarps extend about 2 km (1.3 mi) across the basalt of Mesita Hill; from there north and south, the scarps are formed on older alluvium (unit Qao of Thompson and Machette, 1989) of probable early(?) middle Pleistocene age. North of the volcano for about 6 km (4 mi), the scarps are about 2–3 m high on unit Qao. They are not present on the Holocene floodplain of Culebra Creek, nor to the north across late to middle Pleistocene alluvium and piedmont slope deposits. However, there is a coincident, down-to-the-west fault in upper Oligocene rocks (Conejos Formation) in the eastern part of the San Luis Hills (see Thompson and Machette, 1989) about 8 km (5 mi) northwest of San Acacio (fig. B8.3–1), which may reflect the northern part of a pre-Quaternary Mesita fault.

To the south of Mesita Hill, the fault traverses several ages of alluvial deposits: from young to old, they were mapped as unit Qay (latest Pleistocene, about 12–20 ka), unit Qam (now mapped as unit Qai; about 50–200 ka, late to middle Pleistocene), and unit Qao (about 500±100 ka, middle to early(?) middle Pleistocene). The scarps on these alluvial units are progressively higher and show progressively more surface offset with age. For example, scarps on unit Qao are 7–8 m high between Mesita Hill and Rio Costilla; scarps on unit Qai are commonly 2–3 m high south of Rio Costilla; and the single scarp mapped on unit Qay is 1.4 m high. The ages used for this slip-rate analysis are broad geologic estimates based on soil development, geomorphic expression, and regional mapping. Although Personius and Machette (1984) reported that the youngest movement on the fault was late Pleistocene (10–130 ka), we suspect that there also has been movement in the latest Pleistocene (10–35 ka) on the basis of the offset of unit Qay.

On the basis of the differential offset of the Quaternary geologic units Qay, Qai, Qao, and Qbx, there are three time intervals that record offset along the Mesita fault. However, subsurface data from ground-water investigations in the late 1970s provide additional information about an older offset (fourth interval) of the Servilleta Basalt by the fault. Water-well data are quite abundant in the San Luis Basin, but most are from the Alamosa subbasin where there are logs for thousands of wells that penetrate as much as 500 m (1,640 ft) of the Alamosa Formation. South of the San Luis Hills, there are far fewer holes drilled for water, and few go deeper than 150 m (492 ft). Nevertheless, this is a valuable data set for tracking the depth and configuration of the Servilleta Basalt, which is a regionally extensive set of Pliocene basalt flows that form an important marker bed in basin-fill sediment of the Santa Fe Group.

In addition to the domestic and limited agricultural water-well data for the Costilla Plain, a drilling program was conducted as part of a provocative water play in the late 1970s. At that time, the San Marcos Pipeline Company (later to be acquired by Enron) proposed to mine 15,000-acre-ft of ground water from the Costilla Plain and pipe it over La Veta Pass to its proposed San Marco coal-slurry plant in Walsenberg (see Zorich-Erker Engineering, Inc., 1980, v. 1, p. 2). There it would be used to pipe coal slurry to Texas for use in power-generation plants. This is just one of the many water plays that the San Luis Basin has and will continue to suffer through as water and energy demands grow in the western United States. In order to develop its well field, the San Marcos Pipeline Company drilled 33 test and production wells on and around the north side of Mesita Hill.

Zorich-Erker Engineering, Inc. (1980) used its drill-hole data and previously drilled water-well data to structure contour the top of the Servilleta Basalt and make several cross

sections. Cross section A-A' extends west to east across the Costilla Plain and crosses the Mesita fault about 2 km (1.3 mi) north of Mesita Hill. The map interpretation is based on the assumption that the uppermost Servilleta Basalt flow in each well is coeval. However, recent mapping by Thompson and others (2007) shows there are multiple flows intercalated with sediment of the Santa Fe Group, and it suggests that down-to-the-west faults (such as the Mesita and Sangre de Cristo) may limit the lateral extent of the flows coming from the west. For example, cross section A-A' in Zorich-Erker Engineering, Inc. (1980, pl. 3) shows about 42 m of offset on the Mesita fault, assuming that the upper Servilleta Basalt (unit Tsb) is the same on both sides. Conversely, if the upper flow were restricted to the west (downthrown) side of the fault, then the second (lower) flow to the west might correlate to the upper flow to the east. In that case, the offset on unit Tsb would be about 53 m. These subsurface offsets of the Servilleta Basalt are substantially more than reported by Epis (15 m, 1977) or Burroughs (15–30 m, 1978), which were based on less robust data. For the purposes of this discussion, we use an offset of 42–53 m for the Servilleta Basalt as measured from our interpretations of cross section A-A'.

Fault Slip Rates

The Mesita fault is one of the few extensional faults in the Rio Grande rift that has multiple offset and age data. It is relatively common to have paleoseismic slip data for multiple late Pleistocene or Holocene faulting events, and occasionally a comparison with an older dated unit; however, in this case we have four estimates of fault offset for Quaternary units and an additional estimate for offset of the 4.0±0.3 Ma Servilleta basalt.

We have plotted the offset versus age data in figure B8.3–2. The long-term slip rate for the Mesita fault is about 0.012 mm/yr (or m/k.y.) and is based on 12 m of differential offset between unit Qay (1.4 m) and unit Qbx (about 13 m). The younger units generally fall on this long-term rate line, mainly owing to large age error limits used. In addition, the 42–53 m of estimated offset on the 4.0±0.3 Ma Servilleta Basalt (unit Tsb) falls right on line. The Pliocene offset rate for the Mesita fault is 0.012 mm/yr (using 48 m of offset in 4 m.y.), virtually the same as the 1.0 m.y. rate. Admittedly, the slip rate on the Mesita fault is slow, but it is typical of intrabasin faults that are secondary to faster-moving range-bounding faults, such as the Sangre de Cristo and Wasatch fault zones (see chapters C and H, this volume)

For comparison, we also plotted the 50-k.y. slip rate that Crone and Machette (2005) determined for the central Sangre de Cristo fault zone as a result of trenching at Rito Seco Creek (Crone and others, 2006), located about 5 km (3 mi) northeast of San Luis, Colo. This rate is about 0.17 mm/yr—more than an order of magnitude faster than the Mesita fault. The late Pleistocene rate of the central Sangre de Cristo fault zone is comparable to the long-term rates that Kirkham (2005) calculated using the Servilleta Basalt (about 0.13 mm/yr) and middle Miocene volcanic rocks (about 0.145 mm/yr).

The Mesita fault is only 22 km long (in middle Quaternary deposits), and thus it is probably not capable of generating extremely large earthquakes (**M**>7) or large surface offsets (that is, >2 m). If one uses 1.5 m as a characteristic offset for earthquakes in the **M** 6.5–6.9 range, then the offset recorded in unit Qay (1.4 m) might reflect a single faulting event of this

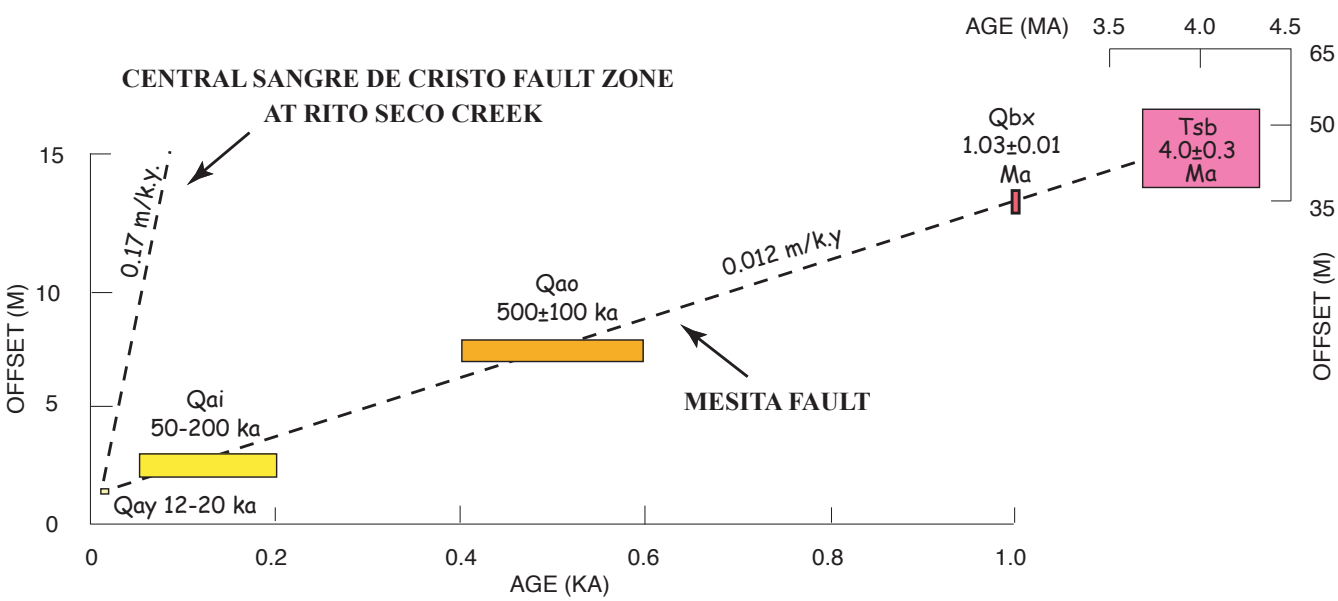

Figure B8.3–2. Amounts of offset of geologic units and slip rates for the Mesita fault. Age of Mesita basalt flow (unit Qbx) is precise, whereas age of Servilleta Basalt (unit Tsb) is range for dated flows in area. Dashed lines indicate average slip rate of Mesita fault for past 1.0 m.y., versus central Sangre de Cristo fault zone (past 50 k.y.) near San Luis, Colo. (see Crone and others, 2005, 2006). Unit Tsb is offset 42–53 m (138–173 ft) as measured from cross-section A-A′ in Zorich-Erker Engineering, Inc. (1980, plate 3).

magnitude. Similarly, the 3-m offset in unit Qai could be the result of 2 events and the 7–8 m offset in unit Qao could be the result of 5 events. Using 500 ka for unit Qao, yields a "back of the envelope" recurrence interval of >100 to 125 k.y. for the Mesita fault (that is, 4 events in a maximum of 500 k.y.). Similar low slip rates have been documented for relatively inactive intrabasin faults in the Rio Grande rift of New Mexico (Machette, 1998) and the Basin and Range province of Utah and Nevada (Machette, 2005).

The Sunshine Valley fault to the south in northern New Mexico (see chapter C), which may be an en echelon, opposite-sense extension of the Mesita fault, shows offset amounts and patterns in late to middle Pleistocene alluvium that are similar to offsets in the Mesita fault, and thus it probably also has extremely low slip rates.

Stop B9 — Landslides and the Sangre de Cristo fault Zone Along San Pedro Mesa

Speaker: Michael Machette
Location: Entrance to Melby Ranch (Wild Horse Mesa) on Colo. Highway 159, about 3.2 km south of Colo. Highway 248 to Mesita, Colo.
Garcia 7.5' quadrangle
GPS: NAD27, Zone 13, 453790 m E., 4102500 m N.
Elevation: 7,666 ft (2,337 m) asl (at entrance to Melby Ranch)

Synopsis

This stop provides a convenient place to view and discuss landslides and the southern Sangre de Cristo fault zone, which bounds the western margin of San Pedro Mesa—the high (8,500–8,900 ft or 2,590–2,713 m asl) basalt-covered surface to the east. The nearly 1,000-ft- (300-m-)high western escarpment of San Pedro Mesa is riddled with landslides, some quite massive (that is, many square kilometers in area). Faulting and landsliding have left large blocks of the Pliocene Servilleta Basalt at various altitudes and orientations. Landslides, rockfalls, colluvium, and ramps of eolian sand obscure the underlying problem unit—poorly consolidated sediment of the Santa Fe Group. To the west of us is the Costilla Plain, an extremely large, coalesced alluvial fan-piedmont slope complex that was deposited by Culebra Creek in middle Pleistocene time. Drillhole logs show that downdropped flows of Servilleta Basalt (4.0±0.3 Ma) are 30–50 m beneath the Costilla Plain, having been displaced about 300–400 m by the Sangre de Cristo fault zone and buried by Santa Fe Group sediment in the past 4 m.y.

Introduction

Stop B9 is just east of Highway 159 (Fort Garland to Questa) and near the western base of San Pedro Mesa, at the parking area for Melby Ranch Estates (formerly Wild Horse Mesa Estates). This a real-estate company that has developed several thousand 5- to 35-acre parcels on San Pedro Mesa. Most of the lots have been sold, and many continue to be resold either through this real-estate company, by others in the area, or by individual owners. Power is available on limited parts of the mesa, mainly along a western power line and along the eastern margin of the mesa. There are no County-supplied utilities (such as sewer, water, phone, or electric), so many of the homes are "off the net" (self-supporting). There have been no successful domestic water wells drilled on the mesa, and numerous 600 ft (183 m) deep wells have proven dry. However, the developer allows homeowners to haul water from his wells east of the mesa. There are fewer than 30 year-round households on the mesa and perhaps an equal number of summer-only residents.

Local Geology

The western margin of San Pedro Mesa, the high (8,500–8,900 ft or 2,590–2,713 m asl) basalt-covered plateau to the east of this stop, is structurally controlled by uplift along the northern part of the southern Sangre de Cristo fault zone, whereas the eastern margin is controlled by down-to-the east movement on the San Luis fault zone (on the east side of the mesa). For the most part, these fault zones underlie extensive landslide deposits all along the mesa's margins, but where the southern Sangre de Cristo fault zone crosses into New Mexico it is largely is coincident with the bedrock-alluvial contact along the east margin of Sunshine Valley (see stop C7 and chapter I, this volume).

Faulting has downdropped large blocks of Pliocene Servilleta Basalt, and landsliding has broken and jostled these blocks into various orientations. The combination of landslides, rock falls, colluvium, and ramps of eolian sand have obscured the poorly consolidated basin-fill sediment (unit Tsf, lower part of the Santa Fe Group, Pliocene to upper Oligocene) that typically underlies the basalt. Although it is poorly exposed, sparse road cuts indicate that most of the basin-fill sediment beneath San Pedro Mesa consists of moderately oxidized siltstone, sandstone, and lesser amounts of sandy pebble conglomerate.

To the west of this stop is the Costilla Plain, which was named by Upson (1939, 1971) for the small community of Costilla, N. Mex. (fig. C–1, chapter C, this volume). The Costilla Plain is an extremely large coalesced alluvial fan-piedmont slope that extends from Culebra Creek south to the subtle drainage divide between Costilla and Ute Mountain, in northernmost New Mexico (see discussion of this area in chapter C). The plain is underlain by old alluvium (unit Qao) deposited by the Rio Culebra in middle Pleistocene time. This alluvium consists of sandy pebble to small-cobble gravel at the north end of San Pedro Mesa, but becomes finer downstream (west and southwest) to pebbly sand near the Colorado–New Mexico border. The alluvium is unconformable on the upper part of the Santa Fe Group (unit QTsf), which is Pliocene to middle Pleistocene in this region (see mapping of Machette and others, 2007, and Thompson and others, 2007). In general, Quaternary alluvium (units Qay, Qai, and Qao; fig. B9–1) is coarser grained than the underlying basin-fill sediment as a result of having been deposited by higher energy, glacially fed streams. Conversely, the basin-fill sediment is relatively fine grained (primarily sandstone, siltstone, and claystone) having been deposited in quieter water, distal alluvial fan, fluvial, or playa environments. These same relations are apparent in the Sunshine Valley of northern New Mexico (see also stop C4).

Landslide Deposits

Three general types of landslides were mapped around the margins of San Pedro Mesa (fig. B9–2) by Thompson and others (2007). They include (1) younger landslide deposits (unit Qlsy) that show hummocky terrain, closed depressions, angular blocks of basalt, and localized accumulations of eolian sand and other cover deposits; (2) older landslide deposits (unit Qlso) that show subdued terrain, integrated drainage, fewer and more subangular blocks of basalt, and discontinuous mantles of eolian sand, colluvium, and alluvium; and (3) massive (as much as 2 km long) relatively intact rotated blocks of basalt than have either slid into place (unit Tsb[lb]) or have been faulted into place (unit Tsb) along strands of the southern Sangre de Cristo fault (see following discussion).

The most recent movement of these landslide deposits is considered to be middle to late Pleistocene (Thompson and others, 2007), although they have probably been mobile throughout much of the past 4 m.y. Figure B9–3 shows and aerial view of these landslide deposits. Their morphology, which is a guide for mapping, is quite apparent and disparate. In general, the younger landslide deposits extend further onto the Costilla Plain and generally cover strands of the fault zone that displace the older landslide deposits. This is not to

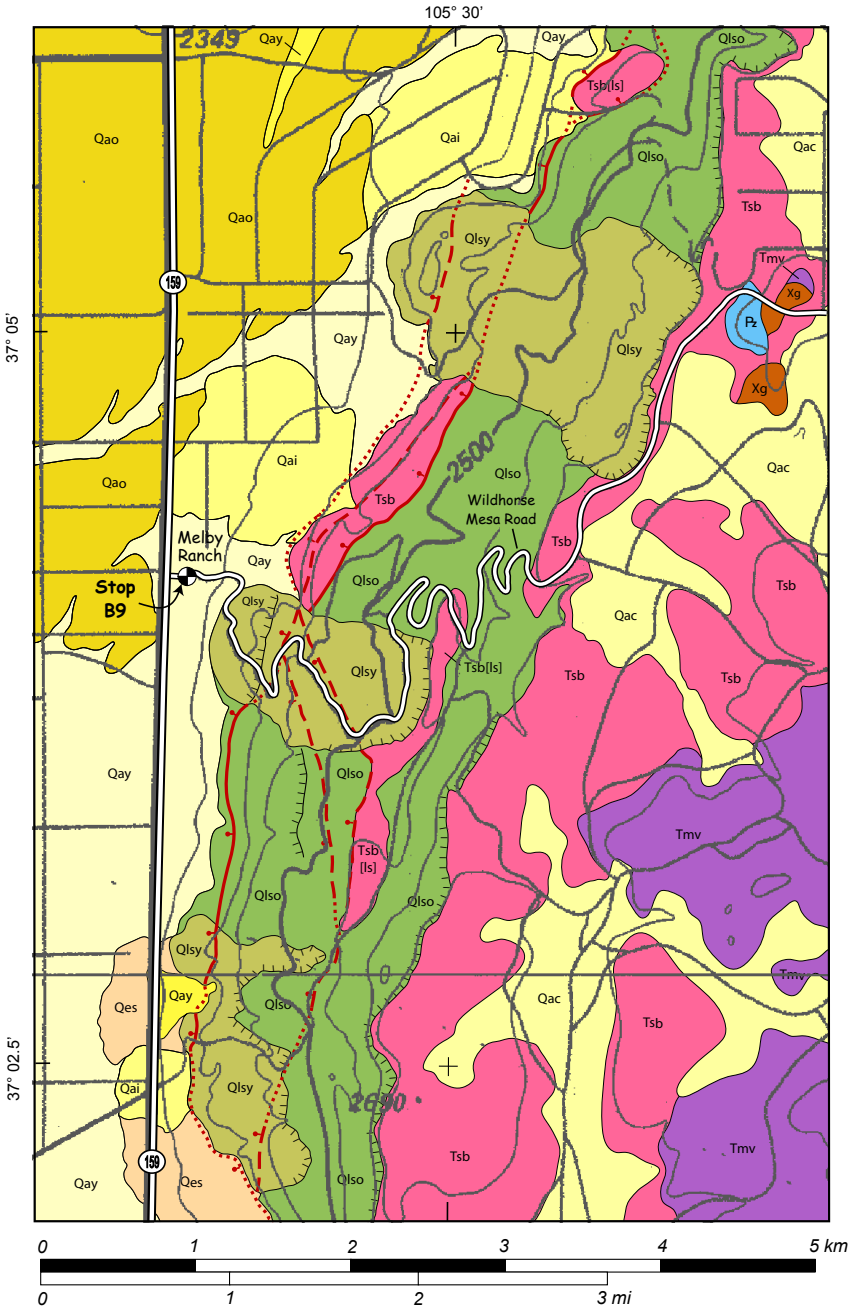

Figure B9–1. Western part of San Pedro Mesa. Quaternary traces of the Sangre de Cristo fault zone are shown in red. Map units: Xg, Early Proterozoic granite; Pz, Paleozoic rocks; Tmv, Miocene(?) volcanic rocks; Tsb, Pliocene Servilleta Basalt ([ls], landslide blocks); Qlso, older landslides; Qlsy, younger landslides; Qao, old alluvium; Qay, young alluvium; Qac, alluvium and colluvium; Qes, eolian sand. Geology simplified from Thompson and others, 2007. Base scanned from 1:100,000-scale Alamosa 30 x 60-minute sheet with metric contours.

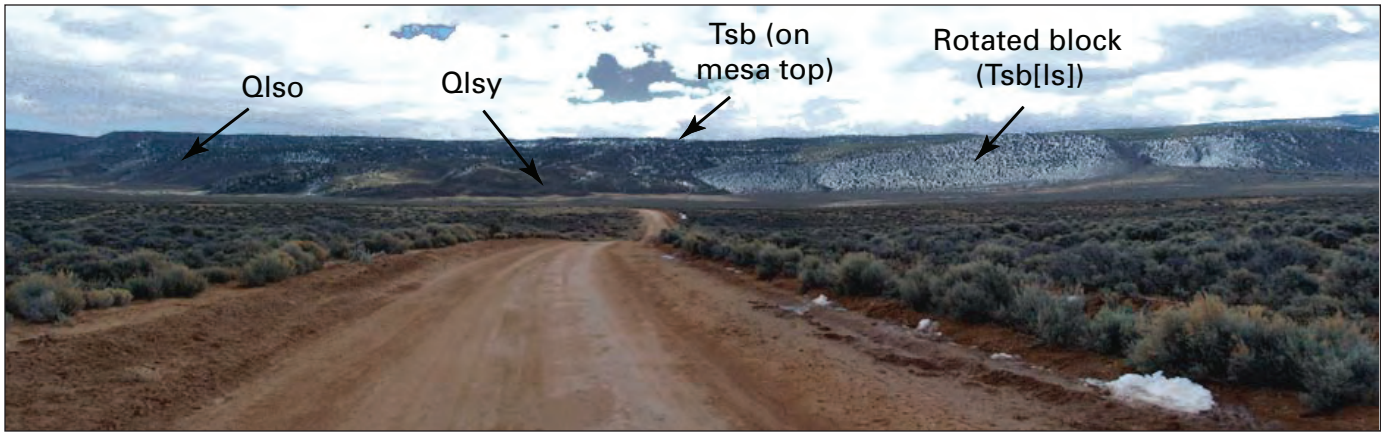

Figure B9–2. Panoramic view of west side of San Pedro Mesa. View to the east, taken from Highway 159 about 1 mi (1.6 km) north of stop B9 (see fig. B9–3). Labels: Qlso, older landslides; Qlsy, younger landslides; Tsb, Servilleta Basalt (about 4 Ma); Tsb[ls], landslide block of Servilleta Basalt.

say that the younger landslides are not faulted, but rather that discrete fault scarps are rarely preserved within the relatively weak, unconsolidated landslide debris. For example, Machette and others (2006) have documented very young movement (about 300 years old) along the Nephi segment of the Wasatch fault zone in central Utah. Massive landslide deposits about 1 km north of their Willow Creek trench site and due east of Mona, Utah, show no definitive traces, yet the fault is mapped up to the margins of the landslide. The Mona landslide is late Pleistocene in age (see Hardy and others, 1997) as shown by Lake Bonneville shorelines (>14.5 ka) on the distal (western) end of the landslide.

Conversely, most of the older landslide deposits (unit Qlso) marginal to San Pedro Mesa along the southern Sangre de Cristo fault zone have linear fronts (fig. B9–3), suggesting that they are faulted. No prominent fault scarps were noted during their mapping by Thompson and others (2007) owing to colluvial and eolian deposits that have accumulated at the base of steep landslide toes. In many instances, photograph lineaments that mark the fault zone are related to vegetation and soil-texture changes. However, because nontranslational landslides commonly have lobate forms when deposited, the linearity of their toes strongly suggests structural control.

Southern Sangre de Cristo Fault Zone

San Pedro Mesa is bounded by the northern part of the southern Sangre de Cristo fault zone, which is one of three fault zones that make up the larger Sangre de Cristo fault system (see chapter I). At the northern end of the mesa, the Servilleta Basalt is offset by numerous strands of the fault as it splays out (like a horse's tail) and changes trend from north-south to more north-northwesterly (see fig. B8.3–1 and mapping of Thompson and others, 2007). The westernmost strand of the fault zone abuts the San Acacio fault, which is one of two intrabasin faults in this part of the Costilla Plain. South of San Pedro Mesa (near Costilla, N. Mex.; see stop C7), the southern Sangre de Cristo fault zone emerges from landslide deposits and forms the bedrock-alluvial contact in the Sunshine Valley. Although this portion of the fault zone has more typical Basin and Range morphology, when mapped in detail it shows multiple surface traces with a complex rupture pattern (C.A. Ruleman, unpub. mapping, 2007).

San Pedro Mesa represents a Pliocene land surface that is now uplifted as a prominent horst block. It is bordered by the southern Sangre de Cristo fault zone on the west and by the San Luis fault zone on the east. The Sanchez graben lies just to the east of the horst—it is bordered by the central Sangre de Cristo fault zone on the east and the San Luis fault zone on the west (see new mapping by Thompson and others, 2007). The Sanchez graben is filled by Neogene sediment and Miocene to upper(?) Oligocene volcanic rocks that lie on Precambrian rock encountered at about 6,230 ft (1,900 m) depth in the Energy Operating Co. Williamson No. 1 well (R.M. Kirkham, written commun., 2005; see Thompson and others, 2007, for location of well, depths, and source of data). This well indicates that there is a minimum of 2,134 m (7,000 ft) of structural relief on the Precambrian rock across the San Luis fault zone. Conversely, Precambrian rock is exposed high in the Culebra Range to the east of the Sanchez graben and somewhere at depth beneath the Costilla Plain, west of the southern Sangre de Cristo fault zone.

The western escarpment of San Pedro Mesa rises southward 13 mi (21 km) to the State line, with the southernmost remnant of basalt preserved on an unnamed mesa about 5 mi (8 km) south of Costilla, N. Mex. (see discussion at stop C7). At the northern end of the mesa (near the north-south to east-west bend in Highway 159; fig. B8.3–1), the Servilleta Basalt is at basin level. It rises gently to the south, so that at the radio tower (about 10 mi to the north of stop B9) it is about 70 m (230 ft) above the Costilla Plain. At stop B9, the top of the mesa is at about 8,600 ft (2,621 m) asl, roughly 900 ft (275 m) above us. From here south to the State line, the top

the mesa climbs gently about 340 ft (104 m) to an elevation of about 8,940 ft (2,725 m) asl, or roughly 1,220 ft (372 m) above the Costilla Plain. Thus, San Pedro Mesa appears to be a northward-tilted ramp that transfers motion from the southern Sangre de Cristo fault zone in New Mexico to the central Sangre de Cristo fault zone in Colorado (see discussion in chapter H, this volume).

South of Costilla, N. Mex., San Pedro Mesa continues as an unnamed surface to the north side of Cedro Canyon (see fig. C–1, chapter C, this volume). This mesa is covered by the southernmost remnant of the Servilleta Basalt on the uplifted (footwall) block of the southern Sangre de Cristo fault zone. The basalt (unit Tsb) was dated at 4.3 Ma by Lipman and Reed (1989) by whole-rock K-Ar methodology. The basalt rests on an ancient land surface that Menges (1988) traced south into a prominent bench on the range front and used as a paleodatum to estimate uplift along the southern Sangre de Cristo fault zone (see further discussion in chapter H).

Little is known about the rupture history of the southern Sangre de Cristo fault zone. Kelson and others (2004) have conducted the only paleoseismic investigation of this fault zone at a site near Taos, N. Mex. (see also chapter I). Dating of the most recent event was poorly constrained, but they concluded that the fault had latest Pleistocene movement. Conversely, scarp morphology studies along the New Mexico portion of the fault zone indicated Holocene rupture to Menges (1988) and Personius and Machette (1984), and recent mapping by C.A. Ruleman (unpub. mapping, 2007) (see stop C6) documents Holocene ruptures. As previously mentioned, we didn't find any fault scarps formed on alluvial deposits along San Pedro Mesa; thus, we are unable to estimate the time of the most recent faulting event. However, on the basis of the fault's expression in landslide deposits, we suspect that the New Mexico portion of the fault zone may have latest Pleistocene movement.

For comparison, the central Sangre de Cristo fault zone offsets latest Pleistocene alluvium at the mouth of Rito Seco Creek, which is located about 3 mi (4.8 km) northeast of San Luis, Colo., and about 14 mi (22 km) north-northeast of this stop. A paleoseismic investigation by Crone and others (2006) dates the most recent movement at Rito Seco Creek at about 9 ka and documents four discrete surface faulting events in the past 50 k.y. The paleoseismic record at that site suggests slip rates of about 0.17 mm/yr and average recurrence intervals of roughly 12 k.y. (Crone and Machette, 2005). As such, the Sangre de Cristo fault system is the most active and longest Quaternary fault in the Rio Grande rift, which extends from central Colorado to northern Mexico.

Subsurface Geology

Drill-hole logs (Zorich-Erker Engineering, Inc., 1980) show that the uppermost flows of Servilleta Basalt are 30–50

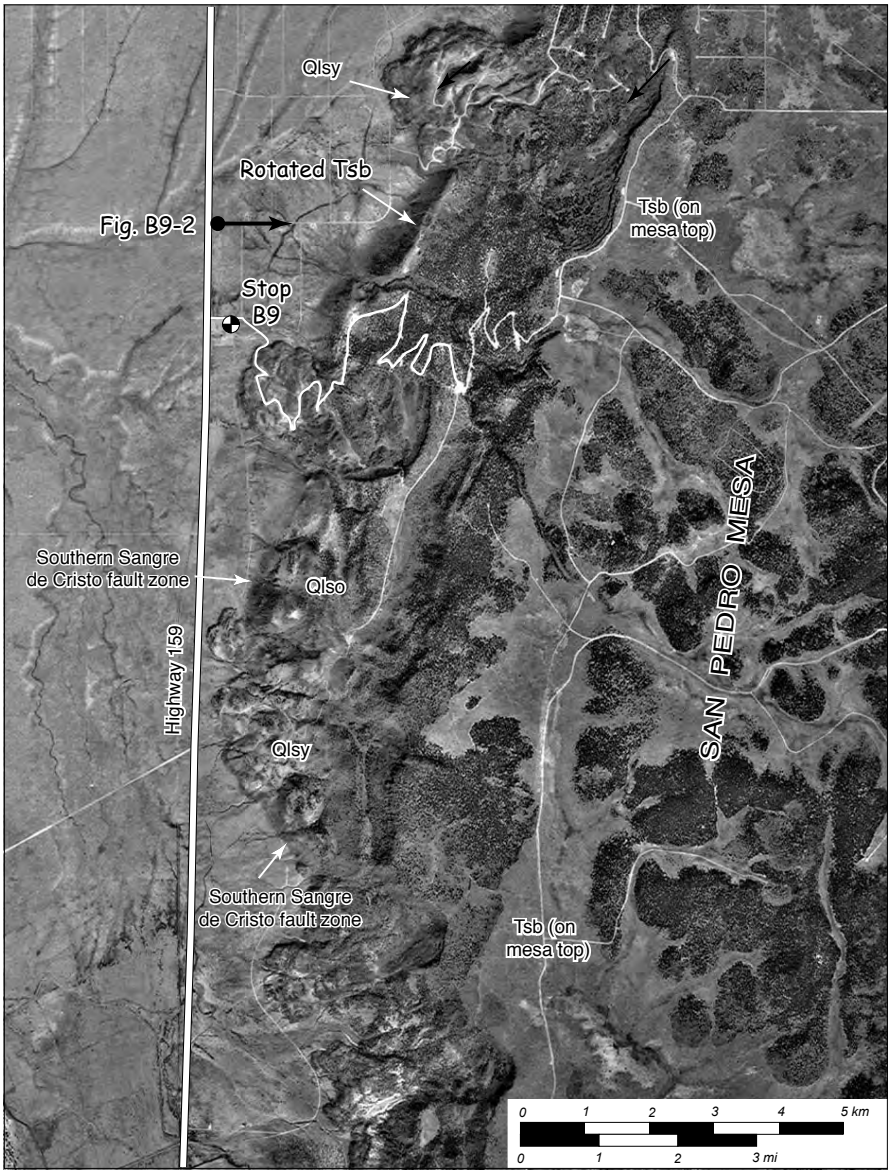

Figure B9–3. Landslides along west side of San Pedro Mesa. Compare with geologic map shown in figure B9–1. Map units: Qlsy, younger landslides; Qlso, older landslides; Tsb, Servilleta Basalt (about 4 Ma). Scanned image is from USGS HAP aerial photograph 428–112, 9–16–83, 1:80,000 scale.

m (100–165 ft) beneath the Costilla Plain and they increase in depth to the east towards the southern Sangre de Cristo fault zone. These relations are shown diagrammatically in figure B9–4, which is a west-northwest–east-southeast section that crosses the Costilla Plain about 2 km north of stop B9. The cross section suggests that there has been about 300–400 m (1,000–1,300 m) of offset along the fault zone in the past 4 m.y. (We use 4.0±0.3 Ma for the probable age range of Servilleta Basalt in this area.) The relations shown in this cross section are quite similar to those of the Sunshine Valley (fig. C7–5), with the exception that Pliocene Lake Sunshine occupied an east-tilted block that abuts southern Sangre de Cristo fault zone. Lake Sunshine is analogous to Lake Alamosa but was not as long lived. As mentioned previously, there is little net offset of the Servilleta Basalt at the northwest end of the San Pedro Mesa, but the 300–400 m of offset along the Colorado portion suggests long-term slip rates of 0.075–0.10 mm/yr of the southern Sangre de Cristo fault zone (compare with New Mexico rates, stop C7 and chapter J, this volume).

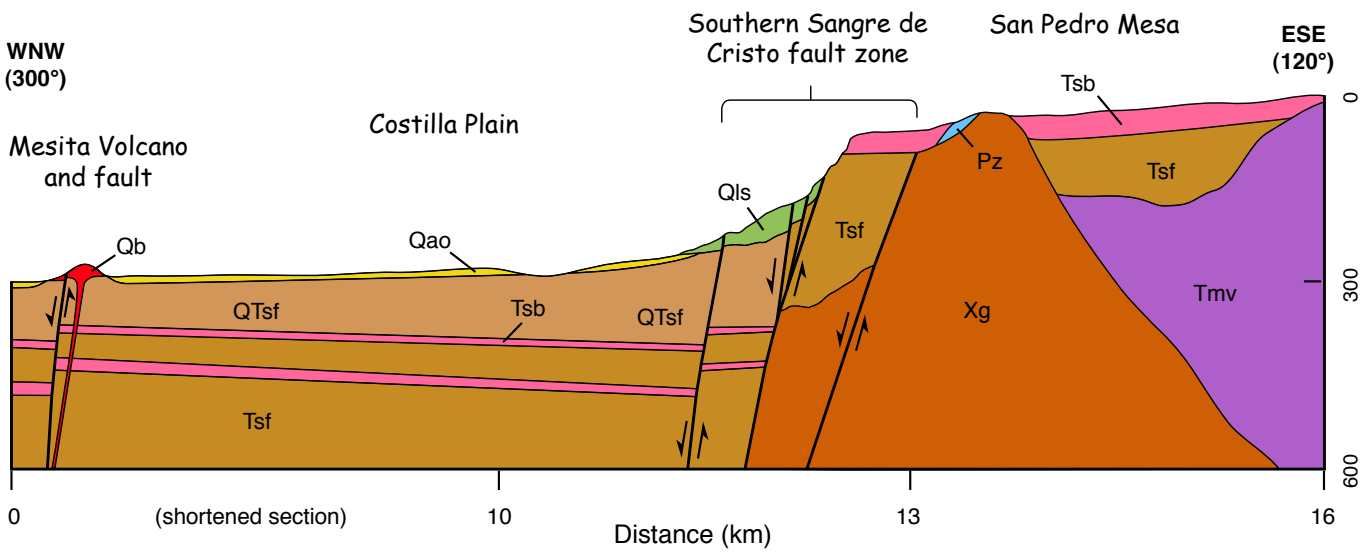

Figure B9–4. Diagrammatic cross section of the Costilla Plain and San Pedro Mesa. Map units: Qls, landslides (Quaternary); Qao, older alluvium (middle Pleistocene); Qb, Mesita basalt (1.0 Ma); QTsf, Santa Fe Group, upper part (middle Pleistocene to Pliocene); Tsb, Servilleta Basalt (about 4 Ma); Tsf, Santa Fe Group, lower part (Pliocene to upper Oligocene); Tmv, middle(?) Miocene volcanic rocks; Pz, Paleozoic sandstone; Xg, Early Proterozoic granitic rock. Based on unpublished geologic mapping of Michael Machette and Ren Thompson (2007) and drill-hole data of Zorich-Erker Engineering, Inc. (1980). Depths (in meters) are exaggerated about 3x and Costilla Plain part of section (0–11 km) is shortened to fit on cross section.

References Cited

Appelt, R.M., 1998, $^{40}Ar/^{39}Ar$ geochronology and volcanic evolution of the Taos Plateau volcanic field, northern New Mexico and southern Colorado: Socorro, New Mexico Institute of Mining and Technology, M.S. thesis, 58 p.

Birkeland, P.W., 1999, Soils and Geomorphology, 3d ed.: New York, Oxford University Press, 430 p.

Burroughs, R.L., 1972, Geology of the San Luis Hills, south-central Colorado: Albuquerque, University of New Mexico, Ph.D. dissertation, 139 p.

Burroughs, R.L., 1978, Alamosa to Antonito, Colorado (p. 33–36, in Northern rift guide 2, Alamosa, Colorado—Santa Fe, New Mexico), *in* Hawley, J.W., ed., Guidebook to Rio Grande rift in New Mexico and Colorado: New Mexico Bureau of Mines and Mineral Resources Circular 103, 241 p.

Colton, R.B., 1976, Map showing landslide deposits and late Tertiary and Quaternary faulting in the Fort Garland–San Luis area, Colorado: U.S. Geological Survey Open-File Report 76–185, scale 1:250,000.

Crone, A.J., and Machette, M.N., 2005, Paleoseismic activity on the Sangre de Cristo fault near San Luis, Colorado: Geological Society of America Abstracts with Programs, v. 37, no. 7, p. 558 (Paper 256–2).

Crone, A.J., Machette, M.N., and Mahan, S.A., 2006, Paleoseismic investigation of Rito Seco site, central section of the Sangre de Cristo fault zone, Colorado—Data related to late Quaternary surface faulting on the Sangre de Cristo fault, Rito Seco site, Costilla County, Colorado: U.S. Geological Survey Scientific Investigations Map SI–2955, 1 oversize pl. (http://pubs.usgs.gov/sim/2006/2955).

Currey, D.R., 1990, Quaternary palaeolakes in the evolution of semidesert basins, with special emphasis on Lake Bonneville and the Great Basin, U.S.A., *in* Davis, O.K., ed., Paleoenvironments of arid lands: Palaeogeography, Palaeoclimatology, Palaeoecology, v.76, no. 3–4, p.189–214.

Endlich, F.M., 1877, Part I—Geology, Chap. II—San Luis Valley, *in* F.V. Hayden's Ninth Annual Report of the United States Geological and Geographical Survey of the Territories . . . for the year 1875: Washington, D.C., Government Printing Office, p. 140–149, and plate XVII.

Epis, R.C., 1977, Surface and subsurface geology of the Mesita volcano area, Costilla County, Colorado, *in* Zorich-Erker Engineering, Inc., Ground water availability of the San Marco property near Mesita in Costilla County, Colorado: Report submitted to San Marco Pipeline Company, Denver, Colorado, dated September, 30, 1980, v. III, Appendix A, 20 p., plus map and cross section.

Giegengack, R.F., 1962, Recent volcanism near Dotsero, Eagle County, Colorado: Boulder, University of Colorado, M.S. thesis, 54 p.

Gosse, J.C., and Phillips, F.M., 2001, Terrestrial in situ cosmogenic nuclides—Theory and application: Quaternary Science Reviews, v. 20, no. 14, p. 1475–1560.

Hardy, K.M., Mulvey, W.E., and Machette, M.N., 1997, Surficial geologic map of the Nephi segment of the Wasatch fault zone, eastern Juab County, Utah: Utah Geological Survey Map 170, 14 p. pamphlet, 1 plate, 1:50,000 scale.

Johnson, R.B., 1969, Geologic map of the Trinidad 1 x 2 degree quadrangle, south-central Colorado: U.S. Geological Survey Miscellaneous Investigations Map I–558, scale 1:250,000.

Kelson, K., Bauer, P.W, Love, D., Connell, S.D., Mansell, M., and Rawling, G., 2004, Initial paleoseismic and hydrologic assessment of the southern Sangre de Cristo fault at the Taos Pueblo site, Taos, New Mexico: New Mexico Bureau of Geology and Mineral Resources Open-File Report 476, 46 p.

Kirkham, R.M., 2006, Surprises in the Culebra graben, a major sub-basin within the San Luis basin of the Rio Grande rift: Geological Society of America Abstracts with Programs, v. 38, no. 6, p. 14.

Kirkham, R.M., Brister, B.S., Grauch, V.J.S., and Budahn, J.R., 2005, Culebra graben—A major intrarift structure in the San Luis Basin, Rio Grande rift: Geological Society of America Abstracts with Programs, v. 137, no. 6, p. 14 (Paper 8–4).

Kirkham, R.M., and Rogers, W.P., 1981, Earthquake potential in Colorado: Colorado Geological Survey Bulletin 43, 171 p., 3 pls.

Kunk, M.J., Budahn, J.R., Unruh, D.M., Stanley, J.O., Kirkham, R.M., Bryant, Bruce, Scott, R.B., Lidke, D.J., and Streufert, R.K., 2002, $^{40}Ar/^{39}Ar$ ages of late Cenozoic volcanic rocks within and around the Carbondale and Eagle collapse centers, Colorado—Constraints on the timing of evaporite related collapse and incision of the Colorado River, *in* Kirkham, R.M., Scott, R.B., and Judkins, T.W., eds., Late Cenozoic evaporite tectonism and volcanism in west-central Colorado: Geological Society of America Special Paper 366, p. 213–234.

Lal, D., 1991, Cosmic ray labeling of erosion surfaces—In-situ nuclide production rates and erosion models: Earth and Planetary Science Letters, v. 104, p. 424–439.

Lanphere, M.A., Champion, D.E., Christiansen, R.L., Izett, G.A., Obradovich, J.D., 2002. Revised ages for tuffs of the Yellowstone Plateau volcanic field—Assignment of the Huckleberry Ridge Tuff to a new geomagnetic polarity event: Geological Society of America Bulletin 114, p. 559–568.

Licciardi, J.M., Kurz, M.D., Clark, P.U., and Brook, E.J., 1999, Calibration of cosmogenic ^{3}He production rates from Holocene lava flows in Oregon, USA, and effects of the Earth's magnetic field: Earth and Planetary Science Letters, v. 172, p. 261–271.

Lipman, P.W., and Mehnert, H.H., 1979, The Taos Plateau volcanic field, northern Rio Grande rift, New Mexico, *in* Reicker, R.C., ed., Rio Grande rift—Tectonics and magmatism: American Geophysical Union, Washington D.C., p. 289–311.

Lipman, P.W., and Reed, J.C., Jr., 1989, Geologic map of the Latir volcanic field and adjacent areas, northern New Mexico: U.S. Geological Survey Miscellaneous Investigations Series Report I–1907, 2 sheets, 1:48,000 scale.

Lisiecki, L.E., and Raymo, M.E., 2005, A Pliocene-Pleistocene stack of 57 globally distributed benthic δ^{18}O records: Paleooceanography, v. 20, no. 1, 17 p., doi:10.1029/2004PA001071.

Machette, M.N., 1978, Dating Quaternary faults in the southwestern United States using buried calcic paleosols: U.S. Geological Survey Journal of Research, v. 6, no. 3, p. 369–381.

Machette, M.N., 1985, Calcic soils of the southwestern United States, *in* Weide, D.L., ed., Soils and Quaternary geology of the southwestern United States: Geological Society of America Special Paper 203, p. 1–21.

Machette, M.N., 1998, Contrasts between short- and long-term records of seismicity in the Rio Grande rift—Important implications for seismic-hazards analysis in areas of slow extension, *in* Lund, W.R., ed., Western States Seismic Policy Council (WSSPC) Basin and Range Province Seismic-Hazards Summit, Proceedings: Utah Geological Survey Miscellaneous Publication 98–2, p. 84–95.

Machette, M.N, 2005, Summary of the late Quaternary tectonics of the Basin and Range province in Nevada, eastern California, and Utah, *in* Lund, W.R., ed., Basin and Range Province Seismic Hazards Summit II, Western States Seismic Policy Council, Reno, Nevada, May 16–91, 2004, Proceedings: Utah Geological Survey Miscellaneous Publication 05–2 (CD-ROM), 18 p., 12 full-color figures, 2 tables.

Machette, M.N., Crone, A.J., Personius, S.F., Dart, R.L., Lidke, D.J., Mahan, S.A., and Olig, S.S., 2006, Paleoseismology of the Nephi segment of the Wasatch fault zone, Juab County, Utah—Preliminary results from two large exploratory trenches at Willow Creek: U.S. Geological Survey Scientific Investigations Map 2966, 2 oversize plates (http://pubs.usgs.gov/sim/2006/2966).

Machette, M.N., Long, T., Bachman, G.O., and Timbel, N.R., 1997, Laboratory data for calcic soils in central New Mexico—Background information for mapping Quaternary deposits in the Albuquerque Basin: U.S. Geological Survey Open-File Report 96–772, 60 p.

Machette, M.N., and Marchetti, D.W., 2006, Pliocene to middle Pleistocene evolution of the Rio Grande, northern New Mexico and southern Colorado: Geological Society of America Abstracts with Programs, v. 38, no. 6, p. 36 (Paper 18–2).

Machette, M.N., and Personius, S.F., 1984, Map showing Quaternary and Pliocene faults in the east part of the Aztec 1° x 2° quadrangle and west part of the Raton 1° x 2° quadrangle, northern New Mexico: U.S. Geological Survey Miscellaneous Field Studies Map MF–1465–B, scale 1:250,000 with 14-page pamphlet.

Machette, M.N., and Thompson, R.A., 2005, Preliminary geologic map of the northwestern part of the Alamosa ½° x 1° quadrangle, Alamosa and Conejos Counties, Colorado: U.S. Geological Survey Open-File Report 2005–1392, 1 sheet, 1:50,000 scale.

Machette, M.N., Thompson, R.A., and Drenth, B.J., 2007, Geologic map of the San Luis quadrangle, Costilla County, Colorado: U.S. Geological Survey Scientific Investigations Map 2963, 1 sheet, 1:24,000 scale (http://pubs.usgs.gov/sim/2007/2963).

Marchetti, D.W., and Cerling, T.E., 2005, Cosmogenic ^{3}He exposure ages of Pleistocene debris flows and desert pavements in Capitol Reef National Park, Utah: Geomorphology, v. 67, no. 3–4, p. 423–435.

Marchetti, D.W., Cerling, T.E., and Lips, E.W., 2005. A glacial chronology for the Fish Creek drainage of Boulder Mountain, Utah, USA: Quaternary Research, v. 64, p. 264–271.

Menges, C.M., 1988, The tectonic geomorphology of mountain-front landforms in the northern Rio Grande rift near Taos, New Mexico: Albuquerque, University of New Mexico, unpublished Ph.D. dissertation, 339 p.

O'Connor, J.E., 1992, Hydrology, hydraulics, and geomorphology of the Bonneville flood: Geological Society of America Special Paper 274, 83 p.

Personius, S.F., and Machette, M.N., 1984, Quaternary and Pliocene faulting in the Taos Plateau, northern New Mexico, *in* Baldridge, S.W., Dickerson, P.W., Riecker, R.E., and Zidek, Jiri, eds., Rio Grande rift—Northern New Mexico: New Mexico Geological Society 35th Annual Field Conference Guidebook, p. 83–90.

Reheis, M.C., Sarna-Wojcicki, A.M, Reynolds, R.L., Repenning, C.A., and Mifflin, M.D., 2002, Pliocene to middle Pleistocene lakes in the western Great Basin—Ages and connections, *in* Hersheler, R., Madsen, D.B., and Currey, D.R., eds., Great Basin aquatic systems history: Washington, D.C., Smithsonian Institution Press, Smithsonian Contributions to the Earth Sciences, v. 33, p. 53–108.

Rogers, K.L., 1984, A paleontologic analysis of the Alamosa Formation (south-central Colorado; Pleistocene, Irvingtonian), *in* Baldridge, W.S., Dickerson, P.W., Riecher, E., and Zidek, J., eds., Rio Grande Rift—Northern New Mexico: New Mexico Geological Society 35th Annual Field Conference Guidebook, v. 35, p. 151–155.

Rogers, K.L., 1987, Pleistocene high altitude amphibians and reptiles from Colorado (Alamosa local fauna: Pleistocene, Irvingtonian): Journal of Vertebrate Paleontology, v. 7, no. 1, p. 82–95.

Rogers, K.L., and Larson, E.E., 1992, Pliocene and Pleistocene sedimentation in south-central Colorado—Opportunity for climate studies: Quaternary International, v. 13/14, p. 15–18.

Rogers, K.L., Larson, E.E., Smith, G.A., Katzman, D., Smith, G.R., Cerling, T.E., Wang, Y., Baker, R.G., Lohmann, K.C., Repenning, C.A., Patterson, P.E., Mackie, G., 1992, Pliocene and Pleistocene geologic and climatic evolution in the San Luis Valley of south-central Colorado: Palaeogeography, Palaeoclimatology, Palaeoecology, v. 94, no. 1–4, p. 55–86.

Rogers, K.L., Repenning, C.A., Forester, R.M., Larson, E.E., Hall, S.A., Smith, G.A., Anderson, Elaine, and Browen, T.J., 1985, Middle Pleistocene (Late Irvingtonian: Nebraskan) climatic changes in south-central Colorado: National Geographic Research, v. 1, no. 4, p. 535–563.

Sarna-Wojcicki, Andrei M., Pringle, M.S., and Wijbrans, J., 2000, New $^{40}Ar/^{39}Ar$ age of the Bishop Tuff from multiple sites and sediment rate calibration for the Matuyama-Brunhes boundary: Journal of Geophysical Research, v. 105, no. B9, p. 21,431–21,444.

Sharp, W.D., Ludwig, K.R., and Hellstrom, J., 2005, U-series dating targets in arid and semi-arid environments: Geological Society of America Abstracts with Programs, v. 37, no. 7, p. 479, Paper 216–5.

Siebenthal, C.E., 1910, Geology and water resources of the San Luis Valley, Colorado: U.S. Geological Survey Water-Supply Report 240, 128 p.

Thompson, R.A., and Lipman, P.W., 1994a, Geologic map of the Los Pinos quadrangle, Rio Arriba and Taos Counties, New Mexico and Conejos County, Colorado: U.S. Geological Survey Map GQ–1749, scale 1:24,000.

Thompson, R.A., and Lipman, P.W., 1994b, Geologic map of the San Antonio Mountain quadrangle, Rio Arriba County, New Mexico: U.S. Geological Survey Map GQ–1750, scale 1:24,000.

Thompson, R.A., and Machette, M.N., 1989, Geologic map of the San Luis Hills, Conejos and Costilla Counties, Colorado: U.S. Geological Survey Miscellaneous Investigations Series Map I–1906, scale 1:50,000.

Thompson, R.A., Machette, M.N., and Drenth, B.J., 2007, Geologic map of San Pedro Mesa and surrounding area, Costilla County, Colorado: U.S. Geological Survey Open-File Report 2007–1074, 1 sheet, 1:24,000 scale (http://pubs.usgs.gov/ofr/2007/1074).

Upson, J.E., 1939, Physiographic subdivisions of the San Luis Valley, southern Colorado: Journal of Geology, v. 47, no. 7, p. 721–736.

Upson, J.E., 1971, Physiographic subdivisions of the San Luis Valley, southern Colorado, *in* James, H.L., ed., Guidebook of the San Luis Basin, Colorado: New Mexico Geological Society, p. 113–122 (Reprinted from Upson, 1939, with recent notes and bibliography by the author).

Wells, S.G., Kelson, K.I., and Menges, C.M., 1987, Quaternary evolution of fluvial systems in the northern Rio Grande rift, New Mexico and Colorado—Implications for entrenchment and integration of drainage systems, *in* Menges, C., ed., Quaternary tectonics, landform evolution, soil chronologies and glacial deposits—Northern Rio Grande rift of New Mexico: Friends of the Pleistocene—Rocky Mountain Cell Field Trip Guidebook, Oct. 8–11, 1987, p. 55–69.

Zorich-Erker Engineering, Inc., 1980, Ground water availability on the San Marco property near Mesita in Costilla County, Colorado: Denver, Colorado, Report prepared for San Marco Pipeline Company, 3 volumes with plates.

Selected Bibliography on Ventifacts

Breed, C.S., McCauley, J.F., Whitney, M.I., Tchakarian, V.P., and Laity, J.E., 1997, Wind erosion in drylands, *in* Thomas, D.S.G., ed., Arid zone geomorphology, 2d ed.: Chichester, England, Wiley, p. 437–464.

Bridges, N.T., Laity, J.E., Greeley, R., Phoreman, J., and Eddlemon, E.E., 2004, Insights on rock abrasion and ventifact formation from laboratory and field analog studies with applications to Mars: Planetary and Space Science, v. 52, p. 199–213.

Bryan, K., 1931, Windworn stones or ventifacts with a discussion and a bibliography: Washington, D.C., National Research Council Report, Commission on Sediments, 1929–30, p. 29–50.

Greeley, R., Bridges, N.T., Kuzmin, R.O., and Laity, J.E., 2002, Terrestrial analogs to wind-related features at the Viking and Pathfinder landing sites on Mars: Journal of Geophysical Research (Planets), v. 107, no. E1, p. 5–1 to 5–21.

Laity, J.E., 1992, Ventifact evidence for Holocene wind patterns in the east-central Mojave Desert: Zeitschrift für Geomorphologie, Suppl.-Bd., v. 84, p. 73–88.

Laity, J.E., 1994 Landforms of aeolian erosion, *in* Abrahams, A., and Parsons, A., eds., Geomorphology of desert environments: London, Chapman and Hall, p. 506–535.

Laity, J.E., 1995, Wind abrasion and ventifact formation in California, *in* Tchakerian, V.P., ed., Desert aeolian processes: London, Chapman and Hall, p. 295–321.

McCauley, J.F., Breed, C.S., Grolier, M.J. and El-Baz, F., 1980, Pitted rocks and other ventifacts in the western desert: Geographical Journal, v. 146, no. 1, p. 84–85.

Needham, C.E., 1937, Ventifacts in New Mexico: Journal of Sedimentary Petrology, v. 7, no. 1, p. 31–33.

Sharp, R.P., 1949, Pleistocene ventifacts east of the Bighorn Mountains, Wyoming: Journal of Geology, v. 57, no. 2, p. 175–195.

Sugden, W., 1968, Ventifacts, *in* Fairbridge, R.W., ed., Encyclopedia of geomorphology: New York, Reinhold Publishing Co., p. 1192–1193.

Wentworth, C.K., and Dickey, R.I., 1935, Ventifact localities in the United States: Journal of Geology, v. 43, no. 1, p. 97–104.

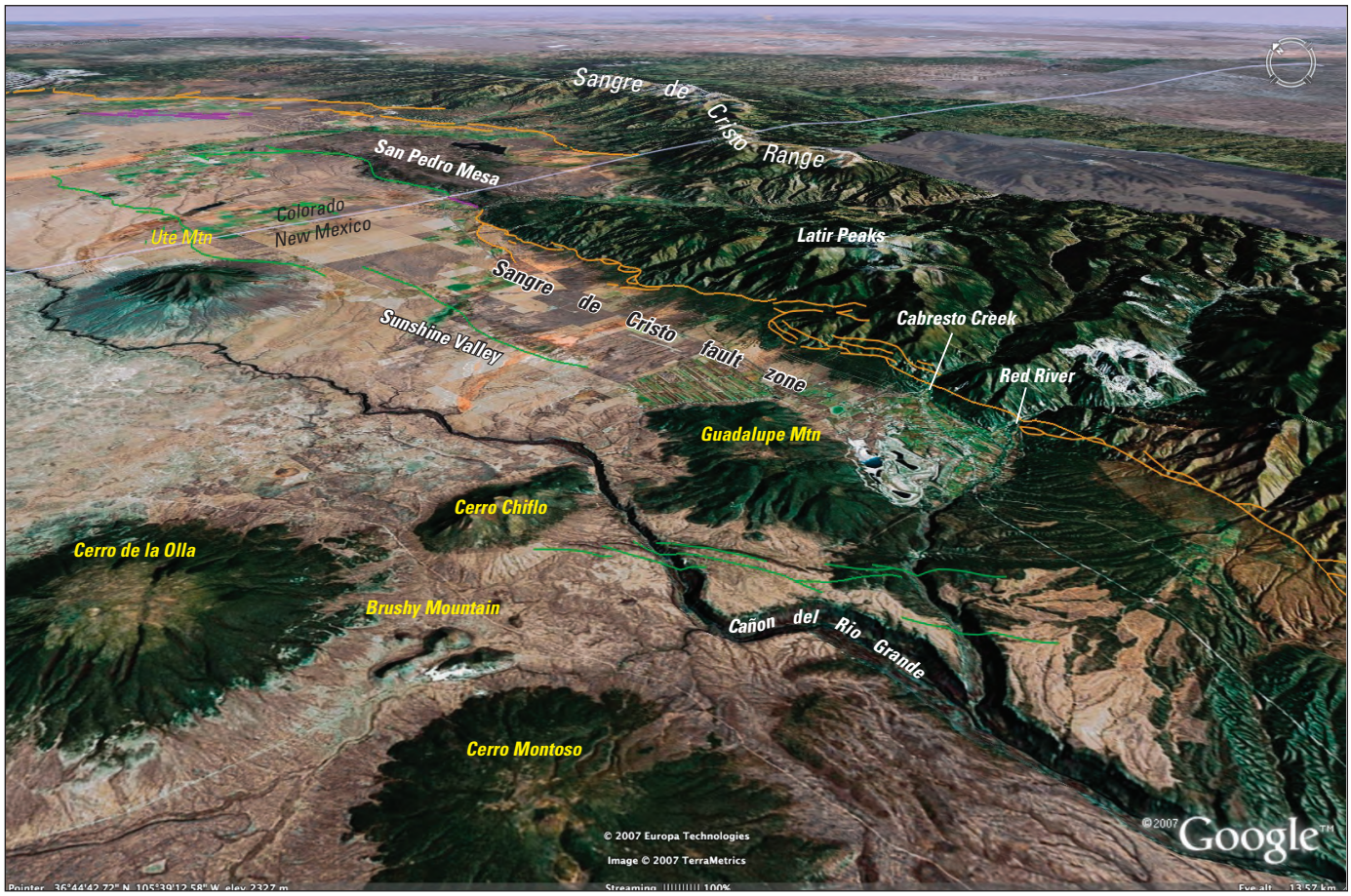

Frontispiece, Chapter C. Oblique aerial view of Sunshine Valley as imaged by Google Earth (v.4.0.1694, beta; © 2007 Europa Technologies, New Mexico; image © 2007 TerraMetrics). Faults shown as green, orange, and magenta lines from USGS Quaternary Fault and Fold Database (http://earthquake.usgs.gov/regional/qfaults/).

Chapter C — Field Trip Day 3 Quaternary Geology of Sunshine Valley and Associated Neotectonics Along the Latir Peaks Section of the Southern Sangre de Cristo Fault Zone

By Cal Ruleman, Ralph Shroba, and Ren Thompson

Overview

Day 3 focuses on our current understanding of the volcanogenic, fluvial, and tectonic development of Sunshine Valley, including the piedmont adjacent to the Latir Peaks–Taos Mountains. We begin by discussing the volcanogenic and fluvial setting of Sunshine Valley and the Rio Grande–Red River system prior to Cañon del Rio Grande incision. This sets the stage for an inspection of the geomorphic and tectonic development and associated landforms of Sunshine Valley related to headward erosion of the Rio Grande River system.

Throughout the day we will traverse multiple surfaces related to changes in the depositional, tectonic, and geomorphic system of Sunshine Valley (fig. C–1). We have interpreted these surfaces of differing age and position as representing a shift from a slowly aggrading, closed-basin system to a degradational, cut-and-fill system with base level controlled by the incision of the Rio Grande River. We will observe and discuss structural controls on the position of the Rio Grande canyon within the basin. At the northern end of Sunshine Valley we will look at scoured channels on Servilleta Basalt (3.66–4.75 Ma) and discuss evidence for basin geomorphic system changes associated with headward erosion of the Rio Grande. We will discuss initiation of canyon erosion and its probable association with Lake Alamosa. Heading east towards the Taos Mountains–Latir Peaks range front of the Sangre de Cristo Range, day 3 will conclude with a look at Quaternary faulting along the Sangre de Cristo fault zone and the probable tectonic controls on piedmont development and morphology. To assist with geologic map reading and understanding map unit correlations, we've provided

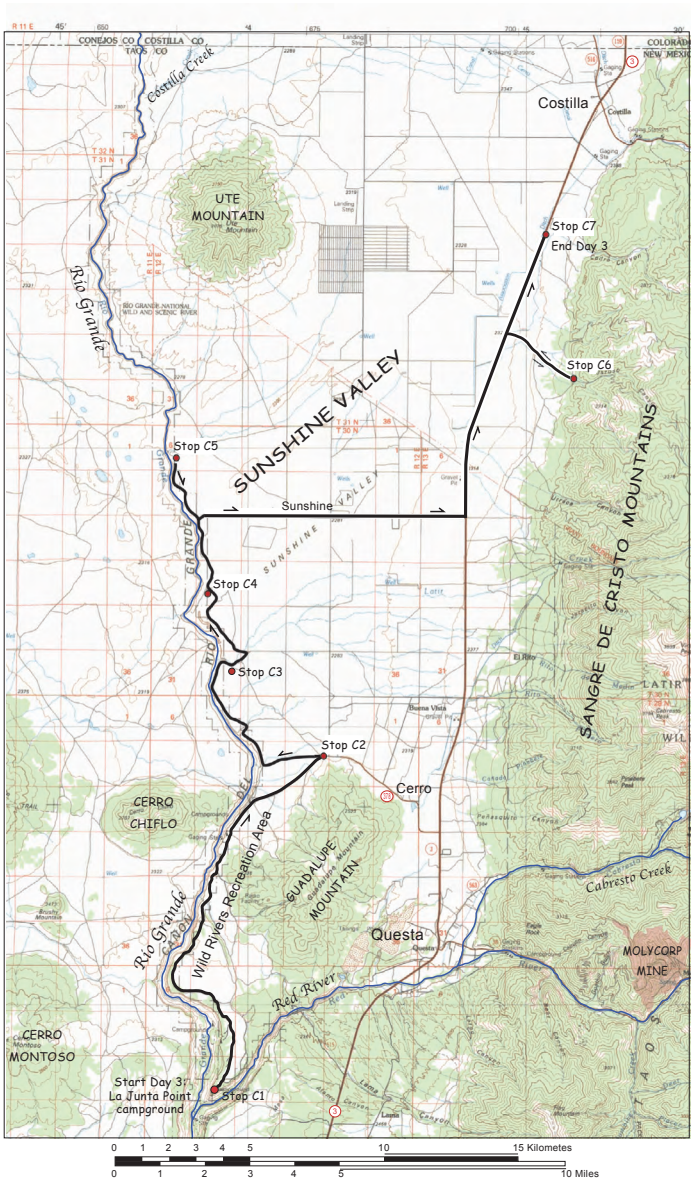

Figure C–1. Index map showing route and stops on field trip day 3.

CHAPTER C

a correlation of map unit figure to accompany all figures (fig. C–2).

Acknowledgments

We would like to give our appreciation to the staff at Wild and Scenic Rivers for providing the beautiful campsite at La Junta Point. Their assistance with our accommodations has made our last night of the field trip a delight. We also thank the Bureau of Land Management for the maintenance of roads and access across Sunshine Valley and at Urraca Ranch. In addition, we appreciate the constructive and helpful comments of Susan Olig (URS) and Daniel Koning (New Mexico Bureau of Geology and Mineral Resources), who reviewed a preliminary version of this manuscript. However, any errors that may remain are the responsibility of the authors.

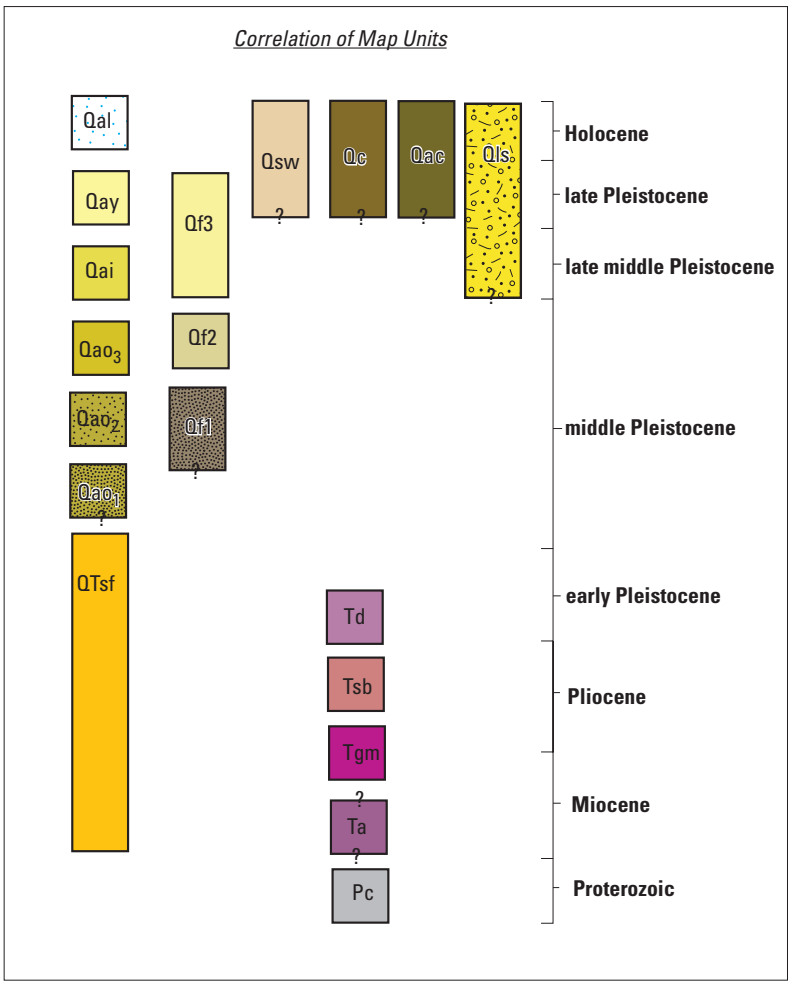

Figure C–2. Correlation of map units for Sunshine Valley.

Stop C1 — Volcanic and Geomorphic Setting of the Sunshine Valley and Taos Plateau

Speakers: Ren Thompson and Cal Ruleman
Start time: 7:30 am
Duration: 30 minutes
Location: La Junta Overlook Campground, Wild Rivers and Scenic Rivers BLM Park and Campground, about 6 mi southwest of Questa, N. Mex.
Guadalupe Mountain 7.5' quadrangle
GPS: NAD27, Zone 13, 438735 m E., 4056803 m N.
Elevation: 7,450 ft asl (approximate at campground)

Synopsis

At this location we will discuss the volcanic stratigraphy of the Servilleta Basalt (3.66–4.75 Ma) exposed in canyon walls and the geomorphic setting prior to canyon incision north of the Rio Grande–Red River confluence. Here we will discuss the Rio Grande's evolution in relation to the Red River–Cabresto Creek terrace suites and correlative units within Sunshine Valley.

Discussion

La Junta Point overlooks the confluence of the Red River and Rio Grande and provides an unparalleled view into the volcanic and sedimentary base deposits exposed in the deeply incised canyons of both drainage systems (fig. C1–1). Prior to capture of the upper Rio Grande drainage system (Wells and others, 1987; Machette and others, chapter G, this volume), the Red River drainage formed the headwaters of the ancestral Rio Grande in northern New Mexico. The thick sedimentary deposits underlying volcanic rocks of the Taos Plateau volcanic field are predominantly alluvial fan gravels of the Red River drainage system that were undercut and slumped as

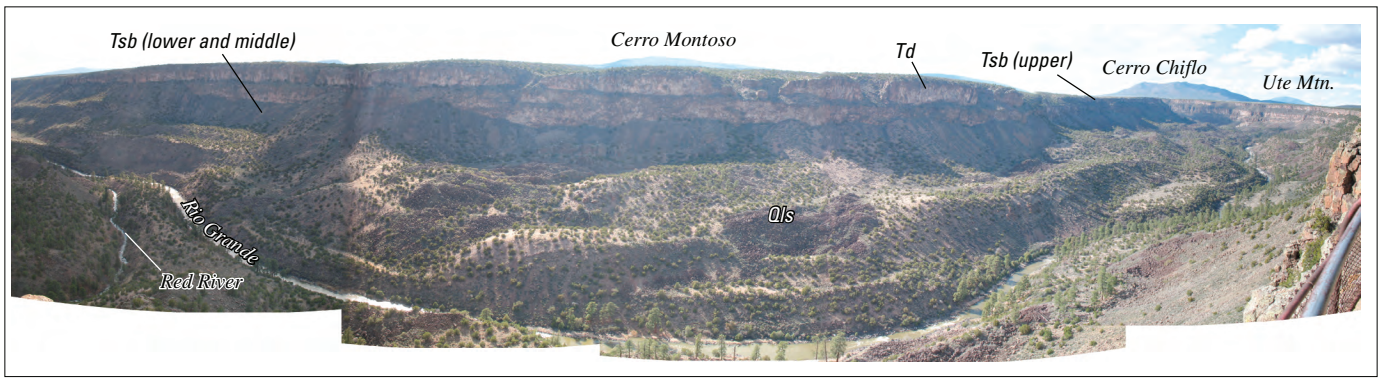

Figure C1–1. Panoramic view of the west wall of the Rio Grande gorge as seen from La Junta Point.

Toreva blocks after incision by the integrated Rio Grande–Red River fluvial system.

The westward-prograding Red River alluvial fan had a profound effect on the syndepositional and postdepositional distribution of volcanic rocks of the Taos Plateau volcanic field (Dungan and others, 1984). Lava flows exposed at the confluence of the Rio Grande and Red River erupted from vent areas to the south and west. These flows pinch out eastward against, and overlie as thin lava flow veneers, the thick sequence of west-sloping fluvial deposits. The volcanic section thickens markedly to the south, away from the topographically high fan deposits; this relation is most notably reflected in the thickening of the composite thickness of the Servilleta Basalt southward toward the "High Bridge" over the Rio Grande gorge, northwest of Taos, N. Mex. The volcanic stratigraphy exposed in the Red River drainage is dominated by lava flows erupted from volcanic centers east of the Rio Grande drainage. These basalts flowed westward and overlie older members of the Servilleta Basalt exposed on the western rim of the Rio Grande gorge rim (McMillan and Dungan, 1986). The complex interplay of volcanism and basin deposition is integral to the interpretation of stratigraphy exposed along the length of the Rio Grande drainage where it incises rocks of unit Taos Plateau volcanic field. The confluence of the Red River and the Rio Grande can be seen in the lower left corner of the photograph in figure C1–1. Alluvial-fan deposits of the ancestral Red River underlie landslide deposits (unit Qls) from river level to the base of the overlying volcanic section. Volcanic rocks of the western gorge rim include (1) a capping flow of Servilleta Basalt (unit Tsbu) visible along the gorge rim near the left and right margins of the photograph, (2) a petrologically atypical, sparsely phyric dacite lava flow (unit Td) from the "UCEM" (Unnamed Cerrito East of Montoso) volcano that forms the gorge rim in the center of the photograph, and (3) basal lava flows of Servilleta Basalt (unit Tsbl) that overlies alluvial-fan deposits.

Proximal to Questa, the Red River and Cabresto Creek emerge from the Sangre de Cristo Mountains and form two deeply incised canyons and the headwaters of the ancestral Rio Grande. This fluvial system has an associated suite of seven pre-Holocene terraces ranging in elevation from 7,660 to 7,320 ft above sea level (Pazzaglia and Wells, 1990). The oldest terrace (unit Qt1) is formed on sediment of the Santa Fe Group (>640 ka) at an elevation of 7,660 ft. It includes a capping coarse-grained gravel veneer. Pedogenic soils on this terrace tread are characterized by stage III–IV carbonate development, indicative of >250 ka deposits (Machette, 1985). Pazzaglia (1989) mapped this surface as unit Qt2 and assigned an age of 300–600 ka on the basis of soil morphology and regional correlations. The unit Qt2 surface is inset into a surface grading to the youngest of the three pre-Rio Grande Cañon incision deposits (unit Qao) mapped to the northwest in Sunshine Valley. The highest surface north of Cabresto Creek and south of Red River is correlated with the highest and oldest surface mapped in Sunshine Valley (unit Qao1), characterized by a pebble-gravel cap overlying fine-grained, silty, basin fill sediments of the Santa Fe Group (unit QTsf). This deposit overlies what has been previously called the Lama Formation (Pazzaglia, 1989), which consists of moderately to well sorted, gravelly, silty sands and sandy pebble gravels with carbonate development ranging from stages II to IV. To the north within Sunshine Valley we have differentiated three subunits of this gravel deposit capping the Santa Fe Group: units Qao1, Qao2, and Qao3.

Stop C2 — Highest Depositional Surface Within Sunshine Valley

Speaker: Cal Ruleman and Ralph Shroba
Start time: 8:30 am
Duration: 30 minutes
Location: Fork in road of Wild and Scenic Rivers Road and BLM Rim Road
Sunshine Valley, New Mexico 7.5' quadrangle
GPS: NAD 27, zone 13, 442701E, 4068963N
Elevation: 7,522 ft asl

Synopsis

This promontory on Servilleta Basalt yields a view to the north showing the highest depositional surface across Sunshine Valley (fig. C2–1). To the north, this surface is underlain by Plio-Pleistocene Santa Fe Group capped by less than 2 m of pebbly coarse sand. The gentle to flat slope of this surface grades to the southwest across the river canyon and is interpreted as reflecting the last depositional cycle (units Qao1, Qao2, and Qao3) before deep canyon incision was initiated and entrenchment of subsequent younger deposits occurred. The route we follow north across Sunshine Valley will traverse this older surface several times.

Discussion

We begin our traverse of Sunshine Valley where Servilleta Basalt is exposed on an erosional bedrock surface. To the north, intrabasin faulting has tilted and downdropped the Servilleta Basalt to induce subsequent burial by the Plio-Quaternary Santa Fe Group (>640 ka) (figs. C2–2 and C2–3). This bedrock surface is approximately 7 m (22 ft) above the oldest pebbly coarse sand deposit of unit Qao at this location, mapped as Qao2. We correlate this surface with the oldest portions of the Costilla–Cabresto Plain to the north, as well as with the highest surface proximal to Red River and Cabresto canyons. Younger middle and late Pleistocene deposits are entrenched and inset into this surface by as much as 30 m (100 ft).

A gravel pit to the northeast (UTM NAD27 443041 E, 4069217 N) (fig. C2–3) exposes younger inset deposits with two buried soils beneath late Pleistocene eolian silts and thin fan gravel deposits (unit Qay). The soil sequence exposed here contains a 45-cm-thick Stage III calcic horizon on coarse gravel deposits capped by approximately 60 cm of loess with strong Bt development, interpreted as buried late-middle Pleistocene eolian deposits (unit Qai). We interpret this exposure to indicate that post–unit Qao deposition was limited to eolian infilling of abandoned inset channels in the unit Qao surface. The lack of channel-fill alluvial deposits and the presence of eolian silts indicates that incision dominated the post-middle Pleistocene fluvial setting. The coarser pebble gravel underlying the Bk stage III soil horizon indicates that a fluvial system, probably fed from Cabresto Creek and small drainages to the north, existed at this location until unit Qao was incised. After a period of deep incision occurred, these channels became filled by units Qai- and Qay-correlative eolian and alluvial deposits, respectively.

Figure C2–1. View north across Sunshine Valley and towards Ute Mountain.

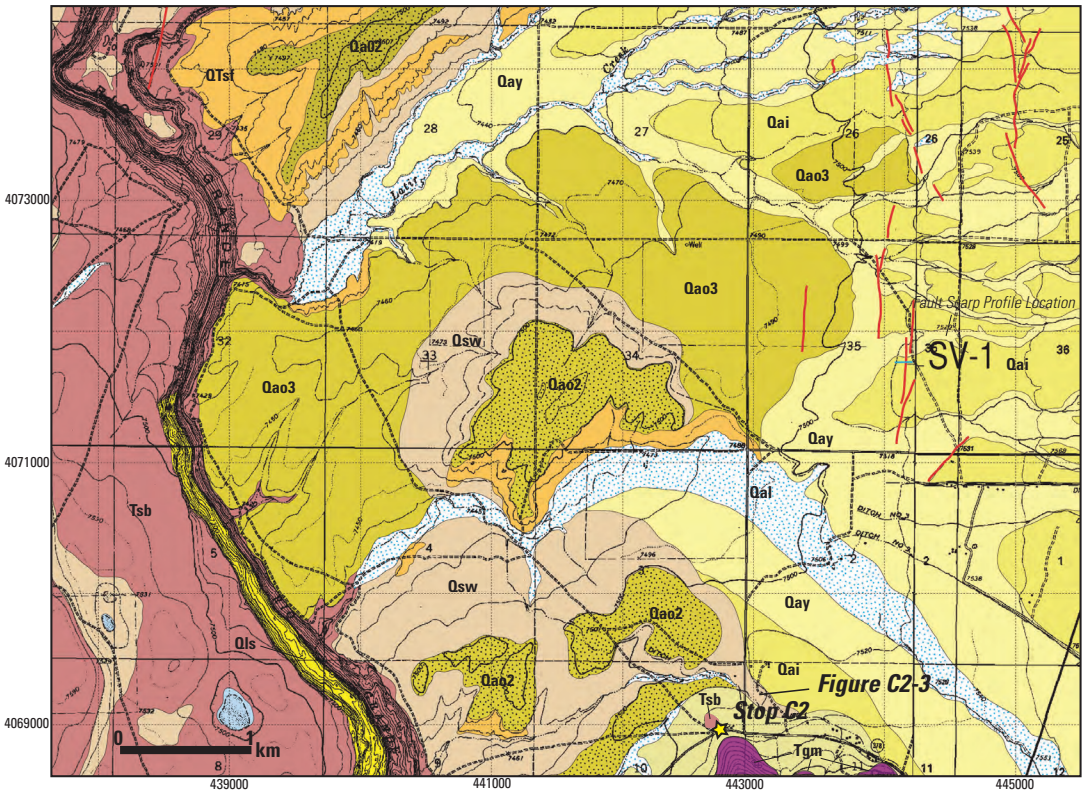

Figure C2–2. Geologic index map for stop C2. Units listed as follows: Qal, Holocene alluvium; Qsw, late Pleistocene and Holocene slopewash deposits; Qls, late Quaternary landslide deposits; Qay, late Pleistocene; Qai, late-middle Pleistocene alluvium; Qao2 and Qao3, middle Pleistocene alluvium; Tsb, Servilleta Basalt; and Tgm, Guadalupe Mountain dacite. Red lines are mapped Quaternary faults. UTM coordinates are given in NAD 27 coordinate system. SV–1 is number of fault scarp profile.

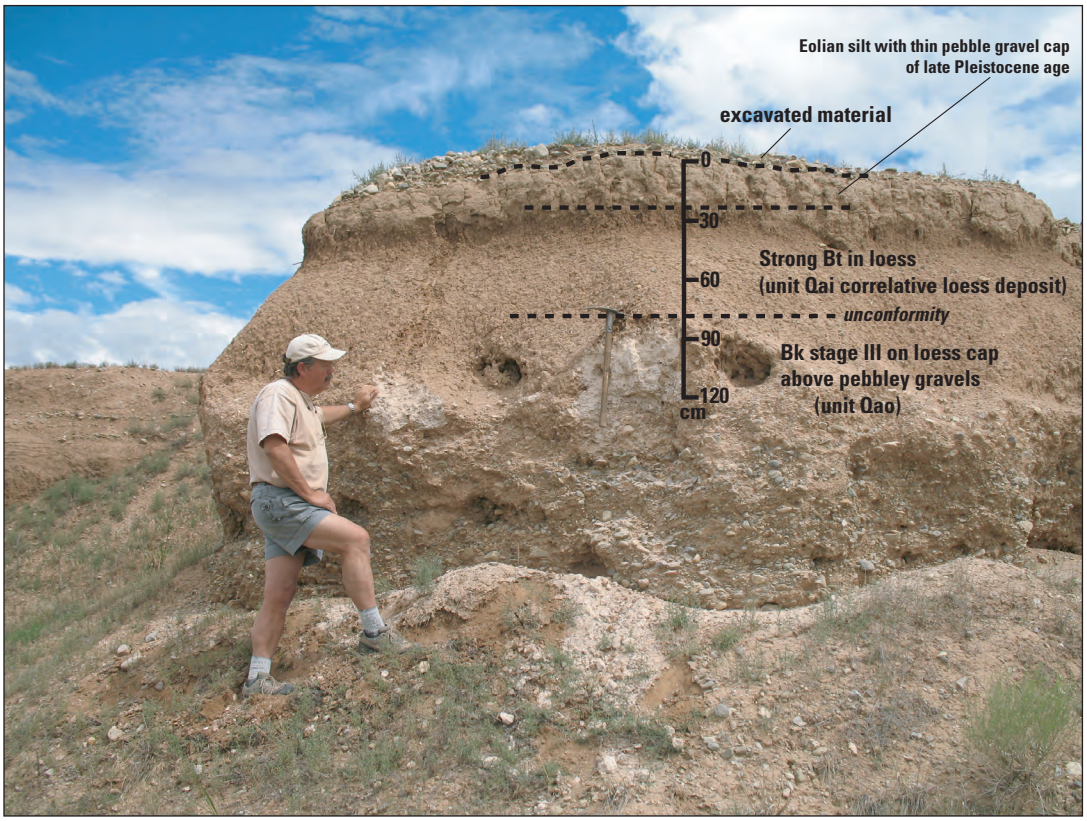

Figure C2–3. Soil sequence exposed in gravel pit northeast of stop C2.

Stop C3 — Faulted Servilleta Basalt (3.66–4.75 Ma) at Latir Creek

Speaker: Cal Ruleman
Start time: 10:00 am
Duration: 30 minutes
Location: Rio Grande Rim Road
Sunshine Valley, New Mexico 7.5' quadrangle
GPS: NAD 27, zone 13, 439447E, 4072188N
Elevation: 7,410 ft asl

Synopsis

Upper Pleistocene and younger alluvium were deposited with an unconformity against an exhumed fault line scarp cut on Servilleta Basalt. Antithetic to the west-dipping southern Sangre de Cristo fault zone along the range front to the east, these antithetic fault strands apparently bound the Sunshine Valley graben along the western basin margin and are considered to be the northern extension of the Gorge fault zone mapped to the south in proximity to Taos and Arroyo Hondo (fig. C3–1).

Discussion

The fault evident at this stop is part of a north-northwest-trending fault zone characterized by east- and west-facing scarps on individual fault strands having displacements of less than 20 m (fig. C3–2). This fault zone roughly coincides with Cañon del Rio Grande, indicating probable fault control on the river's position within the basin as first proposed by Winograd (1959). This fault zone continues to the south where it is the Gorge fault zone (Read and others, 2004) and bounds the western margin of the Taos Plateau near Cañon del Rio Grande (Cordell and Keller, 1984). Read and others (2004) noted that the expression of this fault zone is subtle, but it can be identified by fault scarps, lineaments, and springs. To the south of the confluence of the Red River with the Rio Grande, this fault zone includes the Dunn fault (Dungan and others, 1984) and fault strands splaying off of the Embudo fault (Kelson and Baur, 1998). At stop C3, upper Pleistocene to Holocene alluvium and loess have been deposited with buttress unconformity against an east-facing exhumed fault-line scarp on the Servilleta Basalt.

At stop C3 we have mapped pebbly coarse sand of unit Qao3 on the upthrown side of the fault, and to the north units Qao2 and Qao1 drape across this fault zone as well, indicating that no apparent middle to late Quaternary displacement occurred along this particular fault zone. Thus, we interpret these scarps as exhumed fault-line scarps, concealed by the Santa Fe Group–Lama Formation (>640 ka) and middle Pleistocene alluvium (units Qao1, Qao2, and Qao3) and exhumed by subsequent erosion and incision. Approximately 4 km to the east, intrabasin faults within the central part of Sunshine Valley and range-bounding faults on the east side of Sunshine Valley have late-middle to late Pleistocene displacement, indicating dominant central and eastern basin-margin tectonic activity (fig. C3–3). Mapping of subtle lineaments and escarpments within central Sunshine Valley indicates probable Holocene displacement of <1 m, possibly a product of coseismic displacement associated with large events (>M_w 7.0) along the range-bounding southern Sangre de Cristo fault zone (Ruleman and Machette, chapter J, this volume). Gravity and magnetic data support the presence of this western basin-bounding fault zone as well as a very complex intrabasin fault system (Bankey and others, 2005, 2006) (fig. C3–4).

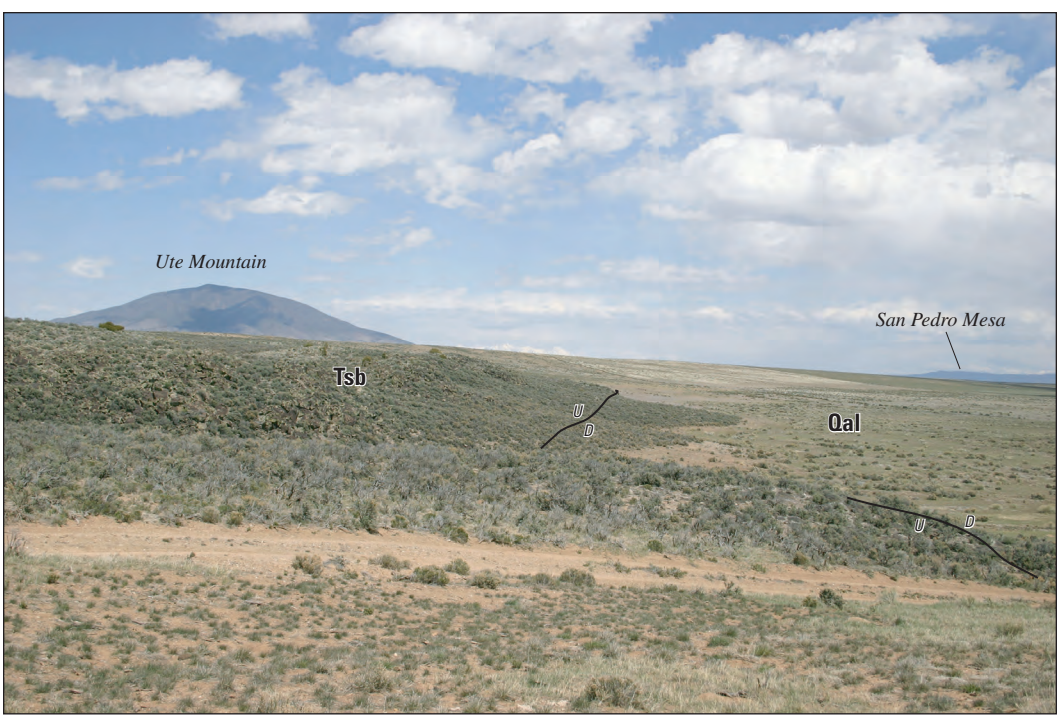

Figure C3–1. View to the north at stop C3. These escarpments on Servilleta Basalt are exhumed fault line scarps with no apparent middle to late Pleistocene displacement.

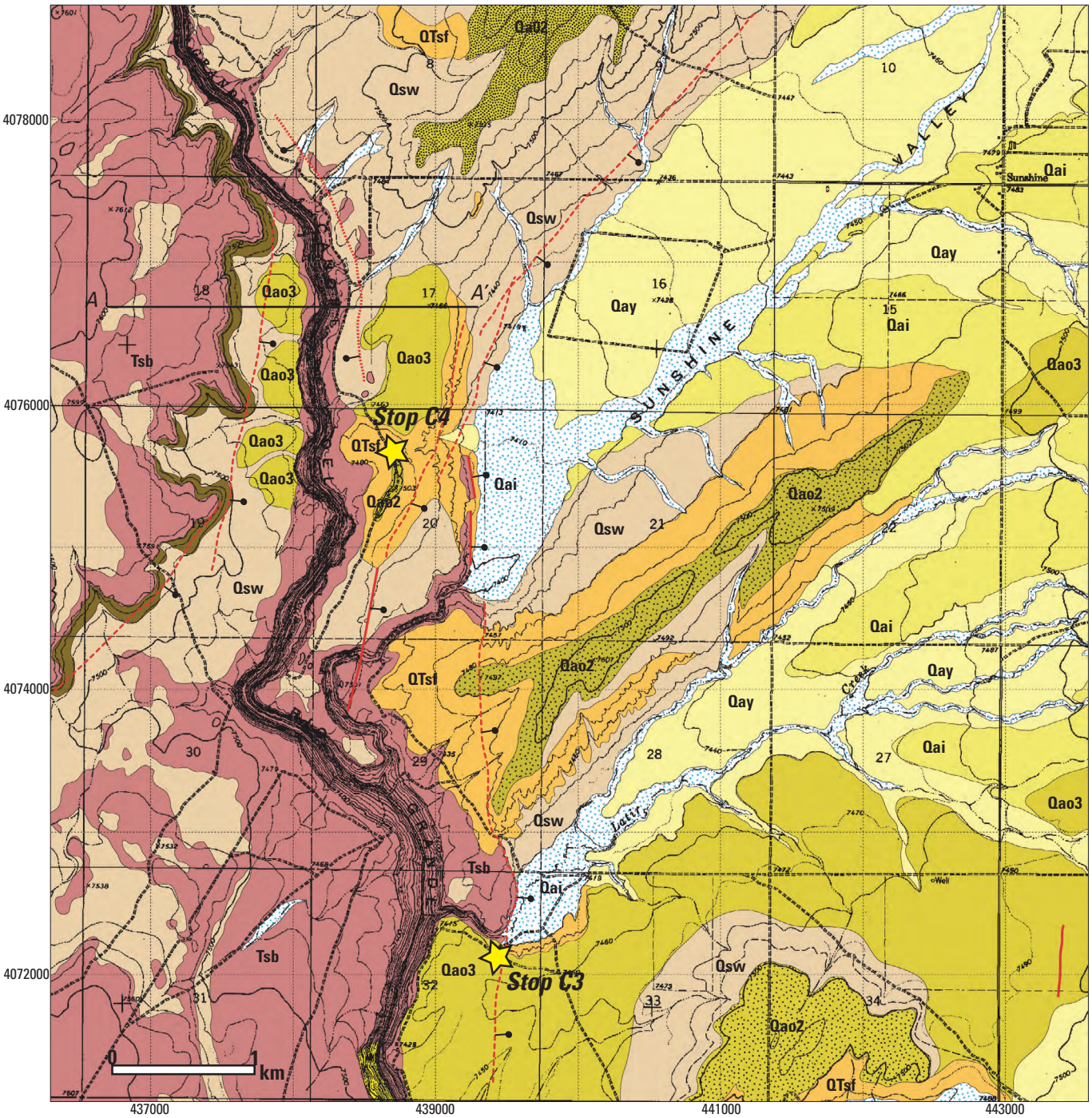

Figure C3–2. Geologic index map of stops C3 and C4. Units listed as follows: Qal, Holocene alluvium and Qsw, late Pleistocene and Holocene slopewash deposits; Qay, late Pleistocene alluvium; Qai, late-middle Pleistocene alluvium; Qao2 and Qao3, middle Pleistocene alluvium; QTsf, Santa Fe Group (>640 ka); and Tsb, Servilleta Basalt. Solid red lines are faults of probable late Pliocene to early Quaternary displacement, dashed where inferred and dotted where concealed. UTM coordinates given in NAD 27 coordinate system.

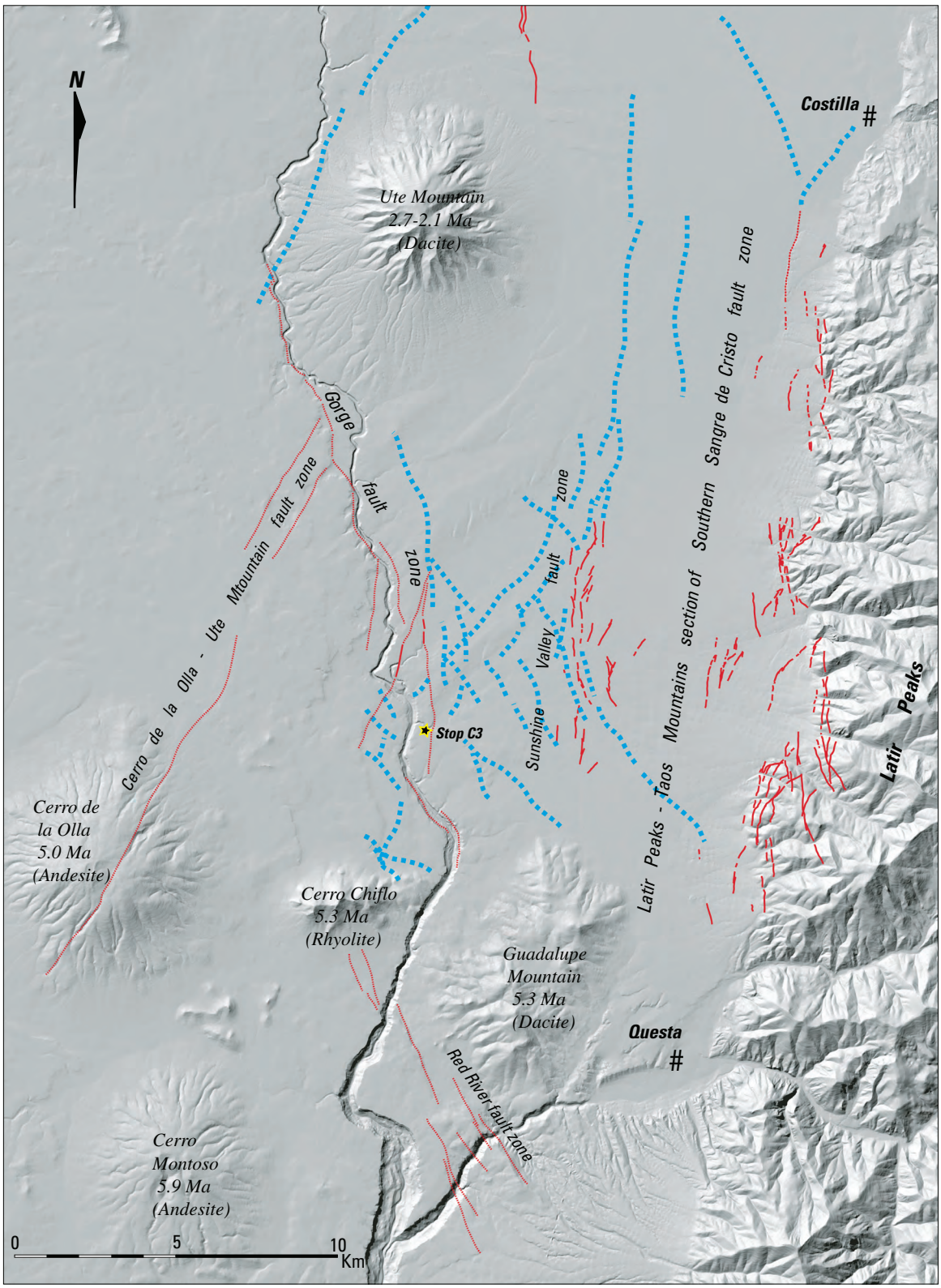

Figure C3–3. Volcanic centers and structural framework of Sunshine Valley (modified from Read and others, 2004). Solid red lines are late-middle Pleistocene to Holocene faults scarps. Dotted red lines are fault scarps and exhumed fault line scarps of middle Pleistocene and older age. Dashed blue lines are faults mapped from our preliminary interpretation of aeromagnetic data from Bankey and others (2005 and 2006). Shaded-relief base map by Ted Brandt (U.S. Geological Survey).

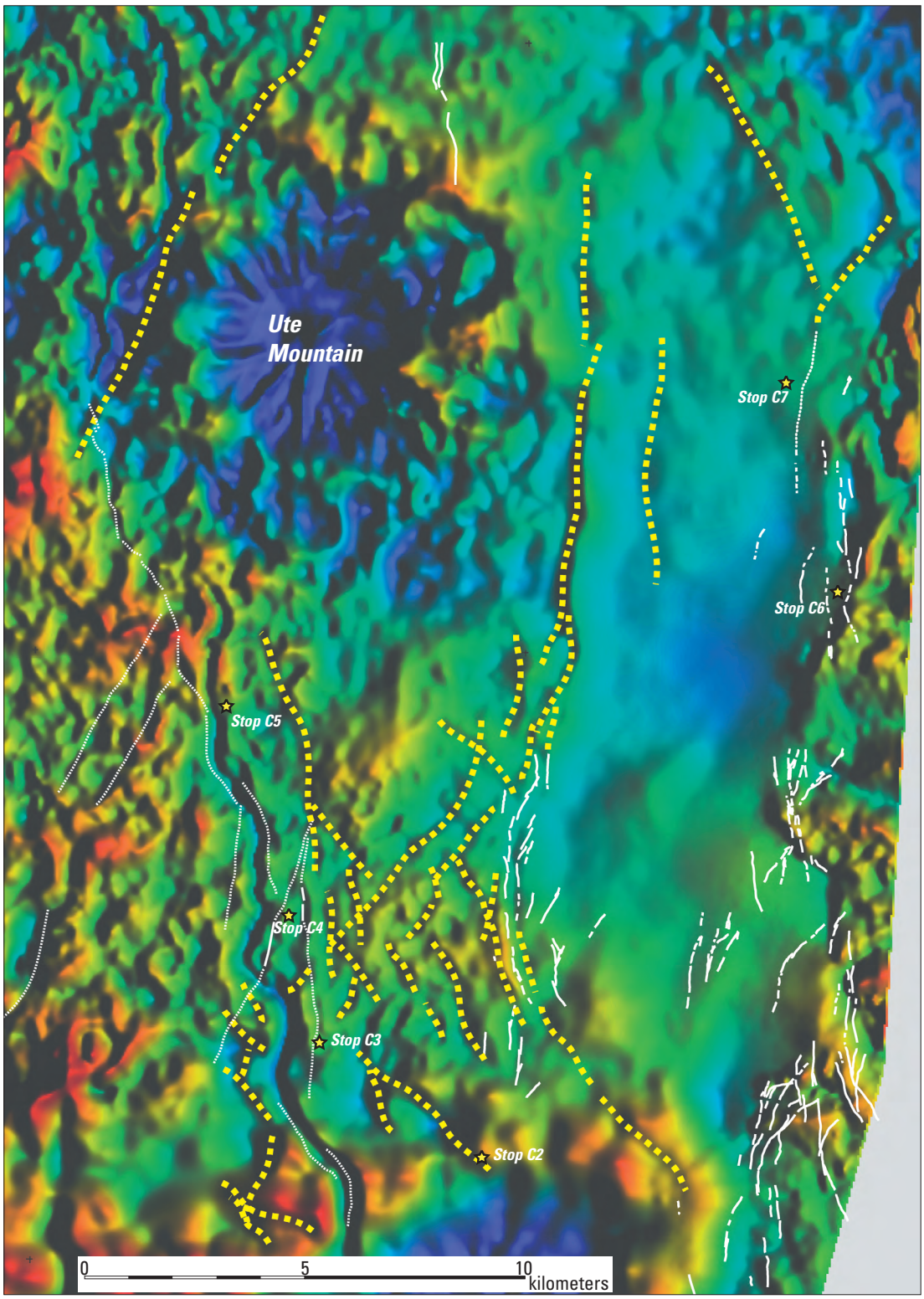

Figure C3–4. Color shaded-relief image of aeromagnetic data merged from two different surveys (Bankey and others, 2005, 2006) and structural framework of Sunshine Valley. The total data range is 2645 nT, with low to high values represented by cool to warm colors, respectively. Illumination is from the east. Data were filtered to enhance details and reduced to the pole to facilitate interpretation. Image courtesy of V.J.S. Grauch (USGS). Solid white lines are late-middle Pleistocene to Holocene fault scarps. Dotted white lines are inferred faults and exhumed fault line scarps. Dashed yellow lines are interpreted faults from aeromagnetic data.

Stop C4 — Old Alluvium (Unit Qao2) Overlying Servilleta Basalt and Santa Fe Formation

Speakers: Ralph Shroba and Cal Ruleman
Start time: 11:00 am
Duration: 30 minutes
Location: Sunshine Valley, New Mexico 7.5' quadrangle
GPS: NAD 27, zone 13, 438745E, 4075600N
Elevation: 7,480 ft asl

Synopsis

At this stop we observe pebbly coarse sand in the basal part of unit Qao2 and underlying silty sand of the Santa Fe Group (unit QTsf) exposed in a shallow gully. Unit Qao2 is the middle unit of three old alluvial units derived from the Sangre de Cristo Mountains that predated the incision of the Cañon del Rio Grande. The top of unit Qao2 is inset about 15 m (50 ft) below the top of the oldest of the three units (unit Qao1) at 7,550 ft asl and is about 13 m above the top of the youngest unit (unit Qao3) at 7,460 ft asl.

Discussion

This inset of units Qao2 and Qao3 below unit Qao1 suggests minor episodes of stream incision and backfilling after the widespread deposition of unit Qao1 but prior to deep canyon cutting by the Rio Grande (fig. C3–2). Late middle Pleistocene alluvium (unit Qai) is the next youngest deposit preserved within the valley and is inset into unit Qao as much as 30 m, suggesting a period of deep incision and extensive erosion between deposition of units Qao and Qai. At this stop, unit Qao2 is about 1.8 m thick and mainly coarse sand. However, granules are abundant and granitic and volcanic pebbles as large as 3–5 cm are common. The upper 5 m of the underlying sediment (Santa Fe Group) is similar in character to Santa Fe Group sediment exposed in other small outcrops north and south of Ute Mountain. Here and at these other outcrops, the Santa Fe commonly consists of very silty, mostly very fine to medium sand; it is consolidated, slightly sticky, and plastic to very plastic, and it has strong brown, reddish yellow, and pink colors (7.5YR 5/6, 6/6, and 7/4, dry; Munsell, 1994). The abundance of medium sand and finer material in the Santa Fe suggests deposition in a low-energy, closed-basin environment. The low point of the basin was between Cerro Chiflo and Guadalupe Mountain at an elevation between about 7,480 and 7,640 ft, about 8 mi (13 km) southeast of here.

About 0.4 km northeast of here, alluvium of unit Qao3 is about 3.4 m thick; it consists of 1.3 m of subangular pebble sandy gravel rich in volcanic and granitic pebbles (commonly as large as 3–4 cm) overlain by 2.1 m of pebbly sand. These deposits overlie slightly silty, mostly very fine to fine sand of the Santa Fe Group (unit QTsf). The top of unit Qao3 projects across the Cañon del Rio Grande (fig. C4–1), which indicates a preincision age for the entire Qao alluvial sequence.

NOTE 1: Along our drive to stop C5, follow the route on geologic index map to identify local intrabasin faults and topographic relations among Quaternary deposits. These faults form a shallow, north-trending graben system, which the Rio Grande has incised and eroded, leaving most of the grabens with very subtle expression.

NOTE 2: Lunch at stop C5: 12:00 pm

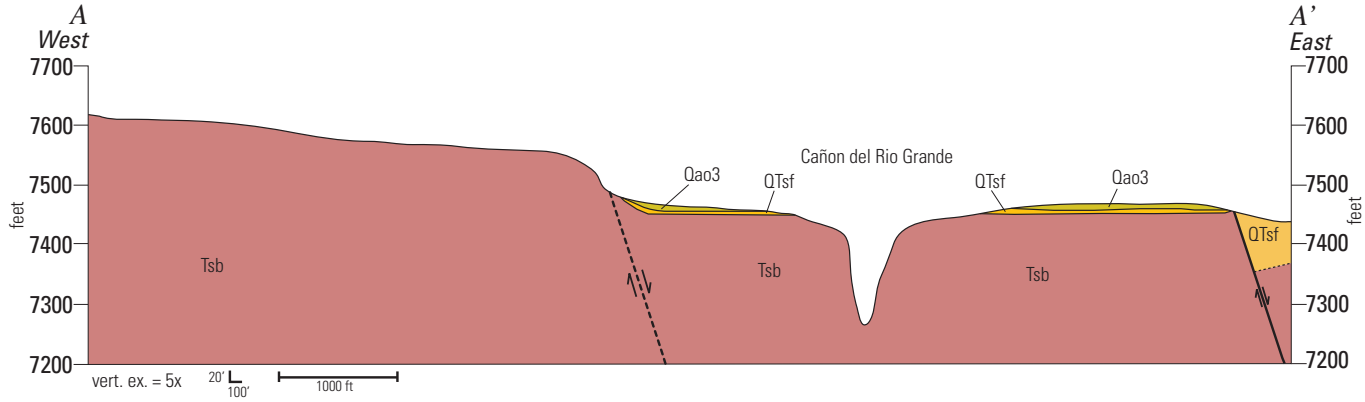

Figure C4–1. Cross section A-A' within north of stop C4 (see figure C3–2 for exact location). Units listed as follows: Qao3, middle Pleistocene alluvium; QTsf, Oligocene to middle Quaternary sediment of Santa Fe Group (25 Ma–640 ka); and Tsb, Pliocene Servilleta Basalt (4.5–3.66 Ma).

Stop C5 — Ute Mountain Volcanic Rocks and Fan Deposits and Surficial Geology of Northern Sunshine Valley

Speakers: Ren Thompson and Ralph Shroba
Start time: 12:30 pm
Duration: 30 minutes
Location: Rio Grande Rim Road north of Sunshine Valley Road junction
Ute Mountain, New Mexico 7.5' quadrangle
GPS: NAD 27, zone 13, 437402E, 4079845N
Elevation: 7,450 ft asl

Synopsis

At this stop we will discuss (1) the lithologic composition and volcanic history of Plio-Pleistocene Ute Mountain, (2) the genesis and inferred ages of the fan deposits that flank the mountain, and (3) the inferred timing of canyon incision by the Rio Grande (fig. C5–1).

Discussion

The view to the north of here is dominated by Ute Mountain, the northernmost dacite volcano in the Taos Plateau volcanic field. Rising to an elevation of nearly 10,100 ft, Ute Mountain towers above the floor of Sunshine Valley and is a prominent landform visible from much of the southern San Luis Valley. The eroded edifice of Ute Mountain consists of a series of a monolithologic dacite lava domes, spines, and flows that all are cut by radial dikes that form prominent ridges that emanate from the summit. The eruptive age of Ute Mountain is poorly constrained by $^{40}Ar/^{39}Ar$ ages of 2.7 and 2.1 Ma (Appelt, 1998), making this volcano the youngest of the large eruptive centers of the Taos Plateau volcanic field. The dacite edifice is built upon an older eroded olivine andesite volcano of unknown age that crops out low on the flanks of Ute Mountain and in the Rio Grande gorge (Cañon del Rio Grande) immediately to the west of this stop (figs. C5–2 and C5–3). This unnamed andesite volcano locally predates the eruption of Servilleta Basalt, because lava flows exposed in the Rio Grande gorge lap onto the lower flanks of this andesitic shield (unit Ta). The Tertiary andesite lava flows exposed in the Rio Grande gorge near this location have well-developed primary pahoehoe flow textures and thus are extremely unusual, and perhaps unique, in the geologic record.

Alluvial fans, composed chiefly of debris-flow deposits of three age groups, form a wide coalesced piedmont apron on the lower flanks of Ute Mountain (fig. C5–1). These deposits record the late erosional history of the dacite volcano. On the southwest flank of Ute Mountain, the oldest exposed alluvial fan deposits (unit Qf1) overlie alluvium correlated with unit Qao1 (chapter K, this volume). The top of unit Qf1 and that of intermediate-age fan deposits (unit Qf2) project above the steep-sided lower part of the Cañon del Rio Grande (fig. C5–4). Although deposits of units Qf1 and Qf2 have not been recognized west of the Rio Grande, unit Qao3 (youngest and lowest of the three alluvial units of middle Pleistocene age) is exposed on both sides of the Cañon del Rio Grande (fig. C4–1). These relationships suggest that the deposition of units Qf1 and Qf2 may predate major canyon cutting by the Rio Grande. Geomorphic position as well as stage I and II carbonate morphology on subsurface clasts (Machette, 1985) suggests that unit Qf3 is probably equivalent or partly equivalent in age to nearby alluvial units Qay (Pinedale age) and Qai (Bull Lake age) (Cal Ruleman, unpub. mapping, 2007). On the southeast side of Ute Mountain, deposits of unit Qf3 appear to be graded to deposits of unit Qay. The inferred ages and geomorphic position of unit Qf3 suggest that the deposition of this unit postdates major canyon cutting, which began about 440 ka (chapter B, this volume).

At this location, river-scoured Servilleta Basalt is overlain by a thin veneer of pebbly sand. This scoured surface is correlated with a surface about 0.75 mi (1.2 km) northwest of here (on the west side of the Rio Grande) where we have obtained five samples for ^{3}He surface-exposure dating. The ^{3}He surface-exposure ages will help to constrain the time of initial incision of the Cañon del Rio Grande along this reach of the river. Thin deposits of gravelly alluvium of unit Qao3 are exposed on both sides of the Cañon del Rio Grande and thus predate major canyon cutting by the Rio Grande. Younger alluvial deposits (units Qay of late Pleistocene age and Qai of late-middle Pleistocene age) are inset into older alluvial deposits (units Qao1, Qao2, and Qao3) as much as 30 m, suggesting a period of widespread incision and erosion postdating deposition of unit Qao and predating deposition of unit Qai, as seen at stop C4. This period of rapid incision corresponds with base-level changes driven by the incision of the Rio Grande.

At this location, Cañon del Rio Grande is roughly 40 m (130 ft) deep. Assuming a long-term fluvial erosion rate of 0.15 mm/yr (15 cm/ka) (Dethier, 2001), the initial timing of canyon incision would be on the order of <600 ka. This roughly estimated age is in accord with the time of the draining of Lake Alamosa, located about 40 km (25 mi) north of here, at about 440 ka (chapter G, this report), assuming that an initial outburst of Lake Alamosa would have created more rapid incision rates before flow stabilized.

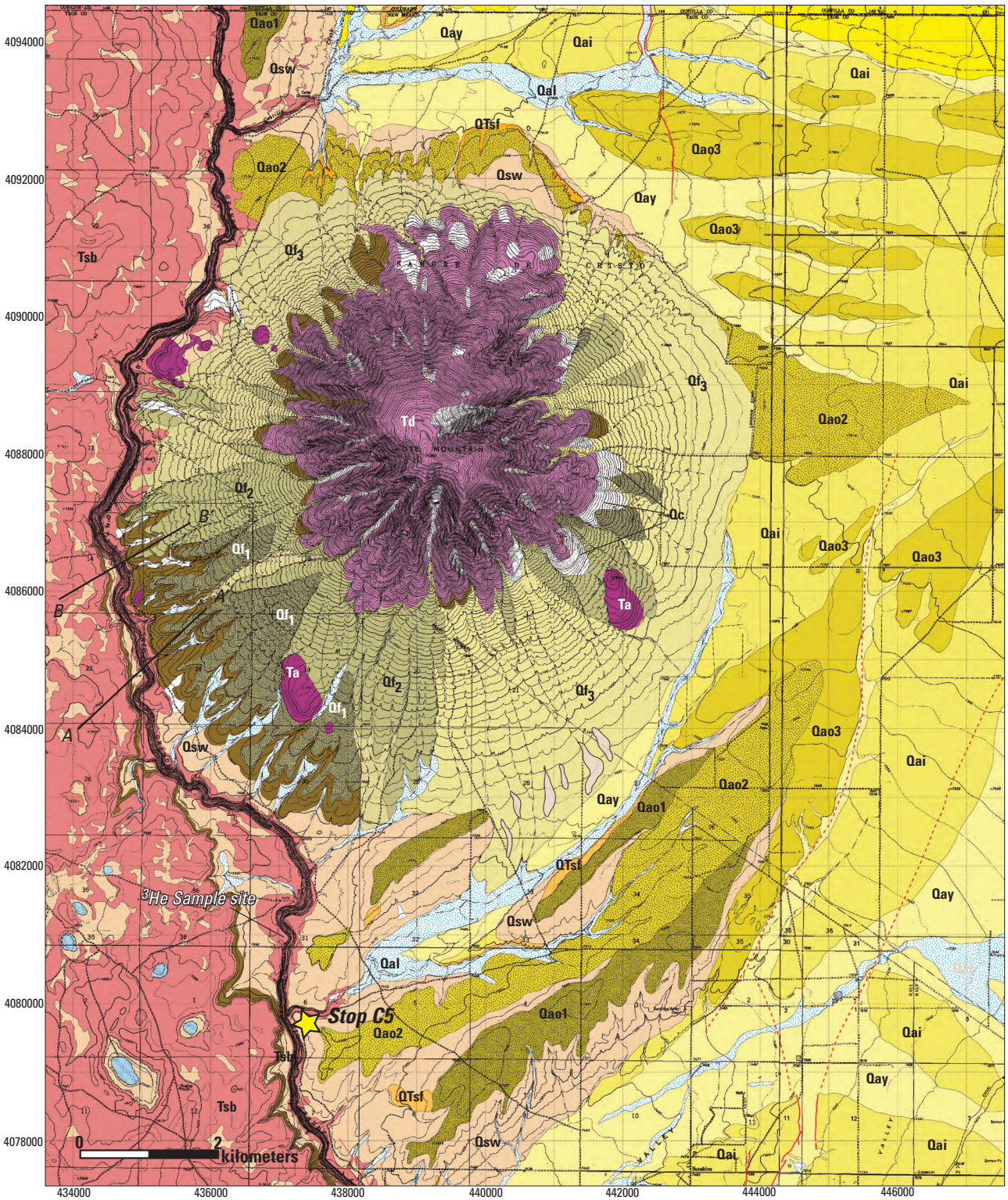

Figure C5–1. Geologic index map of stop C5 showing volcanic flows and alluvial fans associated with Ute Mountain. Units listed as follows: Qf3, late-middle and late Pleistocene fan alluvium; Qf2, upper middle Pleistocene fan alluvium; Qf1, lower middle Pleistocene fan alluvium; Qal, Holocene alluvium; Qay, late Pleistocene alluvium; Qai, late-middle Pleistocene alluvium; Qao1, Qao2, and Qao3, middle Pleistocene alluvium; Qc, Pleistocene colluvium; Qsw, late Pleistocene and Holocene slopewash deposits; Tsb, Servilleta Basalt; and Ta, andesite (early? Pliocene).

Figure C5–2. View east toward Ute Mountain from west side of Rio Grande gorge. The topographic high on the right-hand shoulder of Ute Mountain is an erosional remnant of an olivine andesite volcano that underlies the dacite volcano of Ute Mountain (unit Ta). In the foreground are terraces developed on Servilleta Basalt (unit Tsb), remnants of paleochannels incised in the basalt surface prior to entrenchment in the present-day gorge.

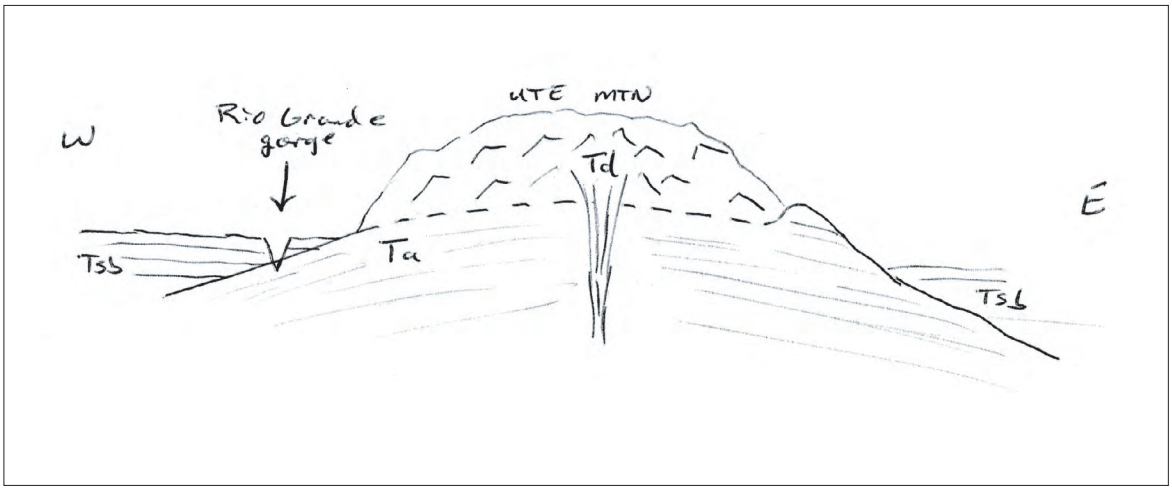

Figure C5–3. Sketch of west-east cross section through Ute Mountain showing generalized stratigraphic relations of Servilleta Basalt (unit Tsb), Ute Mountain dacite (unit Td), and buried andesite volcano (unit Ta) of unknown age.

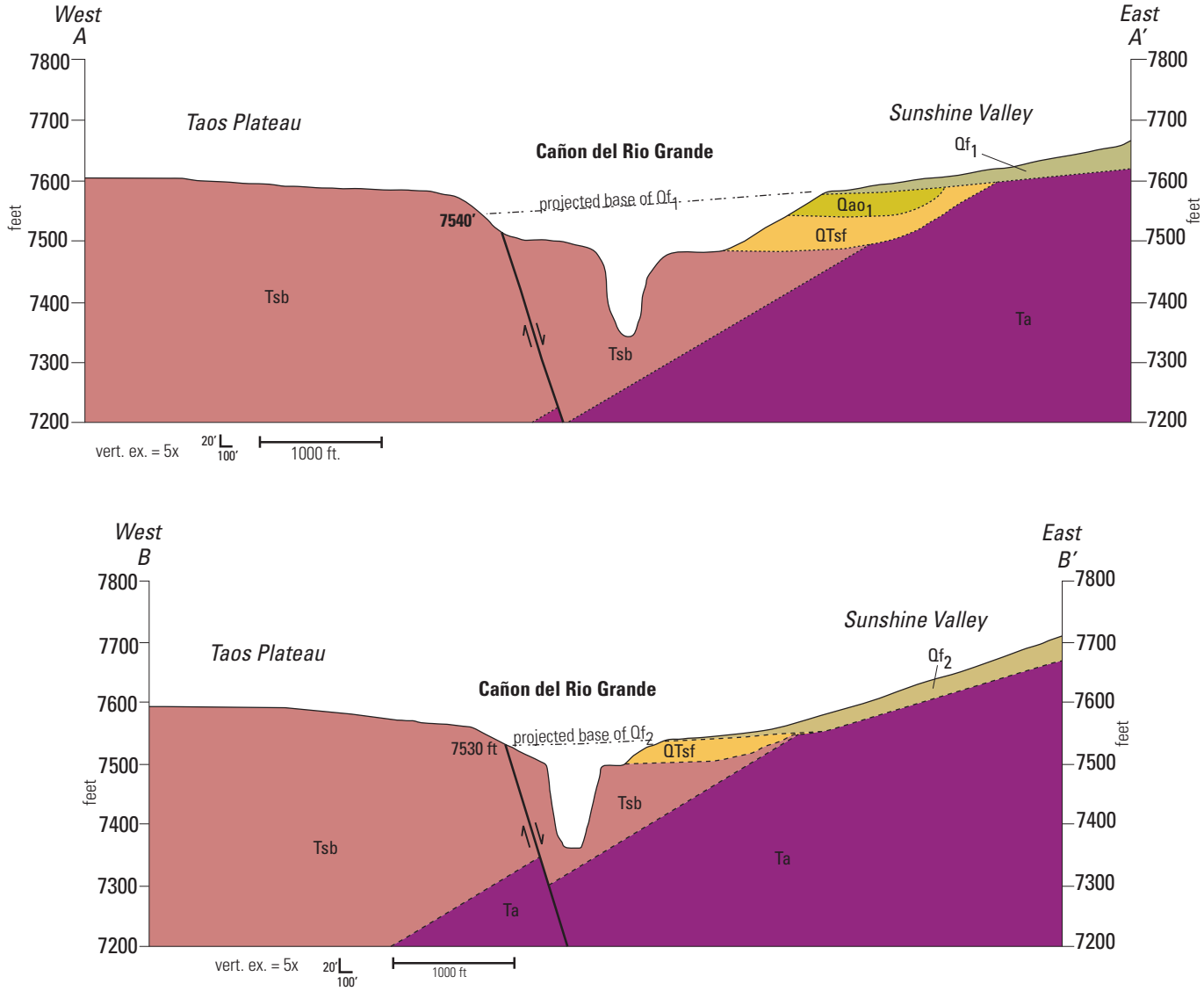

Figure C5–4. Cross sections A-A' and B-B' across Cañon del Rio Grande. Locations of cross sections shown on figure C5–1. Units listed as follows: Qf2 and Qf1, middle Pleistocene fan alluvium; QTsf, upper Oligocene to middle Quaternary Santa Fe Group (25 Ma–640 ka); Tsb, Pliocene Servilleta Basalt (3.66–4.5 Ma); and Ta, xenocrystic basaltic andesite of unknown age (>4.5 Ma).

Stop C6 — Faulted Alluvium at Jaroso Canyon, Latir Peaks Section of the Southern Sangre de Cristo Fault Zone

Speaker: Cal Ruleman
Start time: 1:15 pm
Duration: 1 hour
Location: Urraca Ranch Wildlife Management Area (BLM)
Costilla, New Mexico 7.5' quadrangle
GPS: NAD 27, zone 13, 451684 m E, 4082445 m N
Elevation: 8,080 ft asl

Synopsis

Along this section of the Sangre de Cristo fault zone between El Rito and Jaroso Canyon, we have mapped fault scarps on late-middle Pleistocene to Holocene deposits. This section of the fault zone is characterized by range-front and piedmont scarps that have 0.4–8.2 m of surface offset on units Qay and Qai deposits. As you enter the Wildlife Management Area you will see subtle, north-trending piedmont scarps of probable coseismic origin which are synthetic to the main range-bounding fault.

At the fan head, a large range-front fault scarp on late-middle Pleistocene alluvium has 5.3 m of surface offset. South of Jaroso Canyon, range-front fault scarps are at the bedrock-colluvium contact, where locally Holocene debris flows and colluvial deposits are offset 1–2 m. North of Jaroso Canyon, remnants of late-middle Pleistocene alluvium (unit Qai) are mapped proximal to the range front on the hanging wall of the southern Sangre de Cristo fault zone (fig. C6–1).

Discussion

At this location, soils on the upper surface of the fault scarp are correlative with those mapped on late-middle Pleistocene deposits (unit Qai) estimated to be 125–150 ka (Machette, 1985; Thompson and Machette, 1989) in the region. The composite soil is characterized by a 40-cm-thick Bt horizon formed in a pebble gravel (unit Qai) overlying a 30–50-cm-thick stage III Bk horizon with perhaps >200 k.y. of soil development (unit Qao) conformably beneath (fig. C6–2). Owing to leaching of carbonate at these elevations and moisture regimes, the maturity of these buried calcic soils further supports the antiquity of this surface. Buried stage III calcic horizons are found within the scarp slope, further indicating a probable >200 ka age for the faulted deposit (fig. C6–3). The fault scarp here has a surface offset of 5.3 m (fig. C6–4) and is probably the result of two or three surface rupturing events.

To the north of this stop, across Jaroso Creek, stage III calcic soils are found buried by about 1 m of late-middle and late Pleistocene alluvium on the downthrown side of the range-front fault (fig. C6–5). The fault scarp at this location has a surface offset of 7.8 m (fig. C6–6). As exposed along the arroyo shown in fig. C6–5, unit Qao is buried beneath unit Qai on the downthrown side, but unit Qao underlies the surface on the upthrown side. We correlate the surface on the upthrown

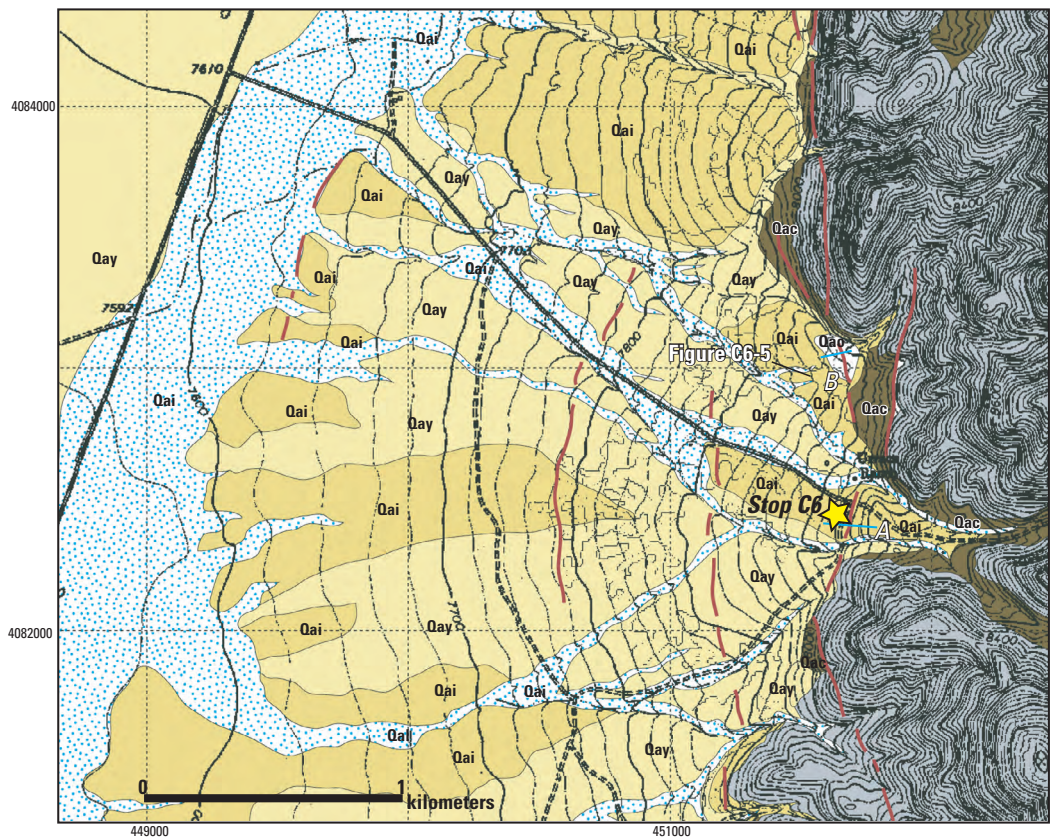

Figure C6–1. Geologic index map to stop C6. Units listed as follows: Qal, Holocene alluvium; Qay, late Pleistocene alluvium; Qai, late-middle Pleistocene alluvium; Qao, middle Pleistocene alluvium; and Qac, late Pleistocene and Holocene range-front alluvium-colluvium undivided. Fault scarps shown with red lines and fault scarp profiles shown as blue lines.

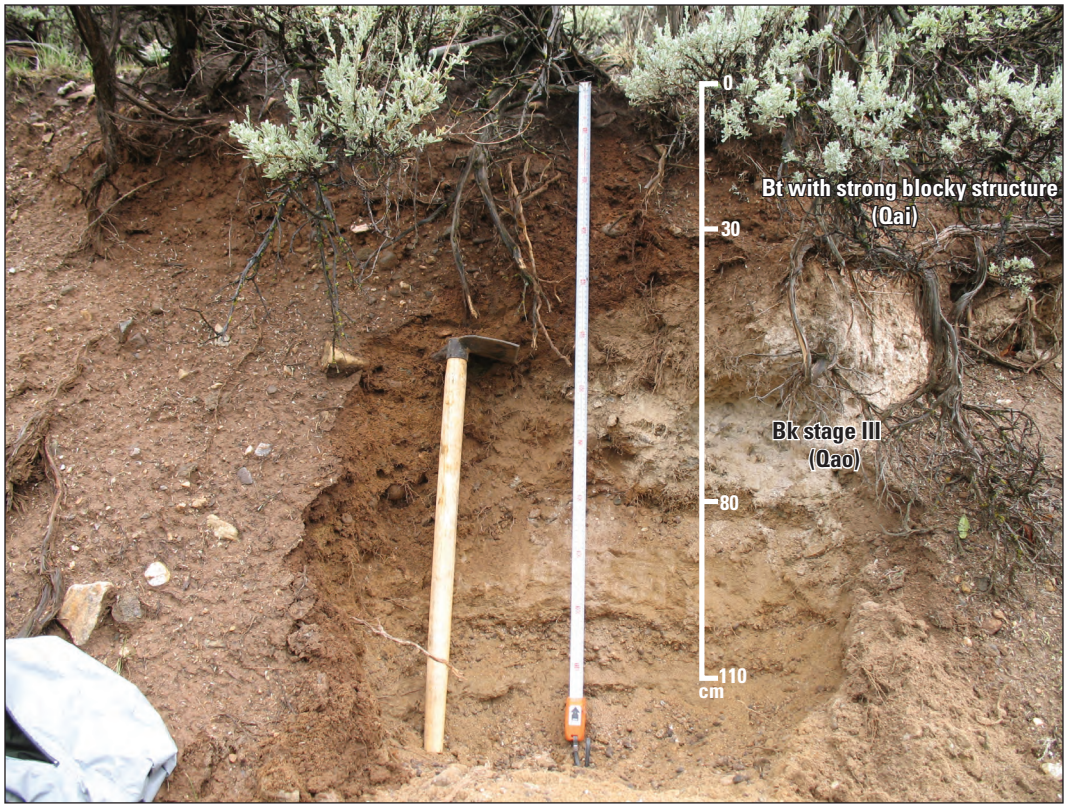

Figure C6–2. Soil on unit Qai-correlative loess overlying Bk stage III soil formed on unit Qai sandy pebble alluvium on upthrown side of fault at Jaroso Canyon.

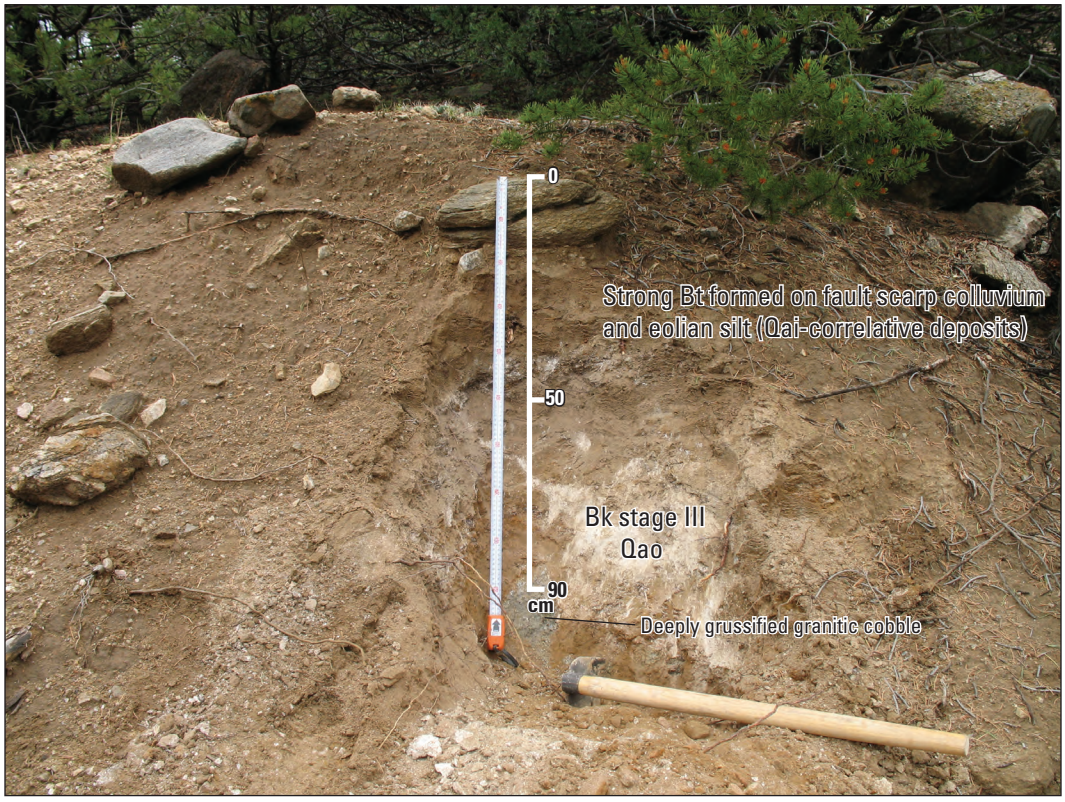

Figure C6–3. Buried soil on downthrown side of fault exposed in road cut at Jaroso Canyon. Similar soil sequence as seen in figure C6–2 with thicker deposition of unit Qai-correlative fault scarp colluvium and eolian silt.

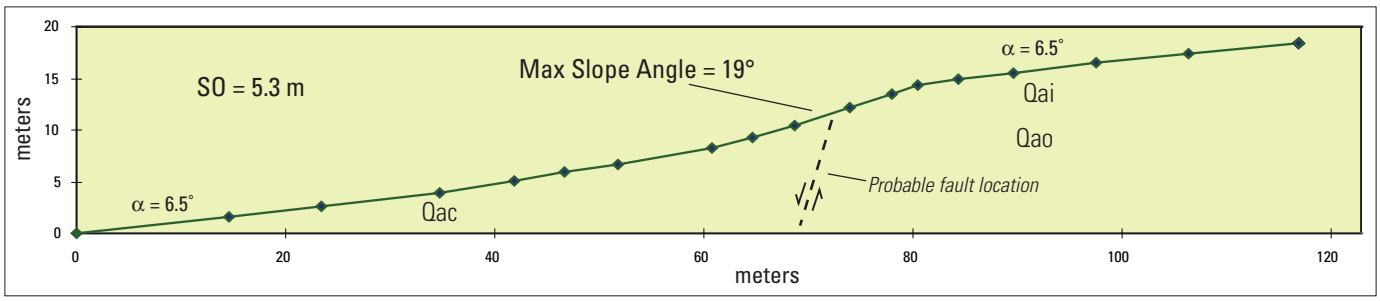

Figure C6–4. Fault scarp profile A at Jaroso Canyon. The profile was measured across late-middle Pleistocene deposits (unit Qai), Bull Lake equivalent (130,000 ka) on the footwall and late Pleistocene to Holocene fault-derived alluvium-colluvium (unit Qac). Far-field slope of offset geomorphic surface shown as the symbol α.

side with the deposit buried by late-middle Pleistocene alluvium shown in figure C6–5, resulting in an estimated surface offset of 10–12 m on >200 ka deposits.

The presence of these older surfaces proximal to the range front is an indication that during late Pleistocene time, alluvial processes at Jaroso Canyon were dominated by fan head incision and alluvial progradation, rather than by range-front aggradation. Less than 2 m of deposits correlative with units Qai and Qay have been deposited on the downthrown side of the fault, and they are mostly localized fault scarp colluvium and slopewash.

The observed 5.3–7.8 m of surface offset on unit Qai (130 ka) yields an average late-middle Pleistocene to Holocene slip rate of 0.04–0.06 mm/yr. Range-bounding normal faults with these slow slip rates are typically characterized by highly sinuous, embayed range fronts with skeletal basal faceted spurs, whereas faults scarps are rare or discontinuous (Bull, 1977, 1984; McCalpin, 1996). Since the faulting occurs at the range front and has slow slip rates and long recurrence intervals (>30 k.y.), accommodation space is not developed proximal to the mountain-piedmont junction, leading to the dissection of older fanhead surfaces and basinward progradation of younger alluvium (Bull, 1977). Thus, the piedmont fan morphology along this section of the Sangre de Cristo fault zone seems to support a late-middle Pleistocene (<150 ka) slip rate of 0.01–0.1 mm/yr.

Contrary to this conclusion about late-middle Pleistocene slip rates along the Latir Peaks section of the southern Sangre de Cristo fault zone, the range-front morphology along this section of the Sangre de Cristo fault zone is characterized by a precipitous, linear range front with well-defined, basal faceted spurs. These features indicate relative slip rates an order of magnitude greater (> 0.1 mm/yr; dePolo, 1998) than those quantified from late-middle Pleistocene to Holocene datums. Menges (1990) determined a post-Pliocene

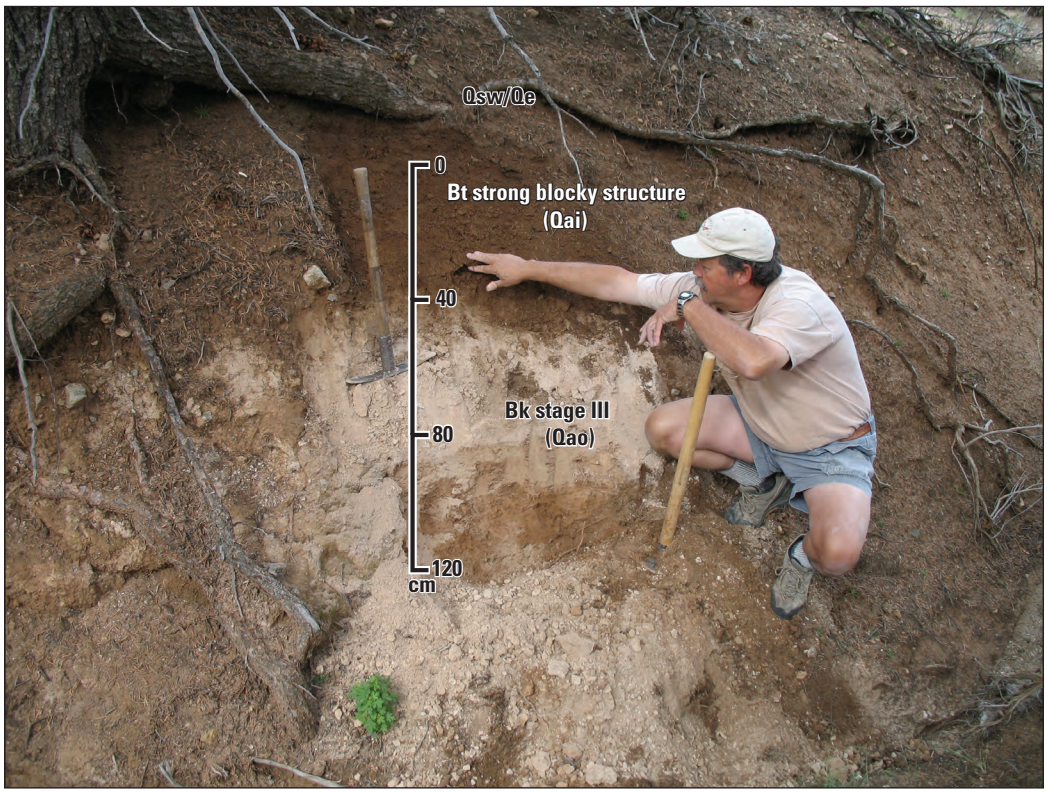

Figure C6–5. Soil profile north of Jaroso Canyon. This soil sequence is buried by about 20–30 cm of late Pleistocene slopewash deposits and eolian silt (unit Qsw/Qe).

slip rate of 0.12 to 0.26 mm/yr on the basis of a correlation between bench heights above faceted spurs along the range front and displaced Servilleta Basalt on top of San Pedro Mesa. The shorter term slip rates (<150 ka) suggest a decrease from the average long-term slip rate. The disparity in slip rates derived from offset late Quaternary deposits and range-front morphology suggests that the steep, faceted range-front morphology is a relict of greater pre–late-middle Pleistocene slip rates along the range-bounding fault (see Ruleman and Machette, chapter J, this volume).

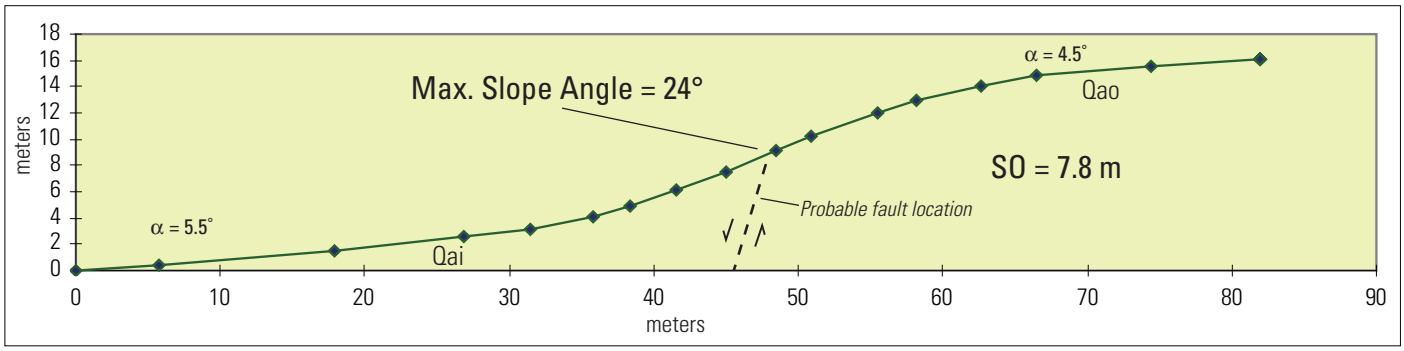

Figure C6–6. Fault scarp profile B at Jaroso Canyon on vertically offset middle Pleistocene deposits (unit Qao). Less than 1 m of Bull Lake-equivalent deposits (unit Qai) and younger late Pleistocene deposits have been deposited above unit Qao on the downthrown side. The far-field slope of the displaced geomorphic surface is indicated by the symbol α.

Stop C7 — Piedmont fault scarp on Cedro Canyon fan

Speaker: Cal Ruleman
Start time: 2:45 pm
Duration: 15 minutes
Location: Highway 522, south of Costilla, N. Mex.
Costilla, New Mexico 7.5' quadrangle
GPS: NAD 27, zone 13, 450667E, 4087722N
Elevation: 7,720 ft asl

Synopsis

Looking east from this stop, we see faulted alluvium of the Cedro Canyon fan complex. Faults that transect this complex have scarps as much as 10 m high on units Qao and Qai (Machette and Personius, 1989) (figs. C7–1 and C7–2). Scarp heights decrease to the north to 2 m, where the fault is buried by latest Pleistocene and Holocene alluvium. No apparent late Pleistocene or Holocene displacement has occurred along this strand of the Latir Peaks section of the southern Sangre de Cristo fault zone. Soils on the upper surface of the Cedro Canyon fan have Bk stage II–III development, whereas deposits in the hanging wall are humic, fine-grained silts, sands, and pebbly gravels of late Pleistocene to Holocene age. At the Cedro Canyon fan head, we found a Bk stage III soil horizon (unit Qao) buried by 2.6 m of late-middle Pleistocene alluvium (unit Qai) and late Pleistocene alluvium (unit Qay), indicating that localized fanhead aggradation has occurred at the range front. No scarps have been identified along the main range-bounding fault. However, the fault could be at the bedrock-colluvium junction. On the skyline, Servilleta Basalt (3.66–4.75 Ma) caps San Pedro Mesa providing a datum to quantify long-term slip rates through well log correlation.

Discussion

At the mouth of Cedro Canyon, a coarse-grained, cobble-boulder gravel with a 60-cm-thick Bt/Bk stage I soil horizon (unit Qai) unconformably overlies a Bk stage III horizon formed on a pebbly sand (unit Qao). This deposit is overlain by approximately 2 m of finer grained sandy-cobble alluvium (unit Qay) (fig. C7–3). We interpret the Bk stage II–III soils exposed along the crest of the intrabasin fault scarp to be characteristic of middle Pleistocene deposits mapped within the region (unit Qao) and correlative with the Bk stage III soil buried at the canyon mouth (fig. C7–4). These features indicate that range front faulting of the original Qao surface has backtilted the deposit 1°–2° and induced aggradation of younger deposits (units Qai and Qay) at the fanhead.

The strong Bt horizon formed in the overlying pebbly gravel and loess is characteristic of soils on late-middle Pleistocene deposits (unit Qai). This exposure is similar to

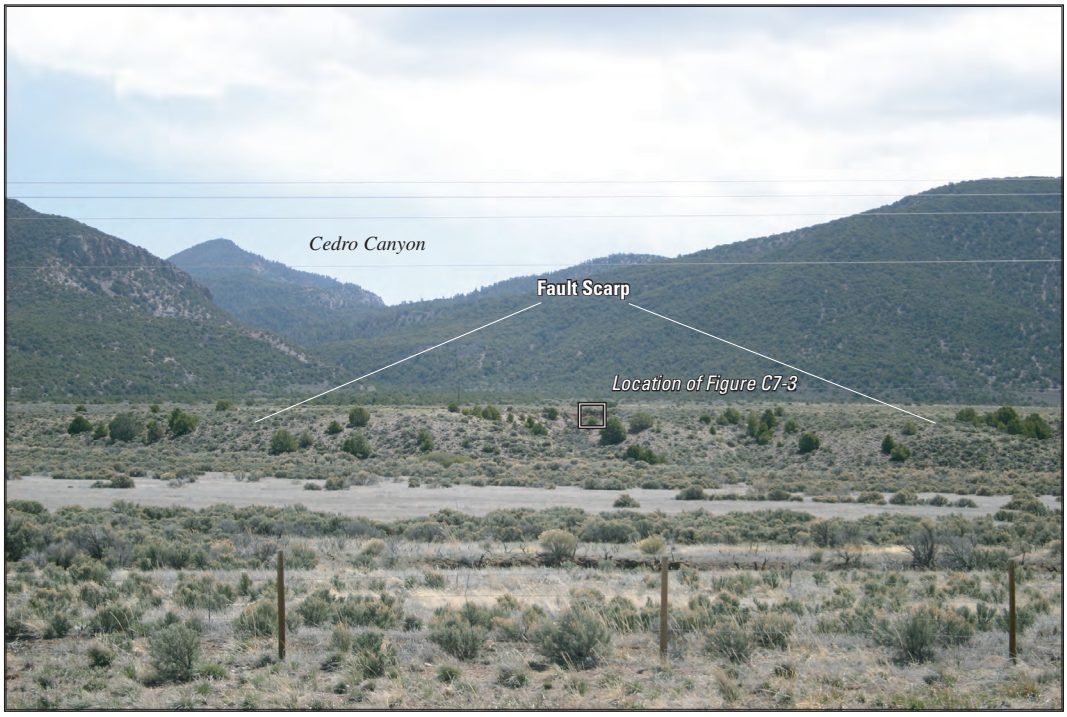

Figure C7–1. View east from stop C7 toward Cedro Canyon.

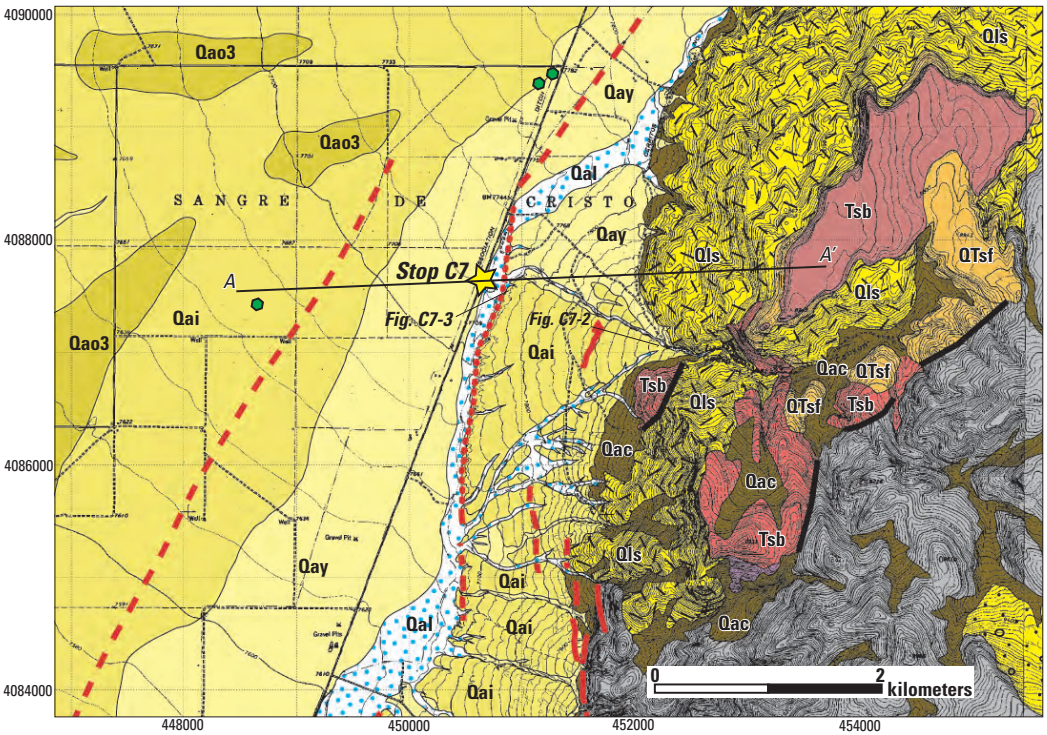

Figure C7–2. Geologic index map for stop 7. Units mapped listed as follows: Qal, Holocene alluvium; Qay, late Pleistocene alluvium; Qai, late-middle Pleistocene alluvium (130,000 ka); Qao3, middle Pleistocene alluvium; Qls, middle and late Pleistocene landslide debris undifferentiated; Qac, late Pleistocene to Holocene alluvium-colluvium undivided; QTsf, Pio-Quaternary Santa Fe Formation; and Tsb, Servilleta Basalt. Faults shown in red, dashed where inferred and dotted where concealed. Green polygons are locations of wells used to constrain cross section A-A'.

that found at Urraca Ranch, where unit Qai overlies unit Qao. Subsequent fluvial trimming of the scarp and deposition of late Pleistocene and Holocene sediments on the hanging wall leaves the amount of offset on Qai uncertain. On the basis of fault scarp profiles from Machette and Personius (1984) and soil development on unit Qao on the upper surface, we can infer that a minimum of 8–10 m of surface offset has occurred on a datum older than 200 ka, yielding a minimum slip rate of 0.05–0.1 mm/yr. This estimated slip rate is consistent with slip rates estimated at Jaroso Canyon.

Wells drilled to the north and west of stop C7 show Servilleta Basalt (unit Tsb) (3.66–4.75 Ma) at depth (fig. C7–2). This unit is correlated with the basalt flows capping the uplifted block of San Pedro Mesa. Lipman and Reed (1989) mapped Servilleta Basalt capping the southern end of San Pedro Mesa as the Cerro flow and dated it at (4.3 Ma). Well data logged in 1959, 1997, and 1998 show two flows of the Servilleta Basalt in the subsurface; either might correlate with the 4.3 Ma flow and allow us to estimate a minimum slip rate for the past 4.3 Ma. By inferring that flows in the hanging wall within the subsurface are either correlative withor younger than the Cerro flow cappin; San Pedro Mesa, two minimum throw calculations can be estimated across the fault, a minimum of 2,000 ft and preferred minimum of 2,200 ft (fig. C7–5). The offset has been rounded owing to uncertainties in flow thickness and precise tilt calculations on the Servilleta Basalt. For comparison, refer to figure B8–4 from Machette (this volume) for cross sections approximately 17 km to the north showing displacement and slip rates estimated by offset on the Servilleta Basalt.

For the minimum throw, we use the base of the Cerro flow on San Pedro Mesa as the footwall datum. The surface elevation of San Pedro Mesa is 8,943 ft at this location. We subtract an approximate average flow thickness of 50 ft to get an elevation of 8,900 ft for the base of the flow on the footwall. A tilt of 5° on the basalt projected to the west approximately 6,500 ft contributes an additional 500 ft to the base of the flow, yielding an elevation of 9,400 ft. Using well log B (fig. C7–5) to determine the hanging wall datum, we start with a surface elevation of 7,782 ft. The top of the upper flow was reached at 398 ft in the subsurface, an elevation of 7,384 ft, rounded to 7,400 ft for our estimations. This elevation (7,400 ft) is subtracted from the projected base of the Cerro flow (9,400 ft), yielding a net throw of 2,000 ft, or 610 m. Six hundred and ten meters of throw during 4.3 m.y. yields a long-term slip rate (since 4.3 Ma) of 0.14 mm/yr.

The preferred minimum amount of throw across the fault is based on the projected footwall base of the Cerro flow (9,400 ft) and subtracting the elevation of the base of the second flow recorded in log B (588 ft) (fig. C7–5). This base depth subtracted from the surface elevation (7,782 ft) yields an elevation of 7,194 ft, which is rounded to 7,200 ft for our purposes. This elevation (7,200 ft) is subtracted from the projected footwall base of the Cerro flow (9,400 ft) to quantify a net throw of 2,200 ft, or 670 m, for the last 4.3 m.y. A long-term slip rate determined from the preferred minimum throw is estimated to be 670 m/4.3 m.y. or 0.16 mm/yr. These long-term slip rates are correlative with those quantified by Menges (1990a,b), for this section of the Sangre de Cristo fault zone, of 0.12–0.26 mm/yr.

By comparing our estimated long-term slip rates with slip rates estimated for the past <200 k.y., we see that the Latir Peaks section of the southern Sangre de Cristo fault zone has dramatic changes in slip rates over shorter periods of time. On the basis of the fault scarp morphology, surface offset on relative-age deposits, and late-middle Pleistocene to Holocene piedmont morphology, long-term slip rates are potentially two times as great as slip rates quantified for the late-middle Pleistocene to present along this section. We propose that the Sangre de Cristo fault system, consisting of northern, central and southern zones, has similar long-term slip rates (>1 Ma) that may be double the short-term rates (<200 ka) for an individual zone. During these shorter periods of time (<200 ka), stress is transferred from one zone to another, reducing the seismic hazard along one and increasing it along another (see Ruleman and Machette, chapter J, this volume).

Figure C7–3. Cedro Canyon fanhead exposure in stream cutbank. Stratigraphy is interpreted as late Pleistocene alluvium (unit Qay) over late-middle Pleistocene (unit Qai) alluvium overlying a Bk stage III horizon in middle Pleistocene alluvium (unit Qao).

Figure C7–4. Soil exposure at crest of piedmont fault scarp on Cedro Canyon fan complex.

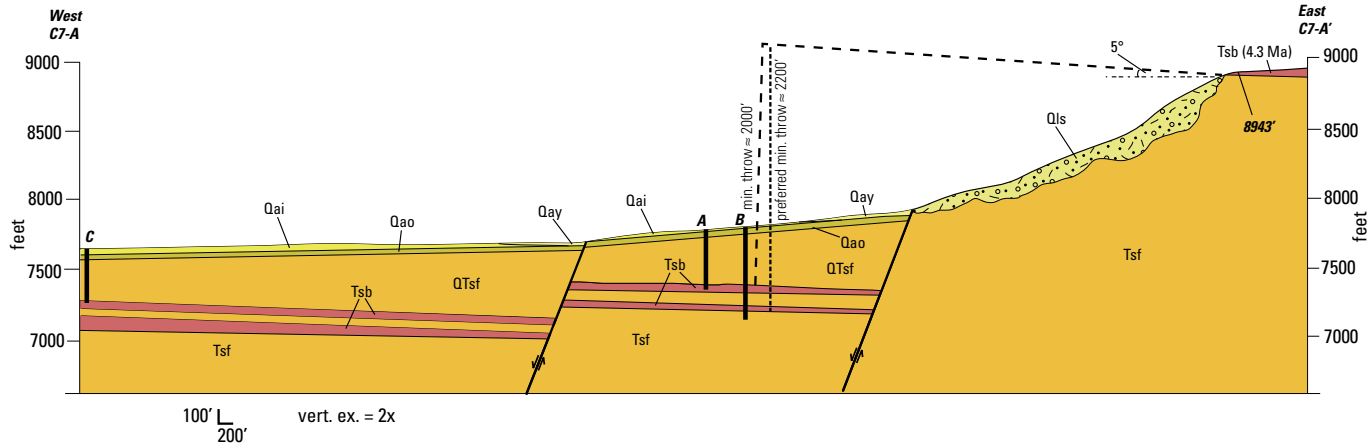

Figure C7–5. Cross section A-A' showing offset Servilleta Basalt (unit Tsb, 3.66–4.75 Ma). Units shown as follows: Qay, late Pleistocene alluvium; Qai, late-middle Pleistocene alluvium; Qao, middle Pleistocene alluvium; Qls, middle to late Pleistocene landslide debris; QTsf/Tsf, Santa Fe Group (>640 ka); and Tsb, Servilleta Basalt. Age of Servilleta Basalt (unit Tsb) on San Pedro Mesa from Lipman and Reed (1989). Well logs A, B, and C record Servilleta Basalt at 415–460 ft, at 398–456 ft/539–588 ft, and at 387–405 feet, respectively.

References Cited

Appelt, R.M., 1998, $^{40}Ar/^{39}Ar$ geochronology and volcanic evolution of the Taos Plateau volcanic field, northern New Mexico and southern Colorado: Socorro, New Mexico Institute of Mining and Technology, M.S. thesis, 58 p.

Bankey, Viki, Grauch, V.J. S., Drenth, B., and Geophex, Inc., 2006, Digital data from the Santa Fe East and Questa–San Luis helicopter magnetic surveys in Santa Fe and Taos Counties, New Mexico, and Costilla County, Colorado: U.S. Geological Survey Open-File Report 2006 –1170, available at http://pubs.usgs.gov/of/2006/1170/.

Bankey, Viki, Grauch, V.J.S., Webbers, A., and PRJ, Inc., 2005, Digital data and derivative products from a high-resolution aeromagnetic survey of the central San Luis Basin, covering parts of Alamosa, Conejos, Costilla, and Rio Grande Counties, Colorado, and Taos County, New Mexico: U.S. Geological Survey Open-File Report 2005–1200, available at http://pubs.usgs.gov/of/2005/1200/.

Bull, W.B., 1977, The alluvial fan environment: Progress in Physical Geography, v. 1, p. 222–270.

Bull, W.B., 1984, Tectonic geomorphology: Journal of Geological Education, v. 32, p. 310–324.

Cordell, L., and Keller, G.R., 1984, Regional structural trends inferred from gravity and aeromagnetic data in the New Mexico–Colorado border region, *in* Baldridge, S.W., Dickerson, P.W., Ricker, R.E., and Zidek, J., eds., Rio Grande rift—Northern New Mexico: New Mexico Geological Society 35th Annual Field Conference, Guidebook, p. 21–23.

dePolo, C.M., 1998, A reconnaissance technique for estimating the slip rates of normal-slip faults in the Great Basin, and application to faults in Nevada, U.S.A.: Reno, University of Nevada, PhD. dissertation, 199 p.

Dethier, D.P., 2001, Pleistocene incision rates in the western United States calibrated using Lava Creek B tephra: Geology, v. 29, no. 9, p. 783–786.

Dungan, M.A., Muehlberger, W.R., Leininger, L., Peterson, C., McMillan, N.J., Gunn, G., Lindstrom, M., and Haskin, L., 1984, Volcanic and sedimentary stratigraphy of the Rio Grande Gorge and the Late Cenozoic geologic evolution of the southern San Luis Valley, *in* Baldridge, S.W., Dickerson, P.W., Ricker, R.E., and Zidek, J., eds., Rio Grande rift—Northern New Mexico: New Mexico Geological Society 35th Annual Field Conference, Guidebook, p. 157–170.

Lipman, P.W., and Reed, J.C., 1989, Geologic map of the Latir volcanic field and adjacent areas, northern New Mexico: U.S. Geological Survey Miscellaneous Investigations Series Map I–1907, scale 1:48,000.

Machette, M.N., 1985, Calcic soils of the southwestern United States, *in* Weide, D.L., ed., Cenozoic History of the southern Rocky Mountains: Geological Society of America Special Paper 203, p. 1–21.

Machette, M.N., and Personius, S.F., 1984, Map of Quaternary and Pliocene faults in the eastern part of the Aztec 1° x 2° quadrangle and the western part of the Raton 1° x 2° quadrangle, northern New Mexico: U.S. Geological Survey Miscellaneous Field Studies Map MF–1465–B, 14 p., 1 plate.

McCalpin, J.P, 1996, Applications of paleoseismic data to seismic hazard assessment and neotectonic research, *in* McCalpin, J.P., ed., Paleoseismology: London, Academic Press, p. 439–494.

McMillan, N.J., and Dungan, M.A., 1986, Magma mixing as a petrogenetic process in the development of the Taos Plateau volcanic field, New Mexico: Journal of Geophysical Research, v. 91, no. B6, p. 6029–6045.

McMillan, N.J., and Dungan, M.A., 1988, Open-system magmatic evolution of the Taos Plateau volcanic field, northern New Mexico: Journal of Petrology, v. 29, no. 3, p. 527–557.

Menges, C.M., 1990a, Late Quaternary fault scarps, mountain-front landforms, and Pliocene-Quaternary segmentation on the range-bounding fault zone, Sangre de Cristo Mountains, New Mexico: Geological Society of America Reviews in Engineering Geology, v. 8, p. 131–156.

Menges, C.M., 1990b, Late Cenozoic rift tectonics and mountain-front landforms of the Sangre de Cristo Mountains near Taos, northern New Mexico, *in* Bauer, P.W., Lucas, S.G., Mawer, C.K., and McIntosh, W.C., eds., Tectonic development of the southern Sangre de Cristo Mountains, New Mexico: New Mexico Geological Society 41st Annual Field Conference, Guidebook, p. 113–122.

Munsell, 1994, Munsell soil color charts revised edition: New Windsor, Macbeth Division of Kollmorgan Corporation.

Pazzaglia, F.J., 1989, Tectonic and climatic influences on the evolution of Quaternary depositional landforms along a segmented range-front fault, Sangre de Cristo Mountains, north-central New Mexico: Albuquerque, University of New Mexico, M.S. thesis, 210 p., 1 plate.

Pazzaglia, F.J., and Wells, S.G., 1990, Quaternary stratigraphy, soils and geomorphology of the Northern Rio Grande rift, *in* Bauer, P.W., Lucas, S.G., Mawer, C.K., and McIntosh, W.C., eds., Tectonic development of the southern Sangre de Cristo Mountains, New Mexico: New Mexico Geological Society 41st Annual Field Conference, Guidebook, p. 423–430.

Personius, S.F., and Machette, M.N., 1984, Quaternary and Pliocene faulting in the Taos Plateau region, northern New Mexico, *in* Baldridge, S.W., Dickerson, P.W., Ricker, R.E., and Zidek, J., eds., Rio Grande rift—Northern New Mexico: New Mexico Geological Society 35th Annual Field Conference, Guidebook, p. 83–90.

Read, A.S., Bauer, P.W., Thompson, R.A., Kelson, K.I., and Muehlberger, W.R., 2004, The Taos Plateau and Rio Grande Gorge, *in* Brister, B.S., Bauer, P.W., Read, A.D., and Lueth, V.W., eds., Geology of the Taos region, New Mexico Geological Society 55th Annual Field Conference, Guidebook, p. 1–36.

Thompson, R.A., and Machette, M.N., 1989, Geologic map of the San Luis Hills area, Conejos and Costilla Counties, Colorado: U.S. Geological Survey Miscellaneous Investigations Series Map I–1906, scale 1:50,000.

Wells, S.G., Kelson, K.I., and Menges, C.M., 1987, Quaternary evolution of fluvial systems in the northern Rio Grande rift, New Mexico and Colorado—Implications for entrenchment and integration of drainage systems, *in* Menges, C.M., Enzel, Y., Harrison, B., eds., Quaternary tectonics, landform evolution, soil chronologies and glacial deposits—Northern Rio Grande rift of New Mexico: Friends of the Pleistocene Rocky Mountain Cell Guidebook, p. 95–109.

Winograd, I.J., 1959, Ground-water conditions and geology of Sunshine Valley and western Taos County, New Mexico, U.S. Geological Survey Technical Report 12, 70 p., 2 plates.

Ground-Water Age and Flow at Great Sand Dunes National Monument, South-Central Colorado

By Michael G. Rupert and L. Neil Plummer

CHAPTER D

USGS
science for a changing world

Ground-Water Age and Flow at Great Sand Dunes National Monument, South-Central Colorado

By Michael G. Rupert and L. Niel Plummer

Great Sand Dunes National Monument (hereinafter called Great Sand Dunes) is located in south-central Colorado along the eastern edge of the San Luis Valley (fig. 1). The San Luis Valley is bounded by the Sangre de Cristo Mountains to the east and the San Juan Mountains to the west. Great Sand Dunes has an altitude ranging from about 7,500 to 10,300 feet and receives annual average precipitation of about 11 inches near the Great Sand Dunes Headquarters (fig. 2).

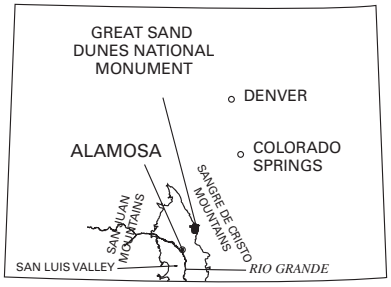

Figure 1. Location of the Great Sand Dunes National Monument, south-central Colorado.

The predominant feature in Great Sand Dunes is the 30 square-mile main dune field (fig. 2) which rises up to 750 feet above the valley floor. The age of the dunes is estimated to be between 2,000 and 12,000 years old (Chatman and others, 1997). Composition of the sand indicates the predominant source is the San Juan Mountains to the west. The sand was transported to the San Luis Valley by the Rio Grande and other local streams and then carried by prevailing southwesterly winds to the Sangre de Cristo Mountain front. The shape of the Sangre de Cristo Mountains acts as a sand trap (Chatman and others, 1997).

The Sand Dunes Need Water

As incongruous as it might seem, existence of the sand dunes is dependent on water (Chatman and others, 1997). Two streams flowing from the Sangre de Cristo Mountains, Medano Creek on the east and southeastern edge, and Sand Creek on the northwestern edge (fig. 2), transport the sand southwestward around the perimeter of the dunes and deposit the sand on the upwind side, where prevailing winds transport the sand northeastward toward the Sangre de Cristo Mountains again. The rate of sand transport northeastward by wind generally is the same as the rate of sand transport southwestward by water; together, the two mechanisms maintain the dune field in a state of quasi-equilibrium (Chatman and others, 1997). Streamflows typically are largest during spring snowmelt, which corresponds with the period of greatest sand transport by the creeks.

An important ecological feature of Great Sand Dunes are wetlands associated with interdunal ponds and depressions that nearly intersect the water table near the western edge of the dune field. The interdunal ponds and depressions provide important habitat for a variety of species that depend on a wetland habitat in an otherwise desert environment. The interdunal ponds are of special concern because their numbers have decreased markedly in recent years. The relatively sudden disappearance of ponds appears to indicate a considerable change in Great Sand Dunes hydrology. The existence and natural maintenance of the dune field and the interdunal ponds are dependent on maintaining ground-water levels at historic elevations.

Two Aquifers Exist at Great Sand Dunes National Monument

A shallow aquifer and a deep aquifer are the two principal aquifers at Great Sand Dunes. All the water in Medano and Sand Creeks, except what is lost to evapotranspiration, infiltrates into the ground to recharge the shallow aquifer. The shallow and deep aquifers are separated by an impermeable layer of clay about 8 feet thick. Wells V and Y, located near the western edge of Great Sand Dunes (fig. 2), intercept the clay layer about 300 feet below the land surface. It is not known if the deep aquifer extends eastward all the way to the Sangre de Cristo Mountain front.

How Old is Water in the Shallow Aquifer?

Ground water in the shallow aquifer is much younger than ground water in the deep aquifer (Rupert and Plummer, 2004). Water first seeps down to the shallow aquifer from Medano and Sand Creek (fig. 2). Ground water near Medano and Sand Creeks probably is only a few years old. The ground water then travels in a southwesterly direction, underneath the main dune field. Additional water from precipitation on the dune field moves down to and mixes with the ground water underneath the main dune field. Ground water in the shallow aquifer also travels to springs that discharge to Big and Little Spring Creeks on the west side of

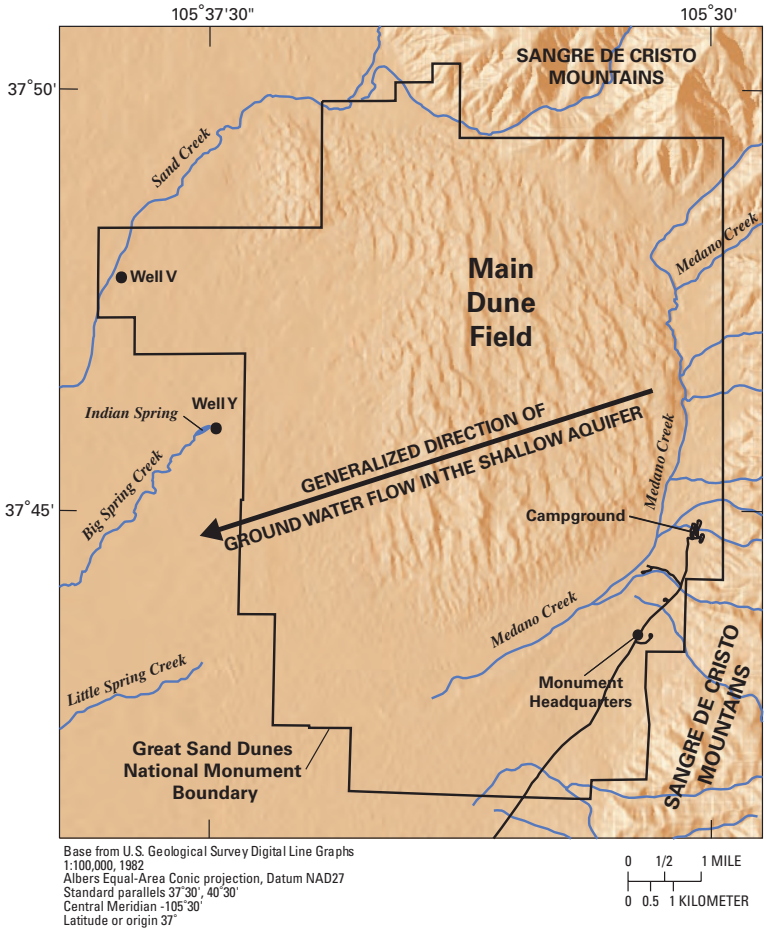

Figure 2. Shaded relief map of the Great Sand Dunes National Monument, south-central Colorado.

Great Sand Dunes. Ground-water age dating using chlorofluorocarbons (Freon™) and tritium (an isotope of hydrogen) indicate that it takes more than 60 years for ground water to travel underneath the dune field from Medano and Sand Creeks to Big and Little Spring Creeks (Rupert and Plummer, 2004).

How Old is Water in the Deep Aquifer?

Using carbon-14 geochemical dating methods, the age of ground water sampled from well Y, which is completed in the deep aquifer and is near the western edge of the dune field (fig. 2), is about 30,000 years before present (plus or minus 3,000 years) (Rupert and Plummer, 2004). This age was determined using methods similar to those used to date charcoal found in firepits of archeological sites. The last major ice advance (Wisconsin) during the ice age peaked about 20,000 years before present (U.S. Geological Survey, 1992); ground water from the deep aquifer is older than that.

References

Chatman, M., Sharrow, D., and Valdez, A., 1997, Water resources management plan, Great Sand Dunes National Monument, Colorado: National Park Service, Water Resources Division, 197 p.

Rupert, M.G., and Plummer, L.N., 2004, Ground-water flow direction, water quality, recharge sources, and age, Great Sand Dunes National Monument and Preserve, south-central Colorado, 2000-2001: U.S. Geological Survey Scientific Investigations Report 2004–5027, 32 p.

U.S. Geological Survey, 1992, The great ice age: U.S. Geological Survey General Interest Publication, ISBN 0-16-036025-0, 8 p. Accessed May 29, 2002, at URL http://pubs.usgs.gov/gip/ice_age/

Dating and Stratigraphy of Middle to Late Holocene Eolian Sand Deposits in the San Luis Basin, East of Alamosa, Colorado

By Michael N. Machette and Kathy Puseman[1]

[1]Paleo Research Institute, Inc., Golden, Colorado

CHAPTER E

Abstract

The Baca Lane pit (field-trip stop A9, this volume) exposes four depositional units within an eolian sand dune. As part of his reconnaissance mapping of the Alamosa 1:100,000-scale sheet during the summer of 2005, the senior author made a quick description of this sand sequence, sampled charcoal and other organic matter from three buried soils, and noted archeological materials associated with a prehistoric hearth site. Charcoal samples were separated from three of the four buried soils that mark depositional hiatuses in the sequence of eolian sands. The charcoal samples, which were radiocarbon dated at about 2800 cal yr, 3900 cal yr, and 5560 cal yr, record a much longer sequence than is normally exposed in the basin (see various field trip stops in chapter A, this volume). Faunal and floral remains in these samples reveal paleovegetation that is consistent with that of the present, and archeological evidence indicates prehistoric occupation of this site between 2.8 ka and 5.6 ka.

Introduction

The Baca Lane pit is one of the few places in the Alamosa area where we can see a sequence of stratified Holocene eolian sand deposits separated by well-formed, organic-rich soils (buried A horizons). This area, and in particular the southeast corner of County Road 6S and Road S116 (Baca Lane, see fig. A9–1, chapter A, this volume), is characterized by largely stabilized sand dunes and interspersed blowouts that expose playa-like organic rich sediment. The presence of charcoal, locally abundant, and a hearth site on one of the buried soils indicates that the organic-rich horizons were at the surface and occupied by prehistoric man.

Local Geology

The Baca Lane pit is located north of U.S. Highway 160, which is the main highway across the San Luis Valley. From east to west, it connects the cities of Fort Garland, Alamosa on the Rio Grande, Monte Vista, and Del Norte. The pit is about 0.9 mi (1.5 km) north of the highway and about 6.5 mi (10 km) east of Alamosa, on the southwest side of a northwest-southeast-trending string of eolian sand dunes (fig. A9–1, chapter A, this volume). A low escarpment to the east separates eolian sand and underlying upper Pleistocene to Holocene fluvial sediment (at and west of site) from a gentle west-sloping piedmont covered by eolian-dune and cover sands (Holocene to upper Pleistocene). The piedmont is largely a relict basin floor of ancient Lake Alamosa (chapter G, this volume) of middle Pleistocene age. The escarpment is fluvial (see field trip stop A8) and, to the south, its height increases to about 25 m where it is known as Hansen Bluff (see field trip stop B7, chapter B, this volume). The lacustrine and interbedded fluvial sediment that underlie the piedmont are part of the Alamosa Formation, which is considered to be an informal, upper member of the Santa Fe Group (middle Pleistocene to late Oligocene, Michael Machette and Ren Thompson, unpub. mapping, 2007).

Baca Lane Pit

During the summers of 2004 and 2005, the senior author made a quick description of the sand sequence, photographed the site, sampled organic materials and charcoal from buried soils, and noted archeological materials associated with a prehistoric hearth site. Four samples of organic-rich sand were submitted to Paleo Research Institute, Inc., Golden, Colo., and processed

by Kathy Puseman (table E–1). Charcoal, bones and bone fragments, and plant fragments were separated from three of the four sampled soils, and one sample contained archeological materials (small rock flakes, burned bone fragments, and fish bones).

Flotation of bulk soil material (R1, R2, R3, and R4) from the Baca Lane pit (site BA–MM04–25) resulted in recovery of charcoal and other charred botanic remains suitable for radiocarbon dating. All of the dating was performed by the Woods Hole Oceanographic Institute (WHOI) National Ocean Sciences Accelerator Mass Spectrometry Facility (NOSAMS; see http://nosams.whoi.edu/index.html). Rabbitbrush charcoal in samples R2 and R4, saltbush charcoal in sample R2, greasewood charcoal in samples R2 and R4, and *Chenopodiaceae* (Goosefoot family) charcoal in samples R1, R2, and R4 all were present in sufficient quantities (>0.007 g) for accelerator mass spectrometry (AMS) radiocarbon analysis. Only sample R3 yielded insufficient charcoal or other organic materials for dating.

Stratigraphic Units

Unit 1

In the borrow-pit wall, which is crescent shaped and faces south, the sand sheets lap over one another in a southeasterly direction, which likely reflects the predominant wind and sand-transport direction at this site during middle and late Holocene time (figs. E–1 and E–2). The upper surface of the excavated dune is covered with modern eolian sand (unit 1) that is sparsely vegetated but anchored by woody shrubs (such as *Artemisia sp*., *Atriplex sp*., and *Sarcobatus sp.*). This unit contained no obvious datable materials (charcoal, fossils, or organic matter) and thus was not sampled or described in any detail.

Unit 2

The uppermost sampled A horizon is formed in the top of unit 2 of the dune sequence. This sample, R1 (BA–MM04–25R1, fig. E–1 and tables E–2, E–3), was collected from an interval 85 to 90 cm below the modern land surface. Sample R1 is from a weakly consolidated light-brown eolian sand (weak A horizon with abundant charcoal in the top of unit 2) that is about 1.2 m thick here (fig. E–1*B*). Unit 2 thickens to the southeast where it fills an intradune low. Conversely, unit 2 is not present on the crest of the dune; instead, older sand (unit 3) forms the northwestern core of this dune (fig. E–1*B*).

Unit 3

The buried soil formed in the top of unit 3 (and buried by unit 2) is characterized by a moderately well developed, light gray A horizon. The soil is best exposed in the northeast part of the pit, below and to right of the sample locality (R1, 2.8 ka A horizon on unit 2). Unit 2 is about 1.2 cm thick at the locality where we sampled for charcoal (between R1 and R2, fig. E–2 and fig. A9–1, chapter A, this volume). The A horizon in the top of unit 3 has been disturbed by a prehistoric fire pit (hearth) that is buried by sand of unit 2.

Charcoal separated from the hearth in the basal part of unit 2 (R2, fig. E–1B) has an AMS radiocarbon age of 3,590±55 ^{14}C yr B.P. (NOSAMS no. OS–52750, table E–2. The radiocarbon ages were calendar corrected using the radiocarbon calibration program (CALIB REV. 5.1, 2005 of Stuiver and Reimer; see also Stuiver and Reimer, 1993). Using a 2-sigma error, sample R2 yielded calendar-corrected age ranges as follows:

1. 3720–3804 cal yr B.P. (13 percent of calibration curve),
2. 3807–4002 cal yr B.P. (80 percent of calibration curve; age reported herein), and
3. 4034–4080 cal yr B.P. (6 percent of calibration curve).

The second range (3807–4002 cal yr B.P.) is most likely to be correct, so we use an age of 3905±98 cal yr B.P. for the age of charcoal in the hearth pit in the A horizon in the top of unit 3 or the base of unit 2 (buried hearth). For the purposes of further discussion, this age range will be treated as 3.9±0.1 ka. This age brackets unit 3 as older than 3.9 ka and unit 2 as 3.9 ka and younger (fig. E–2).). The charcoal submitted for analysis was *Atriplex* (saltbush or shadscale; table E–4), although a variety of other floral and faunal remains were also identified.

A second portion (R3) of the A horizon formed in the top of unit 3 was sampled in the northern part of the pit. Here, unit 3 is overlain by an eroded section of unit 2 (no soil), and sand of unit 1. Separation of organic components of sample R3 yielded rootlets (probably modern), fragments of unidentified hardwood charcoal too small to date (<0.001g), as well as a fragment of bone, an ostracode shell (wind transported), and insect remains (table E–5). Therefore, we were not able to recover datable materials from this soil (unit 3, fig. E–2).

The minimum age of eolian sand unit 3 is limited by the 3905±98 cal yr B.P. age of charcoal in the hearth pit that rests on the A horizon of unit 3. For the purposes of further discussion, this age range will be treated as 3.9±0.1 ka.

Unit 4

The oldest and stratigraphically lowest eolian sand deposit (herein referred to as unit 4) is exposed in the west half of the pit (left-hand side of figs. E–1 and E–2). Unit 4 has a thick, dark silty to clayey A horizon with abundant charcoal. The high silt and clay contents of the A horizon and the

Table E-1. Basic information for samples collected at stop A9, this volume.

[Paleo Research, Inc. is a for-profit company that specializes in the separation and identification of materials for radiocarbon dating, archaeology, and environmental studies]

Paleo Research Institute, Inc. Total Number of Samples: Four
2675 Youngfield Street Delivered: August 12, 2005
Golden CO 80401 Complete: September 19, 2005
Phone: 303–277–9848; Fax: 303–462–2700 Analyst: Kathy Puseman
Client: Michael N. Machette, U.S. Geological Survey, *machette@usgs.gov*

SITE INFORMATION

Site Name: Baca Lane Pit Site No. BA–MM04–25

Location: Baldy 7.5' quadrangle, south central Colorado. UTM coordinates (NAD 27): UTM Zone 13, 433910m E, 4148955 m N. NW¼ NW¼ Sec. 2, T. 37 N., R. 11 E. Alamosa County, Colo. East side of Rd. S116 (Baca Lane), about 2.0 mi north of Colorado State Highway 160, 6.5 mi east of Alamosa, Colo. Elevation: 7,530 ft. Feature description: Eolian sand dune complex, multiple buried A (soil) horizons. About 4 m of section exposed in abandoned borrow (sand) pit.

Environment/vegetation: Semiarid (est. 9 inch MAP), sagebrush, four-wing saltbush is dominant vegetation.

Cultural affiliation: Cultural (Holocene) artifacts are associated with several of the land surfaces (A horizons) that are buried, including a small hearth with flakes and burned bones.

Provenience for samples: Sand-dune complex derived from older floodplain deposits of the Rio Grande, San Luis Basin.

Site description: All four samples are from the same location (pit).

R1 (BA–MM04–25R1) is the highest sample from the section. Charcoal and plant fragments collected from interval 85–90 cm below the modern land surface. The sample is weakly consolidated light-brown eolian sand (unit 2) with abundant charcoal. Weak soil (A horizon) development; not rich in organic matter. Unit 2 is 1.2 m thick here.

R2 (BA–MM04–25R2) is the second highest sample from the section. Abundant, large pieces of charcoal in a pocket (hearth) in A horizon of unit 3, buried by unit 2.

R3 (BA–MM04–25R3) is the third highest sample in the section. Sampled thick, very organic rich A horizon of unit 3, which is overlain by loose eolian and well-stratified sandy silt (unit 2). Sample from interval 15–20 cm below top of unit 3. Can't trace west to R4, but believe that R3 is stratigraphically higher than R4.

R4 (BA–MM04–25R3) is the lowest sample in the section. Sampled a 10–15 cm thick A horizon (near top of unit 4) that is composed of silty sand with very fine medium blocky peds with soft, 2–3 mm diameter carbonate nodules. Contains sparse charcoal below sampled position. Top of unit 4; well stratified sand (unit 3) overlies this sample.

Dates: None known

Maps: Baldy 7.5' topographic quadrangle map

Photos: Available from collector

WORK REQUESTED: Separate charcoal for radiocarbon analysis. Identify plant type when possible.

Table E–2. Radiocarbon age determinations from charcoal samples at stop A9.

[Reported radiocarbon ages have 1-sigma errors; calendar-corrected ages have 2-sigma errors. The radiocarbon ages were calendar corrected using the radiocarbon calibration program (CALIB REV. 5.1, 2005 of Stuiver and Reimer; see also Stuiver and Reimer, 1993)]

USGS sample number	Date reported	NOSAMS accession number	$\delta^{13}C$	Fraction modern	FM error	Radiocarbon ages and errors (^{14}C yr B.P.)	Calendar ages and errors (cal yr B.P.)
BA–MM04–25R1 (soil on unit 2)	2/27/2006	OS–52749	–23.38	0.7148	0.0032	2700±35	2804±54
BA–MM04–25R2 (hearth, base of unit 2)	2/27/2006	OS–52750	–11.21	0.6393	0.0045	3590±55	3905±98
BA–MM04–25R4 (soil on unit 4)	2/27/2006	OS–52751	–25.62	0.549	0.0030	4820±45	5560±90

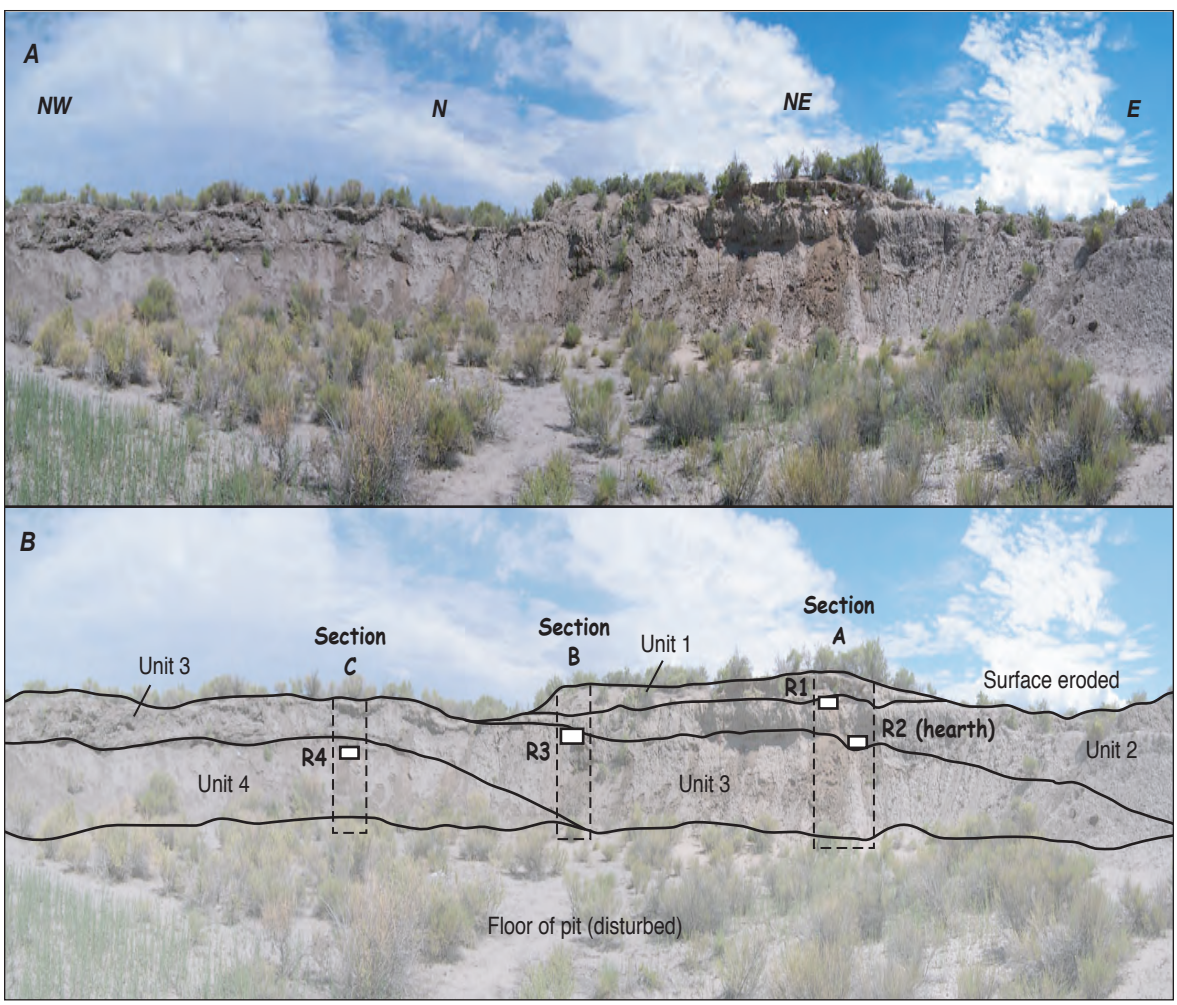

Figure E–1. South-facing wall of the Baca Lane pit (sand borrow pit). *A*, Panoramic view toward the northwest (on left) sweeping to the east (on right). *B*, Overlay showing stratigraphic units (dark lines) exposed in the Baca Lane pit. Soil samples R1 through R4 (white boxes) collected from eolian sand units 2, 3, and 4. Total vertical exposure in the pit is about 4 m below the top of the modern dune surface. Vertical exaggeration of image, 1.5x.

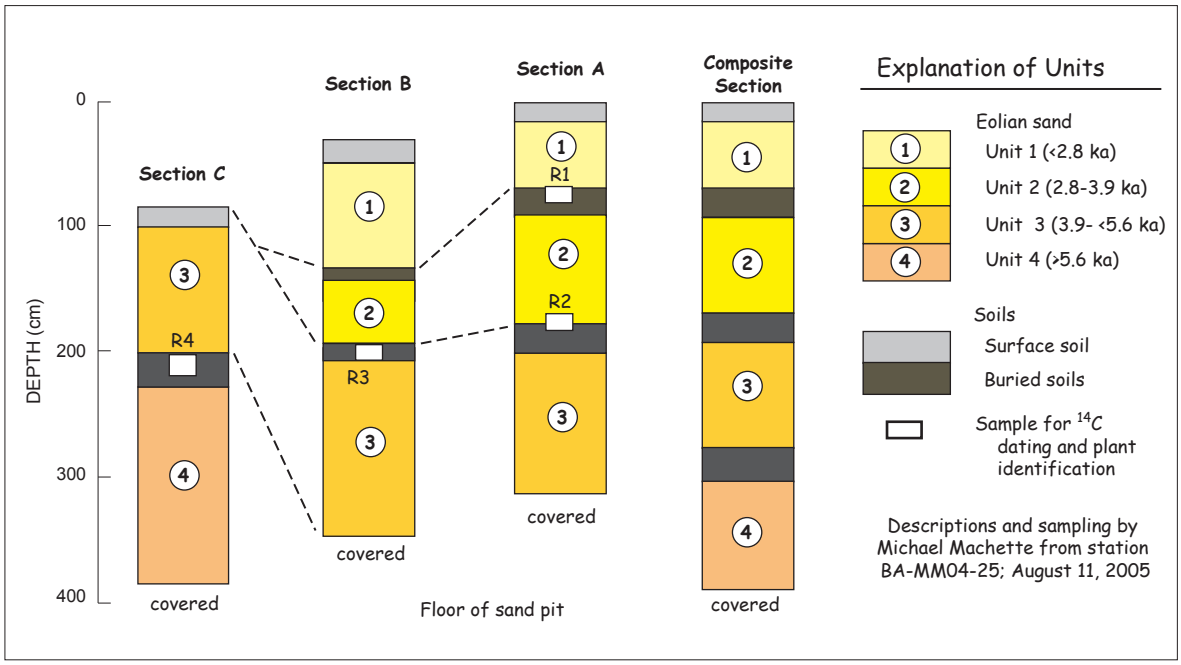

Figure E–2. Stratigraphic sections and sample localities at the Baca Lane pit, east of Alamosa, Colo.

Table E–3. Materials identified from sample R1 (BA–MM04–25R1).

[Analyses by Kathy Puseman and Jamie Dexter of Paleo Research Institute, Inc. Abbreviations: W, whole; F, fragment; X, presence noted in sample; *, indicates number recovered. Material shown in bold was submitted for dating]

Identification	Material	Charred		Uncharred		Material weight or abundance
		W	F	W	F	
Floral remains						
Chenopodium (goosefoot)	Seed	1	17			
Rootlets					X	Moderate
Charcoal or wood						
Chenopodiaceae (Goosefoot family)	**Charcoal**		**20**			**0.025 g**
Nonfloral remains						
Bone ≥2 mm - mostly fish bone			53		6	
Bone <2 mm - mostly fish bone			X		X	Numerous
Fish vertebrae ≥1 mm		35	38			0.311 g
Fish vertebrae <1 mm			X			Moderate
Fish scale					42*	
Flake					5	
Insect	Chitin				5	
Shell					X	Few

Table E–4. Materials identified from sample R2 (BA–MM04–25R2).

[Analyses by Kathy Puseman and Jamie Dexter of Paleo Research Institute, Inc. Abbreviations: W, whole; F, fragment; X, presence noted in sample; *, indicates number recovered. Material shown in bold was submitted for dating]

Identification	Material	Charred		Uncharred		Material weight or abundance
		W	F	W	F	
Floral remains						
Chenopodium (goosefoot)	Seed	7	80			
Oxalis (wood sorrel)	Seed	1	1			
Portulaca (purslane)	Seed	3	1			
Sporobolus (dropseed grass)	Caryopsis	3				
Rootlets					X	Moderate
Charcoal or wood						
Chenopodiaceae (Goosefoot family)	Charcoal		40			0.784 g
***Atriplex* (saltbush or shadscale)**	**Charcoal**		**3**			**0.038 g**
Sarcobatus vermiculatus (greasewood)	Charcoal		13			0.140 g
Chrysothamnus (rabbitbush)	Charcoal		19			0.098 g
Unidentified ≥2 mm	Charcoal		X			0.215 g
Nonfloral remains						
Bone ≥2 mm			6			0.467 g
Bone <2 mm			X		X	Few
Snail shell				4	1	

Table E–5. Materials identified from sample R3 (BA–MM04–25R3).

[Analyses by Kathy Puseman and Jamie Dexter of Paleo Research Institute, Inc. Abbreviations: W, whole; F, fragment; X, presence noted in sample; *, indicates number recovered. Material shown in bold was submitted for dating]

Identification	Material	Charred		Uncharred		Material weight or abundance
		W	F	W	F	
Floral remains						
Rootlets					X	Few
Charcoal or wood						
Unidentified hardwood, small	Charcoal		2			<0.001 g
Nonfloral remains						
Bone			1			
Insect	Chitin				5	
Ostracode shell					1	
Sand					X	

upward fining of unit 4 suggests that this sediment is a result of deflation of dry lake sediment (playa sediment) from an upwind source. The lower, sandier parts of unit 4 must have been deposited when older sands (earlier than unit 4) became unstable (less vegetated), but the lakes still remained moist enough to preclude erosion.

Charcoal separated from the upper part of unit 4 (R4, fig. E–1*B*) has an AMS radiocarbon age of 4,820±45 ^{14}C yr B.P. (NOSAMS no. OS–52751, table E–2). Using a 2-sigma error, this date yielded a unique calendar-corrected age range of 5470–5650 yr B.P. (i.e., 5560±90 cal yr B.P.). We submitted a large piece of unidentified hardwood charcoal for analysis (table E–6), although a variety of floral remains, charred wood and fragments of bone and snails were also identified. For the purposes of further discussion, this age range will be treated as 5.6±0.1 ka. Therefore, unit 4—the oldest eolian sand exposed in the Baca Lane pit—is older than about 5.6 ka. The deeper (exposed) parts of unit 4 could be dated by optical stimulation luminescence (OSL) techniques.

Environments During the Late and Middle Holocene

Climatic and environmental conditions at the Baca Lane site appear to have fluctuated from moist (shallow lakes or ponds) and stabilized (vegetated) landscapes to dry and unstable (poorly vegetated) landscapes at least four times (we recorded four sand units) during the past 6,000 years. During moister conditions, the sand was stable and soil organic matter accumulated at or near the surface of the dunes. Without OSL dating of the eolian sand, we cannot estimate how long it took each unit to accumulate (intervals of instability and sand transport) or the duration of soil formation (intervals of stability and minimal sand transport). Nevertheless, it appears that, on average, these sand dunes persisted for periods of about 1–2 k.y. before becoming unstable.

Table E–6. Materials identified from sample R4 (BA–MM04–25R4).

[Analyses by Kathy Puseman and Jamie Dexter of Paleo Research Institute, Inc. Abbreviations: W, whole; F, fragment; X, presence noted in sample; *, indicates number recovered. Material shown in bold was submitted for dating]

Identification	Material	Charred		Uncharred		Material weight or abundance
		W	F	W	F	
Floral remains						
Chenopodium	Seed		1			
Portulaca	Seed	1				
Sporobolus	Caryopsis	1				
Rootlets					X	Few
Charcoal or wood						
Chenopodiaceae - friable, with pits and fissures	Charcoal		7			0.053 g
Sarcobatus vermiculatus	Charcoal		1			0.006 g
Chrysothamnus	Charcoal		10			0.030 g
Unidentified hardwood >2 m	**Charcoal**		**X**			0.015 g
Unidentified <2 mm	Charcoal		X			
Nonfloral remains						
Bone ≥1 mm			2		1	
Bone <1 mm			X		X	Few
Insect	Chitin				6	
Snail shell			3	1	2	

Paleovegetation During Stable Intervals

The recovered charcoal came from local shrubs (*Chenopodiaceae, Atriplex, Sarcobatus,* and *Chrysothamaus*) that likely were burned as fuel sources by the prehistoric occupants of the site. Charred seeds of *Chenopodium* (goosefoot), *Portulaca* (purslane), *Sporobolus* (dropseed) and *Oxalis* (wood sorrel) were found in the samples that were processed. During prehistoric times, humans appear to have occupied this area during the late summer or fall season when these seed resources are available for harvesting. Charred bone fragments in all four samples most likely reflect the processing of meat and fish (sample R1). Samples R1, R2, and R4 encompass a time span of 2.8 ka to about 5.56 ka, which equates to late and middle Holocene time.

Acknowledgments

We appreciate the constructive and helpful comments of Ralph Shroba (USGS) and Laura Strickland (USGS) who reviewed a preliminary version of this manuscript. However, any errors that may remain are the responsibility of the authors.

References Cited

Stuiver, M., and Reimer, P.J., 1993, Extended ^{14}C database and revised CALIB 3.0 ^{14}C age calibration program: Radiocarbon, v. 35, no. 1, p. 215–230.

Late Pleistocene to Early Holocene Paleoecology of the Mr. Peat Wetland Deposit, Alamosa County, Colorado

By R. Randall Schumann and Michael N. Machette

CHAPTER F

Abstract

The Mr. Peat wetland deposit occupies a west-trending, slightly entrenched, unnamed stream valley located about 16 km (10 mi) east of the city of Alamosa and 2 km (1.3 mi) south of U.S. Highway 160. The peats lie in a late-glacial-age paleovalley that is underlain by well-bedded fluvial sand and pea-size gravel. In the summer of 2006, we excavated four trenches in these deposits to better understand the timing, duration, and environment of peat accumulation, the age of underlying fossil-bearing alluvial deposits, and the age and origin of overlying tufaceous paleospring deposits. Radiocarbon dating of the peats show that most of the deposits accumulated from 13.4 ka cal yr B.P. to about 11.3 ka cal yr B.P., but organic accumulation continued until middle Holocene time (4.3–6.7 ka cal yr B.P.), whereas locally overlying tufaceous spring deposits started to accumulate at about 6.7 ka cal yr B.P. and continued until about 3.9 ka cal yr B.P. The deposit was mined for its peat resources during the 1970s and 1980s.

Introduction

The Mr. Peat wetland deposit is located south of U.S. Highway 160, the main highway across the San Luis Valley (fig. F–1). The pit is about 16 km (10 mi) east of the city of Alamosa and 2 km (1.3 mi) south of the highway, occupying a west-trending, slightly entrenched, unnamed stream valley. The deposit is approximately 3 km (1.9 mi) long, as much as 0.5 km (0.3 mi) wide, and it lies at an elevation of approximately 2,313 m (7,590 ft) near the geographic center of the deposit. The stream valley is incised into gently west-sloping piedmont covered by eolian dune and cover sands of late Pleistocene and Holocene age. The piedmont is largely a relict basin floor of ancient Lake Alamosa (see chapter G in this volume) of middle Pleistocene age. Shallow lacustrine and interbedded fluvial sediment that underlie the piedmont constitute the uppermost part of the Alamosa Formation (middle Pleistocene to Pliocene), which is considered to be an informal, upper

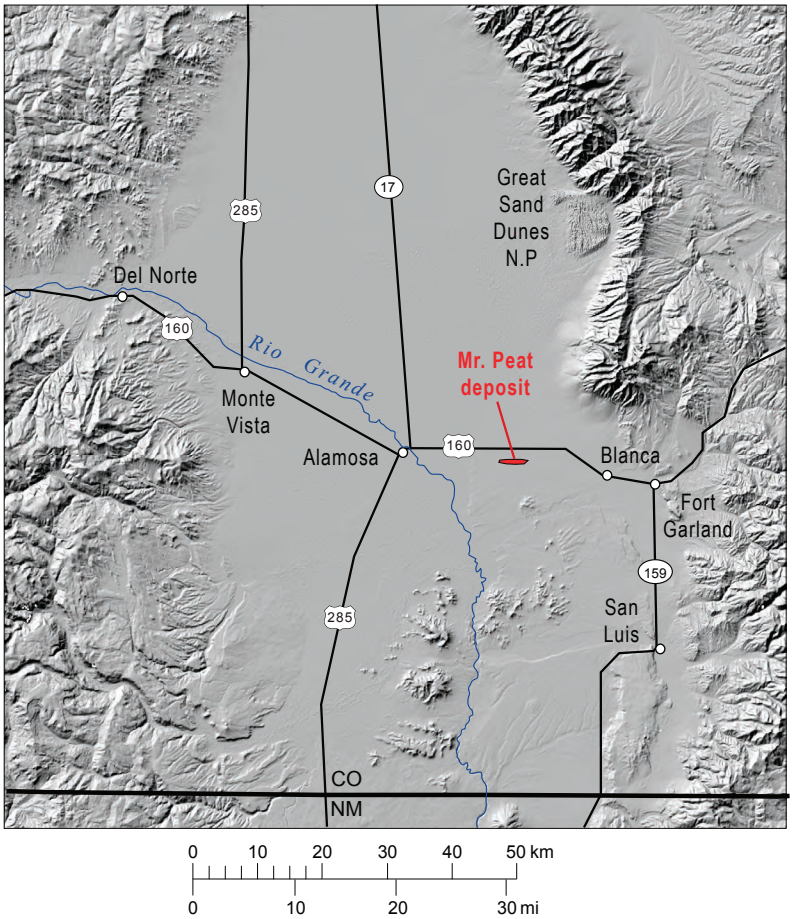

Figure F–1. Generalized map of central San Luis Valley showing location of the Mr. Peat pit.

Figure F–2. Sign at entrance to the Mr. Peat pit.

member of the Santa Fe Group (middle Pleistocene to late Oligocene; Michael Machette and Ren Thompson, unpub. mapping, 2007). The peat deposits were commercially mined in the 1970s and 1980s (fig. F–2). An examination of the geologic history of this deposit was undertaken as part of field investigations related to geologic mapping in the Alamosa 30' x 60' quadrangle.

Vegetation

Vegetation in the floor of the San Luis Valley consists primarily of greasewood (*Sarcobatus vermiculatus*), rubber rabbitbrush (*Chrysothamnus nauseosus*), and grasses such as alkali sacaton (*Sporobolus airoides*), saltgrass (*Distichlis spicata*), and Indian ricegrass (*Oryzopsis hymenoides*). The Rio Grande, other perennial streams, and regularly flooded marshes, lakes, and playas support aquatic and shoreline emergent vegetation such as pondweeds (*Potamogeton spp.*), spikerush (*Eleocharis palustris*), hardstem bulrush (*Schoenoplectus acutus*), cattail (*Typha latifolia*), and American three-square (*Scirpus pungens*). Low-lying basins or playas with irregular or short-duration flooding contain saltgrass or western wheatgrass (*Pascopyrum smithii*) or both. Narrowleaf cottonwood (*Populus angustifolia*), coyote willow (*Salix exigua*), and mountain willow (*Salix monticola*) are common along riparian areas in the valley floor.

Alluvial fans along the valley margins tend to be gravelly and support pinyon pine (*Pinus edulis*), Gambel oak (*Quercus gambelii*), needle-and-thread grass (*Stipa comata*), and short-grass steppe vegetation that reflect the greater precipitation and milder winter temperatures of this zone compared with the valley bottom. Many of the streams on these alluvial fans support riparian forests of narrowleaf cottonwood (*Populus angustifolia*), with shrub understories of willows (*Salix spp.*), western birch (*Betula occidentalis*), ocean spray (*Holodiscus discolor*), and wild rose (*Rosa woodsii*).

Vegetation of the Sangre de Cristo Mountains is typical of the southern Rocky Mountains, including mixed forests of Douglas fir (*Pseudotsuga menziesii*) and ponderosa pine (*Pinus ponderosa*), occasional stands of white fir (*Abies concolor*) at lower elevations, and Engelmann spruce (*Picea engelmannii*) and subalpine fir (*Abies lasiocarpa*) at higher elevations. Aspen (*Populus tremuloides*) is present throughout the study area at elevations over 8,500 ft. (This section is summarized from Rocchio, 2004).

Stratigraphy

In the summer of 2006 we excavated four trenches (approximately 2–3 m deep and 5–7 m long and designated A through D) near the eastern end of the Mr. Peat pit, in order to better understand the depositional environments of the wetland deposits, the age of underlying fossil-bearing alluvial deposits, and the age and origin of overlying spring deposits (fig. F–3).

The wetland deposits are underlain by at least, but probably considerably more than, 3 m of poorly to moderately indurated, bedded fluvial sediments ranging from pebbly or gravelly sand (clasts commonly about 1 cm diameter, maximum 5–7 cm diameter) representing channel bed facies to finely laminated silt and clay channel-margin and overbank deposits (fig. F–4). The coarser grained layers and lenses are commonly iron stained, indicating postdepositional subsurface water throughflow. These fluvial sands underlie the wetland deposits in all four pits. The nature of the deposits and the geometry of the valley suggest that at the time of deposition, the valley was occupied by a sand-bed meandering river that headed in the Sangre de Cristo Mountains and flowed westward into the Rio Grande.

The wetland deposit overlies the fluvial sediment and has three main facies (fig. F–5). The lowermost of these comprise dark brown to black, mucky peat with abundant plant root, stem, and moss fragments, probably deposited in a shallow pond or lake environment with slow-moving or stagnant water. A fragment of *Salicaceae* (willow or cottonwood) wood was found in a sample of this unit (Puseman, 2006). The contact with the underlying fluvial deposits appears gradational in trench A but is relatively sharp in the other trenches.

Above the mucky peat is an orangish- to reddish-brown (5YR 4/4), “woody” peat that is composed almost entirely of fresh-appearing plant fragments. The contact with the underlying mucky peat is gradational except in trench A, in which the two units are separated by about 5 cm of grayish-brown, parallel-bedded silt.

A light to dark gray, low density, organic silt “black-mat” type of deposit overlies the woody peat in trenches A and B, and it overlies mucky peat in trench C. The contact between the underlying unit and the organic silt is generally sharp

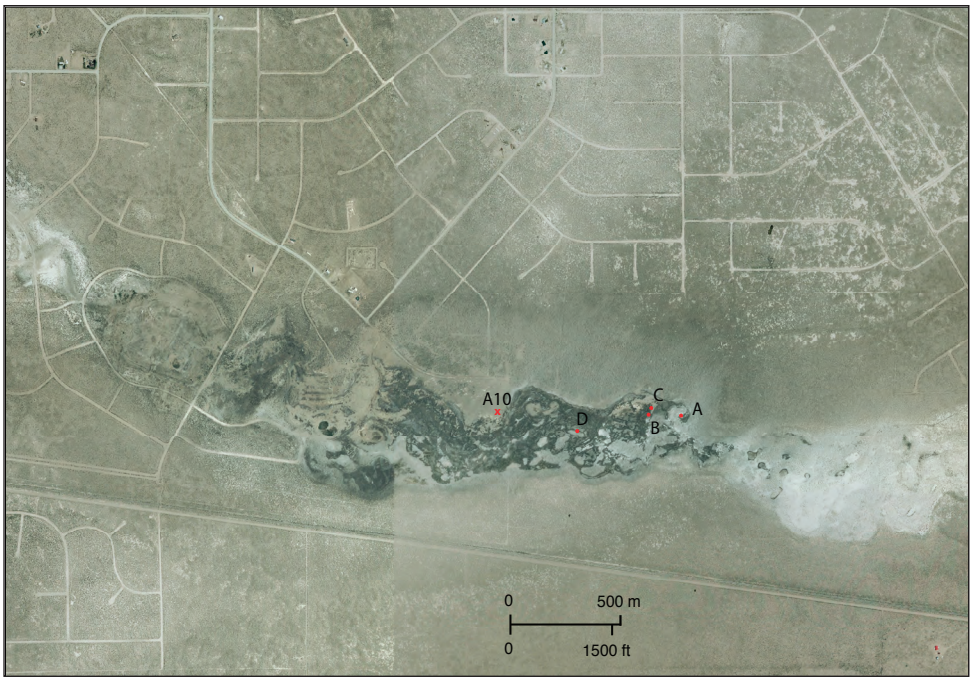

Figure F–3. Aerial photograph of the Mr. Peat deposit showing locations of trenches and stop A10.

and smooth. The silt is massive and blocky, with no visible bedding or other sedimentary structures, and it is composed largely of silt-sized quartz and feldspar grains (loess?) that are loosely cemented by organic matter. Numerous small, elongate white crystals, possibly calcite or gypsum, were also found in samples of this unit (MRP–A5, MRP–B4) (fig. F–4). This unit is commonly exposed at the surface, where it forms a topographically irregular surface marked by a subpolygonal pattern of desiccation cracks that are typically filled with windblown sand and silt (fig. F–6). Total organic carbon contained in a sample of this material (MRP–A5, fig. F–4), determined by coulometric methods, is approximately 8 percent, corresponding roughly to 15–20 percent organic matter in the unit. Organic-rich, mineral-matter-dominated layers accumulated in spring-fed environments have been termed “black mats” (Haynes, 1968, Quade and others, 1998), “sapropelic silt” (for example, Holliday, 1985), or “peaty mud” (for example, Safford, 1981). We use the term “organic silt” in this report as a generic, strictly descriptive term.

In the eastern (upstream) part of the valley, the peats are locally to widely overlain by tufa deposits. At the site of our trenching, the tufas are concentrated in round, domed mounds that are from 25 cm to as much as 1 m thick (figs. F–7 and F–8). Downstream, the tufas become thinner, less continuous, and more layer like, and they are absent altogether in the western part of the deposit. X-ray diffraction analysis of a tufa sample (MRP–A6, fig. F–4) indicates that it is composed almost entirely of calcite, with lesser amounts of intercalated quartz and feldspar, most likely introduced as windblown sand and silt (loess). A mantle of locally derived eolian deposits consisting of quartz and feldspar sands and of reworked fragments (typically granule size) of tufa and peat form a discontinuous cover over the entire area. Thickness of the eolian cover ranges from zero to as much as a meter. Eolian sand and silt commonly fills desiccation cracks in the surface of the organic silt layer and tufa mounds (fig. F–6).

Sample Analyses

Twelve samples from the Mr. Peat pit were submitted for radiocarbon dating: 2 from natural exposures and the remainder (10) from the 4 trenches (table F–1). The woody peats contained whole, fresh pieces of plant matter, which were hand picked after ultrasonic cleaning in distilled water. All of the remaining samples were separated by Kathy Puseman of Paleo Research Institute, Inc. (see chapter E in this volume). Each sample was added to approximately 3 gallons of hot water, stirred until a strong vortex formed, and then poured through a 150-micron mesh sieve. The process was repeated until all floating material was removed from the sample. The floated samples were weighed and then passed through a series of graduated screens to separate datable material and to sort the remains (Puseman, 2006).

Snail shell fragments were found in the tufa samples, whereas organic matter, wood fragments, or charcoal were concentrated from the remaining samples of organic silt and peat. All of the concentrated materials (organic and inorganic) were sent to the radiocarbon laboratory at Woods Hole Oceanographic Institute for accelerator mass spectrometry (AMS) radiocarbon dating. In addition, four samples of sand were collected for optically stimulated luminescence (OSL) dating of sediment that did not contain datable organic matter. The OSL ages were determined by Shannon A. Mahan (USGS).

Radiocarbon dating indicates that most of the peat deposits accumulated from 13.4 ka cal yr B.P. to about 11.3 ka cal yr B.P., but organic accumulation continued on until middle Holocene time (4.3–6.7 ka cal yr B.P.). The locally overlying tufaceous spring deposits started to accumulate at about 6.7 ka cal yr B.P. and continued until at least 3.9 ka cal yr B.P. (table F–1, fig. F–4), but carbonate-rich spring water was likely the major water source for the underlying organic silt deposits, as indicated by the abundant evaporite mineral fragments observed in samples of the organic silt. A thin peaty sand layer in the alluvium about 1.4 m below the base of the main peat layer in trench C (sample

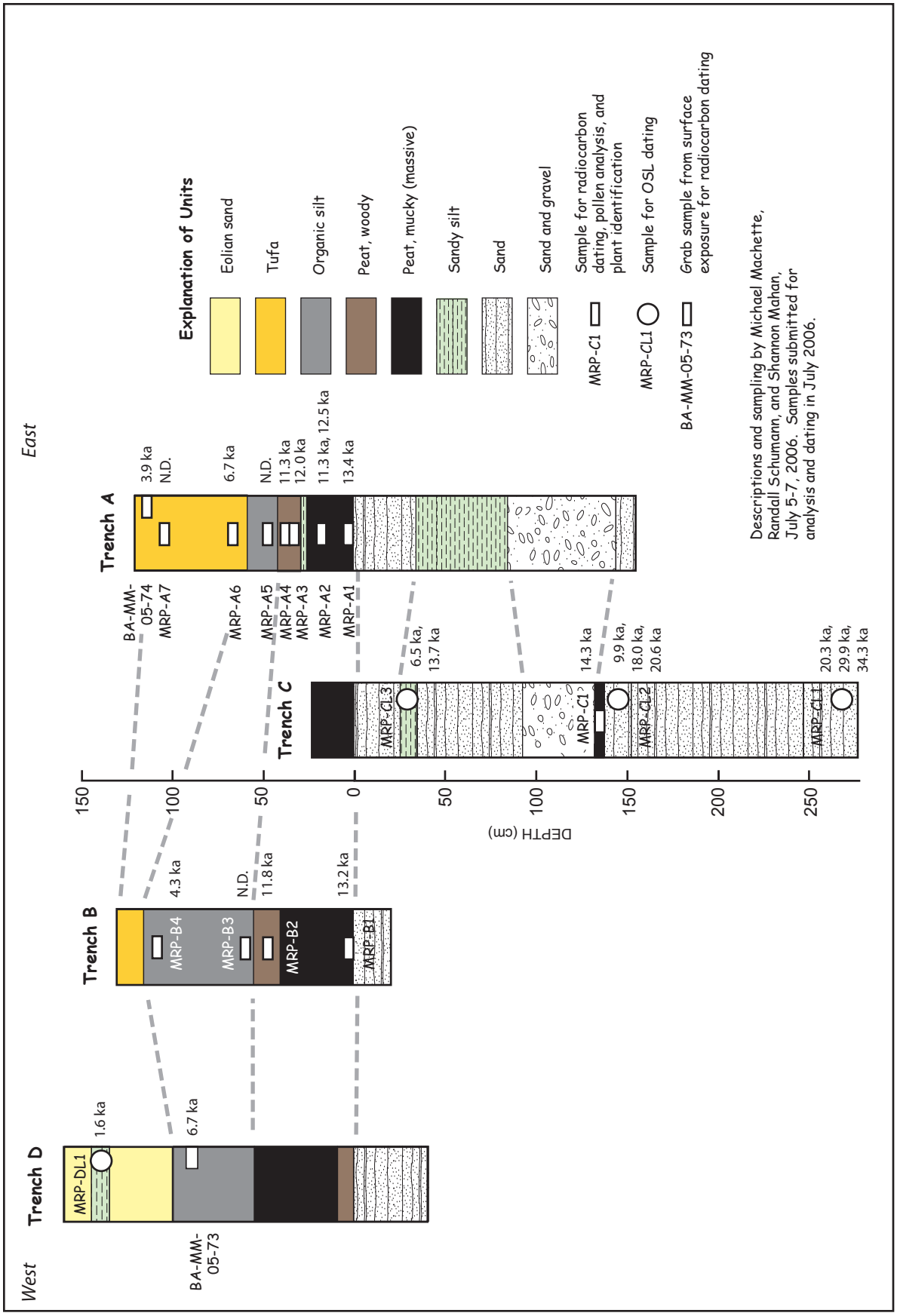

Figure F–4. Sampled stratigraphic sections at the Mr. Peat pit, Alamosa, Colorado. Radiocarbon and luminescence ages are in ka (thousands of years ago). Abbreviation: N.D., not dated.

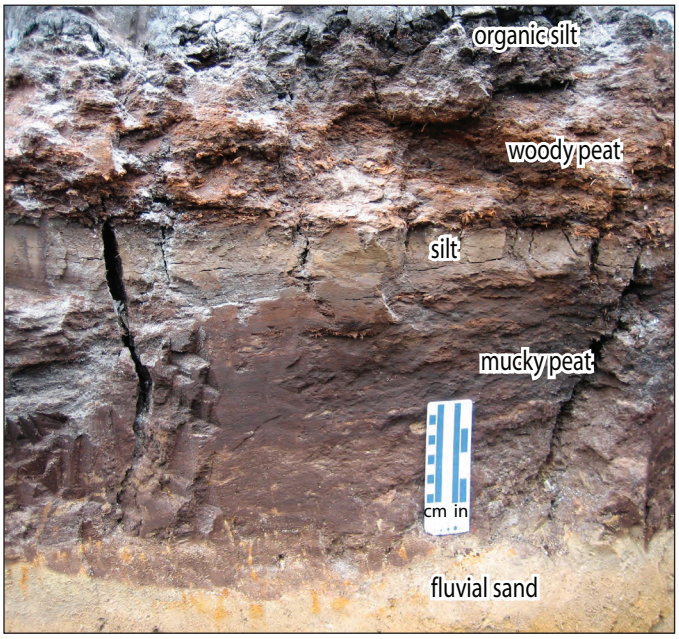

Figure F–5. Major units in trench A. Similar units are present in the other trenches. Each black bar at far left of scale is 1 cm; each black bar at far right is 1 in.

Figure F–6. Surface exposure of "organic silt" layer with eolian sand- and silt-filled desiccation cracks.

Figure F–7. Tufa mound at top of section in trench A. Each red or white section of tape measures 20 cm.

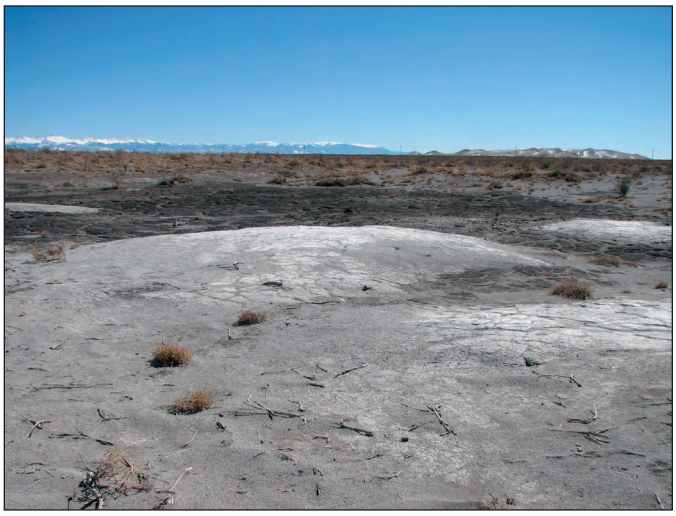

Figure F–8. Tufa mounds at surface near east end of the Mr. Peat pit.

Table F–1. Radiocarbon age determinations from samples collected at the Mr. Peat pit.

[Samples arranged in descending stratigraphic order (see fig. F–4). Reported radiocarbon ages have 1-sigma errors; calibrated ages (in calendar years) have 2-sigma errors. The radiocarbon ages were calibrated using the radiocarbon calibration program (CALIB REV. 5.1, 2005 of Stuiver and Reimer; see also Stuiver and Reimer, 1993)]

USGS sample number	Material dated	Depth	Date reported	NOSAMS accession number	$\delta^{13}C$	$\delta^{14}C$	Radiocarbon ages and errors (^{14}C yrs B.P.)	Calibrated ages and errors (cal yrs B.P.)	Ages used for discussion (ka)
BA–MM05–74	Snail shell in tufa	Grab sample	2/21/06	OS–53176	–6.72	–363.8	3580±30	3875±37	3.9
MRP–A6	Snail shell in tufa	53–60 cm	11/16/06	OS–57406	–7.25	–522.4	5880±45	6701±46	6.7
MRP–A4	Woody peat	80–85 cm	9/29/06	OS–56477	–28.93	–712.7	9960±40	11334±125	11.3
MRP–A3	Woody peat	85–90 cm	9/28/06	OS–56395	–27.9	–722.1	10250±55	12031±76	12.0
MRP–A2(2)	Moss in mucky peat	100–105 cm	12/7/06	OS–57712	–34.1	–711.6	9930±60	11322±82	11.3
MRP–A2(1)	Stems and roots in mucky peat	100–105 cm	12/6/06	OS–57672	–26.36	–733.2	10550±40	12436±35 12636±54	12.5
MRP–A1	Mucky peat	115–120 cm	12/7/06	OS–57714	–29.77	–766.2	11600±65	13428±80	13.4
MRP–B4	Organic silt	20–25 cm	1/4/07	OS– 57942	–26.15	–385.2	3850±85	4314±93	4.3
MRP–B2	Woody peat	80–85 cm	10/5/06	OS–56641	–27.53	–718.8	10150±55	11780±67 11915±59	11.8
MRP–B1	Mucky peat	125–130 cm	11/24/06	OS–57499	–25.8	–758.3	11350±45	13228±43	13.2
MRP–C1	Stems and roots in alluvium	155–160 cm	12/7/06	OS–57740	–27.82	–787.2	12350±60	14288±171	14.3
BA–MM05–73	Organic silt	Grab sample	3/22/06	OS–53707	–25.97	–522.2	5880±50	6700±49	6.7

MRP–C1) yielded an age of 14.3 ka cal yr B.P. (the oldest radiocarbon date reported for our samples), whereas luminescence dating of the alluvium in the same trench yielded both stratigraphically consistent and inconsistent ages depending on the method used (see table F–2*A*, *B*). For example, the OSL and infrared-stimulated luminescence (IRSL) analyses for sample MRP–CL–3 yielded ages of 6.5 ka and 13.7 ka average, respectively, yet the sand must date between 13.2 ka and 14.3 ka on the basis of radiocarbon analyses (table F–1). In this case, the IRSL dating approach yielded the better age. Likewise, dates from sample MRP–CL–2 range from 9.9 ka (OSL) to 20.6 ka (IRSL, table F–2), but they should be about 14.3 ka (see fig. F–4). Finally, sample MRP–CL–1 is dated at 20.3 ka (OSL) to 34.3 ka (IRSL), which is stratigraphically consistent with its position 2.8 m below the base of the peats (dated at 13.2 ka) (fig. F–4). Thus, the luminescence ages provide general limits on the latest Pleistocene fluvial sediment, and both methods yielded stratigraphically consistent (older with increasing depth) ages. However, the luminescence ages differ by method and are not consistent with the more conventional radiocarbon date of 14.3 ka.

In general, the radiocarbon dates are in proper stratigraphic order: the oldest dates come from the basal mucky peat and the youngest dates come from the organic silt and coeval tufa deposits. The young eolian sand that overlies peat and organic silt in trench D yielded an OSL age of 1.6 ka (late Holocene, table F–2).

Samples of organic-rich units in trenches A and B (samples MRP–A1 through A5, B1–B4; fig. F–4) were examined for pollen and microfossils by Robert S. Thompson (USGS). The samples from the mucky and woody peats contain abundant pollen from plants that flourish in wetland environments, including sedge and bulrush (Cyperaceae) and lesser amounts of shallow pond-type vegetation such as pondweed (*Potamogeton*). The mucky and woody peats also contain abundant sagebrush (*Artemisia*), saltbush (Chenopodiaceae/*Amaranthus*), ragweed (*Ambrosia* type), greasewood (*Sarcobatus*), and grass (Gramineae) pollen, indicating an open, xerophytic regional environment similar to that of today, but all of the samples contain moderate amounts of spruce (*Picea*) pollen as well, which may indicate that the climate of the valley floor was cooler and wetter than at present. Pine (*Pinus*) pollen is present in moderate amounts in all of the samples, suggesting its regional, but not necessarily local, presence. Pine pollen is relatively sturdy and can survive transport from distant sources better than many other types of pollen. The *Pinus* pollen in the organic silt sample is broken and fragmented, suggesting that either the organic silt has been highly reworked or that the pollen has been transported from a distance. The organic silt layer, which is typically above the more organic peats, does not contain abundant wetland plant pollen. However, a significant number of *Pseudoschizaea* microfossils were found in sample MRP–A5 from this unit, indicating that the organic silt accumulated in a warm, wet environment, possibly with seasonal drying (Scott, 1992).

Discussion and Conclusions

On the basis of these studies, we suggest that during the late Pleistocene, glacier- and snowmelt-runoff-fed streams flowing west into the Rio Grande entrenched and backfilled valleys. By about 20,000 years ago, these stream channels had aggraded to within 5–10 m of the surface of the piedmont through which they incised. A shift from deposition of fluvial sand and gravel to wetland deposits suggests that the surface stream ceased flowing at about 13.5 ka years ago (indicated by radiocarbon dates at the base of the wetland deposits). High water tables on the piedmont intersected the paleostream valley and probably caused persistent spring discharge that might have been localized by faulting in the underlying fine-grained sediment of the Alamosa Formation. The mucky-peat unit likely accumulated in a sluggish or stagnant water environment, with pondweed and bulrush vegetation suggesting that the paleovalley was a shallow pond or lake at the time. This environment persisted for approximately 1,000 years, giving way to a peatland environment (the woody peat facies) in which the ground was probably perennially saturated but not necessarily submerged.

Peat accumulation ceased approximately 11,000 years ago, suggesting a shift from submerged or perennially saturated wetland to a “wet meadow” that may have been seasonally dry in some years. A drying of the valley floor would have allowed mobilization of eolian sand and silt (probably derived from glacial outwash), which was blown into the wetland, but organic matter continued to accumulate owing to the input of spring water. This wetland would have been an ideal feeding and watering area for large mammals such as bison and mastodon and thus a likely hunting and camping site for early humans. Mastodon tooth and tusk fragments were found at the Mr. Peat site, and many early human campsites from the Folsom period have been identified in the San Luis Valley (Jodry and others, 1989; see also stop B5).

The presence of evaporites in the organic silt suggest that during this period the local water table may have been at or above the ground surface at some times and in the shallow subsurface at others. It is also possible that the evaporite crystals in the organic silt may have formed later if the water table remained high enough for the deposit to remain perennially wet until much later. Pollen analysis of sediments from Como Lake in the Sangre de Cristo Mountains indicates that regional treeline rose to a level approximately 200 m higher than at present about 11,000 years ago in response to significant climatic warming (Jodry and others, 1989). Additional pollen records from Head Lake, on the valley floor, suggest that the regional water table remained high until at least 9,500 years ago, probably owing in part to increased summer precipitation during this period (Jodry and others, 1989). A warmer climate would have reduced winter snowpack and glacier extents, curtailing streamflow, whereas increased summer precipitation in the valley may have helped to keep the water table high in the valley-fill sediments.

Table F–2. Gamma spectrometry, cosmic and total dose rates, equivalent doses, and ages for samples from the Mr. Peat pit, Alamosa, Colorado. *A*, Data for blue-light optically stimulated luminescence (OSL) dating of fine sand grains (250–180 micron) using the single-aliquot additive dose (SAR) technique. *B*, Data for infrared-stimulated luminescence dating (IRSL) of polymineral, fine silt grains (4–11 microns) using the multiple-aliquot additive dose (MAAD) technique.

[Samples arranged in descending stratigraphic order (see fig. F–4)]

A

Sample number	Unit and trench	K (percent)	Th (ppm)	U (ppm)	Water content[a] (percent)	Cosmic dose rate[b] (Gy/ka)	Total dose rate[c] (Gy/ka)	De[d] (Gy)	N[e]	Age (ka)
MRP–DL–1	Coppice dune, trench D	0.50± 0.03	1.45± 0.10	0.61± 0.04	10±1.0	0.40±0.04	1.01±0.04	1.72± 0.07	26 (35)	1.6±0.1
MRP–CL–3	Upper bed, trench C	2.73± 0.07	7.36± 0.32	2.72± 0.11	9±1.0	0.32±0.04	3.52±0.08	22.7± 0.95	24 (30)	6.5±0.3
MRP–CL–2	Middle bed, trench C	2.73± 0.12	7.08± 0.23	2.54± 0.11	10±1.0	0.27±0.03	3.42±0.07	33.9± 1.47	18 (20)	9.9±0.5
MRP–CL–1	Lower bed, trench C	2.99± 0.09	5.22± 0.22	1.57± 0.10	4±0.5	0.23±0.03	3.45±0.08	69.8± 1.71	27 (35)	20.3± .7

B

Sample number	Unit and trench	K (percent)	Th (ppm)	U (ppm)	Water content[a] (percent)	Cosmic dose rate[b] (Gy/ka)	Total dose rate[c] (Gy/ka)	De[d] (Gy)	Age (ka)
MRP–CL–3	Upper bed, trench C	2.73± 0.07	7.36± 0.32	2.72± 0.11	9±1.0	0.32±0.04	4.75±0.10	65.6±2.09	13.6±0.9
									13.8±0.9
MRP–CL–2	Middle bed, trench C	2.73± 0.12	7.08± 0.23	2.54± 0.11	10±1.0	0.27±0.03	4.59±0.09	94.5±3.67	18.0±1.1
								82.5±2.78	20.6±1.5
MRP–CL–1	Lower bed, trench C	2.99± 0.09	5.22± 0.22	1.57± 0.10	4±0.5	0.23±0.03	4.36±0.10	130±4.50	29.9±1.6
								149±4.90	34.3±1.8

[a]From field moisture; ages based on 15–20 percent moisture content (except DL1, measured at field moisture of 10 percent), mid-way between field and saturation moisture values.

[b]Cosmic doses and attenuation with depth were calculated using the methods of Prescott and Hutton (1994).

[c]Total dose rate based on 15–20 percent water content (except –DL1, measured at 10 percent).

[d]Reported at 1-sigma error, fit to exponential and linear regression curves, and calculated as a weighted mean.

[e]Number (N) of replicated equivalent dose estimates (De) used to calculate the mean. Second number is total measurements made including failed runs with unusable data.

Radiocarbon dates from samples of the organic silt and the tufa indicate that accumulation of the two units was essentially coeval. Although the tufa deposits are stratigraphically above the organic silt layer in the trenches we excavated, the tufas are not laterally continuous; they occur as localized mounds at points of spring discharge. Westward (downstream) of the tufa mounds, the organic silt is stratigraphically the uppermost unit, except where it is locally covered by younger eolian deposits (fig. F–4). The youngest sample of tufa we collected was a surface grab sample from the vicinity of trench A, dated at approximately 3875 cal yr (table F–1), indicating that springs continued to flow until at least that time. Ground-water levels probably lowered gradually in response to arid climatic conditions, but they also may have been responding to a local lowering of base level as the nearby Rio Grande River entrenched into the valley floor sediments. Ground-water withdrawals for irrigation, which began in the middle 19th Century but became quite large by the 1950s, probably accelerated lowering of the regional water table to its current level and was thus the final factor responsible for dewatering of the wetland.

Seasonally high water tables appear to have persisted in the vicinity of the Mr. Peat wetland deposit well into the 20th Century. A series of aerial photographs from the late 1930s and 1941 show standing water on the meadow surface (fig. F–9), and a description from a soil survey in which observations were made during the 1960s notes that the peat is “normally moist in the upper 2 to 3 feet” and “the water table is in the sand substratum” (Pannell and others, 1973). At that time the surface vegetation was described as mostly sedges and rushes, and the land was used for grazing; prior to the 1960s, it was used to grow hay (Pannell and others, 1973). Orthophotographs from the soil survey, flown in 1969, show that the site was used as a meadow or pastureland at that time. Another aerial photograph from 1985 depicts the postmining surface of the Mr. Peat deposit. These photographs broadly bracket the period of peat mining as beginning no earlier than 1970 and essentially ending no later than 1985. A comparison of the aerial photographs in figure F–9, combined with on-the-ground observations, indicates that the western part of the deposit was most extensively mined. The topmost soil layer was either scraped off during mining or is, in fact, the “organic silt” layer, which compacted and cracked as it dewatered.

Acknowledgments

Thanks are due to Shannon Mahan, Bob Thompson, Dan Muhs, Laura Strickland, Richard Pelltier, Gary Skipp, and Josh Freeman, all from the USGS in Denver, who analyzed samples, made helpful comments and suggestions, and contributed data to this report. All but the hand-picked carbon samples were separated by Kathy Puseman of Paleo Research Institute, Inc., (Golden, Colo.). Mr. Adrian Absmeier (Alamosa, Colo.) very kindly allowed us access to the property. In addition, we appreciate the constructive and helpful comments of James Otton (USGS) and Robert Thompson (USGS), who reviewed a preliminary version of this manuscript. However, any errors that may remain are the responsibility of the authors.

References Cited

Haynes, C.V., Jr., 1968, Geochronology of late Quaternary alluvium, *in* Morrison, R.B., and Wright, H.E. (eds.), Means of correlation of late Quaternary successions: Salt Lake City, University of Utah Press, p. 345–353.

Holliday, V.T., 1985, Archeological geology of the Lubbock Lake site, southern High Plains of Texas: Geological Society of America Bulletin, v. 96, p. 1483–1492.

Jodry, M.A., Shafer, D.S., Stanford, D.J., and Davis, O.K., 1989, Late Quaternary environments and human adaptation in the San Luis valley, south-central Colorado, *in* Harmon, Eric J., ed., Water in the valley—A 1989 perspective on water supplies, issues, and solutions in the San Luis Valley, Colorado: Colorado Ground-Water Association 8th Annual Field Trip, Guidebook, p. 189–208.

Pannell, J.P., Yenter, J.M., Woodyard, S.O., and Mayhugh, R.E., 1973, Soil survey of Alamosa area, Colorado: U.S. Department of Agriculture Soil Conservation Service, 122 p.

Prescott, J.R., and Hutton, J.T., 1994, Cosmic-ray contributions to dose rates for luminescence and ESR dating—Large depths and long-term time variations: Radiation Measurements, v. 23, p. 497–500.

Puseman, K., 2006, Examination of samples for radiocarbon datable material from the Mr. Peat pit, south-central Colorado: Paleo Research Institute Technical Report 05–99/06–67, 10 p.

Quade, J., Forester, R.M., Pratt, W.L., and Carter, C., 1998, Black mats, spring-fed streams, and late-glacial-age recharge in the southern Great Basin: Quaternary Research, v. 49, p. 129–148.

Rocchio, J., 2004, Survey of critical wetlands and riparian areas in southern Alamosa and Costilla Counties, San Luis Valley, Colorado: Colorado State University, Colorado Natural Heritage Program Report, 206 p.

Safford, T., 1981, Alluvial geology and archeological potential of the Texas southern High Plains: American Antiquity, v. 46, p. 548–565.

Scott, L., 1992, Environmental implications and origin of microscopic *Pseudoschizaea* Thiergart and Frantz Ex R. Potonie emend. in sediments: Journal of Biogeography, v. 19, p. 349–354.

Stuiver, M., and Reimer, P.J., 1993, Extended ^{14}C database and revised CALIB 3.0 ^{14}C age calibration program: Radiocarbon, v. 35, no. 1, p. 215–230.

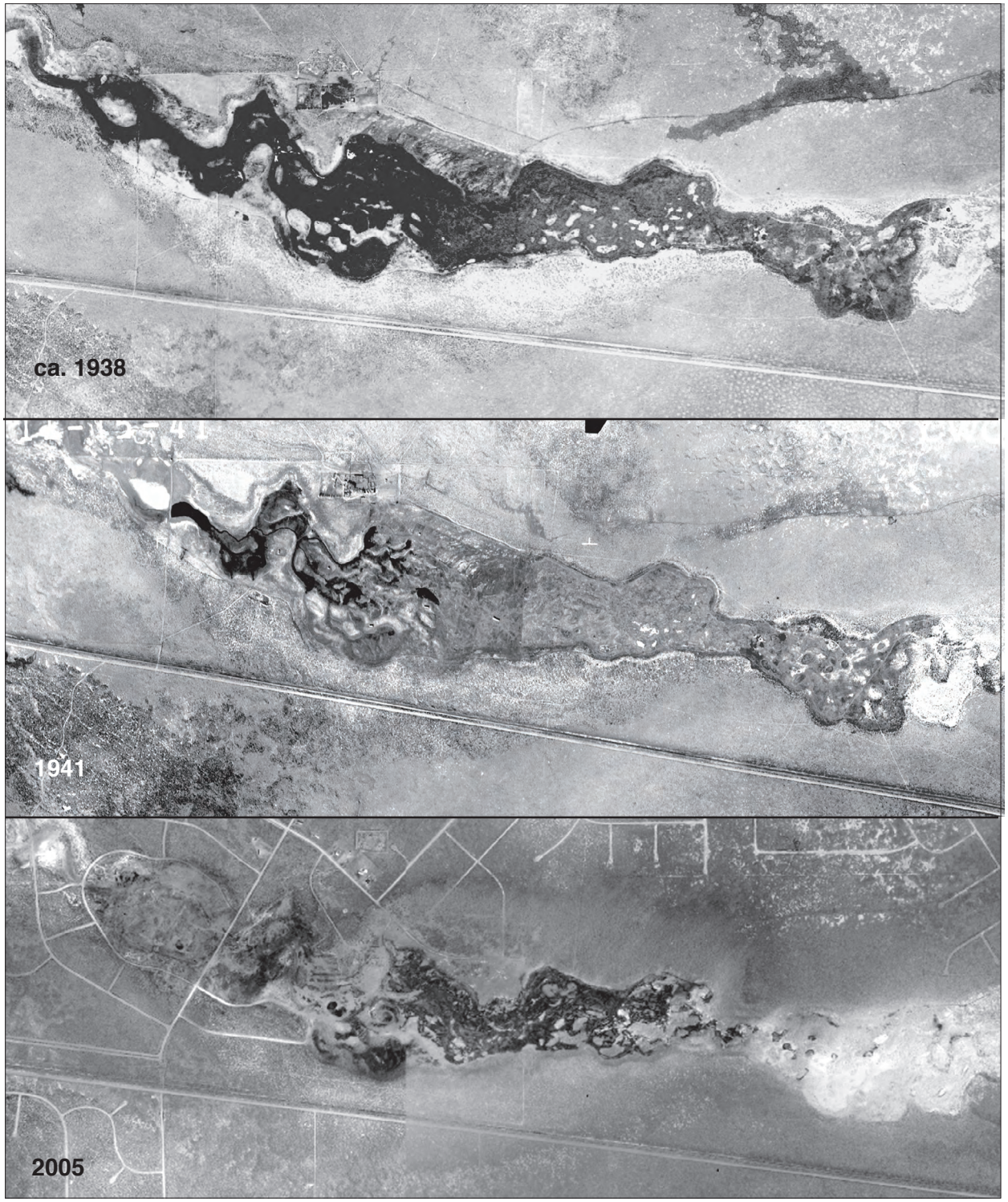

Figure F–9. Aerial photographs of the Mr. Peat deposit showing premining (ca. 1938, 1941) and postmining (2005) surfaces of the deposit. Darkest areas on the earlier two photographs appear to be standing water, whereas the dark areas on the lower photograph are the dry surface of the organic silt layer. USDA Soil Conservation Service photographs date from 1938, and 1941; 2005 photograph from USDA National Agriculture Imagery Program (NAIP). East-west width of each photograph is roughly 3 km.

Ancient Lake Alamosa and the Pliocene to Middle Pleistocene Evolution of the Rio Grande

By Michael N. Machette, David W. Marchetti,[1] and Ren A. Thompson

[1]Department of Natural and Environmental Science, Western State College of Colorado, Gunnison, Colo. 81231

CHAPTER G

Abstract

From Pliocene to middle Pleistocene time, a large, high-altitude lake occupied most of the San Luis Valley of southern Colorado. This ancient lake accumulated sediments that Siebenthal (1910) designated as the Alamosa Formation, for which it is herein named.

The existence of this lake was first postulated in 1822 and proven in 1910 from well logs. It was one of the largest high-altitude lakes in North America, comparable only to historic Lake Texcoco in the Valley of Mexico. Lake Alamosa persisted for about 3 m.y., expanding and contracting and filling the valley with sediment until about 440 ka, when it overtopped a low sill on Oligocene volcanic rocks of the San Luis Hills. The resulting overflow cut a deep gorge, coursed southward, and flowed into the Rio Grande, entering at what is now the mouth of the Red River.

The key to this new interpretation is the discovery of still-extant shoreline deposits, including spits, barrier bars, and lagoons nestled among bays and in backwater positions on the northern margin of the San Luis Hills, southeast of Alamosa, Colo.

Alluvial and lacustrine sediment nearly filled the basin prior to lake overflow, which happened sometime around 440 ka as estimated from a ^{3}He surface-exposure age of about 439±6 ka on a boulder of reworked basalt and from strong calcic soils on barrier bars and spits at 2,330–2,340 m (7,645 ft–7,676 ft). Overtopping of the lake's hydrologic sill may have been stimulated by high lake levels during marine oxygen-isotope stage 12, which was one of the most extensive middle Pleistocene glacial episodes. This integration expanded the Rio Grande's drainage basin by nearly 18,000 km^2 to include the high-altitude, glaciated San Juan, Sawatch, and Sangre de Cristo Mountains.

Study Area

The San Luis Valley of southern Colorado and northern New Mexico is a windswept, high-altitude sedimentary basin within the northern part of the Rio Grande rift. The basin extends from the Taos Plateau on the south to Poncha Pass on the north (fig. G–1). The foothills of the San Juan Mountains bound it on the west and the Sangre de Cristo Mountains on the east. This somewhat desolate valley is the home to the oldest surviving town in Colorado (San Luis, established in 1851) and the newest national park (Great Sand Dunes). The nearly level floor of the valley belies its origin—that of an ancient lake basin which has been alluded to but poorly documented for nearly two centuries. The main objective of this paper is to demonstrate the extent and age of ancient Lake Alamosa and to describe how its demise led to the final evolutionary development in the Rio Grande drainage system.

Paleolakes preserve important evidence of past climates, geomorphic relations, and sedimentary processes. As such, the ancient lake in the San Luis basin provides a record of a high-altitude lacustrine environment rarely seen in North America. Additionally, this lake plays an important part in regional drainage evolution, a fact that is often overlooked or underappreciated in the literature.

The San Luis Basin is one of many linked structural basins that form the Rio Grande rift, which extends from central Colorado to northern Mexico. The western margin of the basin is largely passive, whereas the eastern margin is marked by the Sangre de Cristo fault system—the longest Quaternary fault within the rift (see discussion in chapter J, this volume; and U.S. Quaternary fault and fold database at http://earthquake.usgs.gov/regional/qfaults/). The San Luis Hills, about 20 km southeast of Alamosa (fig. G–1), is a horst block of Oligocene volcanic and volcaniclastic rocks that have San Juan volcanic field affinities but that were locally erupted within the rift. The San Luis Basin is mainly an east-tilted half graben with internal structural complexities, although few of these are preserved at the surface. New aeromagnetic

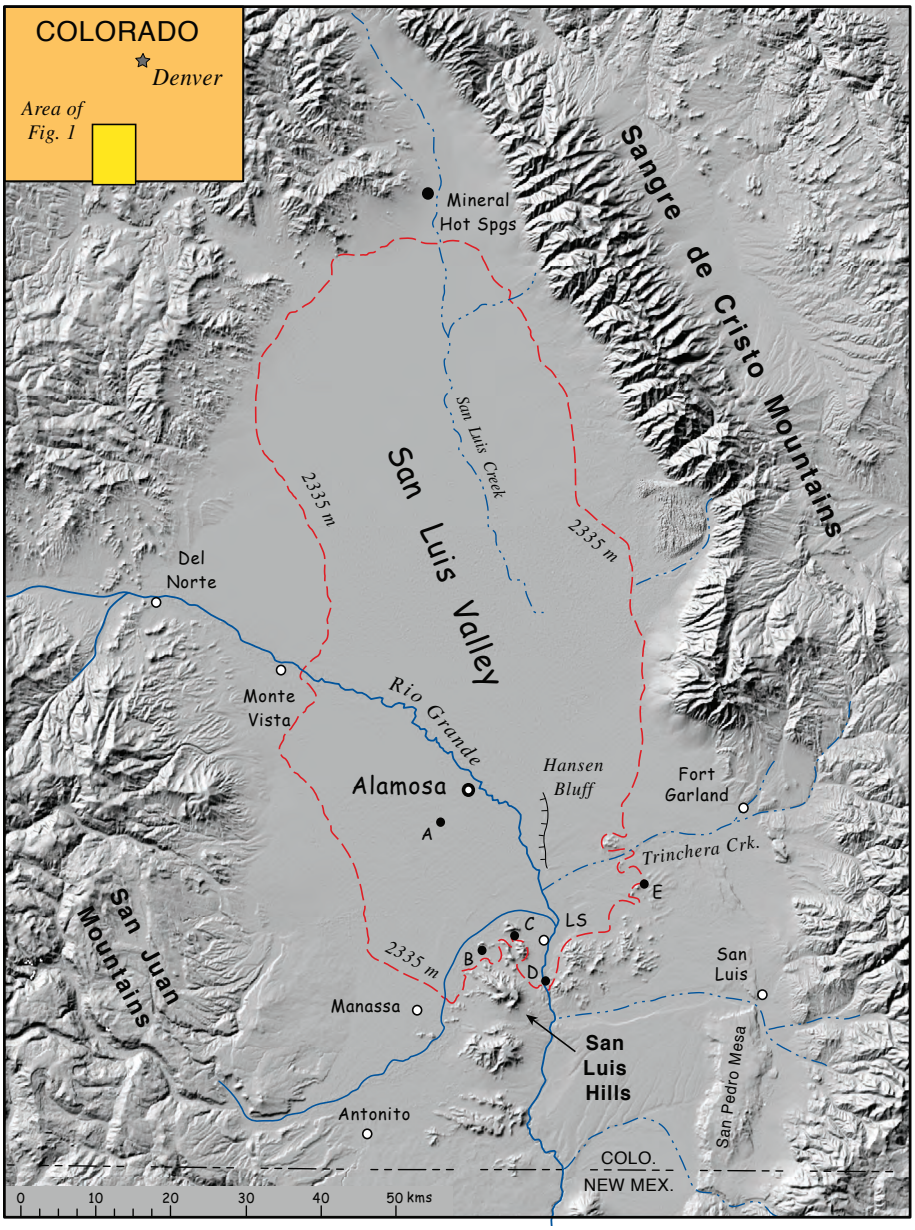

Figure G–1. Index map showing the San Luis Basin of southern Colorado and locations mentioned in the text. A-E are key localities for dating and reconstructing the lake's history.

data for the entire basin south of Alamosa (Bankey and others, 2005) show numerous intrarift faults that partition the basin into hydrologic compartments. Although the entire San Luis Basin now lies within the Rio Grande drainage basin, its geomorphology and surficial geology change markedly at the San Luis Hills (Thompson and Machette, 1989). To the north, the valley is nearly flat floored, rising gently from 2,285 m (7,500 ft) along the river to above 2,500 m (8,200 ft) at the mountain front. South of the San Luis Hills, the valley is largely covered by Pliocene basalts of the Servilleta Formation (hereafter referred to as the Servilleta Basalt; Lipman and Mehnert, 1979) and the Rio Grande flows in an ever-deepening gorge as it makes its way south into New Mexico and eventually to the Gulf of Mexico.

Previous Work

Lake Alamosa's discovery harkens back nearly two centuries. In 1821–22, three decades prior to settlement of the San Luis Valley, Jacob Fowler made his way up the Rio Grande on a hunting and trapping expedition. Fowler was a keen observer of topography, geography, and geology. His journals include this prescient passage that is particularly relevant to the lake:

> *"I Have no doubt but the River from the Head of those Rocks up for about one Hundred miles Has once been a lake of about from forty to fifty miles Wide and about two Hundred feet deep—and that the running and dashing of the Watter Has Woren a Way the Rocks So as to form the present Chanel."* (Cited in Siebenthal, 1910, p. 112–114.)

Jacob Fowler made this keen observation from the San Luis Hills (probably in the Fairy Hills, above the river's gorge), looking northward into the San Luis Valley. As we will show, Jacob Fowler accurately forecast the size, depth, and overflow of the lake—185 years ago.

In 1910, Claude Siebenthal proposed the existence of an unnamed Pliocene-Pleistocene lake in the San Luis Valley of southern Colorado. Siebenthal (1910) was studying the hydrology of this water-rich agricultural area and had examined hundreds of water-well drilling logs as part of his assessment. Of key interest to him was the presence of tight clays ("blue clays" in the logs) that form aquitards in the lower confined layer, whereas the upper unconfined layer was composed of more permeable alluvium (sand and gravel). At this time (early 20th Century) wells that penetrated blue clay in the lower confined layer were typically artesian. Siebenthal (1910) inferred that the blue clays were lacustrine, showed their extent in this ancient lake, and named its sedimentary deposits the "Alamosa Formation."

Siebenthal (1910) found the field evidence for his lake at Hansen Bluff, a 20-m-high exposure about 10 km southeast of Alamosa. In the 1980s, paleontologist Karel Rogers and colleagues conducted multidisciplinary studies of the Alamosa Formation at Hansen Bluff (Rogers and others, 1985, 1992) and documented that the exposed section of fluvial and lacustrine sediment was mainly early Pleistocene (Irvingtonion) in age (see stop B7, chapter B, this volume). These sediments contain abundant vertebrate fossils, two Pleistocene volcanic ashes, and a paleomagnetic record that spans the Brunhes-Matuyama polarity boundary at 780 ka. However, in the nearly 100 years since Siebenthal's work, no one had found surficial expression of this lake or documented its maximum altitude or lateral extent, mainly because the Quaternary deposits of the basin had not been mapped in detail.

New Evidence of the Lake

Machette's previous mapping in the Lake Bonneville Basin of Utah led him to suspect that shorelines and coarse-grained, near-shore deposits of this ancient lake might be preserved on bedrock. A likely area to look for such deposits was along the north side of the San Luis Hills, which had been mapped by Thompson and Machette (1989). During new mapping of the Alamosa ½° x 1° sheet (Machette and Thompson, 2005), we found several exposures of near-shore lacustrine and shoreline deposits. The first evidence came from the Bachus pit (fig. G–1, location A; stop B1, chapter B, this volume), which is located about 6 km southwest of Alamosa at an altitude of about 2,300 m (7,550 ft). This active sand pit exposes about 4 m of finely laminated silts and sands and sandy pebble gravels that we interpret as shallow, near-shore lacustrine deposits. Then we examined adjacent bedrock areas above 2,300 m and found unequivocal shoreline spits (stop B3, chapter B, this volume) perched on the back (south) side of Saddleback Mountain (fig. G–2), about 15 km to the southeast of the Bachus pit and at the southern end of Lake Alamosa, as we'll see later.

Key Locations

The shoreline features coincide with wave-eroded bedrock knobs and hills at altitudes around 2,330–2,335 m (7,645–7,660 ft) and suggest that the ancient lake reached the minimum overflow elevation of 2,335 m (7,660 ft) in the San Luis Hills. Other well-preserved bars, spits, and lagoons between bedrock-core hills were found at similar elevations, both west and east of the Rio Grande. Distinct spits at 2,330–2,335 m (7,645–7,660 ft, fig. G–2) wrap around the leeward, southern, side of Saddleback Mountain (fig. G–1, location B) and Sierro del Ojita (fig. G–1,

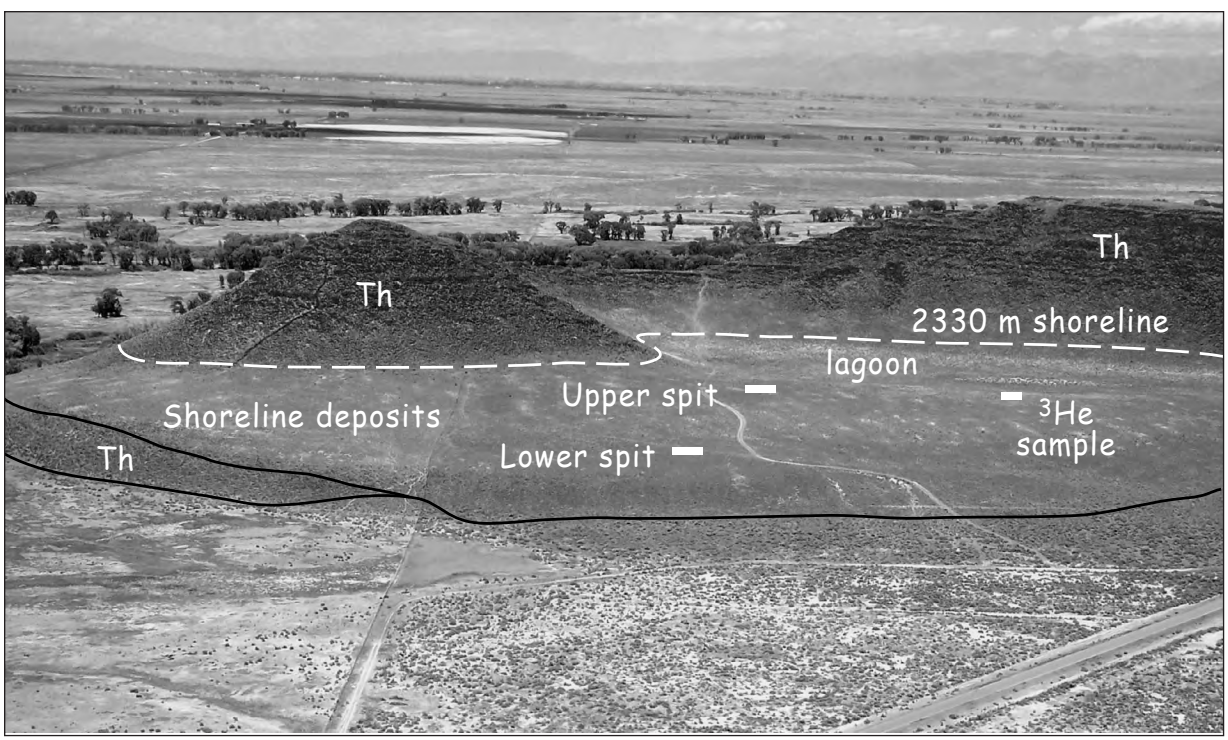

Figure G–2. Oblique aerial photograph of shoreline spits on Saddleback Mountain (location B, fig. G–1). The 2,300-m shoreline is cut across 26-Ma basalts of the Hinsdale Formation (Th); spits and a lagoon formed on the leeward (south) side of the mountain ridge. White boxes are locations of soil pits and basalt boulder sampled for ^{3}H surface-exposure dating.

location C), and a well-preserved, kilometer-long spit (stop B4, chapter B, this volume) lies on the eastern side of the Rio Grande (fig. G–1, location D), just above the basin's outlet near the small town of Lasauses, Colo. (see Machette and Thompson, 2005).

Barrier bay-mouth bars and back-bar lagoons of the ancient lake are still preserved in the southeastern part of the lake basin, both north and south of Trinchera Creek. These features span a narrow but slightly higher elevation range, primarily from 2,330 to 2,340 m (7,645–7,675 ft) (fig. G–3). At most locales, there is a single bar-lagoon complex, but pairs of these features are preserved at the Appleblossum Lane location (fig. G–1, location E; stop B5, chapter B, this volume).

The dozen large constructional lake features that we've found are not well exposed, so we excavated four pits to assess soil development as a relative-age tool. These pits exposed strongly developed, 0.75- to 1-m-thick calcic soils (stops B3.1 and B3.2, chapter B, this volume) that have stage III morphologies (see Birkeland, 1999). The amount of calcium carbonate in these soils is impressive in that they persist at high elevations, close to the pedocal-pedalfer soil boundary in the semiarid San Luis Valley (see discussion of soils at stop B3.2, chapter B, this volume). These soils probably persist owing to persistent relatively dry (semiarid) climate in the basin during the Quaternary. Conversely, soils above 2,500 m (8,200 ft) in the adjacent foothills rarely show significant accumulations of calcium carbonate owing to enhanced mobility of soil carbonate in colder temperatures and to leaching owing to increased precipitation, soil moisture, and lower vegetation zones (soil acidity) during glacial times.

Extent of Lake

Around 450,000 years ago, Lake Alamosa was forming shoreline features at its maximum elevation of about 2,335±5 m (7,660±15 ft). At this elevation, Lake Alamosa would have occupied most of the San Luis Valley north of the San Luis Hills (fig. G–1). This valley is a prime agricultural area for production of potatoes, barley, and hay. Thousands of wells have been drilled in the basin, and the majority of these are (or were) flowing as shown by Siebenthal (1910) and on USGS topographic maps. A quick tabulation of flowing versus standard wells shows that 95 percent of the artesian wells lie at or below the maximum paleoshoreline elevation. This is no coincidence because the aquitard (or aquitards) for pressuring the wells are lake bottom clays in the Alamosa Formation. Also, there are a variety of unusual geomorphic and hydrologic features at or slightly above the maximum paleoshoreline elevation, such as the abundant ponds and springs at Monte Vista Wildlife Refuge.

At its full extent, Lake Alamosa extended almost 105 km north-south and 48 km east-west (2335 m contour, fig. G–1). As such, it was one the largest high-altitude lakes in North America, comparable to historic Lake Texcoco in the Valley of Mexico. However large and long lived, since its overflow and draining at 440 ka, most of the geomorphic evidence of Lake Alamosa (such as shorelines on alluvial fans) has been eroded or buried by younger alluvium or eolian deposits.

The age and extent of ancient Lake Alamosa have practical importance because during high stands of the lake (glacial

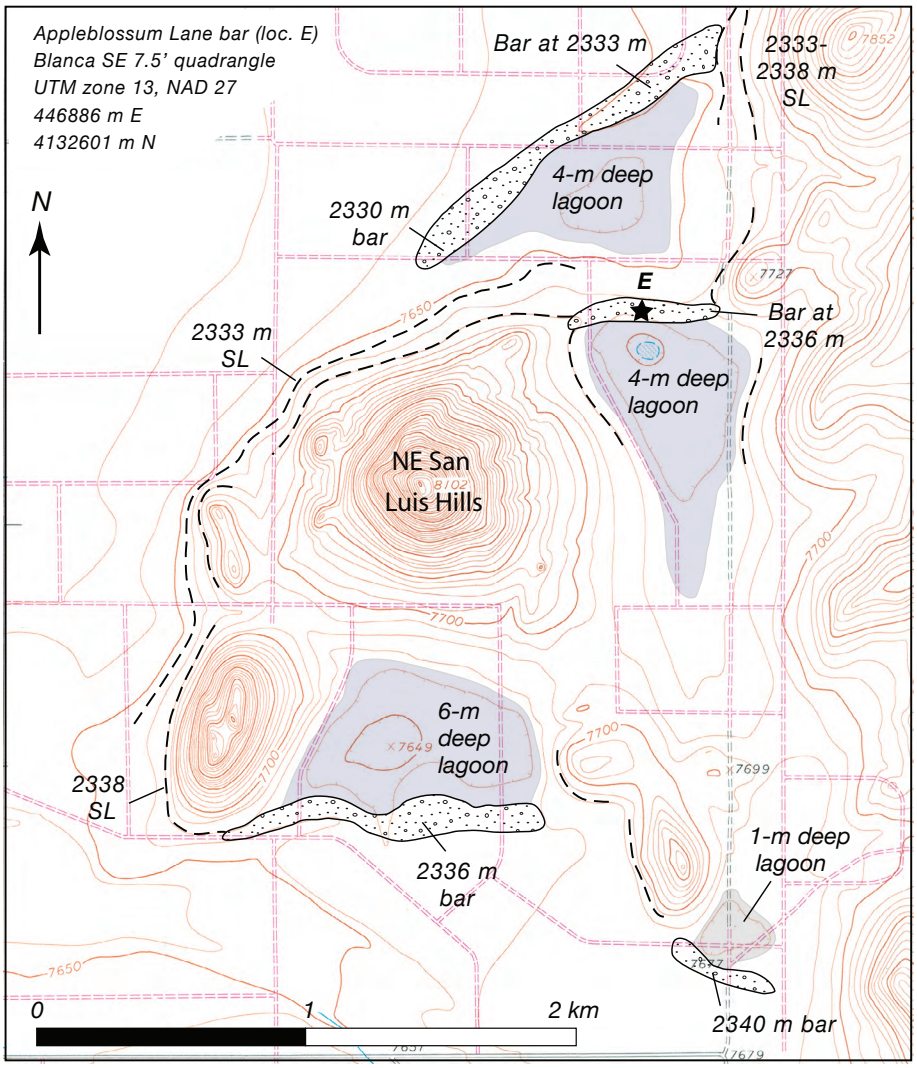

Figure G–3. Barrier bars and lagoons preserved along northeast margin of the San Luis Hills. Appleblossum Lane bar is labeled E, as on figure G–1.

times) silt and clay were deposited in the deeper parts of the basin. These fine-grained lacustrine sediments (the blue clay of drillers' logs) form the aquitards within the confined aquifer (the Alamosa Formation) in the basin and are the source of most agricultural waters.

As part of his work on the lake, Siebenthal (1910) plotted the locations of water wells in the Alamosa portion (subbasin) of the San Luis Basin. He noticed that most of the flowing (artesian) wells were concentrated in the central, lower parts of the basin (see area of flowing wells, plate 1, Siebenthal, 1910), whereas nonflowing wells were located at higher elevations (mountainward). After identifying the highest shoreline of Lake Alamosa at 7,760 ft (about 2,335 m), we plotted this contour against the locations of wells (artesian and nonartesian) and springs in the basin (fig. G–4). Roughly 95 percent of all artesian wells (as shown on USGS 1:100,000-scale topographic maps) in the basin lie within the 7660 ft contour. However, this contour is more restricted than that of the high shoreline owing to postlake deposition. For example, sedimentation by the Rio Grande has built a gigantic alluvial fan that spreads almost entirely across the Alamosa subbasin. Thus, the paleodatum of 7,660 ft (at which the shorelines formed) must lie buried beneath postlake alluvium and mountainward of the lake's extent as shown on figure G–4. Using this argument, we plotted the probable location of the buried shoreline level as a dashed line on figure G–4. As can be seen from the figure, virtually all of the artesian wells lie within this dashed line. Thus, the extent of artesian wells is virtually coincident with Lake Alamosa's highest shoreline. And it follows that the lake's shoreline restricted the deposition of tight, fine-grained deposits (blue clays) and, thus, aquitards in the Alamosa Formation. Recognizing the lake's maximum extent and its likely control by climatic conditions in the closed-basin's drainage area allows one to construct an improved geoclimatic sedimentation model for the Alamosa Formation. Currently, most groundwater assessments for the basin use a simple, multilayer model with little or no interfingering of lacustrine and alluvial materials and virtually no structural control on potential subsurface water flow paths.

Dating Lake Alamosa's Shoreline Deposits

Lake Alamosa persisted from the middle Pliocene to middle Pleistocene. Using sedimentation rates at Hansen Bluff, Rodgers and others (1985) suggested that this part of the section might be as young as 700,000 yr (see discussion for stop B7, chapter B, this volume). However, they did not recognize a significant lacuna at the top of the section where coarse-grained sandy fluvial gravels with stage III calcic soils are unconformable on sediment of the Alamosa Formation. From our study of the bluffs (see stop B7), it appears that the uppermost part of the Alamosa Formation (about <670 ka) has been locally removed by erosion and subsequent deposition of old alluvium (unit Qao, Machette and Thompson, 2005, 2007) that predates the overflow of the lake.

In order to date the upper spit at Saddleback Mountain (fig. G–2), which is stop B3 on the Friends of Pleistocene trip (see chapter B, this volume), we sampled the largest intact (but

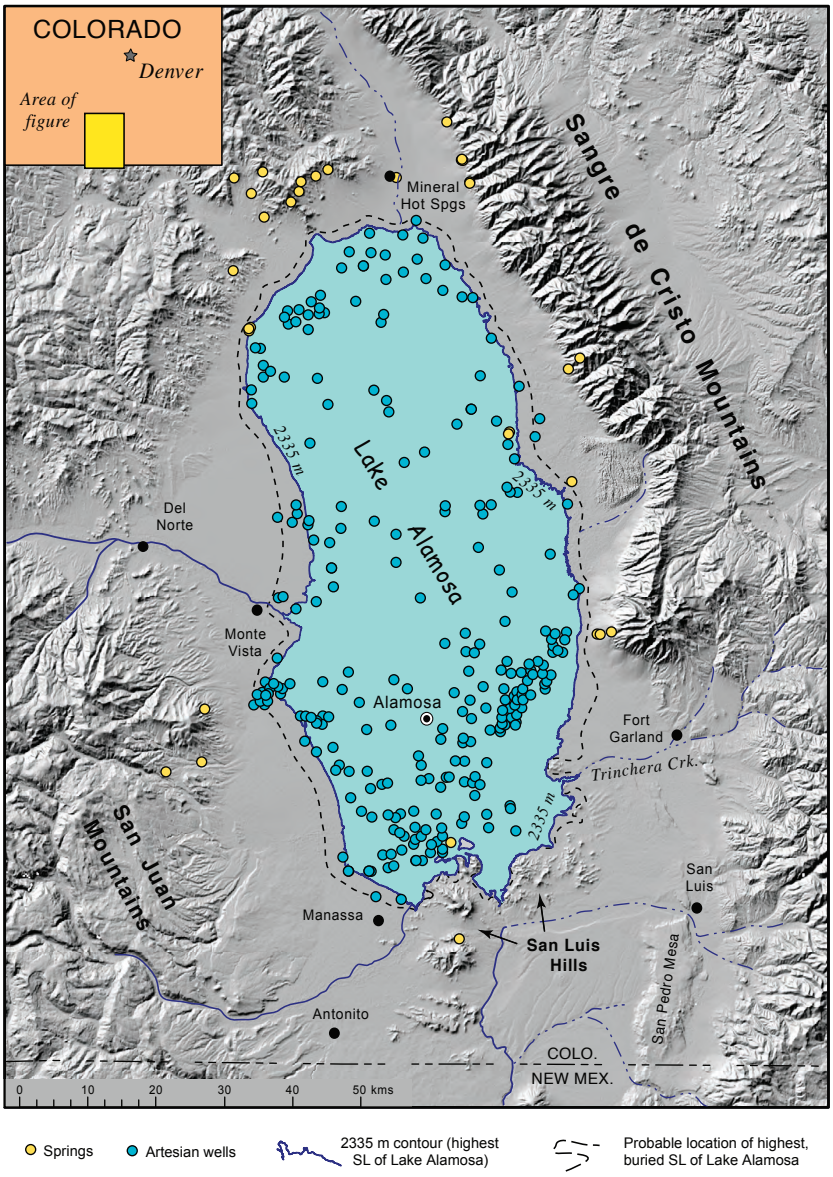

Figure G–4. San Luis Basin showing projected extent of Lake Alamosa, its buried shoreline (SL), and artesian wells and springs.

transported) boulder that showed minimal effects from erosion, such as spalling or eolian erosion (ventifacts are common at this site). The basalts of Saddleback Mountain are perfect for surface-exposure dating with ^{3}He isotopes because they contain phenocrysts of olivine and pyroxenes, two minerals that retain cosmogenic He isotopes. At this locality, the spits are composed almost entirely of reworked basalt boulders and lacustrine sand that has been transported southward around the leeward side of the bedrock hills. The larger basalt boulders are 1 m in diameter, of which 30–40 cm is exposed above ground surface.

The ^{3}He and ^{4}He concentrations were measured at the University of Utah Noble Gas Laboratory on a MAP-251 noble gas mass spectrometer. Gas was released using a modified Turner furnace heated to >1,400°C. SAES getters removed reactive gases; Ar and Ne were cryogenically separated from He. Air contamination was avoided by measuring He concentrations under ultrahigh vacuum (<10^{-8} torr) and using Ne concentrations as a check for possible leakage. The ^{3}He and ^{4}He amounts were standardized against Yellowstone Park gas (MM) at 16.5 R_A, where R_A is the ^{3}He/^{4}He ratio in air (1.39 x 10^{-6}). Furnace blanks were typically 0 to 3 x 10^5 atoms for ^{3}He and near background values (1 x 10^8 to 1 x 10^9 atoms) for ^{4}He. The detection limit for ^{3}He in this system is about 50,000 atoms (table G–1).

Pyroxene separated from the surface layer of a large basalt boulder yielded a preliminary ^{3}He exposure age of 439±6 ka (table G–2). This age was determined using the total ^{3}He concentration and an absolute ^{3}He production rate of 116 atoms gram^{-1} year^{-1} (Licciardi and others, 1999) that was scaled to the samples altitude and latitude using Lal (1991) (table G–1). Pyroxenes from rocks with older (>1–2 Ma) crystallization ages can have significant noncosmogenic ^{3}He from nucleogenic reactions on ^{6}Li (^{6}Li (n, α) ^{3}H→^{3}He). Marchetti and Cerling (2005) and Marchetti and others (2005) used samples shielded from cosmic radiation to account for noncosmogenic ^{3}He in pyroxenes from intermediate volcanic rocks exposed on the western edge of the Colorado Plateau. These volcanic rocks are remarkably similar in crystallization age (~25 Ma) and petrology to the sample we dated in this study. Applying the ^{3}He/^{4}He shielded correction of Marchetti and others (2005) to the He data of the sample changes the exposure age slightly from 439 to 431±6 ka (table G–2). Using the ^{3}He surface-exposure age of 439 ka, we conclude that the spit was deposited at about 440 ka, towards the end of a major glacial episode (marine oxygen-isotope stage 12) that ended between 452 ka and 427 ka (see fig. G–5).

We recognize that our dating of the lake spits is based on only a single cosmogenic surface exposure age and assessments of relative soil development (see stop B3.2), so we are pursuing three additional dating techniques to help constrain the timing of lake's overflow:

1. Terrestrial cosmogenic nuclide (TCN) profile dating using ^{3}He isotopes. This technique uses small gravel clasts collected through a vertical profile at least 2–3 m deep, and it

Table G–1. Sampling data for ^{3}He surface-exposure dating of basalt.

Sample number	Latitude (°N)	Longitude (°W)	Altitude (m)	Topo shielding factor	Self shielding factor	Total shielding factor	^{3}He production rate (atoms g^{-1} yr^{-1})*
PS–MM05–72c	37.262416	105.842416	2,324	0.999	0.942	0.941	598

*Determined using an absolute ^{3}He production rate of 116 atoms g^{-1}yr^{-1} (Licciardi and others, 1999) that was scaled using Lal (1991).

No corrections for potential snow shielding applied to production rate. Topo, topographic.

Table G–2. He isotope data for cosmogenic surface-exposure dating of basalt.

Sample number	$^4He_{total}$ (10^{12} atoms g^{-1})	$^3He_{total}$ (10^6 atoms g^{-1})	^{3}He/^{4}He fusion	^3He_c (10^6 atoms g^{-1})	^3He_c (percent)	Exposure age (ka)±2σ
PS–MM05–72c	22.92±0.06	262.5±3.5	1.15 x 10^{-5}	262.5±3.5	100	439±6
PS–MM05–72c*	22.92±0.06	262.5±3.5	1.15 x 10^{-5}	257.7±3.5	98.2	431±6

*Sample corrected using an estimated ^{3}He/^{4}He correction. The ^3He_c (cosmogenic) component was determined using the following relationship: $^3He_c = {}^3He_{total} - ({}^4He_{total}$ x ^{3}He/^{4}He shielded), where ^{3}He/^{4}He shielded ratio is 2.08x10^{-6} (Marchetti and others, 2005).

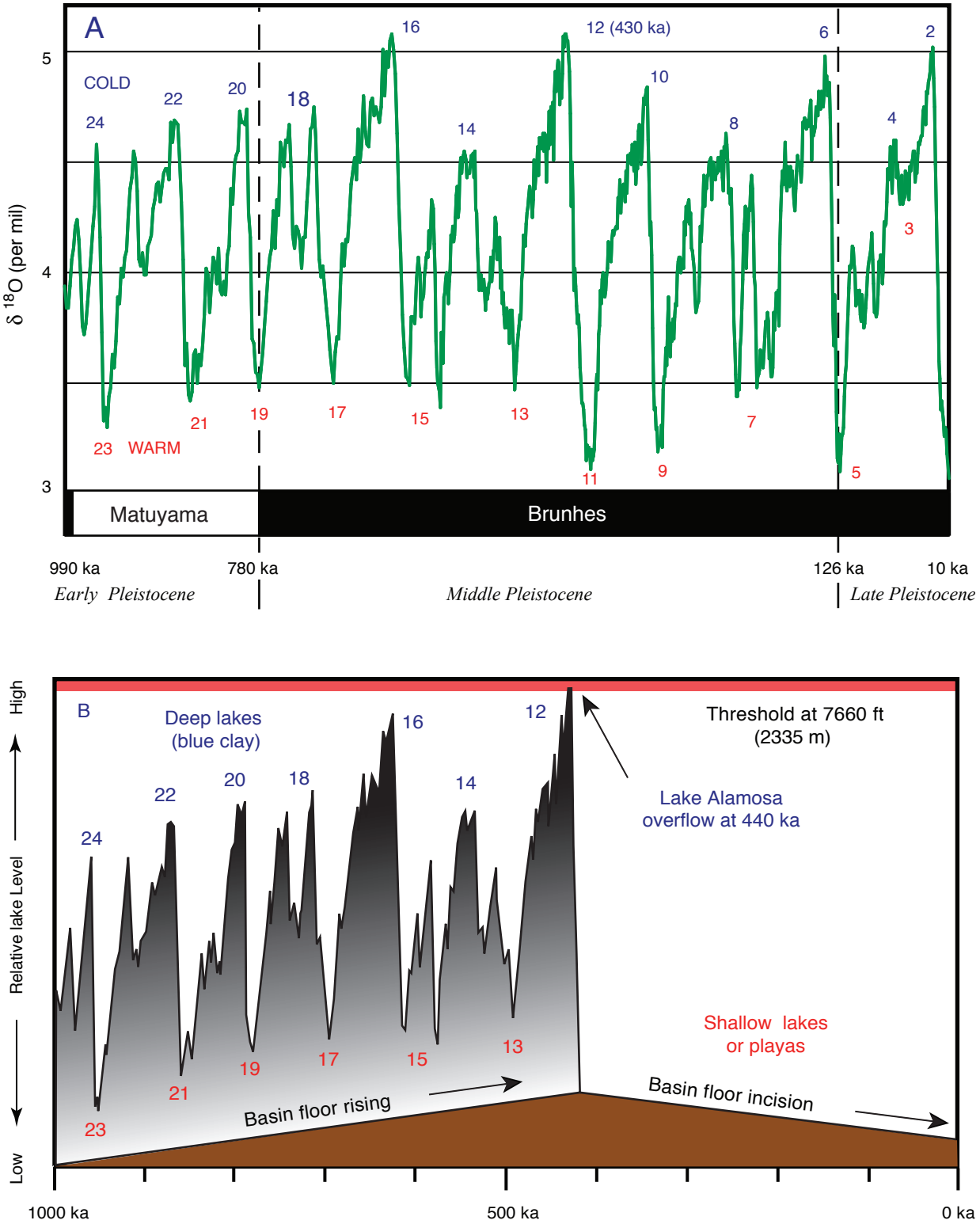

Figure G–5. Marine oxygen-isotope curve and its relation to Lake Alamosa. *A*, OIS curve from Lisiecki and Raymo (2005) showing changes in oxygen-18 isotope concentrations in benthic fauna and related glacial and interglacial stages. *B*, OIS curve from part *A* superposed on an aggrading basin floor. The basin floor was incised after overflow of Lake Alamosa.

can date deposits as old as 1 Ma if they contain olivine or pyroxene.

2. Terrestrial cosmogenic nuclide profile dating using ^{36}Cl isotopes. These analyses are being performed by the PRIME Lab at Purdue University (Lafayette, Indiana), and the modeling work is being done in cooperation with Fred Phillips of New Mexico Institute of Mining and Technology (Socorro). This technique uses small gravel clasts collected through a vertical profile at least 2–3 m deep, and it can date deposits as old as 300 k.y.

3. Experimental U/Th dating using laser-ablation mass-spectrometer techniques. These analyses are being done as part of a cooperative project with Warren Sharp at the University of California Berkeley Geoscience Center. This technique uses calcium-carbonate rinds on the base of large clasts. The best rinds are typically in the Bk horizon of a thick calcic soil. The technique can date deposits as old as 750 ka if they have small amounts of detrital thorium and if the carbonate is a closed system (no leaching and reprecipitation).

Climate Changes and Lake Alamosa

Lake Alamosa formed in the high (>2,300 m) altitude San Luis basin, surrounded by mountainous terrain that commonly exceeds 4,000 m (about 13,000 ft) in elevation. Presently, the central low-lying parts of the basin have a cool, semiarid climate. Modern climatic conditions in Alamosa are cool (41°F or 5°C, mean annual temperature (MAT)) and relatively dry (about 7 in. or 180 mm, mean annual precipitation) on average for the year (see http://www.wrcc.dri.edu). However, during full glacial conditions (that is, at 15 ka), the climate was probably much colder than now (that is, <0°C MAT), and it may have been drier according to some studies (see for example, Leonard, 1989; Fall, 1997). Nevertheless, meltwater from the abundant glaciated basins in the San Juan, Sawatch, and Sangre de Cristo Mountains must have supplied adequate water to fill the lake.

Assuming that the lake's level rose and fell synchronously with changing climates, we can use the marine oxygen-isotope record as a proxy for lake level. Lisiecki and Raymo's (2005) summary of marine benthic oxygen-18 records shows regular cyclic oscillations in sea temperature that is directly linked to glacial and interglacial stages. On figure G–5A, we have reproduced their oxygen-isotope stage (OIS) record for the period between 990 ka and 10 ka, which includes the late-early Pleistocene, middle Pleistocene, and late Pleistocene. From the work on Hansen Bluff by Rogers and others (1992) (fig. G–1), we know that the upper part of the Alamosa Formation includes sediment deposited between about 900 ka and 670 ka (see discussion of stop B8, chapter B, this volume), so this section relates directly to climatic conditions and depositional environments during OIS 22-18.

Because Lake Alamosa formed within a closed basin, sedimentation caused the basin floor to aggrade with time. Downdropping along the Sangre de Cristo fault zone may have created additional space for sediments, but this space was restricted to the eastern margin of the San Luis Basin. Thus in the Pleistocene, Lake Alamosa rose from increasing base levels with the passage of time. Maximum shoreline elevations of Lake Alamosa would have increased through time, until the lake could reach the lowest hydrologic threshold in the basin, which is in the San Luis Hills (fig. G–4).

To illustrate the point of increasing base level and overflow, we simply modified Lisiecki and Raymo's (2005) oxygen-18 record (fig. G–5*A*) so that the maximum shoreline levels (at late-glacial maxima) climb though time. Under this scenario, the lake reached the hydrologic sill at the close of OIS 12, which terminated at about 430 ka. Although figure G–5*B* is model driven, we believe that it is no coincidence that our dating of the highest spit of Lake Alamosa (440 ka) is virtually identical to the close of OIS 12, which was one of the most extensive glacial stages in the northern hemisphere in the Quaternary (see fig. G–5*A*). Presumably, meltwater inputs to the lake during the decline of OIS 12 led to high water levels and overflow.

Implications of Overflow

Understanding the temporal and spatial history of Lake Alamosa has important implications for the San Luis Valley and the Rio Grande, which has the largest drainage system in the southern Rocky Mountains. It provides a geologic framework for interpreting the Alamosa Formation, one in which the lake history is characterized by expansions and contractions in response to changing climates during the Quaternary (the past 1.6–1.8 m.y.). Dating the overflow of the lake limits the time of integration of the Rio Grande to the middle Pleistocene (>440 ka). Overflow of the lake and incision of its sill in the Fairy Hills increased the drainage area of the Rio Grande by about 22,000 km^2 (Wells and others, 1987). Prior to 440 ka, the Rio Grande had its most northerly headwaters in the Red River drainage of the Sangre de Cristo Mountains, north of Taos, N. Mex. (fig. G–6).

To illustrate these points, we have reconstructed the Pliocene to middle Pleistocene history of the upper Rio Grande drainage basin as shown in figure G–6. These scenarios are based on our mapping of the Taos Plateau and San Luis Basin and on earlier reconstructions of the Rio Grande's evolution by Wells and others (1987). Between 5 and 4 Ma, massive flood basalts (Servilleta) erupted on the Taos Plateau, completely burying former drainage channels (including any ancestral Rio Grande). By 3.5 Ma, these basalts flowed northward into Colorado, around the western and eastern margins of the San Luis Hills that partially subdivided the San Luis Basin from the Taos Plateau. These flows extended north of Antonito and Fort Garland, possibly closing off any southward drainage

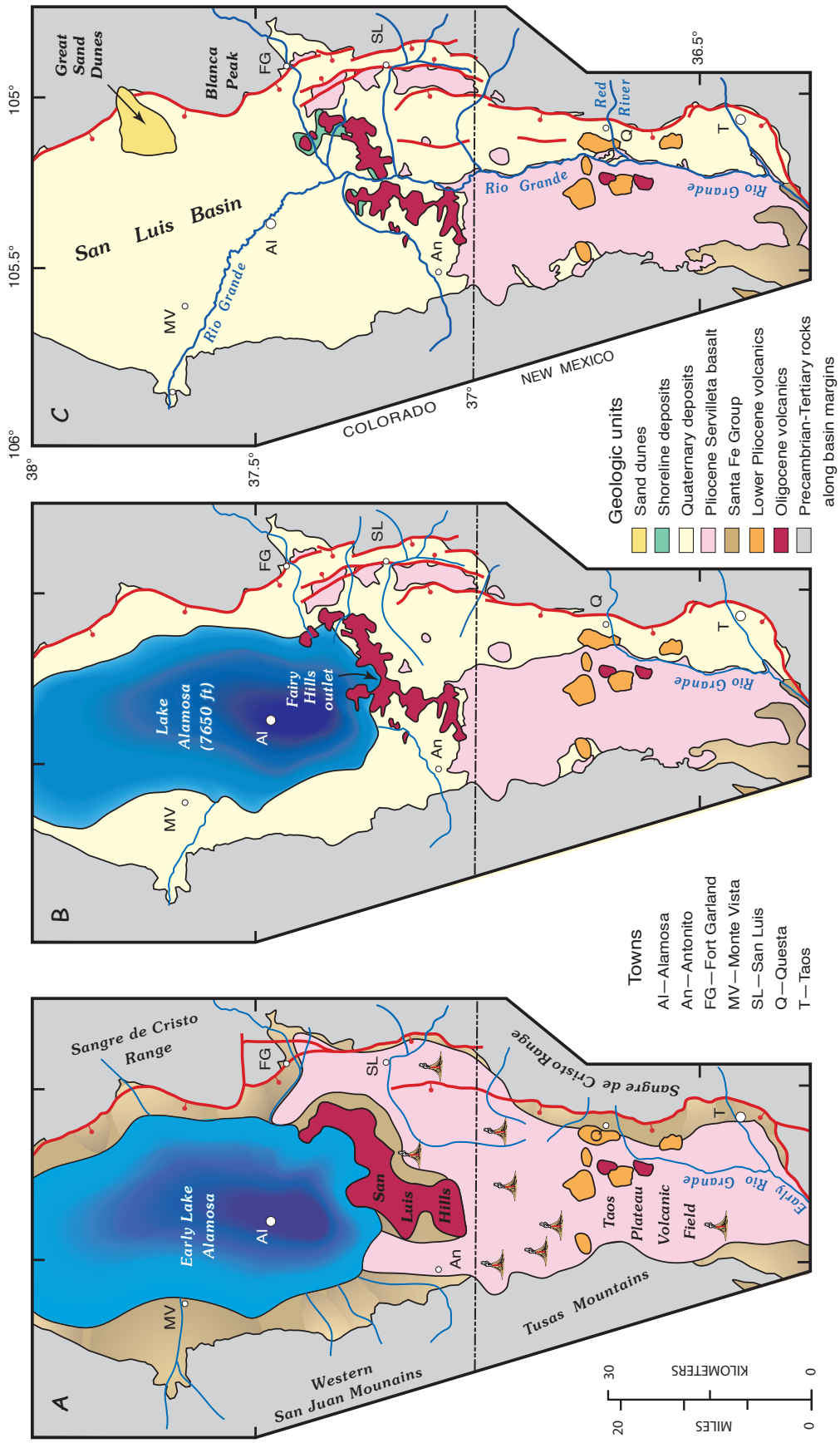

Figure G–6. Simplified geologic map of the San Luis Basin showing generalized geology and drainage patterns for the time intervals of *A*, 3.5–3 Ma; *B*, 440 ka; and *C*, the present.

from the basin (fig. G–6*A*). By 3.5–3 Ma, the basin was filling with sediment of the Alamosa Formation, and Lake Alamosa became a persistent yet variable part of the sedimentologic environment, expanding and contracting in response to the alternating glacial and interglacial climates in the Pleistocene. As a result, the Alamosa Formation has thick impermeable clays in the deep parts of the basin near Alamosa and along the eastern margin of the valley, whereas thinner clay beds interspersed with silt, sand, and gravel were deposited in shallower environments (fig. G–6*B*), such as at Hansen Bluff along the eastern margin of ancient Lake Alamosa.

Around 440 ka (middle Pleistocene), Lake Alamosa reached its highest elevation and had built a series of shorelines, spits, barrier bars, and lagoons (fig. G–6*B*) coincident with the 2,335-m topographic sill in the Fairy Hills (fig. G–1, location D; stop B4, chapter B, this volume). Overflow of the sill led to deep incision through fault-softened and dike-intruded Tertiary volcanic rocks in the Fairy Hills (see mapping of Thompson and Machette, 1989). Lake Alamosa waters flowed southward across the Servilleta Basalt and entered the Rio Grande west of Questa (fig. G–6*B*), which had already incised a modest canyon along the present course of the Red River (former headwater of the Rio Grande). Since integration of the Rio Grande (fig. G–6*C*), the river's 135-m-high knick point has retreated about 8 km north of the Red River to a point east of Brushy Mountain. The Rio Grande gorge is about 165 m deep at the Gorge Bridge (west of Taos, N. Mex.), where it exposes 4.8 to 3.0 Ma basalts interbedded with sediment (Appelt, 1998, table 1). Above the nick point, the Rio Grande has downcut <35 m into the Servilleta Basalt since 440 ka. Wells and others' (1987) careful analysis of the Rio Grande's Quaternary history in New Mexico suggested that integration of the Rio Grande was the result of headward stream erosion and drainage capture by causes that were "unclear and enigmatic" (Wells and others, 1987, p. 63). They considered two possible causes:

1. Overflow of a lake (Sunshine Lake of Winograd, 1959) or restricted drainage areas just north of a paleodrainage divide between Cerro Chieflo and Guadalupe Mountain (Wells and others, 1987, fig. 4a)

2. Regional uplift, which led to increased stream incision and enhanced stream sapping.

However, as a result of our mapping and surface-exposure dating of Lake Alamosa deposits in Colorado, we now believe that integration was a direct result of overflow of Lake Alamosa at 440 ka and not headward capture. Lake water that exited the basin through the Fairy Hills must have flowed along the lowest course out of the San Luis Hills, along the western, distal end of the Costilla Plain and southward along the juncture between west-dipping sediments of the Sunshine Valley and east-dipping flows of Servilleta Basalt (Pliocene, ca. 3.7–4.8 Ma) (see discussion of Rio Grande in chapter C, this volume).

Since 440 ka, Rio Grande has built a large alluvial fan at Monte Vista that effectively further subdivides the San Luis Valley (Alamosa Basin) into northern and southern subbasins. Streams graded to the Rio Grande on the southeast side of the San Luis Basin have cut a series of terraces in response to further river downcutting through the San Luis Hills. The modern Rio Grande is mainly eroding Quaternary deposits west of the river and south of Alamosa, but little of the underlying basin fill of the Alamosa Formation has been removed.

This new history of Lake Alamosa and the Rio Grande has important hydrologic and geologic implications for the San Luis Basin. On a broader basis, it shows that large paleolakes can have a profound influence on the evolution of large river drainage basins and it illustrates the importance and rapidity of overflow events in the Quaternary record.

Acknowledgments

We appreciate the constructive and helpful comments of Steven Colman (University of Minnesota—Duluth), Daniel Muhs (USGS), John Hawley (Hawley Geomatters) and Richard Reynolds (USGS), who reviewed preliminary versions of this manuscript. However, any errors that may remain are the responsibility of the authors.

References Cited

Appelt, R.M., 1998, $^{40}Ar/^{39}Ar$ geochronology and volcanic evolution of the Taos Plateau volcanic field, northern New Mexico and southern Colorado: Socorro, New Mexico Institute of Mining and Technology, M.S. thesis, 140 p.

Bankey, V., Grauch, V.J.S., Webbers, A., and PRJ, Inc., 2005, Digital data and derivative products from a high-resolution aeromagnetic survey of the central San Luis Basin, covering parts of Alamosa, Conejos, Costilla, and Rio Grande Counties, Colorado, and Taos County, New Mexico: U.S. Geological Survey Open-File Report 2005–1200, version 1.0 (CD–ROM).

Birkeland, P.W., 1999, Soils and geomorphology, 3d ed.: New York, Oxford University Press, 430 p.

Fall, P.L., 1997, Timberline fluctuations and late Quaternary paleoclimates in the Southern Rocky Mountains, Colorado: Geological Society of America Bulletin, v. 109, p. 1306–1320.

Lal, D., 1991, Cosmic ray labeling of erosion surfaces: In-situ nuclide production rates and erosion models: Earth and Planetary Science Letters, v. 104, p. 424–439.

Leonard, E.M., 1989, Climate change in the Colorado Rocky Mountains—Estimates based on modern climate at late Pleistocene equilibrium lines: Arctic and Alpine Research, v. 21, no. 3, p. 245–255.

Licciardi, J. M., Kurz, M. D., Clark, P.U., and Brook, E. J., 1999, Calibration of cosmogenic ^{3}He production rates from Holocene lava flows in Oregon, USA, and effects of the Earth's magnetic field: Earth and Planetary Science Letters, v. 172, p. 261–271.

Lipman, P.W., and Mehnert, H.H., 1979, The Taos Plateau volcanic field, northern Rio Grande Rift, New Mexico, *in* Riecker, R.E., ed., Rio Grande rift—Tectonics and magmatism: Washington, D.C., American Geophysical Union International Symposium on the Rio Grande Rift, Proceedings, p. 289–312.

Lisiecki, L.E., and M.E. Raymo, 2005, A Plio-Pleistocene stack of 57 globally distributed benthic d180 records: Paleoceanography, v. 20, PA1003, doi:10.1029/2004PA001071 (http://www.moraymo.us/2005_Lisiecki+Raymo.pdf).

Machette, M.N., and Thompson, R.A., 2005, Preliminary geologic map of the northwestern part of the Alamosa 1/2° x 1° quadrangle, Alamosa and Conejos Counties, Colorado: U.S. Geological Survey Open-File Report 2005–1392, 1:50,000 scale.

Marchetti, D.W., and Cerling, T.E., 2005, Cosmogenic ^{3}He exposure ages of Pleistocene debris flows and desert pavements in Capitol Reef National Park, Utah: Geomorphology v. 67, no. 3–4, p. 423–435.

Marchetti, D.W., Cerling, T.E., and Lips, E.W., 2005, A glacial chronology for the Fish Creek drainage of Boulder Mountain, Utah, USA: Quaternary Research, v. 64, p. 264–271.

Rogers, K.L., Larson, E.E., Smith, G.A., Katzman, D., Smith, G.R., Cerling, T.E., Wang, Y., Baker, R.G., Lohmann, K.C., Repenning, C.A., Patterson, P.E., Mackie, G., 1992, Pliocene and Pleistocene geologic and climatic evolution in the San Luis Valley of south-central Colorado: Palaeogeography, Palaeoclimatology, Palaeoecology, v. 94, no. 1–4, p. 55–86

Rogers, K.L., Repenning, C.A., Forester, R.M., Larson, E.E., Hall, S.A., Smith, G.A., Anderson, Elaine, and Browen, T.J., 1985, Middle Pleistocene (Late Irvingtonion: Nebraskan) climatic changes in south-central Colorado: National Geographic Research, v. 1, no. 4, p. 535–563.

Siebenthal, C.E., 1910, Geology and water resources of the San Luis Valley, Colorado: U.S. Geological Survey Water-Supply Paper 240, 128 p.

Thompson, R.A., and Machette, M.N., 1989, Geologic map of the San Luis Hills, Conejos and Costilla Counties, Colorado: U.S. Geological Survey Miscellaneous Investigations Series Map I–1906, scale 1:50,000.

Wells, S.G., Kelson, K.I., and Menges, C.M., 1987, Quaternary evolution of fluvial systems in the northern Rio Grande rift, New Mexico and Colorado—Implications for entrenchment and integration of drainage systems, *in* Menges, C., ed., Quaternary tectonics, landform evolution, soil chronologies and glacial deposits—Northern Rio Grande rift of New Mexico: Friends of the Pleistocene—Rocky Mountain Cell Field Trip Guidebook, Oct. 8–11, 1987, p. 55–69.

Winograd, I.J., 1959, Ground water conditions and geology of Sunshine Valley and Western Taos County, New Mexico: Technical Report 12, State of New Mexico Office of State Engineer, 70 p.

Geology of Mesita Volcano, Colorado — Eruptive History and Implications for Basin Sedimentation During the Quaternary

By Ren Thompson, Michael Machette, Ralph Shroba, and Cal Ruleman

CHAPTER H

Introduction

The Taos Plateau volcanic field of the central and southern San Luis Valley of Colorado and New Mexico is the largest and longest-lived of the Miocene to Quaternary volcanic fields of the Rio Grande rift. Volcanism of the Taos Plateau volcanic field is predominantly basaltic and is associated with large monogenetic volcanic centers. Rocks ranging in composition from low-silica basalt to high-silica rhyolite are locally present and record a complex, 5 m.y.-long, eruptive history from many eruptive centers; the largest volume of eruptive material was deposited in actively subsiding grabens during the early Pliocene (Lipman and Mehnert, 1979; Appelt, 1998). Mesita Hill, located about 3 km west of the community of Mesita, Colo., on the Costilla Plain (see stop B8, chapter B, this volume), is underlain by volcanic deposits of Mesita volcano—the youngest (1.03 Ma; Appelt, 1998) and only Quaternary volcano of the Taos Plateau volcanic field. Mesita volcano is the last vestige of continental rift volcanism in the San Luis Valley portion of the northern Rio Grande rift. The well-preserved volcanic morphology, exposures created by recent quarrying, and geologic observations and subsurface interpretations (Epis, 1977; Kirkham, 2006) provide rare insight into (1) the eruptive history of Mesita volcano, (2) tectonic control on the eruptive-center location, and (3) stratigraphic constraints on post-1 Ma basin sedimentation of the ancient Culebra and Costilla Creek drainage systems.

Mesita Volcano

Unlike most rift volcanoes of the southern Taos Plateau, Mesita volcano is small (<5 km^2 in areal extent), short lived, and well exposed. Before quarrying, the volcano was a prominent geomorphic feature that protruded above the relatively flat, alluvial surface of the Costilla Plain. The volcano morphology is a classic basaltic shield (referenced to the shape of a warrior's shield) with a summit cone of about 15 m height and 750 m diameter, built on a nearly symmetric lava platform approximately 2.5 km in diameter. The erupted volume of magma is estimated at 0.2 km^3 on the basis of the prequarrying morphology of the volcano; little appears to have been removed by erosion. A geologic map of Mesita Hill is shown in figure H–1 and a topographic map and profile are illustrated in figure H–2.

The volcanic cone, the interior of which is beautifully preserved in the quarry walls, is a natural laboratory of eruptive processes and products. The cone is constructed of interbedded layers of variable-sized volcanic tephra and thin (<1 m) clastigenic (derived primarily from agglutinate) and nonclastigenic lava flows. The predominant fragmental ejecta are cinder or scoria, the glassy lava rock that vesiculated during explosive eruption. Locally, fragmental cinders became welded during rapid burial that retained heat—a result of rapid effusion rates. The cinder of Mesita volcano is typically medium to dark grey in fresh outcrops, but locally it was oxidized to brown and red hues during eruption. Variable dark grey to red transitions in color, observable in the quarry walls, commonly exhibit sharply delineated, crosscutting relations within the volcanic deposits and are likely related to local oxidation resulting from primary and ground-water-induced gas and steam evacuation from fumaroles. Blocks or fragmental solid rock fragments (>64 mm in diameter) ejected from the volcanic vent are intercalated with the cinders and were likely derived from solidified pieces of previously erupted lava flows or are disaggregated ballistic fragments of primary magma ejecta. Volcanic bombs (fig. H–3), ejected from vents in a partially molten state, commonly assume fusiform and spindle shapes during in-flight cooling. Bombs with such shapes are common at Mesita Hill. Less common are breadcrust bombs with fractured surface textures that develop as bomb interiors expand or deform and break or crack the cool, brittle exteriors. Clastigenic lava flows are formed by molten ejecta that agglutinate but remains hot, promoting flowage; the resulting coherent lava flows are typically thin and laterally discontinuous as observed in the quarry walls.

The reconstructed morphology (that is, the morphology before the quarry) of the Mesita cinder cone (as derived from 1935

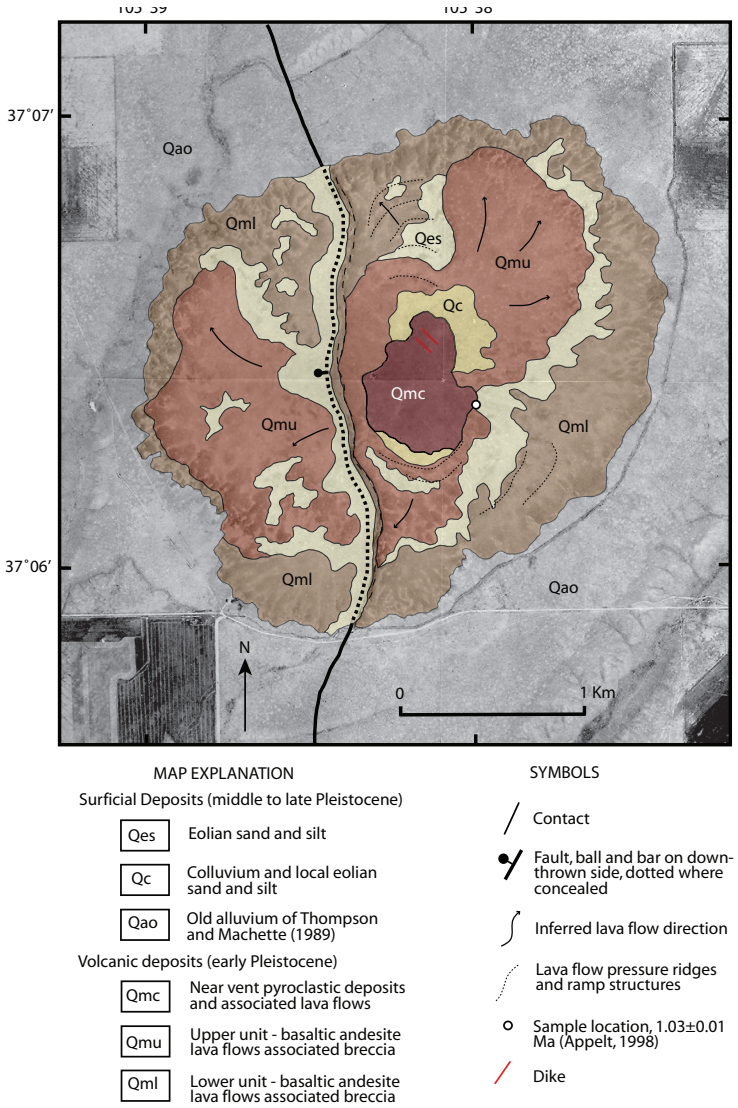

Figure H–1. Geologic map of Mesita volcano. Unpublished geology mapped by Thompson, 2007. Base image from 1936 aerial photography.

aerial photographs and 1967 U.S. Geological Survey topography compiled from 1965 aerial photographs) shows a very small, breeched summit crater immediately southwest of the cone summit and two small, northwest-trending dikes near the north end of the summit cone (figs. H–1 and H–2). All traces of the summit crater and the dikes have subsequently been removed by quarry operations at the Hank and Jake Mine (fig. H–4*A*–*D*; also see stop B8 of chapter B, this volume). The absence of feeder dikes exposed in the quarry walls suggests that the summit cone was the result of a short-lived eruption with little lateral migration of the vent area or feeder system. This suggestion is consistent with the generalized geologic cross section of Epis (1977), which shows a central conduit feeding the Mesita volcano (see stop B8, chapter B, this volume).

The pyroclastic deposits and lava flows observed in quarry walls on the north end of the current pit are subparallel and dip gently north and northeast, away from the inferred primary vent area. Local unconformities, primarily reflecting depositional hiatuses, observed in the quarry walls appear to be the result of migration of depositional centers that may have resulted from local reorientation of the vent geometry or conduit system, or local changes in wind direction during eruption. Such variations in near-vent facies have been well described at the tholeiitic shield volcanoes of Albuquerque Volcanoes National Monument in the Albuquerque Basin of the Rio Grande rift (Smith and others, 1999). No interbedded soil horizons or alluvial deposits are observed in the quarry walls of the Mesita volcano, suggesting that deposition was rapid and nearly continuous throughout the eruptive history of the cone.

The lava platform on which the summit cone rests includes deposits from two eruptive episodes shown on figure H–1 as units Qml (lower) and Qmu (upper). Both map units are predominantly lava flows characterized by blocky to rubbly aa flow-surface textures (fig. H–4*E*, *F*), pressure ridges, and poorly defined flow edges delineating individual flow lobes. The lower unit (Qml) is broadly symmetric about the summit cone (unit Qmc), and the orientations of pressure ridges and flow lobe termini suggest that the lava erupted from a vent area now occupied by the summit cone and overlying lava flows of unit Qmu. Unit Qmu is more areally restricted and volumetrically subordinate to the underlying lava flows (unit Qml), but flow lobes also reflect flow directions radially away from the central summit cone (fig. H–1). In general, lava flows rarely erupt from the summits of cinder cones but are instead typically distributed marginally to the cone, erupting from breeches low on the flanks of cinder or spatter cones. Thus, deposits of map units Qmu and Qmc may be related to the same eruption. Large volumes of nonvesiculated magma erupted as lava flows, such as those of units Qml and Qmu, lack the buoyancy to rise any distance vertically within the cone; such magma capitalizes instead on the inherent instability of the enveloping fragmental deposits and erupts through the cone flanks. The distal reaches of lava flows then reflect local variations in topography; that is, lava always flows downslope. The lack of a preferred flow direction in the lower lava flows of unit Qml suggests that the flows erupted onto a very subdued or nearly flat topographic surface. Subsequent eruptions of lava flows in unit Qmu simply followed the paleotopographic surface created by the undulating and anastomosing lobes of the underlying, slightly older flows of unit Qml. No alluvial or other surficial deposits are observed between the lower and upper map units. It is possible the eruptions of Mesita volcano occurred for a period of perhaps days, weeks, or months.

The lava flows and summit cone deposits of Mesita volcano are petrographically and chemically basaltic andesite and, together with their morphology and inferred eruptive character, are similar to those of other small-volume eruptions of the Taos Plateau volcanic field. The rocks are weakly porphyritic to microporphyritic with pilotaxitic texture. Phenocrysts include

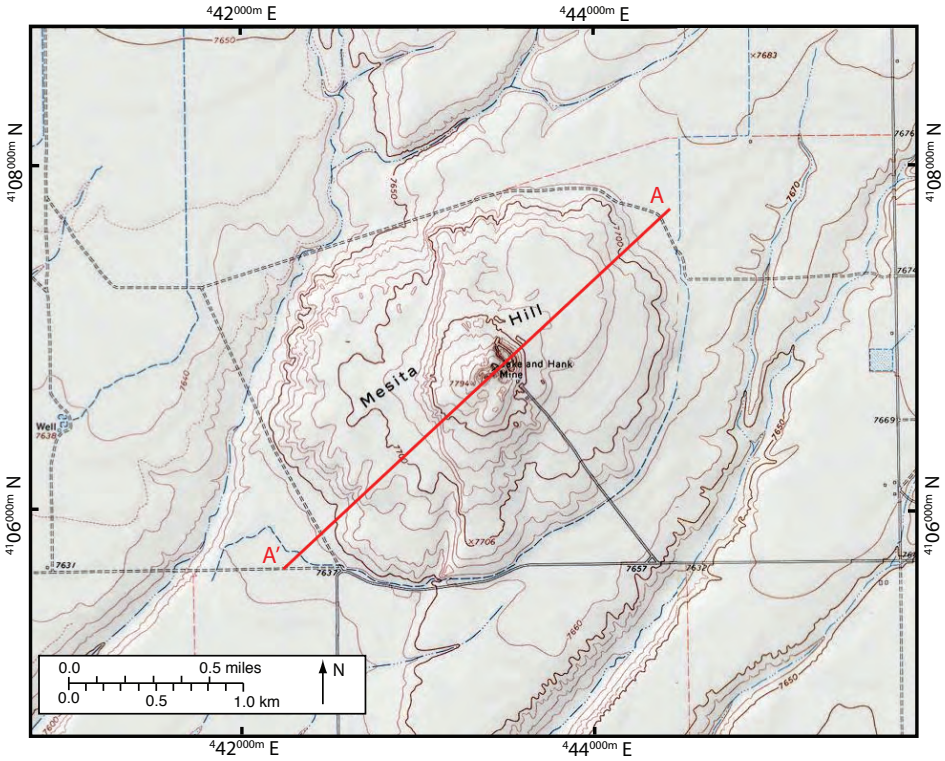

Figure H–2. Topographic map and profile (A'-A) of Mesita volcano, based on Sky Valley Ranch quadrangle 1:24,000-scale U.S. Geological Survey map of Mesita Hill area. Vertical exaggeration, 10.5x.

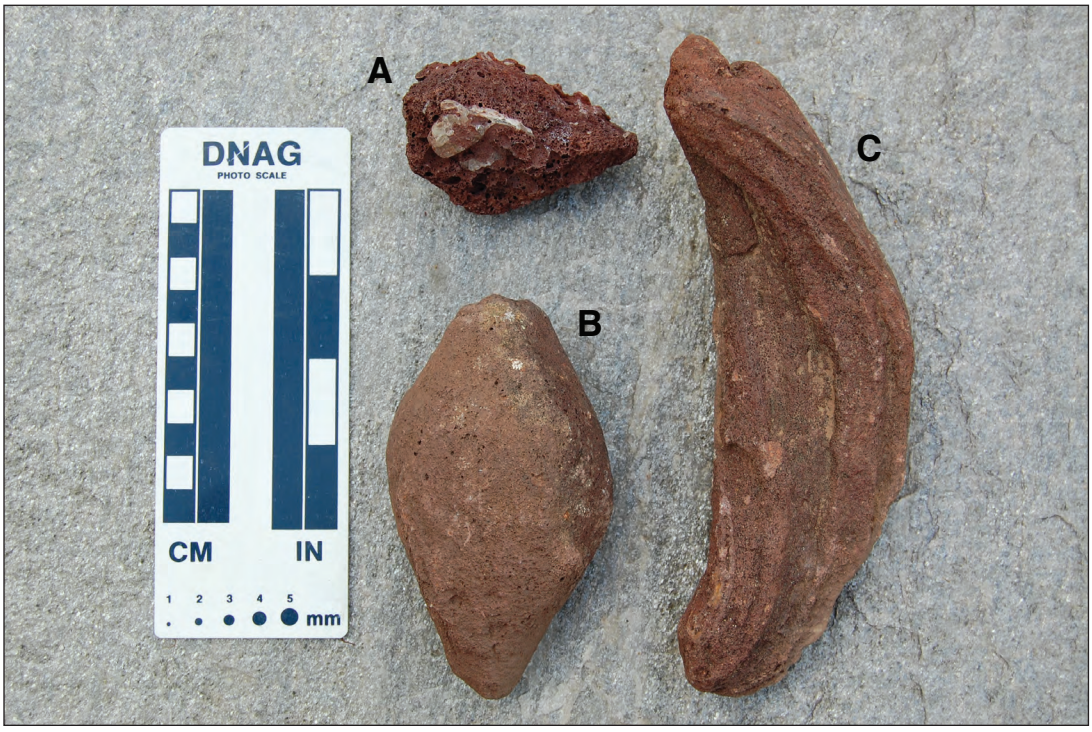

Figure H–3. Volcanic cinder or scoria (A), fusiform bomb (B), and spindle bomb with twisted ends (C) are representative of eruptive material from Mesita volcano. Some rare elongate bombs may be as much as 0.5 m in length. Note large plagioclase xenocryst in A; smaller (2–3 mm) plagioclase and quartz xenocrysts are more typical.

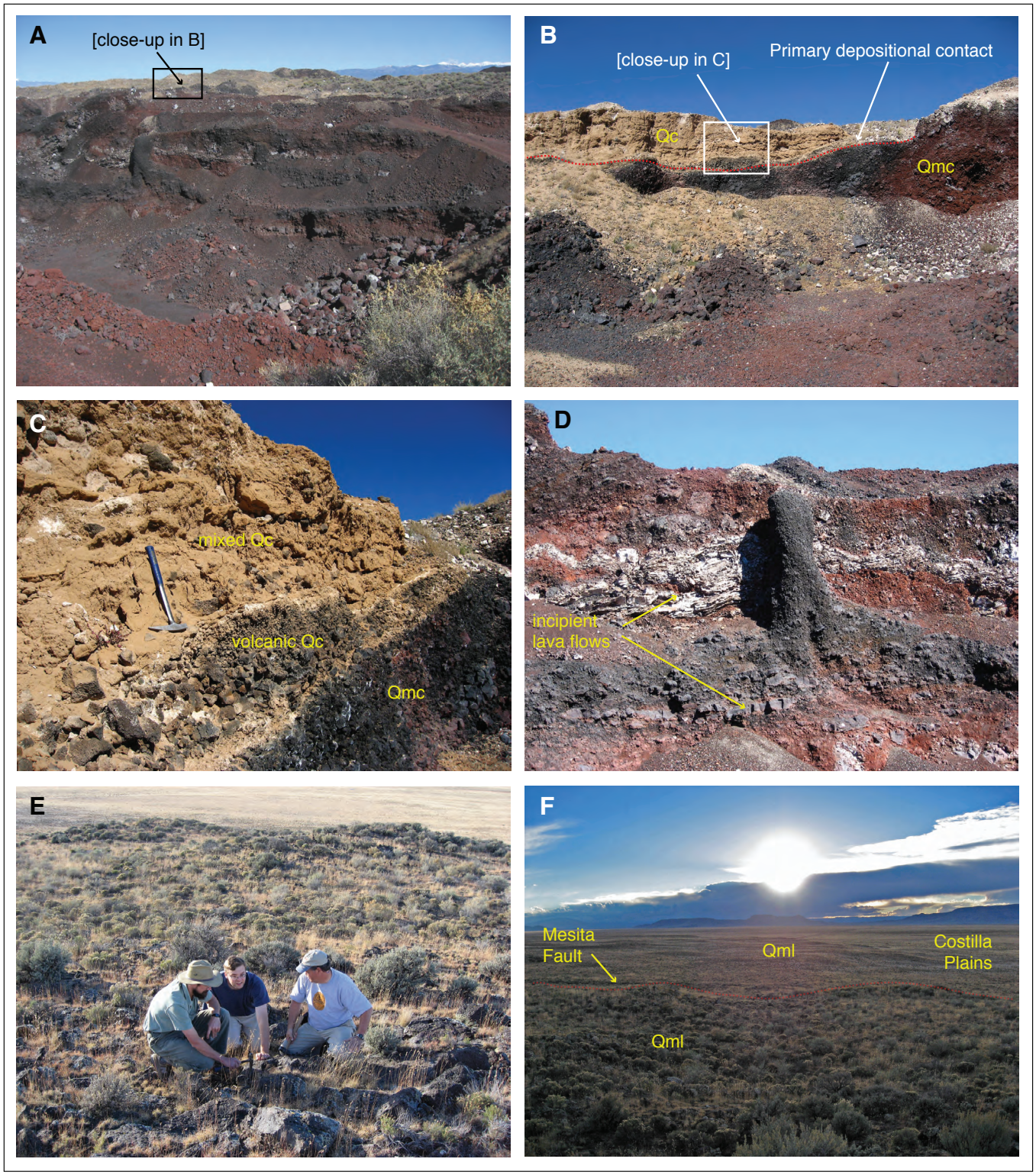

Figure H–4. *A*, View north across quarry pit at Cinder Hill (2007 photograph). *B*, Mixed colluvium and eolian sedimentary deposits (unit Qc) overlying primary volcanic-scoria deposits (unit Qmc). *C*, View of stratigraphic relations between three units: primary volcanic deposits (unit Qmc), volcanic-clast-dominated colluvium (volcanic unit Qc), and matrix-supported mixed aeolian and colluvial deposits (mixed unit Qc). *D*, Gently dipping volcanic scoria, incipient lava flows, and variably oxidized and sintered scoria exposed in east wall of quarry. *E*, Blocky aa flow surface on north flank of Mesita Hill (unit Qml; fig. H–1). Geologists from left to right: Cal Ruleman, David Marchetti, Michael Machette. *F*, View west toward San Luis Hills across nearly horizontal flow surface of unit Qml (Fig. H–2), Mesita fault trace, and Costilla Plain from north end of Mesita Hill.

plagioclase with lesser amounts of olivine in a microcrystalline groundmass of plagioclase, pyroxene, olivine, and iron-titanium oxides. Ubiquitous but rare xenocrysts of plagioclase and lesser quartz can be larger than 1 cm long (fig. H–3) and also are characteristic of other small-volume eruptive centers in the region. As a result, we use the informal term "xenocrystic basaltic andesite" to describe these and similar rocks of the Taos Plateau (Lipman and Mehnert, 1979). Similar deposits from cinder cones have been interpreted as late-stage flank eruptions associated with larger volcanic edifices on the Taos Plateau (Thompson and Lipman, 1994a,b).

Petrographically similar rocks from small cinder cones on the Taos Plateau (to the south) have compositions ranging from basalt to andesite (50.5–57.6 weight (wt) percent SiO_2; 6.4–2.9 wt percent MgO), and the majority are mafic andesite (52–54 wt percent SiO_2 and 4–5 wt percent MgO) (Lipman and Mehnert, 1979; Kinsel, 1985). Xenocryst compositions of the suite range widely; quartz and plagioclase are the predominant assemblage, but these rocks locally contain potassium feldspar, clinopyroxene, and xenolith clots of gabbro and pyroxenite (Kinsel, 1985). All xenoliths and xenocrysts were out of equilibrium with their host magmas as reflected in ubiquitous resorbtion textures, glass inclusions, and mineral overgrowths suggestive of incorporation of cold country rock that partially assimilated within basaltic magma chambers and conduit systems. Kinsel (1985) suggested that many of these inclusions are likely derived from middle and upper Proterozoic crust. In spite of the propensity of these rocks to have excess "old" argon resulting from disaggregation and assimilation of xenocrysts and xenoliths such as those observed at Mesita volcano, Appelt's (1998) $^{40}Ar/^{39}Ar$ age of 1.03±0.01 Ma from the groundmass of a Mesita basaltic andesite yielded a surprisingly reasonable age plateau. Unfortunately, the sample location that Appelt (1998) reported is suspect (see fig. H–1 for an approximate location); nevertheless, it probably reflects the age of the unit Qmu eruptive event and, within error, the age of the entire eruption.

Mesita Fault

Mesita Hill is cut by the down-to-west Mesita fault (figs. H–4*F* and H–5), offsetting lava flows of both units Qml and Qmu (fig. H–1). This fault is one of three down-to-west normal faults that appear to step basinward toward the central basin graben, which is defined by the down-to-east Lasauses fault and the Mesita fault of opposing sense (fig. H–5). Reported offsets of 13 m on the Mesita fault (Thompson and Machette, 1989) reflect the average displacement across both lower and upper lava flow surfaces. The fault offset reflects progressive growth since at least the early Pliocene (4 Ma) based on a 40-m minimum displacement of Pliocene Servilleta basalt flows in the subsurface (see stop B8, chapter B, this volume). The Mesita fault or a similar intrabasin fault projects to the north through the eastern Fairy Hills (Thompson and Machette, 1989), where it cuts upper Oligocene volcanic rocks of the Conejos Formation. Timing of onset of displacement along this structure is not clearly defined owing to diverse stratigraphic facies preserved in volcanic rocks of the Conejos Formation. Regardless of the timing of onset of motion across this fault, the associated

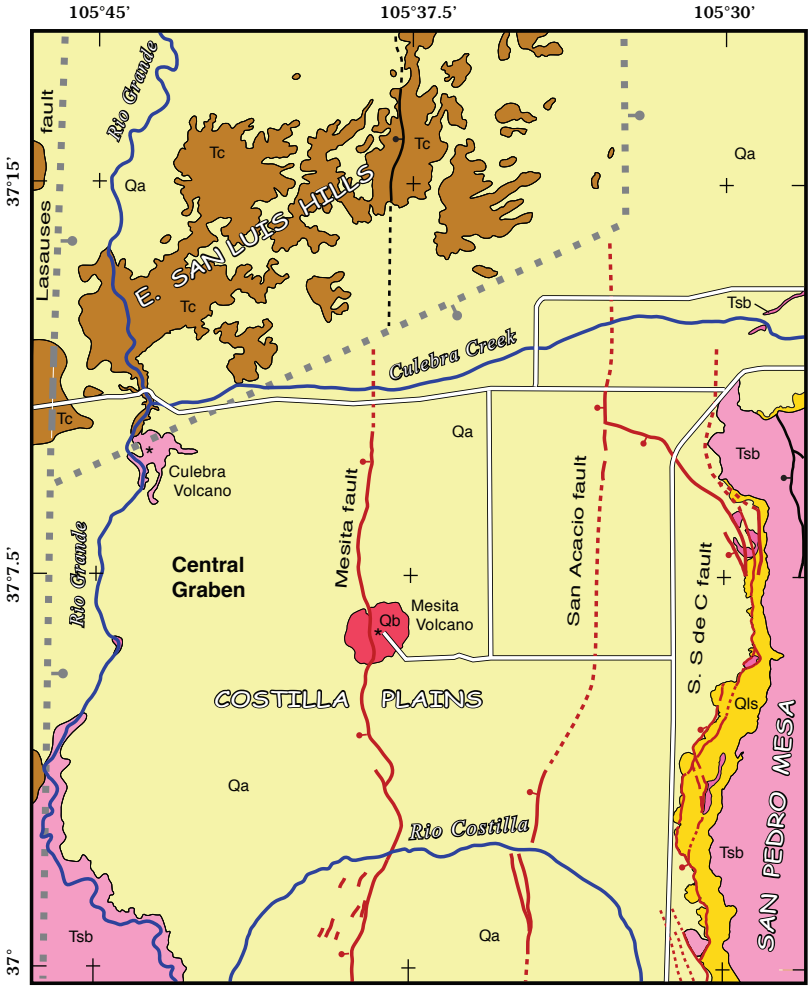

Figure H–5. Generalized geologic map of the Costilla Plain in Colorado showing Quaternary faults (red lines) and older faults (black lines). Major inferred, mostly Neogene, faults that block out the San Luis Hills are shown by thicker gray dashed or dotted lines. Bedrock units: Qb, Mesita basalt (1.0 Ma); Tsb, Pliocene Servilleta Basalt and age-equivalent basaltic rocks of Culebra volcano; Tc, Oligocene volcanic rocks. Quaternary units shown as Qa, with exception of landslide deposits (Qls) along San Pedro Mesa. S. S de C fault, southern Sangre de Cristo fault zone. Geology modified from Thompson and Machette (1989), Machette and others (2007), and Thompson and others (2007).

Quaternary movement and localization of volcanism along the fault is clearly evident.

Recent unpublished mapping by the authors shows a clear proximity of faults to large volcanic edifices (such as Ute Mountain in the northern Taos Plateau volcanic field; see stop C3, chapter C, this volume) although associative relations do not necessarily imply a causal relationship between faulting and eruptive activity. Rather, the proximity of volcanic loci to faults likely represents the ability of magmatic plumbing systems to capitalize on local perturbations of stress fields afforded by faulting and on migration pathways provided by faults. In the Cerros del Rio volcanic field of the Española Basin segment of the Rio Grande rift, the basinward migration of fault activity with constriction of the active zone of extension (Minor and others, 2006) was accompanied by a concomitant basinward migration of basaltic to intermediate-composition volcanic edifices (Thompson, Hudson, and others, 2006; Thompson, Sawyer, and others, 2006). Most eruptions of the Taos Plateau volcanic field occurred during the peak of basaltic volcanism during the Pliocene, and consequently much of the evidence for links to tectonism in the region was buried by younger lava flows and basin-margin sediments. The Quaternary volcanism at Mesita Hill preserves this relation as a result of the short-lived nature of this basaltic eruption during the waning stages of rift volcanism.

Implications for Basin Sedimentation

The volcano of Mesita Hill stands alone on the Costilla Plain, a gently westward-sloping surface of middle Pleistocene age underlain by pebbly to cobbly sand built on older, perhaps early Pleistocene, nearly horizontal silt and sand of the upper part of the Santa Fe Group (Thompson and Machette, 2007). Blanketing the leeward (east) side of lava flows that form the unit Qmu surface and the windward side of the Mesita fault are sedimentary deposits composed predominantly of young (Holocene and late Pleistocene?) eolian silt and sand that contains admixed angular cobble-sized basaltic blocks and scoria from the summit cone and flank lavas of Mesita volcano (unit Qes). Older analogs of middle Pleistocene (unit Qc) are exposed on the summit cone (fig. H–1) and contain well-developed calcic soil horizons within the deposits. These deposits are visible on the north and northeast side of the summit cone from aerial photographs taken during 1936 (fig. H–6) and are locally preserved in the walls of the abandoned quarry (fig. H–4*A,B,C*). The highest preserved outcrop seen on these photos is at an elevation of about 7,775 ft.

Epis (1977) and Kirkham (2006) cite evidence for Quaternary alluvial deposits containing rounded clasts of Precambrian granite in an arkosic sand matrix near the 7,775 ft elevation on the summit cone; much of these deposits have since been removed by mine excavation (see stop B8 discussion, this volume). Our geologic mapping and examination of archival aerial photography suggests that the remaining sedimentary deposits on the north rim of the excavated crater rim (stop B8.2, chapter B, this volume) represent the same stratigraphic unit as those observed and described by Epis and Kirkham. The deposits exposed at the quarry were excavated after 1953 and before 1985 (fig. H–6) and were likely to be accessible to previous researchers during their investigations. A significant and controversial conclusion of both Epis (1977) and Kirkham (2006) is that Mesita Hill was a buried volcanic construct, covered by prograding fan alluvium that is presumably related to the ancestral Culebra and Costilla drainage systems. Burial to at least 7,775 ft (top of mapped deposits) would require basin filling to about 100 ft above the current alluvial surface of the Costilla Plain (a surface underlain by unit Qao of Thompson and Machette, 1989). In this scenario, the current geomorphic form of Mesita Hill would represent an exhumed volcanic feature. This interpretation contradicts three lines of evidence based on recent mapping and examination of primary volcanic features and associated sedimentary deposits discussed below:

(1) Although pebble- to cobble-sized Precambrian clasts are reported by both Epis and Kirkham in their descriptions of alluvial deposits on the summit cone (unit Qmc of fig. H–1), no such clasts are currently observed in preserved deposits at the same stratigraphic level (fig. H–4*A,B,C*). These currently observed deposits are more appropriately interpreted as mostly colluvium with a large component of reworked eolian sediment that composes the sandy matrix.

(2) The interpretation of the volcanic geomorphic feature as “exhumed” requires erosion of the extensive surrounding alluvial deposits yet preservation of the scoriaceous summit cone as an undissected landform. There is no evidence to suggest that the original size of the cone, observable in the 1936 aerial photograph, is distinctly different from its expected original size and shape. Moreover, burial of the undulating, irregular flow surfaces of units Qml and Qmu by fan alluvium (fig. H–4*E,F*) should have left remnants of deposits rich in Precambrian clasts. Only a very limited number of pebble-size clasts are observable on the surfaces of the Qml or Qmu lava flows.

(3) The accumulation of an additional 100 ft of basin-fill alluvial sediment around Mesita Hill would have had dramatic impact on the distal basin morphology and subsequent erosion history. Figure H–7 illustrates the approximate extent of the unit Qao surface mapped by Thompson and Machette (1989) and two topographic profiles projected from the 7,775 ft elevation to points northwest and southwest from Mesita Hill. Based on the projection of the existing surface of unit Qao, the original surface would have extended west of the Rio Grande and intersected the footslope of the San Luis Hills at an approximate elevation of 7,640 ft. Also shown on figure H–7 is the projected elevation of the proposed pre–unit Qao alluvial surface of Epis (1977) and Kirkham (2006); it is based on a slope that parallels the existing unit Qao surface of Thompson and Machette (1989). Finally, we include a second projection to illustrate the effect of variable slope on the proposed pre–unit Qao surface.

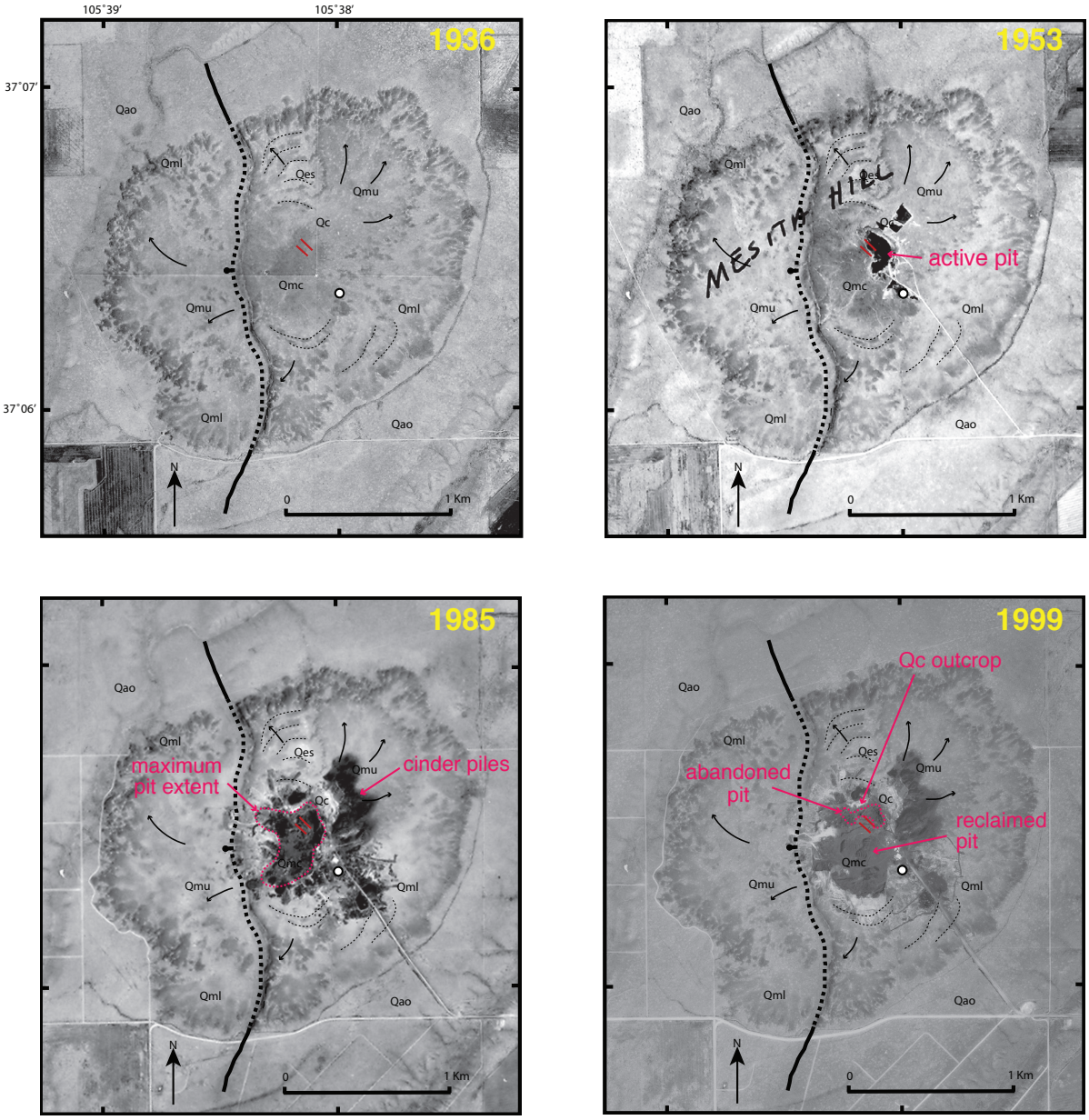

Figure H–6. Aerial photographs from 1936, 1953, 1985, and 1999 (U.S. Geological Survey digital orthophotograph) showing evolution of the cinder quarry at the Hank and Jake Mine on Mesita Hill, Colorado. Geologic map symbols defined on figure H–1.

Southwest of the Costilla Plain, the basin-fill deposits would have spilled into present-day Punche Valley, covered the northern exposures of Servilleta Basalt to an elevation of approximately 7,640 ft, and lapped onto the lower slopes of the southern San Luis Hills (Thompson and Machette, 1989). Remnants of deposits related to the middle Pleistocene unit Qao surface of Thompson and Machette (1989) contain Precambrian clasts (derived from Sangre de Cristo Mountains). West of the Rio Grande they are not observed above an elevation of about 7,640 ft in Punche Valley, but they are preserved at lower elevations. Bedding attitudes of distal alluvial-fan deposits east of the Rio Grande are nearly horizontal suggesting that Punche Valley marks the distal reaches of unit Qao deposition in a depocenter that had aggraded to a nearly horizontal plane by the middle Pleistocene (about 500 ka; see stop B8, chapter B, this volume).

Northwest of Mesita Hill, the proposed basin-fill deposits of Epis (1977) and Kirkham (2006) would have projected above the summit of Culebra volcano, a Pliocene basaltic andesite shield that is bordered on the west by the Rio Grande. The upper flanks of Culebra volcano preserve no evidence for prior burial in the form of Precambrian-rich lag deposits, west

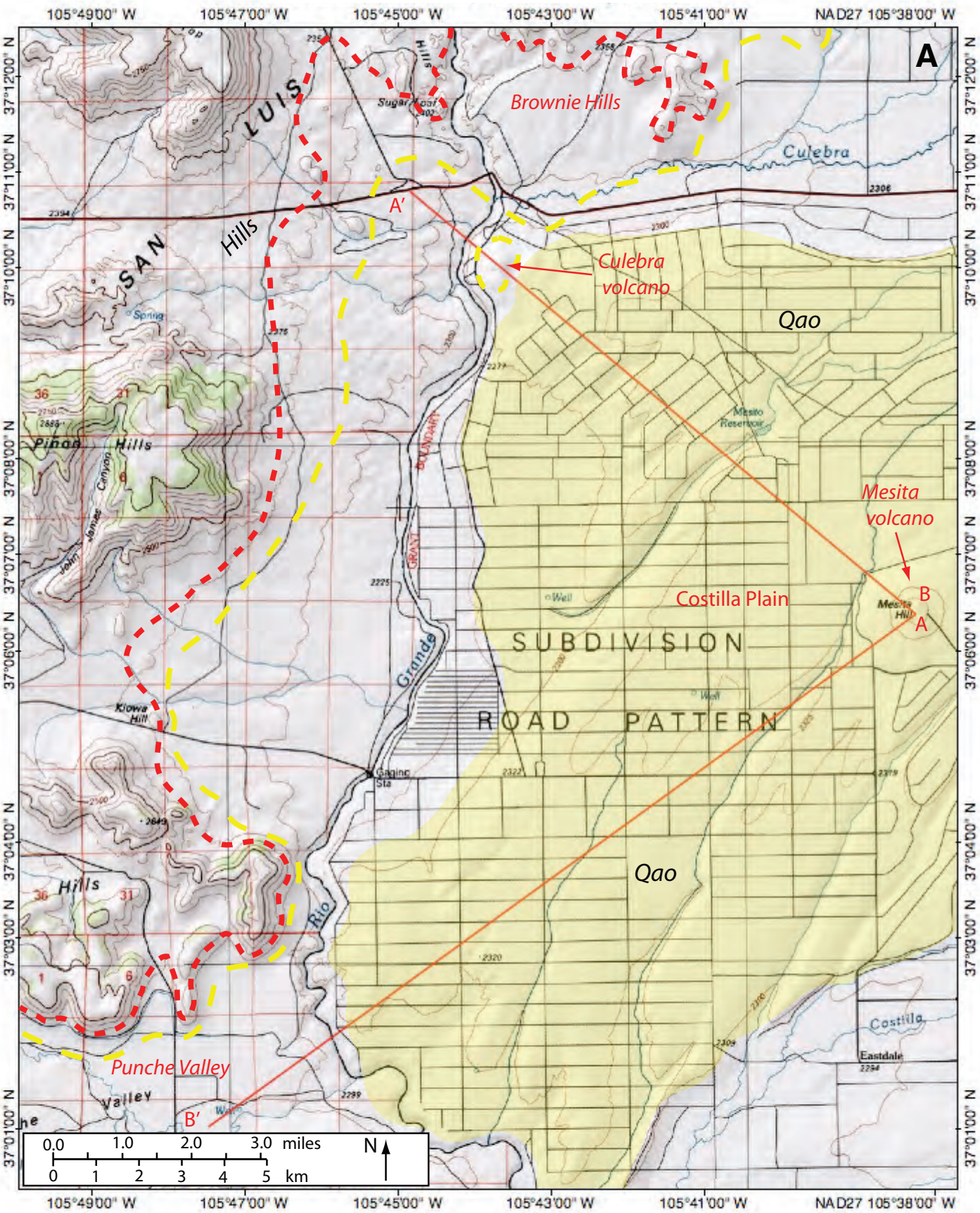
A
Brownie Hills
Culebra
A′
Culebra volcano
Qao
Mesita volcano
B
A
Costilla Plain
SUBDIVISION
ROAD PATTERN
Qao
Punche Valley
B′
SAN LUIS Hills
Pinon Hills
Kiowa Hill
Rio Grande
Costilla
Eastdale
0.0 1.0 2.0 3.0 miles
0 1 2 3 4 5 km
N
105°49'00" W
105°47'00" W
105°45'00" W
105°43'00" W
105°41'00" W
NAD27 105°38'00" W
37°12'00" N
37°11'00" N
37°10'00" N
37°08'00" N
37°07'00" N
37°06'00" N
37°04'00" N
37°03'00" N
37°01'00" N

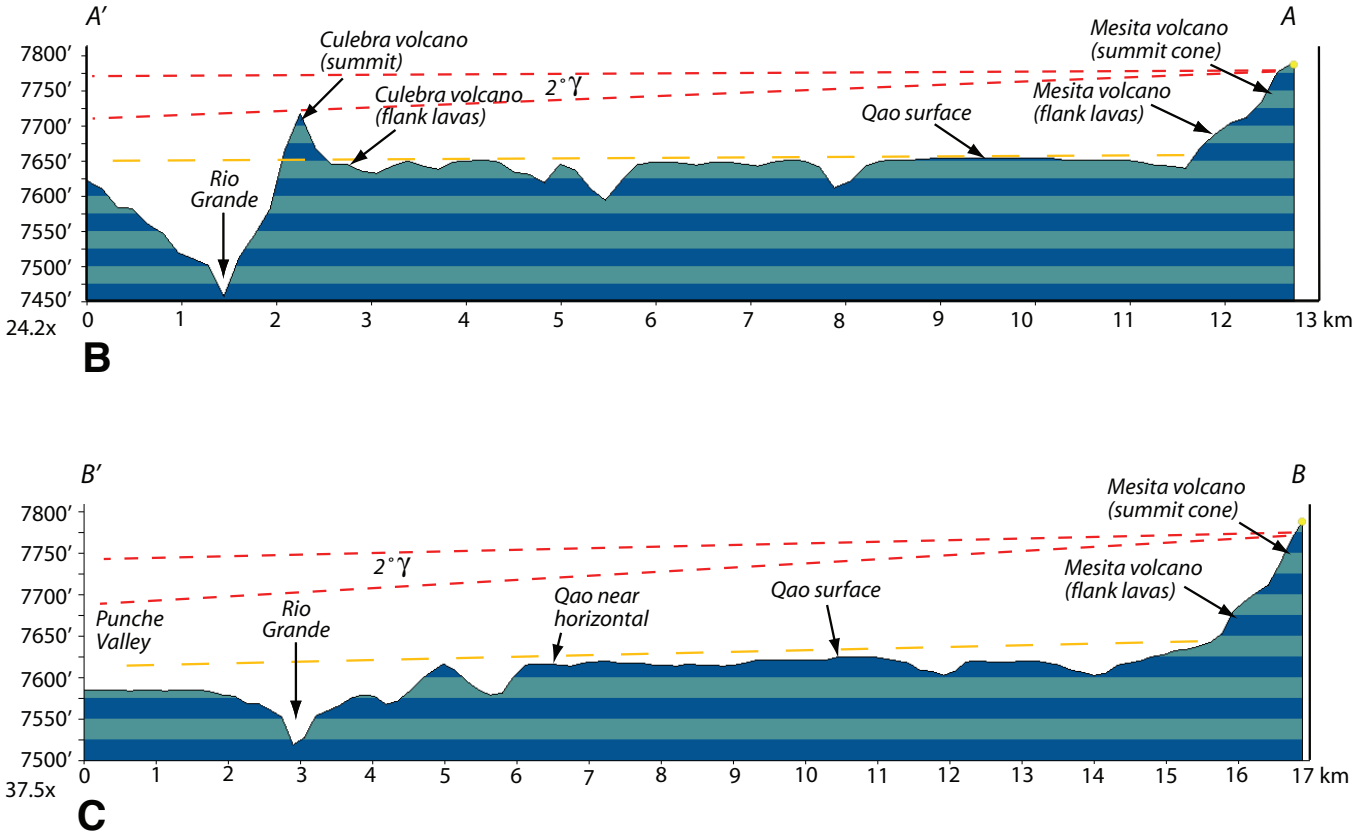

Figure H–7. *A*, Topographic map of the Costilla Plain showing aerial extent of mapped middle Pleistocene deposits (unit Qao in yellow) and profile lines for topographic profiles shown in B and C. Long dash (yellow) line represents projected original distal extent of unit Qao surface based on intersection of top of existing westward-sloping surface with existing topography. Short dash (red) line represents projection of middle Pleistocene volcano at an elevation of 7,775 ft. *B*, Topographic profile for line segment A'-A (vertical exaggeration, 24.2x). Long dash (yellow) line approximates slope of unit Qao surface of Epis (1977) and Kirkham (2006) based on an original slope identical to that observed for preserved unit Qao surface (<1°). Lower short dash (red) line illustrates the effect of variable slope on the projected unit Qao surface of Epis (1977) and Kirkham (2006). *C*, Topographic profile for line segment B'-B (vertical exaggeration, 37.5x). Symbols as in fig H–7B.

of the nearly horizontal lavas at the base of the volcano. These basal lava flows do preserve many subrounded Precambrian clasts believed to be derived from channel deposits of the ancestral Culebra drainage, which flowed across the eastern flanks of the volcano. This observation is consistent with map relations for the distal margins of the unit Qao surface of Thompson and Machette (1989) and the surface projections shown in figure H–7.

A significantly higher level of aggradation associated with the alluvial-fan system built by Rio Culebra would have deposited sediment against the southern margin of Oligocene volcanic rocks in the southeastern Brownie Hills. The southern Brownie Hills has considerable topographic irregularity, which should have preserved remnants of a topographically higher early(?) Pleistocene basin-filling event. In spite of our mapping throughout the area (Thompson and Machette, 1989; 2007), no such remnants have been observed. Additionally, progradation of an alluvial surface into an area now occupied by the canyon of the Rio Grande would imply relatively rapid, post-1.0 Ma deposition of coarse sediment into a basin during an interval of about 500 k.y. during the Pleistocene marked by slow, shallow sedimentation in Lake Alamosa, immediately to the north of the Fairy Hills (see chapter G, this volume). In fact, the northern distal margins of an areally more extensive Pleistocene surface may have extended into the area now underlain by sediments of the 440 ka Lake Alamosa. This interpretation would require that alluvium in the Costilla Plain deposited during the middle Pleistocene and the later part of the early Pleistocene (about 1.0–0.5 Ma) be stripped away prior to deposition of the overlying lake deposits. It's difficult to reconcile the tectonic or climatic drivers for these diverse sedimentation styles and erosion rates in proximity within the same depositional basin.

Conclusion

The Quaternary volcano at Mesita Hill reflects the last gasp of rift volcanism on the Taos Plateau volcanic field. Built on a subhorizontal dipslope of fine-grained sediment of the Santa Fe Group, the basaltic andesite lava flows of the lower flanks reflect the short-lived eruptive history of lava effusion from a central vent area now occupied by the excavated remnants of a low-relief cinder cone forming the volcano's summit. The 1.0 Ma volcano is cut by an active down-to-west graben-bounding fault of the present axial basin that may have served to localize the eruption. The base of the flank lavas were subsequently surrounded by prograding middle Pleistocene alluvial-fan deposits of the ancestral Culebra and Costilla drainage systems that were, in turn, dissected by the same creeks to the north and south of Mesita Hill, respectively, as they adjusted to a lowering base level dictated by the Rio Grande.

Acknowledgments

We appreciate the constructive and helpful comments of Margaret Berry (USGS) and Scott Minor (USGS), who reviewed a preliminary version of this manuscript. However, any errors that may remain are the responsibility of the authors.

References Cited

Appelt, R.M., 1998, $^{40}Ar/^{39}Ar$ geochronology and volcanic evolution of the Taos Plateau volcanic field, northern New Mexico and southern Colorado: Socorro, New Mexico Institute of Mining and Technology, M.S. thesis, 58 p.

Epis, R.C., 1977, Surface and subsurface geology of the Mesita volcano area, Costilla County, Colorado, *in* Zorich-Erker Engineering, Inc., Ground water availability of the San Marco property near Mesita in Costilla County, Colorado: Report submitted to San Marco Pipeline Company, Denver, Colorado, dated September, 30, 1980, Vol. III, Appendix A, 20 p., plus map and cross section.

Kinsel, Eric, 1985, Petrology of the silicic alkalic basalt and xenocrystic basaltic andesite of the Taos Plateau volcanic field, New Mexico: Dallas, Texas, Southern Methodist University, M.S. thesis, 50 p.

Kirkham, R.M., 2006, Surprises in the Culebra graben, a major sub-basin within the San Luis basin of the Rio Grande rift [abs.]: Geological Society of America Abstracts with Program, v. 38, no. 6, p. 14.

Lipman, P.W., and Mehnert, H.H., 1979, The Taos Plateau volcanic field, northern Rio Grande rift, New Mexico, *in* Reicker, R.C., ed., Rio Grande rift—Tectonics and magmatism: Washington D.C., American Geophysical Union, p. 289–311.

Minor, S.A., Hudson, M.R., Grauch, V.J.S., and Sawyer, D.A., 2006, Structure of the Santo Domingo Basin and La Bajada constriction area, New Mexico *in* Minor, S.A., ed., The Cerrillos uplift, the La Bajada constriction, and hydrogeologic framework of the Santo Domingo Basin, Rio Grande rift, New Mexico: U.S. Geological Survey Professional Paper 1720, p. 91–115.

Smith, G.A., Florence, P.S., Castrounis, A.D., Luongo, M., Moore, J.D., Throne, J., and Zelley, K., 1999, Basaltic near-vent facies of Volcan cone, Albuquerque volcanoes, New Mexico: New Mexico Geological Society 50th Field Conference, Guidebook, p. 211–219.

Thompson, R.A., Hudson, M.R., McIntosh, W.C., Miggins, D.P., Grauch, V.J.S., Minor, S.A., Sawyer, D., and Dethier, D.P., 2006, Temporal, stratigraphic and structural controls on the evolution of the Cerros del Rio volcanic field, northern Rio Grande rift, New Mexico [abs.]: Geological Society of America Abstracts with Programs, v. 38, no. 6, p. 37.

Thompson, R.A., and Lipman, P.W., 1994a, Geologic map of the Los Pinos quadrangle, Rio Arriba and Taos Counties, New Mexico and Conejos County, Colorado: U.S. Geological Survey Map GQ–1749, scale 1:24,000.

Thompson, R.A., and Lipman, P.W., 1994b, Geologic map of the San Antonio Mountain quadrangle, Rio Arriba County, New Mexico: U.S. Geological Survey Map GQ–1750, scale 1:24,000.

Thompson, R.A., and Machette, M.N., 1989, Geologic map of the San Luis Hills, Conejos and Costilla Counties, Colorado: USGS Miscellaneous Investigations Series Map I–1906, scale 1:50,000.

Thompson, R.A., and Machette, M.N., 2007, Preliminary geologic map of the Sanchez Reservoir and Garcia quadrangles, Costilla Counties, Colorado: U.S. Geological Survey Open-File Map 2007–1074, scale 1:24,000.

Thompson, R.A., Sawyer, D.A., Hudson, M.R., Grauch, V.J.S., and McIntosh, W.C., 2006, Cenozoic volcanism of the La Bajada constriction area, New Mexico *in* Minor, S.A., ed., The Cerrillos uplift, the La Bajada constriction, and hydrogeologic framework of the Santo Domingo Basin, Rio Grande rift, New Mexico: U.S. Geological Survey Professional Paper 1720–C, p. 43–60.

Zorich-Erker Engineering Inc., 1980, Ground water availability on the San Marco property near Mesita in Costilla County, Colorado: Denver, Colorado, Report prepared for San Marco Pipeline Company, 3 vols. with plates.

Possible Role of Eolian Sediment in the Genesis of Bouldery Debris-Flow Deposits on the Lower Flanks of Ute Mountain, Northern Taos Plateau Volcanic Field, New Mexico

By Ralph R. Shroba, Ren A. Thompson, and Cal Ruleman

CHAPTER I

Introduction

Runoff produced by high-intensity rainfall events on steep slopes in alpine to semiarid areas of the western United States locally generates stream flows, hyperconcentrated flows, and debris flows (for example, Meyer and Wells, 1997; Cannon, 2001; Godt and Coe, 2007). The flow properties of these water-sediment mixtures vary chiefly with sediment concentration, size, and sorting (Costa, 1984; Pierson and Costa, 1987). Stream flows are fully turbulent Newtonian flows (water-sediment mixtures) that exhibit flow behavior unaffected by the low concentration of sediment in transport (Meyer and Wells, 1997; Pierson and Costa, 1987). Hyperconcentrated flows are non-Newtonian flows that appear to flow like a liquid but exhibit low yield strength (resistance to flow) and dampened turbulence, owing chiefly to abundant sediment in transport (Pierson and Costa, 1987). Sediment transported by both stream flow and hyperconcentrated flow moves as separate components carried in suspension by fluid lift and in traction by fluid drag (Costa, 1984), and it can be selectively deposited as a result of decrease in velocity or flow depth (Bull, 1972). Stream-flow deposits commonly are poorly to well sorted, clast supported, and crudely stratified (for example, Meyer and Wells, 1997). Hyperconcentrated-flow deposits have sorting and bedding characteristics intermediate between those of stream-flow and debris-flow deposits (for examples, Pierson and Costa, 1987; Meyer and Wells, 1997), and they commonly consist of poorly sorted granules to boulders in an abundant sandy matrix low in silt- and clay-sized particles (Meyer and Wells, 1997; Cannon, 2001). Debris flows, in contrast, are non-Newtonian flows composed of intergranular fluid and high concentrations of sediment that move as a single phase and exhibit considerable yield strength. They can travel long distances on low slopes and do not separate into solid and liquid phases at the time of deposition (Costa, 1984). Debris-flow deposits commonly are unsorted to very poorly sorted and matrix supported, and they lack internal stratification (for example, Meyer and Wells, 1997).

Fan Deposits at Ute Mountain

Coalescing fan deposits of three age groups form an extensive (about 40 km^2) piedmont apron (or bajada) that surrounds Ute Mountain, the northernmost intermediate-composition volcano of the Taos Plateau volcanic field (fig. I–1). The fan apron commonly is about 0.5–3 km wide, has average slopes of about 2.5°–5.5°, and is slightly incised by a network of shallow ephemeral stream channels that radiate outward from Ute Mountain. Younger fan deposits (unit Qf3) are more extensive on the east and southeast sides of Ute Mountain, whereas intermediate-age and older fan deposits (units Qf2 and Qf1, respectively) are more extensive on the southwest side (fig. I–2). Stage I and II carbonate morphology on clasts in younger fan deposits suggests that these deposits accumulated during the Pinedale and Bull Lake glaciations (Machette, 1985, table 2). These fan deposits probably formed under pluvial climatic conditions associated with these glaciations, which occurred about 12 to >30 ka and 120–170 ka, respectively (Pierce, 2004, and references cited therein). Older fan deposits locally overlie higher, older stream alluvium (unit Qao1). These latter deposits predate major downcutting of the Cañon del Rio Grande, which is interpreted to have occurred after about 440 ka (chapter G and field trip day 3, this volume).

Ute Mountain, which rises to an elevation of about 3,080 m, consists of eroded monolithologic dacite domes, flows, and spires that are locally cut by radial dikes. Clasts (granule-sized and larger particles) in the fan deposits are composed of dacite eroded from Ute Mountain as well as a minor amount of olivine andesite eroded from several small outcrops that locally protrude through the fan deposits near the base of Ute Mountain. These lithologies weather chiefly by physical processes, which produce only a minor amount of sand-sized and finer particles that can be incorporated into the matrix of debris-flow and other surficial deposits.

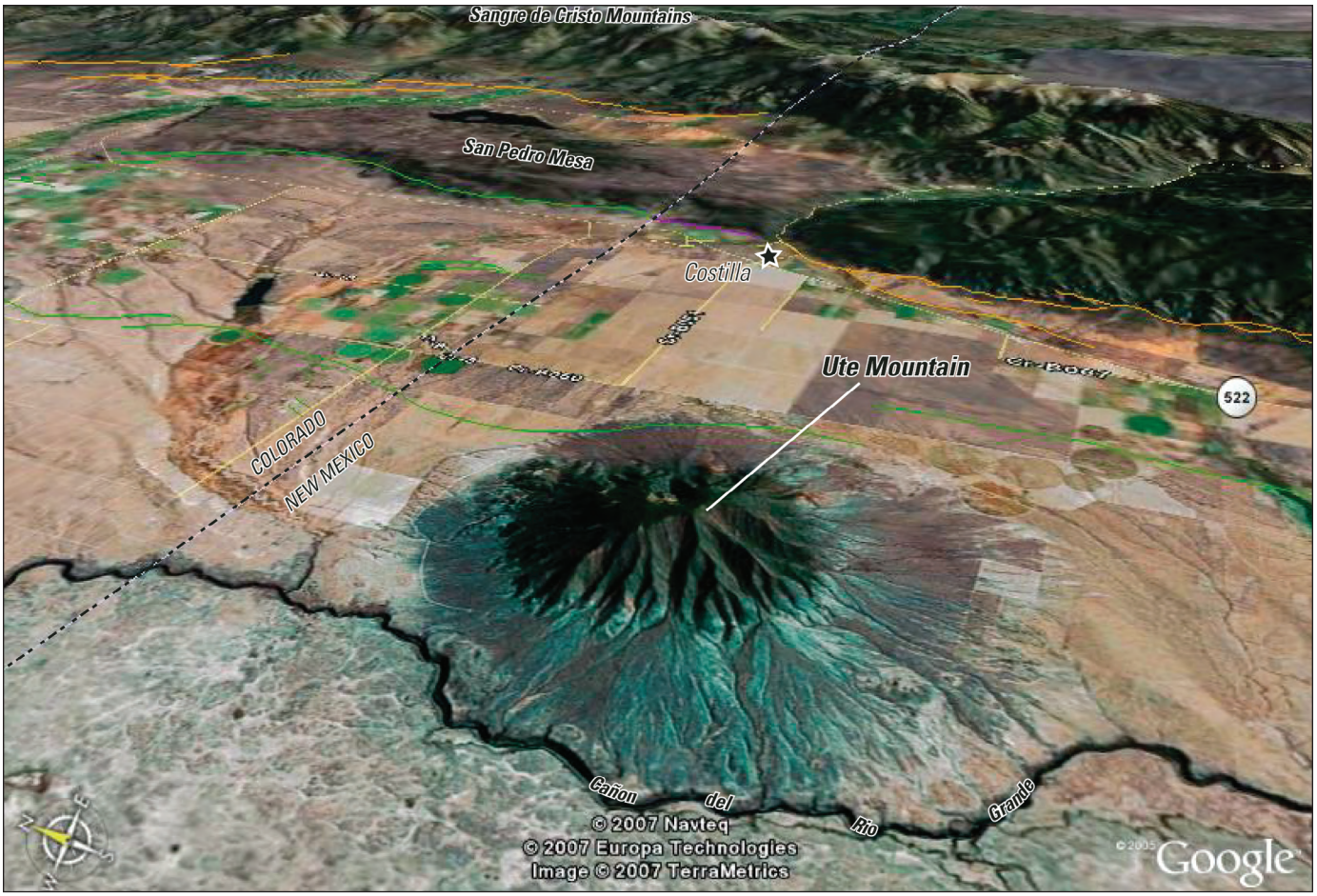

Figure I–1. Oblique aerial view toward the east-northeast of Ute Mountain and adjacent area. Image was obtained from Google Earth. For scale, the distance along the Colorado–New Mexico state line between the Rio Grande and the western margin of San Pedro Mesa is 19 km. Superimposed orange and green lines show locations of mapped faults at the base of San Pedro Mesa and the Sangre de Cristo Mountains. Any use of product, trade, or firm names is for informational purposes only and does not imply endorsement by the U.S. Government.

Fan deposits are locally exposed in small, shallow, widely spaced stream cuts near the lower limit of the fan apron. Grain-size and sorting characteristics of these deposits suggest that they consist of debris-flow deposits along with a subordinate amount of stream-flow (water-laid) deposits within incised channels. Some of the fan deposits probably are hyperconcentrated-flow deposits, because sediment transport at Ute Mountain likely possessed a wide continuum of water-sediment concentrations. Some of the debris-flow deposits on the fan apron probably were eroded by more-fluid late-stage flows and by subsequent sediment-deficient stream flows.

The primary factors that determine flow processes on fans are grain size and areal extent of readily erodable sediment on slopes and in channels (Meyer and Wells, 1997), such as those at Ute Mountain. Much of the sediment in the fan deposits probably was derived from mass-movement deposits on slopes and flash-flood deposits in channels that were mobilized and transported from small (≤1.1 km^2), steep (about 10°–20°) drainage basins on the upper flanks of Ute Mountain by runoff produced by high-intensity and high-volume rainfall events.

Debris-flow deposits near the lower limit of the fan apron commonly consist of unsorted to very poorly sorted, matrix-supported material. Many of the deposits are slightly bouldery and contain abundant cobbles and pebbles; some deposits consist of cobbles and pebbles supported in an abundant sand matrix. Boulders are angular to subangular and commonly 30–90 cm long. Boulders probably decrease in size downslope on the fan apron (Bull, 1972, and references cited therein) and they probably decrease in relative abundance downslope. Clasts make up about 20–70 percent (by volume) of the deposits. Matrix (sand and finer particles) makes up about 30–80 percent (by volume) of the deposits, and it commonly consists of slightly silty to silty, mostly very fine to medium sand and locally very fine to fine sand. These debris-flow deposits form laterally extensive, lobate bodies about 0.5–2 m thick that lack

levees. Levees commonly form on debris-flow deposits that have a relatively high content of boulders (Blair and McPherson, 1998; Blair, 1999a); those near the lower limit of the fan may lack sufficient boulders to form levees. In addition, surface features such as levees may have been muted or obscured by subsequent erosion or deposition of sheetwash deposits.

Shallow ephemeral streams generated chiefly by sediment-charged flash floods deposited many of the stream-flow deposits and probably hyperconcentrated-flow deposits. Near the lower limit of the fan apron, stream-flow deposits commonly consist of poorly sorted, clast-supported, nonbouldery to slightly bouldery gravel that contains abundant cobbles and pebbles. Boulders are subangular and commonly 30–50 cm long. Clasts make up about 80–90 percent (by volume) of the deposits. Matrix makes up about 10–20 percent (by volume), and commonly it consists of very slightly silty, very fine to very coarse sand that locally contains abundant granule-sized particles. Deposits of coarse, open-worked gravel, such as sieve deposits (Hooke, 1967) and boulder berms (Costa, 1984) or boulder jams (Blair, 1987), were not observed but may be locally present in the upper part of the fan apron. Debris-flow and other fan deposits are locally mantled by sheetwash deposits a few tens of centimeters thick. These latter deposits consist of pebbly, plastic, silty, mostly fine to medium and locally very fine to fine sand. The matrix of these deposits may be derived in part from eolian sand. Features characteristic of upper-flow regime sheetflood processes, such as stacked gravelly and sandy couplets and up-fan sloping (antidune) deposits (Blair, 1987, 1999b), were not observed.

Genesis of Debris-Flow Deposits at Ute Mountain

The dacite and minor andesite bedrock at Ute Mountain weather chiefly by physical processes, which produce mostly granule-sized and larger particles. It is likely that these lithologies contribute only a minor portion of the sand and finer particles (about 30–80 percent by volume) in the debris-flow deposits near the lower limit of the fan apron. We suspect that reworked silty eolian sand and silt-rich eolian sediment (loess) are locally important components of the matrix of the debris-flow deposits at Ute Mountain and that they play a key role in the genesis of these deposits. The matrix of these debris-flow deposits is similar in grain size and mineralogy to that of reworked (slightly pebbly) deposits of eolian sand rich in quartz and feldspar that locally underlie some of the debris-flow deposits near the lower limit of the fan apron. The grain size and mineralogy of the <2 mm-sized fractions of reworked eolian sand are similar to those of deposits of silty sand exposed in small nearby outcrops of the upper Santa Fe Group (fig. I–2). Therefore, it is likely that some or much of the silty sand within and below the debris-flow deposits may be reworked by eolian processes from deposits of silty sand in the upper Santa Fe Group. Thick (>3 m) silt-rich deposits, probably loess reworked by sheet flow, are locally present on slopes above washes near the upper limit of the fan apron. Likewise, these silt-rich deposits may also be derived from deposits of the upper Santa Fe Group. These silt-rich deposits consist of slightly sticky, very plastic, slightly sandy silt that contains a minor amount (≥10 percent by volume) of dacite clasts about 0.5–20 cm long. These deposits likely contribute matrix material to the debris flows as well.

Many field and laboratory studies indicate the importance of silt- and clay-sized particles in the genesis of debris flows (for example, Meyer and Wells, 1997; Cannon, 2001; Godt and Coe, 2007; and references cited in these reports). The amount of fine-grained matrix need not be large; for example, the <2-mm-sized fractions of some debris-flow deposits consist of only about 14–16 percent silt (0.5–0.002 mm) and 0–5 percent clay (<0.002 mm) (Cannon, 2001). Primary or reworked deposits of eolian sediment, such as those at Ute Mountain, (1) would retard infiltration and thus promote storm runoff and overland flow on hillslopes, (2) are easily eroded by runoff-related processes, and (3) could be readily entrained within fluid flows by means of progressive sediment bulking and could serve as fine-grained matrix material that promotes the support and transport of granule- to boulder-sized clasts. Silt- and clay-sized particles derived from eolian sediments would help to sustain high pore-fluid pressures in debris-flow slurries (Iverson, 1997, 2003; Meyer and Wells, 1997). High pore-fluid pressures, in turn, would reduce viscosity and internal friction as well as promote flow mobility (Pierson and Costa, 1987; Iverson, 1997). Sediment entrained by overland flow is a dominant mechanism for initiating debris flows and generating debris-flow deposits in steep terrain of the western United States (for example, Meyer and Wells, 1997; Cannon, 2001; Godt and Coe, 2007), and local debris flows may be a dominant mechanism at Ute Mountain.

In addition, the relatively high moisture-holding capacity of primary or reworked loess may locally promote the development of small, thin (≥1 m), infiltration-triggered landslides and small debris flows at Ute Mountain similar to those investigated by Godt and Coe (2007).

Acknowledgments

We appreciate the constructive and helpful comments of James Cole (USGS) and Margaret Berry (USGS), who reviewed a preliminary version of this manuscript. However, any errors that may remain are the responsibility of the authors.

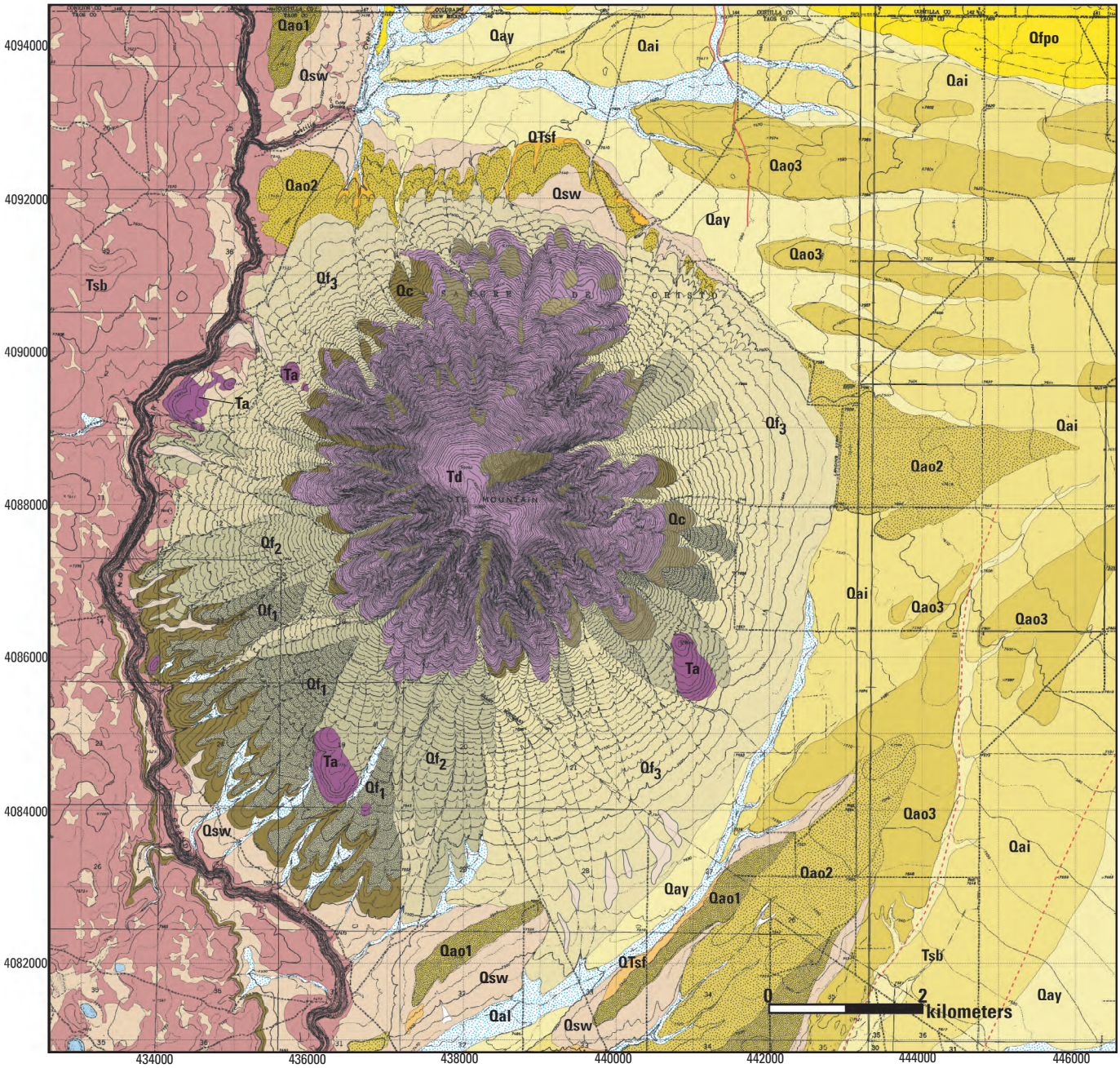

Figure I–2. Generalized geologic map of Ute Mountain and adjacent area. Map units and their known or inferred ages are as follows: Qa, stream alluvium in active channels and flood plains (late Holocene); Qfpo, older flood-plain alluvium (Holocene); Qay, younger stream alluvium (Holocene and late Pleistocene); Qsw, sheetwash deposits (Holocene and late Pleistocene); Qc, colluvium, undivided (Holocene and late Pleistocene); Qf3, younger fan deposits (late and middle Pleistocene); Qai, intermediate-age stream alluvium (middle Pleistocene); Qf2, intermediate-age fan deposits (middle Pleistocene); Qf1, older fan deposits (middle Pleistocene); Qao3, lower older stream alluvium (middle Pleistocene); Qao2, intermediate-height older stream alluvium (middle Pleistocene); Qao1, higher older stream alluvium (middle Pleistocene); QTsf, upper Santa Fe Group (middle Pleistocene to middle (?) Pliocene); Td, dacite (late Pliocene); Tsb, Servilleta Basalt (early Pliocene); Ta, andesite (early? Pliocene). Red lines show locations of known (solid) and inferred (dotted) faults.

References Cited

Blair, T.C., 1987, Sedimentary processes, vertical stratification sequences, and geomorphology of the Roaring River alluvial fan, Rocky Mountain National Park, Colorado: Journal of Sedimentary Petrology, v. 57, p. 1–18.

Blair, T.C., 1999a, Sedimentology of the debris-flow-dominated Warm Spring Canyon alluvial fan, Death Valley, California: Sedimentology, v. 46, p. 941–965.

Blair, T.C., 1999b, Sedimentary processes and facies of the waterlaid Anvil Spring Canyon alluvial fan, Death Valley, California: Sedimentology, v. 46, p. 913–940.

Blair, T.C., and McPherson, J.G., 1998, Recent debris-flow processes and resultant form and facies of the Dolomite alluvial fan, Owens Valley, California: Journal of Sedimentary Research, v. 68, p. 800–818.

Bull, W.B., 1972, Recognition of alluvial-fan deposits in the stratigraphic record, *in* Rigby, J.K., and Hamblin, W.K., eds., Recognition of ancient sedimentary environments: Society of Economic Paleontologists and Mineralogists Special Publication 16, p. 63–83.

Cannon, S.H., 2001, Debris-flow generation from recently burned watersheds: Environmental & Engineering Geoscience, v. 7, p. 321–341.

Costa, J.E., 1984, Physical geomorphology of debris flows, chap. 9, *in* Costa, J.E., and Fleisher, P.J., eds., Developments and applications in Geomorphology: New York, Springer-Verlag, p. 268–317.

Godt, J.W., and Coe, J.A., 2007, Alpine debris flows triggered by a 28 July 1999 thunderstorm in the central Front Range, Colorado: Geomorphology, v. 84, p. 80–97.

Hooke, R. Le B., 1967, Processes on arid-region alluvial fans: Journal of Geology, v. 75, p. 438–460.

Iverson, R.M., 1997, The physics of debris flows: Reviews of Geophysics, v. 35, p. 245–296.

Iverson, R.M., 2003, The debris flow rheology myth, *in* Rickenmann, D., and Chen, C., eds., Debris flow hazards mitigation—Mechanics, prediction, and assessment: Rotterdam, The Netherlands, Millpress, p. 303–314.

Machette, M.N., 1985, Calcic soils of the southwestern United States, *in* Weide, D.L., ed., Soils and Quaternary geology of the southwestern United States: Geological Society of America Special Paper 203, p. 1–21.

Meyer, G.A., and Wells, S.G., 1997, Fire-related sedimentation events on alluvial fans, Yellowstone National Park, U.S.A.: Journal of Sedimentary Research, v. 67, p. 776–791.

Pierce, K.L., 2004, Pleistocene glaciation of the Rocky Mountains, *in* Gillespie, A.R., Porter, S.C., and Atwater, B.F., eds., The Quaternary Period in the United States: Amsterdam, Elsevier, p. 63–76.

Pierson, T.C., and Costa, J.E., 1987, A rheologic classification of subaerial sediment-water flows, *in* Costa, J.E., and Wieczorek, G.F., eds., Debris flows/Avalanches—Process, recognition, and mitigation: Geological Society of America Reviews in Engineering Geology, v. 7, p. 1–12.

An Overview of the Sangre de Cristo Fault System and New Insights to Interactions Between Quaternary Faults in the Northern Rio Grande Rift

By Cal Ruleman and Michael Machette

CHAPTER J

Abstract

On the basis of differences in geomorphic expression, we propose to subdivide the Sangre de Cristo fault system into three distinct parts: the northern Sangre de Cristo fault zone, the central Sangre de Cristo fault zone, and the southern Sangre de Cristo fault zone. In this report, we summarize evidence of Pliocene and Quaternary tectonic activity on these three fault zones as determined by previous studies and by our recent investigations along the Latir Peaks section of the southern Sangre de Cristo fault zone, which further indicates the interaction between two of the three parts. The 50–55 km long Latir Peaks section (in northernmost New Mexico) of this fault zone is characterized by a linear, precipitous range front that has sharp, basal, faceted spurs and scarps that vertically offset alluvium as much as 7.8 m. This study and previous investigations have quantified long-term (about 4 m.y.) slip rates of 0.1–0.2 mm/yr along this section of the southern Sangre de Cristo fault zone. Contrary to these neotectonic assessments, our recent surficial geologic mapping indicates probable late-middle to late Pleistocene vertical tectonic activity rates that are only one-half (0.06 mm/yr) of the previously reported long-term slip rates, suggesting that short-term (<100 k.y.) slip rates change within the long-term tectonic history, as appears to be the case for the northern Sangre de Cristo fault. In comparison, the central Sangre de Cristo fault zone in southern Colorado has a more subdued geomorphic expression than the northern and the southern Sangre de Cristo faults but a higher late Pleistocene slip rate (0.17 mm/yr). Thus, we propose that the foci of tectonic activity on the Sangre de Cristo fault system has shifted from the southern and northern parts of the fault system to the central part during the late Quaternary; before this shift, the ends of the fault system were more active than at present, as shown by their impressive topographic expression.

Introduction

The Sangre de Cristo fault system, which is the structure that bounds the eastern margin of the northern Rio Grande rift in the San Luis Basin, consists of a complex array of range-bounding, piedmont, and intrabasin faults (fig. J–1). This 250-km-long fault system extends from Poncha Pass, Colo., south to near Taos, N. Mex., and is composed of three discrete parts, herein described from north to south. Currently, the U.S. Geological Survey National Seismic Hazard maps divide this fault (that is, fault system) into two faults (that is, two zones): the northern Sangre de Cristo fault and the southern Sangre de Cristo fault, having potential rupture lengths of 185 km and 104 km, respectively (Haller and others, 2002). However, recent paleoseismic investigations, morphometric analyses of scarps and range-fronts, and mapping of geologic structures in the fault zone's footwall that could create asperities in the fault and that could truncate lateral propagation of individual Quaternary faulting events provides criteria for subdividing the fault system into three parts: the northern Sangre de Cristo fault zone, central Sangre de Cristo fault zone, and southern Sangre de Cristo fault zone.

As herein defined, the northern Sangre de Cristo fault zone extends about 104 km from Poncha Pass along the northeastern margin of the San Luis Valley, east of the Great Sand Dunes, to the southern flank of the Blanca Peak massif, a young structure whose uplift may have begun 5 Ma ago (Wallace, 2004). The central Sangre de Cristo fault zone extends about 60 km from the south flank of the Blanca Peak massif through Fort Garland, along the western margin of Culebra Range, and along the east side of the Culebra graben as far south as the northern border of New Mexico. The southern Sangre de Cristo fault zone extends about 96 km from southwest of San Luis, Colo. (where it overlaps the central portion of the fault zone), along the western side of San Pedro Mesa (see chapter B, stop B9) and the Sangre de Cristo Mountains of New Mexico, to southeast of Taos, N. Mex., near the small community of Talpa (Personius and Machette, 1984). Here, it merges with the northeast-trending Embudo fault zone. The following summary of tectonic activity along each part of the Sangre de Cristo fault system is based primarily on

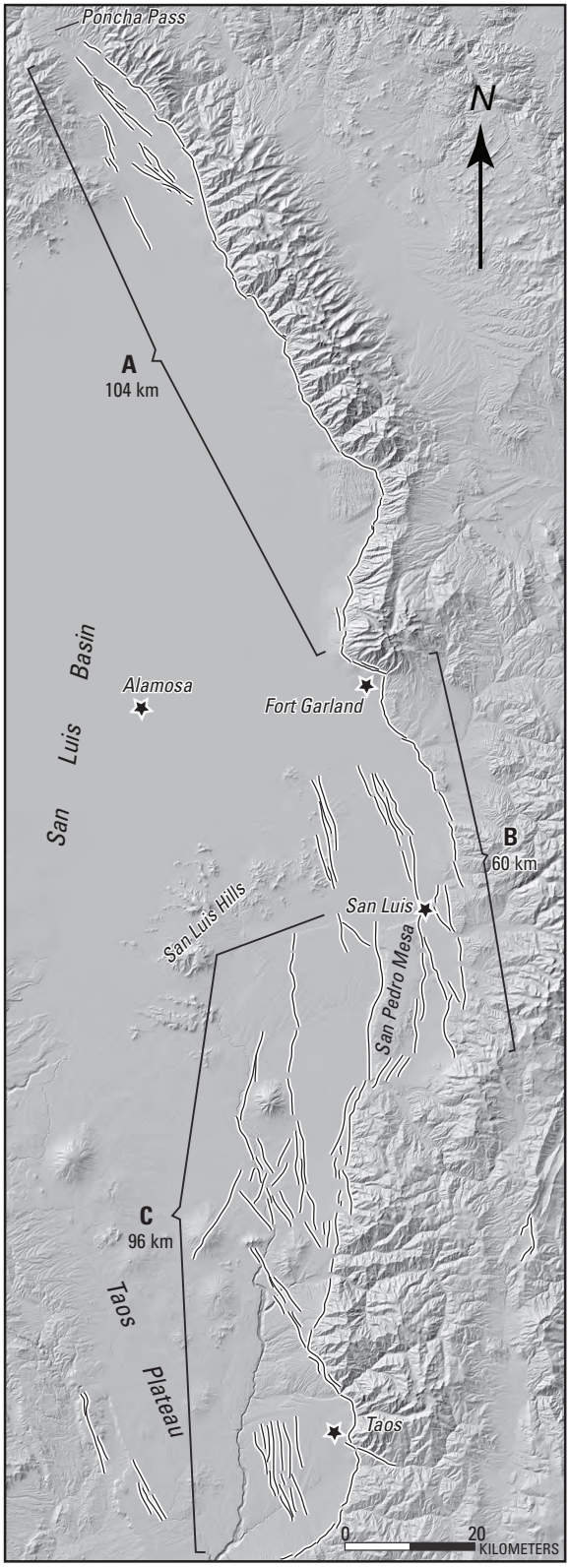

Figure J–1. Sangre de Cristo fault system and fault zone boundaries. Fault zone boundaries shown as follows: A, northern; B, central; C, southern. Fault traces modified from U.S. Geological Survey (2005) and Menges (1990).

modified information from the U.S. Geological Survey's Database of Quaternary faults and folds (U.S. Geological Survey, 2005; http://earthquake.usgs.gov/regional/qfaults/).

Northern Sangre de Cristo Fault Zone

The northern Sangre de Cristo fault zone is characterized by a precipitous, linear range front with well-developed basal faceted spurs, deeply incised canyons in the footwall, and geomorphically fresh fault scarps on late Pleistocene and Holocene deposits (McCalpin, 1982, 1986; Colman and others, 1985). In the San Luis Valley, the deepest part of the San Luis Basin coincides with the northern Sangre de Cristo fault zone (Gaca and Karig, 1965). The northern fault zone has been previously divided into four sections (fig. J–2) listed from north to south: the 19-km-long Villa Grove fault, the 8-km-long Mineral Hot Springs fault, the 80-km-long Crestone section, and the 26-km-long Zapata section (Widmann and others, 2002; USGS, 2005). Average single-event vertical displacements along the northern Sangre de Cristo fault zone range between 1.5 and 2.5 m, which suggest earthquakes having probable moment magnitudes (M_w) of 6.8–7.1 (U.S. Geological Survey, 2005).

The northern end of the northern Sangre de Cristo fault zone is marked by a dramatic narrowing of the San Luis Basin and a potentially active graben that has Quaternary displacement on both east- and west-dipping, basin-bounding faults, the Mineral Hot Springs fault on the west and Crestone section on the east of the fault zone, respectively. The northwest-trending, down-to-the-west Villa Grove fault consists of multiple fault strands that cut obliquely across the basin and connect the Mineral Hot Springs fault with the Crestone section of the northern Sangre de Cristo fault zone. This Villa Grove fault has predominantly southwest-facing scarps (synthetic to the Crestone section) on Pinedale (about 15 ka), Bull Lake (about 130 ka), and pre-Bull Lake equivalent deposits, the latter of which is offset by as much as 14 m (McCalpin, 1981). The Mineral Hot Springs fault has scarps on Bull Lake and Pinedale equivalent deposits (Colman and others, 1985; Kirkham and Rogers, 1981); however, the tectonic origin of these escarpments is uncertain (J.P. McCalpin, 1997, oral commun. cited on http://earthquake.usgs.gov/regional/qfaults/). On the basis of its apparent association with the northern Sangre de Cristo fault zone and the Mineral Hot Springs fault, we include the Villa Grove fault as part of the northern Sangre de Cristo fault zone. It seems probable that the 8-km-long Mineral Hot Springs fault and the 26-km-long Villa Grove fault could rupture coincidently with large events on the Crestone section.

For the northern Sangre de Cristo fault zone and general basin structure, Kellogg (1999) described a "perched basement wedge" of Precambrian metamorphic rocks in the footwall (fig. J–3), resulting from preexisting (Laramide) thrust faulting and Neogene normal faulting. Neogene extensional faulting utilizes preexisting thrust fault planes as reactivated normal

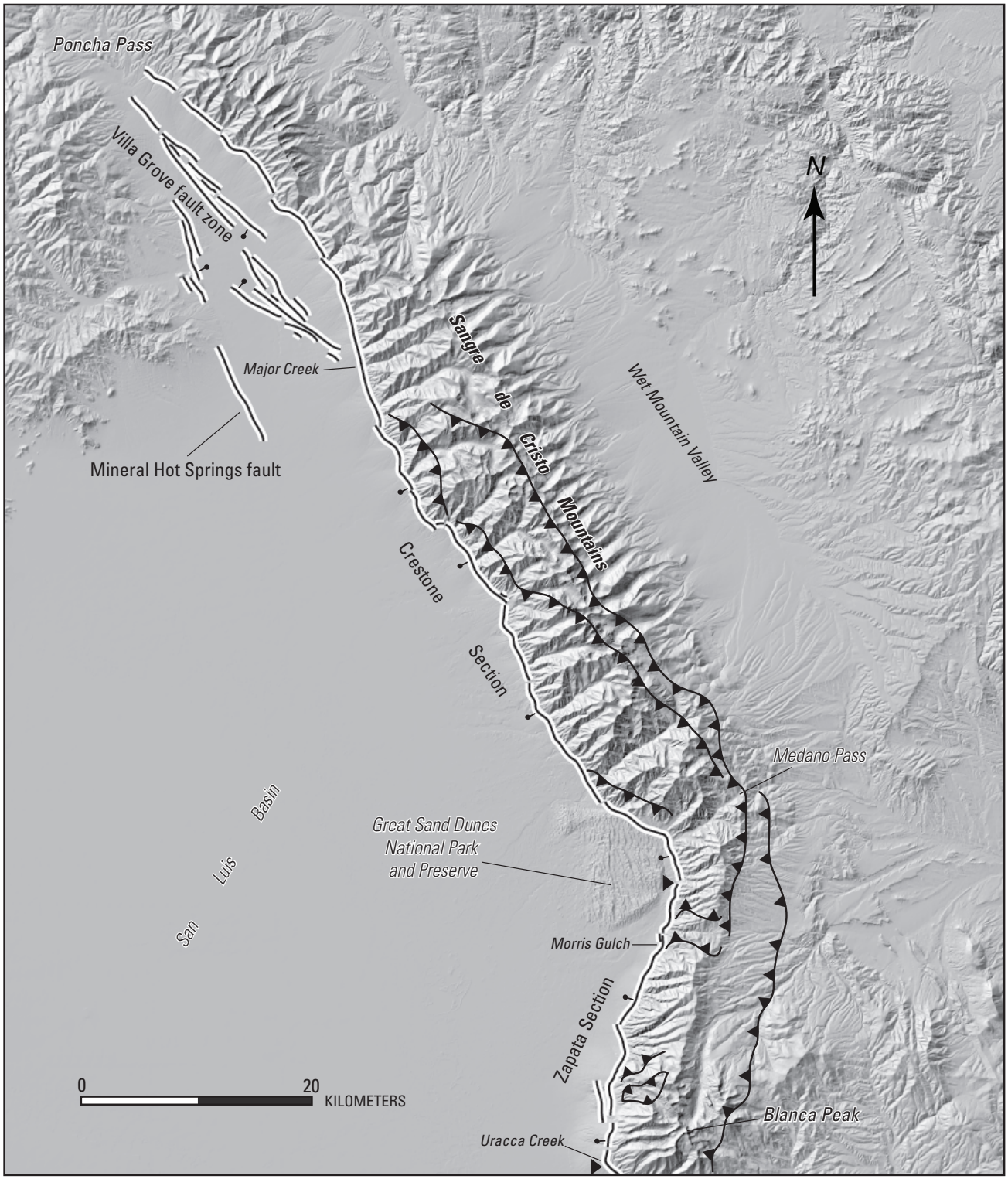

Figure J–2. Shaded relief map of the northern Sangre de Cristo fault zone, showing sections discussed in text. Highlighted black piedmont and intrabasin lines are Quaternary normal faults from the U.S. Geological Survey Quaternary fault and fold database; bar and ball symbol is on downthrown side. Lines with teeth are thrust faults from Tweto (1979). Changes in range-bounding normal fault trends coincide with Laramide thrust faults possibly reactivating thrust ramps as normal faults, creating a "perched basement wedge" (Kellog, 1998). The section boundaries between the Crestone and Zapata sections and the northern and southern fault zones near Great Sand Dunes National Park and Preserve and Urraca Creek are illustrated by a black triangle. Shaded relief map processed and created by Ted Brandt (USGS).

faults. The general geometry of faults developed in the hinge of a fault-propagated fold allows for subsidiary faults to sole into the main basin-bounding fault plane. With large events on the main fault, these subsidiary faults can be activated coseismically (for example, the 1959 Hebgen Lake event, where both the Red Canyon and Hebgen Lake faults were activated during one earthquake).

The Crestone section spans most of the northern Sangre de Cristo fault zone and is the main range-bounding fault from Poncha Pass to Great Sand Dunes National Park and Preserve (GSDNPP). In a trenching study at Major Creek, McCalpin (1986) indicates a surface-rupturing earthquake about 8 ka, a preceding event between 8 and 13 ka, and a still earlier event between 13 and 35 ka. Largely on the basis of surface offsets of Bull Lake and pre–Bull Lake–equivalent deposits, McCalpin also inferred three prior events between 35 ka and 140 ka and possibly 6 to 12 events between 140 ka and approximately 400 ka. From these data, he calculated slip rates that vary markedly during 100 k.y. intervals; three events took place in the last 35 ka and three other events during the preceding 100 ka (35–140 ka). His long-term (>100 k.y.) slip rates are roughly 0.1–0.2 mm/yr; short-term intervals (<100 k.y.) decrease or increase by approximately 50 percent. Such fluctuations in slip rate are well documented on other major Basin and Range faults, particularly the Wasatch fault zone in Utah (Machette and others, 1992).

The Zapata section extends south-southwestward from the Crestone section at the Great Sand Dunes National Park and Preserve, and it creates almost a 90° bend in the fault zone and a deep embayment in the range front. Older structures in the footwall of the fault apparently control the geometry of this embayment as mapped by Tweto (1979) and Bruce and Johnson (1991); preexisting thrust faults may have created asperities in the fault system that could arrest the propagation of fault ruptures. However, precise structural relations and controls on Quaternary normal faulting have not been determined.

Along the Zapata section, McCalpin (1982, 1986) mapped scarps on Pinedale-age deposits that are 4–7 m high, and trenching studies suggest two post-Pinedale surface-rupturing events (McCalpin, 1986, 2006). At Urraca Creek, McCalpin (1986) trenched a piedmont scarp approximately 1.2 km (0.75 mi) northwest of the range front and determined that the most recent event occurred between 5640±100 ^{14}C yr B.P. and 8 ka and produced approximately 2.0 m of vertical displacement. In a more recent study, McCalpin (2006) identified two post-Pinedale events at Morris Gulch of which the most recent event occurred between 5300 and 5500 ^{14}C yr B.P. He notes that the broad time constraints on the most recent event at these two locations allow these scarps to be contemporaneous; however, the potential 2–3 k.y. interval between the most recent events on the Crestone section (at Major Creek) and the Zapata section (at Urraca Creek and Morris Gulch) likely suggest a behavior of fault contagion and interaction, rather than contemporaneous coseismic displacement.

Central Sangre de Cristo Fault Zone

The northern end of the central Sangre de Cristo fault zone is marked by a major eastward step in the range at Blanca Peak. From here, the fault zone extends southward 59 km along the eastern side of the Culebra graben (fig. J–4) (Wallace, 2004; Kirkham and others, 2005) in an area named the Culebra reentrant by Upson (1939). Blanca Peak (14,345 ft), which is the highest peak of the Blanca massif, creates a major salient in the range and is bounded on the south by the 7-km-long Blanca section of the central Sangre de Cristo fault zone. Although it was originally included as a section of the northern Sangre de Cristo fault (Widmann, 2002; U.S. Geological Survey, 2005), we include the Blanca section with the central Sangre de Cristo fault zone on the basis of geomorphic, geometric, and structural data. McCalpin (1982, 1986) reported

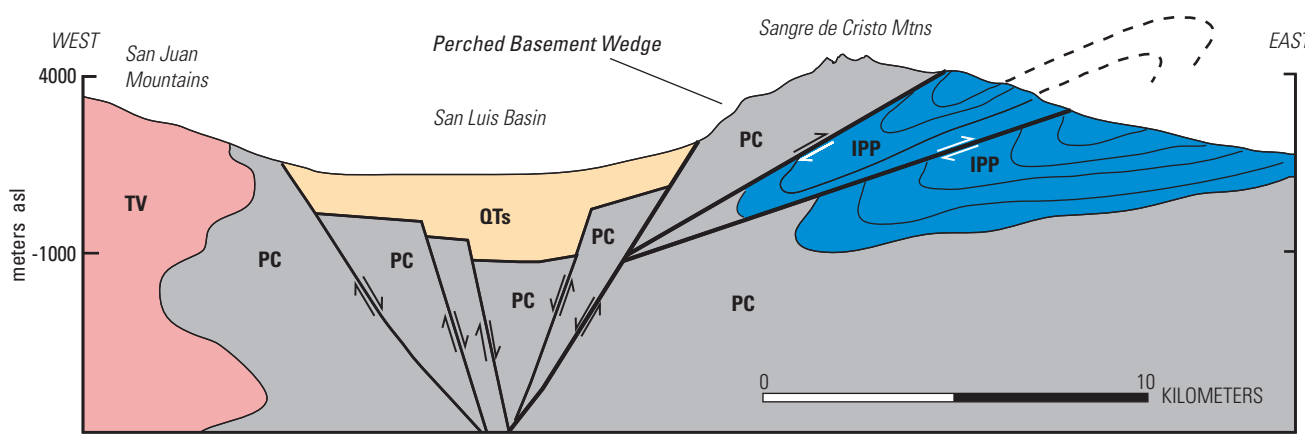

Figure J–3. Schematic cross section showing a perched basement wedge and relations between preexisting thrust faults and Cenozoic normal faults. Arrows indicate sense of motion on faults. Units as follows: PC, Precambrian crystalline rocks; PP, Pennsylvanian and Permian sedimentary rocks; Tv, Tertiary volcanic rocks; QTs, Tertiary and Quaternary basin fill.

that only one post-35 ka event has occurred on the Blanca section and, thus, only one-half of the events recognized along the adjacent northern Sangre de Cristo fault have occurred along this section. In addition, complex bedrock fault structures mapped in the footwall (A.R. Wallace, written commun., 2005) suggest that preexisting structures control the east-west-oriented Quaternary faulting on this section. It has yet to be determined if events on the Blanca section are associated with faulting on the San Luis section of the central Sangre de Cristo fault zone or on the northern Sangre de Cristo fault zone.

From the eastern end of the Blanca section, the San Luis section of the central Sangre de Cristo fault zone turns abruptly south and extends south-southeast through Fort Garland, where scarps of differing heights are formed on middle to latest Pleistocene alluvium. The range front along the San Luis section is much more subdued than along either the northern or southern Sangre de Cristo fault zones. Neogene and Quaternary faulting can be described as a complex right-stepping pattern of range-bounding and intrabasin faults within the Culebra graben (Kirkham and Rogers, 1981; Kirkham and others, 2005; Machette and others, 2007; Thompson and others, 2007). Low-lying foothills underlain by Pliocene to Miocene Santa Fe Group rocks and sediment bound the eastern side of the fault, and the crest of the Sangre de Cristo Mountains is as much as 20 km east of the range-bounding fault. This subdued range-front morphology contrasts with the steep, precipitous front to the range along the northern and southern Sangre de Cristo fault zones. Most of the central Sangre de Cristo fault zone has discontinuous scarps that are best preserved on middle Pleistocene and older deposits (Colman and others, 1985), although more recent mapping by Thompson and others (2007) shows that almost the entire section presents evidence for latest Pleistocene or early Holocene surface rupturing. The overall geomorphic expression of the central Sangre de Cristo fault zone indicates a considerable difference in its long-term Cenozoic tectonic activity rate compared with activity rates in the adjoining northern and southern Sangre de Cristo fault zones.

Crone and Machette (2005) and Crone and others (2006) conducted the only paleoseismic investigation along the central Sangre de Cristo fault zone. They excavated two trenches across the San Luis section at Rito Seco (5 km northeast of San Luis, Colo.) that revealed evidence for four events in the past 50 ka. The most recent event (paoleoevent (PE)1) had a preferred age of 9.0±2.0 ka (optically stimulated luminescence (OSL) and C^{14} dating); earlier events were about 23.4±2 ka (PE2; OSL dating), about 30.3 (PE3; OSL dating), and about 45.0±4.3 ka (PE4; OSL dating). The oldest deposits in the trenches (about 48 ka) have a minimum surface offset of 6.8 m, which suggests a minimum late Pleistocene slip rate of 0.17 mm/yr and recurrence intervals that average about 12 k.y. These late Pleistocene slip rates contrast with the overall (long-term) geomorphic expression of the central Sangre de Cristo fault zone, further suggesting variations in the slip rate of the Sangre de Cristo fault system during the past 5 m.y. (Pliocene to Pleistocene time).

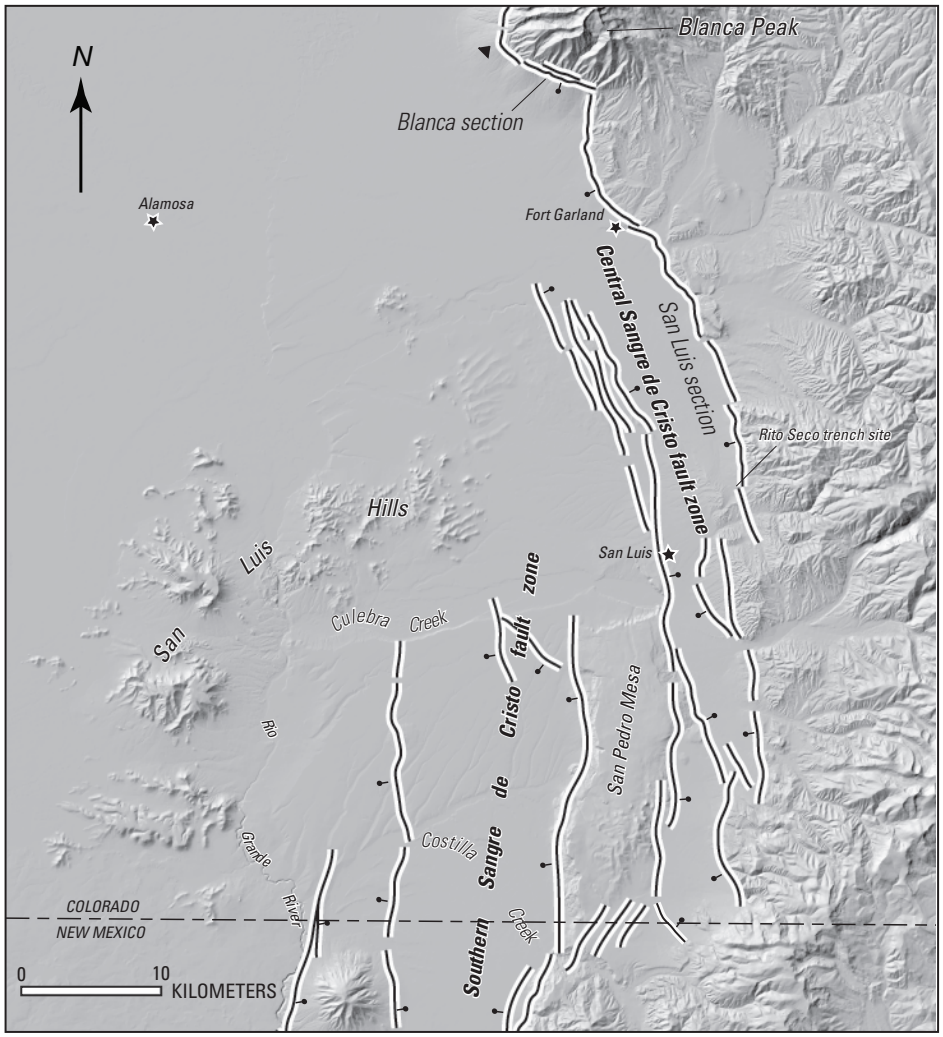

Figure J–4. Central Sangre de Cristo fault zone. Highlighted black lines are Quaternary faults, bar and ball on downthrown side. Section boundary between northern and central fault zones is marked by the black triangle. Heavy white lines along east side of San Luis Hills are older pre-Quaternary faults. Shaded-relief map created by Ted Brandt (USGS).

Southern Sangre de Cristo Fault Zone

The southern Sangre de Cristo fault zone is the only part of the larger fault system that we see in New Mexico on the third day of the Friends of the Pleistocene field trip (see chapter C, this volume). The southern Sangre de Cristo fault zone extends about 96 km from southwest of San Luis, Colo., to near the small community of Talpa, N. Mex. (Personius and Machette, 1984), where it merges with the northeast-trending Embudo fault zone (fig. J–5). Previous work on this part of the fault system has been mainly based on surficial geologic mapping and morphometric analysis of fault scarp profiles (Machette and Personius, 1984; Kelson, 1986; Menges, 1988; Thompson and Machette, 1989), although Kelson and others (2004) trenched the fault near Taos. On the basis of a compilation by Machette and others (1998), the southern Sangre de Cristo fault zone is subdivided into five geometric sections, listed north to south (fig. J–5): San Pedro Mesa (24 km), Urraca (22 km), Questa (18 km), Hondo (22 km), and Cañon (15 km) (U.S. Geological Survey, 2005). There is a major eastward step between the central Sangre de Cristo fault zone and Urraca section, which coincides with the latitude of the southern extent of the Culebra graben. A northeast-trending set of subsidiary Quaternary faults provide a structural link between the southern and the central Sangre de Cristo fault zones across the southern end of San Pedro Mesa (Thompson and others, 2007), but scarps on these faults are largely concealed by late Quaternary landslides that could be of seismogenic origin. On the basis of the geomorphic expression of these fault scarps, morphometric analyses of scarps, and surficial mapping (C.A. Ruleman, unpub. mapping, 2007), we consolidate the Urraca and Questa sections into the new Latir Peaks section of the southern Sangre de Cristo fault zone.

Our studies of the southern Sangre de Cristo fault zone are focused on the northern 64 km of the fault zone (San Pedro and Latir Peaks sections), which contains our map areas in the Alamosa and Wheeler Peak 1:100,000-scale geologic maps, respectively. We make field trip stops at both of these sections. We discuss the San Pedro section at field trip stop B9 (chapter B, this volume), and the Latir Peaks section at field trip stops C6 and C7 (chapter C, this volume).

The San Pedro section has a 24-km-long fault trace that forms the curvilinear western side of San Pedro Mesa, which is capped by Pliocene Servilleta Basalt (4.0±0.3 Ma). Massive landslides largely conceal the fault, but we recognize a few discontinuous scarps on alluvium and colluvium. Thompson and others (2007) mapped offsets of middle and late Pleistocene alluvium; however, the inferred age (latest Pleistocene) for the most recent event is based on the fault being buried by late Pleistocene to Holocene landslides of probable seismogenic origin. Long-term slip rates for this section are based on vertical displacements of the Servilleta Basalt (4.0±0.3 Ma) and range from 0.075 to 0.1 mm/yr (see chapter B, this volume). These long-term rates increase southward towards New Mexico.

The Latir Peaks section of the southern Sangre de Cristo fault zone is about 40 km long. It extends southward from Costilla to San Cristobal, N. Mex. (fig. J–5), as the main range-bounding fault along the Latir Peaks of the Taos Mountains (a local part of the longer Sangre de Cristo Mountains). This section has been previously divided into the Urraca

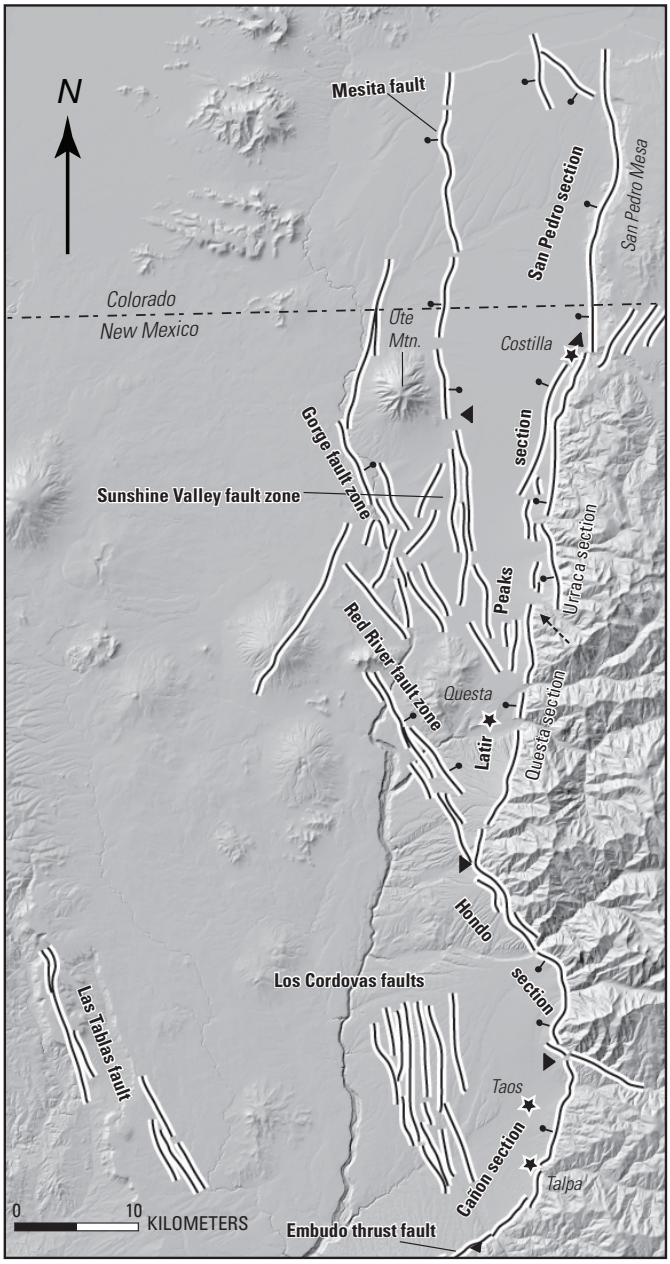

Figure J–5. Quaternary faults along the southern Sangre de Cristo fault zone. Highlighted black lines are Quaternary normal faults with bar and ball on downthrown side. Embudo thrust fault has teeth on the hanging wall. Black triangles mark section boundaries discussed in text. Arrow shows location of previously subdivided Urraca and Questa sections to be consolidated into the Latir Peaks section. Shaded-relief map created by Ted Brandt (USGS).

section (on the north) and Questa section (on the south) (U.S. Geological Survey, 2005), and it includes the Cedro Canyon and Urraca Ranch piedmont faults of Machette and Personius (1984). The Latir Peaks section has a steep, precipitous, linear range front with well-developed faceted spurs, deeply incised canyons on the footwall, and discontinuous range-front and piedmont scarps on late middle Pleistocene to Holocene alluvium and colluvium (Menges, 1987, 1988, 1990). Pazzaglia (1989) mapped range-front deposits along this section of the fault zone and showed offsets in late Pleistocene fan gravels. More-detailed unpublished maps by C.A. Ruleman (2007) show differing ages of faulted deposits and amounts of offset on these deposits, but a detailed paleoseismic study for this section (including trenching and dating) has not been completed.

Range-front scarps are primarily preserved on late-middle Pleistocene alluvium and Holocene colluvium (C.A. Ruleman, unpub. mapping, 2007). Piedmont scarps are mapped on late-middle and late Pleistocene fan deposits (about >130 ka). The lack of well-preserved fault scarps on late Pleistocene alluvium along the range front suggests that late Pleistocene fan-head incision occurred at the canyon mouths and that late Pleistocene deposits prograde into the basin. South of Questa, the fault is expressed as a linear range front with discontinuous, subtle scarps at the bedrock-colluvium junction, which suggests but doesn't require late Quaternary faulting. The adjacent piedmont is deeply dissected with little to no late Pleistocene to Holocene deposition, leaving sparse evidence of latest Quaternary faulting events.

Menges (1990) discusses variations in Pliocene to Quaternary slip rates along this section and notes that long-term (>1 Ma) slip rates are several times greater than those indicated by the late Pleistocene to Holocene record, suggesting temporal changes in slip rates in 100-k.y.-long time spans. In support of his observations, fault scarps on late middle Pleistocene deposits (about >130 ka) have surface offsets between 5.3 and 7.8 m, yielding minimum slip rates of 0.04–0.06 mm/yr for the last 130 k.y. (see stops C6 and C7, chapter C, this volume). However, vertical offset on the Servilleta Basalt (4.6–3.5 Ma; ages of faulted basalt are uncertain because subsurface basalts have not been dated) just south of Costilla, N. Mex. (see stop C7, chapter C, this volume), indicates a long-term slip rate of 0.14–0.16 mm/yr, indicating slip rates that change by a factor of 2–3 during 100-k.y.-long seismic cycles (fig. J–6). A plot of scarp height versus maximum slope angle for fault scarp profiles along the Latir section suggests that only one Holocene event has displaced latest Pleistocene to Holocene deposits, but larger (older) scarps have a steepened bevel caused by this event (fig. J–7). Rough calculations suggest that late Quaternary recurrence intervals are at least 20–40 k.y.

In addition to these observations along the Latir Peaks section, some bedrock escarpments in the footwall block of the range are suspected to be of seismic origin from Quaternary earthquakes on the main range-bounding fault. The continuity of these scarps in rapidly eroding, steep terrain indicates that they were reactivated throughout Bull Lake and Pinedale glacial cycles in order to preserve them. Lipman and Reed (1989) mapped numerous preexisting faults in the Questa caldera complex, which formed during a major 25-Ma caldera eruption. If properly oriented to the modern stress regime, then these preexisting volcanogenic faults might be reactivated and slip during large earthquakes on the Sangre de Cristo fault zone, such as occurred with the interaction of the Red Canyon and Hebgen Lake faults during the 1959 M_s7.5 Hebgen, Mont., earthquake (Myers and Hamilton, 1964). These previously formed volcanogenic faults crosscut and possibly sole into preexisting Laramide thrust faults creating a complex array of faults to be reactivated during large events on the main range-bounding fault as previously described along the northern Sangre de Cristo fault zone.

The 22-km-long Hondo section to the south was previously described and mapped by Kelson (1986) and Menges (1988). The range-front morphology of this section is very similar to that of the Latir Peaks section—it is steep and linear, and it has well-defined basal faceted spurs. Menges (1990) reported early to middle Holocene displacement and documented two slip rates along this section of the southern Sangre de Cristo fault zone: (1) a slow, late-middle Pleistocene to Holocene (about 130 ka to present) rate of 0.03–0.06 mm/yr, and (2) a faster post-Pliocene (<4 Ma) rate of 0.12–0.23 mm/yr (Menges, 1988). The contrast in long-term (>1 Ma) and short-term (<200 ka) slip rates are consistent with rates quantified by Ruleman and others (chapter C, this volume) for the Latir Peaks section and by McCalpin (1982) for the northern Sangre de Cristo fault zone.

To the south, the 15-km-long Cañon section is composed of the Taos Pueblo and Cañon faults of Machette and Personius (1984); as such it extends southward from the Rio Pueblo de Taos to the Rio Grande del Rancho, which is about 1 km south of the small community of Talpa. The boundary between the Hondo and Cañon sections is marked by a salient in the range front that extends about 1.5 km to the northwest. Discontinuous, northwest-facing scarps are present along the range front. This part of the range front has less precipitous basal faceted spurs and canyons are not incised as deeply compared with the area to the north. Previous mapping by Machette and Personius (1984), Kelson (1986), and Menges (1988) indicates that late Pleistocene and possibly Holocene deposits are offset along this section. Machette and Personius (1984) measured scarp heights of 2–5 m on early(?) to late Pleistocene deposits.

Along the Cañon section, Kelson and others (2004) excavated one trench across a scarp on late Pleistocene alluvium near the Taos Pueblo and concluded that one surface-rupturing event occurred between 10 ka and 30 ka, producing 1.5 m of vertical offset. Inconclusive timing of previous events did not allow a recurrence interval to be estimated. However, on the basis of our cursory analyses of their trench maps (Kelson and others, 2004, figs. 4 and 5), it seems unlikely that deposits with Bk stage III+ morphology soil development are offset more than 5–10 m. This development of a calcic horizon suggests that these deposits correlate with

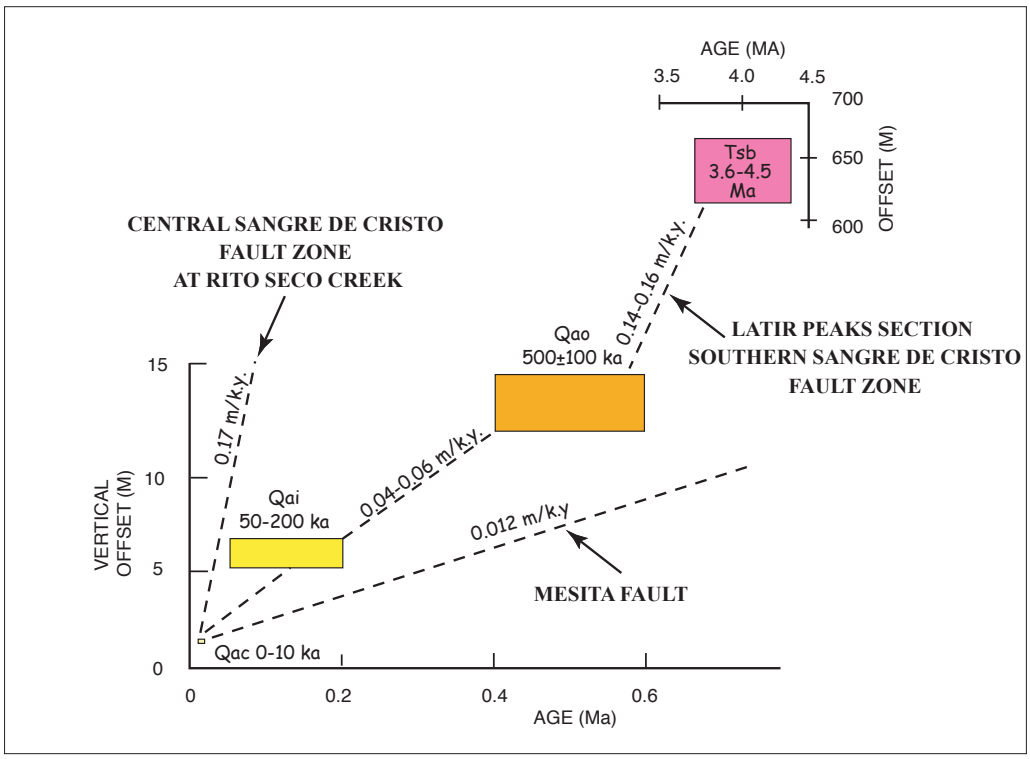

Figure J–6. Surface offset versus age of geologic units along the Latir Peaks section of the southern Sangre de Cristo fault zone, compared with the central Sange de Cristo fault zone and the Mesita fault (see stop B8, chapter B, this volume). Dashed lines indicate average slip rate for past 1.0–4.0 m.y. versus Sangre de Cristo fault zone (past 50 k.y.) near San Luis, Colo. (see Crone and Machette, 2006). The Servilleta Basalt (unit Tsb) is offset 610–670 m (2,000–2,200 ft) as measured from cross section A-A' on fig. C–7 (chapter C, this volume).

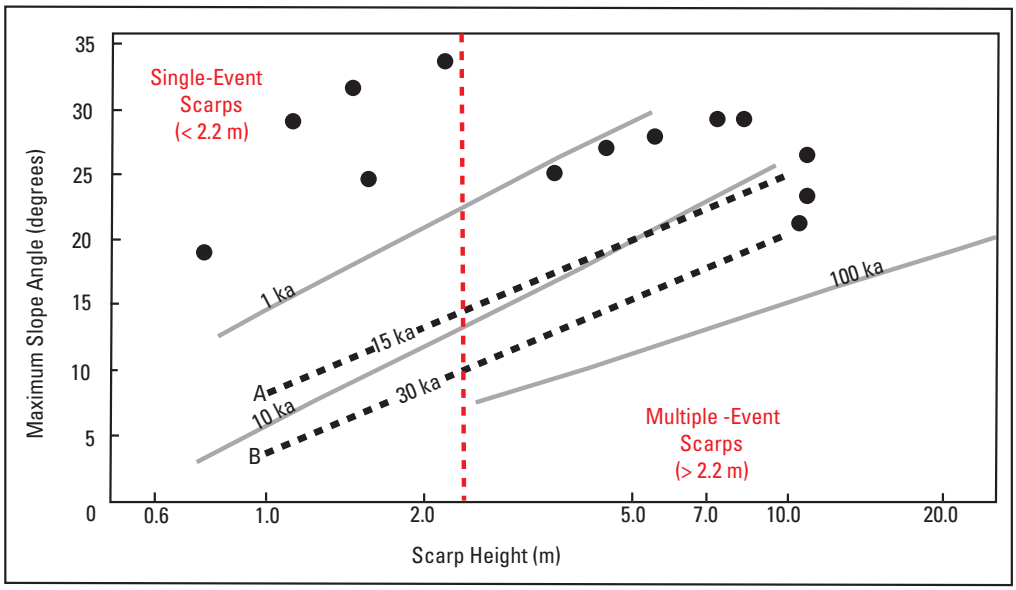

Figure J–7. Scarp height versus maximum slope angle for fault scarps profiled along the Latir Peaks section of the southern Sangre de Cristo fault zone. Solid gray lines are time-regression data from Bucknam and Anderson (1979). Dashed black lines labeled A and B are from Pierce and Colman (1986) and Pierce (1985), respectively.

deposits mapped as late middle Pleistocene and older in the region. With an inferred maximum offset of more than 10 m in >130 k.y., the maximum slip rate since late middle Pleistocene time would be 0.08 mm/yr for the trenched strand of the Cañon section.

Discussion

On the basis of our current understanding of the Sangre de Cristo fault system, we emphasize three main points:

1. We propose to subdivide the fault system into three main parts—the northern Sangre de Cristo, the central Sangre de Cristo, and the southern Sangre de Cristo fault zones;
2. Slip rates on individual sections of these three fault zones have varied throughout the Quaternary and Pliocene; and
3. The overall tectonic geomorphology of the three fault zones suggests marked differences in late Cenozoic fault behavior and leads to inferences about the interaction of these fault zones through time.

Our subdivision of the Sangre de Cristo fault system into three parts is based on geomorphic expression of the range fronts' evidence of Quaternary faulting, the presence of preexisting structures that could subdivide the fault zone, and fault-length parameters constrained by worldwide studies of active normal faulting. As discussed in each fault part's overview, individual sections show differing amounts of offset on deposits of differing ages, thus indicating that these three parts are internally segmented and that apparent interactions occur between sections as stress is relieved from one section and transferred to another following each event. However, we have only a rudimentary understanding of the timing of the most recent event, slip rates, and recurrence intervals for each section; we need more robust data to more clearly define which sections define potential segment rupture boundaries and how adjacent fault sections interact.

Preexisting bedrock structures interpreted from geophysical data and mapped in the footwall of the range-front faults can create asperities that might arrest lateral propagation of individual surface-rupturing earthquakes. On the basis of mapping of these structures, we note changes in Quaternary fault trend and geometry that might reflect control by preexisting faults developed during prior tectonic events and stress regimes.

Subdividing the Sangre de Cristo fault system into these three parts may give us some idea of potential fault rupture lengths that can be compared with observations of rupture characteristics from worldwide studies of active faults. Wells and Coppersmith (1994) show that historic normal-faulting earthquakes have rarely caused surface ruptures that exceed 70 km in length, so it is unlikely that the entire 104-km-long northern Sangre de Cristo fault or the 96-km-long southern Sangre de Cristo fault would rupture during a single earthquake, given the structural complexity of the three parts as previously mentioned. However, Suter and Contreras (2002) reported an historical rupture length of 104 km, but this length is very rare and has not been observed elsewhere. Thus, we conclude that these long structures can be subdivided into rupture sections as we have proposed. For comparison, studies of large (M>7) historic earthquakes in the Basin and Range Province (Doser and Smith, 1989) suggest that they all nucleated below 12 km depth and are composed of multiple subevents with individual rupture lengths <21 km, although the total rupture lengths approached 70 km. A classic example is the Dixie Valley and Fairview Peak earthquakes of December 16, 1954, in north-central Nevada. These two earthquakes occurred only 4 minutes apart, whereas the 1959 M_s7.5, Hebgen Lake, Mont. earthquake was composed of nearly indiscernible subevents (Doser, 1985). Thus, one needs to think of large (M>7) earthquakes as being composed of multiple subevents on individual rupture building blocks.

It is clear that the three individual parts in the large Sangre de Cristo fault system have sections of differing faulting behavior during 100 k.y. cycles, as their geomorphic expression exemplifies. Both the northern and southern Sangre de Cristo fault zones have geomorphic expressions indicative of tectonic activity rates that are as much as twice the calculated late middle Pleistocene to Holocene (<130 ka) slip rates of 0.01–0.09 mm/yr (Bull, 1984). Conversely, the central Sangre de Cristo fault zone has a geomorphic expression indicative of faults with only one-half of its calculated late Pleistocene slip rate (0.17 mm/yr). Lithology must be a major factor in geomorphic expression of the footwall block of Sangre de Cristo fault system. The geomorphic expression of relatively recent rapid uplift along central Sangre de Cristo fault zone is subdued by footwall rocks and sediment composed of easily eroded Santa Fe Group sediment, whereas the slower uplift along the northern and southern Sangre de Cristo faults contrasts with their precipitous footwalls composed predominantly of resistant Precambrian crystalline rock. Thus, we propose that the neotectonic signatures of the northern and southern Sangre de Cristo fault zones represent higher pre-late Quaternary slip rates with a decrease in tectonic activity during the past 130 k.y. As tectonic activity on the northern and southern fault zones decreased during the late Pleistocene, tectonic activity may have shifted to the central fault zone, thereby allowing the accumulated stress to be released on the central Sangre de Cristo fault between the two previously more active fault zones to the north and south, the northern and the southern Sangre de Cristo fault zones, respectively.

Acknowledgments

We appreciate the constructive and helpful comments of Anthony Crone (USGS) and Matthew Morgan (Colorado Geological Survey) who reviewed a preliminary version of this manuscript. However, any errors that may remain are the responsibility of the authors.

References Cited

Bruce, R.M., and Johnson, B.R., 1991, Reconnaissance geologic map of parts of the Zapata Ranch and Mosca Pass quadrangles, Alamosa and Huerfano Counties, Colorado: U.S. Geological Survey Miscellaneous Field Studies Map MF–2168, 1 sheet, scale 1:24,000.

Bucknam, R.C., and Anderson, R.E., 1979, Estimation of fault-scarp ages from a scarp height–slope-angle relationship, Geology, v. 7, p. 11–14.

Bull, W.B., 1984, Tectonic geomorphology: Journal of Geological Education, v. 32, p. 310–324.

Colman, S.M., McCalpin, J.P., Ostenaa, D.A., and Kirkham, R.M., 1985, Map showing upper Cenozoic rocks and deposits and Quaternary faults, Rio Grande rift, south-central Colorado: U.S. Geological Survey Miscellaneous Investigations Map, I–1594, 2 sheets, scale 1:125,000.

Crone, A.J., and Machette, M.N., 2005, Paleoseismic activity on the Sangre de Cristo fault near San Luis, Colorado [abs.]: Geological Society of America Abstracts with Programs, v. 37, no. 7, p. 558.

Crone, A.J., Machette, M.N., and Mahan, S.A., 2006, Paleoseismic investigation of Rito Seco site, central section of the Sangre de Cristo fault zone, Colorado—Data related to late Quaternary surface faulting on the Sangre de Cristo fault, Rito Seco site, Costilla County, Colorado: U.S. Geological Survey Scientific Investigations Map SI–2955, 1 oversize plate (available at: http://pubs.usgs.gov/sim/2006/2955).

Doser, D.I., 1985, Source parameters and faulting processes of the 1959 Hebgen Lake, Montana, earthquake sequence: Journal of Geophysical Research, v. 90, p. 4537–4555.

Doser, D.I., and Smith, R.B., 1989, An assessment of source parameters of earthquakes in the cordillera of the western United States: Bulletin of the Seismological Society of America, v. 79, no. 5, p. 1383–1409.

Gaca, J.R., and Karig, D.E., 1965, Gravity survey in the San Luis Valley area, Colorado: U.S. Geological Survey Open-File Report, unnumbered.

Haller, K.M., Wheeler, R.L., and Rukstales, K., 2002, Documentation of changes in fault parameters for the 2002 National Seismic Hazard maps–Conterminous United States except California: U.S. Geological Survey Open-File Report 02–467, 32 p. (available at: http://pubs.usgs.gov/of/2002/ofr-02-467/).

Kellogg, K.S., 1999, Neogene basins of the northern Rio Grande Rift—Partitioning and asymmetry inherited from Laramide and older uplifts: Tectonophysics, v. 305, p. 141–152.

Kelson, K.I., 1986, Long-term tributary adjustments to base-level lowering northern Rio Grande rift, New Mexico: Albuquerque, University of New Mexico, M.S. thesis, 210 p.

Kelson, K.I., Bauer, P.W., Connell, S.D., Love, D.W., Rawling, G.C., and Mansell, M., 2004, Initial paleoseismic and hydrogeologic assessment of the southern Sangre de Cristo fault at Taos Pueblo, *in* Brister, B.S., Bauer, P.W., Read, A.S., and Lueth, V.W., eds., Geology of the Taos region, New Mexico Geological Society 55th Annual Field Conference, Guidebook, p. 289–299.

Kirkham, R.M., Brister, B.S., Grauch, V.J.S., and Budhan, J.S., 2005, Culebra graben–A major intrarift structure in the San Luis Basin, Rio Grande rift [abs.]: Geological Society of America Abstracts with Programs, v. 36, no. 6, p. 14.

Kirkham, R.M., and Rogers, W.P., 1981, Earthquake potential in Colorado: Colorado Geological Survey Bulletin 43, 171 p.

Lipman, P.W., and Reed, J.C., 1989, Geologic map of the Latir volcanic field and adjacent areas, northern New Mexico, U.S. Geological Survey Miscellaneous Investigations Series Map I–1907, 1:48,000 scale.

Machette, M.N., and Personius, S.F., 1984, Map of Quaternary and Pliocene faults in the eastern part of the Aztec 1° by 2° quadrangle and the western part of the Raton 1° by 2° quadrangle, northern New Mexico: U.S. Geological Survey Miscellaneous Field Studies Map MF–1465–B, 1 sheet, scale 1:250,000.

Machette, M.N., Personius, S.F., Kelson, K.I., Haller, K.M., and Dart, R.L., 1998, Map and database of Quaternary faults and folds in New Mexico: U.S. Geological Survey Open-File Report 98–521, 443 p., 1 plate (1:750,000 scale).

Machette, M.N., Personius, S.F., and Nelson, A.R., 1992, Paleoseismology of the Wasatch fault zone—A summary of recent investigations, conclusions, and interpretations, *in* Gori, P.A., and Hays, W.W., eds., Assessing regional earthquake hazards and risk along the Wasatch Front, Utah: U.S. Geological Survey Professional Paper 1500, chap. A, p. A1–A72.

Machette, M.N., Thompson, R.A., and Drenth, B.J., in press, Geologic map of the San Luis quadrangle, Costilla County, Colorado: U.S. Geological Survey Scientific Investigations Map 2963, 1 sheet, 1:24,000 scale (http://pubs.usgs.gov/sim/2007/2963).

McCalpin, J.P., 1981, Quaternary geology and neotectonics of the west flank of the northern Sangre de Cristo Mountains, south-central Colorado: Golden, Colorado School of Mines, Ph.D. dissertation, 287 p.

McCalpin, J.P., 1982, Quaternary geology and neotectonics of the west flank of the northern Sangre de Cristo Mountains, south-central Colorado: Colorado School of Mines Quarterly, no. 77, 97 p.

McCalpin, J.P., 1986, Quaternary tectonics of the Sangre de Cristo and Villa Grove fault zones, *in* Rogers, W.P. and Kirkham, R.M., eds., Contributions to Colorado seismicity and tectonics—A 1986 update: Colorado Geological Survey Special Publication 28, p. 59–64.

McCalpin, J.P., 2006, Active faults and seismic hazards to infrastructure at Great Sand Dunes National Monument and Preserve: Crestone, Colorado: unpublished report by GEO-HAZ Consulting, Inc., 49 p., 1 oversize plate.

Menges, C.M., 1987, Temporal and spatial segmentation of Plio-Quaternary fault rupture along the base of the western Sangre de Cristo mountain front, northern New Mexico, *in* Menges, C.M., Enzel, Y., and Harrison, B., eds., Quaternary tectonics, landform evolution, soil chronologies and glacial deposits—Northern Rio Grande rift of New Mexico: Friends of the Pleistocene Rocky Mountain Cell Fieldtrip, Guidebook, p. 71–94.

Menges, C.M., 1988, The tectonic geomorphology of mountain-front landforms in the northern Rio Grande rift near Taos, New Mexico: Albuquerque, University of New Mexico, Ph.D. dissertation, 339 p.

Menges, C.M., 1990, Late Quaternary fault scarps, mountain-front landforms, and Pliocene-Quaternary segmentation on the range-bounding fault zone, Sangre de Cristo Mountains, New Mexico, *in* Krinitzsky, E.L., and Slemmons, D.B., eds., Neotectonics in earthquake evaluation: Geological Society of America Reviews in Engineering Geology, v. 8, p. 131–156.

Myers, W.F., and Hamilton, Warren, 1964, Deformation accompanying the Hebgen Lake earthquake of August 17, 1959, U.S. Geological Survey Professional paper 435, p. 37–98.

Pazzaglia, F.J., 1989, Tectonic and climatic influences on the evolution of Quaternary depositional landforms along a segmented range-front fault, Sangre de Cristo Mountains, north-central New Mexico: Albuquerque, University of New Mexico, M.S. thesis, 246 p., scale 1:24,000.

Personius, S.F., and Machette, M.N., 1984, Quaternary and Pliocene faulting in the Taos Plateau region, northern New Mexico, *in* Baldridge, W.S., Dickerson, P.W., Riecker, R.E., and Zidek, J., eds., Rio Grande rift—Northern New Mexico: New Mexico Geological Society 35th Annual Field Conference, Guidebook, p. 83–90.

Pierce, K.L., 1985, Quaternary history of faulting along the Arco segment of the Lost River fault, central Idaho, *in* Stein, R.S., and Bucknam, R.C., eds., Proceedings of Workshop XXVIII on the Borah Peak, Idaho, Earthquake: U.S. Geological Survey Open-File Report 85–290, v. A, p. 195–206.

Pierce, K.L., and Colman, S.M., 1986, Effect of height and orientation (microclimate) on geomorphic degradation rates and processes, late-glacial terrace scarps in central Idaho: Geological Society of America Bulletin, v. 97, p. 869–885.

Suter, Max, and Contreras, Juan, 2002, Active tectonics of northeastern Sonora, Mexico (southern Basin and Range Province) and the 3 May 1887 M_w 7.4 earthquake: Bulletin of the Seismological Society, v. 92, no. 2, p. 581–589.

Thompson, R.A., and Machette, M.N., 1989, Geologic map of the San Luis Hills area, Conejos and Costilla Counties, Colorado: U.S. Geological Survey Miscellaneous Investigations Map I–1906, 1 sheet, scale 1:50,000.

Thompson, R.A., Machette, M.N., and Drenth, B.J., 2007, Geologic map of San Pedro Mesa and surrounding area, Costilla County, Colorado: U.S. Geological Survey Open-File Report 2007–1074, 1 sheet, 1:24,000 scale (*http://pubs.usgs.gov/ofr/2007/1074*).

Tweto, Ogden, 1979, Geologic map of Colorado, U.S. Geological Survey, 1:500,000 scale.

Upson, J.E., 1939, Physiographic subdivisions of the San Luis Valley, southern Colorado: Journal of Geology, v. 47, no. 7, p. 721–736.

U.S. Geological Survey, 2005, Quaternary faults and fold database of the United States: U.S. Geological Survey website, available at *http://earthquake.usgs.gov/qfaults/*.

Wallace, A.R., 2004, Evolution of the southeastern San Luis Basin margin and the Culebra embayment, Rio Grande rift, southern Colorado, *in* Brister, B.S., Bauer, P.W., Read, A.S., and Lueth, V.W., eds., Geology of the Taos region, New Mexico Geological Society 55th Annual Field Conference, Guidebook, p. 121–132.

Wells, D.L., and Coppersmith, K.J., 1994, New empirical relationships among magnitude, rupture length, rupture area, and surface displacement: Seismological Society of America Bulletin, v. 84, p. 974–1002.

Widmann, B.L., Kirkham, R.M., Morgan, M.L., and Rogers, W.P., 2002, Colorado late Cenozoic fault and fold database and Internet map server: Colorado Geological Survey Information Series 60a, available at *http://geosurvey.state.co.us/pubs/ceno/*.

Machette, Coates, Johnson—**Quaternary Geology of the San Luis Basin, Colorado and New Mexico**—Open-File Report 2007–1193